RECZKO, BORIS FRANZ FRIEDRICH

THE GEOCHEMISTRY OF THE SEDIMENTARY ROCKS OF THE PRETORIA GROUP, TRANSVAAL SEQUENCE

PhD **UP** **1994**

The geochemistry of the sedimentary rocks of the Pretoria Group, Transvaal Sequence

by

Boris Franz Friedrich Reczko

Submitted in partial fulfilment of the requirements

of the degree of

DOCTOR OF PHILOSOPHY

in the

Faculty of Science of the

University of Pretoria

December 1994

I, BORIS FRANZ FRIEDRICH RECZKO, hereby declare that this thesis is my own original work, that all assistance and sources of information have been acknowledged, and that this work has not been presented to any other university for the purpose of a higher degree.

Die Wissenschaft ist ein grandioses Abenteuer des Geistes, das nicht auf die Entdeckungen absolut sicherer Theorien ausgeht, sondern auf die Erfindung immer besserer Theorien, die immer strengeren Prüfungen unterworfen werden können.

Karl Popper

Volume 1

ABSTRACT

A total of 1203 samples from all formations of the Pretoria Group, including mainly sedimentary rock samples, some volcanic rocks from the Hekpoort Formation and Machadodorp Volcanic Member as well as diabase sills, were taken from surface outcrops and drillholes in the main Transvaal basin. All samples were analysed for major and trace elements with XRF, 275 selected samples were analysed for boron with ICP-AAS, and 50 selected shale samples were analysed for REE, organic carbon and CO_2 using liquid chromatography and LECO. The mineralogy of selected shale samples was established with XRD. The sedimentary and volcanic sample populations were treated statistically after differentiation in stratigraphic and regional sub-groups, and average element concentration estimates of the sub-groups were established.

Generally, two distinct groups of shales can be differentiated geochemically and mineralogically, i.e. high-Al shales with a predominant kaolinite-mica clay mineral assemblage, and high-Mg-Ca-Na shales with a mica-plagioclase mineral assemblage. The high-Al shales dominate the succession from the base of the Pretoria Group up to the Daspoort Formation, the high-Mg-Ca-Na shales occur mainly in the Silverton and post-Magaliesberg Formations. The shale samples from the Botswana sampling area are somewhat different from this stratigraphic trend, as they contain significant amounts of chlorite, which is only an accessory mineral in other parts of the basin. The geochemistry of the shales generally points to some regional differences, independent of the stratigraphic signature. The Pretoria Group shale estimate (640 samples) is enriched in Al, Th, Cr and Sc, and depleted in Mn, Na, Ca, Sr and some base-metals compared to average shale estimates. The Pretoria Group sandstone estimate (335 samples) is enriched in Cr, Ni and Fe, and depleted in Ca, Na, Ti and K compared to average sandstone estimates.

The geochemistry of the sedimentary rocks of the Pretoria Group shows evidence for complex source terrains, with predominantly granitic and sedimentary sources, as well as, possibly, ultramafic sources. Transport fractionation seems to have influenced the evolving pattern to a certain degree. The syndepositional palaeoclimate is thought to have been humid-hot, at least for the middle part of the Pretoria Group (Hekpoort to Daspoort Formations). The basal part of the Pretoria Group has a similar geochemical pattern (i.e. points to a similar climate), but the possible introduction of reworked and redeposited weathering profiles, related to the depositional hiatus between the Chuniespoort and Pretoria Groups must be considered in any interpretation. Penecontemporaneous volcanic activity and proposed tectonic activity obviates an evaluation of syndepositional climate for the Post-Daspoort formations. The geochemical signature of Pretoria Group sedimentary rocks is indicative of a divergent margin tectonic setting (intracratonic sag, failed rift/aulacogen or passive margin). Asthenospheric upwelling related to a rift tectonic setting could provide a simple explanation for the composition of Pretoria Group volcanic rocks. The geochemistry of boron and REE point to a strong influence of post-depositional processes, namely diagenesis and/or hydrothermal alteration. Mineral assemblages and trace element patterns provide some evidence for local source areas, for at least the lower part of the Pretoria Group. The described geochemical pattern cannot solve the marine/lacustrine nature of the basin.

SAMEVATTING

'n Totaal van 1203 monsters van al die formasies in die Pretoria Groep in die hoofkom van die Transvaal Opeenvolging, sowel as van 'n aantal diabaasplate- en gange is versamel van dagsone en boorgate. Die meeste van die monsters is van sedimentere gesteentes, maar n aantal is van vulkaniese gesteentes van die Hekspoort Formasie en die Machadadorp Lid. Al die monsters is vir hoof- en spoorelemente ontleed deur middel van XRF-spektemetrie, 275 geselekteerde monsters vir boor deur middel van IGP- AA- spektrometrie en 50 geselekteerde monsters vir seldsame aardelemente, organiese koolstof en CO2 deur middel van vloeistof-chromatografie en LECO. Die mineralogie van uitgesoekte skaliemonsters is bepaal deur middel van XRD. Die monsterpopulasies van sedimentêre en vulkaniese gesteentes is verdeel in stratigrafiese en geografiese subgroepe en gemiddelde elementkonsentrasies van die subgroepe is statisties bepaal.

Twee duidelike groepe van skalie kan geochemies en mineralologies onderskei word, nl. hoë-Al skalie met 'n oorwegend kaoliniet- glimmer mineraalversameling, en hoë-Mg-Ca-Na skalie met n oorwegend glimmer-plagioklaas mineraalversameling. Die hoë-Al skalies oorheers die Pretoria Groep vanaf die basis tot by die Daspoort Formasie en die hoë-Mg-Ca-Na skalies oorheers in die Silverton Formasie en die Na-Magaliesberg formasies. Die skaliemonsters van Botswana verskil effens van hierdie stratigrafiese- beheerde tendens deurdat hulle opmerklike chloriet bevat - 'n mineraal wat slegs in ondergeskikte hoeveelhede in ander dele van die kom voorkom. Die geochemie van die skalies vertoon ook sekere regionale verskille, onafhanklik van die stratigrafiese tendens. Die skalie van dei Pretoria Groep (640 monsters) is verryk aan Al, Th, Cr en Sc en verarm aan Mn, Na, Ca, Sr en sommige basismetale vergeleke met skattings vir die gemiddelde skalie. Die sandstene van die Pretoria Groep (335 monsters) is verryk aan Cr, Ni en Fe en verarm aan Ca, Na, Ti en K vergeleke met skattings vir die gemiddelde sandsteen.

Die geochemie van die sedimentêre gesteentes van die Pretoria Groep getuig van 'n komplekse brongebied van oorwegend granitiese en sedimentere en moontlik ook vulkaniese gesteentes. Fraksionering tydens vervoer van die materiaal het oënskynlik die ontwikkelingspatroon van die sedimente tot 'n mate geaffekteer. Die paleoklimaat tydens afsetting was waarskynlik warm en humid, ten minste vir die middelste gedeelte van die Pretoria Groep (Hekpoort tot Daspoort Formasies). Die onderste gedeelte van die Pretoria Groep het soortgelyke kenmerke wat dui op 'n soortgelyke klimaat, maar die moontlike toevoer van herwerkte en herafgesette verweringsmateriaal, verwant aan die afsettingshiaat tussen die Chumiespoort en Pretoria Groep moet in ag geneem word in enige interpretasie. Penekontemporêre vulkaniese aktiwiteit en verwante tektoniese aktiwiteit maak die herkenning van die paleoklimaat tydens die afsetting van die Na-Daspoort formasies onmoontlik. Die geochemiese kenmerke van die sedimentêre gesteentes van die Pretoria Groep dui op 'n tektoniese plasing by 'n divergerende plaatgrens (intrakratoniese afsakking, onvoltooide sinkdal\ aulakogeen of passiewe grens). Astenosferiese opwelling verwant aan 'n sinkdal-tektomiese plasing sou 'n eenvoudige verklaring bied vir die vulkaniese gesteentes van die Pretoria Groep. Die geochemie van boor en die seldsame aardelemente dui op 'n sterk invloed van diagenese en\of hidrotermale verandering na afsetting van die sedimente. Mineraalversamelings en spoorelementkenmerke is getuienis ten gunste van plaaslike brongebiede, ten minste vir dir onderste gedeelte van die Pretoria Groep. Die geochemiese gegewens kan egter nie gebruik word om te besluit of die afsettingskom marien of lakustrien was nie.

CONTENTS

LIST OF FIGURES

LIST OF TABLES

CONTENTS OF APPENDICES (Vol. 2)

(**Note:** Each Appendix has an internal numeration, and contains a detailed list of contents)

CHAPTER 1: INTRODUCTION

1.1 Aims and objectives

This study was undertaken to establish the geochemistry of the sedimentary rocks of the Early Proterozoic Pretoria Group, Transvaal Sequence, including regional and stratigraphic variation in element contents. The geochemical parameters will be used to discuss the depositional palaeoenvironment, syndepositional palaeoclimate, composition of source rocks, tectonic setting, post-depositional events and the economic mineral potential of the investigated rocks. The implications of the geochemistry for existing depositional and structural models will be discussed.

The size of the study area (Chapter 1.2) made it impossible to sample detailed stratigraphic sections everywhere. Accordingly, the sample locations were chosen with respect to investigated areas, where at least the sedimentology and, if possible, structural framework had been established.

It should be emphazised, that the geological implications of the geochemistry form the major aim of this study. Although great importance was attached to precision and accuracy of the element determinations, the choice of analytical procedures was directed by practicality. The analytical procedures used are standard methods in geochemistry, and are therefore only described but not discussed.

1.2 Study area

The study area comprises the main outcrop area of the Pretoria Group in the Transvaal region of South Africa and in eastern Botswana, an oval-shaped basin of 500 km by 200 km (Fig. 1.5.1). The study area stretches from Lobatsi, Botswana, in an ENE-direction to Thabazimbi and in an ESE-direction to Pretoria and Bronkhorstspruit; from Potgietersrus in an easterly direction to Penge and from Penge in a southerly direction to Carolina. It also includes the isolated occurrences of Pretoria Group rocks surrounded by the Bushveld Complex at the Marble Hall, Dennilton, Makeckaan, Rooiberg and Crocodile River Fragments. Samples were not taken in the Potchefstroom Synclinorium to the south of the main Transvaal basin and the Kanye basin in Botswana (Figs. 1.2.1 and 1.5.1).

1.3 General geology

The Transvaal Sequence is preserved in a main Transvaal or Bushveld basin within South Africa, situated in the southern, western, central and eastern Transvaal and in southeastern Botswana between Lobatsi and Ramotsa (Fig. 1.2.1).

The Pretoria Group correlates to a certain degree with the Postmasburg Group of the Griqualand West Sequence (Fig. 1.2.1, Table 1.2.1). However, only the Hekpoort and Ongeluk volcanics show a satisfying geochemical pattern of correlation (Sharpe et al., 1983; Harmer and v. Gruenewaldt, 1991), whereas the sedimentary rocks overlying and underlying these volcanics are distinguished by their different petrography and thicknesses. The term Transvaal 'Supergroup' or 'Sequence' for both sequences (e.g. Beukes, 1986) is avoided, because the lack of any preserved contact between the Transvaal and Griqualand West basins makes the usage of an overall term erroneous according to stratigraphic terminology (SACS, 1980; Eriksson et al., 1993a). In a recent development, the term 'Transvaal Sequence' was withdrawn by SACS due to its possible confusion with to the modern concept of 'sequence stratigraphy', where the term 'sequence' has a different meaning (P.G. Eriksson, 1994, pers. comm.). SACS has subsequently reintroduced the term 'Transvaal Supergroup'.

The Bushy Bend Lava Member at the base of the Timeball Hill Formation (Eriksson et al., in press b) has a preliminary single zircon date of 2350 Ma (Eriksson et al., in press a). Dullstroom volcanics, which are regarded as part of the post-Pretoria Rooiberg Group by Schweitzer (1992) and Eriksson et al. (1993a), are dated at 2089 $\pm$ 26 Ma (Rb-Sr, Schweitzer, 1986). An age constraint of approximately 2400 - 2100 Ma may thus be placed on the Pretoria Group. This is supported by an age determination of 2224 $\pm$ 21 Ma (Rb-Sr, Burger & Coertze, 1975) for the Hekpoort Formation andesites. The upper age limit is supported by an age of 2465 Ma (SHRIMP) for the Kuruman Formation (R. Armstrong, 1993, pers. comm.), which is a time and facies equivalent of the Penge Formation in the Transvaal basin (Beukes, 1983). The Penge Formation is part of the Chuniespoort Group of the Transvaal Sequence, which underlies the Pretoria Group. The total thickness of the Pretoria Group varies between 7000 m in the eastern Transvaal (Button, 1973; Schreiber, 1990), 3300 m in the central Transvaal (SACS, 1980), 1500 m in the western Transvaal

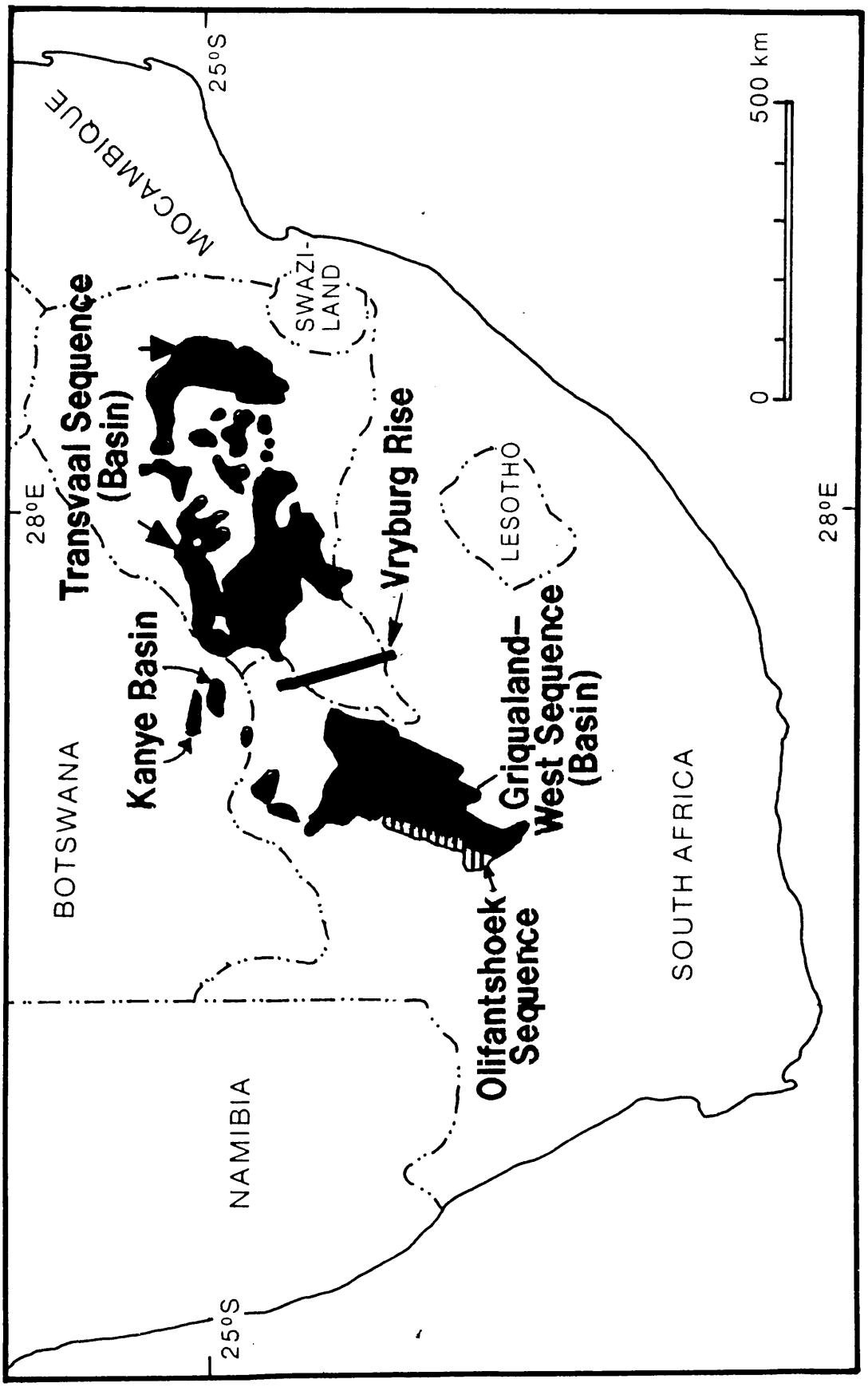

Figure 1.2.1: The geographic position of the Early Proterozoic Transvaal (= Bushveld), Kanye and Griqualand West basins in South Africa.

Overall lithology	Griqualand West Sequence (Basin)	Kanye Basin (Transvaal Sequence) (Botswana)	TRANSVAAL SEQUENCE (Transvaal or Bushveld Basin)	
			S.E. Botswana (Bushveld basin)	South Africa (Transvaal basin)
Volcanic & clastic sedimentary unit				Loskop clastics & volcanics Damwal/Selonsrivier Duitstroom lavas/Smelterskop & Makeckaan clastics (lavas) Leeuwpoort sandstones — Rooiberg Group (sensu lato)
Clastic sediments & volcanics			Woodlands volcanics/clastics	Rayton sandstones & shales & volcanics — Pretoria Group
	Postmasburg Group: Mooiwater dolomites & Manganiferous Hotazel ironstones		Sengoma sandstones	Magaliesberg sandstones
			Sengoma shales	Silverton shales
		Segwagwa Group: Mogapinyana & Gatsepane chert, sandstone & shale	Ditlhojana sandstones/conglomerates	Daspoort sandstones
				Strubenkop shales
	Ongeluk andesites	Tsatsu andesites	Ditlhojana volcanics	Dwaalheuwel/Droogedal sandstones Hekpoort andesite
	Makganyene diamictites	Ditlhojana & Tlaameng shales, sandstones & conglomerates	Ditlhojana shales: conglomerates / shales	Boshoek conglomerates/sandstones shales
			Tsokwane sandstones	sandstone — Timeball Hill
			Lephala: shales / conglomerates/sandstones	shales Roolhoogte conglomerates/ sandstones
Regional unconformity				
Chemical sedimentary unit	Ghaap Group: Koegas Subgroup / Asbesheuwels Subgroup: Griquatown & Kuruman Iron formations	Taupone Group: Masoke ironstone/ferruginous chert	Ramotswa shale	Duitschland carbonates, clastics Penge Iron formations — Chuniespoort Group
		Kgwakgwe chert breccia		
	Campbellrand Subgrp: Campbellrand dolomites	Ramonnedi dolomites	Magopane / Maholobota / Ramotswa: dolomites	Malmani dolomites
	Schmidtsdrif Subgrp: Lokamonna Formation (shale) Boomplaas Form. (dolomite)			
Clastic sediments	Vryburg Formation	Black Reef Formation	Black Reef Formation	Black Reef Formation
Clastic sediments & volcanics (Ventersdorp age)				Pre-Black Reef units - Wolkberg Group & correlates

Table 1.2.1: Correlation of Griqualand West, Kanye and Transvaal basins (modified after Eriksson et al., 1993)

(SACS, 1980) and approximately 3000 m in Botswana (Key, 1983). However, the reported thickness data include post-depositional mafic sills, which are common throughout the stratigraphy, with an increase in number and thickness towards the top of the Pretoria Group (Button, 1973; Sharpe, 1984; Schreiber, 1990). Hence, the real thickness of the Pretoria Group must be smaller than the reported values. The thickness data for the western Transvaal might be underestimated, as the thickness of the Silverton and the Magaliesberg Formations are difficult to estimate due to alluvial cover and mafic intrusive rocks in the Nietverdiend area, which are thought to be related to the Bushveld Complex.

In general, the Pretoria Group consists of alternating mudrocks and thinner recrystallized sandstones, with three interbedded main volcanic units. Figure 1.2.2 gives the generalized lithostratigraphy of the Pretoria Group. Further lithological data and geographical variations of the various formations are listed in Table 1.2.2. It should be mentioned that the post-Magaliesberg Formations are subdivided into Vermont, Lakenvlei, Nederhorst, Steenkampsberg and Houtenbeck Formations in the eastern Transvaal, whereas subdivision was omitted in the central Transvaal (Rayton Formation) and Botswana (Woodlands Formation), where only a single unit is used (Eriksson et al., 1993a). The names for the pre-Woodlands formations in the Bushveld basin in southeastern Botswana (e.g. Key, 1983) are disregarded in this work, due to a very good correlation with the western Transvaal stratigraphy (Piper and Kreimeyer, 1992). The exact startigraphic position of the Makeckaan Formation (Makeckaan Fragment, Fig. 1.5.1) and the Leeuwpoort and Smelterskop Formations (Rooiberg Fragment, Fig. 1.5.1) is uncertain (Rooiberg Group in Table 1.2.1); however, Hartzer (pers. comm., 1994) proposes a late Pretoria Group age based on recent research.

Sedimentary structures are common and well preserved in the Pretoria Group sandstones, particulary ripple marks, planar and trough cross-bedding, and channel-fills. The wide variety of ripple mark types have been used as a depositional enviroment indicator for Pretoria Group sediments (e.g. van der Neut, 1990; Schreiber, 1990). The mudrocks are generally poorly exposed and normaly display few features in outcrop, except for colour-banding and small-scale graded bedding (Schreiber, 1990). Organo-sedimentary structures have been found associated with minor carbonate rocks (Button, 1973), and in black shales of the

FORMATIONS		TRANSVAAL BASIN				INFERRED PALAEO-ENVIRONMENTS
		WEST	CENTRE	EAST	SOUTH	
HOUTENBEK	Mudrocks, sandstones, limestones, tuffaceous mudrocks	Woodlands Formation in far west - interbedded mudrocks & sandstones, some conglomerates, 600 -1200 m	Rayton Formation- interbedded mudrocks & sandstones, minor andesites & dolomites ±1200 m	150-200 m	Absent	Combination of tectonic instability & central basin doming produced separate, probably closed western & eastern basins, with fan, fan-delta, delta & shallow lacustrine sedimentation
STEENKAMPSBERG	Sandstones			450-600 m, erosive base in north		
NEDERHORST	Sandstones Mudrocks, tuffaceous mudsrocks			200-600 m, sandstones are arkosic		
LAKENVLEI	Sandstones			200-250 m, Some arkosic sandstones		
VERMONT	Mudrocks & tuffaceous mudrocks			500-700 m		
MAGALIESBERG	Sandstones (mudrock lenses & interbeds)	120-300 m, significant mudrocks, Sandstones thicken to west & to east	±300 m Subordinate mudrocks thicken to west	±500 m, subordinate mudrocks	Very thin, mostly eroded	Probably represents sandy shoreline to Silverton basin, evidence for fluvial reworking of shoreline deposits as basin shrank
SILVERTON	Sandstone lens Mudrocks, commonly tuffaceous Machadodorp Volcanic Member Mudrocks, commonly tuffaceous	≥100 m dolomites in west at top of formation. Minor reworked tuffs. Total thickness: 400-600 m & thins to west	No significant sandstones Thin pyroclastic & dolomitic/chert member Total thickness ±600 m	Upper mudrocks ±1700 m & thin to north Machadodorp Member ±500 m Lower mudrocks ±250 m	±550 m	Relatively deep basin suspension desposits, tuffaceous shales common, medial pyroclastics in east of basin. Uppermost carbonates in north point to shallower water & far removed sediment sources
DASPOORT	Sandstones	130-200 m pebbly sandstones & mudrocks in far west, thickens to west, locally △	±60 m, pebbly sandstones common, locally ▽	0-±1100m, pebbly sandstones, mudrocks & thicker in north, ironstones & Fe-mudrocks in N.E.	±60 m,pebbly sandstones, mudrocks	Distal fan, fluvial braidplain, with distal shallow basin to east
STRUBENKOP	Mudrocks, lesser sandstones	100-135 m minor sandstones	±110 m, significant sandstones, locally ▽, minor tuffs	±30-100 m, thickens to south	±110 m, thickens to south	Shallow basin, distal to Dwaalheuwel fan systems
DWAALHEUWEL or DROOGEDAL	Diamictite, conglomerate, sandstone	Droogedal - 10-50 m	Absent or very thin	Dwaalheuwel 50-100m, thins to south	Absent	Alluvial fan & fan-delta deposits
HEKPOORT	Basaltic andesite	510-600 m	±400m, Air fall & reworked pyroclastics locally	±25-500 m, pyroclastics common, thins to north	±550-630 m, thickens to south, pyroclastics common	Volcanism, commonly pyroclastic, localised sedimentary interbeds. Uppermost palaeosol
BOSHOEK	Diamictite, conglomerate, sandstone	0-10 m	0-50 m	≥100m large channels	±10 m diamictite	Periglacial till & fan deposits
TIMEBALL HILL	Upper Mudrocks Diamictite/conglomerate lens Klapperkop Quartzite Member Lower mudrocks Bushy Bend Lava Member	Upper mudrocks 200-500 m, thicken westwards, no diamictite lens Quartzites 5-500 m, thicken westwards Lower mudrocks 300-500 m, thicken westwards	Upper mudrocks, ±100-200 m, thick lens of diamictite/conglomerate Quartzites ±30-70 m Lower mudrocks 400-700 m, thin southwards	Upper mudrocks ±400-600 m, arkose wedge in north, thin diamictites, deformed mudrocks Quartzite 0-15-100 m, thins to South Lower mudrocks 400-700 m, thin southwards	Upper mudrocks ±180 m Quartzite 10-90 m, thins southwards Lower mudrocks 140-430m, thicken southwards ≤90 m Bushy Bend Lava Member	Relatively deep periglacial basin subject to suspension sedimentation, turbidites, distal fluvial-deltaic deposition and short-lived periglacial reworked tillite deposition. Basal volcanism in south & widespread fumarolic influence throughout basin & stratigraphy
ROOIHOOGTE	Polo Ground Quartzite Member Mudrock Bevets Conglomerate (breccia) Member	Polo Ground 0-1 Mudrocks 0-150 m Bevets 0-150 m	0-10 m 0-18-250 m 0-150 m	Only Bevets Member, 0-30m, locally quartzite	Sandstone & diamictite ±25 m Mudrocks ±15 m Bevets ±110 m	Basal *in situ* karst-fill, succeeding alluvial fan, fan-delta & shallow periglacial basin
CHUNNIESPOORT GROUP	Iron Formation & dolomite	PALAEOKARST TOPOGRAPHY				

Figure 1.2.2: Lithostratigraphy of the Pretoria Group, illustrating thickness and lithological variation across the Transvaal basin (modified after Eriksson et al., in press a)

Table 1.2.2: Lithology of Pretoria Group formations in the Transvaal basin

Formation	Lithology	BOT	NWT	WF	WT	CT	EF	ET	NET
Mackekaan	Q,ark ss, cong						X		
Rooiberg*)	Q,ark ss,an volc,sh			X					
Houtenbeck	Q,sh,carb,calc sil							X	
Steenkampsberg	Q						X	X	
Nederhorst	Q,ark ss,calc sil,carb,sh							X	
Lakenvlei	Q,ark ss						X	X	X
Vermont	sh,tsh,(carb)						X	X	X
Rayton	Q,volc,cong,(sh)	X	X	X	X	X			
Magaliesberg	Q,(sh,carb)	X	X	X	X	X	X	X	X
Siverton	sh,tsh,volc,carb,(ss,cong)	X	X	X	X	X	X	X	X
Daspoort	Q,(sh)	X	X	X	X	X	X	X	X
Strubenkop	sh,oo,(ss)		X	X	X	X	X	X	
Dwaalheuwel	Q,(sh)		X		X		X	X	X
Hekpoort	and volc,(sh,Q)	X	X	X	X	X	X	X	X
Boshoek	Q,cong,diam				X	X		X	
U.Timeball Hill	sh,ss,diam,(oo)	X	X	X	X	X	X	X	X
Timeball Hill Q	Q,(sh)	X	X	X	X	X	X	X	X
L.Timeball Hill	sh,volc	X	X	X	X	X	X	X	X
Rooihoogte	brec,cong,Q,sh	X	X	X	X	X	X	X	X

Abbreviations: sh = shale; tsh = tuffaceous shale; ss = sandstone; Q = quartzite; cong = conglomerate; ark ss = arkosic sandstone; brec = breccia; volc = volcanic units; and volc = andesitic volcanism; diam = diamictite; carb = carbonate; calc sil = calc-silicate rocks; oo = ironstone; BOT = Botswana; NWT = Northwestern Transvaal; WF = Western Fragments (Crocodile River & Rooiberg); WT = Western Transvaal; CT = Central Transvaal; ET = Eastern Transvaal; NET = Northeastern Tranvaal; EF = Eastern Fragments (Dennilton, Marble Hall & Mackekaan); **Definition of areas see Fig. 1.5.1**; ( ) = minor lithological facies; *) = lower Leeuwpoort and upper Smelterskop Formation; (after P.G. Eriksson, 1994, pers. comm.)

Timeball Hill Formation (Nixon et al., 1988).

Tuffaceous material appears to be interlayered with the fine-grained rocks of the Timeball Hill, Silverton, Vermont, Nederhorst and Houtenbeck Formations (Button, 1973; Schreiber, 1990, Eriksson et al., 1990).

The depositional models proposed for the Pretoria Group formations vary from author to author. The suggested models are summarized in Table 1.2.3. In general, two opposing views can be distinguished:

1. deposition in an epeiric marine environment with accompanying continental facies (e.g. Visser, 1969, 1972; Button, 1973, 1975, 1986; Eriksson, 1973; Button and Vos, 1977; Klop, 1978; Tankard et al., 1982; Beukes, 1983)
2. an intracratonic palaeoenvironment with predominantly fluvial-lacustrine settings and short-lived marine incursions (e.g. Du Toit, 1954; Visser, 1957; Crockett, 1972; Eriksson, 1986, 1988, 1990, 1992; Eriksson et al., 1989, 1991a, 1993a, in press a; van der Neut, 1990; Schreiber, 1990; Eriksson and Clendenin, 1990; Schreiber and Eriksson, 1992; Schreiber et al., 1992).

The tectonic setting of the Pretoria Group is also discussed from different points of view. Figure 1.2.3 gives the position of the Pretoria Group relative to major tectonic features. Eriksson (1990), Eriksson et al. (1991a,b), Schreiber (1990) and Schreiber et al. (1992) propose a rift setting with half-graben developement (Fig. 1.2.4). Their model includes three cycles of initial mechanical rifting in the lower part of the Pretoria Group (up to the Daspoort Formation), thermal subsidence with expansion of the basin during Silverton/Magaliesberg Formation times, and resurgent mechanical subsidence for the post-Magaliesberg Formations. This model is accepted by v. Gruenewaldt and Harmer (1993), who have investigated the volcanic rocks of the Transvaal Sequence and the igneous rocks of the Bushveld Complex, and who have postulated a rift-setting for the volcanics as well as for the Bushveld Complex. The Bushveld Complex is intrusive into the upper Transvaal Sequence, the Pretoria Group forming the floor in most areas. Hatton and Sharpe (1988) and Hatton and v. Gruenewaldt (1990) describe a subduction-related signature of the Bushveld magmas. The subduction zone they postulate is thought to be related to the Limpopo Mobile Belt (Fig. 1.2.3). The proposed associated island arc setting for the Bushveld Complex (Hatton and v. Gruenewaldt, 1990)

Table 1.2.3: Proposed depositional palaeoenvironments for Pretoria Group formations

Formations	Intracratonic Basin	Epeiric Sea
Rayton Fm. & correlates	ETvl & CTvl: shallow lacustrine & wind-tidal flat (shales), fan & fan-delta (s/stones) [2,3,25]; BOT: gravity flow [26,27];	ETvl: beach - intertidal mudflat - shallow marine [6,24]; CTvl: fluvial [5]
Magaliesberg	regressive shoreline [4,19]; tidal [22]; above with marine influence [14,21]; above with fluvial influence [14,23];	delta - beach - shallow marine [6]; fluvial - beach [5];
Silverton	lacustrine delta/fan-delta [4,19]; above with transgressive marine influence [14, 21];	pro-delta [6]
Daspoort	distal fan - fluvial braidplain [3,20];	fluvial - beach [5]; shallow marine / beach barrier [6];
Strubenkop	distal lacustrine [4,19];	shallow marine [5]; tidal flat [6]; ironstones: shallow offshore
Dwaalheuwel	alluvial fan/distal fan [3,18]	shallow marine [6]
Hekpoort (only sediments)	paleosoil [15]; resedimented volcanics [17]; semi-arid, cool climate playa lake [16];	
Boshoek	alluvial [13]; glacial-alluvial [14];	
Upper Time-ball Hill	glacial-lacustrine [14];	glacial - fluvial - marine [12]; ironstones: shallow marine [6,8];
Timeball Hill Quarzite	tidal reworking of delta-front sand (lacustrine delta) [3,4];	tidal reworking of delta-front sands (marine) [6,7,9,10];
Lower Time-ball Hill	resedimentation of distal delta (lacustrine delta) [3,11];	current resedi-mentation of distal delta (marine) [6,7,9,10];
Rooihoogte	Alluvial fan, distal fan lacustrine [1,2,3,4];	transgressive marine [5,6,7,8];

(1= Eriksson, 1988; 2= van der Neut, 1990; 3= Schreiber, 1990; 4= Eriksson & Clendenin, 1990; 5= Visser, 1969; 6= Button, 1973; 7= Button, 1986; 8= Beukes, 1983; 9= Visser, 1972; 10= Eriksson, 1973; 11= Eriksson et al., 1993; 12= Visser, 1971; 13= Schreiber et al., 1990; 14= Eriksson, 1993a; 15= Button, 1979; 16= Martini, 1990; 17= Eriksson & Twist, 1986; 18= Eriksson et al., 1989; 19= Eriksson et al., 1991; 20= Eriksson et al., 1993b; 21= Eriksson, 1992; 22= Eriksson et al., 1987; 23= Reczko et al., 1992; 24= Button & Vos, 1977; 25= Schreiber & Eriksson 1992; 26= Crocket 1969; 27= Crocket 1972;)

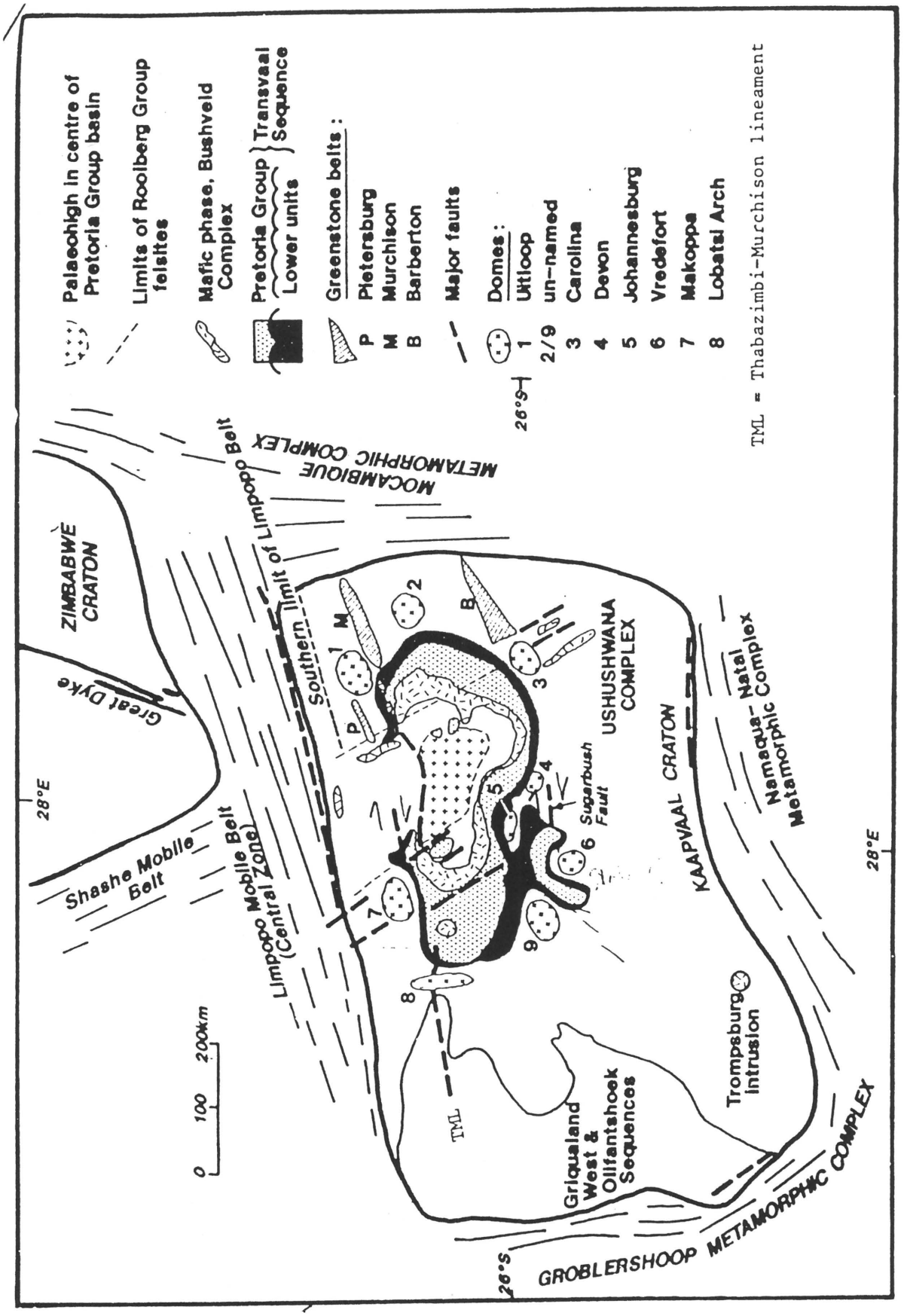

Figure 1.2.3: Geographical position of the Transvaal basin on the Kaapvaal craton and its spatial relation to major structures of the Kaapvaal craton. Modified after Eriksson et al. (1991).

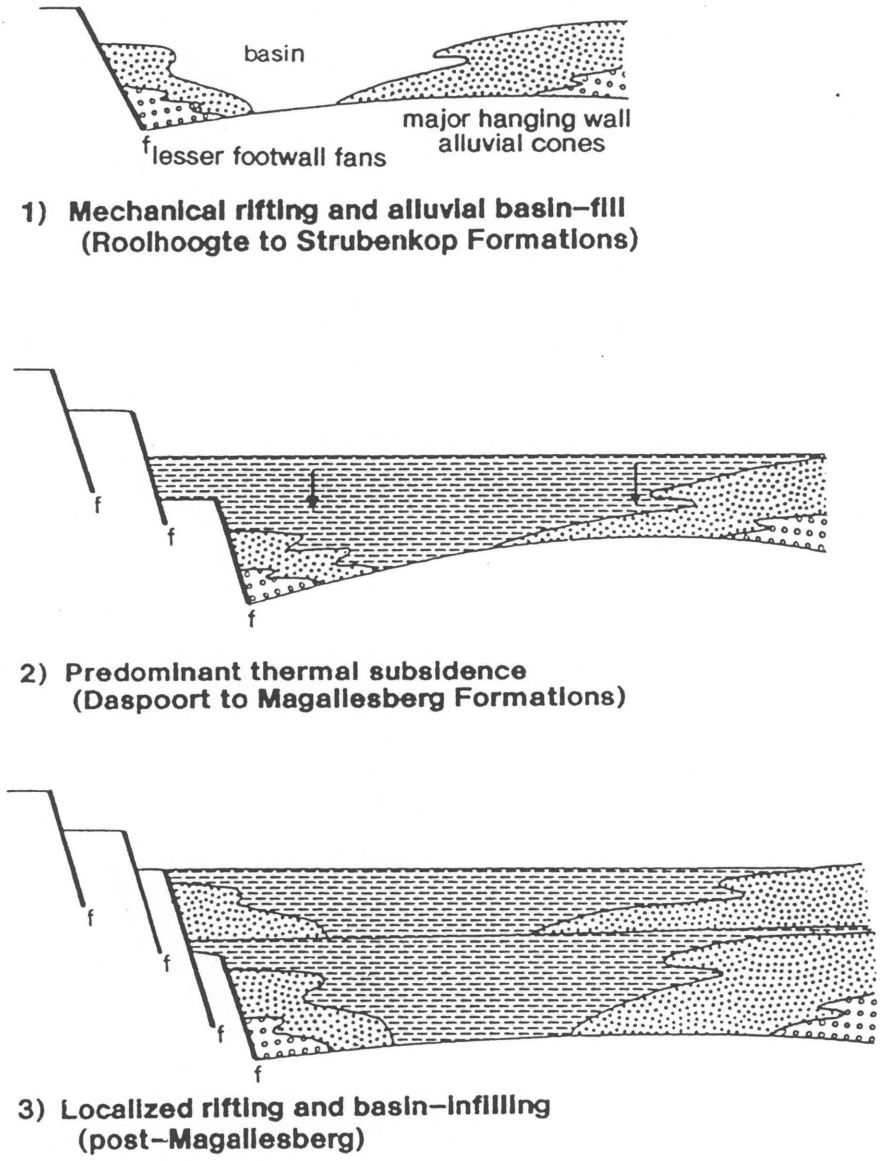

Figure 1.2.4: Tectonic setting of the Pretoria Group proposed by Eriksson (1990) (modified after Schreiber, 1990)

leads to a back-arc depositional model for at least the upper parts of the Pretoria Group (e.g., Hatton, 1993, pers. comm.). However, a revised model by Hatton (1994) suggests the ascent of the Bushveld magmas to be related to a mantle plume, as an active tectonic margin setting is considered to be generally unsatisfactory to account for the composition of the igneous rocks of the Bushveld Complex. Winter (1991) proposed a foreland basin setting for the Pretoria Group, related to a major collisional event in the Limpopo Mobile Belt. This suggestion follows on the earlier work of Button (1975).

Several important post-depositional events affecting the Pretoria Group are distinguished. The emplacement of mafic sills, differentiated into pre-Bushveld, syn-Bushveld and Waterberg-age (= 1600 - 1900 Ma) sills (Sharpe, 1984), and contact-metamorphism related to the emplacement of the Bushveld Complex (e.g. Engelbrecht, 1976, 1986; Wallmach et al., 1989), are the major post-depositional events which would have influenced primary petrography and possibly geochemistry. The frequent occurrence of andalusite-bearing shales and slates in most of the Pretoria Group shale formations and the occurrence of cordierite, amphiboles and garnets in shales near to the Bushveld Complex contact, are thought to be related to the intrusion of the Bushveld magmas (Sharpe, 1984; Engelbrecht, 1976, 1986); this thermal metamorphism had an additional affect on the degree of regional metamorphism of the Pretoria Group sedimentary rocks further away from the contact (Wallmach et al., 1989). However, petrographic, geochemical and sedimentological data of the sedimentary and volcanic rocks of the Pretoria Group show that, apart from the contact aureole, the influence of regional metamorphism is negligible (Eriksson and Clendenin, 1990). The influence of metamorphism related to the Bushveld intrusion is thought to be overestimated by several workers (Wallmach et al., 1989).

References to the economic geology of the Pretoria Group are compiled in Table 1.2.4. Although various types of mineralization are known, none of these occurrences, with the exception of hydrothermal gold and andalusite deposits, are presently of economic importance.

Table 1.2.4: Reported economic mineralisation of Pretoria Group sedimentary and volcanic rocks in the Transvaal basin (modified after Schreiber, 1990)

Hydrothermal Au and Ag, associated with Ag, Bi, Co	stratiform and vertical reefs in the Timeball Hill, Boshoek, Strubenkop, Silverton and Rayton Formations (e.g. Hammerbeck, 1976; Verryn et al., 1991; Boer et al., 1993; Harley and Charlesworth, 1993)
Fe_2O_3/Fe_3O_4	black heavy mineral layers in two horizons in the basal Steenkampsberg Formation (Frick, 1967)
Fe	oolitic ironstones of the Rooihoogte, Timeball Hill, Dwaal Heuwel and Daspoort Formations (Wagner, 1928; Schweigart, 1963, 1965; Button, 1973; Beukes, 1983)
Cu	in association with hydrothermal gold (Hammerbeck, 1976); disseminated in Hekpoort and Machadodorp volcanics (Button, 1973; Hammerbeck, 1976)
Cu/Ni	associated with layered ultramafic intrusions transecting lower Transvaal strata up to Timeball Hill Formation, Uitkomst Complex (Gauert et al., in press)
Pb	galena associated with Ag, Au and ZnS in vertical quartz lode, Daspoort Formation (Hammerbeck, 1976); in quartz veins of the Silverton Formation (Hammerbeck, 1976)
Sulphides	associated with vein quartz in the Timeball Hill Formation (Button, 1973); pyritic speckling in black shales of the Timeball Hill and Silverton Formations; massive sulphide layers in the Timeball Hill Formation (Schweigart, 1963)
C (graphite)	Silverton Formation (Button, 1973)
marble	up to 2.5 m thick layers in the Nederhorst Formation (Hiemstra and van Biljon, 1959)
building stone	argillaceous sandstone of the Nederhorst Formation (Button, 1973)
andalusite \ chiastolite	in argillaceous rocks throughout the stratigraphy (Hammerbeck, 1976)

1.4 Previous Workers

First mention of geochemical analysis of Pretoria Group sedimentary rocks was made by van Biljon (1950), who determined and reported the major element contents of shales, hornfelses, quartzites and limestones of the "Pretoria Series" north of Pretoria. His data comprise sedimentary rocks of the Rayton Formation, Pretoria Group, and of the Rooiberg Group which succeeded Pretoria Group deposition. Schweigart (1963, 1965) determined trace element contents of oolitic ironstones of the "Lower Daspoort Stage" (now: Upper Timeball Hill Formation) semi-quantitatively, to distinguish between ironstone occurrences in the eastern and central part of the basin.

Engelbrecht (1976) gives the chemical analyses of eight metamorphosed sedimentary rocks of the Pretoria Group from the Enzelsberg area, western Transvaal. He concludes that the variation of the SiO_2/Al_2O_3-ratio and the TiO_2-content is related to the syndepositional waterdepth. His evaluation of ACF- and AKF-diagrams and the comparison of the Niggli-norms of the samples resulted in a fourfold subdivision of the sedimentary rocks (Al-rich shales, marls, greywacke-type shales and femic silicate rocks).
Boehmer (1977) analyzed 255 borehole core samples from the Pretoria Group in the Potchefstroom Synclinorium and in the Delmas-Bronkhorstspruit area. Average major element compositions for shales (184 samples, volatile-free) and for a total of 204 sedimentary rocks (comprising of shales, quartzites and ironstones, volatiles included) are reported. Additionally, the average contents of Be, Li, Rb, Cs, Zr, Hf, Cr, and B are given for the shale samples. As the main objectives of Boehmer's Ph.D. thesis (Dept. of Chemistry, University of Pretoria) were the analytical procedures, a geological interpretation of the data was omitted.

Button (1979) describes an exceptionaly well preserved weathering profile (5.20m thickness) at the top of the Hekpoort Formation. He provides geochemical data for the profile (13 samples). The observed geochemistry is interpreted as an indicator for penecontemporaneous weakly oxidizing atmospheric conditions, alkaline palaeogroundwater near the soil surface, and reducing conditions with lower pH down the profile.

Engelbrecht (1986) analysed 54 samples of metamorphosed sedimentary rocks of the Pretoria Group in the western Transvaal. He gives average element concentrations of 8 groups, which were chosen according to their metamorphic mineral assemblage. Meissner (1987) gives the average contents for major and three trace elements of 44 borehole samples of shales from the Silverton Formation.

Condie and Wronkiewicz (1990) give the average Cr/Th-, Co/Th-, Th/Sc-, La/Sc-, Cr/Zr-, La/Yb- and Eu/Eu*-ratios of selected Pretoria Group shales (Timeball Hill, Strubenkop and Silverton Formations). They interpret the variation between the Cr/Th-ratio of the lower (Timeball Hill Formation) and middle part of the Pretoria Group (Strubenkop and Silverton Formations) as being related to a change in provenance rocks following a tectonic event. The similarity of the Cr/Th-ratios of the latter two formations is explained by a homogenous scource and/or efficient sediment mixing (Condie and Wronkiewicz, 1990).

Wronkiewicz and Condie (1990) publish geochemical data (average major and trace element contents) of pelites and quartzites of the Pretoria Group. They conclude that the Pretoria Group pelites were derived from sources rich in granitic components, with lesser contributions from basaltic, tonalitic and komatiitic rocks. The syndepositional climate is postulated to have been similar to the average Phanerozoic climate, with the exception of the Strubenkop shales, which show CIA-patterns (CIA = Chemical Index of Alteration, Nesbitt & Young, 1982) characteristic of sediments derived from chemically weathered detritus. However, Wronkiewicz and Condie (1990) simultaneously infer that chemical weathering of the source areas is responsible for a decrease of K/Rb-ratios of all Pretoria Group pelites compared to the older Ventersdorp Supergroup, Lower Transvaal Sequence (= pre-Pretoria Group) and average Phanerozoic pelites.

Eriksson et al. (1990) report the analyses of 14 samples of the Silverton Formation from the central and western parts of the Transvaal basin. A Silverton Formation average (74 samples) is presented, which additionally comprises the data of Boehmer (1977) and Meissner (1987). Eriksson et al. (1990) interpret this major and trace element geochemistry as providing evidence for mixed basaltic and granitic source rocks and intense source rock weathering. Trace elemements tentatively point to freshwater to brackish water conditions in the

depository. High Mg-Ca mudrocks are related to penecontemporaneous volcanism (Eriksson et al., 1990).

Schreiber (1990) reports the geochemistry of all of the Pretoria Group formations (160 samples) in the eastern Transvaal. According to Schreiber (1990), the CIA-indices point to stable tectonic conditions and little climatic change during the deposition of the lower and middle parts of the Pretoria Group, but increased tectonic instability and climatic changes for the upper part. Various ratios (TiO_2/Al_2O_3, Cr/Zr, Th/Sc) are used for interpreting source rock compositions, which are thought to have been mixed granitic-basaltic, with a greater contribution of granites in the eastern part of the depository than in the central part. Trace element contents and variations favour a brackish to freshwater depositional palaeoenvironment (Schreiber, 1990).

Schreiber et al. (1991) report the geochemistry of 61 sandstone samples of all stratigraphic units of the Pretoria Group from the eastern Transvaal. They argue that the petrography and geochemistry of the sandstones favour an intracratonic palaeoenvironment with mainly fluvial deposition.

Verryn et al. (1991) discuss the geochemistry of strongly altered and mineralized sedimentary rocks of the Rayton Formation at Waaikraal, near Brits, central Transvaal. They provide averages of calc-silicate rocks, quartzites and a magnetite-rich rock, and assume that mobilization of some major elements occurred due to metasomatizing fluids related to the emplacement of the Bushveld Complex.

Eriksson (1992) interprets the content and variation of boron in Pretoria Group sedimentary rocks (data taken from Boehmer (1977) and Schreiber (1990)) as indicating freshwater conditions for the lower and middle part of the Pretoria Group. Extraordinary high values at the base of the Silverton Formation are related by Eriksson (1992) to a marine incursion.

Schreiber et al. (1992) compare the average major element content of mudrocks, quarzitic, arkosic and lithic sandstones and ironstones of the Pretoria Group from the eastern and central Transvaal regions. They interpret the geochemical composition of the sandstones as

being typical of structural depressions in craton interiors and infer increasing tectonic instability towards the top of the Pretoria Group succession. CIA-patterns of the mudrocks are thought to reflect a stable palaeoclimate throughout the deposition of the Pretoria Group, irrespective of a decrease in the CIA-index for the upper stages, thought to have been caused by tectonic instability (e.g. basement uplift and/or continental rifting). Mudrock geochemistry points to predominantly granitic scource rocks with minor contributions from basaltic or ultramafic rocks (Schreiber et al., 1992).

Eriksson et al. (under review a) discuss the influence of andesitic volcanism on the boron concentration of the Pretoria Group sedimentary rocks. They conclude that the increased boron content with stratigraphic height is related to an increase in volcanic activity.
Eriksson et al. (in press c) discuss the geochemistry of shales from the Timeball Hill Formation. They show that the black colouration of the shales is seldom related to the carbon content, but can rather be explained by pigmentation due to iron minerals (e.g. sulphides and limonite). The latter are thought to have been enriched due to exhalative processes.

1.5 Methods of investigation

1.5.1 Sampling and sample preparation

A total of 1203 samples from all formations, including material from the Hekpoort and Machadodorp volcanics, diabase sills and formations of unclear stratigraphic relation (Makeckaan Formation and samples of sedimentary rocks from the Leeuwpoort and Smelterskop Formations, Rooiberg Fragment), were taken from surface outcrops (964 samples) and borehole cores (238 samples). Sample locations are shown in Figures 1.5.1 - 1.5.18, by white dots on a black background. Due to the scale of the sampling maps, a dot represents 1 to 64 samples taken at the locality. The location of geochemical profiles shown in Chapter 3.3 is exemplified by a white line transecting one or more dots. Borehole samples were only taken from Botswana, where the Geological Survey of Botswana kindly provided the cores described by Key (1983). The surface sampling was dictated by availability of outcrops in the selected sampling areas. Only samples with a relatively fresh appearance in

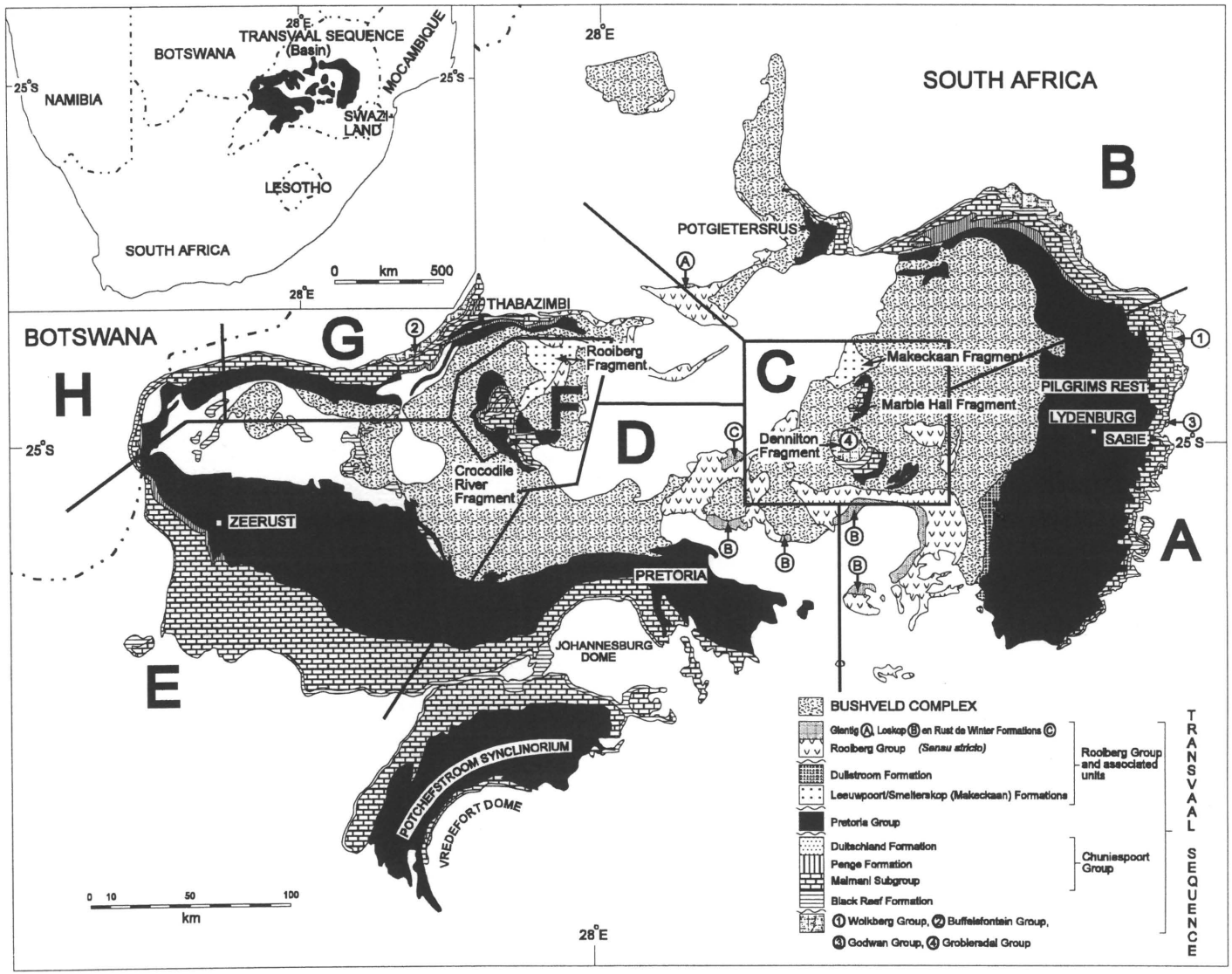

Fig. 1.5.1: Definition of sampling areas: A - eastern Tvl; B - northeastern Tvl; C - eastern Fragments; D - central Tvl; E - western Tvl; F - western Fragments; G - northwestern Tvl; H - Botswana

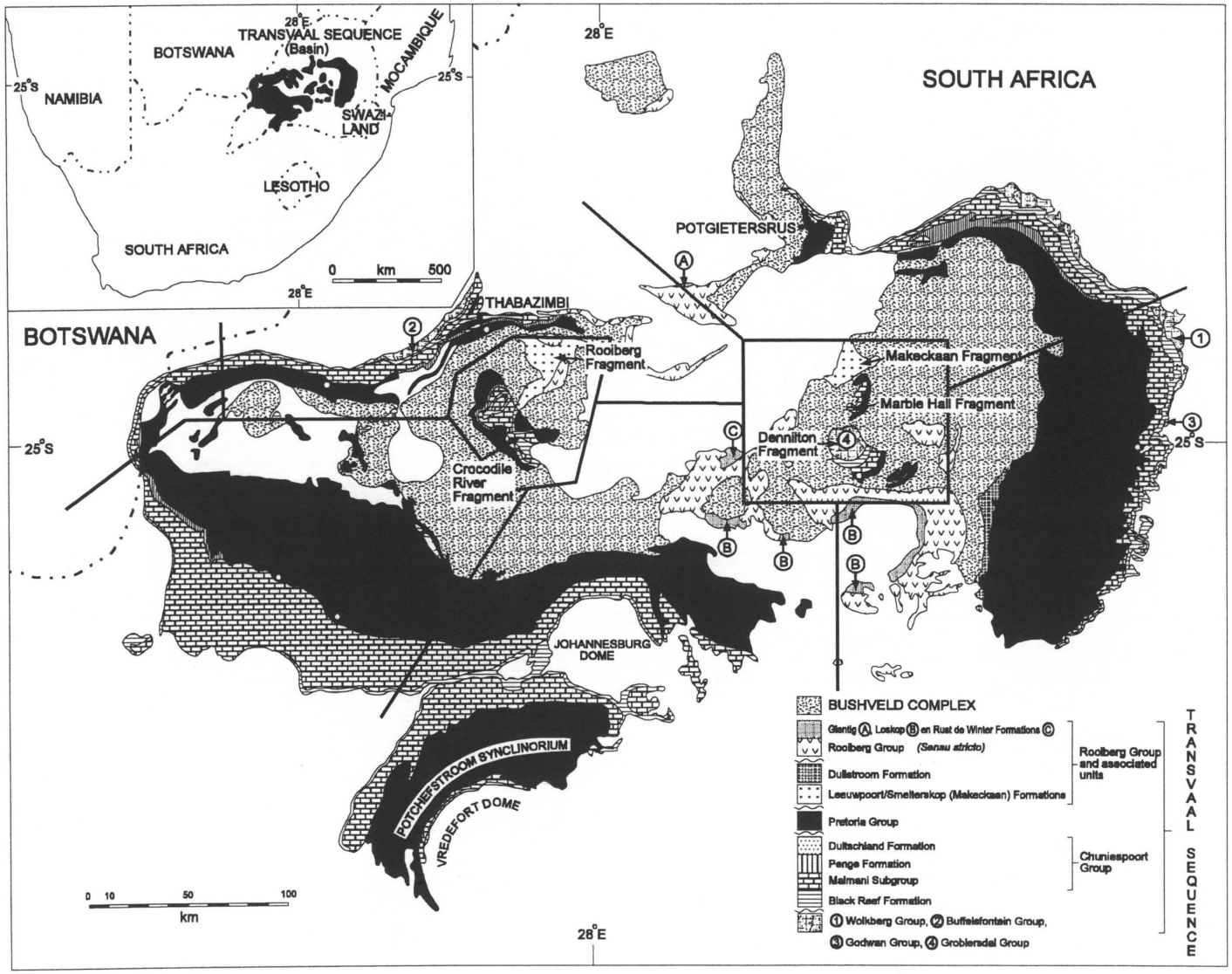

Fig. 1.5.2: Sampling map of the Rooihoogte Formation

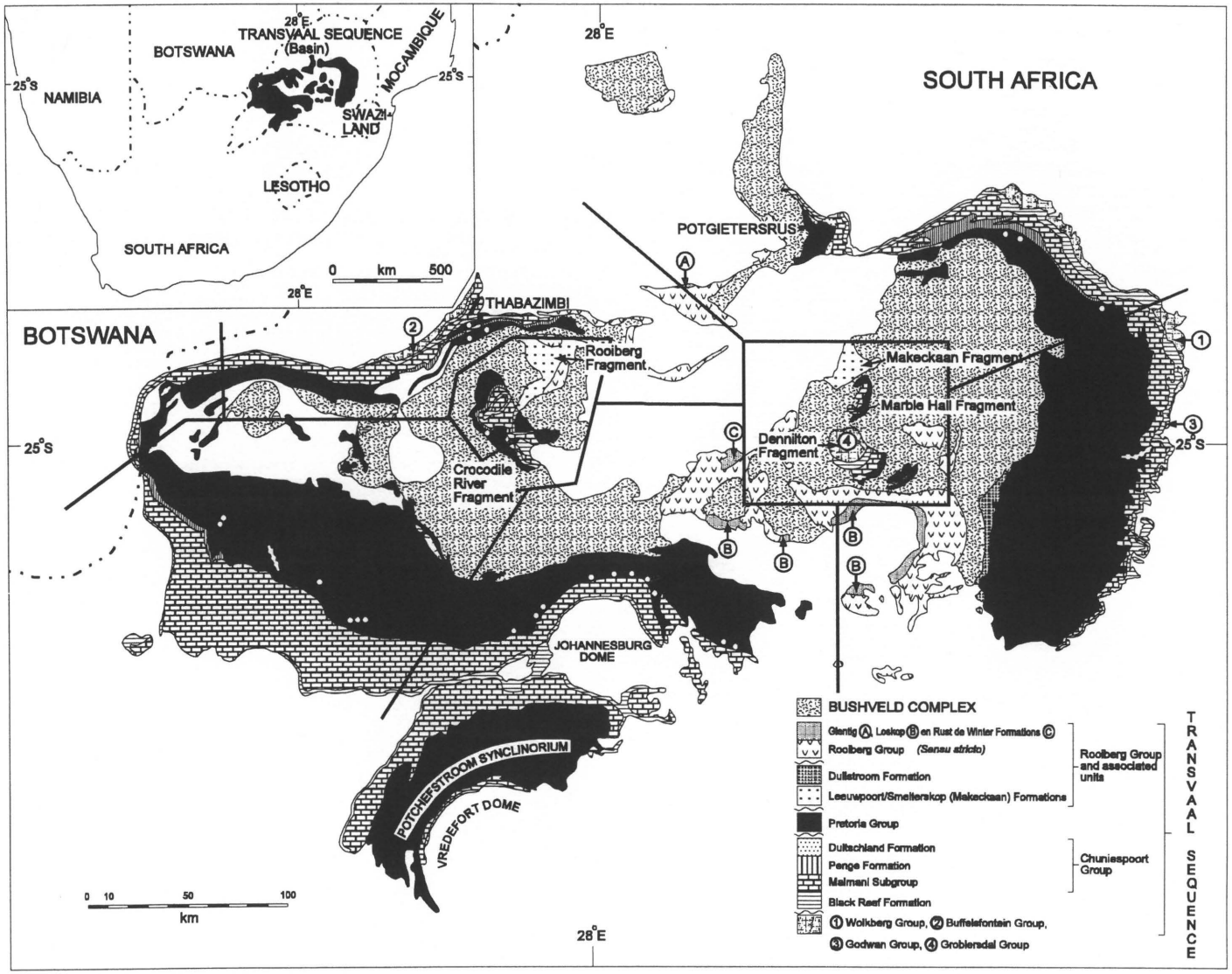

Fig. 1.5.3: Samling map of the Lower Timeball Hill Formation

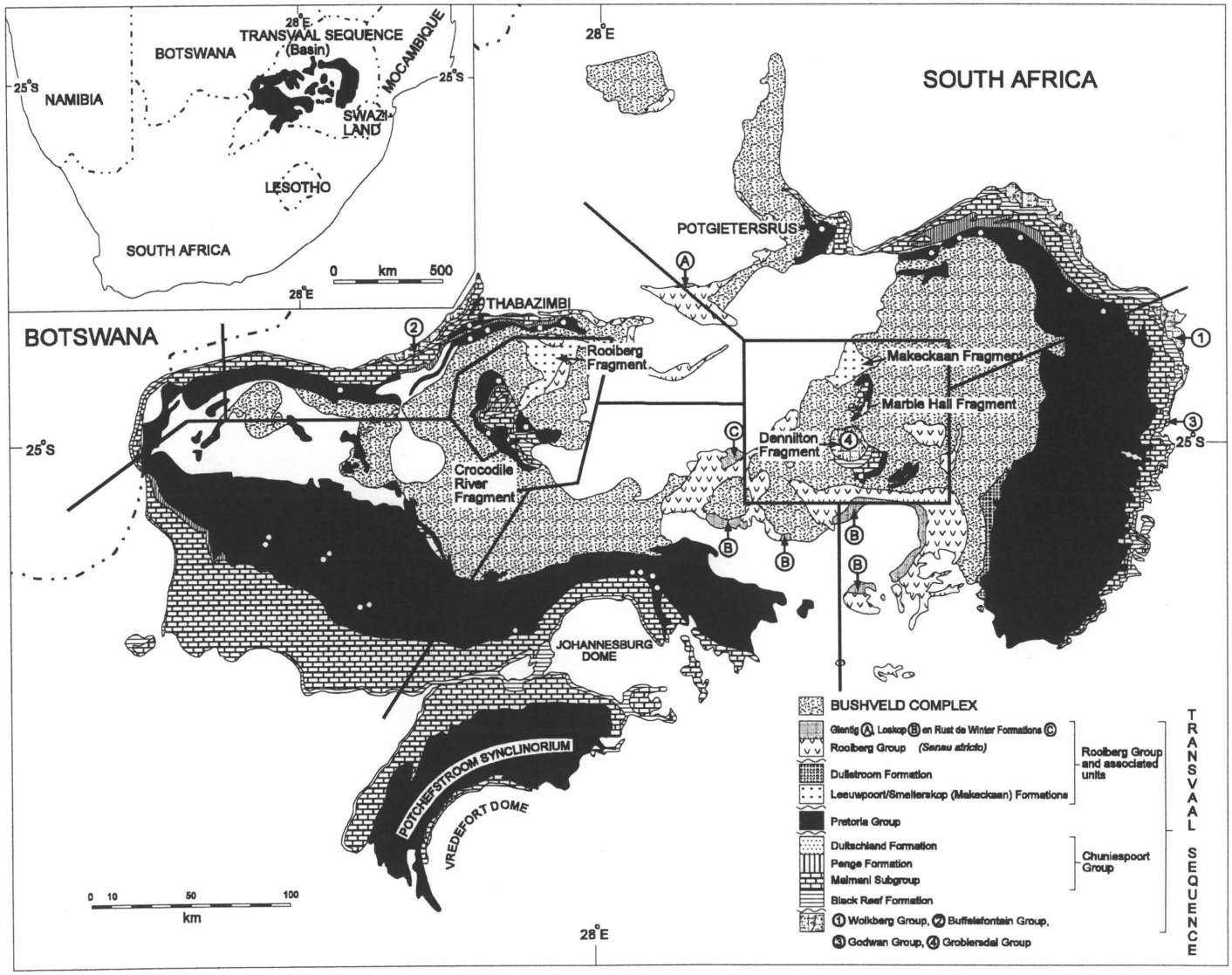

Fig. 1.5.4: Sampling map of the Timeball Hill Quarzites

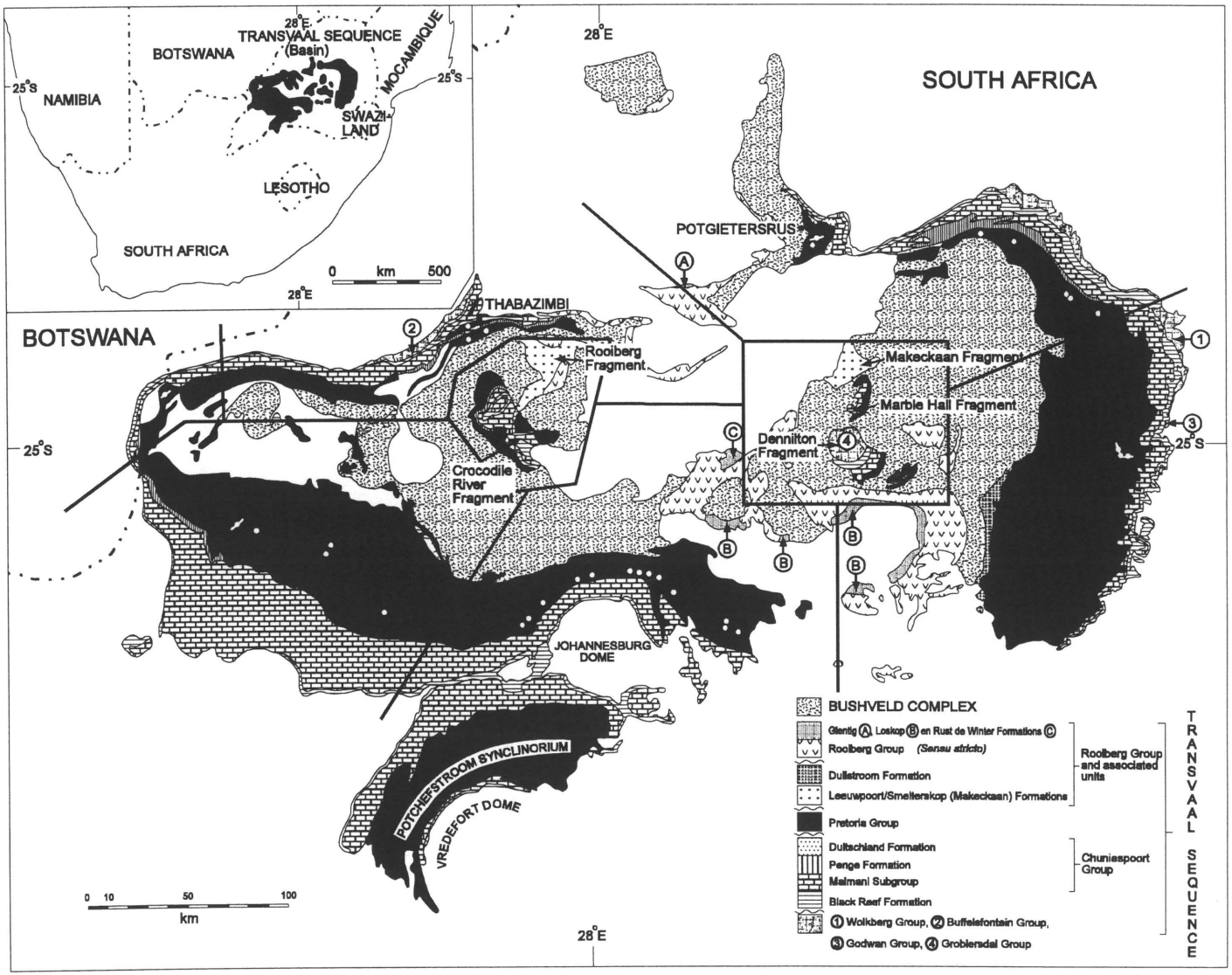

Fig. 1.5.5: Sampling map of the Upper Timeball Hill Formation

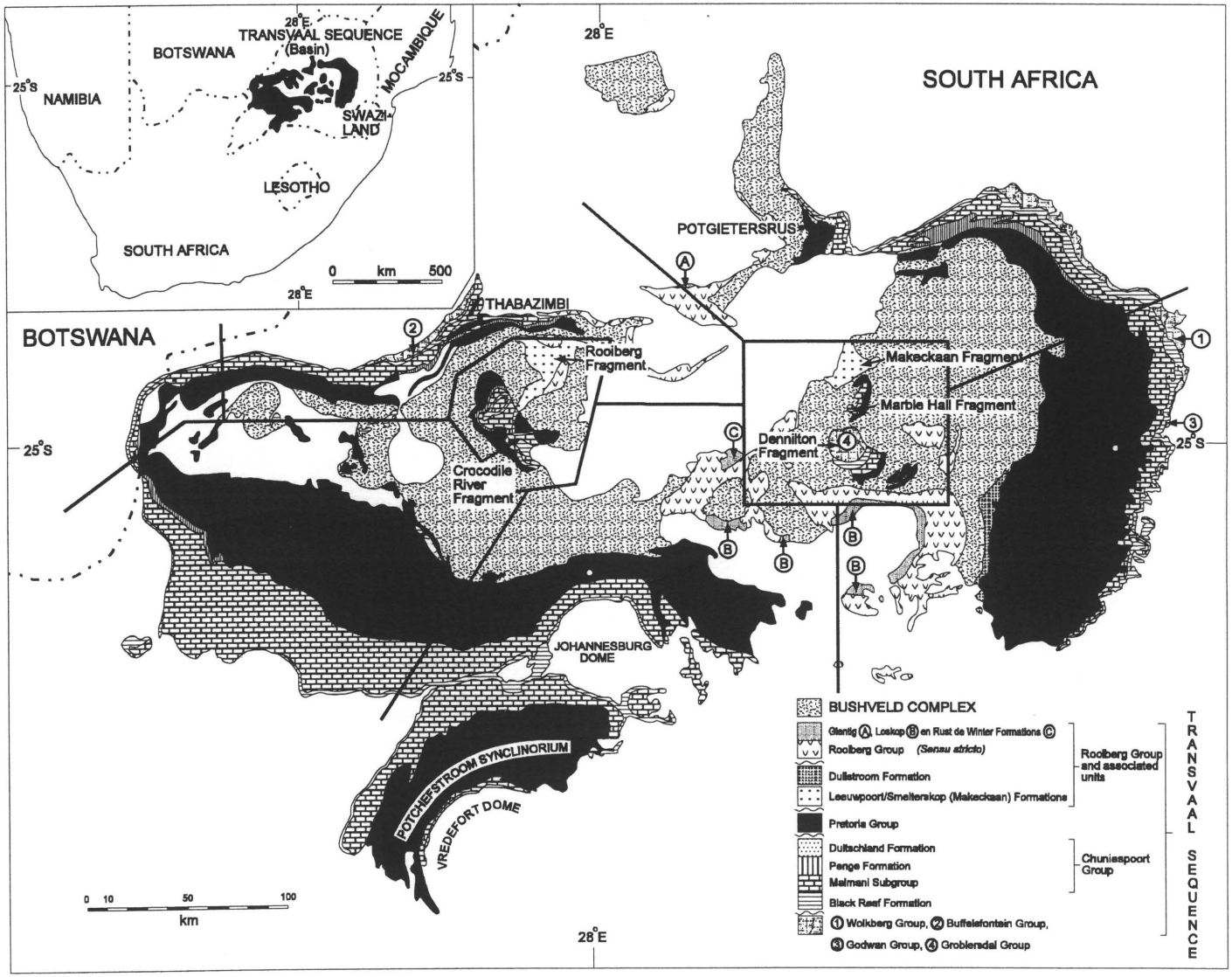

Fig. 1.5.6: Sampling map of the Boshoek Formation

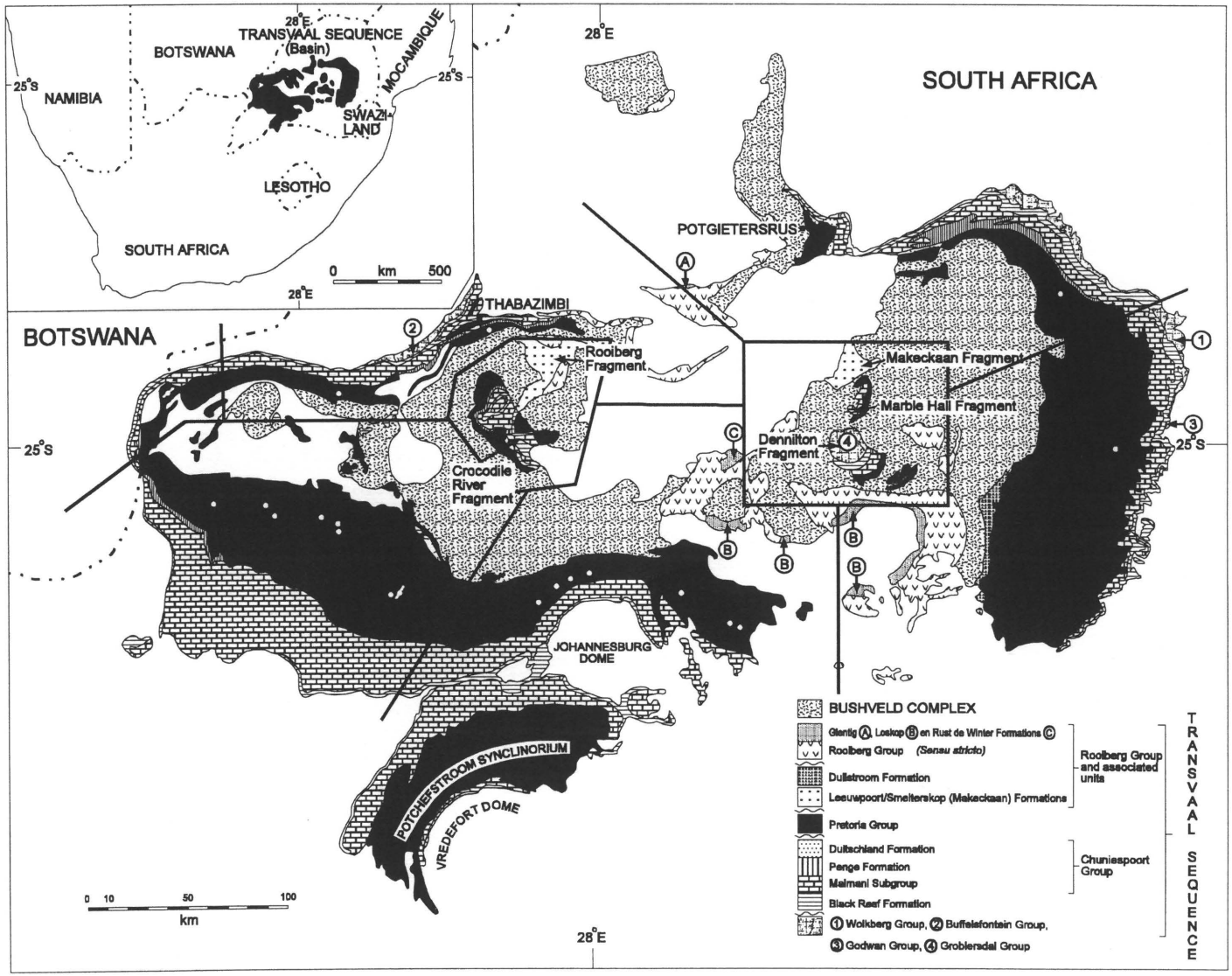

Fig. 1.5.7: Sampling map of the Hekpoort Formation

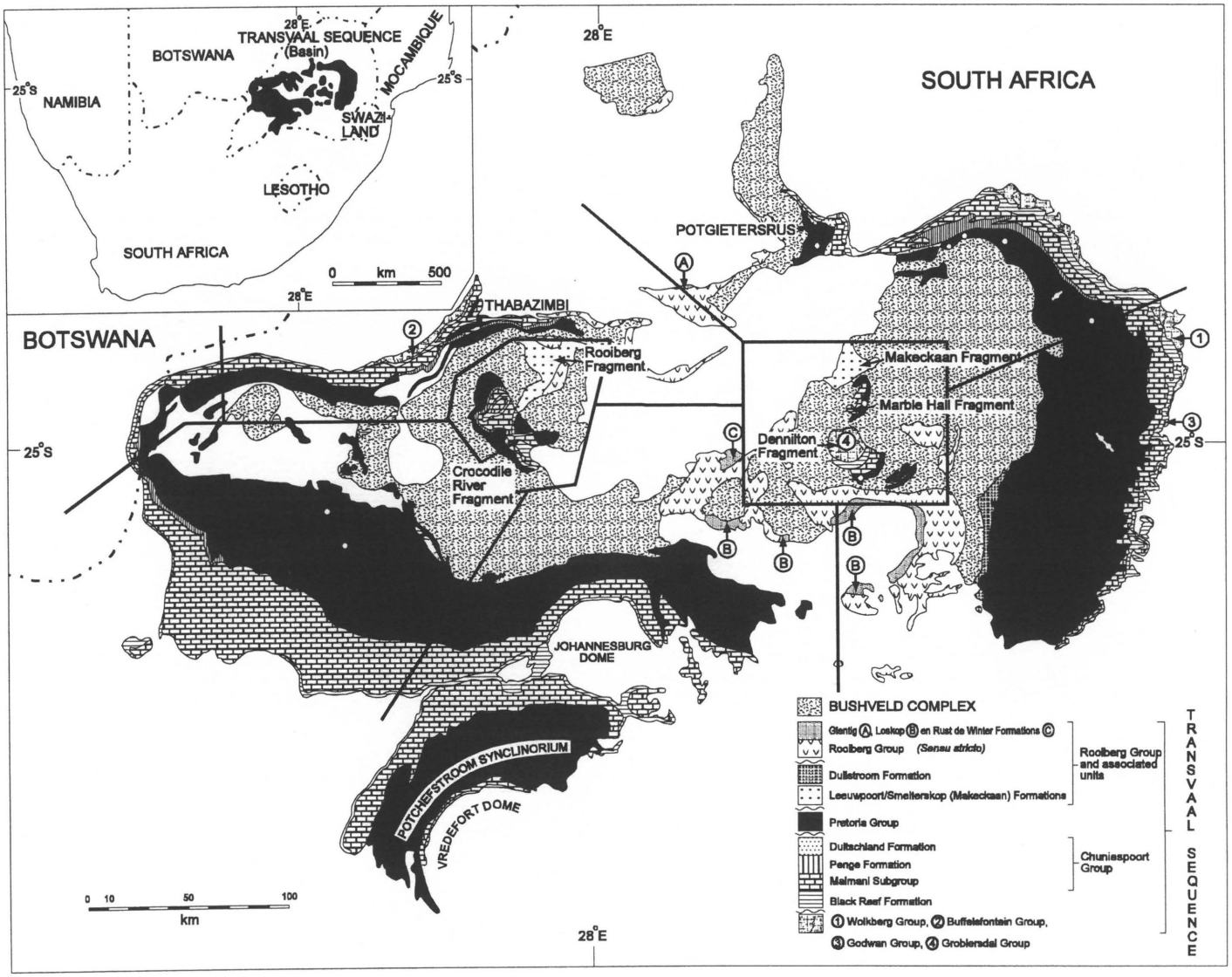

Fig. 1.5.8: Sampling map of the Dwaalheuwel Formation

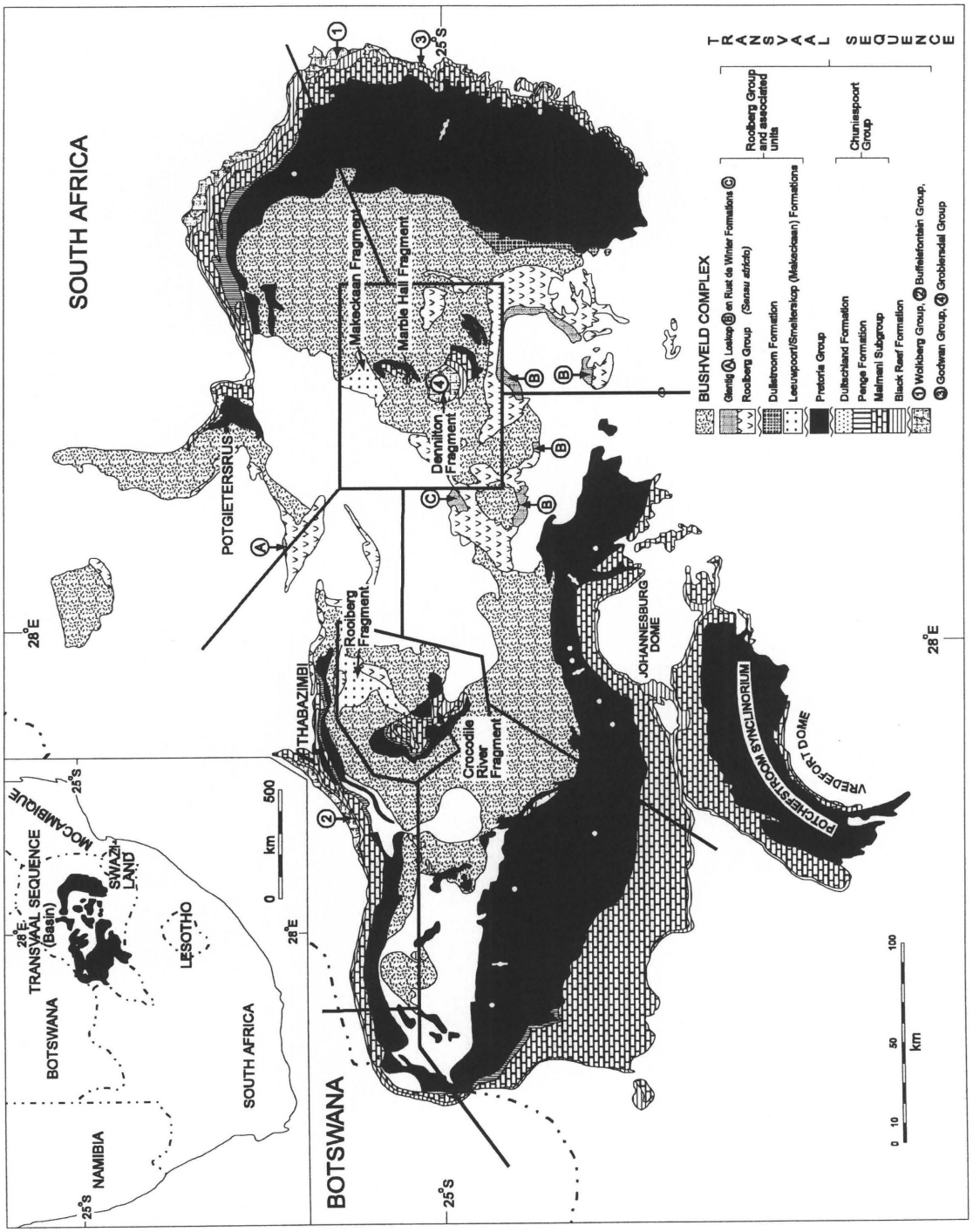

Fig. 1.5.9: Sampling map of the Strubenkop Formation

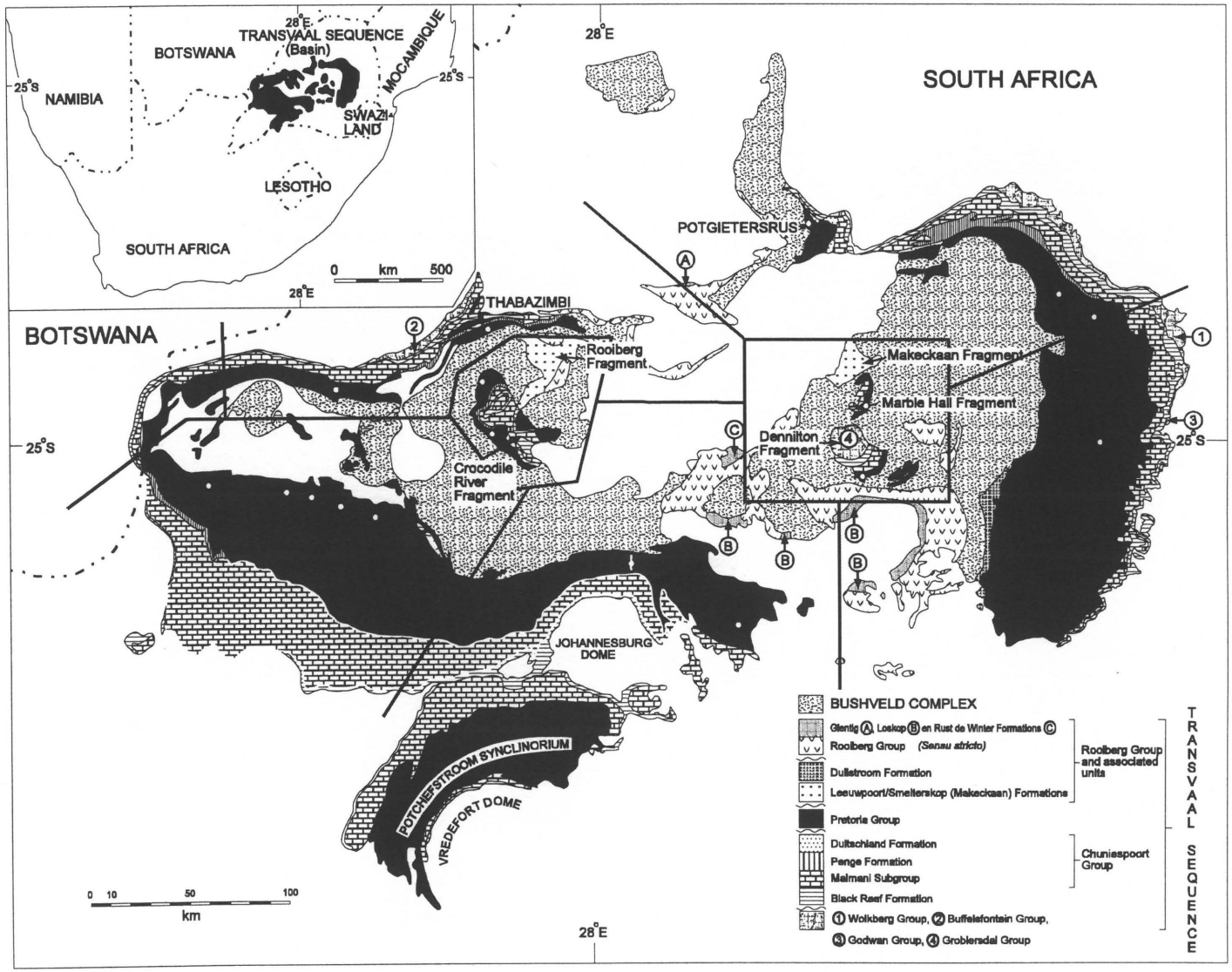

Fig. 1.5.10: Sampling map of the Daspoort Formation

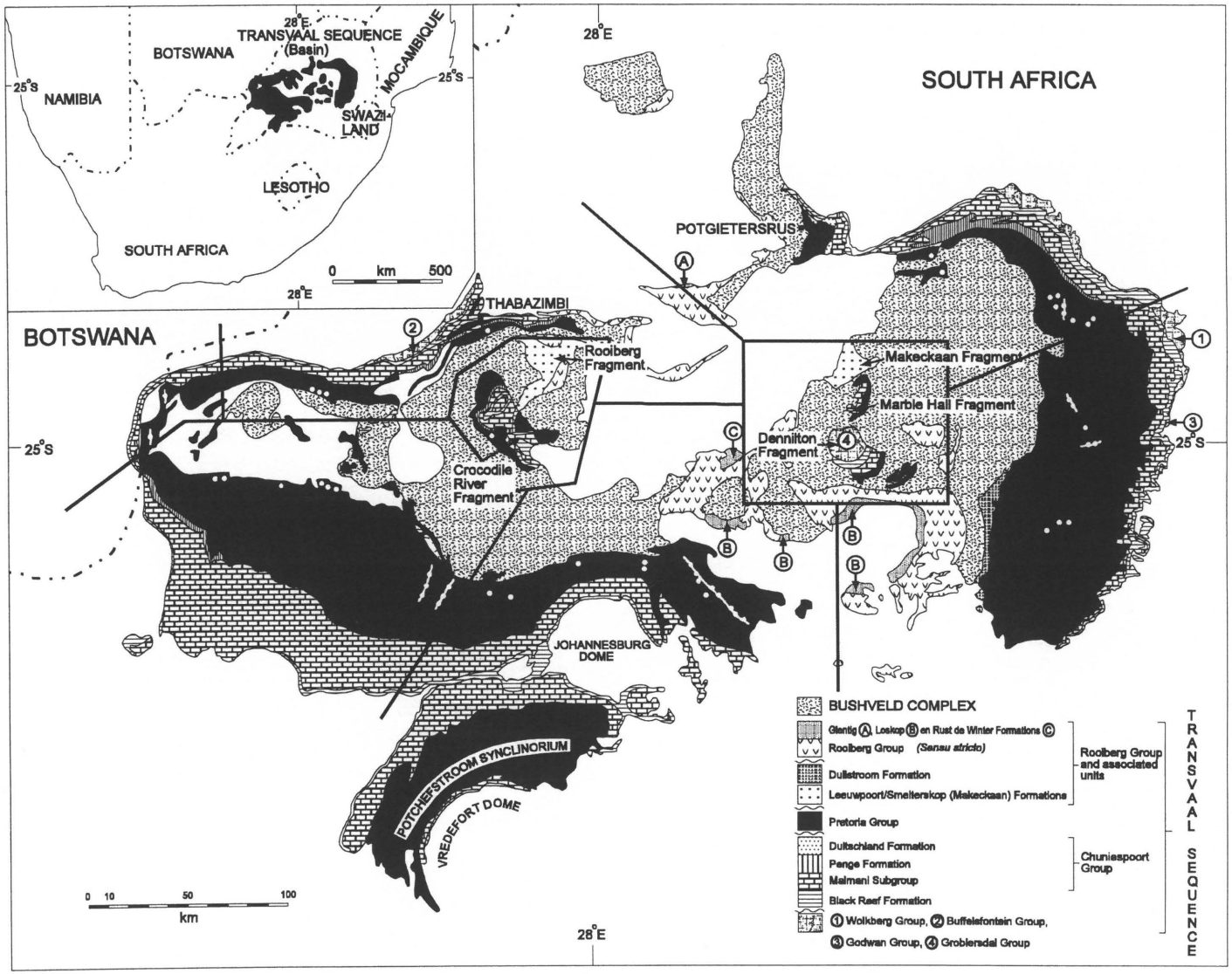

Fig. 1.5.11: Sampling map of the Silverton Formation

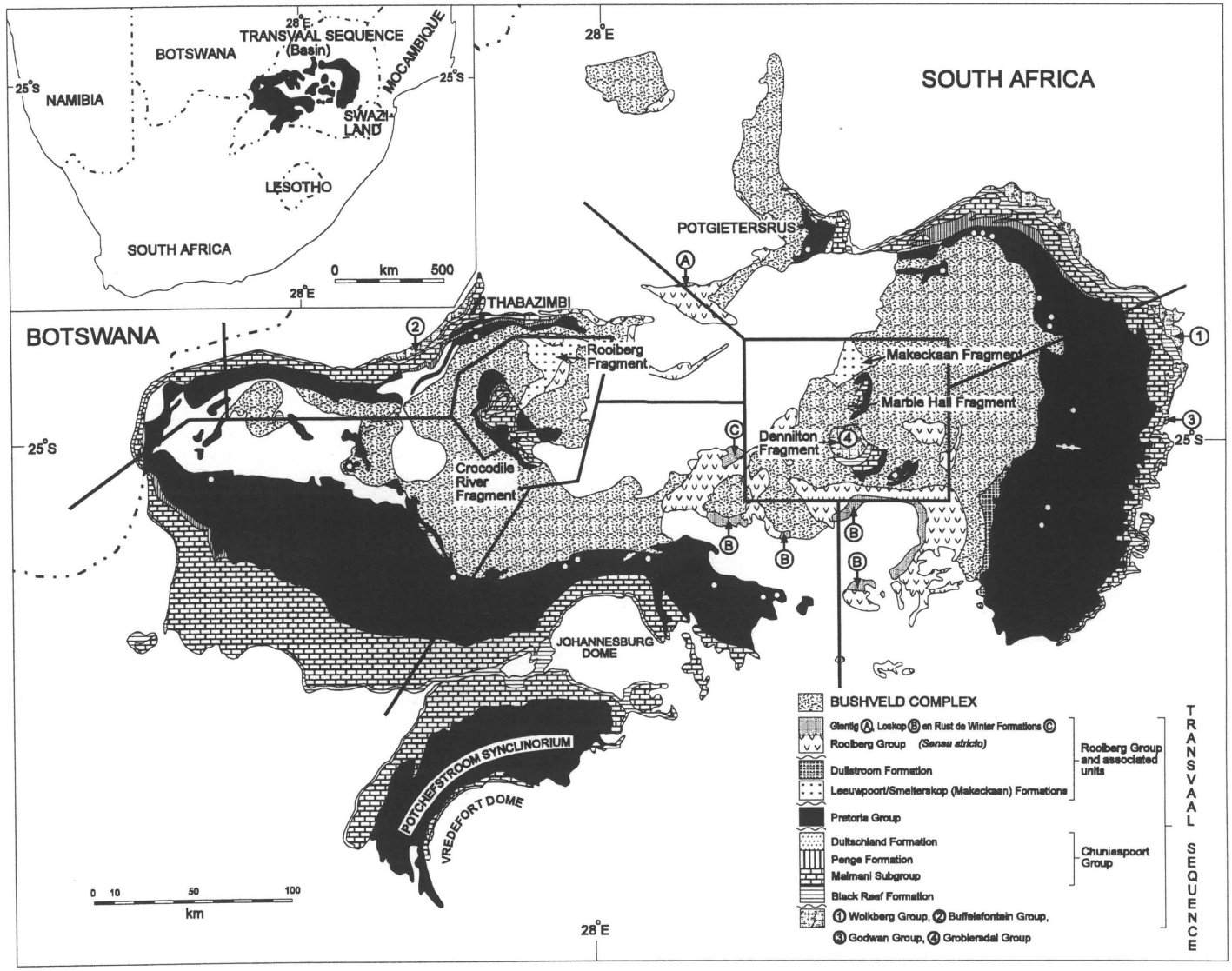

Fig. 1.5.12: Sampling map of the Magaliesberg Formation

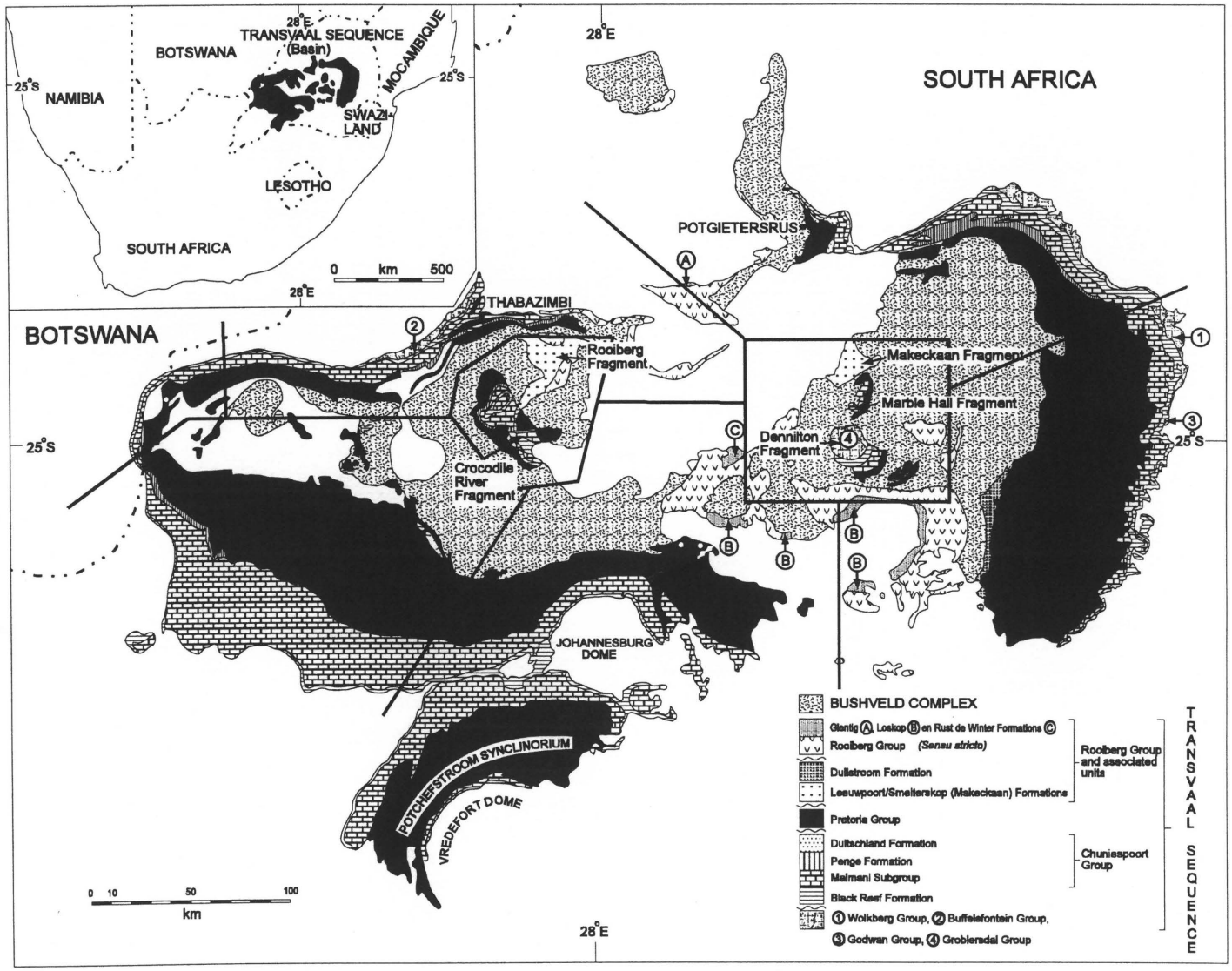

Fig. 1.5.13: Sampling map of the Rayton Formation

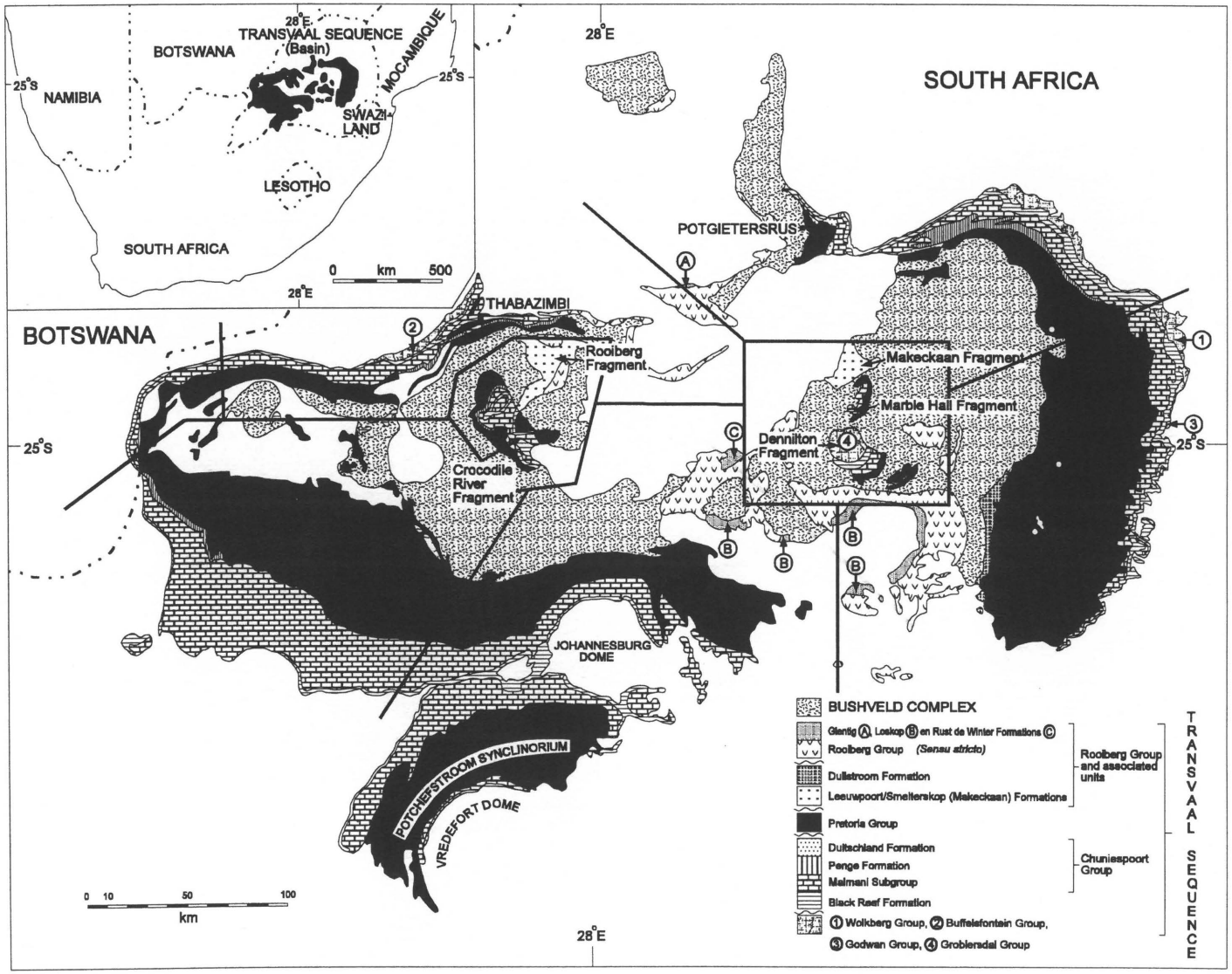

Fig. 1.5.14: Sampling map of the Vermont Formation

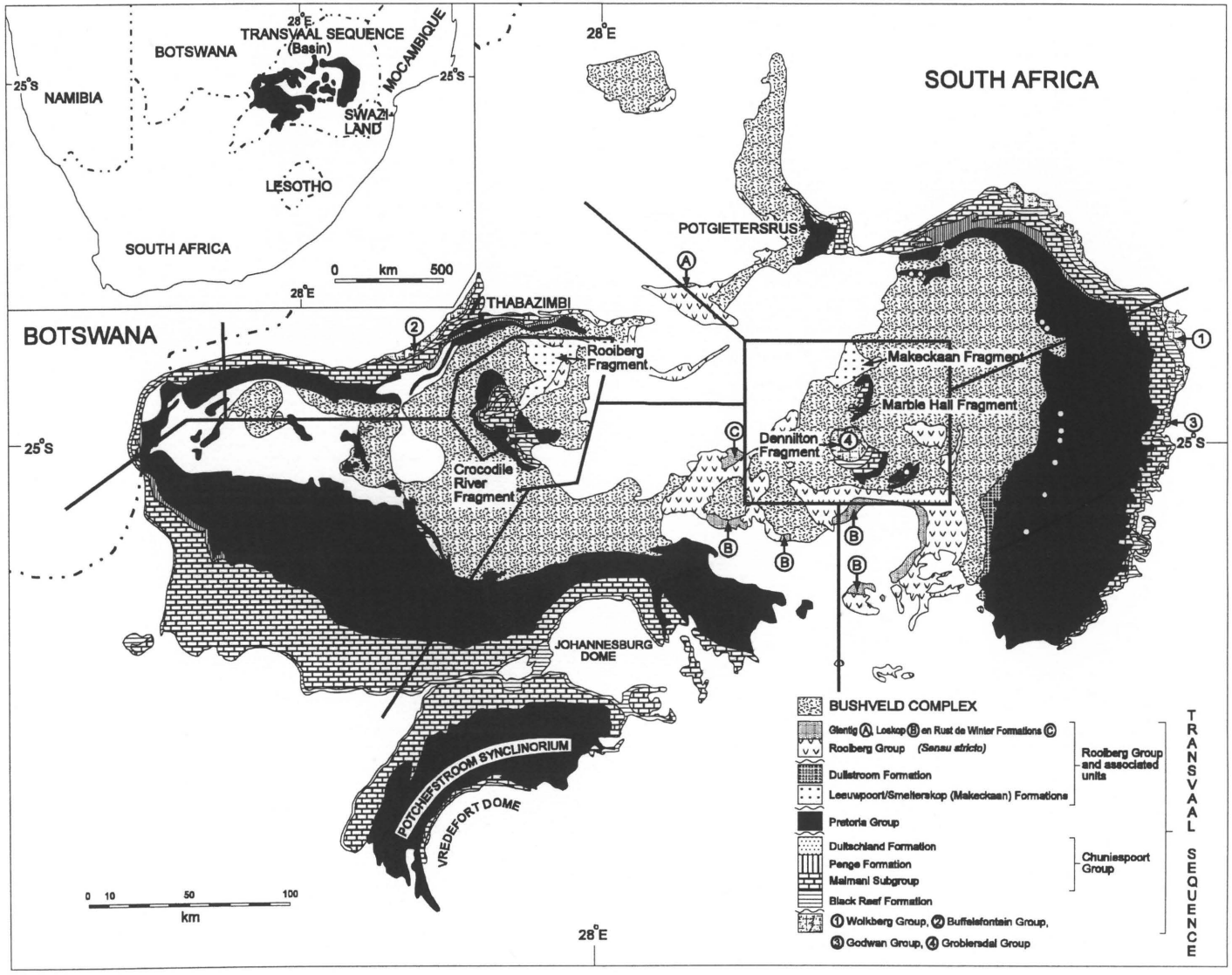

Fig. 1.5.15: Sampling map of the Lakenvlei Formation

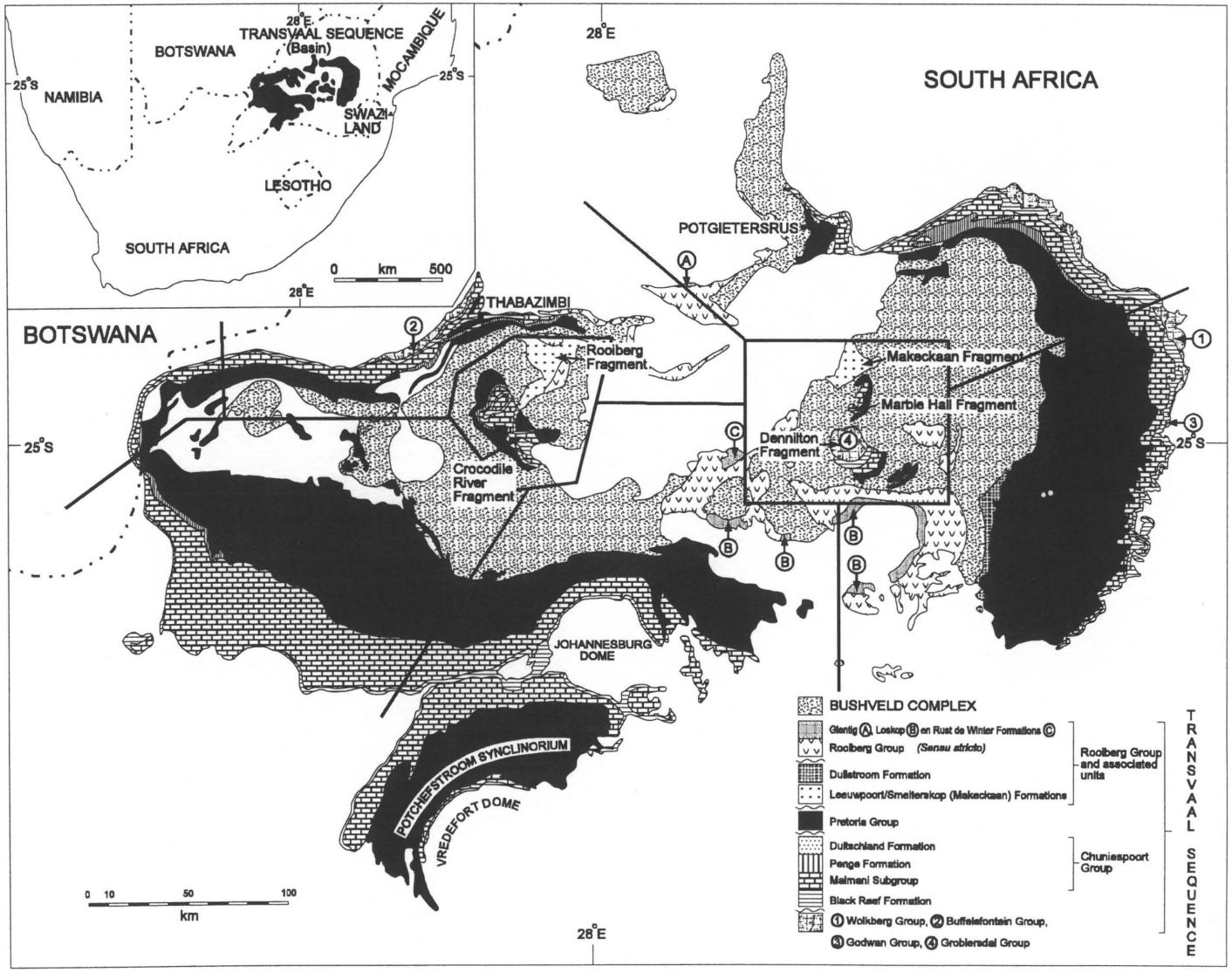

Fig. 1.5.16: Sampling map of the Nederhorst Formation

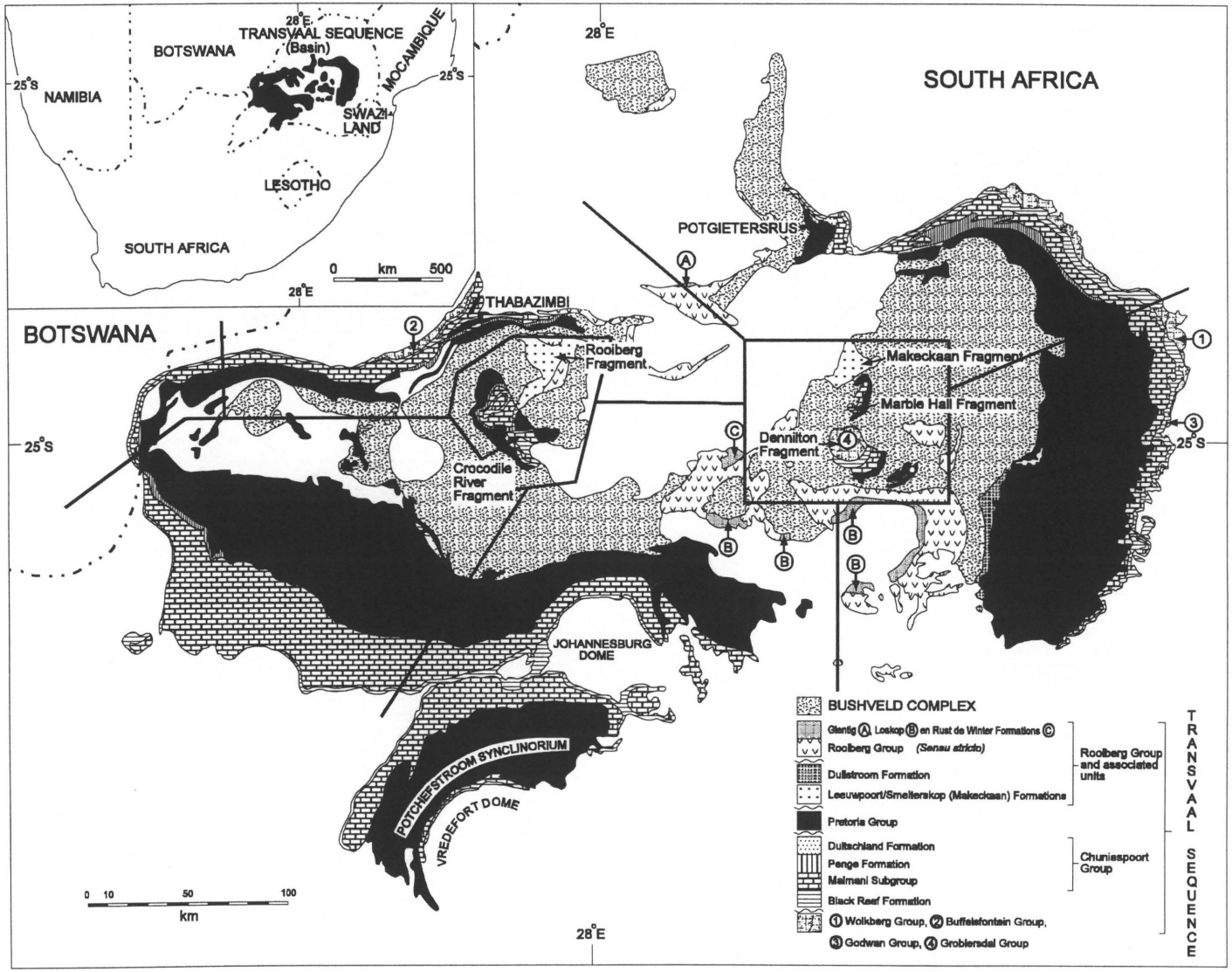

Fig. 1.5.17: Sampling map of the Steenskampsberg Formation

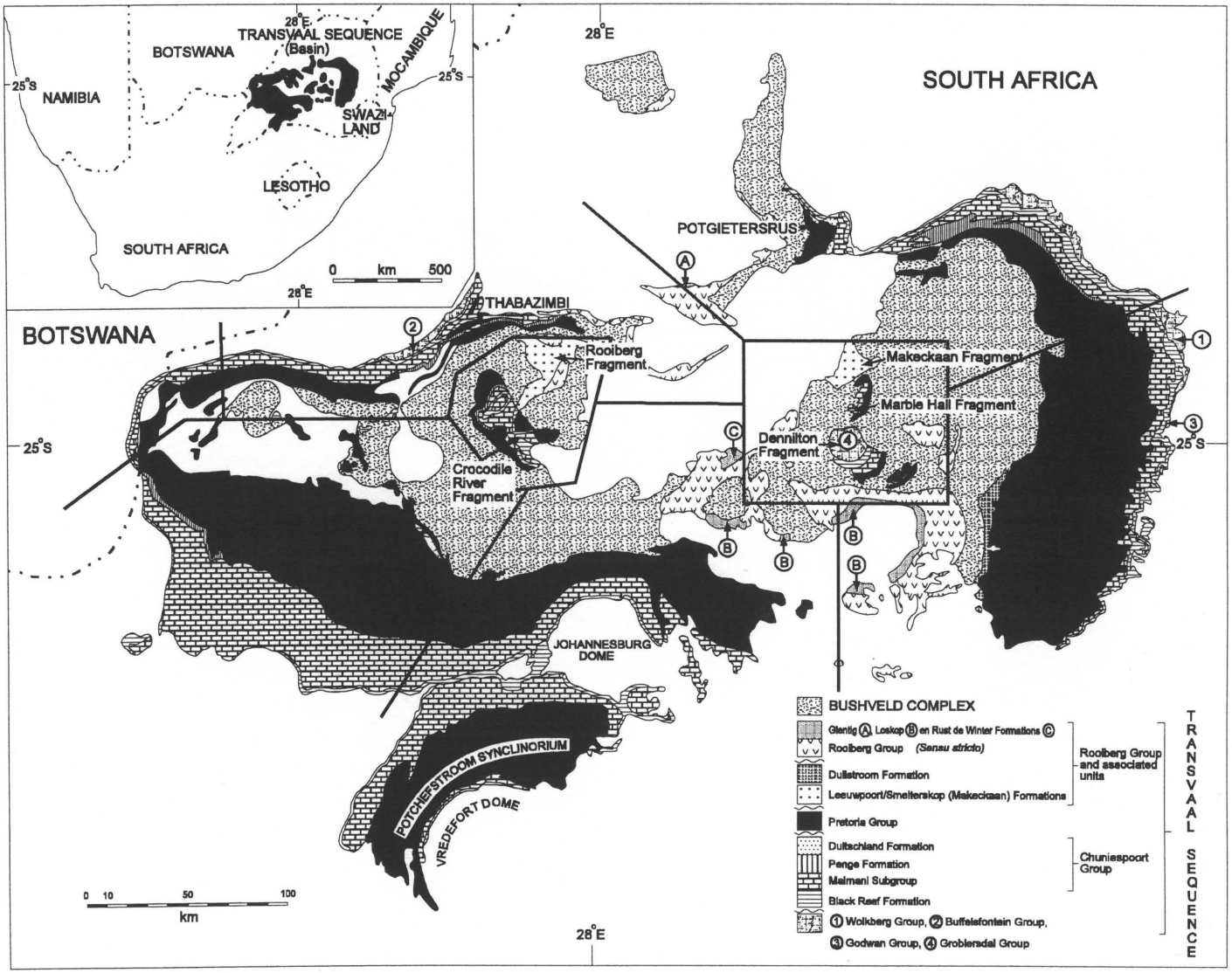

Fig. 1.5.18: Sampling map of the Houtenbek Formation

outcrop were chosen. The surface samples were carefully cleaned of weathering crusts, mud and recent organic matter like algae and roots, and the borehole core samples of cutting debris. The samples were then crushed and ground. The study area as a whole was subdivided into eight regions (Fig. 1.5.1), which will be utilised later in this study.

1.5.2 Analytical procedures

All methods of chemical analysis are subject to analytical errors, which can be thought of as consisting of two main components (Le Maitre, 1982). One is a statistical error or precision which arises from random fluctuations in the analytical procedure, and is thus a measure of the reproducibility of a set of results; the other is a systematic error or accuracy, which is a measure of how close the results are to the true value. All analyses were performed by professional chemists or geochemists. With the exception of the XRF analyses, the long term empirical precision and accuracy of the respective procedure are reported. For the XRF analyses, precision is given as the relative standard error in percent of multiple analyses of a set of samples, and the accuracy as the average observed deviation from several measured standards in percent.

1.5.2.1 X-ray fluorescence (XRF)

All samples were analysed for major and trace elements, using standard x-ray fluorescence techniques on an ARL 8420 spectrometer. The analyses were performed at the University of Pretoria by Dr. Martin Sharpe (Rocklabs CC).

Major elements, except for Na_2O, were analysed on glass discs, following the Norrish fusion method as applied at the Department of Geology, University of Pretoria. Na_2O and trace elements were analysed on compressed powder pellets, pressed at ca. 5 kN.

The trace elements, except for Cr, V, Ba and Sc, were determined using Rh/Comp peak to monitor the mass absorption coefficient. Cr, V, Ba and Sc were calculated from the direct-intensity peak-background counts, with mass absorption coefficients calculated from the major element analyses. All values were corrected by application of interference correction

Table 1.5.1: Measuring conditions of XRF-determinations

Abbreviations: Count.t. = counting time; LLD = lower limit of detection; Prec. = precission, given as the relative standard error of multiple analyses in percent; Acc. = accuracy, given as average observed deviation from a measured standard; LLD in % for major elements and ppm for trace elements; n.a. = not available.

Element	Sample	Crystal	Detector	Count.t.	2Θ	LLD	Prec.	Acc.
SiO_2	Glass Disk	PET	FPC	20 sec	109.21	0.01	± 0.4 %	< 1.1 %
TiO_2	Glass Disk	LIF200	FPC	20 sec	86.14	0.01	± 3.5 %	< 2.2 %
Al_2O_3	Glass Disk	PET	FPC	20 sec	145.01	0.01	± 1.3 %	< 1.6 %
Fe_2O_3	Glass Disk	LIF200	FPC	15 sec	57.52	0.01	± 1.7 %	< 1.7 %
MnO	Glass Disk	LIF200	FPC	10 sec	63.00	0.01	± 7.0 %	< 7.2 %
MgO	Glass Disk	AXO6	FPC	15 sec	21.21	0.01	± 4.8 %	< 1.5 %
CaO	Glass Disk	LIF200	FPC	10 sec	100.19	0.01	± 2.7 %	< 4.1 %
Na_2O	Pressed Pel	AXO6	FPC	15 sec	24.29	0.01	± 7.1 %	< 6.1 %
K_2O	Glass Disk	LIF200	FPC	25 sec	136.67	0.01	± 7.4 %	< 3.1 %
P_2O_5	Glass Disk	GEIII	FPC	20 sec	140.92	0.01	± 6.3 %	<10.7 %
Element	**Peak**	**Crystall**	**Detector**	**Count. t.**	**2Θ**	**LLD**	**Prec.**	**Acc.**
Zn	ZnKα1	LIF200	SC	30 sec	41.38	3 ppm	± 4.4 %	< 2.6 %
Cu	CuKα1	LIF200	SC	30 sec	45.06	3 ppm	± 24.2 %	<13.6 %
Ni	NiKα1	LIF200	FPC	30 sec	48.67	3 ppm	± 9.8 %	<12.7 %
Co	CoKα1	LIF200	FPC	60 sec	52.84	3 ppm	± 13.6 %	< 6.1 %
Ga	GaKα1	LIF200	SC	30 sec	38.95	3 ppm	± 7.7 %	<12.6 %
Mo	MoKα1	LIF200	SC	30 sec	20.33	2 ppm	± 16.2 %	n.a.
Nb	NbKα1	LIF220	SC	30 sec	30.44	2 ppm	± 3.7 %	< 6.1 %
Zr	ZrKα1	LIF220	SC	30 sec	32.10	2 ppm	± 9.2 %	< 9.3 %
Y	YKα1	LIF220	SC	30 sec	33.87	2 ppm	± 1.9 %	< 7.5 %
Sr	SrKα1	LIF220	SC	30 sec	31.91	2 ppm	± 0.3 %	< 2.5 %
Rb	RbKα1	LIF220	SC	30 sec	37.99	2 ppm	± 1.8 %	< 5.0 %
U	ULα1	LIF220	SC	60 sec	37.30	5 ppm	± 8.3 %	n.a.
Th	ThLα1	LIF220	SC	60 sec	39.23	5 ppm	± 5.8 %	< 9.3 %
Pb	PbLα1	LIF220	SC	60 sec	28.26	5 ppm	± 14.5 %	<24.5 %
Cr	CrKα1	LIF220	FPC	100 sec	107.06	14 ppm	± 36.6 %	<20.8 %
V	VKα1	LIF220	FPC	100 sec	123.13	14 ppm	± 6.3 %	< 5.0 %
Ba	BaLα1	LIF200	FPC	100 sec	75.84	16 ppm	± 1.0 %	<15.7 %
Sc	ScKα1	LIF200	FPC	100 sec	97.70	8 ppm	± 12.4 %	<11.7 %
As	AsKß1	LIF200	Sc	50 sec	30.45	10 ppm	n.a.	n.a.
S	SKα	GE III	FPC	100 sec	110.69	50 ppm	± 7.4 %	<22.9 %
Sb	SbKα1	LIF200	Sc	100 sec	13.42	8 ppm	± 25.5 %	n.a.
Sn	SnKα1	LIF200	Sc	50 sec	14.00	8 ppm	n.a.	n.a.
Bi	BiLα1	LIF200	Sc	100 sec	33.01	5 ppm	n.a.	n.a.
W	WLß1	LIF200	Sc	50 sec	37.12	8 ppm	n.a.	n.a.

factors and mass absorption coefficients.

Measuring conditions, lower limit of detection (LLD), precision and accuracy of determinations are compiled in Table 1.5.1. International standards were used for internal calibration. H_2O- (adsorped water) and LOI (loss on ignition) were determined at 130° and 1000° C, respectively.

1.5.2.2 Determination of Boron by inductivley coupled plasma atomic emission spectrometry (ICP-AES)

174 shale and 80 quartzitic sandstone samples (1 g) were melted with an excess of sodium carbonate to ensure complete dissolution, and were then analysed for B by means of ICP-AES at the Atomic Energy Board, Pelindaba. Due to the high salt concentration of the measured solution, the system was rinsed with acid and water after each determination to prevent a build-up of salt precipitates in the system. The lower limit of detection (LLD) is 1 ppm. The precision of the determination is < 10 %, the accuracy ± 5 %. International standards were used for internal calibration.

1.5.2.3 Carbon and Sulphur by infrared (IR) absorption spectrometry

50 shale samples were analysed for total C (C_{total}), inorganic C (C_{inorg}), organic C (C_{org}) and S by means of IR Absorption Spectrometry at the Geological Survey of South Africa, Pretoria. The powdered sample (0.25 g) was burnt in a moisture-free oxygen atmosphere at high temperature (~ 1400° C). The CO_2 and SO_2 gasses were carried through the sulphur IR cell first, and, after removal of SO_2 by a sulphur trap, remaining CO_2 entered the carbon IR cell. In the respective IR detector cell, the absorbed IR energy at the precise wavelength was measured, and compared with the IR energy for the pure oxygen environment, which permits the maximum energy to reach the detector. Since the absorped IR energy is directly related to the content of CO_2 or SO_2, the C and S contents were automatically calculated from the detector reading. The instrument used was a LECO CS 244 Carbon/Sulphur Analyzer. As

the above described method determines only the total C content, the determination procedure was changed for a second run for the analyses of organic carbon. The sample (0.25 g) was combusted in a nitrogen atmosphere at 750° - 1000° C. The low temperature and the N_2-atmosphere prevents development of CO_2 from organic C. The inorganic C content is then measured as described previously, and the organic C content calculated from the difference between C_{total} and C_{org}. The precision of the method is as follows:

S < 5 wt.% : < 3 %
C < 7 wt.% : < 2 %
C > 7 wt.% : < 5 %

The accuracy is shown below:

S < 0.1 wt.% : ± 0.5 %
S > 0.1 wt.% : ± 2 %
C < 0.1 wt.% : ± 0.5 %
C > 0.1 wt.% : < 1 %

Internal standards used for calibration were international standards. The lower limit of detection (LLD) was 0.001 % for S and 0.01 % for C.

The determination of sulphur is problematic with the above procedure. Crystalline and adsorped water (H_2O+,H_2O-) can lead to interference reactions, if all the water is not driven off completely during the initial stage of the heating/burning process. H_2SO_4 can be formed, and a considerable reduction of the measured S content, compared to the real S content, is therefore possible. This reaction can explain the generally lower S-values obtained by IR Absorption Spectrometry compared to the S contents obtained by XRF, as crystalline and/or free water is always an important constituent of the shales analysed. The carbon determination is thought to be unaffected by interference from water, as the high instability at higher temperatures of any H_2CO_3 prevents a similar effect.

1.5.2.4 Potentiometric determination of FeO

50 shale samples were analysed for FeO at the Geological Survey of South Africa, Pretoria.

The sample (1 g) was decomposed in a mixture of dilute H_2SO_4 (1:1) and excess HF (48%) and gently heated in the absence of air. The solution was then rapidly cooled and the crucible containing the solution was plunged into 300 ml of freshly prepared boric acid (5%). After removing the crucible, 15 ml of a 1:1 mixture of sulphuric(15 %) and phoshoric(15 %) acid and 10 drops of barium diphenylamine sulphonate solution indicator (1%) was added. The solution was titrated with standard potassium dichromate solution (0.1 N) until a constant purple colour was achieved. A blank and a reference material of similar chemical and mineralogical composition to the sample were run with the sample through the entire procedure to ensure the correctness of the results. The volume of the titrant used in ml for the sample, minus the volume of titrant used for the blank, was taken to calculate the percentage of FeO in the sample (1 ml 0.1 N $K_2Cr_2O_7 \equiv$ 0.00718g FeO).

Internal standards used for calibration were NIM-G, NIM-D and NIM-N. The lower limit of detection (LLD) is 0.01% FeO. The precision of the determination is:

0.01 wt.% - 2.50 wt.% FeO:	< 3 %
2.50 wt.% - 7.00 wt.% FeO:	< 5 %
> 7.00 wt.% FeO:	< 8 %

The accuracy of the method lies between ± 5 - 15 %, depending on the composition of the geological material (sulphides: ± 50%). The variable accuracy is caused by a variety of interference reactions (J. Trojak, 1993, pers. comm.). As the 50 samples analysed for FeO are shales, with negligible amounts of insoluble minerals like chromite, tourmaline and spinel, the accuracy is assumed to be better than ± 10 % for most of the samples. Only samples with a high content of C_{org} and/or sulphur might have been susceptible to interference reactions. However, recalculations of the major element content after correction for C_{org}, CO_2, S and H_2O+ (Chapter 3.1, Appendix 1b) show a high degree of reliability of the data.

1.5.2.5 Li by Atomic Absorption Spectrometry (AAS)

50 shale samples were analysed for lithium at the Geological Survey of South Africa, Pretoria. The sample (0.5 g) was heated to 1038° C to break down the crystalline structure.

The treated sample was then dissolved with a mixture of conc. HF and conc. H_2SO_4 and fumed with H_2SO_4 to remove HF. The soluble salts were dissolved in warm distilled water and, after cooling, made up to an appropriate volume with distilled water. After adding ~3 ml KCl (0.1 %), the resultant solution was aspirated into an air/acetylene flame of PU 9000 AAS. The Li_2O content was measured at 670 nm by comparison with a suitable reference material, which was carried through the same procedures as the sample. A reagent blank was similarly prepared and used to zero the AAS.

International standards were used for internal calibration. The lower limit of detection is 1 ppm. The accuracy for 3.1 % Li_2O is about 4%. The precision is < 5 %. Ionisation as an interference factor was overcome by the addition of the KCl-solution.

1.5.2.6 Rare Earth Elements (REE) by Liquid Chromatography

50 shale samples were analysed for REE at the Geological Survey of South Africa, Pretoria. The sample (0.5 g) was weighed into a teflon crucible and 10 ml HF (conc.) and 4 ml $HClO_4$ (conc.) were added. The sample/acid mixture was heated for about 12 hours at 80° C and then evaporated to near dryness at 250° C. After cooling, the residue was dissolved again in 2 ml conc. $HCLO_4$, heated at 250° C, and 10 - 12 drops of H_2O_2 (100 v/s) were added to the hot solution to ensure all Ce was reduced to the 3+ oxidation state. The solution was again evaporated to near dryness. After cooling, the residue was dissolved in ammonium acetate (2 M) and quantitatively transferred into 100 ml volumetric flasks and made up to volume. The separation of the REE from the other elements and the measurement of the REE contents was automatically performed by the DIONEX ION CHROMATOGRAPH (Model 2000 i).

Due to the uniqueness and recent development of the automatic procedure, a short description of the method will be given. The prepared ammonium acetate solution (4 ml) is injected into the chromatograph and the cations are concentrated using a cation concentration column (CC-1). The mono- and divalent cations are eluted with ammonium acetate. All metals are then transferred onto a trace metal concentrating column (TMC-1) using HCl as eluent. PDCA (pyridine-2,6-dicarboxylic acid) is used to transfer the REE onto a guard column (CG-5),

while the rest of the transition metals are eluted. Switching over to the oxalate system allows the REE to be washed onto the separator column, where the REE are separated. Detection is achieved by mixing the eluent with a colouring reagent (0.4 mM PAR), allowing for enough time and heat to form the colour complexes, and then to measure the light absorbency. A linear gradient between oxalic acid and di-glycolic acid is used to attain a workable chromatogram. The process described above gives excellent separation results for the REE, except for Ho which exactly co-elutes with Y. The obtained results are automatically captured and processed by an integrator (SPECTRA PHYSICS Mod. 4270). A more detailed description of the separation and analytical procedure is available at the Geological Survey of South Africa, Pretoria.

LLD is 1 ppb for all REE, precision is < 20 %, and accuracy is $\pm$ 10 %. Internal standards for calibration were prepared from stock solutions from ALDRICH CHEMICAL COMPANY INC., Milwaukee, USA.

1.5.3 X-ray diffraction (XRD)

A Siemens D-500 automated X-ray diffractometer, equipped with primary and secondary monochromators, was used for all X-ray measurements, which were performed by Sabine Verryn at the University of Pretoria. The diffractometer includes a 40-position automated sample changer and an IBM compatible computer for operating the diffractometer. The X-ray generator was operated with a copper target X-ray tube (wavelength of 1.5406 Å) at 30 kV and 25 mA. The apertures used in the diffractometer were: two 1° beam apertures, one 0.05° detector aperture, and one 1° diffracted beam aperture. All samples were recorded over the range 5° to 70° 2Θ in 0.05° steps for a 1 sec. counting time per step. All shale samples were run twice, the second run was performed after the samples were exposed to an ethylene/glycol atmosphere for 24 hours. This procedure ensured that the presence of expandible clays (e.g. smectites) could be detected. Raw data files were transferred from the Siemens X-ray diffractometer to a data reduction programme (DIFMAIN) and processed.

1.5.4 Computer software

Statistical tests and mathematical parameters were calculated and performed using the computer software packages CSS, SAS, Grapher and Quattro Pro. Graphical representation was performed with Kemplot, CSS, Quattro Pro and Grapher. Word Perfect was used for word processing, while organisation and layout of the data sets and tables was carried out using Kemfile, CSS, Quattro Pro and Word Perfect.

CHAPTER 2: MATHEMATICAL METHODS

2.1 Descriptive statistics

The basic statistical principles outlined in Chapter 2.1 are compiled largely from Le Maitre (1982) and Sachs (1982, 1992). Various numerical and graphic examples of statistical properties of geochemical data are given by Le Maitre (1982), and are therefore not repeated here. In the following description of statistical procedures, the term 'sample' is not used in a statistical sense, but in a geochemical sense, i.e., the term 'sample' refers to the results of the chemical analysis of a rock specimen.

2.1.1 Introductory remarks

Geochemical investigations are undertaken to establish the composition of a specified rock population, and to draw conclusions about geological parameters controlling the geochemistry of this population. If a rock population were geochemically completely uniform in its characteristics, it would only be necessary to sample and analyse one rock specimen, in order to provide all the geochemical information about the population. However, it is known from experience that every specimen of a defined population will have a different geochemical composition, even if the analytical procedure is absolutely free of error. Hence, quantitative statements are made about geochemical properties of a specified rock population from the data obtained from the composition of various rock specimens. This mathematical process is called statistical inference.

Statistical treatment of variables demands, as a prerequisite, that the population under investigation is sampled randomly, i.e., every object in the population has an equal chance of being collected. Hence, an implicit bias has to be noted for most geochemical investigations, as sampling is restricted to outcrop or borecore material. The following stages of sampling, sample preparation and analysis are prone to related bias (i.e., the sample was not taken randomly) in this investigation:

1. The analysed powder is a sample from a larger amount of crushed rock.
2. The crushed rock is a sample from a specimen.
3. Each specimen collected is a sample from an outcrop, or borecore.
4. Each outcrop selected for collection is a sample of the rock population under investigation.

Although stages 1 and 2 are thought to have been controlled sufficiently to avoid bias, the nature of this investigation generally prohibited a random sampling procedure for stages 3 and 4. It is thought that possible bias was minimised by collecting and analysing a large number of specimens.

2.1.2 Frequency distributions and central value estimation

If values are grouped together in classes, such that each class represents a particular range of values, a histogram can be produced showing the frequency of occurrences of each class, where the frequency may be expressed as the actual number of occurrences in a class, or is expressed as relative frequency, i.e., the actual number in a class divided by the total number. A histogram utilizing the actual number of occurrences is an empirical frequency distribution, whereas the use of relative frequencies leads to an empirical probability distribution. However, the empiric frequency and probability distributions found graphically with the help of histograms have the disadvantage that they are discontinuous distributions, i.e., frequencies are known only for a discrete range of values. As geochemical data consist normally of continuous variables, a continuous distribution in the form of a curve, which is defined by a mathematical formula, is more convenient to use. Although it is possible, in some instances, to interpolate the continuous distribution curve from a histogram, its mathematical expression would still be doubtful. Furthermore, a continuous distribution curve interpolated from a histogram is dependant on the chosen width of the classes, and thus offers non-unique solutions.

In general, the values of an element's concentration in a specific sample population will tend to cluster about a central value and their frequency of occurrence will decline away from this value (Le Maitre, 1982). A central value commonly used for descriptive statistics is the median. The median, $\tilde{x}$, can be defined as the value that divides the distribution into halves.

An estimate of the median is that value in the sequence of individual values, ordered according to size, which divides the sequence in half. Another important statistical parameter of unimodal distributions is the mode, **M**, which is defined as the most frequent sample value. Both median and mode are not influenced by extreme values (Sachs, 1992), but are less efficient from a theoretical statistical point of view (Garrett, 1993).

The shape of a continuous frequency distribution curve can vary considerably. It is assumed for many variables that their population follows a 'normal' distribution (Gauss distribution), which is symmetrical and determined by the mean, μ, and the standard deviation, σ. The mean, μ, of a distribution is estimated by the following expression:

$$\bar{x} = \frac{\Sigma x_i}{n} \qquad \textbf{(2.1)}$$

where $\bar{x}$ is the empiric estimation of μ, **n** the number of variables, and x_i is the ith variable of the sample set with i assuming values from 1 to n. The mean, $\bar{x}$, is also called arithmetic mean. The standard deviation, σ, is calculated as

$$s = \sqrt{\frac{\Sigma(x_i - \bar{x})^2}{(n - 1)}} \qquad \textbf{(2.2)}$$

where **s** is the empiric estimation of σ. As the standard deviation is the square root of the variance, the standard deviation can be looked upon as a parameter expressing the variability of a variable. It should be noted, that **s** is calculated with the term "n - 1" in the denominator, whereas σ is calculated by using the total number "n" in the denominator. Accordingly, σ can be termed the population standard deviation, and **s** the sample standard deviation. It is obvious, that for geochemical purposes only, **s** is a meaningful expression, as the total geochemical population of a rock unit remains an unknown quantity.
The density function of the 'normal' distribution is given by the expression:

$$y = \frac{1}{\sigma\sqrt{2\pi}} \exp\left(\frac{-(x-\mu)^2}{2\sigma^2}\right) \qquad \textbf{(2.3)}$$

Integrating **y** over a particular range of **x** then gives the area under the curve and hence the probability of such a range of values, **x**, occurring. The expression

$$R_{\bar{x}\pm s} = \bar{x} \pm s \qquad \textbf{(2.4)}$$

defines a range $\mathbf{R}_{\bar{x}\pm s}$ around the mean, $\bar{\mathbf{x}}$, which contains 68.3 % of the observed values, $\mathbf{x}_i$, for a normal distribution. In other words, a newly sampled specimen of the population under investigation will fall in the range $\mathbf{R}_{\bar{x}\pm s}$ with a probability of 68.3 %, if the population has a normal distribution. The fundamental significance of the normal distribution is based on the fact that a sum of many independent, arbitrarily distributed random variables is approximately normally distributed (central limit theorem) (Sachs, 1992). The normal distribution can be viewed as a basic tool of mathematical statistics, and many statistical tests require a normal distribution of the variables tested (for example, product moment correlation coefficient, see Chapter 2.2.2.1).

However, geochemical data exhibit various types of distributions. The main types of distributions found in geochemical data, after Le Maitre (1982), are :

A. Symmetrical distributions (incl. normal distributions);
B. Skewed (= asymmetrical) distributions;
C. Polymodal distributions.

It should be noted in this context, that symmetrical and bell-shaped distribution curves are not necessarily normally distributed. The assumption that a symmetrical and bell-shaped curve represents a normal distribution is found in the geochemical literature (for example, Le Maitre, 1982, p. 9), but is not absolutely incorrect. Generally, deviations of the normal distribution, apart from polymodal distributions, are of two distinct types (Sachs, 1992):

I. One of the two tails is lengthened, and the distribution becomes 'skewed' (**skewness**);
II. The maximum of the distribution curve lies higher or lower than that of the normal distribution (**kurtosis**).

Important measures of skewness and kurtosis in a population are the third and fourth moments about the mean, i.e., the average values of $(\mathbf{x}_i - \mu)^3$ and $(\mathbf{x}_i - \mu)^4$ over the whole population. The skewness (Sachs, 1992) is estimated as

$$\alpha_3 = \frac{\Sigma(x_i - \bar{x})^3}{n \cdot s^3} \qquad (2.5)$$

and the kurtosis (Sachs, 1992) as

$$\alpha_4 = \frac{\Sigma(x_i - \bar{x})^4}{n \cdot s^4} - 3 \qquad (2.6)$$

It has to be noted that for the calculation of skewness and kurtosis, **s** has to be calculated with the denominator "**n**" and not with "**n - 1**". For a symmetric distribution, $\alpha_3 = 0$, and for a normal distributions, $\alpha_3 = \alpha_4 = 0$. A positive skewness, i.e. α_3 having a positive value, implies that the right hand part of a distribution is lengthened (left-steep); a negative skewness, i.e. α_3 having a negative value, implies that the principal part of a distribution is concentrated on the right side of a frequency plot and the distribution is lengthened towards lower values of $\mathbf{x_i}$ (left hand part of distribution lengthened and right-steep). Analogously, a distribution with a flatter curve than the normal distribution will have a negative coefficient of kurtosis (i.e. α_4), and a distribution with a higher peak than the normal distribution will have a positive coefficient of kurtosis. The arithmetic mean and the standard deviation can be taken to be the first and second moments of a distribution. Sachs (1992) emphasises that the meaningful calculation of the moments is dependent on the sample size, and mentions '**Tukey's fiver rule**' as an approximation for the number, **n,** of variables necessary to calculate the moments. Tukey's fiver rule states that **n** must exceed $\mathbf{5^k}$ for the calculation of the **k**th moment (Sachs, 1992). A strict application of Tukey's fiver rule had to be omitted in this investigation, but it was attempted to use data sets which were large enough to avoid evidently meaningless statistical calculations, although a few exceptions had to be permitted in the descriptive part (for example, Chapter 3.3.5). It is noted in this context, that estimations of the standard deviation, **s**, (i.e. second moment) of normal and uniform distributions with a similar range show only minor differences for sample sets of $n \leq 12$ (Sachs, 1992).

As mentioned above, geochemical data exhibit various types of distributions. Symmetrical and positively skewed distributions with a more or less defined modal value are most abundant in geochemical data (Le Maitre, 1982). Polymodal distributions are usually confined to data drawn from rock series or occur when a wide variety of rocks are considered together (Le Maitre, 1982, p. 16, Fig. 1.7). The occurrence of polymodal distributions in a geochemical data set points to the existence of more than one underlying population, i.e., the investigated set of specimens may have been drawn from statistically different geochemical populations.

Ahrens (1954) put forward his "fundamental law of geochemistry", which states that "the concentration of an element is log-normally distributed in a specific igneous rock". The log-normal distribution is normally distributed for $\mathbf{ln}\ x_i$. The log-normal distribution is positively skewed and has a positive kurtosis for x_i. The central value, $\bar{x}_{log}$, of a log-normal distribution is expressed as

$$\bar{x}_{log} = antilog\left(\frac{\Sigma \log x_i}{n}\right) \qquad (2.7)$$

with $x_i > 0$. The central value, $\bar{x}_{log}$, is analogous to the median of the normal distribution, i.e., $\mathbf{ln}\ \bar{x}_{log}$ is the 50th percentile of $\mathbf{ln}\ x_i$ in a cumulative frequency plot (Sachs, 1992). It has to be noted that the central value, $\bar{x}_{log}$, is greater than the mode, **M**, of the log-normal distribution for <u>both</u> a normal and logarithmic scale of x_i (Binder, 1962). The dispersion factor of a log-normal distribution (analogous to the standard deviation of the normal distribution) is expressed as

$$s_{log} = antilog\sqrt{\frac{\Sigma (\log x_i)^2 - \frac{(\Sigma \log x_i)^2}{n}}{n-1}} \qquad (2.8)$$

where s_{log} is the dispersion factor. The central mass, R_{log}, of the log-normal distribution (analogous to $R_{\bar{x}\pm s}$ of the normal distribution) is expressed as

$$R_{log} = (\bar{x}_{log}) \cdot (s_{log})^{\pm 1} \quad \textbf{(2.9)}$$

It is obvious that equation (2.7) can also be solved using equation (2.10)

$$\bar{x}_{log} = \bar{x}_{GM} = (\Pi\, x_i)^{\frac{1}{n}} \quad \textbf{(2.10)}$$

where $\bar{x}_{GM}$ is the geometric mean. Both geometric mean, $\bar{x}_{GM}$, and arithmetic mean, $\bar{x}$, are useful descriptive parameters of distributions. The arithmetic mean, $\bar{x}$, is elevated relative to the geometric mean, $\bar{x}_{GM}$, with increasing skewness, α_3, and both will be high relative to the median, $\tilde{x}$ (Garrett, 1993). The relationship of $\bar{x}$, $\tilde{x}$ and $\bar{x}_{GM}$ thus provides for an indirect indication of the skewness of the observed distribution. However, this relationship is dependent on the range of the variables (i.e. x_{max} - x_{min}) and is not easy to quantify. The ratio of "geometric mean $\bar{x}_{GM}$ over arithmetic mean $\bar{x}$", which has a maximum of 1.0, is generally greater than 0.9 for normal distributions (BFF Reczko, unpublished data). For log-normal distributions, this ratio becomes smaller with increasing range and is smaller than 0.9 for ranges $>$ 100 (BFF Reczko, unpublished data).

The use of the geometric mean, $\bar{x}_{GM}$, as a descriptive parameter has the additional advantage that the geometric mean of a ratio of two variables is equal to the ratio of the geometric means of the two variables. The latter peculiarity is of some importance, as ratios are widely used in sedimentary geochemistry, but a comparison of newly acquired data and published data sets has to fail in this regard, as the complete data sets are not reported (e.g, Taylor and McLennan, 1985), and a particular ratio of interest cannot be deduced from the mean concentrations of elements. An analogous calculation of mean ratios from arithmetic mean concentrations is evidently nothing more than a meaningless mathematical exercise, although this procedure is widely used in the geochemical literature (e.g., Wronkiewicz and Condie, 1990; Feng et al., 1993).

The nature of the distributions of geochemical data sets, i.e. symmetrical to strongly skewed, poses implicit problems in the meaningful description of geochemical data sets. Experience shows that distributions of geochemical (and other natural) data deviate more or less strongly

from either normal or log-normal distributions (Le Maitre, 1982; Sachs, 1992). Therefore, the statistical parameters of geochemical data should be chosen according to their descriptive properties, wide range of applications and their comparative aspects. Naturally, the calculation of as many statistical parameters as possible and graphic representation of the distributions, will enhance the knowledge of the empiric geochemical populations under investigation. However, the amount of information obtained by such steps would be immense and confusing. Accordingly, the chosen statistical parameters should describe sufficiently the element distributions investigated, without causing statistical load. Secondly, the descriptive parameters should allow for comparison with published data from similar investigations, and should be easily applicable for further investigations. Thirdly, the descriptive parameters should be chosen for a wide range of applications, e.g. determination of the background range for economic and/or environmental purposes.

The choice of descriptive statistical parameters is thus associated with their properties. For example, arithmetic mean, $\bar{\mathbf{x}}$, and standard deviation, **s**, are sufficient to describe the most important properties of a normal distribution. However, it is essentially unknown, at least before performing additional statistical tests (e.g., χ^2 or Kolmogoroff-Smirnoff tests), if the population in question can be approximated by a normal distribution. As outlined above, many geochemical distributions cannot be approximated by a normal distribution. Although deviations from the normal distribution are indicated by an unusually high or low standard deviation, **s**, relative to the arithmetic mean, $\bar{\mathbf{x}}$, (see also Chapter 2.1.3), the type of deviation remains unknown. Hence, a summarizing table of arithmetic mean, $\bar{\mathbf{x}}$, and standard deviation, **s**, of element concentrations, i.e. the usual form of representation of geochemical data, must be considered insufficient to describe the underlying distribution of a population.

Further statistical manipulations of arithmetic mean, $\bar{\mathbf{x}}$, and/or standard deviation, **s**, (e.g., Taylor and McLennan, 1985; Condie and Wronkiewicz, 1990) can distract attention from highly variable results, which may invalidate the conclusions drawn or, at least, constrain the interpretations derived. For example, the 95 % confidence interval of the arithmetic mean, $\bar{\mathbf{x}}$, of a normal distribution is calculated by the equation

$$R_{\bar{x}\,95\%} = \bar{x} \pm 1.96 \frac{s}{\sqrt{n}} \qquad \textbf{(2.11)}$$

The term $\mathbf{R_{\bar{x}95\%}}$ implies that the arithmetic mean, $\bar{\mathbf{x}}$, lies with a 5 % error probability in this range, if the population is normally distributed. Taylor and McLennan (1985) utilize the "95 % confidence interval" extensively for showing differences of element concentrations and ratios with time, although the data provided by them clearly point to the occurrence of non-normal distributions (i.e., the variation coefficient exceeds the limit for a normal distribution, see Chapter 2.1.3). Hence, element and ratio distributions are compared by using, probably, incorrectly obtained parameters (i.e. an interval around the arithmetic mean, $\bar{\mathbf{x}}$, of at least questionable significance), although a multitude of statistical procedures for comparing distributions and mean values are available (see, for example, Chapter 2.2.1).
Condie and Wronkiewicz (1990) utilize the 'standard deviation of the mean', which is usually termed 'standard error of the mean' and which is calculated by the equation

$$s_{\bar{x}} = \frac{s}{\sqrt{n}} \qquad \textbf{(2.12)}$$

Analogous to $\mathbf{R_{\bar{x}95\%}}$, $\bar{\mathbf{x}} \pm \mathbf{s_x}$ is the 68.3 % confidence interval of the mean, $\bar{\mathbf{x}}$, for normally distributed data. If the $\mathbf{s_{\bar{x}}}$ values given by Condie and Wronkiewicz (1990) are recalculated to account for the standard deviation, **s**, the interpretations made for Pretoria Group shales are questionable, as the ranges $\mathbf{R_{\bar{x}\pm s}}$ (see equation 2.4) of the variables used overlap for the formations investigated. An overlap of $\mathbf{R_{\bar{x}\pm s}}$ parameters does not necessarily imply that a statistical difference has to be rejected, but additional statistical tests would be a prerequisite to conclude any significant differences between $\mathbf{R_{\bar{x}\pm s}}$ parameters. The high variability of the Condie and Wronkiewicz (1990) data (i.e. high **s** relative to $\bar{\mathbf{x}}$) further suggests that the reported ratios have strongly skewed distributions (i.e. are not normally distributed), thereby indicating that the calculation of $\mathbf{s_{\bar{x}}}$ and its use for interpretative purposes is a questionable statistical technique. Furthermore, as Condie and Wronkiewicz (1990) use ratios of presumably negatively correlated elements with concentration differences of a magnitude or more, a strongly skewed nature of the reported ratios can be expected. Hence, a simple comparison of the resulting mean values and statistical derivatives designed for normal

distributions, can be viewed as a fundamentally mistaken approach, as the mean values of skewed distributions are inconclusive estimators of the respective central values.

2.1.3 Variation coefficient

The variation coefficient, **VC**, is defined as the ratio of "standard deviation, **s**, over arithmetic mean, $\bar{x}$," (equation 2.13).

$$VC = \frac{s}{\bar{x}} \qquad \textbf{(2.13)}$$

The variation coefficient, **VC**, can be used as a quick test of the normality of a distribution. Perfect normal distributions have a variation coefficient of less than 0.33, and normality is rejected if the variation coefficient exceeds this value (Sachs, 1992). The derivation of the variation coefficient, **VC**, can be shown by a simple example: A normal distribution with values between 0 and 100 will have an arithmetic mean, $\bar{x}$, of $\sim$50 and a standard deviation, **s**, of $\sim$16.6 (i.e., s = R/6, Sachs, 1992). The variation coefficient, **VC**, would accordingly be $\sim$0.33. The expressiveness of the variation coefficient, **VC**, has two pitfalls:

1. The sample number **n** must be of a considerable size (i.e., $>>$ 100), if the critical value of 0.33 is applied as a quick test on normality (Sachs, 1992).
2. The critical value of 0.33 can only be applied for sample populations with a minimum value of 0.

The latter restriction can be illustrated by adding a constant value of 100 to all variables in the above example of deriving the **VC**. The addition would not alter the variance or standard deviation, **s**, but the arithmetic mean, $\bar{x}$, would rise to $\sim$150 and the **VC** would drop to $\sim$0.11. Although the interpretation of the **VC** would in both cases be correct, i.e. as the **VC** is smaller than or equal to 0.33 the underlying distribution would be considered to be normally distributed; however, the latter example shows that a **VC** of smaller than 0.33 might also occur for non-normal distributions, if the minimum value is $>$ 0. To circumvent this problem, a method based on the approximate standard deviation for normal distributions was developed. This method allows the calculation of a critical value for the variation

coefficient, **VC**, corrected for the sample size, **n**, and the empirical minimum value.

Table 2.1 shows approximations of the standard deviation, **s'**, of normal distributions for different sample sizes as a function of the range, **R**, which is defined as $\mathbf{x_{max}}$ - $\mathbf{x_{min}}$ (Sachs, 1992).

TABLE 2.1: Approximations of the standard deviation, **s'**, of normal distributions for different sample sizes as a function of the range, **R**.

n	~12	20 - 40	~100	≥ 400
s'	**R/√n**	**R/4**	**R/5**	**R/6**

The arithmetic mean, $\bar{x}$, of a normal distribution (and symmetric distributions) can be approximated by

$$\bar{x} = x_{min} + \frac{(x_{max} - x_{min})}{2} = \frac{(x_{max} + x_{min})}{2} \qquad \textbf{(2.14)}$$

where $\mathbf{x_{min}}$ is the lowest and $\mathbf{x_{max}}$ is the highest value of the empiric distribution. Accordingly, the critical value of the **VC** for normal distributions can be estimated by the equation

$$VC_{crit.} = \frac{s'}{\left(\frac{(x_{max} + x_{min})}{2}\right)} \qquad \textbf{(2.15)}$$

where **s'** is the approximation of the standard deviation, **s**, according to Table 2.1. As numerator and denominator of equation (2.15) contain numbers, the equation can be written as

$$VC_{crit.} = r' \cdot \left(\frac{(x_{max} - x_{min})}{(x_{max} + x_{min})}\right) \qquad \textbf{(2.16)}$$

where **r'** is a variable depending on the sample size. Values for **r'** are listed in Table 2.2.

TABLE 2.2: The relation between **n** and **r'**

n	~12	20 - 40	~100	≥ 400
r'	$2/\sqrt{n}$	0.5	0.4	0.33

The values of **r'** in Table 2.2 are equal to the critical value of the **VC** of normal distributions for a respective sample size for $x_{min} = 0$ as the term

$$\left(\frac{(x_{max} - x_{min})}{(x_{max} + x_{min})}\right) = 1 \qquad for \quad x_{min} = 0 \qquad (2.17)$$

Equation (2.17) thus corrects for the 'added constant problem' and has a maximum of 1 for $x \in Ra \geq 0$, i.e. the measured concentrations in geochemistry. The variable **r'** corrects for the sample size, **n**.

It has to be noted that the variation coefficient, **VC**, is not so much a thumb nail test on normality, but rather a quick test on non-normality of an investigated distribution. The **VC** cannot be utilized to identify deviations from the normal distribution due to a high kurtosis (i.e., $\alpha_4 >> 0$, but $\alpha_3 = 0$) or due to the occurrence of a χ^2 distribution. Accordingly, the expressiveness of a **VC** below the critical limit is restricted. However, a **VC** above the critical limit is thought to be a strong indication for the occurrence of a non-normal distribution. Accordingly, the null hypothesis for the described test is defined as:
H_0: the distribution can be normally distributed for $VC \leq VC_{crit.}$,
and the alternative hypothesis as:
H_1: the distribution cannot be normally distributed for $VC > VC_{crit.}$.
It should be mentioned that the case of an empirical VC only marginally exceeding $VC_{crit.}$ is considered inconlusive, and thus further statistial tests would be required. As many statistical tests require normality of the variables as a prerequisite (Sachs, 1992), the **VC** seems to be an ideal tool for a superficial evaluation of the distributions without applying more exact, but time consuming tests (e.g., χ^2 or Kolmogoroff-Smirnoff tests). As the **VC** of most element distributions of Pretoria Group sedimentary rocks point to non-normal distributions, tests requiring normality are generally considered to be inappropriate, if the

data are not transformed (see Chapter 2.2.1).

The variation coefficient **VC** can be utilized further as a statistical tool to compare empirical normal distributions. As the standard error of the variation coefficient is calculated as

$$s_{VC} = \frac{VC}{\sqrt{2n}} \cdot \sqrt{1 + \frac{2(VC)^2}{10^4}} \approx \frac{VC}{\sqrt{2n}} \qquad \textbf{(2.18)}$$

the difference between two variation coefficients can be tested by

$$z' = \frac{|VC_1 - VC_2|}{\sqrt{\frac{(VC_1)^2}{2n_1} + \frac{(VC_2)^2}{2n_2}}} \qquad \textbf{(2.19)}$$

where $\mathbf{z'}$ is evaluated with respect to the standard normal distribution (Sachs, 1992; Tables of the standard normal variable, **z**, are reported by Sachs, 1992, p. 116, Table 25). When $\mathbf{z'}$ is smaller than **z** for the chosen significance level (error probability), the uniformity of the underlying parameters of the variation coefficients cannot be rejected. The test described above needs a sample size, **n**, in excess of 30. Sachs (1992) refers to an exact test and critical limits for small sample numbers; Dornbos and Dijkstra (1983) describe a method to compare several variation coefficients simultaneously. However, the comparison of variation coefficients described above requires normality of the empirical distributions (Sachs, 1992), i.e. variation coefficients which are, at least, below the critical limit.

2.1.4 Descriptive statistical parameters

In this investigation, it was attempted to provide a certain critical minimum number of descriptive statistical parameters, which are compatible with the criteria listed above. Hence, the arithmetic mean, $\bar{\mathbf{x}}$, the standard deviation, **s**, the geometric mean, $\bar{\mathbf{x}}_{\mathbf{GM}}$, the median, $\tilde{\mathbf{x}}$, minimum and maximum concentrations, $\mathbf{x}_{\mathbf{max}}$ and $\mathbf{x}_{\mathbf{min}}$, and the number of analysed specimens, **n**, of a respective element are thought to be the descriptive statistical parameters

which constitute the minimum number of parameters necessary to: (1.) describe the empirical distribution and enable the interpretion of the character of the distribution under investigation (i.e., symmetric or skewed), (2.) provide information about the background concentration, and (3.) compare the concentrations found with values reported from literature. Additionally, the variation coefficient, **VC**, is reported for convenience, although the **VC** can simply be calculated from arithmetic mean, $\bar{x}$, and the standard deviation, **s**.

2.2 Univariate statistical tests

2.2.1 Analysis of variance and LSD-test

The comparison of means of an arbitrary number of groups can be performed by one way analysis of variance. An essential aspect of this technique is the decomposition of the sum of squares of the deviations of the observed values from the overall mean, SS_{total}, into two components:

1. the sum of squares of the deviations of the observed values from the corresponding group means, called "within sample sum of squares" (SS_{within}) or "error sum of squares", and,
2. the sum of squares of the deviations of the group means from the overall mean, weighted by the number of elements in the respective population. This sum is called the "between samples sum of squares" ($SS_{between}$) (Sachs, 1982).

The partitition of SS_{total} is accomplished by

$$SS_{total} = SS_{within} + SS_{between} \qquad \textbf{(2.20a)}$$

$$\sum_{i,j} (x_{ij} - \bar{x})^2 = \sum_{i,j} (x_{ij} - \bar{x}_i)^2 + \sum_{i} n_i (\bar{x}_i - \bar{x})^2 \qquad \textbf{(2.20b)}$$

where x_{ij} is the **j**th value of the **i**th group ($j = 1,\ldots,n_i$; $i = 1,\ldots,k$), n_i is the number of values in the **i**th group, $\bar{x}_i$ is the arithmetic mean of the **i**th group and $\bar{x}$ is the overall arithmetic mean. The sums of squares divided by the respective degrees of freedom are called the mean sum of squares (**MS**) in analysis of variance. The respective degrees of

freedom are '**(n - k)**' for SS_{within}, '**(k - 1)**' for $SS_{between}$, and, accordingly, '**(n - k) + (k - 1)**' for SS_{total}, where **k** is the number of groups and **n** the total number of samples. If all the tested groups originate in the same population, then the variances, i.e. the mean squares MS_{within} and $MS_{between}$ should be about the same size (Sachs, 1982). If this is not so, i.e., if the quotient of $MS_{between}/MS_{within}$ is larger than the critical value (one sided test) of the F-distribution for a specific significance level α, with **v1 = k - 1** and **v2 = n - k** (for example Sachs, 1992, Tables 52 a-f, p. 218 - 226), then the null hypothesis (H_0: the means of the **k** groups are equal) has to be rejected, and the alternative hypothesis that at least two μ_i's are different (H_1: $\mu_i \neq \mu_j$ for some {i,j}) is accepted (Sachs, 1982). **F'** is computed according to

$$F' = \frac{\frac{1}{k-1}\left[\sum_{ij}\frac{x_i^2}{n_i} - \frac{(\Sigma x_{ij})^2}{n}\right]}{\frac{1}{n-k}\left[\sum_{i,j} x_{ij}^2 - \sum_{i}\frac{x_i^2}{n_i}\right]} \qquad \textbf{(2.21)}$$

The prerequisites for this test are

1. Independence of observations within and between all samples;
2. Observations from normally distributed populations with equal (and unknown) variances (Sachs, 1992).

The second prerequisite poses a problem for geochemical data as the distributions are usually non-normal, and the variances might be heterogeneous (see Chapter 2.1.2). To circumvent this problem, the data must be transformed with the aim to obtain normally distributed values with homogeneous variances (Sachs, 1982). For geochemical data, a logarithmic transformation ($\log_{10}$) is usual (e.g., Govett, 1983).

The rejection of the null hypothesis then permits further tests to conclude which mean values differ significantly. A statistical procedure to determine significant differences between mean values is the LSD-test (**L**east **S**ignificant **D**ifference). The LSD-test measures the significance of the empirical difference **Δ** between two means, **a** and **b**, as follows:

$$\Delta_{emp.} = \sqrt{MS_{within}\left(\frac{n_a + n_b}{n_a\, n_b}\right) F_{(1;\, n-k;\, \alpha)}} \qquad (2.22)$$

where the significance level α of the F-distribution is the only unknown variable (Sachs, 1992). After solving equation (2.22), the significance of the difference of two means is expressed as $\mathbf{1 - \alpha}$. For sample groups of equal size (Sachs, 1992), α is calculated as

$$\Delta_{emp.} = \sqrt{\frac{2}{n_i} MS_{within}\, F_{(1;\, n-k\,;\, \alpha)}} \qquad (2.23)$$

2.2.2 Measures of association

2.2.2.1 Correlation analysis

Correlation analysis investigates stochastic relations between random variables of equal importance on the basis of a group of samples (Sachs, 1982). As a statistical parameter of correlation, a correlation coefficient is defined, as a measure of the direction and the strength of the stochastic relationship between two random variables (Sachs, 1992). A widely used statistic to test the linear interdependence of two random variables is the product moment correlation coefficient, ϱ, which is defined as

$$r = \frac{\Sigma\,[(x_i - \bar{x}) \cdot (y_i - \bar{y})]}{\sqrt{\Sigma\,(x_i - \bar{x})^2 \cdot \Sigma\,(y_i - \bar{y})^2}} \qquad (2.24)$$

where $\mathbf{r}$ is an estimate of the product moment correlation coefficient ϱ, $\mathbf{x_i}$ and $\mathbf{y_i}$ are pairs of the tested variables from the same specimen, and $\bar{\mathbf{x}}$ and $\bar{\mathbf{y}}$ are the arithmetic means of the random variables $\mathbf{x}$ and $\mathbf{y}$. The product moment correlation coefficient, ϱ, is a dimensionless quantity with $\mathbf{-1 \leq \varrho \leq 1}$, where a stochastic relationship between two variables is assumed

for $\mathbf{r} \neq 0$, and a functional relationship for $\mathbf{r} = 1$ or $\mathbf{r} = -1$. The significance of the estimator **r** depends strongly on the number of samples in the investigated data set (e.g., Sachs, 1992, p. 540, Table 193).

The prerequisites for the test of two random variables for stochastic independence (null hypothesis) with the product moment correlation coefficient, ϱ, are

1. the stochastic relationship must be linear;
2. the variables must be continuous variables;
3. the variables must be bivariately normally distributed;
4. the variables must be independent pairs of observations (Sachs,1992).

These prerequisites restrict the application of the product moment correlation coefficient, ϱ, on geochemical data, as

A. normally distributed variables are rather exceptional (see Chapter 2.1), and thus bivariate normal distributions (i.e., both variables are normally distributed) can be expected to be uncommon;
B. non-linear relationships might occur and be of interest in the interpretation of geochemical data.

Mutual dependence of sample populations containing non-normally distributed data and/or possibly non-linear relationships between variables can be assessed through Spearman's rank correlation coefficient, ρ (Conover, 1980; Sachs, 1982, 1992), which is calculated by

$$r_s = 1 - \frac{6 \cdot \Sigma\,[R(x_i) - R(y_i)]^2}{n \cdot (n^2 - 1)} = 1 - \frac{6 \cdot T_s}{n \cdot (n^2 - 1)} \qquad \textbf{(2.25)}$$

where $\mathbf{r_s}$ is an estimation of ρ, $\mathbf{R(x_i)}$ and $\mathbf{R(y_i)}$ are the rank of $\mathbf{x_i}$ and $\mathbf{y_i}$ (i.e., $\mathbf{R(x_i)} = 1$ for the smallest $\mathbf{x_i}$, $\mathbf{R(x_i)} = 2$ for the second smallest $\mathbf{x_i}$, and so on, with rank **n** being assigned to the largest $\mathbf{x_i}$), and $\mathbf{T_s}$ represents the entire sum in the numerator (Conover, 1980). If there are no ties (i.e., observations with the same value) in the data, Spearman's $\mathbf{r_s}$ is merely what one obtains by replacing the observations by their ranks, and then computing the product moment correlation coefficient, **r**, on the ranks (Conover, 1980). If there are many ties in the data, equation (2.25) changes to

$$r_{s,t} = 1 - \frac{6 \cdot T_s}{(n^3 - n) - (B_{x'} + B_{y'})} \qquad \textbf{(2.26)}$$

where $\mathbf{r_{s,t}}$ is Spearman's rank correlation coefficient corrected for tied ranks, and $\mathbf{B_x}$, and $\mathbf{B_y}$, are computed as

$$B_{x'} = \frac{1}{2} \cdot \Sigma(t_{x'}^3 - t_{x'}) \qquad \textbf{(2.27a)}$$

$$B_{y'} = \frac{1}{2} \cdot \Sigma(t_{y'}^3 - t_{y'}) \qquad \textbf{(2.27b)}$$

where $\mathbf{t_x}$, and $\mathbf{t_y}$, are the number of ties in consecutive groups of the same rank (Sachs, 1992). Compared to the product moment correlation coefficient, ϱ, Spearman's ρ estimates ϱ with an asymptotic efficiency of $9/\pi^2$ or 91.2 % for very large **n** and a bivariate normal population with $\varrho = 0$ (Sachs, 1982, 1992). For increasing **n** (i.e., $n \geq 100$) and binormally distributed variables, **r** can be estimated from $\mathbf{r_s}$ by using the following equation

$$r_{\backslash} = 2 \sin\left(\frac{1}{6}\pi \cdot r_s\right) \qquad \textbf{(2.28)}$$

Critical values of Spearman's rank correlation coefficient, $\mathbf{r_s}$, are reported by Conover (1980, Table A 10, p.456) and Sachs (1982, Table 103, pp. 398 and 399). The significance of $\mathbf{r_s}$ can also be tested on the basis of the standard normal distribution

$$z' = |r_s| \cdot \sqrt{n - 1} \qquad \textbf{(2.29)}$$

for $\mathbf{n} \geq 100$, or on the basis of Student's t-distribution

$$t' = |r_s| \cdot \sqrt{\frac{n - 2}{1 - r_s}} \qquad \textbf{(2.30)}$$

with **n - 2** degrees of freedon for **n** $\geq$ 30 (Sachs, 1982). If the number of ties is moderate, T_s can be applied as a statistic for stochastic independence (Hotteling-Pabst test, Conover, 1980; critical values ibid., Table A 11, p. 457).

The factual interpretation of correlation analysis is complicated, as even apparently significant stochastic dependence may not point to a causal relation (Sachs, 1982). A significant correlation coefficient may be introduced by:

1. a direct causal (= true) correlation;
2. a joint dependence on a third quantity (simultaneous correlation);
3. heterogeneity of the material (inhomogeneity correlation);
4. the scale of measurement, i.e. the expression of contents as part of a whole necessarily introduces negative correlations (formal correlation or constant sum problem);
5. the treatment of the variables, e.g. their expression as ratios with a third random variable in the denominator leads to the occurrence of index correlations;
6. coincidental correlations of independent variables (McNemar, 1969; Sachs, 1982, 1992 ; Aitchison, 1986; Rollinson, 1992).

Geochemical investigations are prone to all types of 'false' correlations (see above, No. 2.-6.). Hence, utmost care is obligatory in attempts to interpret the occurrence and/or lack of significant correlations. The problem of 'true' and 'false' correlations in the geochemical data of the sedimentary rocks of the Pretoria Group is discussed in some detail in Chapter 3.1.3. Two conclusive examples of apparently meaningless, but highly significant correlations are given by Sachs (1982): The increase in the number of storks and newborn human babies during a certain time period in Sweden, and the long term decrease in the number of stork nests and number of human births in East Prussia are not, with a probability close to certainty, causal correlations!!

2.2.2.2 Regression analysis

In regression analysis, a regression equation is fitted to an observed point cloud (Sachs, 1982). As, in this investigation, regression equations are only computed for graphic

applications, a thorough description and discussion of regression analysis will be omitted. The regression equations are estimated from the investigated population by the method of least squares, with the help of so-called normal equations (Sachs, 1982). Table 2.3 summarizes the regression equations used in this investigation and their simplified mathematical derivations. It is obvious from the equations listed in Table 2.3 that two regression lines exist, the first inferring variable y from x and the second infering x from y. The two regression lines intersect at the center of gravity ($\bar{x}$, $\bar{y}$) and form a 'pair of scissors' (Sachs, 1982). The angle between the linear regression lines (prerequisites: bivariate normal distribution of the variables and linear dependency) is zero for a product moment correlation coefficient, $\varrho = 1$ or $\varrho = -1$, and the angle is 90° for $\varrho = 0$. The product moment correlation coefficient, **r**, can be estimated from the regression equations by

$$r = \sqrt{b_{yx} \cdot b_{xy}} \qquad \textbf{(2.31)}$$

where $\mathbf{b_{yx}}$ and $\mathbf{b_{xy}}$ are the regression coefficients, which are calculated from Table 2.3 with A.) **y** as dependent variable ($\mathbf{b_{yx}}$), and B.) **x** as dependent variable ($\mathbf{b_{xy}}$).

2.3 Multivariate statistical tests

Garrett (1993) discusses the dimensionality problem of multivariate statistical procedures, i.e. how many samples, **n**, are necessary for a specified number of variables, **p**, to obtain a reliable result if multivariate statistical tests on **p** variables are performed. Garrett (1993) concludes that the bare minimum of **n** should be **3p**, but that **10p** would be far more prudent. Garrett (1993) summarizes the dimensionality problem by stressing that, firstly, a fixed multiple cannot be used to give an estimation of the necessary sample size, **n**, as low dimensionalities require a lower ratio of sample size, **n**, to number of variables, **p**, than higher dimensionalities, and, secondly, that the less known about the underlying probability structure, the larger the ratio of sample size, **n**, to number of variables, **p**, should be.

TABLE 2.3: Regression functions and normal equations (after Press et al., 1988; Sachs, 1982, 1992). All functional relations written with **y** as dependent variable; **a** is the intercept on the ordinate; **b** is the slope of the regression line (also called coefficient of regression).

Functional relation	Normal equations
linear $y = a + b \cdot x$	$n \cdot a + b \cdot \Sigma x = \Sigma y$ $a \cdot \Sigma x + b \cdot \Sigma x^2 = \Sigma (xy)$
logarithmic $y = a + b \cdot \ln x$	$n \cdot a + b \cdot \Sigma (\ln x) = \Sigma y$ $a \cdot \Sigma (\ln x) + b \cdot \Sigma (\ln x)^2 = \Sigma (y \cdot \ln x)$
exponential $y = a \cdot e^{bx}$	$n \cdot \ln a + b \cdot \Sigma x = \Sigma (\ln y)$ $(\ln a) \cdot \Sigma x + b \cdot \Sigma x^2 = \Sigma (x \cdot \ln y)$
power $y = a \cdot x^b$	$n \cdot \lg a + b \cdot \Sigma \lg x = \Sigma \lg y$ $\lg a \cdot \Sigma \lg x + b \cdot \Sigma (\lg x)^2 = \Sigma (\lg x \cdot \lg y)$
polynomial $y = b_0 + b_1 \cdot x + b_2 \cdot x^2 + \ldots + b_i \cdot x^i$	$n \cdot b_0 + b_1 \cdot \Sigma x + b_2 \cdot \Sigma x^2 + \ldots + b_i \cdot \Sigma x^i = \Sigma y$ $b_0 \cdot \Sigma x + b_1 \cdot \Sigma x^2 + b_2 \cdot \Sigma x^3 + \ldots + b_i \cdot \Sigma x^{i+1} = \Sigma xy$ $b_0 \cdot \Sigma x^2 + b_1 \cdot \Sigma x^3 + b_2 \cdot \Sigma x^4 + \ldots + b_i \cdot \Sigma x^{i+2} = \Sigma x^2 y$ $\ldots$ $b_0 \cdot \Sigma x^i + b_1 \cdot \Sigma x^{i+1} + b_2 \cdot \Sigma x^{i+2} + \ldots + b_i \cdot \Sigma x^{2i} = \Sigma x^i y$

2.3.1 Cluster analysis

The cluster analysis procedure described here is reported in detail by Backhaus et al. (1990). The starting point of cluster analysis is a raw data matrix with **i** variables and **n** objects.In

a first step, a measurement of similarity or distance between either variables or objects has to be introduced, which is usually done by using a statistic. Two types of similarity statistics can be differentiated:

1. similarity statistics (e.g., product moment correlation coefficient, ϱ);
2. distance statistics (e.g., Euclidean distance, Mahalanobis distance, for definition see Backhaus et al., 1990).

As geochemical data mainly consist of metric variables, a description of the treatment of data with nominal scale is omitted. In this investigation, the product moment correlation coefficient, **r**, is calculated as a measure of similarity and the term '**1 - r**' used for further computations.

The computed similarity (or distance) matrix is then the starting-point of the cluster algorithms. Clustering procedures can be divided by their properties. An overview of clustering procedures is given by Davis (1973) and Backhaus et al. (1990). In this investigation, the 'complete linkage' or 'furthest neighbour' procedure is applied, which is an agglomerative hierarchical procedure. The complete linkage procedure includes the following steps of calculation:

1. The two variables **P** and **Q** with the highest degree of similarity/lowest distance are combined in a cluster.
2. The similarity/distance between the new cluster and the other variables is calculated according to

$$D(R;P+Q) = 0.5 \cdot [D(R,P) + D(R,Q) + | D(R,P) - D(R,Q) |] \quad (2.32)$$

   where **D** depicts a similarity/distance measure of the variables in brackets, and **R** stands for the similarity/distance measure of any other variable.
3. Step 1. is repeated with the newly computed data matrix.
4. Step 2. is repeated for the next cluster.
5. The procedure is repeated until all variables are assigned to one cluster.

The procedure is depicted graphically in the lower figures of the respective cluster analysis diagrams in Appendix 2b. The results of the cluster analysis are shown in the form of a hierarchical tree in the upper figures of Appendix 2b.

The use of the product moment correlation coefficient, **r**, in the performed cluster analysis procedure might be looked upon as questionable (Chapter 2.2.2.1), as the data set contains non-normal distributions. The use of statistical parameters requiring normality is common in multivariate statistic analysis of geochemical data, and a thorough investigation of the influence of non-transformed non-normal data on multivariate statistics seems to be missing. Another problem arises as the sample number **n** required to perform multivariate statistical tests is too low for the number of variables used for some data sets (Garrett, 1993; s.a.). It has to be emphazised that cluster analysis is used in Chapter 3.1.3 as a statistical tool to exemplify graphically groups of elements with similar behaviour concerning their mutual correlations. As cluster analysis in this thesis is not used with the intention of performing an exact statistical test, but rather as a mathematical manipulation for graphic purposes, it is thought that the theoretical problems discussed above can generally be ignored.

2.3.2 Correspondence analysis

The description and theoretical derivation of the correspondence analysis procedure is largely compiled from the more detailed summary of Jöreskog et al. (1976). Correspondence analysis is a method of factor analysis, and combines some advantages of Q-mode and R-mode techniques (e.g., principal component analysis and principle coordinate analysis). An exhaustive account of the theory of correspondence analysis is given by Benzecri (1973). The aim of correspondence analysis is to obtain simultaneously, and on equivalent scales, factor loadings for both objects (i.e., samples) and variables (i.e., elements).

The method, primarily designed for discrete variables, may be applied to continuous distributions by the strategem of dividing the ranges of the variables into discrete pieces (Hill, 1975; Jöreskog et al., 1976). A natural restriction for this procedure is that the data cannot be negative. As a first step, the elements of a raw data matrix $\mathbf{X}_{(n \times p)}$ are divided by the sum of all elements in the matrix

$$b_{ij} = \frac{x_{ij}}{\sum_{i=1}^{n}\sum_{j=1}^{p} x_{ij}} \qquad \textbf{(2.33)}$$

where **n** represents the objects (rows of matrix) and **p** the variables (columns of matrix). The values $\mathbf{b_{ij}}$ transform the data matrix **X** to the data matrix **B**. For convenience later, a diagonal matrix $\mathbf{D_{c(p\ x\ p)}}$, containing the column sums of B in the principal diagonal, and a diagonal matrix $\mathbf{D_r}$, containing row sums of **B** are defined. Finally, the row and column sums are used to transform **B** as follows:

$$W = D_r^{-1/2}\ B\ D_c^{-1/2} \qquad \textbf{(2.34)}$$

The rationale for the transformation of (2.34) is based on the development of a measure of similarity between objects and between variables. The distance between two objects, q and r, is defined as

$$d_{qr}^2 = \sum_{j=1}^{p}\left(\frac{b_{qj}}{b_{q.}\sqrt{b_{.j}}} - \frac{b_{rj}}{b_{r.}\sqrt{b_{.j}}}\right) \qquad \textbf{(2.35)}$$

and the distance between variables i and j is defined as

$$d_{ij}^2 = \sum_{s=1}^{n}\left(\frac{b_{si}}{b_{.i}\sqrt{b_{s.}}} - \frac{b_{sj}}{b_{.j}\sqrt{b_{s.}}}\right) \qquad \textbf{(2.36)}$$

The next step is to calculate a covariance matrix for multinominal variables, which can be derived, in simplified form, by

$$c_{ij} = \sum_{s=1}^{n}\frac{b_{si}b_{sj}}{b_{s.}\sqrt{b_{.i}b_{.j}}} \qquad \textbf{(2.37)}$$

The covariance matrix, **C**, is equivalent to the minor product moment of **W**, defined in (2.34)

$$C = W'W = (D_c^{-1/2}B'D_r^{-1/2})\ (D_r^{-1/2}BD_c^{-1/2}) \qquad \textbf{(2.38)}$$

The major product moment of **W** is

$$G = WW' = (D_r^{-1/2}BD_c^{-1/2})\ (D_c^{-1/2}B'D_r^{-1/2}) \qquad \textbf{(2.39)}$$

and

$$g_{qr} = \sum_{j=1}^{p} \frac{b_{qj}b_{rj}}{b_{.j}\sqrt{b_{q.}b_{r.}}} \qquad \textbf{(2.40)}$$

The factor loadings matrix, **A**, of the minor product moment matrix, **C**, is then obtained from its scaled eigenvectors as follows:

$$C = U\Lambda U' \qquad \textbf{(2.41)}$$

where **U** is the matrix of eigenvectors of **C** and Λ is a diagonal matrix of eigenvalues. Then, it follows that

$$AA' = U\Lambda U' \qquad \textbf{(2.42a)}$$

and

$$A = U\Lambda^{1/2} \qquad \textbf{(2.42b)}$$

The factor loadings matrix, $\mathbf{A}^*$, of the major product moment matrix, **G**, can be developed equivalently from the matrix of eigenvectors, **V**, and the diagonal matrix of eigenvalues, Λ. It can be shown that the non-zero eigenvalues of the major product moment equal those of the minor product moment, so that Λ in both equations contains the same non-zero eigenvalues. However, it is more convenient to derive $\mathbf{A}^*$ from the minor product moment:

$$A^* = V\Lambda^{1/2} = WA\Lambda^{-1} \qquad \textbf{(2.43)}$$

In order to express **A** and $\mathbf{A}^*$ in the same metric, the differential scaling of row and column vectors in **B** must be taken into account, and the rows of **A** are adjusted according to

$$A_a = D_c^{1/2} A \qquad \textbf{(2.44a)}$$

and

$$A_a^* = D_r^{1/2} A^* \qquad \textbf{(2.44b)}$$

$\mathbf{A}_a$ and $\mathbf{A}_a^*$ are now in the common metric of the data matrix **B**. Distances between objects in $\mathbf{A}_a^*$ are the same as those expressed previously. The factor loadings of variables and objects can now be plotted for two chosen factors, i.e. a projection of the multidimensional space is performed in two dimensions. As both objects and variables are in the same metric, a simultaneous presentation of objects (i.e. samples) and variables (i.e. element concentrations) in the same set of coordinate systems is possible. As the first and the second factor contain the most information about the data matrix, these are usually taken for presentation in a plot. The plots can be interpreted in the usual way for factor analytical procedures:

1. objects plotting close to each other represent groups of similar individuals;
2. variables plotting close to each other are interpreted to react similarly.

Correspondence analysis plots have some further interpretative advantages compared to common factor analytical procedures, namely,

A. as the position of objects and variables are to some degree interrelated, mutual dependencies can be interpreted;
B. the angle between two variables is proportional to the product moment correlation coefficient, **r**.

The above description of correspondence analysis requires some basic knowledge of factor analysis, in order to be fully understood. A description of the mathematical derivation of eigenvectors and eigenvalues is beyond the scope of this investigation, although correspondence analysis and other factor analytical procedures can hardly be comprehended without this basic knowledge. A thorough description and discussion of factor analysis and associated procedures is given by Jöreskog et al. (1976) and Backhaus et al. (1990).

CHAPTER 3: DESCRIPTIVE GEOCHEMISTRY

3.1 Introductory remarks

3.1.1 Definition of rock types

All samples were classified within groups, which are generally defined by grain-size, mineralogy (for example calc-silicate rocks), genesis (for example, lavas and tuffs), and/or geochemical peculiarities (Magaliesberg Formation, shales from Bronkhorstspruit). Table 3.1.1 gives an overview of the resulting groups. The differentiation of samples into groups was thought to be of some importance to exclude the apparent geochemical relationships resulting for a combination of groups and/or sub-types. Further subgroups were defined locally for samples with distinct features like macroscopic andalusite or graphite in shales, or shale samples with more than 15 wt.% Fe_2O_3* (Fe_2O_3* = all Fe expressed as Fe_2O_3*).

Table 3.1.1: Subdivision of rocks into groups

GROUP	grain-size	texture	mineralogy	chemistry
shale, unspecified	X		X	
Bronkhorstspruit shales	X		X	X
high Mg-Ca-Na-shale	X		X	X
shale & sandstone, fine-layered	X			
siltstone	X			
sandstone	X		X	
lava		X	X	
tuff		X		
igneous rock (diabase)		X	X	
chert		X		X
calc-silicate rock		X	X	X
ironstone			X	X
conglomerate	X			
breccia	X			
carbonate rock	X			X
vein		X		

3.1.2 Recalculations

Statistical parameters of trace elements of shales, except Mo, As, U, Sb, and Sn, are calculated after setting values below the detection limit to half of this value. Values above the detection limit were taken as reported. This procedure is thought to ensure the calculation of statistically more correct results, as a frequency class with the width of the lower limit of detection is created, and the statistical calculations are performed using the middle value of this class.

As most of the measured values of Mo, As, U, Sb, and Sn are below the lower limit of detection, the use of the above procedure would possibly have led to grossly inflated averages. For these 5 elements, a concentration of 0 was then taken as the calculation value for concentrations below the detection limit. Hence, the reported average concentrations for these elements can be regarded as minimum average concentrations. However, as the average concentrations of these elements are normally below or around the lower limit of detection, their use as an indicator of average concentrations or for evaluation purposes is questionable and limited.

The reported ratios were selected according to their importance for the objectives of this investigation. Most of the ratios chosen from literature have some significance in the evaluation and interpretation of sedimentary basin development, source rocks, syn-depositional environment or syndepositional climate. The calculation of statistical parameters of ratios is problematic. Ratios can only be calculated correctly mathematically, if both respective elements are measured, i.e. each element has a concentration above the lower limit of detection. However, to exclude cases where one of the relevant elements is below the detection limit is questionable, as the statistical parameters of ratios of negatively correlated elements will be affected by the exclusions. For example, a population of shales with chromium contents in excess of 400 ppm and thorium contents below the detection limit may have predominantly mafic or ultramafic source rocks (Condie and Wronkiewic, 1990). In this case, a high value of the one element is accompanied by a very low value of the other element. Hence, an interpretional bias would be introduced if values below the lower limit of detection of one of the elements led to exclusion of the respective case or a group of samples. To circumvent such difficulties, a value equal to the lower limit of detection was

taken, if one element of the ratio is below the detection limit. The resulting ratio can be interpreted as a minimum or maximum value for the respective case, depending on the position of the element below the detection limit in the ratio (i.e. a numerator would give a maximum value and a denominator a minimum value). Cases with both elements below the detection limit were excluded for the calculation of the ratios.

The determination of organic and inorganic carbon, S and FeO in 50 samples allowed the calculation of $H2O^+$. The method of calculation is given in Table 3.1.2 . A further assumption is that pyrite (FeS_2) is the only sulphide mineral. The presence of high amounts of pyrite or iron sulphides in general leads to another problem, as the iron content of pyrite is included in the FeO-value. As sulphur is included in the calculation of the resulting sum of the major elements, this sum would have to be corrected for Fe present in sulphide. As the highest measured amount of S in the 50 samples analysed for FeO was 1.76 %, the overestimation of the Fe^{2+}-concentration expressed as FeO and, consequently, for the sum

Table 3.1.2: Calculation of H2O+

1. $FeO\% * 1.1113 = Fe_2O_{3(FeO)}\%$
2. $Fe_2O_{3(total)}\% - Fe_2O_{3(FeO)}\% = Fe_2O_3\%$
3. $[1.1113 * (FeO\% - (S\% * 1.12))] - [FeO\% - (S\% * 1.12)] + [(S\% * 1.245) - (S\% * 0.871)] = O_{(GOxI)}\%$
4. $LOI_{(determ.)}\% + O_{(GOxI)}\% = LOI_{(true)}\%$
5. $C_{inorg}\% * 3.6641 = CO_2$
6. $LOI_{(true)}\% - (CO_2\% + C_{org}\% + S\%) = H_2O^+$

EXPLANATION:

1. $Fe_2O_{3(FeO)}$ is FeO expressed as Fe_2O_3.
2. $Fe_2O_{3(total)}$ is all Fe expressed as Fe_2O_3.
3. The term (1.1113 * FeO% - FeO%) is sufficient for the calculation of the gain of oxygen during the ignition process during the determination of the LOI in a sulphide-free environment. The presence of iron sulphides leads to an additional gain of oxygen which was calculated with step 3.
   The correction of the LOI with the formula used in step 3 can only be applied if the presence of sulphur minerals other than pyrite (FeS_2) can be excluded. It is presumed that all sulphur is contained in pyrite.
   $O_{(GOxI)}$ stands for "gain of oxygen during ignition".
4. $LOI_{(determ.)}$ stands for the experimentally determined value of LOI, $LOI_{(true)}$ for the calculated value.
5. H_2O^+ is crystalline bound water. - For further discussion see text.

of the major elements, would only be 0.2 % and thus negligible. As the S-contents are much lower for most of the samples, a correction was omitted. The low concentrations of base metals made further corrections for base metal sulphides unnecessary.

3.1.3 Correlation matrices

Correlation coefficients were calculated using the nonparametric method of Spearman (Sachs, 1992). The mathematical procedure, the advantages and disadvantages of this procedure compared to the parametric product moment correlation coefficient are described and discussed in Chapter 2.2.2.1. The interpretation of correlation coefficients and their significances are prone to several errors (Sachs, 1992; see also Chapter 2.2.2.1). The correct evaluation of significant and insignificant correlations presupposes the exclusion of formal, inhomogeneity, simultaneous, and index correlations. The use of correlations for the evaluation of geochemical data sets is problematic, as geochemical data are prone to all of the above mentioned errors.

A good example of an inhomogenity correlation is shown by samples of the Timeball Hill Upper Shale Member from Botswana. The samples were divided macroscopically into shales, alternating shales and sandstones, and fine-grained sandstones. Figure 3.1.1a exhibits the correlation between SiO_2 and Al_2O_3 for the whole data set. However, examination of the plot reveals that the correlation is due to the combination of different groups. Table 3.1.3 shows the correlation coefficients (and their significances) of selected pairs of elements, Figures 3.1.1 a-e the matching plots. It is evident that only the element pair K_2O-Rb (Fig. 3.1.1 e) exhibits a causal (="true") correlation whereas the other element pairs show no correlations in the shale group and changing degrees of correlation for the coarser-grained sample set (i.e. sandstone and alternating shale and sandstone) and the combined data set. The coarser-grained sample sets themselves give another example of an inhomogeneity correlation, as the correlation coefficients for the alternating shale and sandstone group alone are not significant, with the exception of Al_2O_3-K_2O and K_2O-Rb. The relatively high correlation coefficients for SiO_2-TiO_2, SiO_2-Al_2O_3 and SiO_2-K_2O for the coarser-grained rocks are caused by the outlier value with ca. 67% SiO_2 (Fig. 3.1.1 a-c).

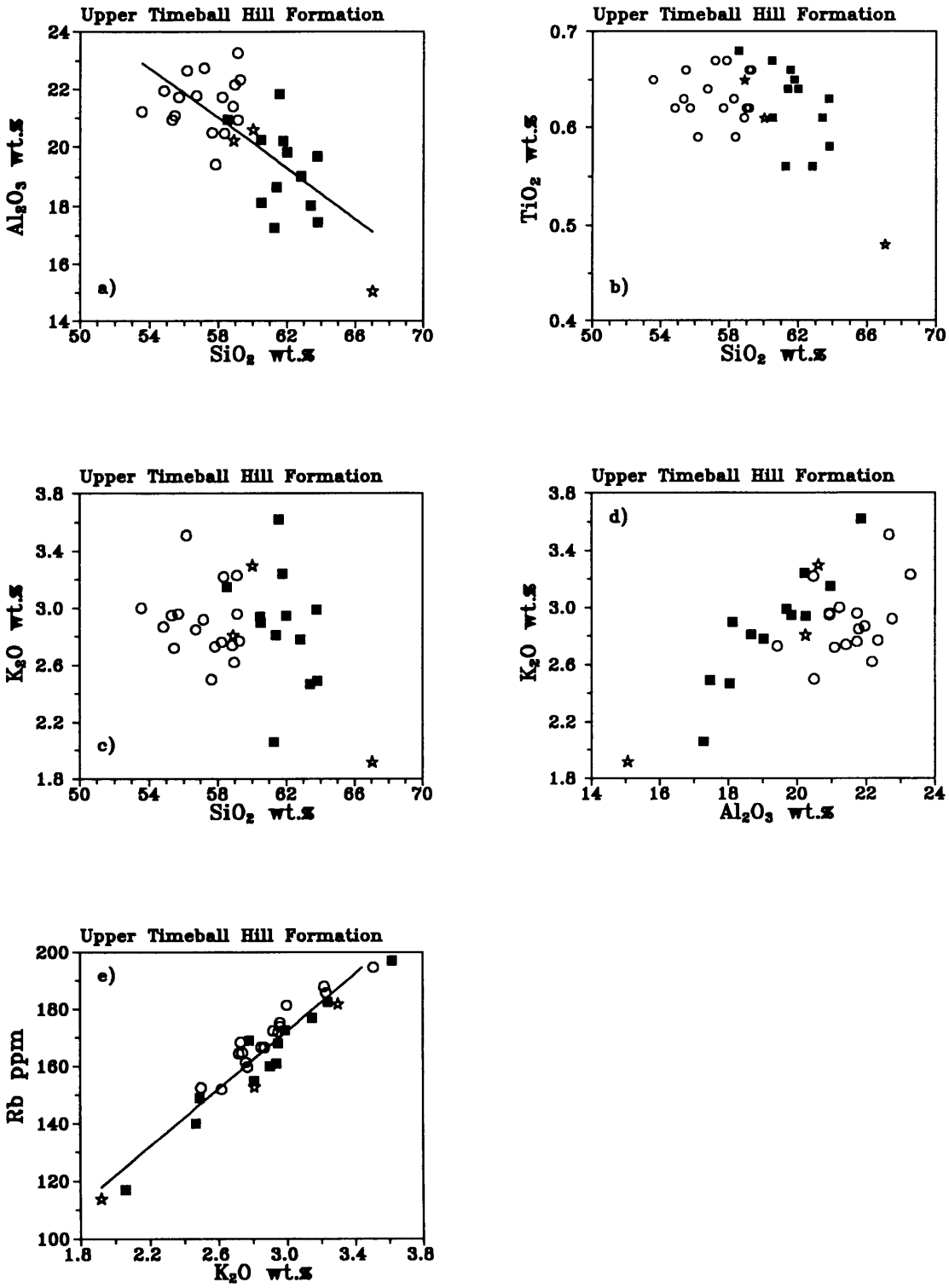

Figure 3.1.1 a-e: Relationship of major and trace elements in a sample set of sedimentary rocks of the Timeball Hill Formation Upper Shale Member from Botswana. Lithological types: ○ = shale; ■ = alternating shale and sandstone; ★ = sandstone

Table 3.1.3 : Correlation coefficients and significance of correlations of selected element pairs of the upper shale member of the Timeball Hill Formation in Botswana. Correlation coefficients were calculated with CSS software, the significance of the product moment correlation coefficient (PMCC) obtained from Sachs (1992); the significance of Spearman's rank correlation coefficient (RANK) was calculated with CSS after adjustment for tied ranks. Legend, sample size **n** and degrees of freedom **df**: **A** = shale, **n** = 17, **df** = 15; **B** = sandstone & alternating shale and sandstone ('coarser grained sample set'), **n** = 15, **df** = 13; **C** = total sample population, **n** = 32, **df** = 30.

		PMCC			RANK		
		A	B	C	A	B	C
SiO_2-TiO_2	cor. coeff.	-0.04	-0.74	-0.48	-0.01	-0.57	-0.28
	significance	n.s.	>99%	>99%	n.s.	>95%	n.s.
SiO_2-Al_2O_3	cor. coeff.	0.09	-0.70	-0.71	0.12	-0.61	-0.64
	significance	n.s.	>99%	>99.9%	n.s.	>95%	>99.9%
SiO_2-K_2O	cor. coeff.	-0.16	-0.56	-0.34	-0.13	-0.42	-0.17
	significance	n.s.	>95%	≈ 95%	n.s.	n.s.	n.s.
Al_2O_3-K_2O	cor. coeff.	0.37	0.93	0.65	0.26	0.88	0.40
	significance	n.s.	>99.9%	>99.9%	n.s.	>99.9%	>95%
K_2O-Rb	cor. coeff.	0.96	0.98	0.96	0.93	0.94	0.92
	significance	>99.9%	>99.9%	>99.9%	>99.9%	>99.9%	>99.9%

Another common problem is the occurrence of formal correlations, as geochemical data sets normally have a compositional form, i.e. the data are expressed as a proportion of a whole. This standard form of data presentation in geochemistry causes pitfalls in correlation analysis for various reasons (e.g. Chayes, 1969; Meisch, 1969; Butler, 1979). Recently, Woronow (1987), Butler and Woronow (1986) and Rollinson (1992) have reviewed the constant sum problem (i.e. appearance of formal correlations in composional data sets) for geochemical data. They recommand the application of the methods described by Aitchinson (1986), namely evaluation by handling the data as a log-ratio variance matrix, a log-ratio covariance matrix and/or centred log-ratio covariance matrix. However, case studies in sedimentary

geochemistry in which Aitchinson's methods have been applied are not available at present. An application of the method was not therefore attempted.

The presence of formal correlations must be assumed for most geochemical data sets. The generally negative correlation of SiO_2 to most of the other elements can be explained as a formal correlation, although occurrences of causal correlations of SiO_2 and other elements are possible. An interpretional overlap between inhomogeneity, formal and causal correlations has to be considered. For example, a negative correlation of SiO_2 to other elements, caused by a varying amount of quartz grains in sediments, can be interpreted as

1. a causal (="true") correlation, if a specific characteristic is tested (e.g. influence of turbidity currents on the geochemical pattern of deep sea sediments);
2. an inhomogeneity correlation, as different petrographical groups of sediments are tested together (e.g. shale, silt and sandstone);
3. a formal correlation, as an increase of the SiO_2-content necessarily leads to a decrease of other major elements.

Interpretations can also be questioned, as the possibility of simultaneous correlations cannot be ruled out (Sachs, 1992), i.e. the correlation between two elements is caused by a third variable, or a causal correlation may be masked by this effect. A good example in the current study for simultaneous correlations is the pattern of correlation of trace elements in the Magaliesberg Formation sandstones (see Appendix 2c). The sandstones of the Magaliesberg Formation are predominantly quartzitic (Schreiber, 1990; Eriksson et al., 1993a). Hence, the occurrence and amount of clay minerals in the matrix of the sandstones controls the distribution of most other elements. The elements which show no significant correlations to other elements (P, Ca, Mn, Co, U, Pb, Sc, As) commonly are mostly below or close to the limit of detection in this data set. The other trace elements, except Cr, are all positively correlated to the remaining major elements as well as to each other, with a significance of generally $> 99.9\%$. Major and trace elements have a negative correlation to SiO_2 (significance generally $> 99.9\%$). The negative correlations to SiO_2 are interpreted as formal correlations for the major elements, and as simultaneous correlations for the trace elements. The positive correlations between major and trace elements are interpreted as simultaneous correlations. As the possibility of a simultaneous correlation in geochemical data of sandstones seems to be implicit, the evaluation of correlation matrices of sandstones in this study was limited to a case study of the variation patterns of the correlation coefficients of

the element pairs SiO_2-Zr and SiO_2-Cr against stratigraphic height.

Another way to circumvent formal correlations is the use of ratios with an element as divisor (e.g. element X and Y are divided by element Z). Ratios are frequently used for representation and evaluation of geochemical data. However, ratio correlation is omitted, because the use of ratios in the way described above can create index correlations (McNemar, 1969), depending on the distribution of the elements.

Correlation matrices of shales were calculated after subdivision of data sets into formations and regions (Fig. 1.5.1). A true correlation was assumed if an element pair showed correlations with the same sign in the regional data sets and also for the total data set of the formation with a significance level of $> 99\%$ (Appendix 2c). The high significance level had to be chosen due to the effects of multiple testing of random samples (Sachs, 1992; p. 183-184). The possibility of an error related to these effects is reduced by taking a higher level of significance (Sachs, 1992). The data sets chosen for correlation usually contain more than 15 samples. Table 3.1.4 is slightly simplified to facilitate a conclusive overview and lists the significant and inferred causal Spearman correlations. It should be mentioned that not all of the correlations (Table 3.1.4) reach the 99% significance level in all regional data sets. Spearman's rank correlation coefficients and their significance levels are tabulated in Appendix 2c. Only the correlation matrices of the total data sets of the formations are recorded in this appendix, as the total of the correlation matrices calculated exceed 500 pages.

The respective data sets of the formations were then processed with the CSS Cluster Analysis option, using only the elements with a significant and presumably causal correlation. The Term 1 - **r** (see Chapter 2.3.1) was taken as a measurment of similarity, and the complete linkage alogarithm was used as amalgamation schedule. It must be emphazised that this process was chosen as a representative method and not as a statistical test (for discussion, see Chapter 2.3.1). The hierarchical trees produced by cluster analytical procedures (Appendix 2b) show a good agreement with the relationships inferred by the Spearman's rank correlation coefficients (Table 3.1.4, Appendix 2c).

Table 3.1.4 : Inferred causal element correlations of Pretoria Group shales

Correlations were grouped where elements showed a similar behaviour, i.e. an element or a group of elements on the left side of the hyphen is (1.) negatively correlated with the elements on the right side of a hyphen in the NEGATIVE CORRELATION column; and (2.) positively correlated with the elements on the right side of the hyphen in the POSITIVE CORRELATION column. Elements of a group in the POSITIVE CORRELATION column are normally positively correlated to each other, whereas groups negatively correlated to a element may have no mutual relationship. The legend for abbreviations of formations is given in Table 3.1.5.

Formation	Negative correlations	Positive correlations
Vrs	Si - Al, Fe, LOI, Zn, Ni, Co; Mg - Ba;	Al - K, Ga, Rb, Th; Ti - Cr, V, Sc, Zn; Fe - Co, Mn, Ni, Cu; Mg - Ca, S;
Vtl	Si - Al;	K - Rb, Ba; Na - Sr; Mn - Co; Mg - Ca; Zn - Ni; Ti - Cr;
Vtq	Si - Al, Ti, P, LOI, Zn, Cu, Ga, Y, Sr, Th, Pb, V;	Al - Ti, K, P, LOI, Zn, Cu, Ga, Y, Sr, Th;
Vtu	Si - Al, Ga;	Al - K, Rb, Nb, Ga, Th; Ti - Cr, V; Mg - Zn; Mn - Co; Zn - Ni; Na - Sr, (Ca);
Vst	Si - Cr, V, Sc;	Al - Ti; K - Ba, Rb, (Na); Mg - Mn, Co, Zn; Cr - V, Sc;
Vsi	Si - Fe, V, Sc;	Fe - Mg, Mn, Ni, Co; Al - Ti, Ga, Nb, Y, K, Rb, Th; Na - Sr, (Ca);
Vm	Si - Al, Ti, K, LOI, Ga, Nb, Y, U, Th, Cr, V; Zr - Fe, Mn, S, Ca, Na;	Fe - Mn, S, Ca, Na, Zn; Al - Ti, K, LOI, Th, Ga, Nb, Y,Cr,V;
Vv		Al - Ga, Nb, Y, Th, (K); Sr - Ca, Na; Zn - Ni, V, Sc;
Vn	Ca, Mg, Mn, LOI - Si, Al, Ti, Fe, K, Na, Sr, Rb, Cr, V, Ga, Zr, Nb, Y, Th;	Ca - Mg, Mn, LOI; Si - Na, K, Sr, Rb; Al - Ti, Fe, Cr, V, Ga, Nb, Y, Th;

The element pairs SiO_2-Zr and SiO_2-Cr were evaluated according to the above mentioned procedure (corresponding correlations of regional and total data sets per formation) for shales and sandstones. A significance level of 95% was chosen for this evaluation. Table 3.1.5 lists the results, arranged according to stratigraphic height. Note, that Table 3.1.5 and 3.1.4 differ because of the changed significance level.

Table 3.1.5 : Sign and significance of SiO_2-Zr and SiO_2-Cr Spearman correlation coefficients in shales and sandstones arranged in ascending stratigraphic order. Significance level is 95%; "n.s." = "not significant"; brackets indicate a trend.

*): Correlation coefficients of SiO_2-Cr of the shales of the Silverton Formation exhibit a positive trend in the western part of the basin and a negative trend in the eastern part of the basin.

Abbreviation of formations: Vrs = Rooihoogte Fm.; Vtl = Timeball Hill Fm. Lower Shale Member; Vtq = Timeball Hill Fm. Quartzite Member; Vtu = Timeball Hill Fm. Upper Shale Member; Vdw = Dwaalheuwel Fm.; Vst = Strubenkop Fm.; Vdq = Daspoort Fm.; Vsi = Silverton Fm.; Vm = Magaliesberg Fm.; Vry = Rayton Fm.; Vv = Vermont Fm.; Vlq = Lakenvlei Fm.; Vn = Nederhorst Fm.; Vsq = Steenkampsberg Fm.

Formation	SiO_2-Zr Shales	SiO_2-Zr Sandstones	SiO_2-Cr Shales	SiO_2-Cr Sandstones
Vsq		-		+
Vn	+		+	
Vlq		-		+
Vv	n.s.		n.s.(-)	
Vry		-		+
Vm	n.s.	-	-	+
Vsi	n.s.(+)	n.s.(-) -	n.s.*)	+
Vdq				n.s.(-)
Vst	n.s.(+)	-	-	
Vdw				n.s.(-)
Vtu	n.s.(+)	-	n.s.(-)	
Vtq	n.s.(-)		-	n.s.
Vtl	n.s.(+)	-	-	
Vrs	n.s.(-)		n.s.(-)	n.s.

The negative correlation of SiO_2-Zr in sandstones may represent a simultaneous correlation, and was therefore excluded from the interpretation. The positive correlation between SiO_2-Cr in the upper parts of the stratigraphy of the Pretoria Group merits special mention. A simultaneous correlation can be ruled out, as Cr is the only element positively correlated to SiO_2 in these data sets, except for the Nederhorst Formation, where Si is positively correlated to a number of elements (Table 3.1.4). As the probabilities of a formal or inhomogenity correlation with a positive sign are considered to be negligible for the element pair SiO_2-Cr, the relationship is thought to represent a causal correlation.

3.1.4 Mineralogy

The mineralogy of 77 shale samples was determined with XRD. Results of XRD analysis are listed in Table 3.1.6 a-c. The absence of expandable clay minerals was shown by randomly performed tests. Illite is listed together with micas.

Apart from quartz, mica and kaolinite are the main minerals present in the samples examined. Chlorite is common in the Botswana samples, absent in the western and central Transvaal samples and occurs sporadically in the eastern Transvaal (Fig. 1.5.1) material. The plagioclase contents are high in the Silverton and Vermont Formation samples, but this mineral is virtually absent in the lower part of the Pretoria Group, except for minor amounts in three samples from the Timeball Hill Lower Shale Member. Chloritoid was found as a major phase in the Strubenkop Formation and occurs frequently in formations up to the Silverton Formation. Pyrophyllite is a major phase of the Timeball Hill Formation. Amphibole occurs as a minor phase throughout the Pretoria Group, although an increase towards the top of the Pretoria Group is noticeable.

Table 3.1.6 a: Mineralogy of selected samples determined with XRD

Sample	Area	Form	Code	Qz	Mic	Kao	Chl	Plg	Clo		
ET-355	ETvl	Vv	160	xxx	xxx		xx	xxx		Amp	
ET-353	ETvl	Vv	160	xxx				xxx		**Trm**	
ET-351	ETvl	Vv	160	xx	xx	xx		xxx		**Amp**	
ET-349	ETvl	Vv	101	xxx	xxx	xxx	xx	?x			
ET-347	ETvl	Vv	101	xxx	xxx						
ET-372	ETvl	Vsil	160	xxx	xxx	x		xxx			
ET-368	ETvl	Vsil	160	xxx	xxx		x	xxx			
ET-363	ETvl	Vsil	160	xxx	xxx			xxx			
ET-360	ETvl	Vsil	160	xxx	xxx			xxx			
ET-357	ETvl	Vsil	160	xxx	xxx	xxx		xxx			
ET-282	ETvl	Vsib	101	xxx	xxx	xxx					
ET-280	ETvl	Vsib	101	xxx	xxx	xxx			xx		
ET-278	ETvl	Vsib	101	xxx	xxx	xxx					
ET-274	ETvl	Vsib	101	xxx	xxx	xxx		?x	xx	?Amp	Hem
ET-271	ETvl	Vsib	101	xxx	xxx	xxx		?x		?Amp	
ET-197	ETvl	Vtl	101	xxx	xxx	xx				?Amp	
ET-191	ETvl	Vtl	101	xxx	xxx		xxx			**Pph**	
ET-187	ETvl	Vtl	101	xxx	xxx	xxx	xx	?x			
ET-180	ETvl	Vtl	101	xxx	xx	xx			xxx	Hem	
ET-173	ETvl	Vtl	101	xxx	xxx						

Abbreviations for AREA: BOT = Botswana; WTvl = Western Transvaal; CTvl = Central Transvaal; ETvl = Eastern Transvaal (Fig. 1.5.1). Abbreviations for Formations (Fm.): see Table 3.1.5; Vsib = Silverton Fm. Boven Shale Member; Vsim = Silverton Fm. Machadodorp Member; Vsil = Silverton Fm. Lydenburg Shale Member. Frequency of occurrence: XXX = major; XX = common; X = minor; ?X = trace; Bold + Underlined = major; Bold = common; normal = minor; ? = trace.

Abbreviations for minerals: Qz = Quartz; Mic = Mica; Kao = Kaolinite; Chl = Chlorite; Plg = Plagioclase; Clo = Chloritoid; Pph = Pyrophyllite; And = Andalusite; Stp = Stilpnomelane; Hem = Hematite; Amp = Amphibole; Pyr = Pyrite; Sta = Staurolite; Sid = Siderite; Mgn = Magnesite; C = Carbon; Act = Actinolite; Trm = Tremolite; Car = Carbonate; Dps = Diopside; Ver = Vermiculite; Pal = Palygorskite; OPx = Orthopyroxene; Talc = Talc; Mag = Magnetite; Ocl = Orthoclase; Ves = Vesuvianite; CPx = Clinopyroxene; Gib = Gibbsite; Goe = Goethite.

Code: 101 = shale, unspecified; 160 = high-Mg-Ca-Na shale; 180 = alternating shale and sandstone; 330 = Bronkhorstspruit shales (Vm); 791 = calc-silicate rock; 504 = low-Si sandstone; 310 = iron oolites; 610 = tuff

Table 3.1.6 b: Mineralogy of selected samples determined with XRD (Legend for abbreviations and codes see Table 3.1.6 a)

Sample	Area	For.	Code	Qz	Mic	Kao	Chl	Plg	Clo		
ST-308	BOT	Vsi	101	xxx	xx	xxx	xx	xx			
ST-313	BOT	Vsi	101	xxx	xxx	xxx	xx	xx			
ST-322	BOT	Vsi	101	xxx	xxx	xxx	xxx	?x		**Sid**	
ST-337	BOT	Vsi	160	xxx	xxx	xxx	xx	xx		**Pyr**	**Mgn**
ST-360	BOT	Vsi	101	xxx	xxx	xxx	?x				
ST-202	BOT	Vtu	101	xxx	xx	xxx			xx		
ST-206	BOT	Vtu	101	xxx	xxx	xxx	xx			**Pph**	
ST-214	BOT	Vtu	101	xxx	xxx	xxx	xx			**Pph**	
ST-221	BOT	Vtu	180	xxx	xxx	xxx	xx			**Pph**	
ST-232	BOT	Vtu	180	xxx	xxx	xxx				?Car	
G-302	BOT	Vtl	101	xxx	xxx	xxx				?Amp	
G-305	BOT	Vtl	101	xxx	xxx	xxx	xxx				
G-308	BOT	Vtl	101	xxx	xxx	xxx	xx			Amp	?Hem
G-312	BOT	Vtl	101	xxx	xxx	xxx	xxx	xx		?Sta	
G-315	BOT	Vtl	101	xxx	xx	xxx	xx	x			
WT-164	WTvl	Vsi	101	xxx	xxx			xx		**Act**	
WT-165	WTvl	Vsi	160	xxx				xxx		**Amp**	?Pyr
WT-166	WTvl	Vsi	101	xxx	xxx					**C**	
WT-167	WTvl	Vsi	101	xxx	xxx	xx		xxx		**C**	
WT-168	WTvl	Vsi	101	xxx	xxx	xxx				**And**	
UV-127	CTvl	Vst	101	xxx	xxx	xx					
UV-126	CTvl	Vst	101	xxx	xxx						
UV-125	CTvl	Vst	101	xxx	xx	xx			xxx	**Hem**	
UV-124	CTvl	Vst	101	xxx	xxx	xx			xxx		
UV-123	CTvl	Vst	101	xxx	xx				xxx	Amp	
UV-131	CTvl	Vtl	101	xxx	xxx	xxx	?x				
UV-135	CTvl	Vtl	101	xxx	xxx	xxx					
UV-134	CTvl	Vtl	101	xxx	xxx	xxx					
UV-132	CTvl	Vtl	101	xxx	xxx	xxx					
UV-133	CTvl	Vtl	101	xxx	xxx		?x			?Stp	

Table 3.1.6 c: Mineralogy of selected samples determined with XRD (Legend for abbreviations and codes see Table 3.1.6 a)

Sample	Area	For.	Code	Qz	Mic	Kao	Chl	Plg	Clo		
ET-183	ETvl	Vtl	101	xxx	xxx	x	xxx	x	xxx		
ET-199	ETvl	Vtl	101	xxx	xxx	xxx					
ET-174	ETvl	Vtl	610	xxx	xxx					?Dps	
ET-175	ETvl	Vtl	610	xxx	xxx	xxx				**Hem**	
ET-224	ETvl	Vtu	101	xxx	xxx	?x	xxx				
ET-148	NTvl	Vtu	101	xxx	xxx		x	xxx			
ET-267	ETvl	Vdq	101	xx	xxx		xxx	?x			
ET-109	NTvl	Vsib	160	xxx	xxx			xxx			
ET-111	NTvl	Vsib	160	xxx				xxx		Dps	
ET-112	NTvl	Vsim	101	xxx						**Car**	**Ver**
ET-364	ETvl	Vsil	160	xxx				xxx		**Amp**	?Pal
ET-126	NTvl	Vsi	101	xxx	xxx					**Amp**	?OPx
ET-133	NTvl	Vsi	101	xxx	xxx			xxx			
ET-346	ETvl	Vv	160	xxx				xxx		**Amp**	
ET-352	ETvl	Vv	160	?x		?x				**Talc**	
ET-382	ETvl	Vv	101	xxx	xxx					?OPx	
ET-330	ETvl	Vn	791		xx	xx				**Car**	**Dps**
ET-341	ETvl	Vn	101	xxx	xx	?x	?x			**Amp**	**Ocl**
ET-343	ETvl	Vn	791				xxx			**Dps**	**Ves**
ET-345	ETvl	Vn	791			xxx				**Dps**	**Ves**
ET-333	ETvl	Vn	791	xx				xx	**Talc**	**Trm**	**Car**
ST-342B	BOT	Vsi	310	xx		xx			**Hem**	**Pyr**	Sid
ST-351	BOT	Vsi	310	xx		xx				**Hem**	Sid
ET-201	ETvl	Vtq	504	xxx	xxx	xx				CPx	Gib
UVS-122	CTvl	Vm	330		xxx	xxx				**Goe**	
UVS-11	CTvl	Vm	330		xx	xxx				Goe	?Talc
UVS-113	CTvl	Vm	330	xxx		x				Hem	?Mag

3.2 Estimates of average element contents of various "standard" shales and sandstones

The geochemistry of the Pretoria Group sedimentary rocks will be compared with various estimates of average shales and sandstones, compiled in Tables 3.2.1 a-e. Table 3.2.1a contains a short definition of the estimates, the source of the data and the relevant abbreviations used in Tables 3.2.1 b-e. FeO was recalculated to Fe_2O_3 where neccessary. The loss on ignition (LOI) was corrected for FeO expressed as Fe_2O_3.

Geosynclinal Average Shale, Platform Average Shale, Average Platform Sandstone (all Wedepohl, 1971) and Average Shale (Clarke, 1924, op. cit. Wedepohl, 1971) were recalculated on a carbonate-free basis. The composition of the assumed carbonate was estimated by taking 80 mol.% Ca and 20 mol.% Mg to obtain the hypothetical mineral $(Ca_{0.8},Mg_{0.2})CO_3$. The chosen proportions of Ca and Mg are supposed to reflect the average composition of calcitic and dolomitic materials, which can be presumed to be the prevalent calcareous components in sedimentary rocks, independent of their authigenic or allogenic origin.

The Post-Archaean Average Shale (Taylor and McLennan, 1985) was recalculated to 100 as the volatile-free sum is not 99.9 % as stated in their treatise (p. 28), but only 97.87 %. Trace element data and ratios of the Post-Archaean Average Shale are slightly different in Taylor and McLennan (1985) between their Table 2.9 (p.28) and their Table 5.2 (p.100). Trace element data of this Post-Archaean Average Shale were thus taken from Taylor and McLennan's (1985) Table 2.9, ratios from their Table 5.2. The 1 σ standard deviation for ratios of Post-Archaean Average Shale, Archaean Average Shale, Early Archaean Average Shale and Late Archaean Average Shale (all Taylor and McLennan, 1985) was recalculated from the reported '95 % confidance interval', using equation (2.11) in Chapter 2.1.2.

The calculation of average ratios from reported estimates was omitted, although various authors use this method to obtain average estimates of ratios (e.g., Feng et al., 1993; Wronkiewicz and Condie, 1990; see Chapter 2.1.2 for a thorough discussion).

Table 3.2.1a: References for estimates of element contents and ratios in Tables 3.2.1b-e

1)	**GAS:**	Geosynclinal Average Shale (Wedepohl, 1971); for recalculation 'carbonate-free' all carbonate was assumed in $(Ca_{0.8},Mg_{0.2})CO_3$, 'volatile-free' was calculated from carbonate-free estimate.
2)	**PAS:**	Platform Average Shale (Wedepohl, 1971); for recalculation 'carbonate-free' all carbonate was assumed in $(Ca_{0.8},Mg_{0.2})CO_3$, 'volatile-free' was calculated from carbonate-free estimate;
3)	**PAAS:**	Post-Archaean Average Shale (Taylor and McLennan, 1985); original volatile-free major element data were recalculated to 100 (Taylor and McLennan, 1985, p. 28, Sum = 97.87) and the LOI included;
4)	**RLPS:**	Average Russian Late Proterozoic Shale (Ronov and Migdisov, 1971);
5)	**REPS:**	Average Russian Early Proterozoic Metamorphic Shale (Ronov and Migdisov, 1971);
6)	**PAMS:**	Pontiac Average Metamorphic Shale (Feng et al., 1993);
7)	**ACPS:**	Average Canadian Proterozoic Shale (Cameron and Garrels, 1980);
8)	**AvS:**	Average Shale (Clarke, 1924);
9)	**NASC:**	North American Shale Composite (Gromet et al., 1984);
10)	**AAS:**	Archaean Average Shale (Taylor and McLennan, 1985);
11)	**UCC:**	Present-day Upper Continental Crust (Taylor and McLennan, 1985);
12)	**AS:**	Average Shale (Turekian and Wedepohl, 1961);
13)	**EAAS:**	Early Archaean Average Shale (Taylor and McLennan, 1985)
14)	**LAAS:**	Late Archaean Average Shale (Taylor and McLennan, 1985)
15)	**ASS:**	Average Sandstone (Turekian and Wedepohl, 1961)
16)	**AvSS:**	Average Sandstone (Clarke, 1924); for recalculation 'carbonate-free' all carbonate was assumed in $(Ca_{0.8},Mg_{0.2})CO_3$;
17)	**APSS:**	Average Platform Sandstone (Wedepohl, 1971); for recalculation 'carbonate-free' all carbonate was assumed in $(Ca_{0.8},Mg_{0.2})CO_3$;
18)	**AREPSS:**	Average Early Proterozoic Sandstone (Ronov and Migdisov, 1971);
19)	**ARLPSS:**	Average Late Proterozoic Sandstone (Ronov and Migdisov, 1971);

TABLE 3.2.1b: Various estimates of major element data of shales in weight %

	GAS[1)] ☼	PAS[2)] ☼	PAAS[3)] #	RLPS[4)] #	REPS[5)] #	PAMS[6)] #
SiO_2	60.47	58.27	60.32	57.65	58.42	62.01
TiO_2	0.80	0.90	0.96	0.86	0.79	0.63
Al_2O_3	17.14	17.35	18.15	17.04	16.63	16.50
Fe_2O_3(t)	7.09	7.74	6.94	7.78	9.82	6.18
MnO	0.09	0.09	0.10	0.11	0.15	0.09
MgO	2.42	2.52	2.12	2.38	4.12	3.60
CaO	0.90	1.14	1.25	1.20	2.34	2.42
Na_2O	1.64	0.92	1.16	0.93	1.57	3.71
K_2O	3.70	4.02	3.55	4.18	3.08	2.92
P_2O_5	0.16	0.12	0.15	0.09	0.09	0.14
LOI	5.57	6.94	5.31	7.89	3.12	1.60

	GAS[1)] ↕	PAS[2)] ↕	PAAS[3)] ↕	RLPS[4)] ↕	REPS[5)] ↕	ACPS[7)] ↕
SiO_2	64.05	62.61	64.17	62.51	60.22	66.90
TiO_2	0.85	0.97	1.02	0.93	0.81	0.78
Al_2O_3	18.15	18.64	19.31	18.48	17.14	16.67
Fe_2O_3(t)	7.51	8.32	6.64	8.44	10.12	5.87
MnO	0.10	0.10	0.11	0.12	0.16	0.06
MgO	2.56	2.71	2.25	2.58	4.25	2.59
CaO	0.95	1.23	1.33	1.30	2.41	0.83
Na_2O	1.74	0.99	1.23	1.01	1.62	1.50
K_2O	3.92	4.32	3.78	4.53	3.18	4.97
P_2O_5	0.17	0.13	0.16	0.10	0.09	0.14

	AvS[8)] ↕	NASC[9)] ↕	AAS[10)] ↕	UCC[11)] ↕
SiO_2	64.21	64.80	60.40	66.00
TiO_2	0.72	0.70	0.80	0.50
Al_2O_3	17.02	16.90	17.10	15.20
Fe_2O_3(t)	6.71	5.66	9.50	4.50
MnO	0.50	0.06	0.10	0.08
MgO	2.70	2.86	4.30	2.20
CaO	3.44	3.53	3.20	4.20
Na_2O	1.44	1.14	2.10	3.90
K_2O	3.58	3.97	2.30	3.40
P_2O_5	0.19	0.13	-.-	-.-

☼: Carbonate-free
#: *Volatiles included*
↕: *Volatile-free*

Table 3.2.1c: Various estimates of major element data of average sandstones in weight %

	AvSS[16)]#	APSS[17)]#	AREPSS[18)]#	ARLPSS[19)]#
SiO_2	78.70	70.00	78.81	72.78
TiO_2	0.25	0.58	0.28	0.56
Al_2O_3	4.80	8.20	8.71	9.79
Fe_2O_3(t)	1.43	4.17	3.21	4.90
MnO	0.03	0.06	0.04	0.09
MgO	1.20	1.90	1.65	1.67
CaO	5.50	4.30	1.45	1.37
Na_2O	0.45	0.58	0.60	0.69
K_2O	1.30	2.10	1.30	2.94
P_2O_5	0.08	0.10	0.05	0.07
LOI	6.30	7.69	2.72	4.87

	AvSS[16)]☼	APSS[17)]☼	AREPSS[18)]↕	ARLPSS[19)]↕
SiO_2	88.39	76.84	82.01	76.72
TiO_2	0.28	0.64	0.29	0.59
Al_2O_3	5.39	9.00	9.06	10.32
Fe_2O_3(t)	1.61	4.58	3.34	5.17
MnO	0.03	0.07	0.04	0.10
MgO	0.33	1.31	1.72	1.76
CaO	0.46	0.36	1.51	1.44
Na_2O	0.51	0.64	0.62	0.73
K_2O	1.46	2.31	1.35	3.10
P_2O_5	0.09	0.11	0.05	0.07
LOI	1.46	4.16	-.-	-.-

#: all volatiles included

☼: recalculated carbonate-free

↕: recalculated volatile-free

Table 3.2.1d: Various estimates for trace elements of average shales and sandstones in ppm

	AS[12]	NASC[9]	PAAS[3]	ACPS[7]	AAS[10]	PAMS[6]	UCC[11]	ASS[15]
Zn	95			114			71	16
Cu	45			75	150		25	<10
Ni	68	58	55	57	100		20	2
Co	19	26		22	40		10	0.3
Ga	19			20	15		17	12
Mo	2.6		1.0	4	1.0		1.5	0.2
Nb	11		19		9	8.7	25	<0.1
Zr	160	200	210		120	150	190	220
Y	26		27	25	18	14	22	40
Sr	300	142	200	69	180	405	350	20
Rb	140	125	160	174	60	111	112	60
U	3.7	2.7	3.1	6	1.6	2.7	2.8	0.45
Th	12	12	15		6.3	7.9	11	1.7
Pb	20		20	22	20	19	20	7
Cr	90	125	110	105	205	222	35	35
V	130		150	188	135	119	60	20
Ba	580	636	650	492	575	747	550	<100
Sc	13	15	16	16	20	16	11	1
As	13	28		23			1.5	1
S	2400							170
Sb	1.5	2.1		1.3			0.2	<0.1
Sn	6.0		4.0	2.6	5.5		5.5	<1
B	100			25	65		15	35
Li	66			60		78	20	15
La	92	31.1	38		20	27	30	30
Ce	59	66.7	80		42	57	64	92
Pr	5.6		8.9		4.9	6.7	7.1	8.8
Nd	24	27.4	32		20	26	26	37
Sm	6.4	5.6	5.6		4.0	4.5	4.5	10
Eu	1.0	1.2	1.1		1.2	1.1	0.88	1.6
Gd	6.4		4.7		3.4	3.6	3.8	10
Tb	1.0	0.85	0.77		0.57	0.46	0.64	1.6
Dy	4.6		4.4		3.4	2.8	3.5	7.2
Er	2.5		2.9		2.1	1.6	2.3	4.0
Tm	0.2		0.4		0.30	0.24	0.33	0.3
Yb	2.6	3.1	2.8		2.0	1.5	2.2	4.0

Table 3.2.1e: Various estimates for element ratios of average shales

(All confidence intervals are 1 δ standard deviation; ¶: Sum of REE in ppm; ∞: Recalculated from 95 % confidence interval of mean; subscript "n": normalised to chondrite; $REE_{(t)}$: sum of all rare earth elements in ppm; Eu/Eu*: europium anomaly)

	PAAS[3]	AAS[10]	EAAS[13]	LAAS[14]	PAMS[9]
K_2O/Na_2O	1.8	0.76			0.86 ± 0.46
SiO_2/Al_2O_3					3.83 ± 0.63
Th/Sc	1.0 ± 0.43∞	0.43 ± 0.24∞			
K/Rb					251 ± 162
Cr/V	0.9 ± 0.29∞		5.3 ± 2.16∞	1.5 ± 0.84∞	
V/Ni	2.1 ± 0.58∞		0.51 ± 0.61∞	1.7 ± 1.92∞	
Ni/Co	2.6 ± 0.57∞		11.6 ± 3.37∞	3.0 ± 1.86∞	
Th/U	4.8 ± 1.3∞	3.8 ± 1.03∞			3.5 ± 1.1
Ba/Th					101 ± 59
La/Sc	2.7 ± 1.28∞	1.3 ± 0.68∞			
Th/La	0.36	0.3			
LREE/HREE	10 ± 4.27∞	7.4 ± 4.27∞			12.3 ± 3.6
Gd_n/Yb_n					2.0 ± 0.5
Eu/Eu*	0.65 ± 0.09∞	0.99 ± 0.17∞			0.89 ± 0.18
$REE_{(t)}$¶	185 ± 64∞	102 ± 52∞			133 ± 48

3.3 Geochemistry of the Pretoria Group Formations

3.3.1 Rooihoogte Formation

The major element geochemistry of the shales of the Rooihoogte Formation (Tables 3.3.1.1 and 3.3.1.2) exhibits major deviations from average shale estimates (Table 3.2.1b) only for the oxides of Ca and Na, which are depleted more than tenfold. MgO and TiO_2 are slightly depleted, SiO_2 and $Fe_2O_3(t)$ slightly enriched, although the latter depletions and enrichments cannot be regarded as a significant deviation from the average shale estimates.

Element	n	MEAN	STD ±	GM	MEDIAN	RANGE	VC
SiO_2	43	61.34	6.85	61.01	60.10	53.44 - 88.44	0.11
TiO_2	43	0.69	0.17	0.66	0.72	0.18 - 0.90	0.25
Al_2O_3	43	17.18	3.83	16.57	17.90	6.15 - 24.50	0.22
Fe_2O_3*	43	9.30	4.24	7.80	9.82	0.74 - 26.98	0.46
MnO	43	0.12	0.18	-	0.06	<LLD - 1.01	1.50
MgO	43	2.19	1.54	-	2.23	<LLD - 4.59	0.70
CaO	43	0.08	0.10	-	0.02	<LLD - 0.36	1.25
Na_2O	43	0.04	0.06	-	0.02	<LLD - 0.28	1.50
K_2O	43	3.59	1.33	3.00	3.56	0.02 - 6.45	0.37
P_2O_5	43	0.10	0.05	-	0.09	<LLD - 0.23	0.50
H_2O^-	43	0.65	1.41	0.33	0.28	0.07 - 9.33	2.17
LOI	43	4.75	1.26	4.56	4.80	1.34 - 9.17	0.27
Zn	43	119	147.0	82	96	6 - 981	1.24
Cu	43	63	50.3	47	46	5 - 215	0.80
Ni	43	99	72.5	76	100	4 - 472	0.73
Co	43	22	13.9	16	25	<3 - 64	0.63
Ga	43	22	5.5	21	23	4 - 34	0.25
Mo	43	2.6 *)	3.4	-	2.0	<2 - 16	1.31
Nb	43	17	4.0	16	18	6 - 22	0.24
Zr	43	160	38.0	156	158	67 - 281	0.24
Y	43	33	9.1	31	33	11 - 57	0.28
Sr	43	32	13.2	29	33	3 - 77	0.41
Rb	43	171	52.8	145	176	<2 - 292	0.31
U	43	10	3.8	-	11	<5 - 17	0.38
Th	43	21	6.1	19	22	<5 - 30	0.29
Pb	43	24	15.6	19	20	<5 - 30	0.29
Cr	43	196	58.7	182	217	39 - 287	0.30
V	43	140	30.0	135	147	31 - 184	0.21
Ba	43	1761	2670.4	1103	1040	311 - 14706	1.52
Sc	43	18	5.7	17	17	<8 - 32	0.32
As	43	5.7 *)	14.9	-	<LLD	<10 - 67	2.61
S	43	558	1002.2	322	302	62 - 5129	1.80
Sb	43	0.8 *)	2.4	-	<LLD	<8 - 9	3.00
Sn	43	1.1 *)	3.1	-	<LLD	<8 - 13	2.82
B	25	54	34.7	46	47	11 - 180	0.64

Table 3.3.1.1: Average element concentrations of Rooihoogte Formation shales

(n = number of samples; 'MEAN' = arithmetic mean; 'STD ±' = 1 σ standard deviation; 'GM' = geometric mean; 'MEDIAN' = median; 'VC' = variation coefficient; average major element concentrations are reported in weight %, average trace element concentrations in ppm; 'Fe_2O_3*' is all Fe expressed as Fe_2O_3; *) = arithmetic mean below detection limit; LLD = lower limit of detection)

Table 3.3.1.2: Average major element concentrations of Rooihoogte Formation shales recalculated to 100 % volatile-free.

Element	n	MEAN	STD ±	RANGE
SiO_2	43	64.77	6.34	58.51 - 90.78
TiO_2	43	0.73	0.18	0.18 - 0.97
Al_2O_3	43	18.18	4.08	6.22 - 25.65
Fe_2O_3*	43	9.87	4.56	0.76 - 28.99
MnO	43	0.13	0.19	<LLD - 1.11
MgO	43	2.31	1.63	<LLD - 4.83
CaO	43	0.08	0.11	<LLD - 0.38
Na_2O	43	0.04	0.06	<LLD - 0.29
K_2O	43	3.79	1.38	0.02 - 6.66
P_2O_5	43	0.10	0.05	<LLD - 0.24

The average trace element contents of the Rooihoogte Formation shales (Table 3.3.1.1) show depletion for As and Sr; Cr, Ba and U are enriched compared with average shale estimates (Table 3.2.1d). Th and Ni show slight enrichment. Cr and Ni have average contents similar to Archaean Average Shales (Taylor and McLennan, 1985).

The statistical parameters of the ratios of the Rooihoogte Formation shales are shown in Table 3.3.1.4a. The K_2O/Na_2O-ratio mirrors the Na_2O-depletion and is enriched significantly compared with average shale estimates (Table 3.2.1e). Th/Sc is slightly increased, the trace element ratios Cr/V, V/Ni and Ni/Co resemble Late Archaean Average Shales (Taylor and McLennan, 1985), particularly if the geometric mean is compared with the average estimates. The Th/U-ratio is considerably lower than Post-Archaean Average Shales and Archaean Average Shales (both Taylor and McLennan, 1985). Interestingly, Ronov and Migdisov (1971) report a similar decrease of Th/U for Lower Proterozoic metamorphosed sedimentary rocks of the Russian Platform.

The sandstones of the Rooihoogte Formation (Tables 3.3.1.3 and 3.3.1.4b) are enriched in Fe_2O_3(t) and depleted in MgO, CaO, Na_2O and K_2O compared with average sandstone estimates (Table 3.2.1c). Zn, Cu, Ni, Mo, Nb, Cr, V Ba, Sc, and Co are enriched, Ga, Zr, and Y are depleted compared with an average sandstone estimate (Table 3.2.1d) of Turekian and Wedepohl (1961).

Element	n	MEAN	STD ±	GM	MEDIAN	RANGE	VC
SiO_2	14	81.02	14.14	79.82	81.43	60.15 - 97.57	0.17
TiO_2	14	0.22	0.24	-	0.13	<LLD - 0.69	1.09
Al_2O_3	14	5.26	5.09	3.27	3.51	0.85 - 17.67	0.97
Fe_2O_3*	14	8.86	7.44	4.54	7.86	0.22 - 22.86	0.84
MnO	14	0.07	0.10	-	0.04	<LLD - 0.39	1.43
MgO	14	0.68	1.34	-	0.03	<LLD - 3.84	1.97
CaO	14	0.07	0.15	-	<LLD	<LLD - 0.51	2.14
Na_2O	14	0.01	0.01	-	<LLD	<LLD - 0.02	1.00
K_2O	14	0.64	1.16	-	0.23	<LLD - 3.66	1.81
P_2O_5	14	0.08	0.05	-	0.08	<LLD - 0.18	0.63
H_2O^-	14	0.28	0.31	0.15	0.14	0.02 - 1.09	1.11
LOI	14	2.45	1.89	1.44	2.51	0.11 - 5.45	0.77
Zn	14	43	48.6	24	23	5 - 169	1.13
Cu	14	22	28.1	-	13	<3 - 108	1.28
Ni	14	40	39.8	-	28	<3 - 116	1.00
Co	14	5.7	6.3	-	3.5	<3 - 18	1.11
Ga	14	6.4	7.4	-	5.0	<3 - 22	1.16
Mo	14	6.4	2.9	-	7.0	<2 - 10	0.45
Nb	14	5.2	4.4	-	4.5	<2 - 14	0.85
Zr	14	126	103.2	93	97	32 - 353	0.82
Y	14	14	7.4	12	14	4 - 25	0.53
Sr	14	12	17.6	-	4.5	<2 - 69	1.47
Rb	14	39	63.2	-	8.5	<2 - 186	1.62
U	14	2.9 *)	4.1	-	<LLD	<5 - 10	1.41
Th	14	3.9 *)	6.1	-	<LLD	<5 - 19	1.56
Pb	14	4.0 *)	4.5	-	2.5	<5 - 11	1.13
Cr	14	171	72.2	156	161	74 - 297	0.42
V	14	93	65.0	-	85	<14 - 202	0.70
Ba	14	251	303.8	138	115	25 - 994	1.21
Sc	14	7.6 *)	7.4	-	8.5	<8 - 20	0.97
As	14	4.4 *)	11.7	-	<LLD	<10 - 39	2.66
S	14	629	1223.9	-	221	<50 - 4539	1.95
Sb	14	0.6 *)	2.4	-	<LLD	<8 - 9	4.00
Sn	14	1.4 *)	3.7	-	<LLD	<8 - 11	2.64
B	4	28	21.0	22	24	10 - 53	0.75

Table 3.3.1.3: Average element concentration of Rooihoogte Formation sandstones

(n = number of samples; 'MEAN' = arithmetic mean; 'STD ±' = 1 σ standard deviation; 'GM' = geometric mean; 'MEDIAN' = median; 'VC' = variation coefficient; average major element concentrations are reported in weight %, average trace element concentrations in ppm; 'Fe_2O_3*' is all Fe expressed as Fe_2O_3; *) = arithmetic mean below detection limit; LLD = lower limit of detection)

Table 3.3.1.4a: Average ratios of Rooihoogte Formation shales

(NOTE: ratios corrected as described in Chapter 3.1.2)

Ratio	n	MEAN	STD ±	GM	RANGE	VC
CIA	43	81.5	4.6	81.4	74.0 - 99.5	0.06
Fe/V	43	496	367	404	28 - 2559	0.74
K_2O/Na_2O	39	184	130	124	2 - 445	0.71
SiO_2/Al_2O_3	43	4.1	2.5	3.7	2.5 - 14.4	0.61
Cr/Th	43	10.6	7.0	9.3	1.9 - 48.5	0.66
Th/Sc	43	1.32	0.61	1.17	0.16 - 3.00	0.46
Cr/Zr	43	1.24	0.36	1.17	0.28 - 1.80	0.29
Co/Th	43	1.25	1.20	0.84	0.11 - 6.4	0.96
Al_2O_3/TiO_2	43	26	9	25	15 - 72	0.35
Al_2O_3/K_2O	43	13.4	53.4	5.5	3.2 - 355	3.99
K/Rb	43	171	26	169	83 - 243	0.15
K/Ba	43	31	21	23	1 - 90	0.68
Ti/Ni	43	94	201	52	10 - 1184	2.14
Cr/V	43	1.39	0.31	1.35	0.53 - 2.19	0.22
V/Ni	43	3.46	8.05	1.78	0.31 - 46	2.33
Ni/Co	43	5.89	5.19	4.60	0.80 - 27.77	0.88
Zr/Nb	43	10.4	4.8	9.8	5.9 - 31.2	0.46
Th/U	43	2.13	0.85	1.98	0.50 - 5.00	0.40
Ba/Rb	43	13.8	25.6	7.5	2.2 - 156.3	1.86
Ba/Sr	43	50	50	38	15 - 248	1.00
Ba/Th	43	108	205	56	18 - 1135	1.90
Al/Zr	43	589	149	563	134 - 1029	0.25
Ti/Zr	43	26.2	5.8	25.4	8.1 - 35.4	0.22

Another important lithological type of the Rooihoogte Formation is conglomerate, which can be found near the base of the Formation (Bevets Conglomerate Member, e.g. Eriksson et al. 1993) and interlayered with shales in the upper part of the Rooihoogte Formation (Eriksson 1988). The SiO_2-content of the conglomerates (Appendix 2a) is on average higher than the SiO_2-content of the sandstones of the Rooihoogte Formation. The trace element contents are generally low with the exception of Cr (ϕ 170 ppm), B (ϕ 90 ppm) and Mo (ϕ 6.3 ppm). The chemical composition of basal chert breccias in the Rooihoogte Formation is highly variable. Pure chert breccias with SiO_2-contents of up to 98 wt.% and calcareous breccias (CaO: 40.9 wt.%; SiO_2: 12 wt.%) were sampled in this study (Appendix 1a).

Table 3.3.1.4b: Average ratios of Rooihoogte Formation sandstones

(NOTE: ratios are not corrected, i.e. a sample was excluded from calculation of the average ratio if one or both elements are below the detection limit; n.c. = not calculated)

RATIO	n	MEAN	STD ±	GM	RANGE	VC
CIA	14	89.0	8.6	88.6	76.7 - 100.0	0.10
SiO_2/Al_2O_3	14	44	43	24	3 - 113	0.98
lg SiO_2/Al_2O_3	14	1.38	n.c.	n.c.	n.c.	n.c.
K_2O/Na_2O	5	84	77	55	18 - 183	0.92
lg Na_2O/K_2O	5	-1.74	n.c.	n.c.	n.c.	n.c.
Ti/Zr	13	12.8	14.4	7.1	0.9 - 50.5	1.13
Ti/Cr	13	8.6	8.3	4.1	0.4 - 27.5	0.97
Al/Zr	14	258	209	186	18 - 693	0.81
Al_2O_3/TiO_2	13	49	45	36	11 - 143	0.92
Al_2O_3/K_2O	12	17.4	15.3	11.7	3.8 - 47.7	0.88
K/Rb	11	174	92	148	31 - 332	0.53
K/Ba	12	19	10	15	3 - 31	0.53
K/Sr	12	526	468	304	35 - 1321	0.89

The generally poor outcrops of the Rooihoogte Formation only permitted the sampling of one complete geochemical profile, at the Long Tom Pass, eastern Transvaal (Fig. 3.3.1.3). Additionally, two partial profiles were taken from bore-cores drilled in Botswana (see Fig. 1.5.2 for location of profiles). A detailed petrographic description of the bore-cores is given by Key (1983). Conglomerates interlayered in shales are correlated with the Bevets Conglomerate Member by Key (1983). However, a field visit to the drilling area established a profile for the Rooihoogte Formation in Botswana, which is similar to the western Transvaal stratigraphy (P.G. Eriksson, 1993, pers. comm.): a basal chert breccia is succeeded by the Bevets Conglomerate Member and the conglomerates are overlain by sandstones. The top of the succession is built up by poorly outcropping shales, and is concluded by a sandstone (Polo Ground Member). The sandstone succeeding the Bevets Conglomerate Member has a thickness of several metres in the Lobatse area. This sandstone unit thickens towards the eastern part of the Transvaal basin (up to 150 m) and can also be observed in the Kanye Basin near Jwaneng (> 90 m thickness from bore-core data, Reczko 1992). The shales in the Jwaneng area contain conglomerate lenses, similar in thickness and lithology to the conglomerate lenses in the western Transvaal described by Eriksson (1988).

As the borecores described by Key (1983) do not transect the sandstone succeeding the Bevets Conglomerate Member, it is inferred that the conglomerate units of the bore-cores are correlates of the conglomerate lenses in the upper shale unit found in the western Transvaal (Eriksson, 1988) and in the Kanye Basin (B. F. F. Reczko, unpublished data). This interpretation of the stratigraphy is consistent with field observations. The geochemical profiles shown in Figures 3.3.1.1 and 3.3.1.2, accordingly, are interpreted in this way.

The Botswana bore-cores contain three petrographic units, conglomerate, sandstone and shale. Bore-core 1 (Figure 3.3.1.1) shows a fairly constant pattern for most major and trace elements and ratios, except for changes related to petrographic changes (i.e., the two lowermost, coarser-grained samples) and a certain degree of variability for some elements and ratios above the oxidation base (= limit of weathering)(e.g., SiO_2, Al_2O_3, MnO, Na_2O, K_2O, Cr, Ba). The oxidation base is marked by a major increase of Zn (> 900 ppm). MgO decreases sharply towards the surface. Cr/Th and Th/Sc show opposing trends throughout the bore-core.

The geochemical profile of bore-core 2 (Figure 3.3.1.2) exhibits an even more constant pattern than the bore-core 1 geochemical profile. Samples above the oxidation base only show significant variability for MgO and Zn. The latter element is again strongly enriched at the oxidation base (> 200 ppm), and MgO decreases towards the surface. The conglomerate lens in the lower part of the profile (depth just above 110 m) divides the distributions of K_2O, Th, Th/Sc and K/Rb in two distinct trends. MnO and Fe_2O_3(t) are strongly enriched in shales adjacent to the top of the conglomerate lens. Other changes in major and trace elements at this level largely reflect the coarser petrography of these quartz pebble conglomerates.

The geochemical profile from the eastern Transvaal contains four petrographic types (breccia, sandstone, conglomerate and shale) and is shown in Figure 3.3.1.3. Most stratigraphic changes in element contents are related to petrographic changes. Extremely high values of TiO_2 (>2 wt.%) and K_2O (>7 wt.%) were observed in the conglomerate unit, accompanied by moderate increases of Al_2O_3, P_2O_5, MgO, CaO and Na_2O. A chert breccia in the middle part of the profile contains more than 600 ppm Zr. The geochemical profile has an

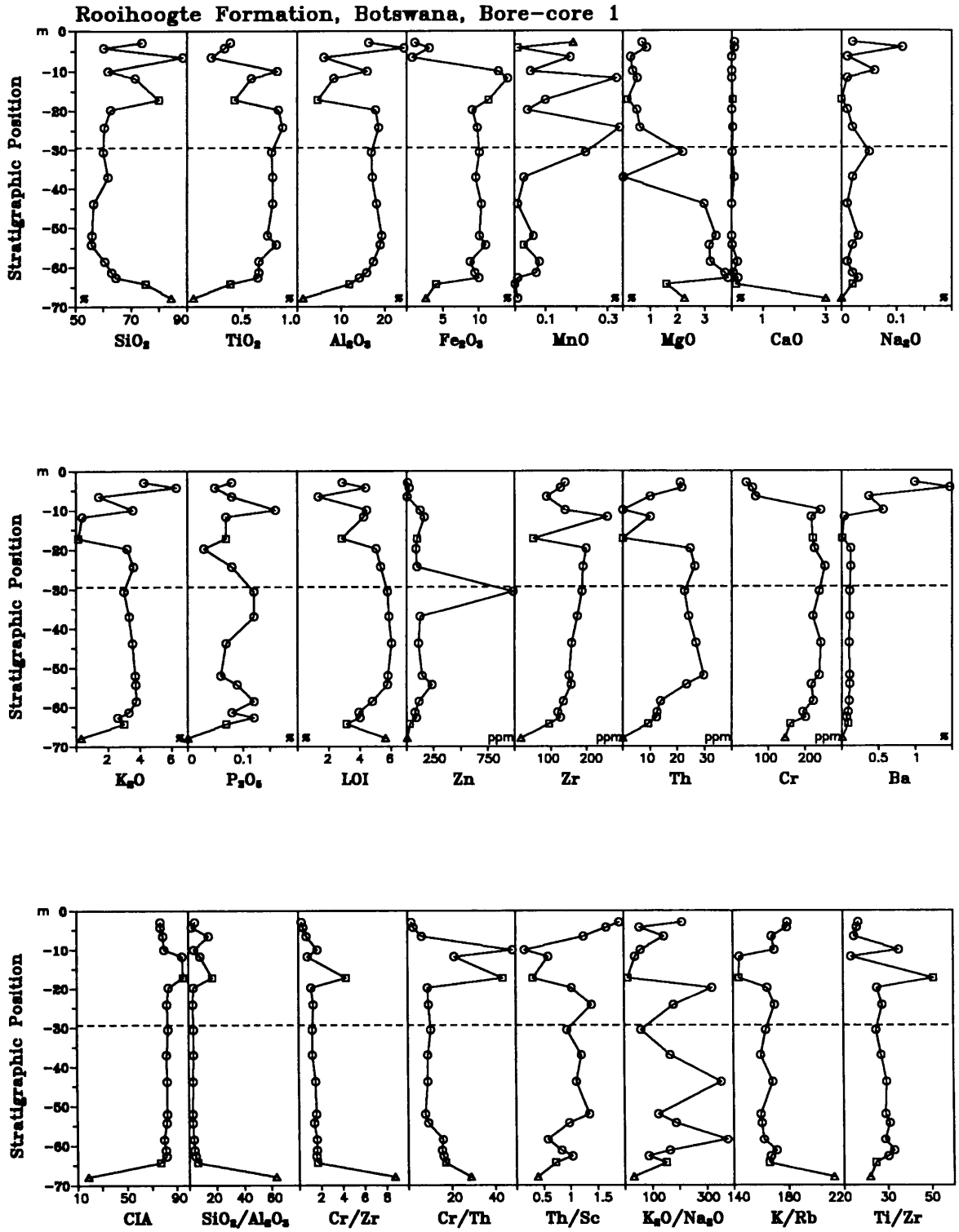

Figure 3.3.1.1: Partial geochemical profile of borehole 1 from the Rooihoogte Formation, Botswana. Lithological types: Δ = conglomerate; □ = sandstone; ○ = shale. Dashed line = oxidation base of borehole.

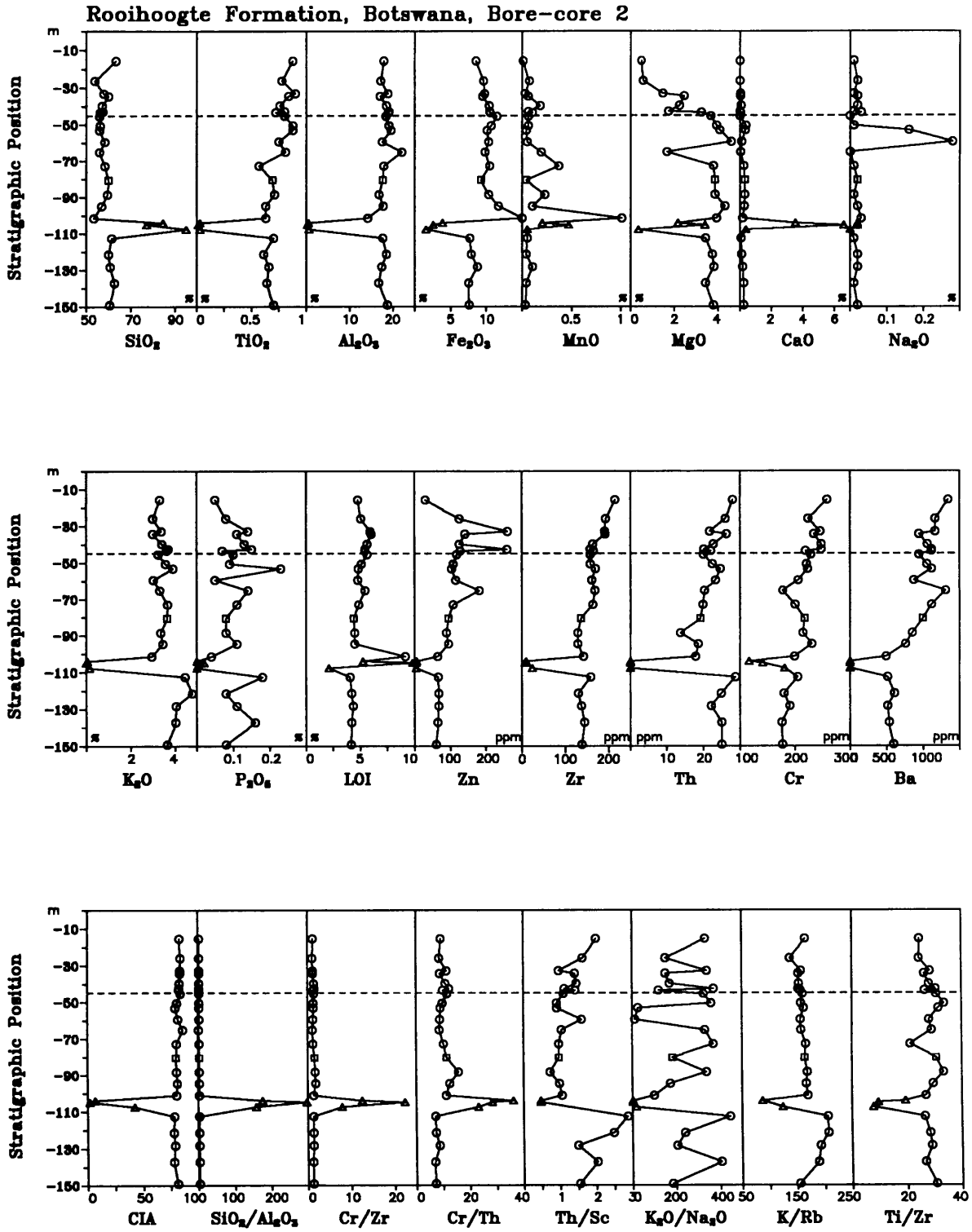

Figure 3.3.1.2: Partial geochemical profile of borehole 2 from the Rooihoogte Formation, Botswana. Lithological types: Δ = conglomerate; □ = sandstone; ○ = shale. Dashed line = oxidation base of borehole.

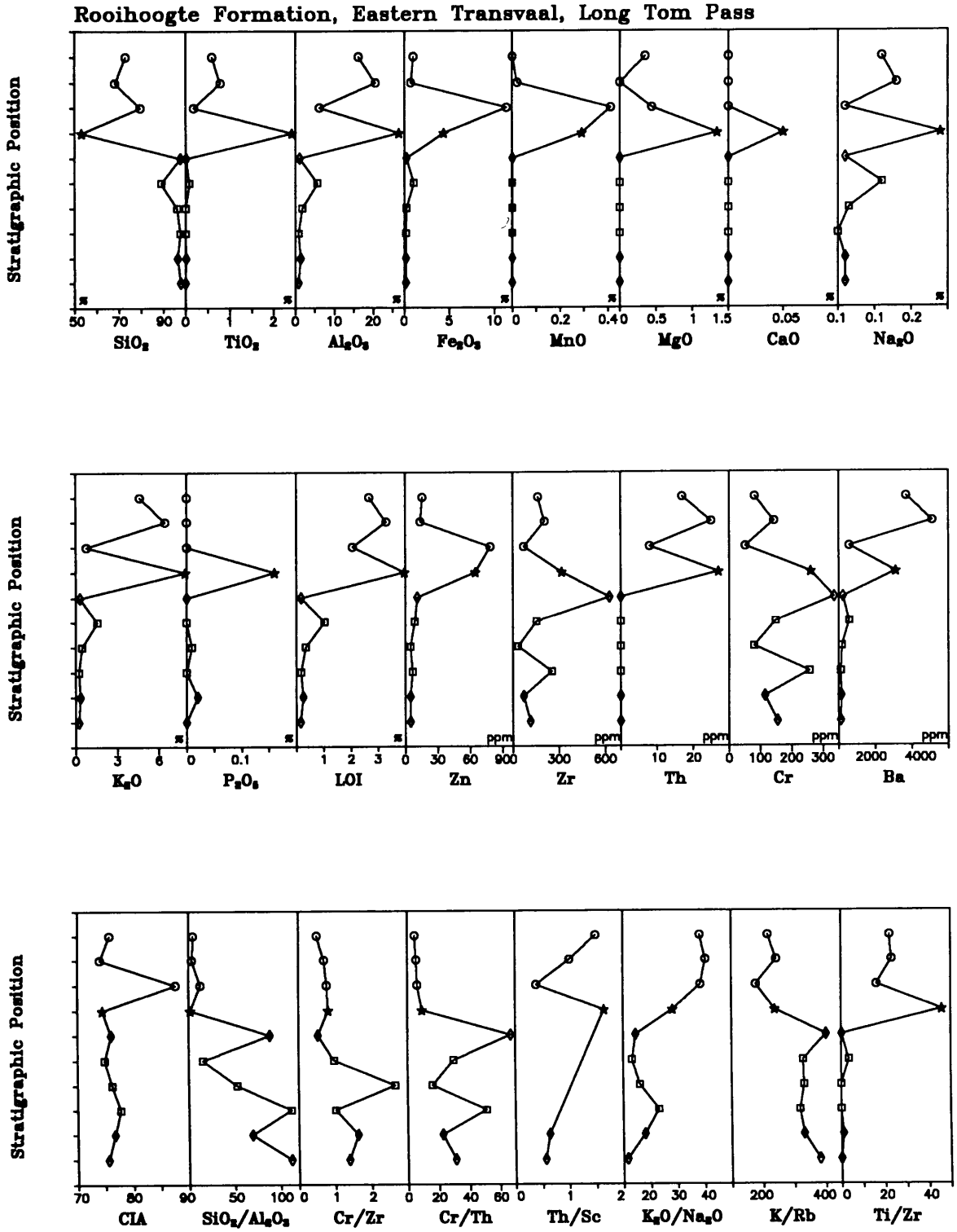

Figure 3.3.1.3: Geochemical profile of the Rooihoogte Formation, Long Tom Pass, eastern Transvaal. Lithological types: ★ = conglomerate; □ = sandstone; ○ = shale; ◇ = breccia. Vertical scale = ± 50 m in total.

approximate thickness of 50 m and can be broadly correlated with Rooihoogte Formation profile No. 5 of Schreiber (1990, p. 16). The conglomerate bed can most likely be correlated with Schreiber's (1990) medium-grained sandstone 'with pebbly sandstone interbeds' at the base of the Rooihoogte shales, and not with the underlying conglomerate bed.

3.3.2 Timeball Hill Formation Lower Shale Member

The Timeball Hill Formation consists of three distinct members throughout the study area, a lower shale unit, a middle sandstone and/or quartzite unit (Klapperkop Member) and an upper shale unit. Each unit is described separately in this investigation.

The major element geochemistry of the Lower Timeball Hill Shale (Tables 3.3.2.1 and 3.3.2.2) exhibits deviations from average shale estimates (Table 3.2.1b) for Al_2O_3, MgO, CaO and Na_2O. The latter three elements are depleted, and Al_2O_3 is enriched compared to average shale estimates. Fe_2O_3(t) is slightly, but not significantly enriched. The average C_{org}-content (Table 3.3.2.4) is low, although black shales are common at the base of the Lower Timeball Hill Shales. Co and Sr are depleted, Ga, U, Th, and Cr enriched (Table 3.3.2.1) compared to average shale estimates (Table 3.2.1d). Zn is slightly depleted, Ba slightly enriched. The average REE-contents (Table 3.3.2.4) are considerably higher than average shale estimates, except for Ce. The variation coefficients of the enriched REE suggest the occurrence of strongly skew distributions for most REE. The geometric means, as a better estimate for the central value of strongly skewed distributions (see Chapter 2.1.2), of the REE are very similar to the North American Shale Composite (Gromet et al., 1984; Table 3.2.1d) and the Post-Archaean Average Shale (Taylor and McLennan, 1985; Table 3.2.1d). If the geometric mean is taken as a fair estimate of the average REE-contents of the Lower Timeball Hill Shale, only La is significantly enriched. K2O/Na2O, LREE/HREE, Th/Sc, and Th/La are enriched, Th/U is depleted (Tables 3.3.2.3 and 3.3.2.4) compared to Archaean Average Shale and Post-Archaean Average Shale (Taylor and McLennan, 1985; Table 3.2.1d). The Σ REE (Table 3.3.2.4) is slightly higher than the Post-Archaean Average Shale estimate of Taylor and McLennan (1985), although the geometric mean shows a good correspondence (Timeball Hill Lower Shale Member: GM 186 ppm; PAAS: ϕ 185 ppm).

Element	n	MEAN	STD ±	GM	MEDIAN	RANGE	VC
SiO_2	120	57.38	7.66	56.87	56.42	37.96 - 78.92	0.13
TiO_2	120	0.74	0.14	0.72	0.72	0.28 - 1.33	0.19
Al_2O_3	120	21.44	5.00	20.78	21.39	5.31 - 33.62	0.23
Fe_2O_3*	120	9.17	3.54	8.43	9.21	1.14 - 23.61	0.39
MnO	120	0.03	0.04	-	0.02	<LLD - 0.25	1.33
MgO	120	0.96	1.23	0.53	0.58	0.03 - 5.35	1.28
CaO	120	0.10	0.13	-	0.05	<LLD - 0.58	1.30
Na_2O	120	0.47	0.43	-	0.34	<LLD - 2.69	0.92
K_2O	120	3.35	0.90	3.12	3.33	0.05 - 6.29	0.27
P_2O_5	120	0.13	0.09	-	0.12	<LLD - 0.58	0.69
H_2O^-	120	0.81	0.91	0.48	0.41	0.03 - 4.50	1.12
LOI	120	4.96	1.30	4.78	4.80	1.32 - 9.20	0.26
Zn	120	76	90.3	56	63	9 - 934	1.19
Cu	120	44	34.7	34	33	4 - 188	0.79
Ni	120	67	53.3	56	56	9 - 509	0.80
Co	120	14	11.5	9.4	11	<3 - 75	0.82
Ga	120	29	7.8	27	28	<3 - 51	0.27
Mo	120	1.7	2.7	-	<LLD	<2 - 19	1.59
Nb	120	17	3.1	17	17	5 - 26	0.18
Zr	120	169	47.6	164	159	80 - 415	0.28
Y	120	34	15.7	31	30	11 - 122	0.46
Sr	120	92	52.0	77	82	4 - 316	0.57
Rb	120	173	56.0	160	170	5 - 402	0.32
U	120	8.3	4.7	-	9	<5 - 22	0.57
Th	120	22	6.2	21	23	<5 - 34	0.28
Pb	120	24	14.2	20	21	<5 - 77	0.59
Cr	120	186	79.3	171	201	46 - 733	0.43
V	120	164	57.0	156	154	37 - 510	0.35
Ba	120	979	1014.8	818	775	73 - 9799	1.04
Sc	120	17	5.9	15	16	<8 - 36	0.35
As	120	19	56.7	-	12	<10 - 460	2.41
S	120	325	851.3	163	151	<50 - 7280	2.62
Sb	119	2.9	5.9	-	<LLD	<8 - 25	2.03
Sn	119	2.5	5.2	-	<LLD	<8 - 23	2.08
B	38	72	40.8	63	59	22 - 206	0.57

Table 3.3.2.1: Average element concentration of shales from the Lower Timeball Hill Shale (n = number of samples; 'MEAN' = arithmetic mean; 'STD ±' = 1 σ standard deviation; 'GM' = geometric mean; 'MEDIAN' = median; 'VC' = variation coefficient; average major element concentrations are reported in weight %, average trace element concentrations in ppm; 'Fe_2O_3*' is all Fe expressed as Fe_2O_3; *) = arithmetic mean below detection limit; LLD = lower limit of detection)

Table 3.3.2.2: Average major element concentrations of shales from the Lower Timeball Hill Formation Shales recalculated to 100 % volatile-free.

Element	n	MEAN	STD ±	RANGE
SiO_2	119	61.23	7.38	41.73 - 81.89
TiO_2	119	0.78	0.15	0.29 - 1.46
Al_2O_3	119	22.95	5.56	5.51 - 36.96
Fe_2O_3*	119	9.67	3.61	1.20 - 25.25
MnO	119	0.03	0.04	<LLD - 0.26
MgO	119	1.02	1.29	0.03 - 5.61
CaO	119	0.11	0.14	<LLD - 0.61
Na_2O	119	0.50	0.45	<LLD - 2.91
K_2O	119	3.56	0.95	0.05 - 6.85
P_2O_5	119	0.14	0.10	<LLD - 0.60

Tuffaceous material is interlayered with the argillaceous rocks of the Lower Timeball Hill Shales in the eastern Transvaal. The tuffaceous layers only have a thickness of one to two meters, but a distinct geochemistry (Appendix 1a). Base metals are strongly enriched (Zn: ϕ 399 ppm; Cu: ϕ 263 ppm; Ni: 514 ppm; Co: ϕ 127 ppm) as well as Cr (ϕ 1258 ppm), As (ϕ 319 ppm) and Zr (ϕ 316 ppm). Al_2O_3, Fe_2O_3 and K_2O are enriched, SiO_2, Na_2O, CaO and MgO are strongly depleted. The average S-content is low.

Four complete geochemical profiles were sampled in the Lower Timeball Hill Shales (see Fig. 1.5.3 for location of profiles). The petrograghy of the Botswana bore-core is described in detail by Key (1983). The bore-core contains two petrographic units, shale and sandstone. The geochemical profile of the Botswana bore-core data is shown in Figure 3.3.2.1. The pattern of elements and ratios in this geochemical profile is rather complicated. The sandstone sample (at $\approx$ 70 m depth) seems to divide the profile in two parts, although a distinct pattern is only obvious for MgO. The two samples below the sandstone sample introduce some variability for Al_2O_3, Fe_2O_3, MnO and K_2O. Substantial amounts of CaO and Na_2O are only found in the lower part of the profile. Zn again exhibits an anomalously high value ($>$ 900 ppm) close to the oxidation base. The sandstone sample has a low Zr- and high Cr-content. The uppermost sample in the profile may have been affected by surface weathering.

Table 3.3.2.3: Average ratios of shales from the Lower Timeball Hill Formation Shales

(NOTE: ratios corrected as described in Chapter 3.1.2)

Ratio	n	MEAN	STD ±	GM	RANGE	VC
CIA	119	82.5	4.4	82.4	72.1 - 99.0	0.05
Fe/V	119	402	122	375	17 - 783	0.30
K_2O/Na_2O	117	16.1	33.8	9.5	1.2 - 350	2.10
SiO_2/Al_2O_3	119	3.0	1.6	2.7	1.4 - 14.9	0.53
Cr/Th	119	10.0	13.8	8.3	4.0 - 146.9	1.38
Th/Sc	119	1.42	0.58	1.30	0.17 - 3.25	0.41
Cr/Zr	119	1.20	0.68	1.05	0.23 - 6.43	0.57
Co/Th	119	0.80	1.48	0.49	0.10 - 15.03	1.85
Al_2O_3/TiO_2	119	30	6	29	11 - 61	0.20
Al_2O_3/K_2O	119	8.0	10.4	6.7	3.4 - 106.2	1.30
K/Rb	119	164	27	161	83 - 253	0.17
K/Ba	119	34	11	32	4 - 65	0.32
Ti/Ni	119	93	64	78	10 - 460	0.69
Cr/V	119	1.19	0.62	1.10	0.30 - 6.79	0.52
V/Ni	119	3.69	5.27	2.81	0.29 - 56.67	1.43
Ni/Co	119	7.65	8.89	5.44	1.00 - 79.60	1.16
Zr/Nb	119	10.4	3.9	9.9	5.9 - 27.9	0.38
Th/U	118	2.75	1.26	2.47	0.64 - 6.60	0.46
Ba/Rb	119	6.1	5.8	5.1	1.5 - 42.4	0.95
Ba/Sr	119	15	19	11	3 - 163	1.27
Ba/Th	119	55	87	39	3 - 754	1.58
Al/Zr	119	718	236	671	134 - 1136	0.33
Ti/Zr	119	27.2	6.6	26.4	10.3 - 47.9	0.24

The eastern Transvaal profile is shown in Figure 3.3.2.2. The profile contains two petrographic units, shale and tuffaceous material, and has a thickness of approximately 500 m. Apart from anomalous values caused by the geochemistry of the tuffaceous material, no distinct trend is obvious in the profile. However, Na_2O seems to increase towards the top of the profile, although the highest values are recorded for the middle part. The geochemistry of the four lowermost shale samples deviates from the geochemistry of the other shales. The former shales are enriched in SiO_2, Ba and the K_2O/Na_2O ratio, and depleted in Al_2O_3, CaO, Na_2O, P_2O_5, Th, Ti/Zr and CIA (= Chemical Index of Alteration, Nesbitt and Young, 1982). The tuffaceous material is distinguished by an enrichment in Zn, $Fe_2O_3(t)$, MnO, Zr, Cr and Cr/Zr, and is concentrated at the base of this profile.

Table 3.3.2.4: Average element concentrations and ratios of selected shale samples of the Timeball Hill Formation Lower Shale Member

(n = number of samples; 'MEAN' = arithmetic mean; 'STD ±' = 1 σ standard deviation; 'GM' = geometric mean; 'MEDIAN' = median; 'VC' = variation coefficient; average major element concentrations (i.e. FeO to S_{XRF}) are reported in weight %, average trace element concentrations in ppm; n.c. = not calculated; subscript N = concentration normalised to chondrite; $Ce/Ce^* = Ce_N/[(La_N + Pr_N)/2]$; Σ REE = sum of REE in ppm; NOTE: ratios corrected as described in Chapter 3.1.2; LLD = lower limit of detection)

Element	n	MEAN	STD ±	GM	MEDIAN	RANGE	VC
FeO	15	2.83	3.46	-	1.64	<LLD - 9.71	1.22
Fe_2O_3	15	4.85	3.31	3.27	6.73	0.35 - 9.10	0.68
CO_2	15	0.36	0.20	0.28	0.33	0.07 - 0.84	0.56
C_{org}	15	0.15	0.35	-	0.05	<LLD - 1.41	2.33
H_2O^+	15	4.72	1.15	4.56	4.89	2.22 - 6.16	0.24
S_{leco}	15	0.04	0.16	-	<LLD	<LLD - 0.63	4.00
S_{xrf}	15	0.03	n.c.	n.c.	n.c.	<LLD - 0.73	n.c.
Li	15	49	28.4	33	55	1 - 85	0.58
La	15	60.6	42.6	50.1	44.9	19.2 - 155	0.70
Ce	15	76.8	29.7	72.0	77.4	36.9 - 155	0.39
Pr	15	13.7	13.3	10.0	8.5	2.6 - 51.1	0.97
Nd	15	47.7	50.7	33.2	30.1	6.8 - 204	1.06
Sm	15	8.2	8.3	6.2	5.4	2.3 - 35.1	1.01
Eu	15	1.7	1.9	1.2	1.0	0.4 - 7.9	1.12
Gd	15	6.5	6.8	5.0	4.3	2.5 - 29.4	1.05
Tb	15	1.0	0.9	0.8	0.7	0.4 - 4.1	0.90
Dy	15	5.2	4.8	4.3	4.0	2.6 - 21.8	0.92
Er	15	2.8	2.3	2.4	2.3	1.6 - 10.7	0.82
Tm	15	0.4	0.3	0.3	0.3	0.2 - 1.4	0.75
Yb	15	2.8	1.9	2.5	2.4	1.5 - 9.3	0.68
La/Sc	15	4.27	4.68	3.01	2.78	0.75 - 19.40	1.10
Th/La	15	0.52	0.27	0.46	0.47	0.17 - 1.20	0.52
Ba/La	15	40.5	81.3	21.0	19.4	5.3 - 332.2	2.01
LREE/HREE	15	14.81	7.17	13.60	12.74	8.25 - 31.04	0.48
K2O/ΣREE	15	214	104	191	198	64 - 423	0.49
Gd_N/Yb_N	15	1.72	0.65	1.62	1.44	1.03 - 3.34	0.38
La_N/Sm_N	15	5.23	0.97	5.13	5.42	2.78 - 6.85	0.19
Ce/Ce*	15	0.767	0.240	0.716	0.885	0.207 - 1.082	0.31
Eu/Eu*	15	0.650	0.101	0.642	0.648	0.365 - 0.818	0.16
C_{org}/S	15	3.31	2.50	2.33	2.63	0.34 - 8.61	0.76
ΣREE	15	227	149.4	193	185	77 - 609	0.66

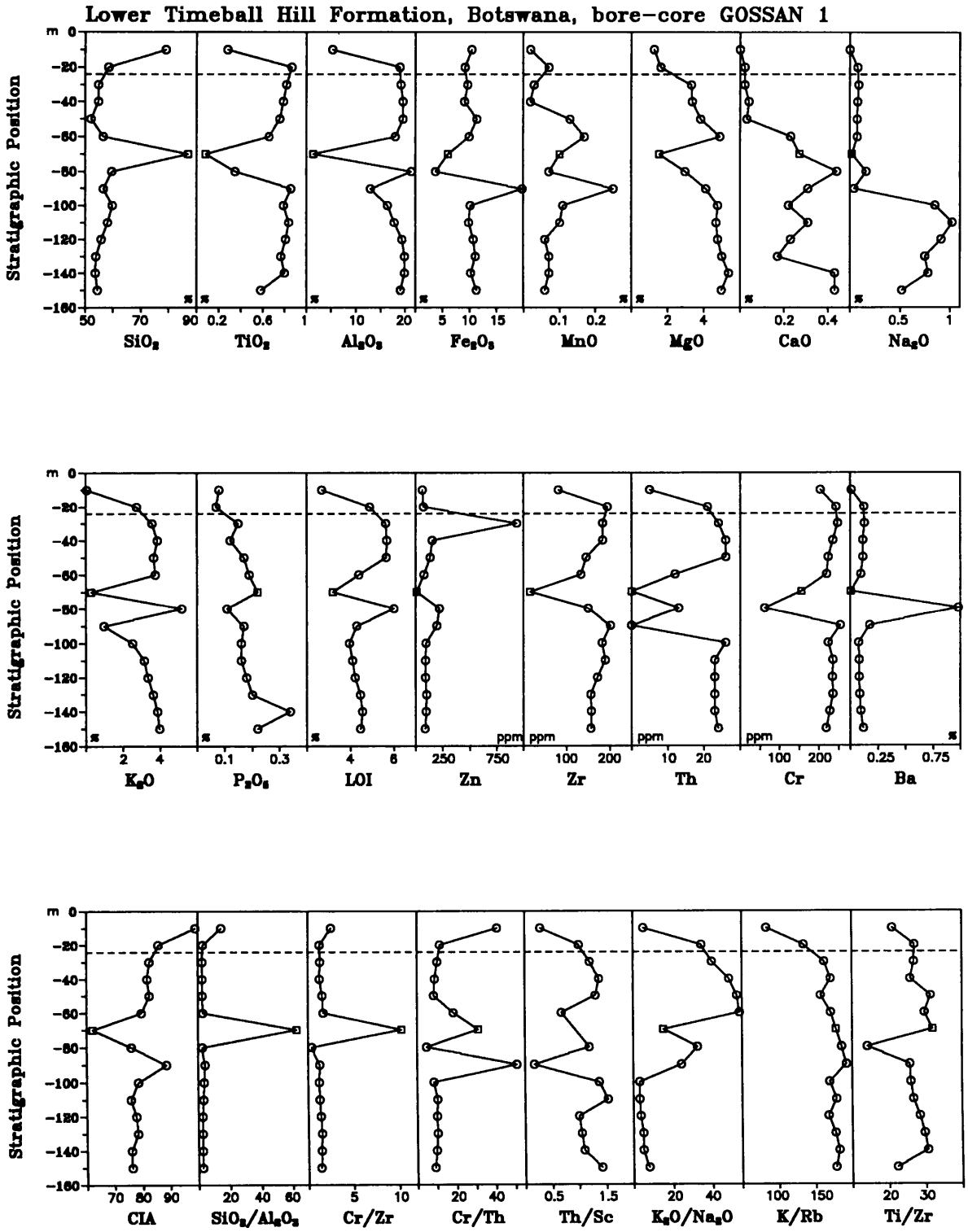

Figure 3.3.2.1: Geochemical profile of the Timeball Hill Formation Lower Shale Member, bore-core, Botswana. Lithological types: □ = sandstone; ○ = shale. Dashed line = oxidation base of borehole.

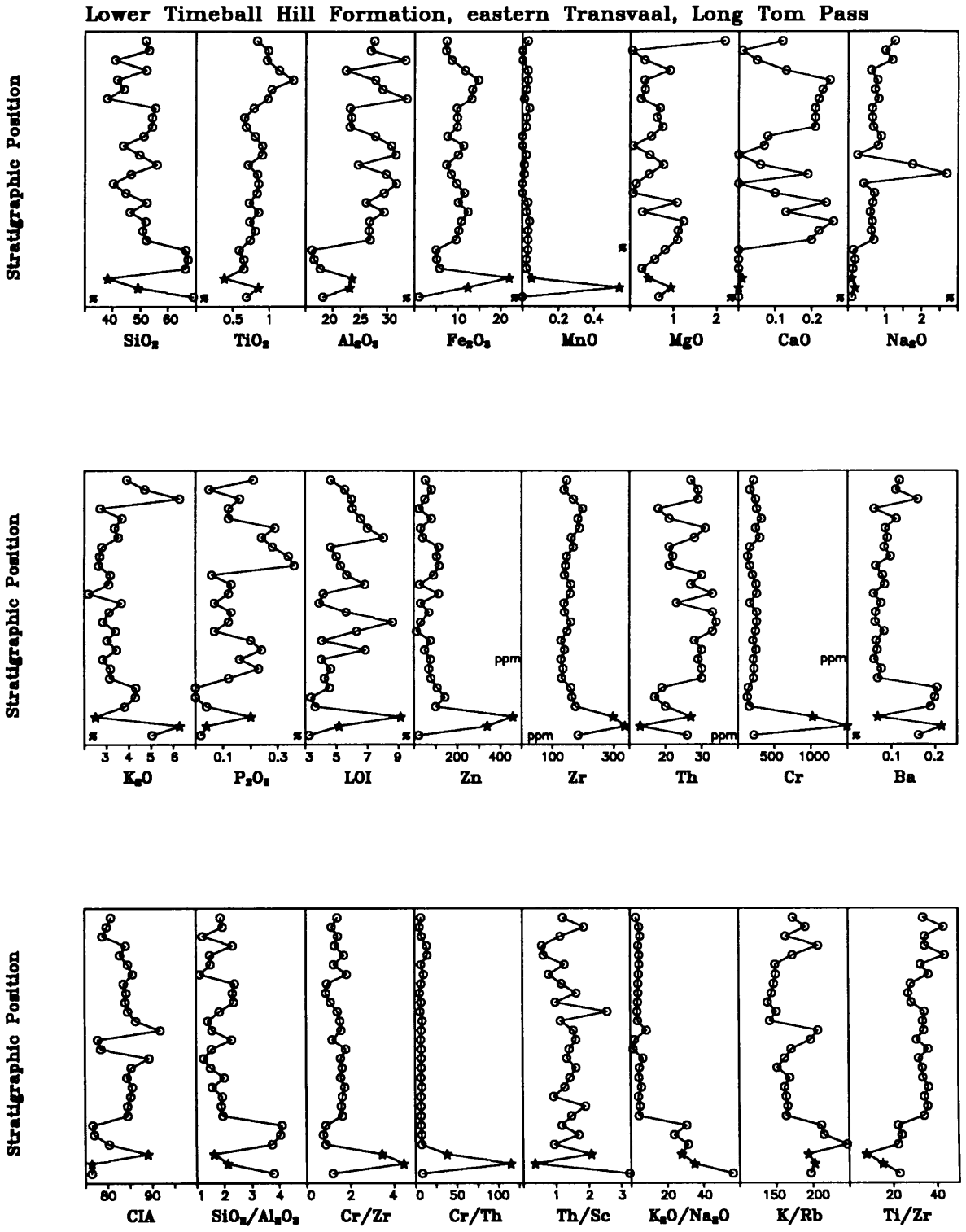

Figure 3.3.2.2: Geochemical profile of the Timeball Hill Formation Lower Shale Member, Long Tom Pass, eastern Transvaal. Lithological types: ★ = tuffaceous material; ○ = shale. Vertical scale = ± 500 m in total.

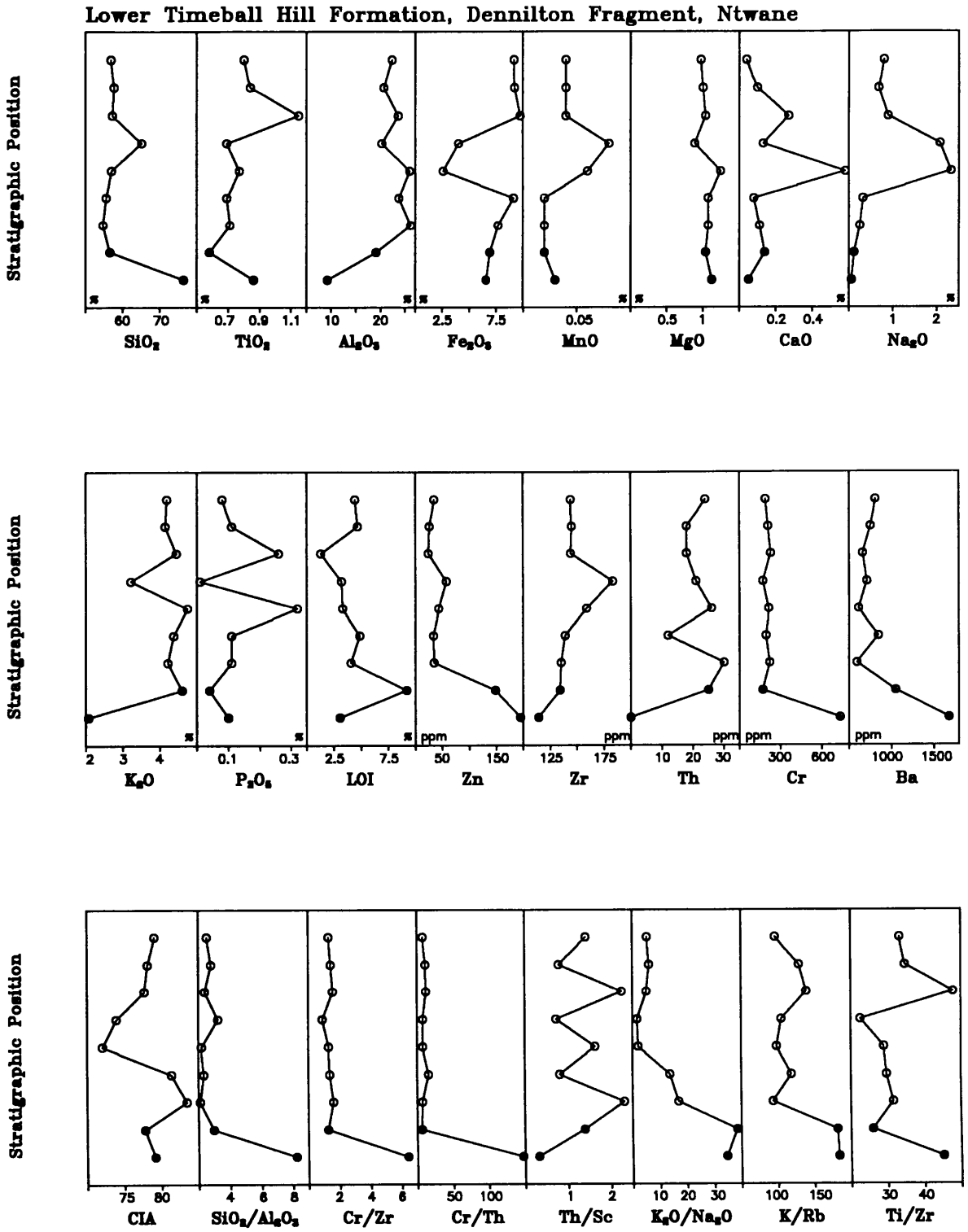

Figure 3.3.2.3: Geochemical profile of the Timeball Hill Formation Lower Shale Member, Ntwane, Dennilton Fragment. Lithological types: ○ = shale; ● = black shale. Vertical scale = ± 250 m.

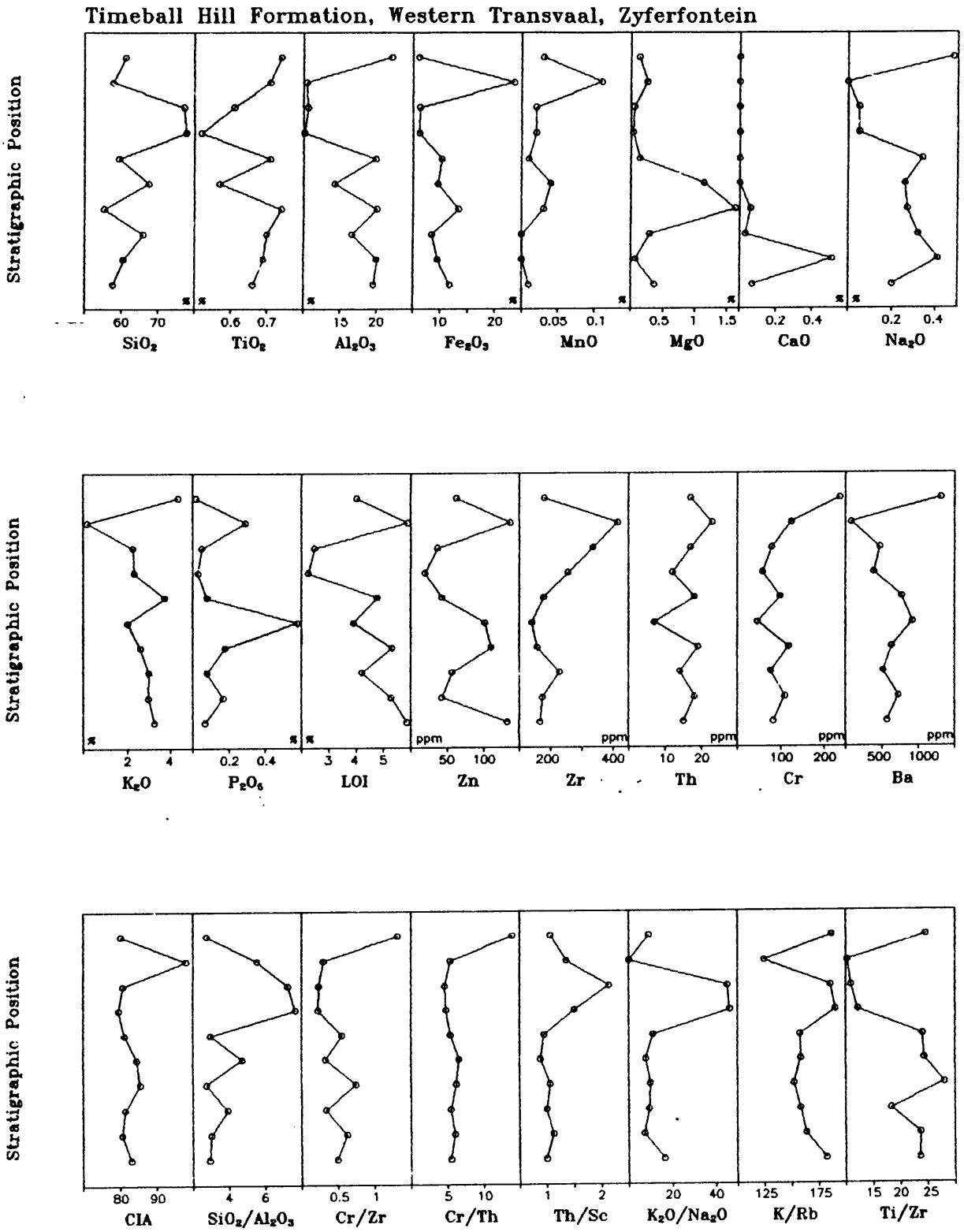

Figure 3.3.2.4: Geochemical profile of the Timeball Hill Formation Lower Shale Member, Zyferfontein, western Transvaal. Lithological types: ○ = shale. Vertical scale = ± 350 m in total.

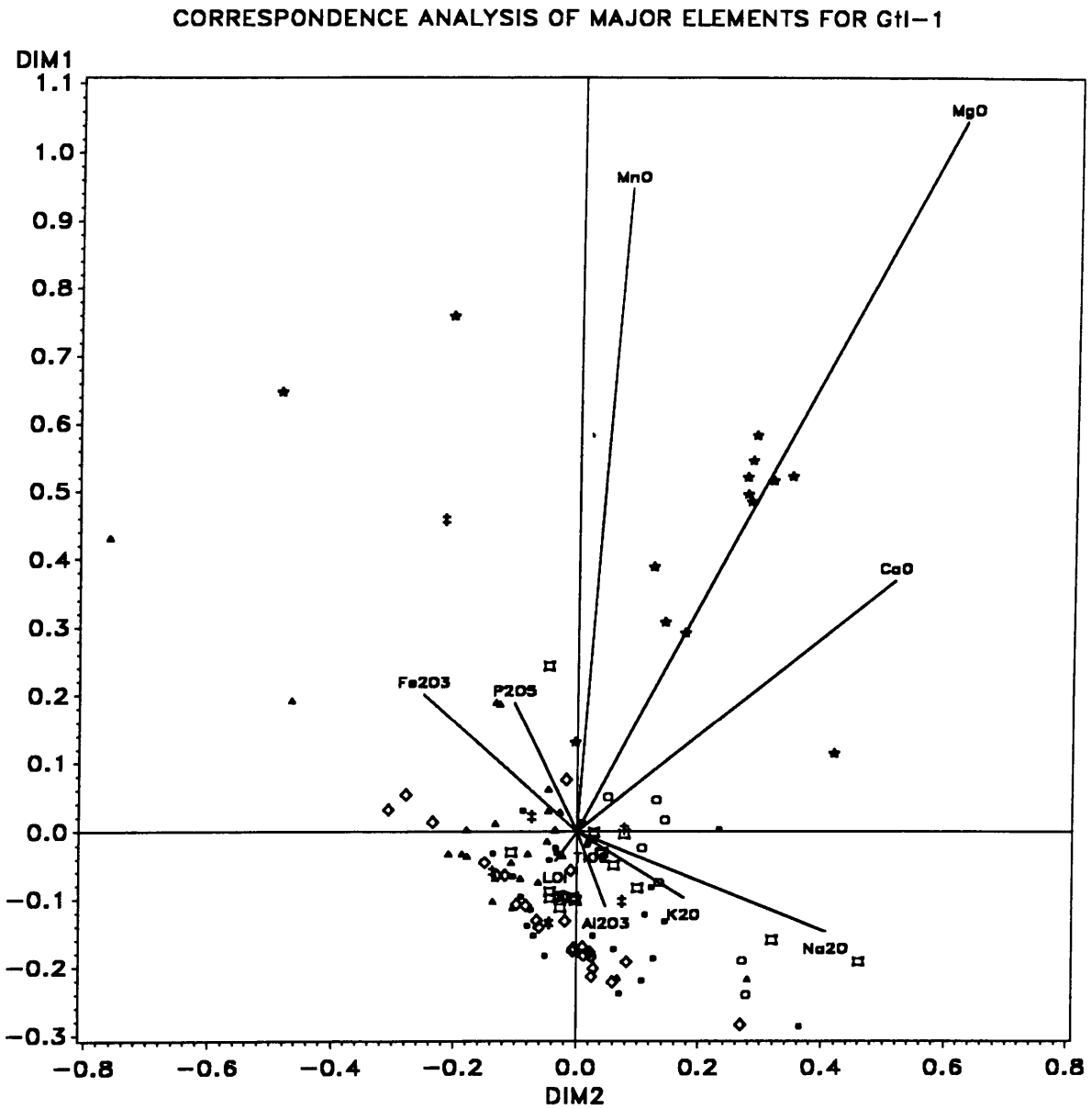

Figure 3.3.2.5: Correspondence analysis of major elements (except SiO_2) of shales for the Lower Timeball Hill Formation. Symbols for sampling areas: ● (red) = eastern Transvaal; ○ (red) = northeastern Transvaal; □ (violet) = eastern fragments; ◇ (green) = central Transvaal; ▲ (blue) = western Transvaal; † (blue) = western fragments; ‡ (blue) = northwestern Transvaal; ★ (yellow) = Botswana. Definition of sampling areas is shown in Figure 1.5.1. DIM 1 and DIM 2 are the values of the factor loadings of the samples and variables for the first and second factor (see Chapter 2.3.2). Angles between lines connecting a variable and the point (0,0) are proportional to the product moment correlation coefficient of these variables.

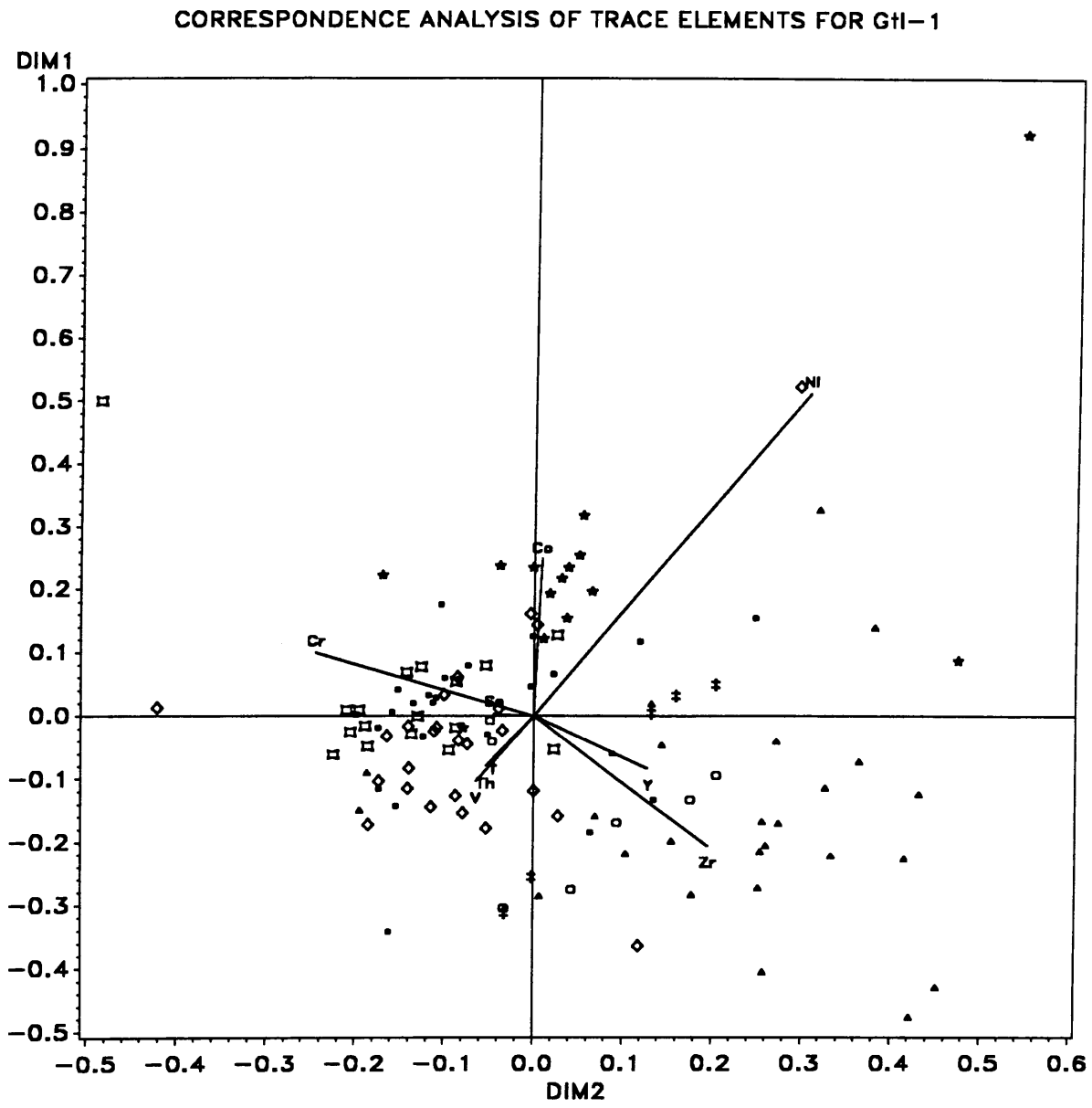

Figure 3.3.2.6: Correspondence analysis of selected trace elements of shales for the Lower Timeball Hill Formation. Symbols for sampling areas: ● (red) = eastern Transvaal; ○ (red) = northeastern Transvaal; □ (violet) = eastern fragments; ◇ (green) = central Transvaal; ▲ (blue) = western Transvaal; † (blue) = western fragments; ‡ (blue) = northwestern Transvaal; ★ (yellow) = Botswana. Definition of sampling areas is shown in Figure 1.5.1. DIM 1 and DIM 2 are the values of the factor loadings of the samples and variables for the first and second factor (see Chapter 2.3.2). Angles between lines connecting a variable and the point (0,0) are proportional to the product moment correlation coefficient of these variables.

The Dennilton Fragment geochemical profile (Fig. 3.3.2.3) has an approximate thickness of 250 m. The profile contains two petrographic units, shale and black shale. The Na_2O-content exhibits an overall increase towards the top of the succession with peak values in the middle part. The black shale samples at the bottom of the profile show increased SiO_2, Ba, Cr, Zn, K/Rb, and K_2O/Na_2O contents and are depleted in Al_2O_3 and, to a minor extent, in K_2O, Th, and Zr. The black shales have extraordinary high As-contents (up to 460 ppm, not shown in the profile). The overall geochemical pattern of the Dennilton Fragment profile is quite similar to the eastern Transvaal profile (Fig. 3.3.2.2).

The western Transvaal geochemical profile (Fig. 3.3.2.4) contains shales as the sole lithotype. The profile has an approximate thickness of 350 m, including diabase sills. The geochemical pattern is complicated for most elements due to the occurrence of partial trends (e.g., TiO_2 exhibits an increase in the lower part of the profile, decreases in the middle part and increases again in the upper part). Na_2O and Al_2O_3 decrease throughout the profile, except for the uppermost sample. A comparison of the western Transvaal geochemical profile with the Botswana geochemical profile (Fig. 3.3.2.1) shows a good fit for the trends of Na_2O and CaO. Both oxides have substantial abundances in the lower part of the respective profiles only. Most other elements and ratios of the western Transvaal geochemical profile exhibit trends comparable to the patterns of the lower part of the Botswana geochemical profile.

Correspondence analysis was performed on major and selected trace elements. A detailed description of the mathematical background is found in Chapter 2.3.2. In Chapter 3 correspondence analysis is used to investigate regional variations and, if possible, to show regional geochemical differences defined by a combination of elements. To obtain meaningful results, only samples of a defined grain-size, i.e. shales or sandstones, were tested together.

Correspondence analysis for major elements (Si excluded) of the Lower Timeball Hill Shales (Fig. 3.3.2.5) distinguishes the Botswana shale samples as a separate group. Grouping patterns for the other areas are less obvious. Correspondence analysis for selected trace elements (Fig. 3.3.2.6) clearly shows defined fields for most regions. The shales from the eastern Transvaal and the eastern fragments occupy the same cluster. This result corresponds to the comparison of the respective geochemical profiles (see above). With the exception of

the Botswana and northeastern Transvaal samples, a systematical east-west trend of variation is indicated.

3.3.3 Timeball Hill Quartzites (Klapperkop Member)

The major element geochemistry of the Timeball Hill Quartzites/Sandstones (Table 3.3.3.1) shows a higher average SiO_2-content compared to average sandstone estimates (Table 3.2.1c). The other major elements are depleted, except Fe_2O_3(t). The trace elements (Table 3.3.3.1) Ni, Cr, Mo, and Co are enriched compared with average sandstone estimates (Table 3.2.1d), whereas Zr, Y, Rb and B are depleted.

Shale bands of varying thickness are interlayered with the quartzites. This shales (Tables 3.3.3.2 and 3.3.3.3) have increased average contents of Al_2O_3 and P_2O_5 and a high, but not significantly increased, Fe_2O_3(t)-content compared with average shales (Table 3.2.1b). MgO, CaO and MnO are strongly, and Na_2O moderatly depleted. The trace elements (Table 3.3.3.2) Cr, Mo, Th, U, and Ba are enriched, Zn, Ni, and Co depleted compared with average shales (Table 3.2.1d). The K2O/Na2O-ratio (Table 3.3.3.4) is significantly higher than the values reported for Post-Archaean Average Shale and Archaean Average Shale (Taylor and McLennan, 1985, Table 3.2.1e). The ratios Cr/V, Ni/Co and V/Ni (Table 3.3.3.4) show some inconsistencies. The average Cr/V-ratio lies between ratios reported for Post-Archaean Average Shale and Late Archaean Average Shale (Taylor and McLennan, 1985), the Ni/Co-average between Early Archaean Average Shale and Late Archaean Average Shale (Taylor and McLennan, 1985), and the V/Ni-average exceeds all reported ratios significantly (Table 3.2.1e). The Th/U-average is, similar to Rooihoogte Formation shales and Lower Timeball Hill Shales, lower than either Post-Archaean Average Shale or Archaean Average Shale (Taylor and McLennan, 1985; Table 3.2.1e).

A conglomerate bed sampled in the northeastern Transvaal has a P_2O_5-content of more than 12 wt.%. The enrichment in P_2O_5 is accompanied by high CaO, Sr, and Cr contents (Appendix 1a).

Element	n	MEAN	STD ±	GM	MEDIAN	RANGE	VC
SiO_2	43	93.64	9.43	93.03	96.56	53.22 - 98.83	0.10
TiO_2	43	0.12	0.20	-	0.05	<LLD - 0.84	1.67
Al_2O_3	43	2.41	5.30	1.11	1.01	0.14 - 27.45	2.20
Fe_2O_3*	43	2.29	2.62	1.45	1.26	0.30 - 12.33	1.14
MnO	43	0.01	0.01	-	<LLD	<LLD - 0.06	1.00
MgO	43	0.14	0.42	-	<LLD	<LLD - 2.04	3.00
CaO	43	0.01	0.02	-	<LLD	<LLD - 0.10	2.00
Na_2O	43	0.07	0.17	-	0.02	<LLD - 0.88	2.43
K_2O	43	0.36	0.87	-	0.07	<LLD - 4.54	2.42
P_2O_5	43	0.04	0.04	-	0.03	<LLD - 0.16	1.00
H_2O^-	43	0.07	0.06	-	0.05	<LLD - 0.30	0.86
LOI	43	0.63	0.97	0.39	0.35	0.02 - 4.88	1.54
Zn	43	10	9.3	-	7	<3 - 44	0.93
Cu	43	4.8	12.5	-	0	<3 - 65	2.60
Ni	43	6.6	12.9	-	3	<3 - 69	1.96
Co	43	5.0	4.1	-	4	<3 - 24	0.82
Ga	43	2.3 *)	6.9	-	<LLD	<3 - 33	3.00
Mo	43	10	12.4	-	9	<2 - 86	1.24
Nb	43	2.3	4.0	-	2	<2 - 18	1.74
Zr	43	7.8	68.8	59	57	22 - 336	0.88
Y	43	6.3	7.8	-	4	<2 - 42	1.24
Sr	43	14	24.2	-	7	<2 - 125	1.73
Rb	43	16	45.1	-	5	<2 - 225	2.82
U	43	2.0 *)	3.7	-	<LLD	<5 - 12	1.85
Th	43	2.5 *)	5.9	-	<LLD	<5 - 29	2.36
Pb	43	6.7	20.7	-	<LLD	<5 - 133	3.09
Cr	43	155	49.7	146	147	38 - 249	0.32
V	43	37	31.6	-	28	<14 - 152	0.85
Ba	43	125	249.8	-	50	<16 - 1508	2.00
Sc	43	3.3 *)	5.8	-	<LLD	<8 - 19	1.76
As	43	5.8 *)	13.6	-	<LLD	<10 - 69	2.35
S	43	55	192.3	-	<LLD	<50 - 1256	3.50
Sb	43	0.6 *)	2.2	-	<LLD	<8 - 11	3.67
Sn	43	1.0 *)	4.1	-	<LLD	<8 - 24	4.10
B	1	4	-	-	-	-	-

Table 3.3.3.1: Average element concentrations of sandstones from Timeball Hill Quartzite (n = number of samples; 'MEAN' = arithmetic mean; 'STD ±' = 1 σ standard deviation; 'GM' = geometric mean; 'MEDIAN' = median; 'VC' = variation coefficient; average major element concentrations are reported in weight %, average trace element concentrations in ppm; 'Fe_2O_3*' is all Fe expressed as Fe_2O_3; *) = arithmetic mean below detection limit; LLD = lower limit of detection)

Element	n	MEAN	STD ±	GM	MEDIAN	RANGE	VC
SiO_2	12	57.31	11.03	56.34	56.85	40.17 - 82.46	0.19
TiO_2	12	0.71	0.20	0.68	0.72	0.22 - 0.98	0.28
Al_2O_3	12	21.74	6.56	20.51	22.34	6.87 - 31.64	0.30
Fe_2O_3*	12	9.60	2.56	9.27	9.29	6.14 - 13.49	0.27
MnO	12	0.01	0.01	-	0.01	0 - 0.05	1.00
MgO	12	0.24	0.27	-	0.19	0 - 1.06	1.13
CaO	12	0.05	0.04	-	0.05	0 - 0.12	0.80
Na_2O	12	0.61	0.39	0.50	0.45	0.13 - 1.33	0.64
K_2O	12	2.98	0.95	2.81	2.88	0.98 - 4.77	0.32
P_2O_5	12	0.23	0.10	0.19	0.25	0.02 - 0.33	0.44
H_2O^-	12	0.78	0.46	0.68	0.72	0.23 - 1.96	0.59
LOI	12	5.31	1.56	5.05	5.56	2.08 - 7.46	0.29
Zn	12	35	14.6	31	38	7 - 58	0.42
Cu	12	37	23.3	27	38	<3 - 83	0.63
Ni	12	30	13.5	26	31	3 - 52	0.45
Co	12	6.0	2.5	5.4	5.5	<3 - 9	0.42
Ga	12	25	13.4	19	26	<3 - 54	0.54
Mo	12	7.3	5.6	-	5.5	<2 - 19	0.77
Nb	12	16	6.9	13	17	<2 - 29	0.43
Zr	12	174	59.3	164	174	79 - 292	0.34
Y	12	34	25.6	28	31	8 - 108	0.75
Sr	12	159	117.5	109	124	5 - 403	0.74
Rb	12	158	74.6	105	169	<2 - 275	0.47
U	12	9.6	5.6	-	11	<5 - 20	0.58
Th	12	21	9.7	18	21	<5 - 34	0.46
Pb	12	21	13.6	17	20	<5 - 48	0.65
Cr	12	178	37.3	174	185	120 - 248	0.21
V	12	149	44.4	142	142	67 - 220	0.30
Ba	12	1073	1141.6	800	782	287 - 4531	1.06
Sc	12	16	6.8	14	15	<8 - 28	0.43
As	12	12	14.6	-	10	<10 - 50	1.22
S	12	281	101.4	267	263	158 - 541	0.36
Sb	12	1.9 *)	4.5	-	<LLD	<8 - 12	2.37
Sn	12	1.6 *)	3.8	-	<LLD	<8 - 11	2.38
B	1	46	-	-	-	-	-

Table 3.3.3.2: Average element concentrations of shales from Timeball Hill Quartzite

(n = number of samples; 'MEAN' = arithmetic mean; 'STD ±' = 1 σ standard deviation; 'GM' = geometric mean; 'MEDIAN' = median; 'VC' = variation coefficient; average major element concentrations are reported in weight %, average trace element concentrations in ppm; 'Fe_2O_3*' is all Fe expressed as Fe_2O_3; *) = arithmetic mean below detection limit; LLD = lower limit of detection)

Table 3.3.3.3: Average major element concentrations of shales from the Timeball Hill Quartzites recalculated to 100 % volatile-free.

Element	n	MEAN	STD ±	RANGE
SiO_2	12	61.13	10.56	44.55 - 84.76
TiO_2	12	0.77	0.22	0.23 - 1.09
Al_2O_3	12	23.38	7.36	7.06 - 34.40
Fe_2O_3*	12	10.31	2.90	6.50 - 15.01
MnO	12	0.01	0.01	<LLD - 0.05
MgO	12	0.25	0.28	<LLD - 1.11
CaO	12	0.05	0.04	<LLD - 0.13
Na_2O	12	0.65	0.42	0.13 - 1.48
K_2O	12	3.20	1.06	1.01 - 5.19
P_2O_5	12	0.24	0.11	0.02 - 0.37

Table 3.3.3.4a: Average ratios of shales from the Timeball Hill Quartzites

(NOTE: ratios corrected as described in Chapter 3.1.2)

Ratio	n	MEAN	STD ±	GM	RANGE	VC
CIA	12	83.4	1.9	83.4	80.2 - 87.2	0.02
Fe/V	12	475	139	456	279 - 712	0.29
K_2O/Na_2O	12	6.3	2.7	5.6	1.8 - 9.4	0.43
SiO_2/Al_2O_3	12	3.3	2.8	2.8	1.3 - 12.0	0.85
Cr/Th	12	10.4	6.5	9.3	6.0 - 27.1	0.63
Th/Sc	12	1.44	0.56	1.26	0.19 - 2.13	0.39
Cr/Zr	12	1.14	0.48	1.06	0.59 - 2.35	0.42
Co/Th	12	0.36	0.22	0.30	0.09 - 0.80	0.61
Al_2O_3/TiO_2	12	30.7	4.4	30.4	25.3 - 39.7	0.14
Al_2O_3/K_2O	12	7.4	1.2	7.3	5.4 - 10.1	0.16
K/Rb	12	1028	3053	209	113 - 10722	n.c.
K/Ba	12	32	13	29	9 - 60	0.41
Ti/Ni	12	237	350	158	66 - 1339	1.48
Cr/V	12	1.28	0.50	1.23	0.94 - 2.78	0.39
V/Ni	12	7.99	11.01	5.56	2.06 - 42.67	1.38
Ni/Co	12	5.54	3.52	4.5	0.75 - 14.05	0.64
Zr/Nb	12	13.6	10.8	11.6	7.2 - 46.7	0.79
Th/U	11	2.17	0.65	2.08	1.36 - 3.09	0.30
Ba/Rb	12	30	83	7.2	2 - 295	2.77
Ba/Sr	12	16	32	7.3	3 - 117	2.00
Ba/Th	12	51	38	43	24 - 142	0.75
Al/Zr	12	702	240	663	346 - 1077	0.34
Ti/Zr	12	26.0	8.5	24.7	15.4 - 43.2	0.33

Table 3.3.3.4b : Average ratios of sandstones from the Timeball Hill Quartzites

(NOTE: ratios are not corrected, i.e. a sample was excluded from calculation of the average ratio if one or both elements are below the detection limit; n.c. = not calculated)

Ratio	n	MEAN	STD ±	GM	RANGE	VC
CIA	43	82.0	11.1	81.2	50.6 - 99.6	0.14
SiO_2/Al_2O_3	43	134	132	84	1.9 - 705	0.99
lg SiO_2/Al_2O_3	43	1.92	n.c.	n.c.	n.c.	n.c.
K_2O/Na_2O	30	8.8	9.2	5.2	0.3 - 42	1.05
lg Na_2O/K_2O	30	-0.72	n.c.	n.c.	n.c.	n.c.
Ti/Zr	35	11.3	18.1	6.1	1.0 - 102.8	1.60
Ti/Cr	35	5.5	7.8	2.8	0.3 - 35.0	1.42
Al/Zr	43	161	185	99	8 - 982	1.15
Al_2O_3/TiO_2	35	34.8	39.9	18.7	1.1 - 207	1.15
Al_2O_3/K_2O	35	25.3	56.1	9.5	2.3 - 246.5	2.22
K/Rb	28	197	87	178	55 - 418	0.44
K/Ba	33	26	26	16	2 - 111	1.00
K/Sr	35	228	269	125	9 - 1494	1.18

Two complete geochemical profiles were sampled in the Timeball Hill Quartzite (see Fig 1.5.4 for location of the profiles). The eastern Transvaal geochemical profile (Figure 3.3.3.1) contains two petrographic types, sandstone and shale. The approximate thickness of the profile is 100 m, including diabase sills. The profile only shows a clear pattern for the K_2O/Na_2O-ratio, which decreases from bottom to top. Even the petrographic differences are not distinctly mirrored by the geochemical variation.

The eastern fragment geochemical profile (Figure 3.3.3.2) has an approximate thickness of 70 m. The petrography consists exclusively of recrystallized quartzites with high SiO_2-contents. Minor variations of the SiO2-content are accompanied by diametrically opposed variations of Al_2O_3 and K_2O. The Cr-contents are extraordinarily high, similar to the eastern Transvaal profile.

Correspondence analysis was performed for the quartzite/sandstone litho-type of the Timeball Hill Quartzites. Correspondence analysis of the major elements (except Si) shows an unsystematic spread of samples along the DIM 1-axis, and a fairly low variability for most samples on the DIM 2-axis with exception of the northwestern Transvaal samples (Figure

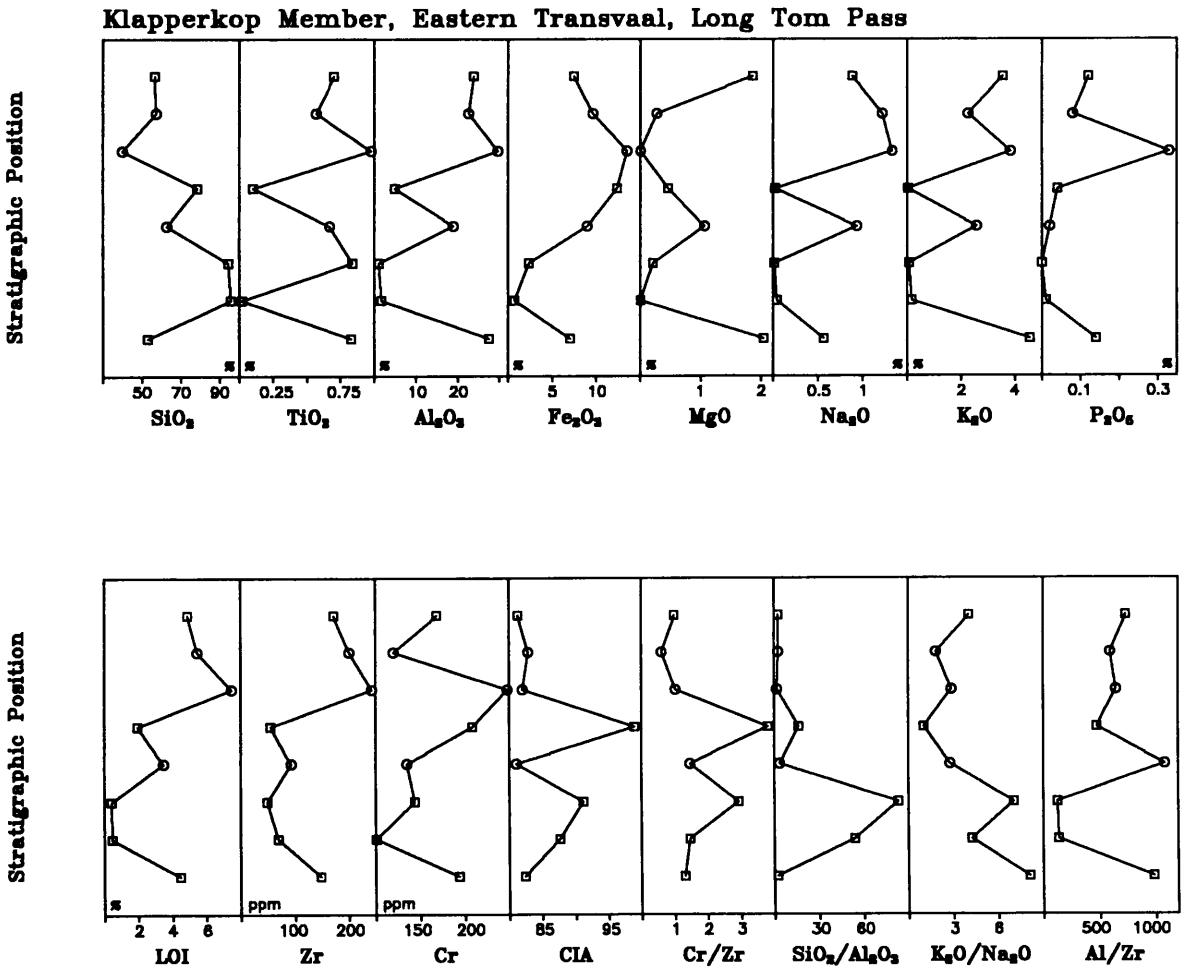

Figure 3.3.3.1: Geochemical profile of the Timeball Hill Quartzites, Long Tom Pass, eastern Transvaal. Lithological types: □ = sandstone; ○ = shale. Vertical scale = ± 100 m in total.

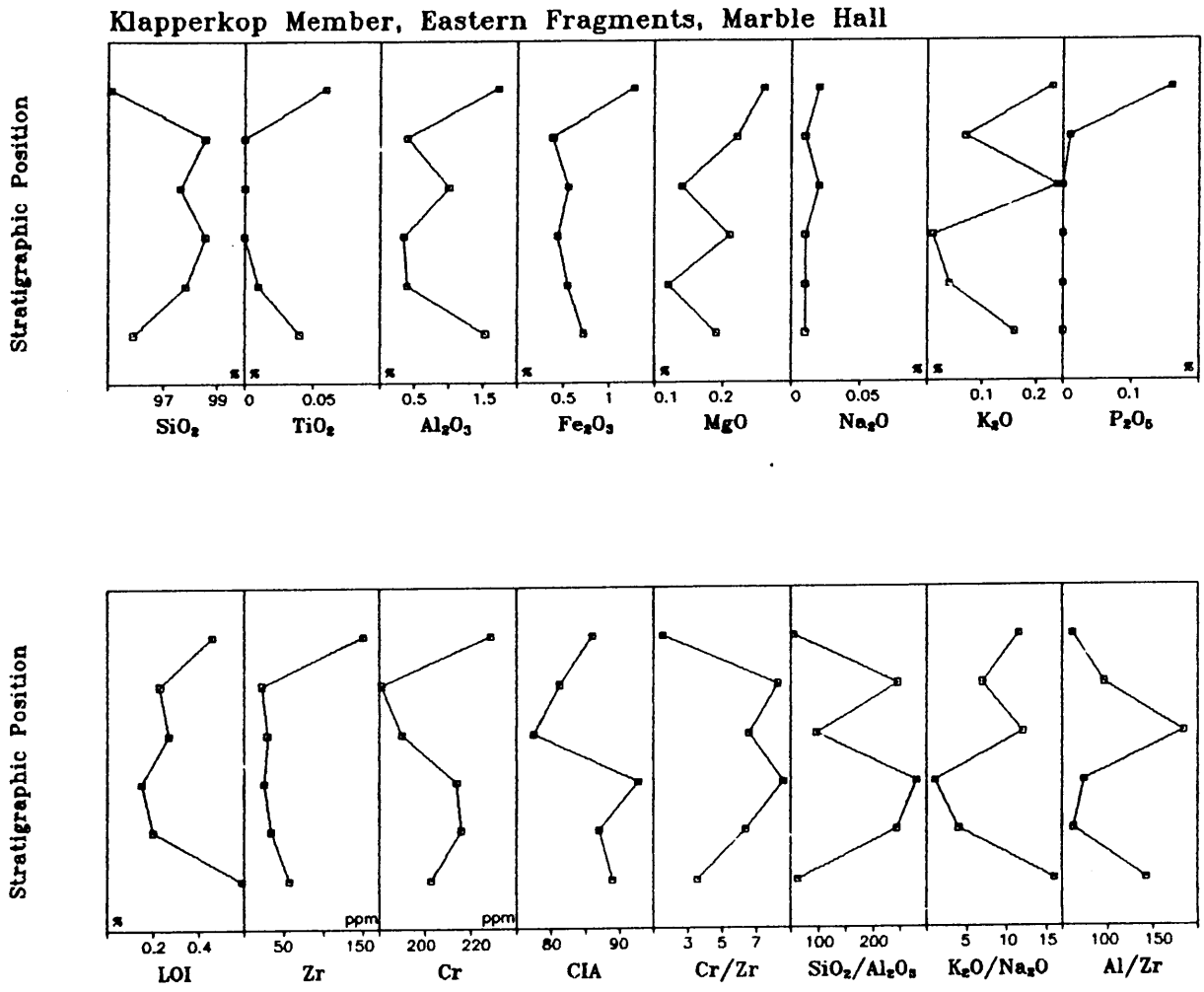

Figure 3.3.3.2: Geochemical profile of the Timeball Hill Quartzites, Marble Hall, eastern fragments. Lithological type: □ = quartzite. Vertical scale = ± 70 in total.

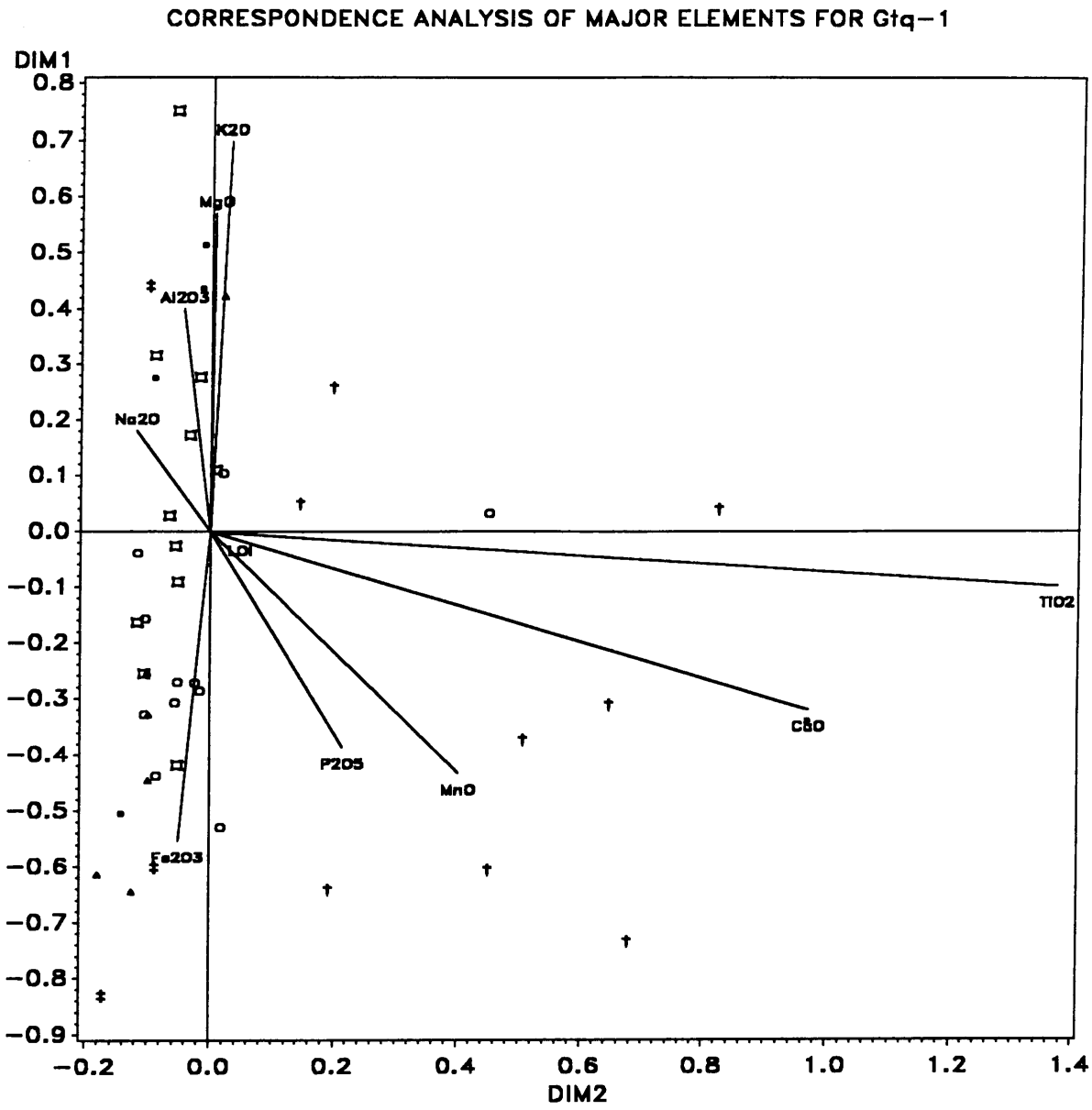

Figure 3.3.3.3: Correspondence analysis of major elements (except SiO_2) of sandstones for the Timeball Hill Quartzites. Symbols for sampling areas: ● (red) = eastern Transvaal; ○ (red) = northeastern Transvaal; □ (violet) = eastern fragments; ◇ (green) = central Transvaal; ▲ (blue) = western Transvaal; † (blue) = western fragments; ‡ (blue) = northwestern Transvaal; ★ (yellow) = Botswana. Definition of sampling areas is shown in Figure 1.5.1. DIM 1 and DIM 2 are the values of the factor loadings of the samples and variables for the first and second factor (see Chapter 2.3.2). Angles between lines connecting a variable and the point (0,0) are proportional to the product moment correlation coefficient of these variables.

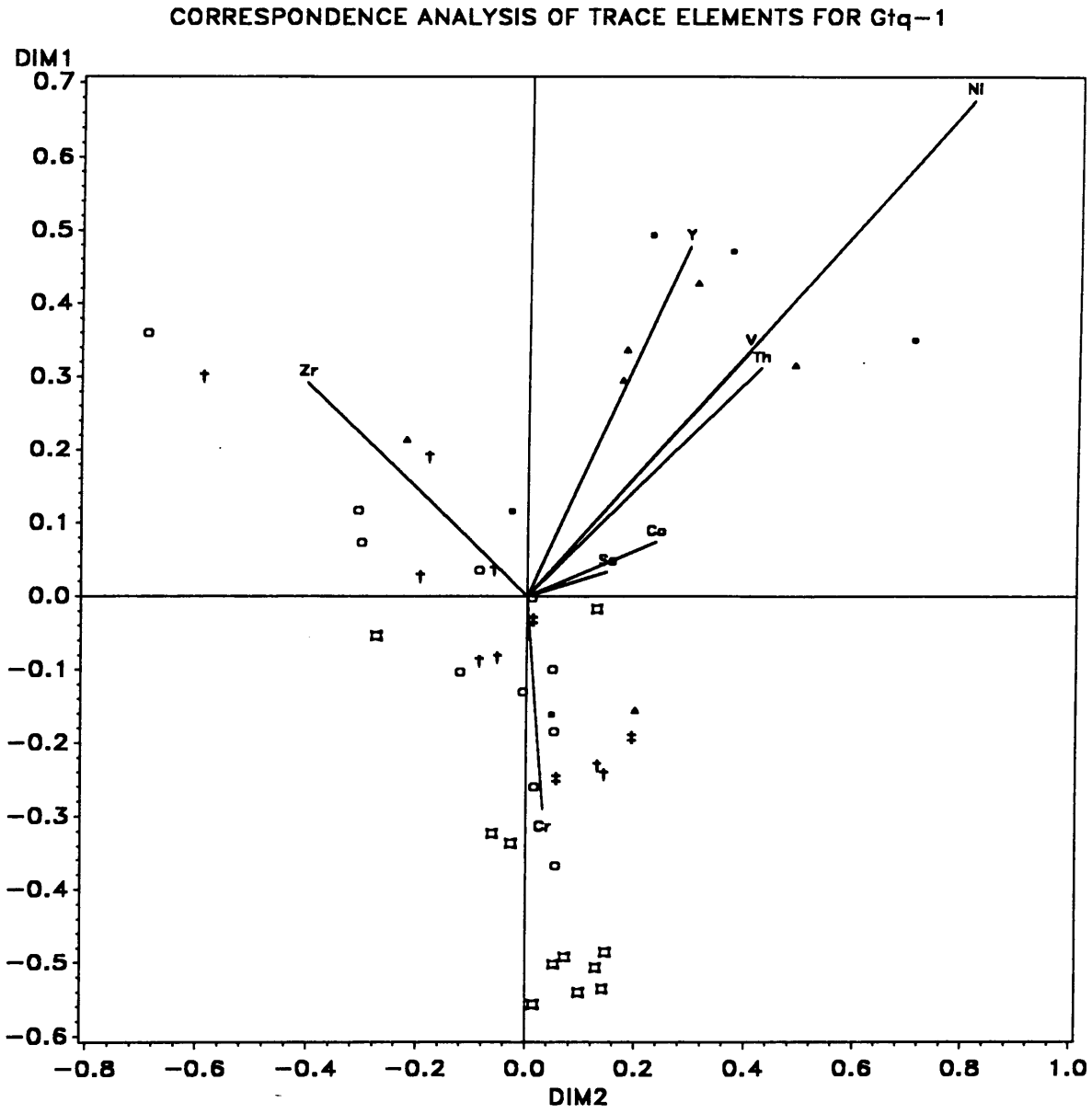

Figure 3.3.3.4: Correspondence analysis of selected trace elements of sandstones for the Timeball Hill Quartzites. Symbols for sampling areas: ● (red) = eastern Transvaal; ○ (red) = northeastern Transvaal; □ (violet) = eastern fragments; ◇ (green) = central Transvaal; ▲ (blue) = western Transvaal; † (blue) = western fragments; ‡ (blue) = northwestern Transvaal; ★ (yellow) = Botswana. Definition of sampling areas is shown in Figure 1.5.1. DIM 1 and DIM 2 are the values of the factor loadings of the samples and variables for the first and second factor (see Chapter 2.3.2). Angles between lines connecting a variable and the point (0,0) are proportional to the product moment correlation coefficient of these variables.

3.3.3.3). The correspondence analysis plot of selected trace elements for the quartzite/sandstone lithotype shows a well defined cluster of the eastern fragment samples (Figure 3.3.3.4). Other clusters are less well defined, although it seems as if a differentiation in broader regional categories is possible: northeastern and northwestern Transvaal samples spread from the position of Zr towards the eastern fragment cluster. Western fragment samples are in the lower part of this trend, close to the eastern fragment cluster. Hence, the observed pattern may indicate a systematical geochemical change from north to south. The bulk of 'southern' samples, i.e. from the western Transvaal and eastern Transvaal sampling areas, cluster in the upper right corner of the plot, thereby further indicating variations on a north-south axis.

3.3.4 Timeball Hill Formation Upper Shale Member

The major element geochemistry of the Upper Timeball Hill Shales (Tables 3.3.4.1, 3.3.4.2 and 3.3.4.4) exhibits deviations from average shale estimates (Table 3.2.1b) for Al_2O_3, CaO, MgO, and Na_2O. The latter three oxides are depleted, while Al_2O_3 is enriched. The P_2O_5-content reaches 2.3 wt.%, although the average content is not significantly higher than average shale estimates. The trace element geochemistry (Table 3.3.4.1) is similar to average shale estimates (Table 3.2.1d). Ga, U, and Th are enriched, Cr and Pb show minor enrichment. Zn, Cu, and Co are slightly depleted, but, as the standard deviations of these elements indicate a substantial uncertainty, it is unclear if these depletions are significant. The REE (Table 3.3.4.4) have a very low variability, especially if it is considered that the average REE-contents were calculated from only five samples containing two petrographical groups ('shale' and 'alternating shale and sandstone'). The LREE-averages (and geometric means) are similar to the Post-Archaean Average Shale (Taylor and McLennan, 1985) and the North American Shale Composite (Gromet et al., 1984; Table 3.2.1d), except for La, which is enriched. The HREE and Eu are slighly depleted compared with the Post-Archaean Average Shale (Taylor and McLennan, 1985). The Σ REE-average (ϕ 186 ppm) indicates a resemblance to the Post-Archaean Average Shale (Taylor and McLennan, 1985, ϕ 185 ppm).

Average element ratios of shales from the Timeball Hill Formation Upper Shale Member are listed in Tables 3.3.4.3 and Tables 3.3.4.4, and can be compared to ratios reported from

Element	n	MEAN	STD ±	GM	MEDIAN	RANGE	VC
SiO_2	124	59.03	5.02	58.82	58.95	38.93 - 76.65	0.09
TiO_2	124	0.70	0.14	0.68	0.68	0.21 - 1.02	0.20
Al_2O_3	124	20.39	3.51	20.05	20.90	8.87 - 32.61	0.17
Fe_2O_3*	124	8.36	2.42	8.06	8.19	4.35 - 21.92	0.29
MnO	124	0.03	0.02	-	0.02	<LLD - 0.11	0.67
MgO	124	0.87	0.64	-	0.85	<LLD - 2.27	0.74
CaO	124	0.29	0.46	-	0.12	<LLD - 3.00	1.59
Na_2O	124	0.62	0.48	-	0.48	<LLD - 3.27	0.77
K_2O	124	3.20	1.12	2.85	3.17	0.05 - 6.87	0.35
P_2O_5	124	0.15	0.23	-	0.10	<LLD - 2.30	1.53
H_2O^-	124	1.20	1.60	1.79	0.78	0.13 - 12.71	1.33
LOI	124	4.56	1.00	4.54	4.59	2.36 - 8.01	0.22
Zn	124	70	33.9	61	71	13 - 171	0.48
Cu	124	36	23.5	29	35	3 - 198	0.65
Ni	124	58	29.4	51	53	10 - 178	0.51
Co	124	12	8.2	8.5	11	<3 - 42	0.68
Ga	124	27	4.7	26	28	10 - 40	0.17
Mo	124	1.4 *)	2.2	-	<LLD	<2 - 10	1.57
Nb	124	17	9.6	16	15	10 - 89	0.57
Zr	124	173	47.3	167	164	51 - 341	0.27
Y	124	34	20.6	31	28	15 - 182	0.61
Sr	124	139	163.7	109	113	6 - 1772	1.18
Rb	124	172	59.2	153	172	<2 - 477	0.34
U	124	7.1	5.6	-	7	<5 - 31	0.79
Th	124	20	5.7	19	20	<5 - 52	0.29
Pb	124	29	36.0	22	25	<5 - 388	1.24
Cr	124	157	74.3	145	154	<14 - 584	0.47
V	124	148	31.6	144	148	20 - 239	0.21
Ba	124	777	441.9	690	681	<16 - 1494	0.57
Sc	124	16	5.5	15	16	<8 - 35	0.34
As	124	12	18.3	-	<LLD	<10 - 104	1.53
S	124	498	1299.2	196	173	<50 - 10780	2.61
Sb	124	1.3 *)	3.9	-	<LLD	<8 - 20	3.00
Sn	124	2.6 *)	5.3	-	<LLD	<8 - 22	2.04
B	36	72	20.7	68	74	21 - 106	0.29

Table 3.3.4.1: Average element concentrations of shales from Upper Timeball Hill Fm.

(n = number of samples; 'MEAN' = arithmetic mean; 'STD ±' = 1 σ standard deviation; 'GM' = geometric mean; 'MEDIAN' = median; 'VC' = variation coefficient; average major element concentrations are reported in weight %, average trace element concentrations in ppm; 'Fe_2O_3*' is all Fe expressed as Fe_2O_3; *) = arithmetic mean below detection limit; LLD = lower limit of detection)

Table 3.3.4.2: Average major element concentrations of shales from the Upper Timeball Hill Formation recalculated to 100 % volatile-free.

Element	n	MEAN	STD ±	RANGE
SiO_2	124	63.00	4.56	47.45 - 80.47
TiO_2	124	0.74	0.15	0.21 - 1.21
Al_2O_3	124	21.81	3.90	9.07 - 35.73
Fe_2O_3*	124	8.94	2.66	4.57 - 23.92
MnO	124	0.03	0.02	0 - 0.12
MgO	124	0.93	0.68	0 - 2.46
CaO	124	0.31	0.49	0 - 3.14
Na_2O	124	0.66	0.51	0 - 3.43
K_2O	124	3.42	1.21	0.05 - 7.53
P_2O_5	124	0.16	0.25	0 - 2.51

Table 3.3.4.3: Average ratios of shales from the Upper Timeball Hill Formation

(NOTE: ratios corrected as described in Chapter 3.1.2)

Ratio	n	MEAN	STD ±	GM	RANGE	VC
CIA	124	80.6	5.0	80.4	60.8 - 97.1	0.06
Fe/V	124	413	166	392	198 - 1521	0.40
K_2O/Na_2O	123	9.7	25.0	6.0	0.04 - 278	2.58
SiO_2/Al_2O_3	124	3.0	1.0	2.9	1.4 - 8.2	0.33
Cr/Th	124	9.9	14.2	7.6	0.3 - 117	1.43
Th/Sc	124	1.32	0.71	1.2	0.26 - 6.51	0.54
Cr/Zr	124	1.00	0.64	0.86	0.06 - 4.64	0.64
Co/Th	124	0.69	0.62	0.49	0.08 - 3.44	0.90
Al_2O_3/TiO_2	124	30.2	6.1	29.5	14.6 - 54.4	0.20
Al_2O_3/K_2O	124	9.9	20.6	7.0	3.5 - 177.4	2.08
K/Rb	124	157	37	154	80 - 415	0.24
K/Ba	124	37	11	34	0.2 - 81	0.30
Ti/Ni	124	94	67	80	11 - 569	0.71
Cr/V	124	1.05	0.42	0.99	0.20 - 3.28	0.40
V/Ni	124	3.32	2.37	2.83	0.80 - 18.70	0.71
Ni/Co	124	7.60	7.66	5.46	1.14 - 41.00	1.01
Zr/Nb	124	11.3	4.3	10.5	1.7 - 32.7	0.38
Th/U	122	2.75	1.05	2.54	0.46 - 6.00	0.38
Ba/Rb	124	7.7	31.0	4.50	1.7 - 346	4.03
Ba/Sr	124	9	13	6	0.1 - 105	1.44
Ba/Th	124	44	38	37	0.8 - 375	0.86
Al/Zr	124	667	186	636	195 - 1071	0.28
Ti/Zr	124	25.5	7.1	24.4	6.1 - 45.0	0.28

Table 3.3.4.4: Average element concentrations and ratios of selected shale samples of the Upper Timeball Hill Formation

(n = number of samples; 'MEAN' = arithmetic mean; 'STD ±' = 1 σ standard deviation; 'GM' = geometric mean; 'MEDIAN' = median; 'VC' = variation coefficient; average major element concentrations (i.e. FeO to S_{XRF}) are reported in weight %, average trace element concentrations in ppm; n.c. = not calculated; subscript N = concentration normalised to chondrite; $Ce/Ce^* = Ce_N/[(La_N + Pr_N)/2]$; Σ REE = sum of REE in ppm; NOTE: ratios corrected as described in Chapter 3.1.2; LLD = lower limit of detection)

Element	n	MEAN	STD ±	GM	MEDIAN	RANGE	VC
FeO	5	4.41	2.68	2.41	4.98	0.10 - 6.69	0.61
Fe_2O_3	5	2.49	3.68	0.52	0.54	0.01 - 8.74	1.48
CO_2	5	0.50	0.26	0.44	0.55	0.22 - 0.81	0.52
C_{org}	5	0.43	0.70	0.18	0.13	0.04 - 1.68	1.63
H_2O^+	5	4.58	0.64	4.54	4.60	3.65 - 5.23	0.14
S_{leco}	5	0.01	0.02		0.003	<LLD - 0.04	2.00
S_{xrf}	5	0.06	n.c.	n.c.	n.c.	n.c.	n.c.
Li	5	105	49	94	101	41 - 169	0.47
La	5	49.8	2.2	49.8	51.2	46.7 - 51.7	0.04
Ce	5	78.2	8.4	77.9	80.0	69.6 - 89.6	0.11
Pr	5	9.1	0.9	9.0	9.2	8.1 - 10.3	0.10
Nd	5	31.1	3.5	30.9	30.9	25.8 - 35.0	0.11
Sm	5	5.0	0.5	5.0	5.3	4.2 - 5.3	0.10
Eu	5	0.8	0.16	0.8	0.9	0.6 - 1.0	0.20
Gd	5	3.5	0.6	3.5	3.7	2.9 - 4.2	0.17
Tb	5	0.6	0.11	0.6	0.6	0.4 - 0.7	0.18
Dy	5	3.4	0.6	3.3	3.4	2.7 - 4.2	0.18
Er	5	2.0	0.3	2.0	2.0	1.7 - 2.5	0.15
Tm	5	0.3	0.05	0.3	0.3	0.3 - 0.4	0.17
Yb	5	2.3	0.3	2.3	2.3	2.0 - 2.8	0.13
La/Sc	5	4.22	1.61	3.98	3.89	2.42 - 6.47	0.38
Th/La	5	0.41	0.02	0.41	0.41	0.39 - 0.43	0.05
Ba/La	5	10.9	1.6	10.8	11.0	8.9 - 13.2	0.15
LREE/HREE	5	14.6	2.2	14.5	15.0	11.7 - 17.3	0.15
K2O/ΣREE	5	161	17	160	158	142 - 181	0.11
Gd_N/Yb_N	5	1.22	0.10	1.21	1.22	1.07 - 1.32	0.08
La_N/Sm_N	5	6.34	0.88	6.29	6.08	5.55 - 7.75	0.14
Ce/Ce*	5	0.810	0.075	0.807	0.781	0.733 - 0.930	0.09
Eu/Eu*	5	0.566	0.072	0.562	0.582	0.449 - 0.644	0.13
C_{org}/S	5	4.56	3.48	3.62	3.55	1.14 - 10.41	0.76
ΣREE	5	186	8.2	186	189	174 - 195	0.04

average shale estimates (Table 3.2.1e). The K_2O/Na_2O-ratio is significantly higher than the value for Post-Archaean Average Shale (Taylor and McLennan, 1985). Th/U and Ba/Th are depleted and La/Sc is enriched compared to Post-Archaean Average Shale and Archaean Average Shale (Taylor and McLennan, 1985), and to Pontiac Average Metamorphic Shale (Feng et al., 1993). The Cr/V-average is similar to the value reported for the Post-Archaean Average Shale (Taylor and McLennan, 1985), Ni/Co resembles more Early Archaean Average Shale and Late Archaean Average Shale (Taylor and McLennan, 1985). V/Ni is significantly higher than all averages reported by Taylor and McLennan (1985). The LREE/HREE-average is higher than the corresponding value for the Post-Archaean Average Shale (Taylor and McLennan, 1985), largely due to an increased La-content. The Eu-anomaly (expressed as Eu/Eu*) is steeper in the Upper Timeball Hill Formation than in the Post-Archaean Average Shale (Taylor and McLennan, 1985), i.e., the Eu/Eu*-average is smaller than the reported value.

The average element concentration of 'alternating shale and sandstone' and 'sandstone' lithotypes is given in Appendix 2a. Both lithotypes have a similar major and trace element geochemistry. It should be noted that the major element geochemistry of the sandstone lithotype resembles rather average shale estimates (Table 3.2.1b) than average sandstone estimates (Table 3.2.1c).

Two complete and two partial geochemical profiles were sampled in the Upper Timeball Hill Shales (for location of profiles see Fig. 1.5.5). The Botswana bore-core geochemical profile (Figure 3.3.4.1) contains three petrographic types, shale, alternating shale and sandstone, and sandstone. The geochemical pattern of the profile is divided into two parts, a lower part consisting of the coarser-grained fraction and an upper part comprising fine-grained material. SiO_2, MgO, Zr, Cr, Zn, and the ratios Cr/Zr, Cr/Th, and Ti/Zr exhibit an obvious change in content or pattern at the transition between lower and upper parts of the profile. MgO, Zn, and Cr/Th decrease in each part of the profile, the transition being marked by an increase. SiO_2, Zr, Cr, Cr/Zr and Ti/Zr are relativly stable in each part (except for the four lowermost samples in the lower part), but differ in their respective contents. Na_2O and K/Rb decrease, K_2O/Na_2O increases throughout the profile. Al_2O_3 only increases in the lower part and is fairly stable in the upper part.

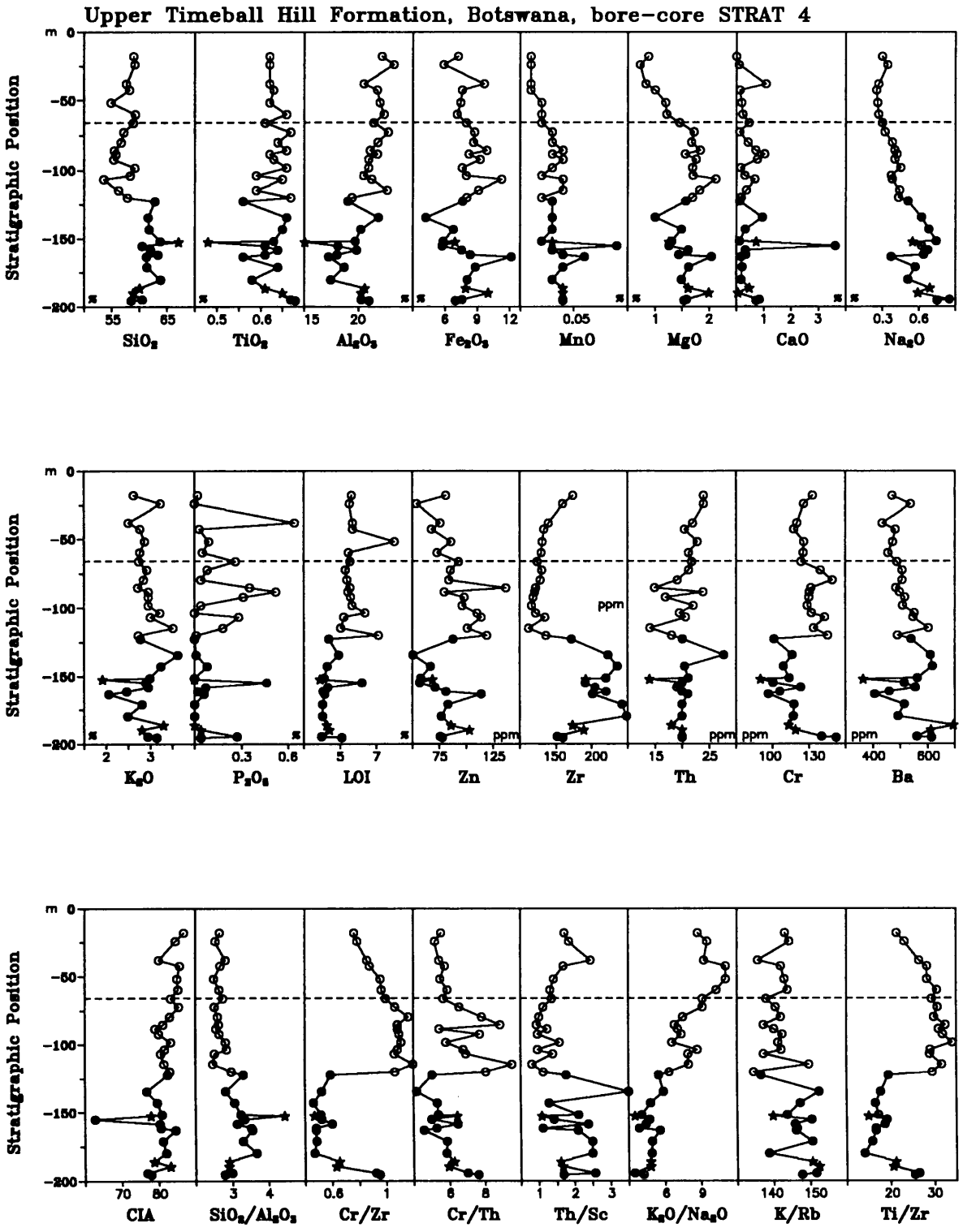

Figure 3.3.4.1: Geochemical profile of the Timeball Hill Formation Upper Shale Member, borehole, Botswana. Lithological types: ★ = sandstone; ○ = shale; ● = alternating shale and sandstone. Dashed line = oxidation base of borehole.

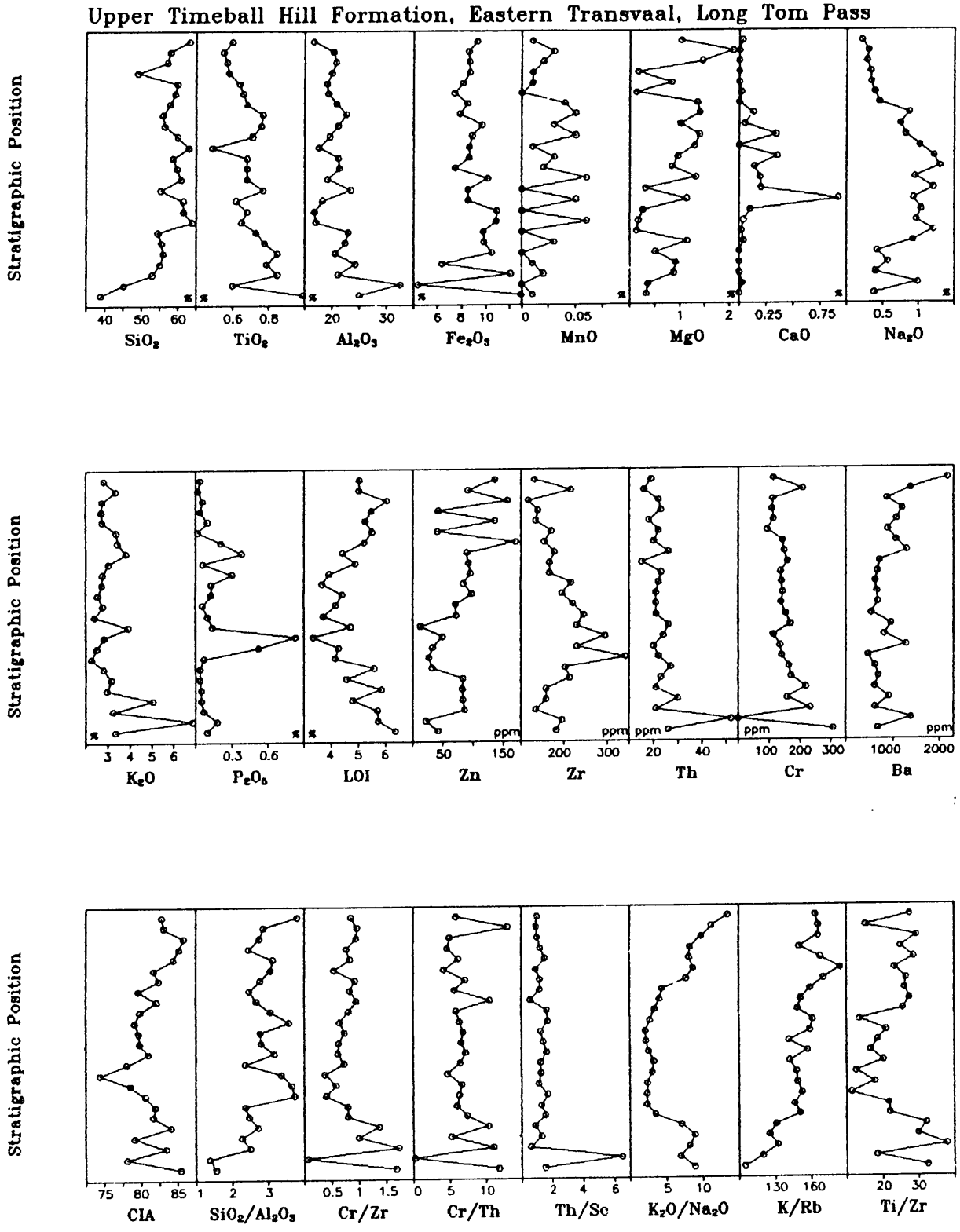

Figure 3.3.4.2: Geochemical profile of the Timeball Hill Formation Upper Shale Member, Long Tom Pass, eastern Transvaal. Lithological type: ○ = shale. Vertical scale = ± 600 m in total.

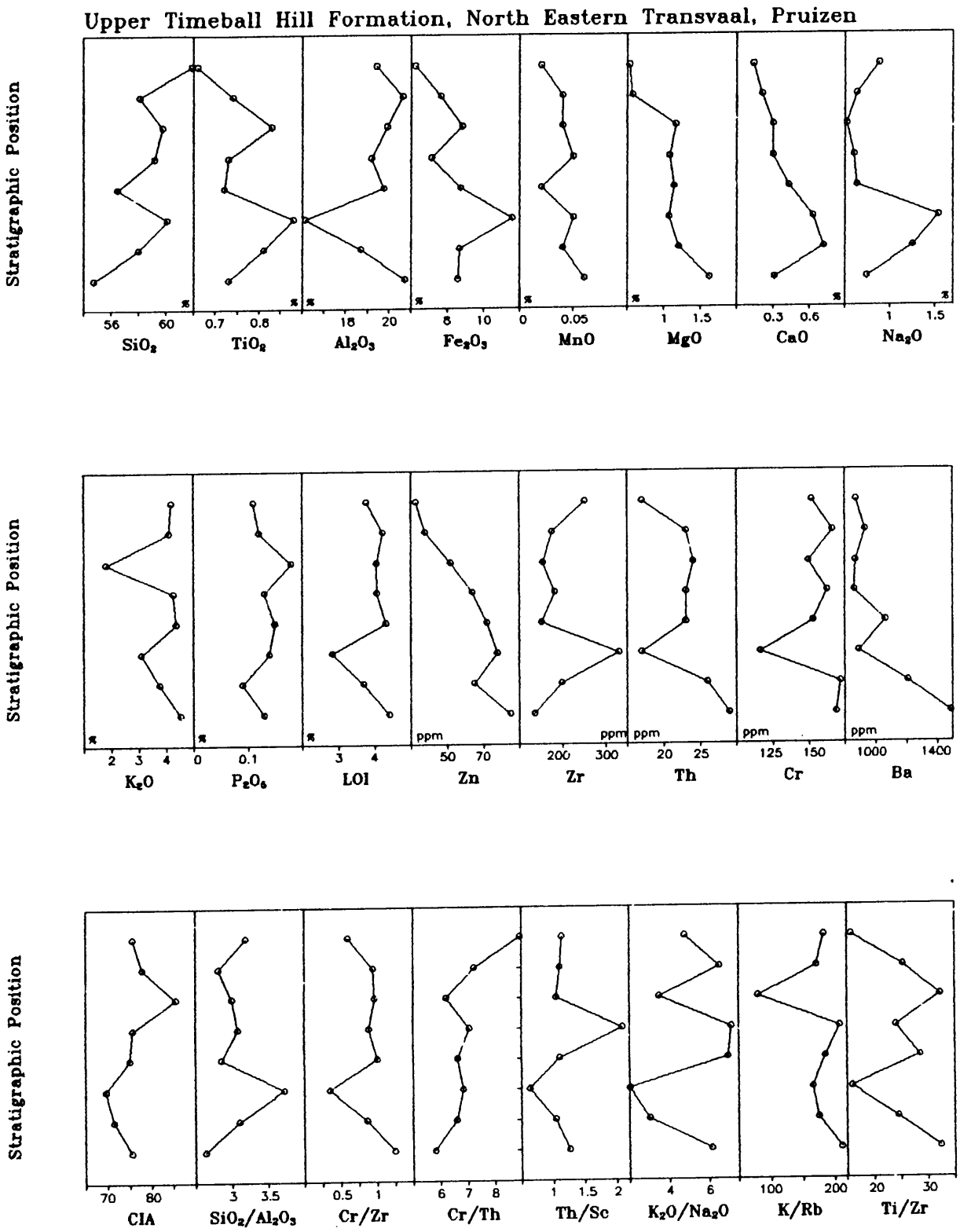

Figure 3.3.4.3: Partial geochemical profile of the Timeball Hill Formation Upper Shale Member, Pruizen, northeastern Transvaal. Lithological type: ○ = shale. Vertical scale = ± 80 m in total.

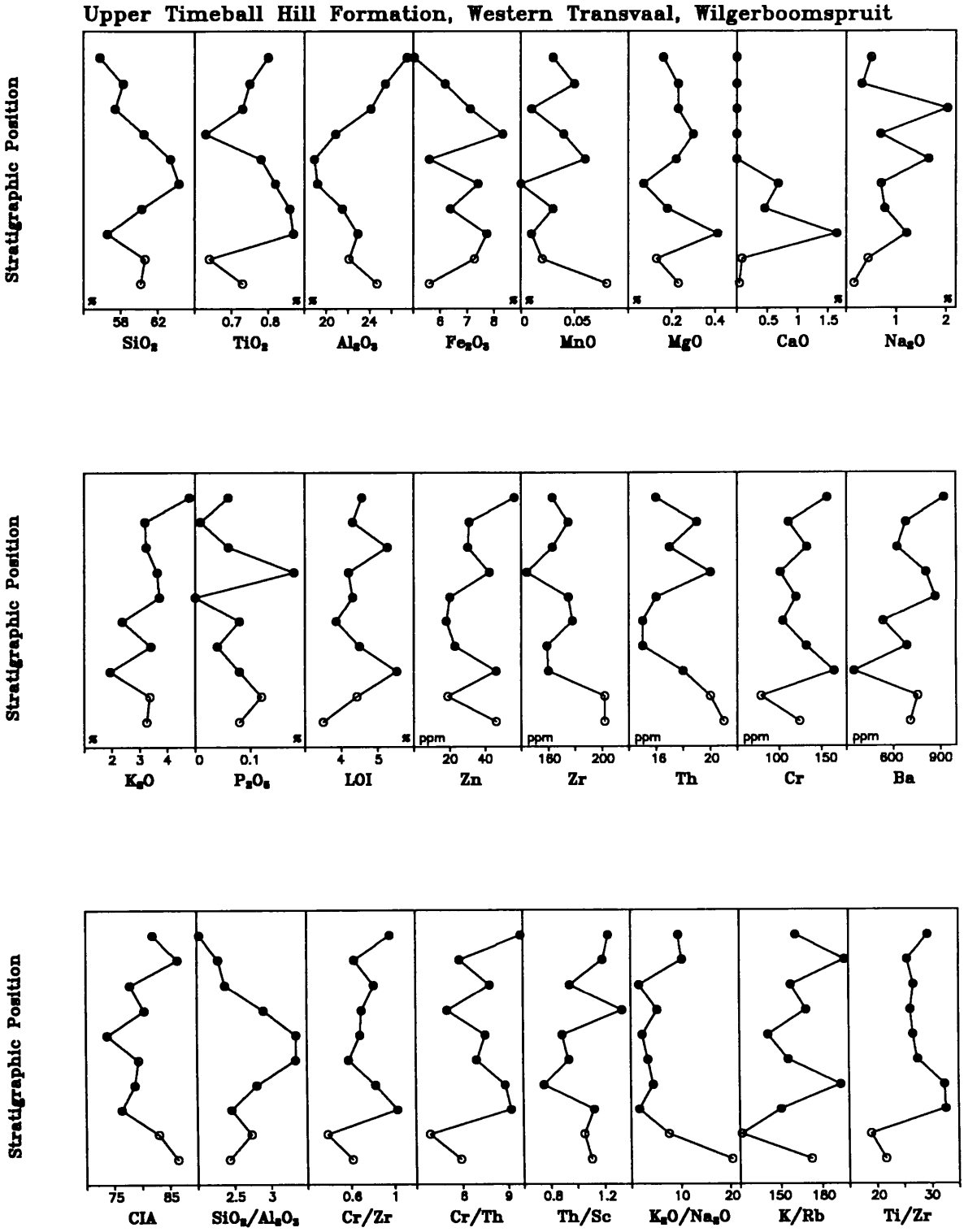

Figure 3.3.4.4: Partial geochemical profile of the Timeball Hill Formation Upper Shale Member, Wilgerboomspruit, western Transvaal. Lithological types: ○ = shale; ● = andalusite shale. Vertical scale = ± 100 m in total.

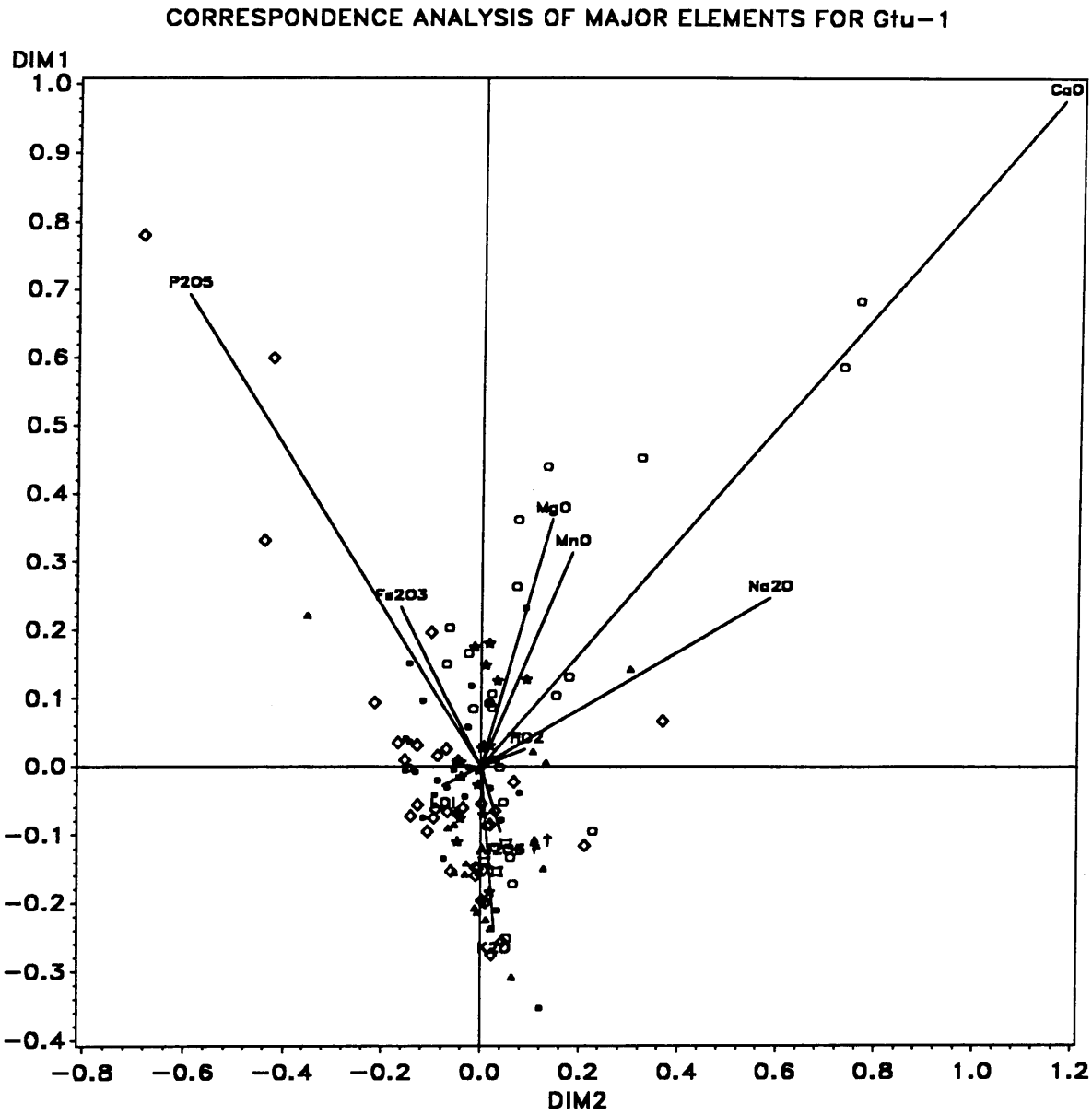

Figure 3.3.4.5: Correspondence analysis of major elements (except SiO_2) of shales for the Timeball Hill Formation Upper Shale Member. Symbols for sampling areas: ● (red) = eastern Transvaal; ○ (red) = northeastern Transvaal; □ (violet) = eastern fragments; ◇ (green) = central Transvaal; ▲ (blue) = western Transvaal; † (blue) = western fragments; ‡ (blue) = northwestern Transvaal; ★ (yellow) = Botswana. Definition of sampling areas is shown in Figure 1.5.1. DIM 1 and DIM 2 are the values of the factor loadings of the samples and variables for the first and second factor (see Chapter 2.3.2). Angles between lines connecting a variable and the point (0,0) are proportional to the product moment correlation coefficient of these variables.

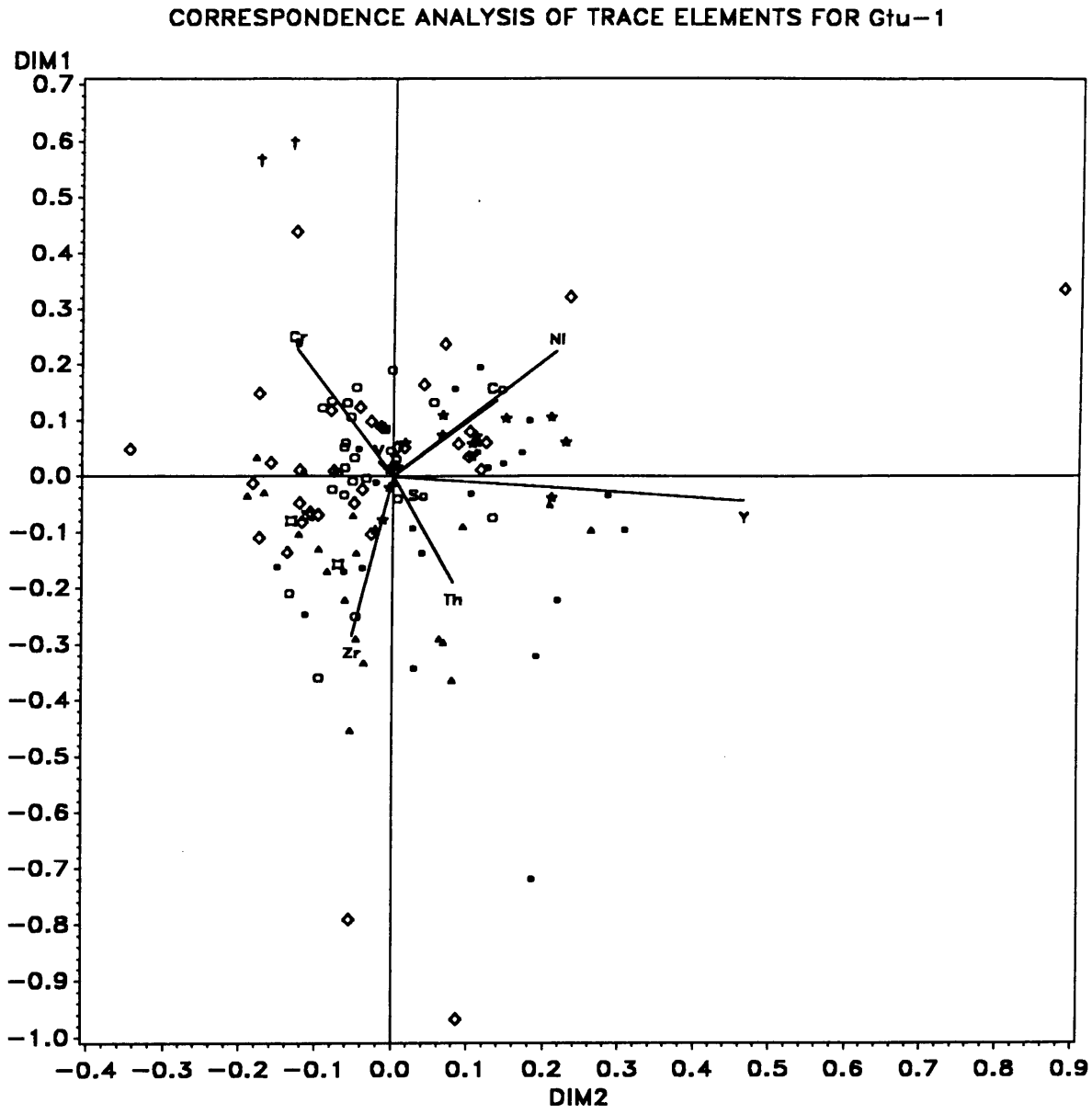

Figure 3.3.4.6: Correspondence analysis of selected trace elements of shales for the Timeball Hill Formation Upper Shale Member. Symbols for sampling areas: ● (red) = eastern Transvaal; ○ (red) = northeastern Transvaal; □ (violet) = eastern fragments; ◇ (green) = central Transvaal; ▲ (blue) = western Transvaal; † (blue) = western fragments; ‡ (blue) = northwestern Transvaal; ★ (yellow) = Botswana. Definition of sampling areas is shown in Figure 1.5.1. DIM 1 and DIM 2 are the values of the factor loadings of the samples and variables for the first and second factor (see Chapter 2.3.2). Angles between lines connecting a variable and the point (0,0) are proportional to the product moment correlation coefficient of these variables.

The eastern Transvaal geochemical profile (Figure 3.3.4.2) only contains shales as a petrographical type. The approximate thickness of the profile is 600 m, including diabase sills. The upper part of the profile can be correlated with profile 13 of Schreiber (1990, p. 36). The profile starts with a ferrugenous shale and shows some variability for some elements and ratios in the four lowermost samples. TiO_2 and Al_2O_3 decrease, whereas K/Rb increases throughout the profile. Other patterns are indistinct or only partialy developed, e.g. the decrease of Na_2O in the upper part of the profile. MgO and Zn have a high variability close to the top of the profile.

The northeastern Transvaal geochemical profile (Figure 3.3.4.3) contains only shales. The profile is taken from the uppermost part of the Upper Timeball Hill Shale Member and has an approximate thickness of 80 m. MgO, CaO, Zn, and Ba exhibit an overall decrease, SiO_2 and Cr/Th an increasing pattern upwards. The increase in Cr/Th might be not substantial if the scale for Cr/Th is considered. Cr and Th show a fairly well defined positive correlation, diametrically opposed to the trend for Zr.

The western Transvaal geochemical profile (Figure 3.3.4.4) has an approximate thickness of 100 m and is taken from the middle part of the Upper Timeball Hill Shale Member. The profile contains two shale types, shale and andalusite-shale. The profile shows no apparent trends. The element contents and ratios are relatively stable, if the scale is considered. Only Zr and Ti/Zr are sensitive to the petrographic differences.

Correspondence analysis for major and trace elements (Figure 3.3.4.5 and 3.3.4.6) could not establish geographic differences with certainty. Some degree of separation is shown for the shales of the northern sampling areas (northeastern Transvaal and Botswana) compared to the southern sampling areas (central, western and eastern Transvaal) (Figure 3.3.4.5).

3.3.5 Boshoek Formation

The major element geochemistry of the Boshoek Formation sandstones (Table 3.3.5.1) is similar to average sandstone estimates (Table 3.2.1c), although strongly depleted in CaO and Na_2O, and slightly depleted in MgO and K_2O. Base metals, Cr, U, Ba, and Mo are enriched

Element	n	MEAN	STD ±	GM	MEDIAN	RANGE	VC
SiO_2	5	83.52	10.83	82.90	89.30	65.46 - 91.47	0.13
TiO_2	5	0.19	0.17	0.14	0.16	0.03 - 0.47	0.90
Al_2O_3	5	6.26	4.62	5.16	4.01	2.48 - 13.86	0.74
Fe_2O_3*	5	4.99	2.72	4.28	5.66	1.84 - 7.79	0.55
MnO	5	0.01	0.01	-	0.01	<LLD - 0.03	1.00
MgO	5	0.75	0.85	-	0.29	<LLD - 2.00	1.13
CaO	5	0.06	0.13	-	<LLD	<LLD - 0.30	2.17
Na_2O	5	0.07	0.08	-	0.04	<LLD - 0.21	1.14
K_2O	5	0.96	1.44	-	0.36	<LLD - 3.44	1.50
P_2O_5	5	0.03	0.03	-	0.03	<LLD - 0.07	1.00
H_2O^-	5	0.68	0.92	0.34	0.34	0.06 - 2.30	1.35
LOI	5	2.13	0.98	1.95	2.02	1.11 - 3.43	0.46
Zn	5	34	27.4	26	21	10 - 76	0.81
Cu	5	24	14.5	-	27	<3 - 38	0.60
Ni	5	24	20.1	17	16	4 - 57	0.84
Co	5	9.0	3.4	8.5	7	6 - 14	0.38
Ga	5	7.2	7.1	-	5	<3 - 18	0.99
Mo	5	4.4	4.0	-	7	<2 - 8	0.91
Nb	5	7.6	4.8	6.7	5	5 - 16	0.63
Zr	5	127	104.3	100	80	39 - 302	0.82
Y	5	10	4.9	9.2	8	6 - 18	0.49
Sr	5	18	16.1	14	13	5 - 46	0.89
Rb	5	58	93.9	-	20	<2 - 223	1.62
U	5	3.6 *)	3.5	-	5	<5 - 8	0.97
Th	5	8.0	5.8	-	8	<5 - 16	0.73
Pb	5	23	19.6	-	17	<5 - 52	0.85
Cr	5	141	21.5	140	141	114 - 174	0.15
V	5	67	40.8	55	68	22 - 107	0.61
Ba	5	326	364.8	161	140	38 - 858	1.12
Sc	5	2.8 *)	6.3	-	<LLD	<8 - 14	2.25
As	5	2.6 *)	5.8	-	<LLD	<10 - 13	2.23
S	5	153	115.0	-	171	<50 - 308	0.75
Sb	5	2.2 *)	4.9	-	<LLD	<8 - 11	2.23
Sn	5	-	-	-	-	<LLD	-
B	2	9.0	-	-	-	8 - 10	-

Table 3.3.5.1: Average element concentrations of sandstones from the Boeshoek Formation.

(n = number of samples; 'MEAN' = arithmetic mean; 'STD ±' = 1 σ standard deviation; 'GM' = geometric mean; 'MEDIAN' = median; 'VC' = variation coefficient; average major element concentrations are reported in weight %, average trace element concentrations in ppm; 'Fe_2O_3*' is all Fe expressed as Fe_2O_3; *) = arithmetic mean below detection limit; LLD = lower limit of detection)

Table 3.3.5.2: Average ratios of Boshoek Formation sandstones

(NOTE: ratios are not corrected, i.e. a sample was excluded from calculation of the average ratio if one or both elements are below the detection limit; n.c. = not calculated)

Ratio	n	MEAN	STD ±	GM	RANGE	VC
CIA	5	89.4	9.5	89.0	75.0 - 98.3	0.11
SiO_2/Al_2O_3	5	19.9	12.3	16.1	4.7 - 36.0	0.62
lg SiO_2/Al_2O_3	5	1.22	n.c.	n.c.	n.c.	n.c.
K_2O/Na_2O	3	19.1	11.7	16.8	9.0 - 32.0	0.61
lg Na_2O/K_2O	3	-1.22	n.c.	n.c.	n.c.	n.c.
Ti/Zr	5	8.5	2.8	8.1	4.6 - 12.0	0.33
Ti/Cr	5	8.2	7.4	5.8	1.3 - 20.7	0.90
Al/Zr	5	276	39	273	240 - 337	0.14
Al_2O_3/TiO_2	5	42.5	23.8	38.3	22.6 - 82.7	0.56
Al_2O_3/K_2O	4	20.9	27.5	11.8	4.0 - 62.0	1.32
K/Rb	4	153	19	152	128 - 170	0.12
K/Ba	4	20	11	17	9 - 33	0.55
K/Sr	4	345	266	215	30 - 621	0.77

compared with average sandstone estimates (Table 3.2.1d), while Zr and Y are depleted. The expressiveness of the statistical parameters presented in Tables 3.3.5.1 and 3.3.5.2 is limited, as only five samples were taken from the Boshoek Formation. The statistical parameters were calculated to ensure consistency in the way of presentation.

3.3.6 Hekpoort Formation

The major element geochemistry of the shales interlayered and immediately overlying (= an inferred palaeosol; Button, 1973; Holland, 1984) the Hekpoort Formation (Tables 3.3.6.1 and 3.3.6.2) show major deviations from average shale estimates (Table 3.2.1b). Al_2O_3 is strongly enriched, TiO_2 moderately so, and SiO_2, MgO, MnO, and Na_2O are depleted. The average CaO-content is higher than average shale estimates (Table 3.2.1b). However, the average CaO-content is biased by one extreme value of 15.08 wt.%. As the average CaO-content of the Hekpoort Formation shales without the extreme value is only 0.61 wt.% and the median of the total population (n = 13) is only 0.18 wt.% (Table 3.3.6.1), CaO is considered to be generally depleted compared to average shale estimates (Table 3.2.1b). The average trace element contents of the Hekpoort Formation shales (Table 3.3.6.1) exhibit depletion for Zn, Co, As, and, moderate depletion for Pb. The trace elements Ni, Y, Cr, V, Sc, and B are stronly enriched, and U, Th, and Ga moderately so. Cr and Ni have average contents similar to Archaean Average Shale (Taylor and McLennan, 1985).

Average element ratios of the Hekpoort Formation shales are listed in Table 3.3.6.3. The K_2O/Na_2O-ratio is greatly increased compared to Post-Archaean Average Shale (Taylor and McLennan, 1985, see Table 3.2.1e). The Th/U-ratio is significantly lower than values reported for either Post-Archaean Average Shale and Archaean Average Shale (Taylor and McLennan, 1985). The Th/Sc-average of the Hekpoort Formation lies between estimates for Post-Archaean Average Shale and Archaean Average Shale (Taylor and McLennan, 1985). The trace element ratios Cr/V, V/Ni and Ni/Co exhibit no clear pattern. Cr/V resembles Post-Archaean Average Shale (Taylor and McLennan, 1985), V/Ni is higher than reported values for Post-, Early and Late Archaean Average Shale (Taylor and McLennan, 1985), and Ni/Co is similar to Early Archaean Average Shale (Taylor and McLennan, 1985).

Sandstones occur only occasionally in the Hekpoort Formation. The average composition of Hekpoort Formation sandstones is listed in Appendix 2a. The Hekpoort Formation sandstones have relatively low average SiO_2-contents, and are enriched in Al_2O_3 and Fe_2O_3, and strongly so in Cr, Cu, Co, Ni and V compared to average sandstone estimates (Tables 3.2.1 c and d). A geochemical profile of a borehole in Botswana is shown in Figure 3.3.6.1. The

Element	n	MEAN	STD ±	GM	MEDIAN	RANGE	VC
SiO_2	13	53.04	6.25	52.69	54.60	44.33 - 62.87	0.12
TiO_2	13	1.09	0.41	0.95	0.99	0.51 - 1.90	0.38
Al_2O_3	13	27.15	8.04	24.76	25.29	14.99 - 37.51	0.30
Fe_2O_3*	13	6.84	3.59	4.33	7.22	1.39 - 12.33	0.53
MnO	13	0.04	0.07	-	0.02	<LLD - 0.25	1.75
MgO	13	1.02 [1)]	1.44	-	0.40	<LLD - 5.23	1.41
CaO	13	1.72 [2)]	4.31	-	0.18	<LLD - 15.08	2.51
Na_2O	13	0.57	0.49	-	0.39	<LLD - 1.32	0.86
K_2O	13	3.31	2.31	2.20	2.95	0.04 - 8.04	0.70
P_2O_5	13	0.11	0.06	0.09	0.10	0.01 - 0.23	0.55
H_2O^-	13	0.26	0.17	0.21	0.18	0.07 - 0.55	0.65
LOI	13	4.36	1.95	3.96	4.38	1.70 - 8.70	0.45
Zn	13	35	39.9	23	15	8 - 148	1.14
Cu	13	41	46.4	23	26	3 - 165	1.13
Ni	13	92	81.4	76	78	38 - 354	0.89
Co	13	12	12.4	7	8	<3 - 38	1.03
Ga	13	28	6.3	27	28	14 - 37	0.23
Mo	13	1.2 *)	2.1	-	<LLD	<2 - 7	1.75
Nb	13	15	4.1	15	15	6 - 20	0.27
Zr	13	206	61.6	195	229	76 - 295	0.30
Y	13	68 [3)]	108.3	44	36	14 - 426	1.59
Sr	13	128	125.2	94	96	28 - 508	0.98
Rb	13	167	115.4	106	135	<2 - 407	0.69
U	13	6.9	3.6	-	8	<5 - 11	0.52
Th	13	20	5.8	19	20	8 - 26	0.29
Pb	13	17	15.6	11	14	<5 - 55	0.92
Cr	13	201	128.8	159	175	35 - 459	0.64
V	13	307	178.3	270	253	148 - 694	0.58
Ba	13	542	464.1	415	414	75 - 1945	0.86
Sc	13	37	19.2	32	35	14 - 83	0.52
As	13	1.4 *)	5.0	-	<LLD	<10 - 18	3.57
S	13	289	360.2	170	146	<50 - 1296	1.25
Sb	13	2.4 *)	5.8	-	<LLD	<8 - 16	2.42
Sn	13	3.5 *)	5.6	-	<LLD	<8 - 14	1.60
B	3	264	32.1	263	281	227 - 284	0.12

Table 3.3.6.1: Average element concentrations of shales from the Hekpoort Formation

(n = number of samples; 'MEAN' = arithmetic mean; 'STD ±' = 1 σ standard deviation; 'GM' = geometric mean; 'MEDIAN' = median; 'VC' = variation coefficient; average major element concentrations are reported in weight %, average trace element concentrations in ppm; 'Fe_2O_3*' is all Fe expressed as Fe_2O_3; *) = arithmetic mean below detection limit; LLD = lower limit of detection). 1) ϕ MgO without extreme value of 5.23 wt.% = 0.67 wt.%; 2) ϕ CaO without extreme value of 15.08 wt.% = 0.61 wt.%;

Table 3.3.6.2: Average major element concentrations of shales from the Hekpoort Formation recalculated to 100 % volatile-free.

ELEMENT	NO.	MEAN	STD ±	RANGE
SiO_2	13	55.83	5.94	48.33 - 64.48
TiO_2	13	1.15	0.43	0.52 - 1.98
Al_2O_3	13	28.71	8.78	15.33 - 39.17
Fe_2O_3*	13	7.23	3.79	1.46 - 12.61
MnO	13	0.04	0.07	0 - 0.26
MgO	13	1.06	1.47	0 - 5.35
CaO	13	1.77	4.43	0 - 15.52
Na_2O	13	0.59	0.49	0 - 1.35
K_2O	13	3.49	2.41	0.04 - 8.40
P_2O_5	13	0.12	0.07	0.01 - 0.25

Table 3.3.6.3: Average ratios of the shales in the Hekpoort Formation

(NOTE: ratios corrected as described in Chapter 3.1.2)

Ratio	n	MEAN	STD ±	GM	RANGE	VC
CIA	13	78.9	16.6	76.7	36.7 - 94.0	0.21
Fe/V	13	228	160	147	17 - 475	0.70
K_2O/Na_2O	11	7.1	3.8	5.9	0.9 - 15.8	0.54
SiO_2/Al_2O_3	13	2.2	0.9	2.0	1.2 - 3.7	0.41
Cr/Th	13	10.6	8.0	8.6	3.5 - 28.7	0.76
Th/Sc	13	0.72	0.55	0.58	0.24 - 1.86	0.76
Cr/Zr	13	0.99	0.65	0.82	0.32 - 2.37	0.66
Co/Th	13	0.75	0.99	0.45	0.15 - 3.80	1.32
Al_2O_3/TiO_2	13	25.9	4.5	25.5	19.7 - 34.1	0.17
Al_2O_3/K_2O	13	39.7	107.8	11.8	4.0 - 398.3	2.72
K/Rb	13	165	17.5	164	130 - 191	0.11
K/Ba	13	54	26.2	44	4.4 - 89.8	0.49
Ti/Ni	13	93	40.2	81	12 - 176	0.43
Cr/V	13	0.82	0.57	0.59	0.15 - 1.75	0.70
V/Ni	13	4.36	2.52	3.57	0.42 - 9.69	0.58
Ni/Co	13	12.68	10.68	8.99	2.47 - 31.44	0.84
Zr/Nb	13	13.5	2.0	13.4	10.3 - 17.9	0.15
Th/U	13	2.68	1.04	2.52	1.60 - 4.60	0.39
Ba/Rb	13	6.1	9.7	3.7	1.6 - 37.7	1.59
Ba/Sr	13	6.3	4.9	4.4	0.2 - 20.5	0.78
Ba/Th	13	28	23	22	9 - 97	0.82
Al/Zr	13	729	197	706	489 - 1109	0.27
Ti/Zr	13	32.2	7.4	31.3	20.1 - 40.2	0.23

borehole was drilled near Ramotswa (see Fig. 1.5.7 for location of profile), where the Hekpoort Formation has an approximate thickness of 400m (Key, 1983). The profile comprises the upper third of the Hekpoort Formation in this area. A detailed lithological description of the bore-core is given by Key (1983). The bore-core samples comprise four petrographic lithotypes (Key, 1983), mafic to andesitic volcanics, sandstones, shales and 'felsic' rocks. The geochemical pattern is generally characterised by these differences in petrography and exhibits individual trends for each type. The volcanic unit at the bottom of the profile (below 100 m depth) shows an overall upward decrease in SiO_2. The uppermost five volcanic samples in this basal volcanic unit have an unusual character, exhibiting a sharp increase in TiO_2, Al_2O_3, K_2O, Zr, Cr and Ba, and a strong depletion in MnO, MgO, CaO and Zn compared to the underlying volcanics (Fig. 3.3.6.1). MnO, LOI, and Zn are strongly enriched in the sample immediately below these five volcanic samples. Fe_2O_3 is variable and Na_2O and Th increase moderately in the top five volcanic samples. The division of the basal volcanic unit into a geochemically distinct upper (= uppermost five samples) and lower part is mirrored by the CIA, i.e., the ratio of immobile to mobile elements. It is noteworthy, that Ti/Zr and Th/Sc, i.e., ratios of immobile elements, show no separation into an upper and lower part in the basal volcanic unit.

The sandstone samples (70-100 m below surface), which include an interlayered volcanic rock sample, are characterised by relatively low SiO_2-contents, and an increase of Fe_2O_3 (up to 30 wt.%) towards their top. Key (1983) describes the sandstones as volcaniclastic, and the interlayered volcanic rock as an andesite with lenticular shaped clasts of felsic material and reaction rims around the clasts.

The overlying shales (50-70 m below surface) have a consistent geochemical pattern, with only minor changes in element contents. SiO_2, Zr and Cr decrease moderately upwards, and Ti/Zr increases moderately towards the top of the shales. The uppermost lithology, 'felsic rock' according to Key (1983), is difficult to evaluate, as geochemical differences from the underlying shales are only apparent for SiO_2, K_2O, Ba, and the K_2O/Na_2O-ratio. On an overall geochemical basis, it might not thus be appropriate to distinguish between 'felsic rock' and shale. Whereas specific volcanic features are not apparent from the description by Key (1983) and were not encountered in the present investigation, clastic sedimentary features like fine- to medium-scaled bedding are equally unsuitable to exclude the volcanic association inferred by Key (1983).

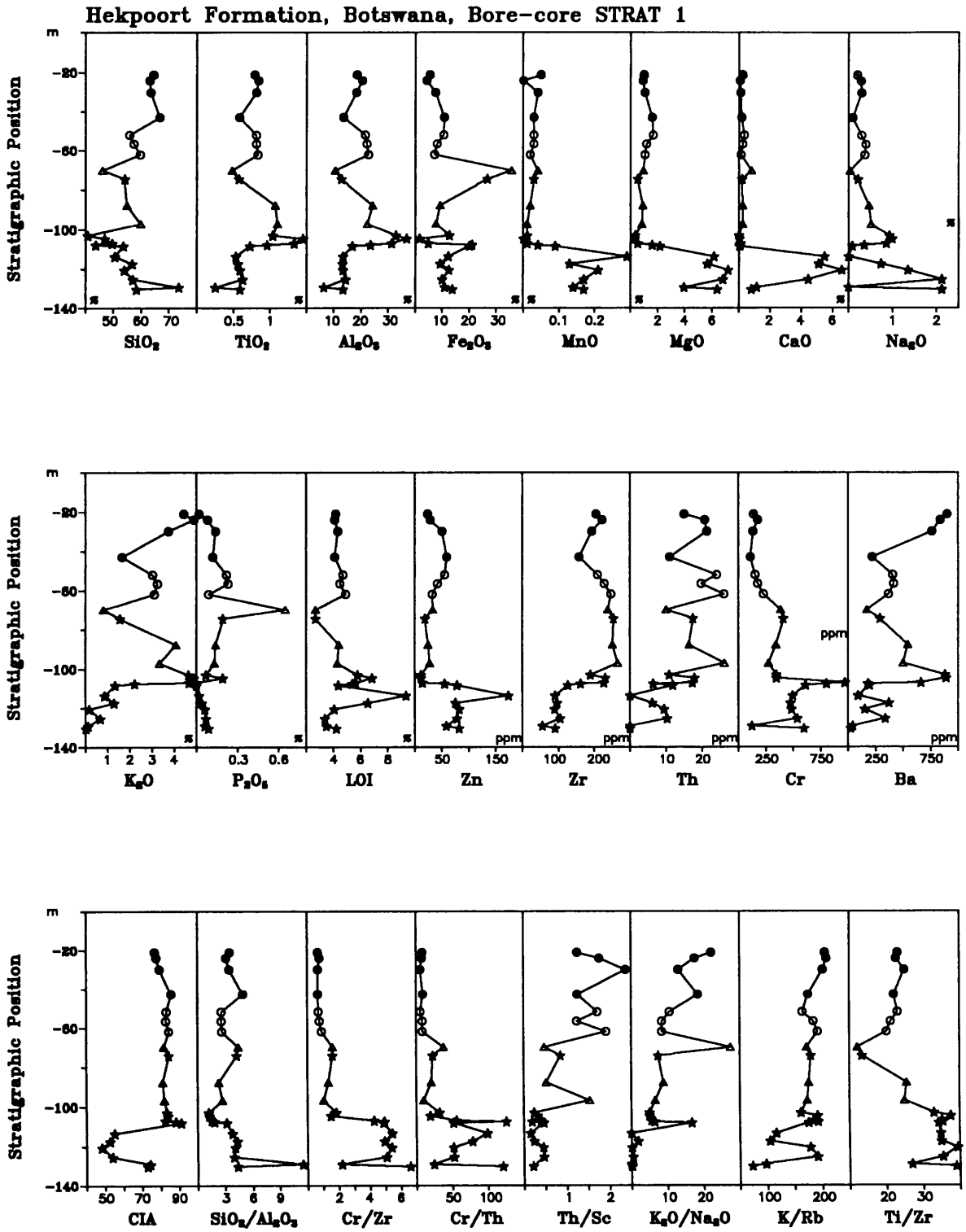

Figure 3.3.6.1: Geochemical profile of the Hekpoort Formation, borehole STRAT 1, Botswana. Lithological types: ★ = andesites; Δ = sandstone; ○ = shale; ● = 'felsic' rock.

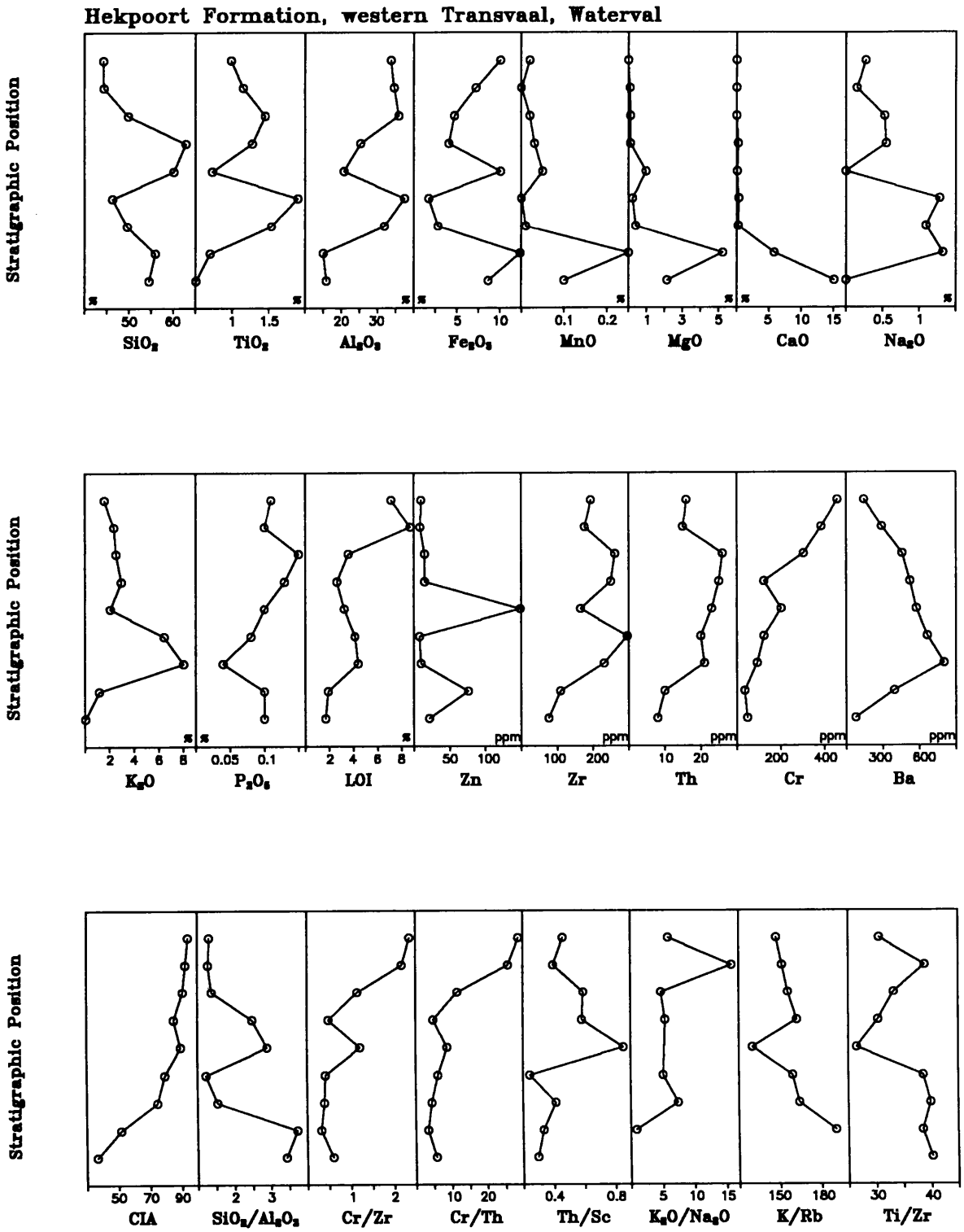

Figure 3.3.6.2: Geochemical profile from a shale bed in the uppermost part of the Hekpoort Formation, Waterval, western Transvaal. Lithological type: ○ = shale. Vertical scale = ± 20 m in total.

A geochemical profile (see Fig. 1.5.7 for location of the profile) of samples from a shale bed in the western Transvaal, which occurs between the Hekpoort andesites and the succeeding Dwaalheuwel Formation sandstones, has an approximate thickness of 20 m (Fig. 3.3.6.2). These shales have an unusual geochemistry, with extremly high Al_2O_3-contents (5 samples $>$ 30 wt.%) and low SiO_2-contents. TiO_2 reaches 2 wt.%. Cr increases linearly throughout the profile. TiO_2, Zr, Th, and CIA increase in the lower part of the profile, Cr/Zr and Cr/Th in the upper part. K/Rb decreases throughout the profile, Th/Sc decreases in the upper part after a sharp increase in the middle of the profile. The variability of most elements and ratios is high, if the profile thickness (only 20 m) is considered. Due to their stratigraphic position below the normally erosively-based Dwaalheuwel sandstones, these shales are inferred to belong to the Hekpoort Formation.

3.3.7 Dwaalheuwel Formation

The major element geochemistry of the sandstones of the Dwaalheuwel Formation (Table 3.3.7.1) shows a comparatively good correlation with the carbonate-free average sandstone estimate of Clarke (1924) (Table 3.2.1c), except for CaO and Na_2O, which are strongly depleted. Compared to other average sandstone estimates (Table 3.2.1c), the Dwaalheuwel Formation is moderately enriched in SiO_2 and, accordingly, depleted in the other major elements (see Chapter 3.1.4 for a discussion of formal correlations). The trace elements Co, Mo, Nb, Cr and Ba are strongly enriched, Ni and V moderately so, and Zr and Y are depleted compared to average sandstone estimates (Table 3.2.1d). A strong increase of the average U-content can be inferred, but, as the calculated mean lies below the detection limit, this cannot be confirmed beyond doubt. Noteworthy is the average Cr-content, which is 4.5-times enriched compared to average sandstone estimates.

Shale beds are occasionally interlayered in the sandstones/quartzites of the Dwaalheuwel Formation. The major element geochemistry of the Dwaalheuwel shales (see Appendix 2a) exhibits strong depletion of SiO_2 (ϕ 50.8 wt.%), CaO (ϕ 0.02 wt.%), and moderate depletion of Na_2O and MgO. Al_2O_3 (ϕ 25.7 wt.%) and Fe_2O_3 (ϕ 12.1 wt.%) are enriched compared to average shale estimates (Table 3.2.1b). The trace elements Ni, Cr, Ga, U, Th, Rb, Pb,

Element	n	MEAN	STD ±	GM	MEDIAN	RANGE	VC
SiO_2	34	86.92	11.38	86.10	92.19	57.48 - 98.13	0.13
TiO_2	34	0.16	0.19	-	0.10	<LLD - 0.83	1.19
Al_2O_3	34	6.21	6.27	3.48	3.40	0.16 - 24.00	1.01
Fe_2O_3*	34	2.55	2.13	1.68	1.95	0.23 - 7.25	0.84
MnO	34	<0.01	0.01	-	0	<LLD - 0.02	-
MgO	34	0.33	0.40	-	0.17	<LLD - 1.24	1.21
CaO	34	0.03	0.07	-	0	<LLD - 0.31	2.33
Na_2O	34	0.14	0.20	-	0.08	<LLD - 1.09	1.43
K_2O	34	1.34	1.69	-	0.61	<LLD - 7.08	1.26
P_2O_5	34	0.04	0.08	-	0.02	<LLD - 0.48	2.00
H_2O^-	34	0.26	0.51	0.09	0.08	0.01 - 2.56	1.96
LOI	34	1.43	1.28	0.93	0.77	0.15 - 4.27	0.90
Zn	34	12	13.7	-	8	<3 - 79	1.14
Cu	34	11	20.0	-	3	<3 - 85	1.82
Ni	34	12	17.6	-	5	<3 - 80	1.47
Co	34	3.6	1.7	-	4	<3 - 8	0.47
Ga	34	6.5	8.4	-	4	<3 - 29	1.29
Mo	34	6.1	3.1	-	7	<2 - 12	0.51
Nb	34	4.5	4.9	-	4	<2 - 16	1.09
Zr	34	124	94.3	93	98	5 - 379	0.76
Y	34	11	11.4	-	7	<2 - 55	1.07
Sr	34	19	21.8	13	14	3 - 117	1.15
Rb	34	60	75.1	-	33	<2 - 322	1.25
U	34	3.2 *)	4.2	-	<LLD	<5 - 13	1.31
Th	34	4.4 *)	6.2	-	<LLD	<5 - 20	1.41
Pb	34	13	42.9	-	6	<5 - 253	3.30
Cr	34	158	46.5	151	157	41 - 290	0.29
V	34	42	32.2	-	29	<14 - 163	0.77
Ba	34	357	431.1	-	284	<16 - 2274	1.21
Sc	34	5.4 *)	7.2	-	<LLD	<8 - 27	1.33
As	34	-	-	-	<LLD	<10	-
S	34	122	222.5	-	72	<50 - 1091	1.82
Sb	34	0.3 *)	1.7	-	<LLD	<8 - 10	5.66
Sn	34	1.4 *)	4.1	-	<LLD	<8 - 19	2.93
B	8	23	15.7	17	20	2 - 46	0.68

Table 3.3.7.1: Average element concentrations of sandstones from the Dwaalheuwel Formation. (n = number of samples; 'MEAN' = arithmetic mean; 'STD ±' = 1 σ standard deviation; 'GM' = geometric mean; 'MEDIAN' = median; 'VC' = variation coefficient; average major element concentrations are reported in weight %, average trace element concentrations in ppm; 'Fe_2O_3*' is all Fe expressed as Fe_2O_3; *) = arithmetic mean below detection limit; LLD = lower limit of detection)

Table 3.3.7.2 : Average ratios of Dwaalheuwel Formation sandstones

(NOTE: ratios are not corrected, i.e. a sample was excluded from calculation of the average ratio if one or both elements are below the detection limit; n.c. = not calculated)

Ratio	n	MEAN	STD ±	GM	RANGE	VC
CIA	34	78.3	7.25	78.0	69.1 - 99.1	0.09
SiO_2/Al_2O_3	34	59	107	25	2.4 - 607	1.81
lg SiO_2/Al_2O_3	34	1.39	n.c.	n.c.	n.c.	n.c.
K_2O/Na_2O	31	14.4	13.8	7.5	0.33 - 59.0	0.96
lg Na_2O/K_2O	31	-0.88	n.c.	n.c.	n.c.	n.c.
Ti/Zr	32	7.4	5.5	5.9	1.3 - 30.2	0.74
Ti/Cr	32	6.9	7.4	4.0	0.4 - 28.0	1.07
Al/Zr	34	261	172	199	34 - 770	0.66
Al_2O_3/TiO_2	32	48	31.4	39	9.0 - 129.5	0.65
Al_2O_3/K_2O	32	19.3	48.2	6.8	3.2 - 254.3	2.50
K/Rb	28	194	52	187	111 - 288	0.27
K/Ba	31	35	27	25	3.7 - 100	0.77
K/Sr	32	529	381	355	11 - 1262	0.72

V, Ba and Sc are fairly strongly (>1.5 times) enriched, and B and Rb moderatly so, compared to average shale estimates (Table 3.2.1d). Zn and Sr are depleted. Cr has an average content (ϕ 303 ppm) about 3 times higher than average shale estimates and is even enriched compared to Archaean Average Shales (Taylor and McLennan, 1985). K2O/Na2O, V/Ni, and Ni/Co (Appendix 2a) are enriched, and Th/U and SiO_2/Al_2O_3 depleted compared to average shale estimates (Table 3.2.1e).

Two complete geochemical profiles were sampled in the Dwaalheuwel Formation (see Fig. 1.5.8 for location of profiles). The northeastern Transvaal geochemical profile (Fig. 3.3.7.1) contains three lithological units, sandstone, carbonate rock, and high-Fe shale. The approximate thickness of the profile is 90 m. No systematic pattern is apparent. The variability in the profile is mainly determined by lithological differences.

The eastern Transvaal geochemical profile (Fig. 3.3.7.2) has an approximate thickness of 80 m and contains only sandstone samples. A sedimentological profile of the sampling site is given by Schreiber (1990, p. 81). The geochemical pattern is without apparent trends. However, most element patterns can be correlated broadly with the northeastern Transvaal geochemical profile (Fig. 3.3.7.1), although differences in absolute values may be substantial (e.g. SiO_2).

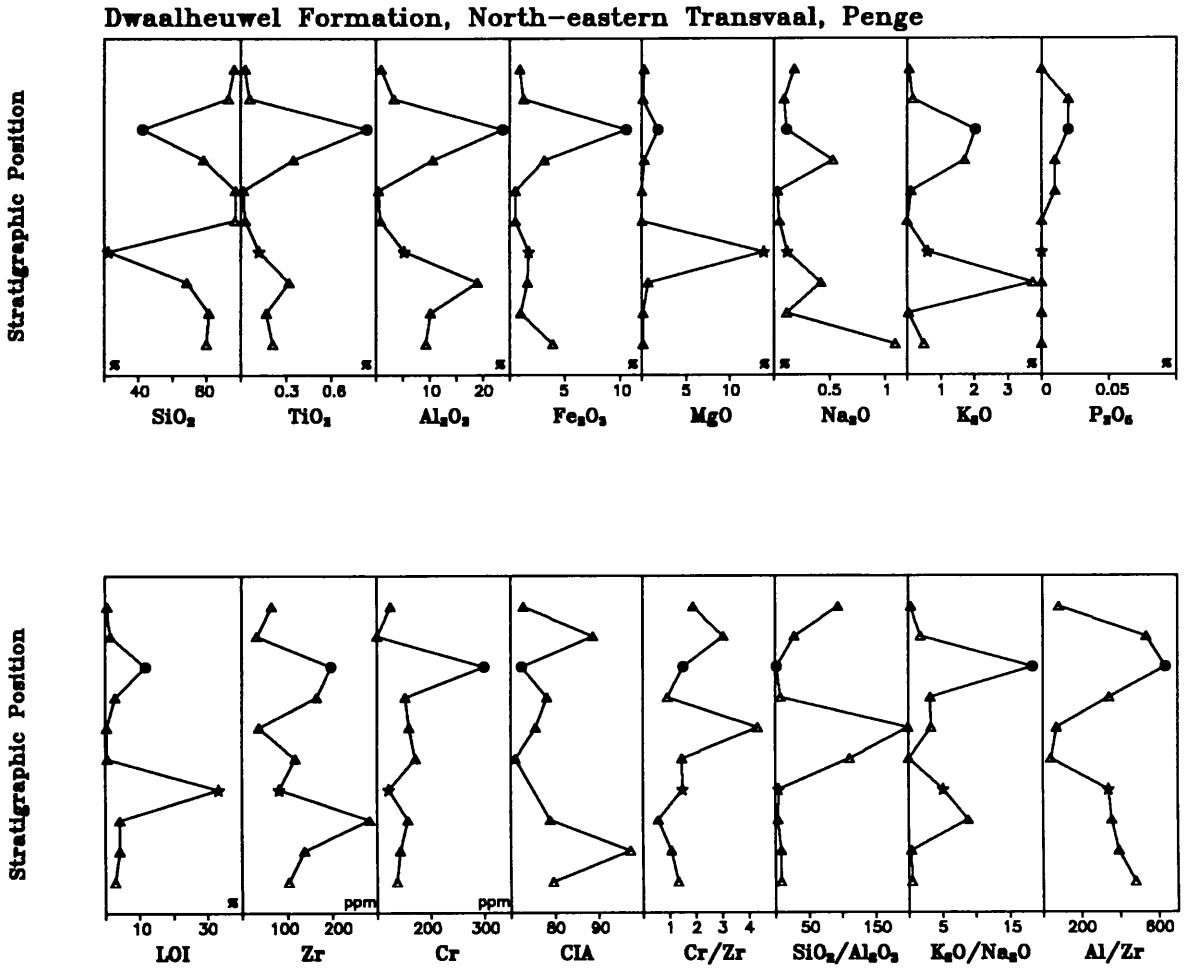

Figure 3.3.7.1: Geochemical profile of the Dwaalheuwel Formation, Penge, northeastern Transvaal. Lithological types: ★ = carbonate rock; Δ = sandstone; ● = high-Fe shale. Vertical scale = ± 90 m in total.

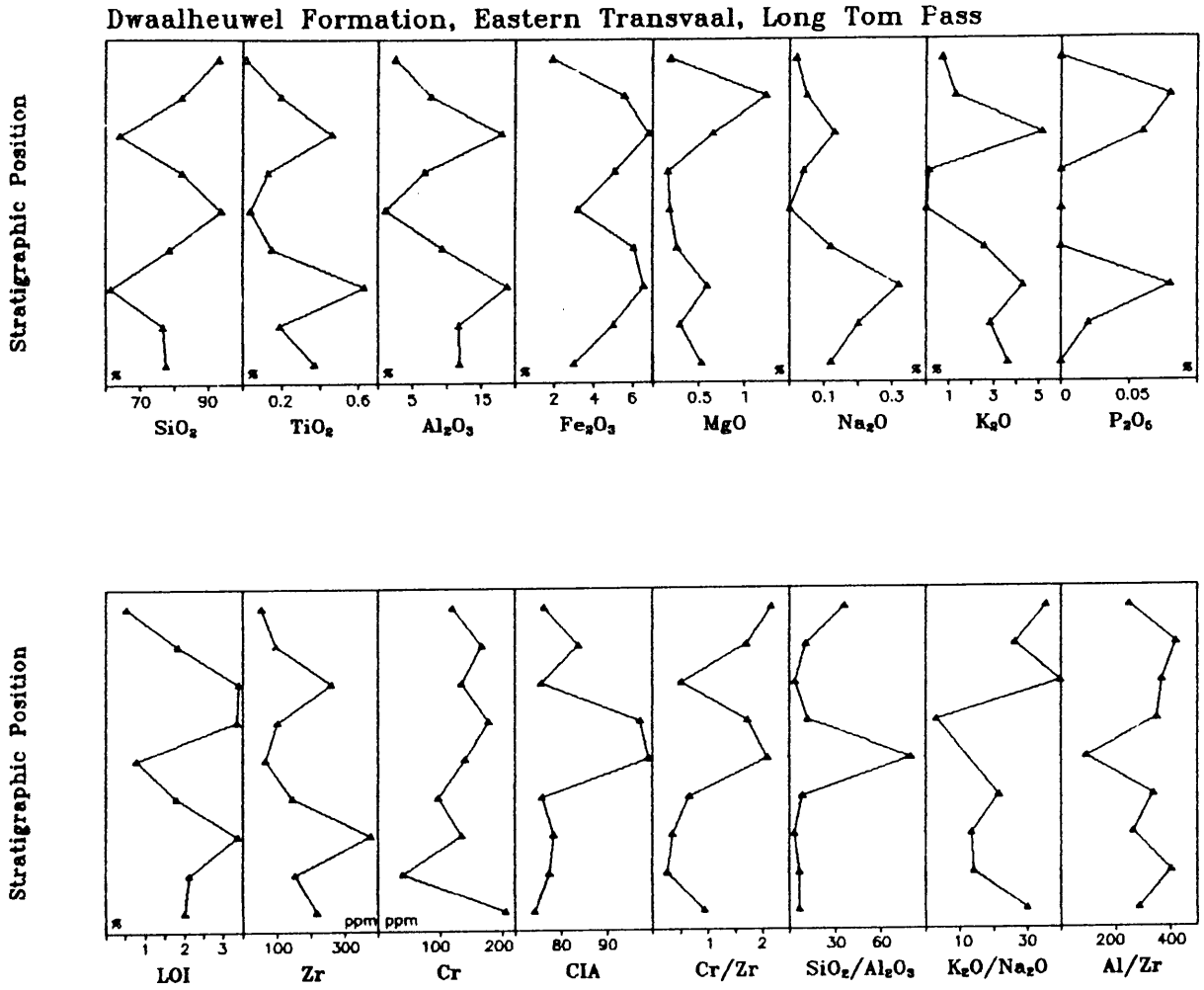

Figure 3.3.7.2: Geochemical profile of the Dwaalheuwel Formation, Long Tom Pass, eastern Transvaal. Lithological type: Δ = sandstone. Vertical scale = ± 80 m in total.

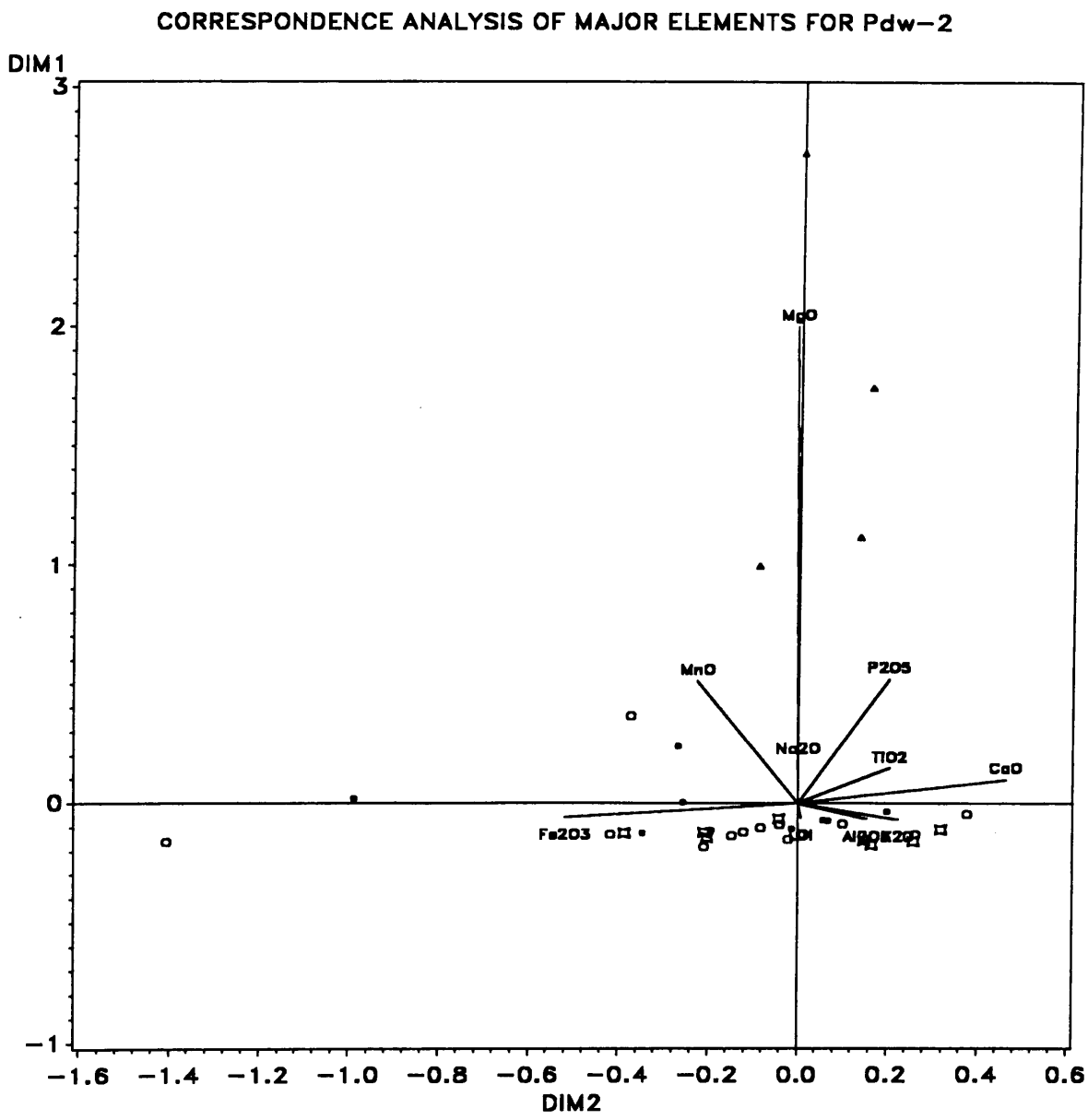

Figure 3.3.7.3: Correspondence analysis of major elements (except SiO_2) of sandstones from the Dwaalheuwel Formation. Symbols for sampling areas: ● (red) = eastern Transvaal; ○ (red) = northeastern Transvaal; □ (violet) = eastern fragments; ◇ (green) = central Transvaal; ▲ (blue) = western Transvaal; † (blue) = western fragments; ‡ (blue) = northwestern Transvaal; ★ (yellow) = Botswana. Definition of sampling areas is shown in Figure 1.5.1. DIM 1 and DIM 2 are the values of the factor loadings of the samples and variables for the first and second factor (see Chapter 2.3.2). Angles between lines connecting a variable and the point (0,0) are proportional to the product moment correlation coefficient of these variables.

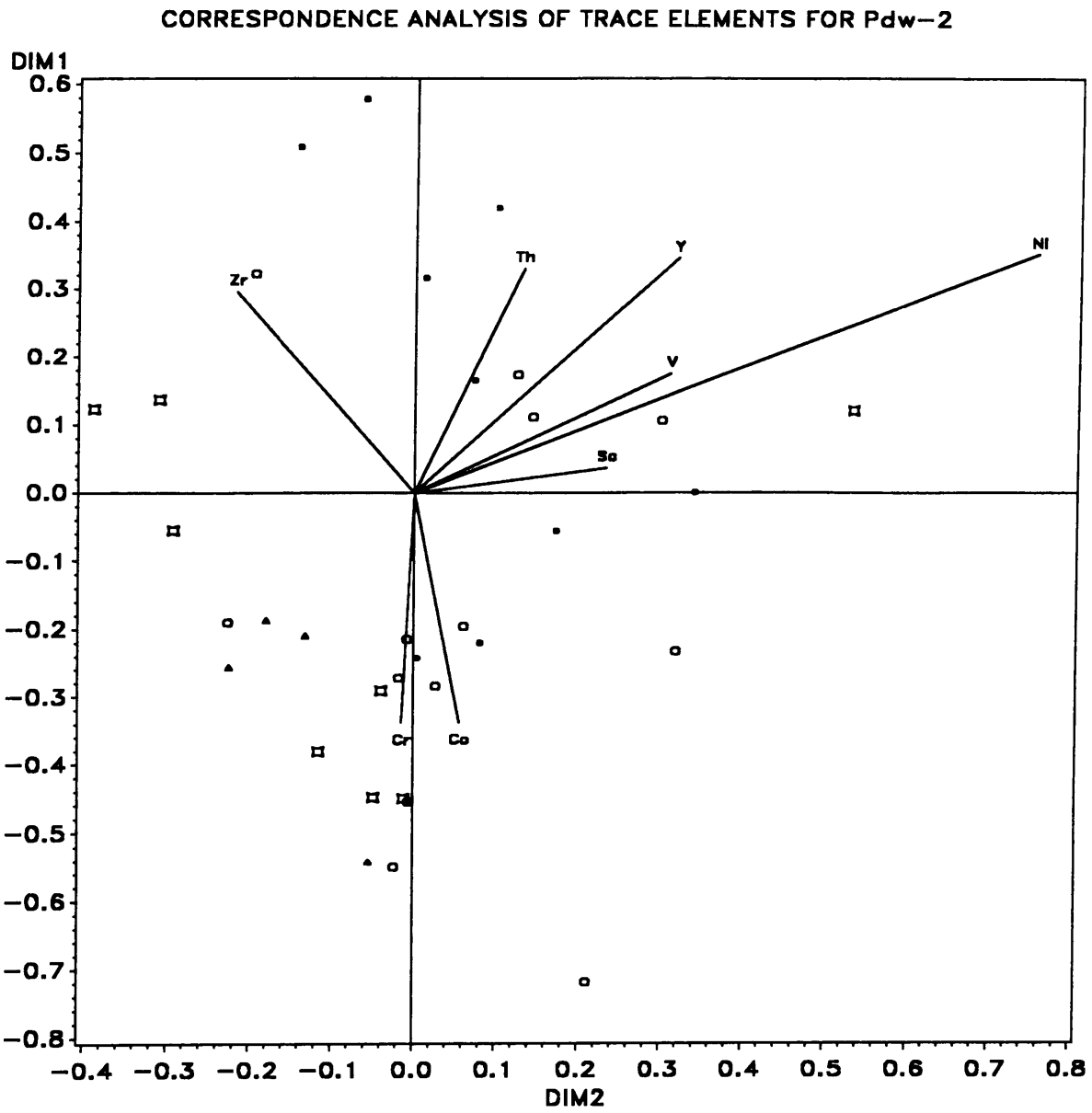

Figure 3.3.7.4: Correspondence analysis of selected trace elements of sandstones from the Dwaalheuwel Formation. Symbols for sampling areas: ● (red) = eastern Transvaal; ○ (red) = northeastern Transvaal; □ (violet) = eastern fragments; ◇ (green) = central Transvaal; ▲ (blue) = western Transvaal; † (blue) = western fragments; ‡ (blue) = northwestern Transvaal; ★ (yellow) = Botswana. Definition of sampling areas is shown in Figure 1.5.1. DIM 1 and DIM 2 are the values of the factor loadings of the samples and variables for the first and second factor (see Chapter 2.3.2). Angles between lines connecting a variable and the point (0,0) are proportional to the product moment correlation coefficient of these variables.

Correspondence analysis for major elements of the sandstones of the Dwaalheuwel Formation (Fig. 3.3.7.3) exhibits, to a certain degree, a separated geochemical pattern for the western Transvaal samples, which are seperated along dimension 1 from the bulk of the other samples. Correspondence analysis for the trace elements (Fig. 3.3.7.4) gives somewhat ambiguous results, with an unclear separation of western Transvaal and eastern fragment samples from eastern and northeastern Transvaal samples.

3.3.8 Strubenkop Formation

The major element geochemistry of the shales of the Strubenkop Formation (Tables 3.3.8.1, 3.3.8.2 and 3.3.8.4) deviates from average shale estimates (Table 3.2.1b) for SiO_2, MgO, MnO, K_2O, CaO and Na_2O, which are moderately to strongly depleted, and for Al_2O_3 and Fe_2O_3(t), which are enriched. Only traces of C_{org} and CO_2 are present. Zn, Co, Rb and Sr are depleted, Cr, Ni, Ga, V, Sc, Th, U, and Y are enriched (Table 3.3.8.1). Cr, Ni, and Sc have average contents similar to Archaean Average Shale (Taylor and McLennan, 1985), although slightly elevated compared to this average. The average REE-contents of Strubenkop Formation shales (Table 3.3.8.4) are similar to the estimate for Post-Archaean Average Shale (Taylor and McLennan, 1985), except for Ce, which is depleted. The depletion of $REE_{(t)}$ compared to Post-Archaean Average Shale (Taylor and McLennan, 1985) can be related to the depletion of Ce. The C_{org}/S-ratio is significantly lower than in modern marine sedimentary rocks, which have a constant ratio of about 6.6 - 10 (Maynard, 1983). K_2O/Na_2O and Th/La are enriched compared to Post-Archaean Average Shale (Taylor and McLennan, 1985), Th/U and La/Sc depleted (Table 3.2.1e). The Cr/V-ratio (Table 3.3.8.3) lies between estimates for Post-Archaean Average Shale and Late Archaean Average Shale (Taylor and McLennan, 1985), V/Ni is strongly enriched compared to other average shale estimates (Table 3.2.1e), and Ni/Co has a similar average to that of Early Archaean Average Shale (Taylor and McLennan, 1985).

Another lithotype frequently encountered in the Strubenkop Formation is siltstones. The average element concentrations of this lithotype are given in Appendix 2a. Compared to the geochemistry of the Strubenkop shales, the siltstones are distinguished by strongly increased SiO_2-contents and depletion of most other major and trace elements.

Element	n	MEAN	STD ±	GM	MEDIAN	RANGE	VC
SiO_2	55	54.09	9.50	52.79	56.08	16.08 - 65.63	0.18
TiO_2	55	0.87	0.22	0.84	0.83	0.28 - 1.37	0.25
Al_2O_3	55	23.01	4.68	22.51	22.76	10.97 - 34.25	0.20
Fe_2O_3*	55	13.39	11.98	10.80	9.55	1.96 - 34.21	0.89
MnO	55	0.03	0.03	-	0.02	<LLD - 0.12	1.00
MgO	55	0.54	0.42	0.40	0.43	0.03 - 2.21	0.78
CaO	55	0.07	0.13	-	0.01	<LLD - 0.79	1.86
Na_2O	55	0.31	0.29	-	0.25	<LLD - 1.20	0.94
K_2O	55	2.45	1.43	1.91	2.37	0.15 - 5.87	0.58
P_2O_5	55	0.17	0.14	-	0.14	<LLD - 0.69	0.82
H_2O^-	55	0.58	0.45	0.44	0.37	0.09 - 1.63	0.78
LOI	55	4.23	1.56	3.90	4.46	1.01 - 7.75	0.37
Zn	55	64	47.7	48	51	6 - 246	0.75
Cu	55	66	54.4	50	47	10 - 310	0.82
Ni	55	104	103.8	82	77	23 - 717	1.00
Co	55	14	11.0	9.2	10	<3 - 46	0.79
Ga	55	29	5.0	29	29	20 - 39	0.17
Mo	55	2.6	3.6	-	2	<2 - 19	1.39
Nb	55	16	3.2	16	17	6 - 22	0.20
Zr	55	215	40.5	211	221	97 - 295	0.19
Y	55	40	7.4	39	39	19 - 59	0.19
Sr	55	98	71.6	80	87	15 - 421	0.73
Rb	55	119	61.3	96	121	9 - 245	0.52
U	55	6.0	4.1	-	6	<5 - 14	0.68
Th	55	19	5.8	19	19	9 - 36	0.31
Pb	55	21	17.7	17	16	<5 - 102	0.84
Cr	55	254	110.1	236	227	100 - 638	0.43
V	55	222	116.1	202	176	118 - 606	0.52
Ba	55	552	246.8	484	556	93 - 1077	0.45
Sc	55	25	9.9	23	22	12 - 54	0.40
As	55	0.4 *)	2.1	-	<LLD	<10 - 11	5.25
S	55	187	88.7	172	178	73 - 624	0.47
Sb	55	2.8 *)	6.1	-	<LLD	<8 - 27	2.18
Sn	55	2.9 *)	5.4	-	<LLD	<8 - 17	1.86
B	7	99	34.0	94	100	48 - 161	0.34

Table 3.3.8.1: Average element concentrations of shales from the Strubenkop Formation

(n = number of samples; 'MEAN' = arithmetic mean; 'STD ±' = 1 σ standard deviation; 'GM' = geometric mean; 'MEDIAN' = median; 'VC' = variation coefficient; average major element concentrations are reported in weight %, average trace element concentrations in ppm; 'Fe_2O_3*' is all Fe expressed as Fe_2O_3; *) = arithmetic mean below detection limit; LLD = lower limit of detection)

Table 3.3.8.2: Average major element concentrations of shales from the Strubenkop Formation recalculated to 100 % volatile-free.

Element	n	MEAN	STD ±	RANGE
SiO_2	55	57.00	10.01	17.23 - 69.08
TiO_2	55	0.92	0.23	0.28 - 1.40
Al_2O_3	55	24.23	4.82	11.76 - 36.25
Fe_2O_3*	55	14.09	12.57	2.08 - 68.91
MnO	55	0.03	0.03	0 - 0.12
MgO	55	0.57	0.44	0.03 - 2.41
CaO	55	0.07	0.14	0 - 0.82
Na_2O	55	0.33	0.30	0 - 1.28
K_2O	55	2.59	1.53	0.15 - 6.22
P_2O_5	55	0.17	0.14	0 - 0.74

Table 3.3.8.3: Average ratios of shales from the Strubenkop Formation

(NOTE: ratios corrected as described in Chapter 3.1.2)

Ratio	n	MEAN	STD ±	GM	RANGE	VC
CIA	55	87.5	6.3	87.3	77.8 - 98.5	0.07
Fe/V	55	405	149	375	51 - 796	0.37
K_2O/Na_2O	49	11.4	10.1	8.3	1.1 - 53.5	0.89
SiO_2/Al_2O_3	55	2.4	0.6	2.3	1.3 - 3.9	0.25
Cr/Th	55	14.2	7.1	12.7	4.4 - 38.8	0.50
Th/Sc	55	0.91	0.43	0.80	0.24 - 1.85	0.47
Cr/Zr	55	1.31	0.98	1.12	0.44 - 5.50	0.75
Co/Th	55	0.81	0.85	0.54	0.09 - 4.40	1.05
Al_2O_3/TiO_2	55	27.2	5.4	26.8	19.5 - 55.1	0.20
Al_2O_3/K_2O	55	18.5	26.7	11.8	4.0 - 174.6	1.44
K/Rb	55	167	27	165	108 - 249	0.16
K/Ba	55	38	26	33	8 - 174	0.68
Ti/Ni	55	74	43	61	6 - 206	0.58
Cr/V	55	1.21	0.34	1.17	0.69 - 2.67	0.28
V/Ni	55	3.06	2.07	2.45	0.22 - 10.45	0.68
Ni/Co	55	11.49	10.94	8.24	1.65 - 53.43	0.95
Zr/Nb	55	13.8	2.6	13.6	9.5 - 23.1	0.19
Th/U	55	2.93	1.19	2.69	1.15 - 5.61	0.41
Ba/Rb	55	5.7	3.4	5.0	1.2 - 18.2	0.60
Ba/Sr	55	7.6	5.4	6.0	0.5 - 33.7	0.71
Ba/Th	55	30.5	15.9	26.1	4.4 - 91.7	0.52
Al/Zr	55	579	142	565	346 - 1268	0.25
Ti/Zr	55	24.3	4.8	23.9	14.2 - 36.9	0.20

Table 3.3.8.4: Average element concentrations and ratios of selected shale samples of the Strubenkop Formation

(n = number of samples; 'MEAN' = arithmetic mean; 'STD ±' = 1 σ standard deviation; 'GM' = geometric mean; 'MEDIAN' = median; 'VC' = variation coefficient; average major element concentrations (i.e. FeO to S_{XRF}) are reported in weight %, average trace element concentrations in ppm; n.c. = not calculated; subscript N = concentration normalised to chondrite; Ce/Ce* = $Ce_N/[(La_N + Pr_N)/2]$; Σ REE = sum of REE in ppm; NOTE: ratios corrected as described in Chapter 3.1.2; LLD = lower limit of detection; 1) expressiveness of VC doubtful due to small sample size)

Element	n	MEAN	STD ±	GM	MEDIAN	RANGE	VC
FeO	5	4.25	4.73	2.37	2.13	0.56 - 11.85	1.11
Fe_2O_3	5	5.52	2.56	4.96	6.31	2.34 - 7.85	0.46
CO_2	5	0.06	0.02	0.06	0.07	0.04 - 0.07	0.33
C_{org}	5	<0.01	-	-	-	<LLD - 0.01	-
H_2O^+	5	5.41	0.93	5.34	5.30	4.13 - 6.51	0.17
S_{leco}	5	16 ppm	21.9	-	<LLD	<LLD - 40	1.37
S_{xrf}	5	180 ppm	18.6	179	177	161 - 199	0.10
Li	5	17	17.6	9.7	12	1 - 47	1.04
La	5	39.6	20.2	34.6	48.4	14.8 - 62.5	0.51
Ce	5	55.3	29.9	48.5	49.3	25.4 - 87.1	0.54
Pr	5	8.3	4.3	7.2	9.3	3.1 - 13.2	0.52
Nd	5	29.9	15.7	26.0	32.9	10.9 - 48.8	0.53
Sm	5	5.6	2.2	5.2	5.5	3.1 - 8.5	0.39
Eu	5	1.08	0.45	1.0	1.1	0.6 - 1.7	0.42
Gd	5	4.7	1.3	4.6	4.7	3.2 - 6.4	0.28
Tb	5	0.78	0.13	0.77	0.8	0.6 - 0.9	0.17
Dy	5	4.7	0.6	4.6	4.4	4.1 - 5.6	0.13
Er	5	2.6	0.3	2.6	2.5	2.5 - 3.2	0.12
Tm	5	0.38	0.08	0.37	0.4	0.3 - 0.5	0.21
Yb	5	2.7	0.3	2.7	2.7	2.3 - 3.2	0.11
La/Sc	5	2.12	1.04	1.91	1.86	1.14 - 3.29	0.49
Th/La	5	0.79	0.52	0.67	0.43	0.42 - 1.55	0.66
Ba/La	5	19.5	11.9	16.7	12.0	8.9 - 33.5	0.61
LREE/HREE	5	9.95	5.11	8.77	10.56	3.70 - 16.89	0.51
K2O/ΣREE	5	197	154	151	102	68 - 380	0.78
Gd_N/Yb_N	5	1.43	0.40	1.39	1.41	0.96 - 2.08	0.28
La_N/Sm_N	5	4.27	0.97	4.18	4.50	3.01 - 5.54	0.23
Ce/Ce*	5	0.71	0.18	0.69	0.67	0.52 - 0.96	0.25
Eu/Eu*	5	0.62	0.05	0.61	0.62	0.56 - 0.68	0.08
C_{org}/S	5	0.58	0.05	0.58	0.61	0.50 - 0.62	0.09
ΣREE	5	155.6	73.4	140.3	161.9	74.8 - 238	0.47

Two complete and two partial profiles were sampled in the Strubenkop Formation (see Fig. 1.5.9 for location of profiles). Additionally, the local geochemical variation of Strubenkop Formation shale samples was studied below and above an intrusive mafic sill.

The eastern Transvaal geochemical profile (Fig 3.3.8.1) at Long Tom Pass (see Fig. 1.5.9 for location) has an approximate thickness of 45 m and contains two lithological units, shales in the lowermost part of the profile and siltstones in the middle and upper parts. Except for the shales, the profile is lithologically comparable to Profile 2 of Schreiber (1990, p. 104). The major element variation (except for CaO and Na_2O) as well as the variations of Zn, Th and Ba, are dependent on lithology. Two groups of element patterns can be identified: (1) TiO_2, Al_2O_3, K_2O, LOI and Th are negatively correlated with SiO_2 and Ba, and (2) Fe_2O_3, MnO, MgO, P_2O_5 and Zn increase in the lowermost shale samples and have a low, but stable, content in the siltstone samples. Zr-contents are generally high, with a maximum of 600 ppm in a siltstone sample, which also shows considerable enrichment in TiO_2, Cr and Th compared to the other siltstone samples. The K_2O/Na_2O ratio decreases from bottom to top of the profile, with low variability in the middle part of the profile. Ti/Zr discriminates between the rocktypes.

The central Transvaal geochemical profile (Fig. 3.3.8.2) from Scheerpoort (see Fig. 1.5.9 for location of the profile) has an approximate thickness of 90 m and contains only shale. A differentiation was made for shales with less than 15 wt.% Fe_2O_3(t) (open circle) and a high-Fe shale with more than 15 wt.% Fe_2O_3(t) (filled square). TiO_2 exhibits a linear upward decrease throughout the profile, and Al_2O_3 has a fairly well defined negative correlation to SiO_2. Other element patterns are complicated. The variability of most elements is small, if the scale is considered. Fe_2O_3(t), MgO and MnO show some degree of similarity in their pattern. Cr and Th are considerably enriched compared to Average Shale estimates (Table 3.2.1d). Cr/Zr and Cr/Th are positively correlated to each other, and negatively correlated to Th/Sc. Cr/Th, Cr/Zr, and Ti/Zr are enriched in the single high-Fe sample. The CIA generally decreases upwards throughout the profile, with the exception of the high-Fe shale sample. However, the CIA for all samples is enriched compared to the North American Shale Composite (Nesbitt and Young, 1982).

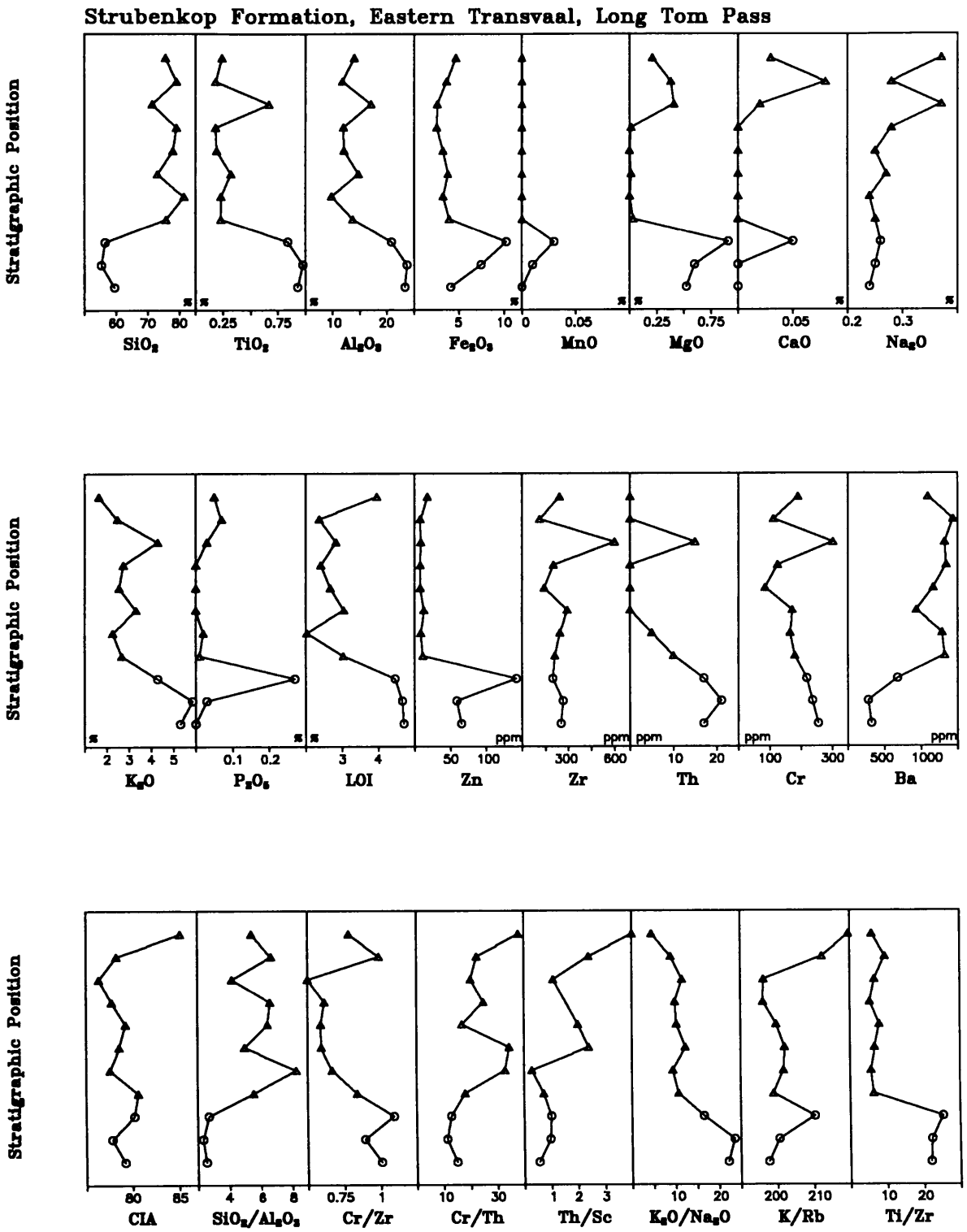

Figure 3.3.8.1: Geochemical profile of the Strubenkop Formation, Long Tom Pass, eastern Transvaal. Lithological types: ○ = shale; Δ = siltstone. Vertical scale = ± 45 m in total.

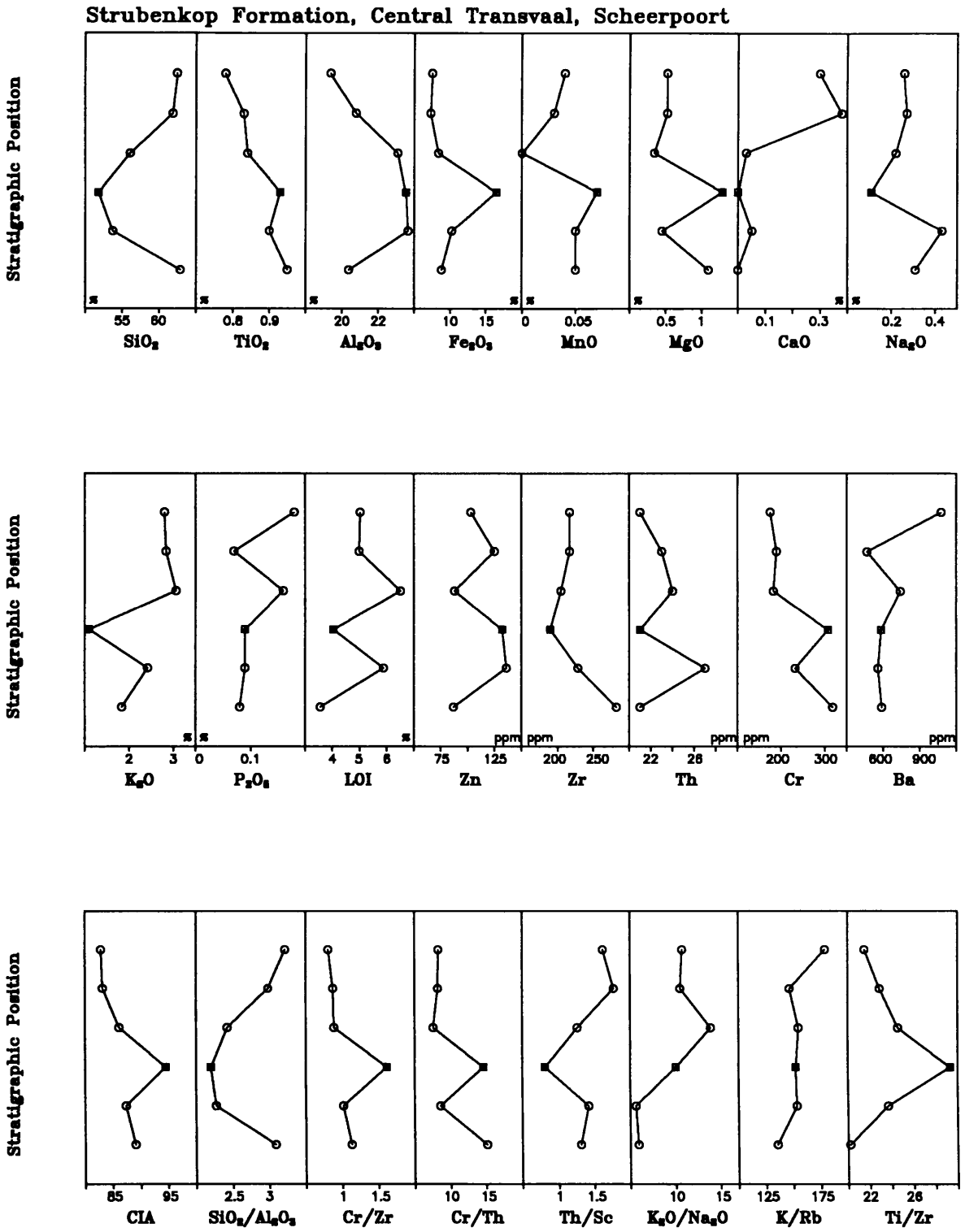

Figure 3.3.8.2: Geochemical profile of the Strubenkop Formation, Scheerpoort, central Transvaal. Lithological types: ○ = shale; ■ = high-Fe shale (Fe_2O_3* > 15 wt.%). Vertical scale = ± 90 m in total.

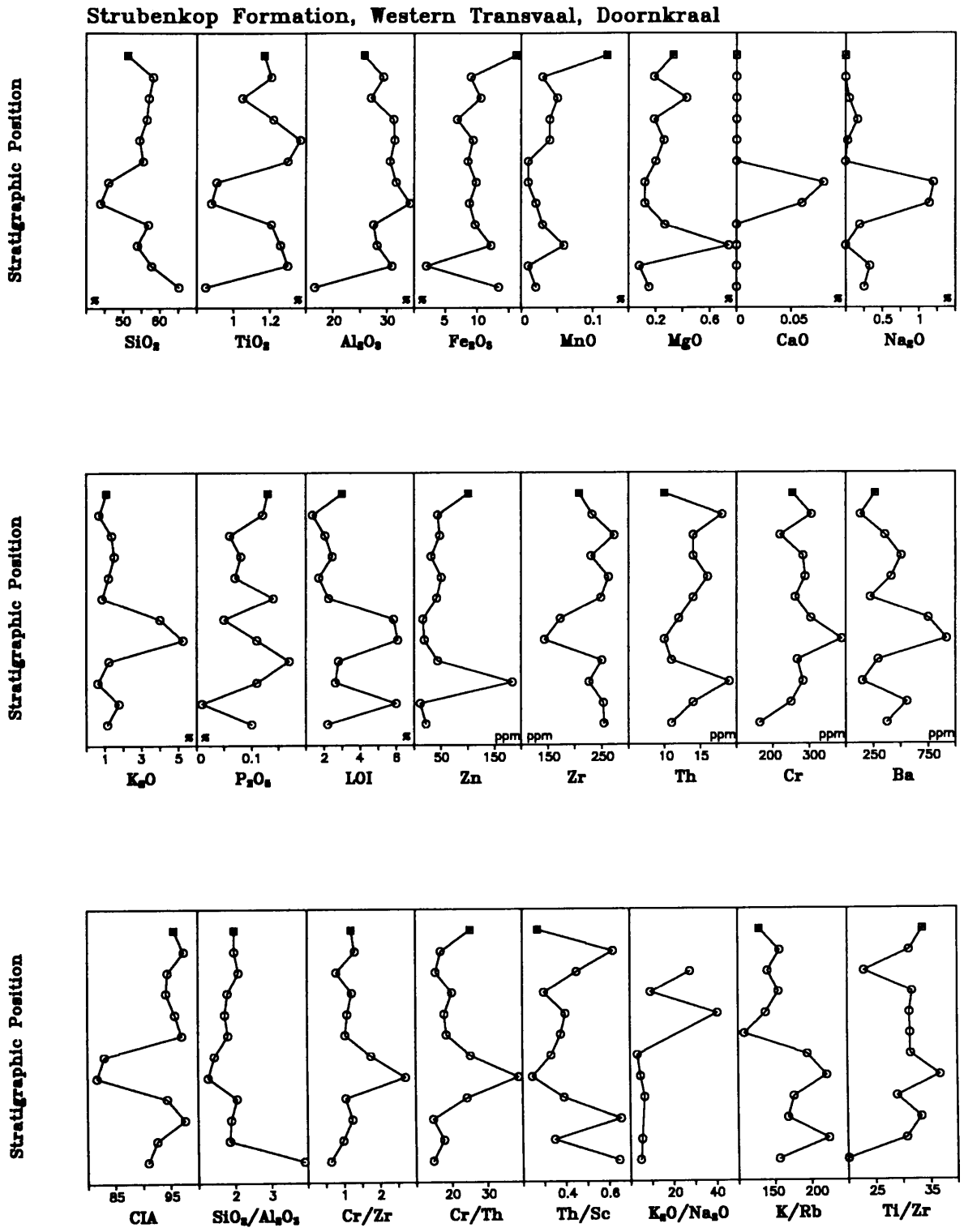

Figure 3.3.8.3: Partial geochemical profile of the Strubenkop Formation, Doornkraal, western Transvaal. Lithological types: ○ = shale; ■ = high-Fe shale (Fe_2O_3* > 15 wt.%). Vertical scale = ± 40 m in total.

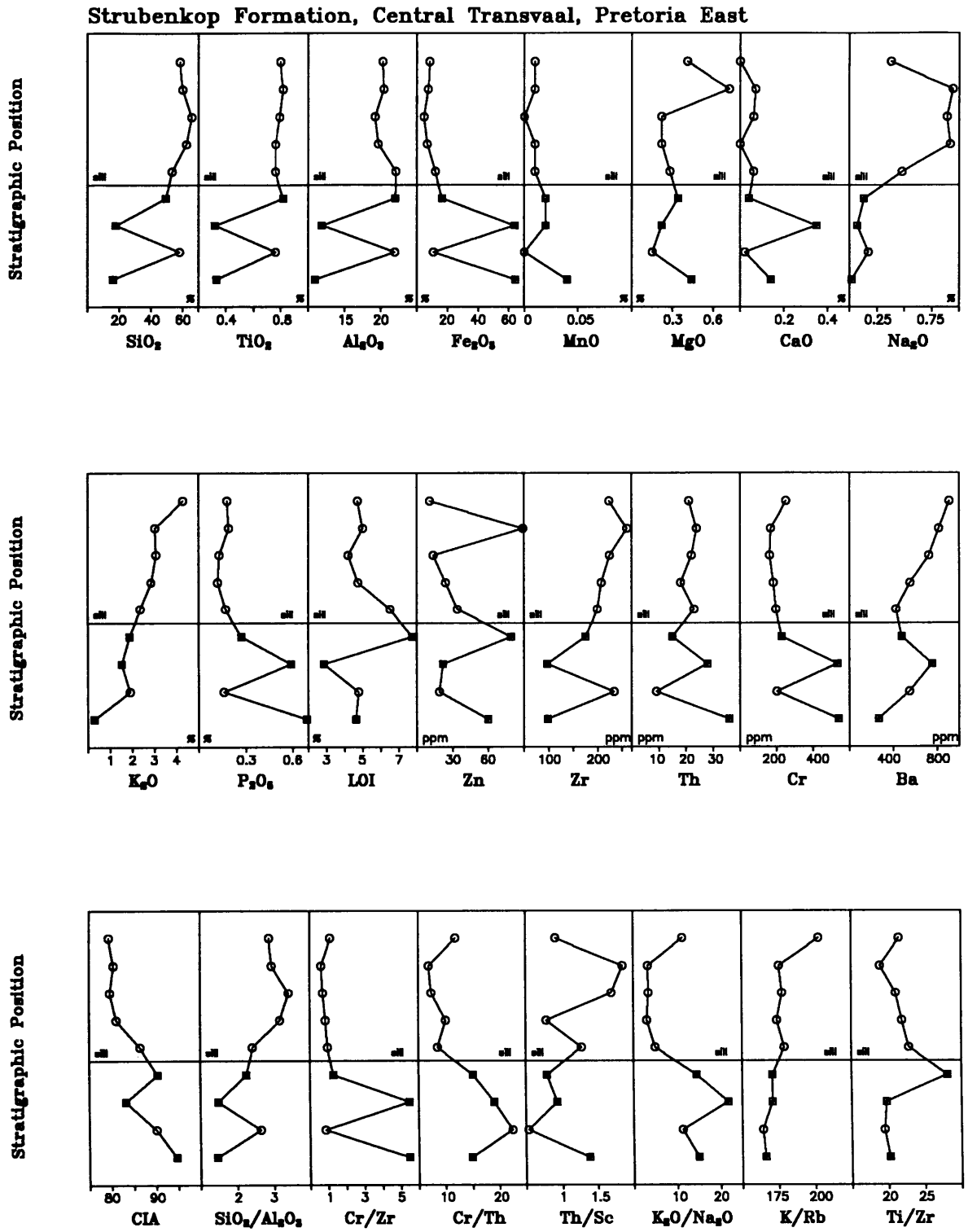

Figure 3.3.8.4: Partial geochemical profile of the Strubenkop Formation, Pretoria East, central Transvaal. Lithological types: ○ = shale; ■ = high-Fe shale (Fe_2O_3* > 15 wt.%). Line = position of mafic sill. Vertical scale = ± 40 m in total.

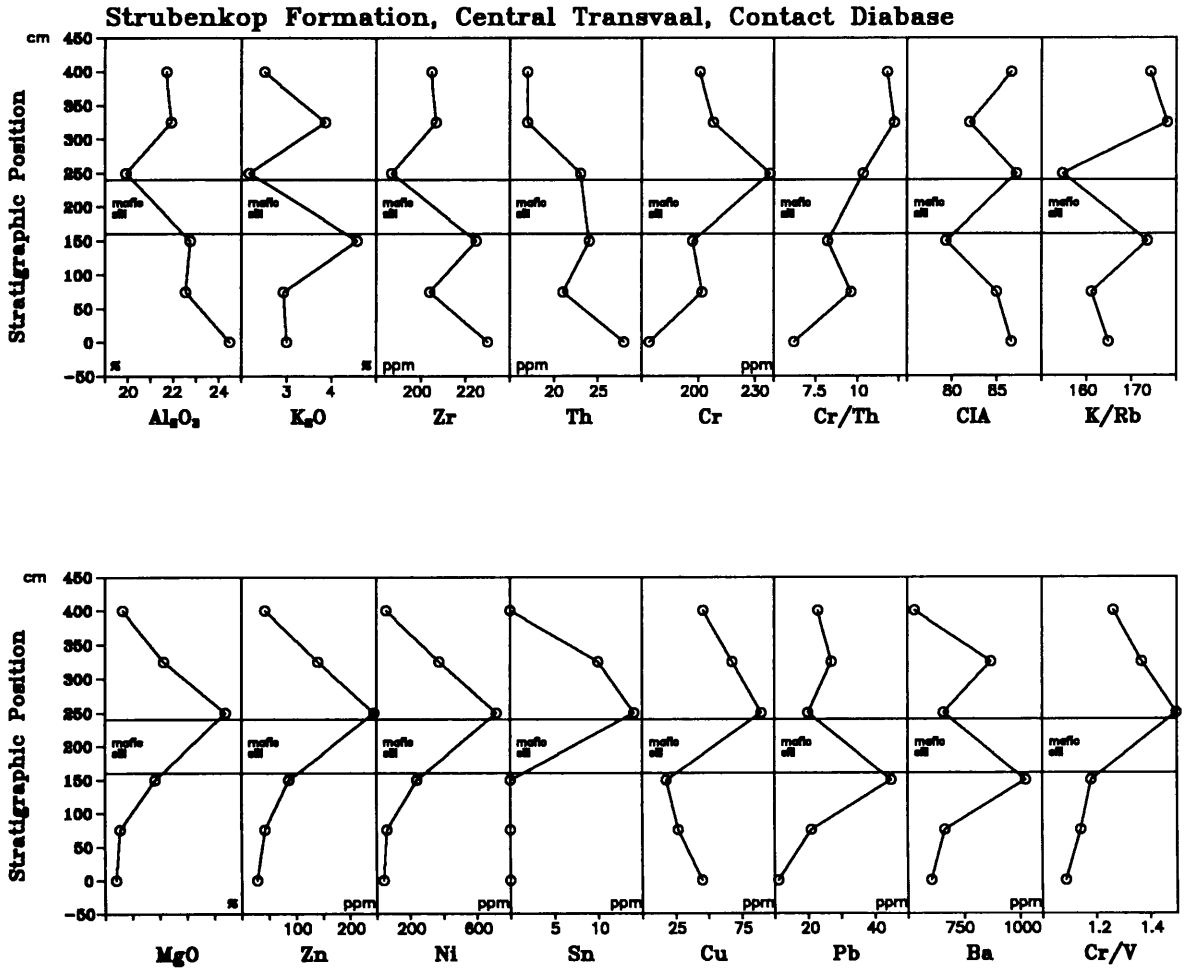

Figure 3.3.8.5: Geochemical variation of Strubenkop Formation shales in contact to a mafic sill. Pretoria East, central Transvaal. Lithological types: ○ = shale. Only relative stratigraphic height shown, with respect to sill.

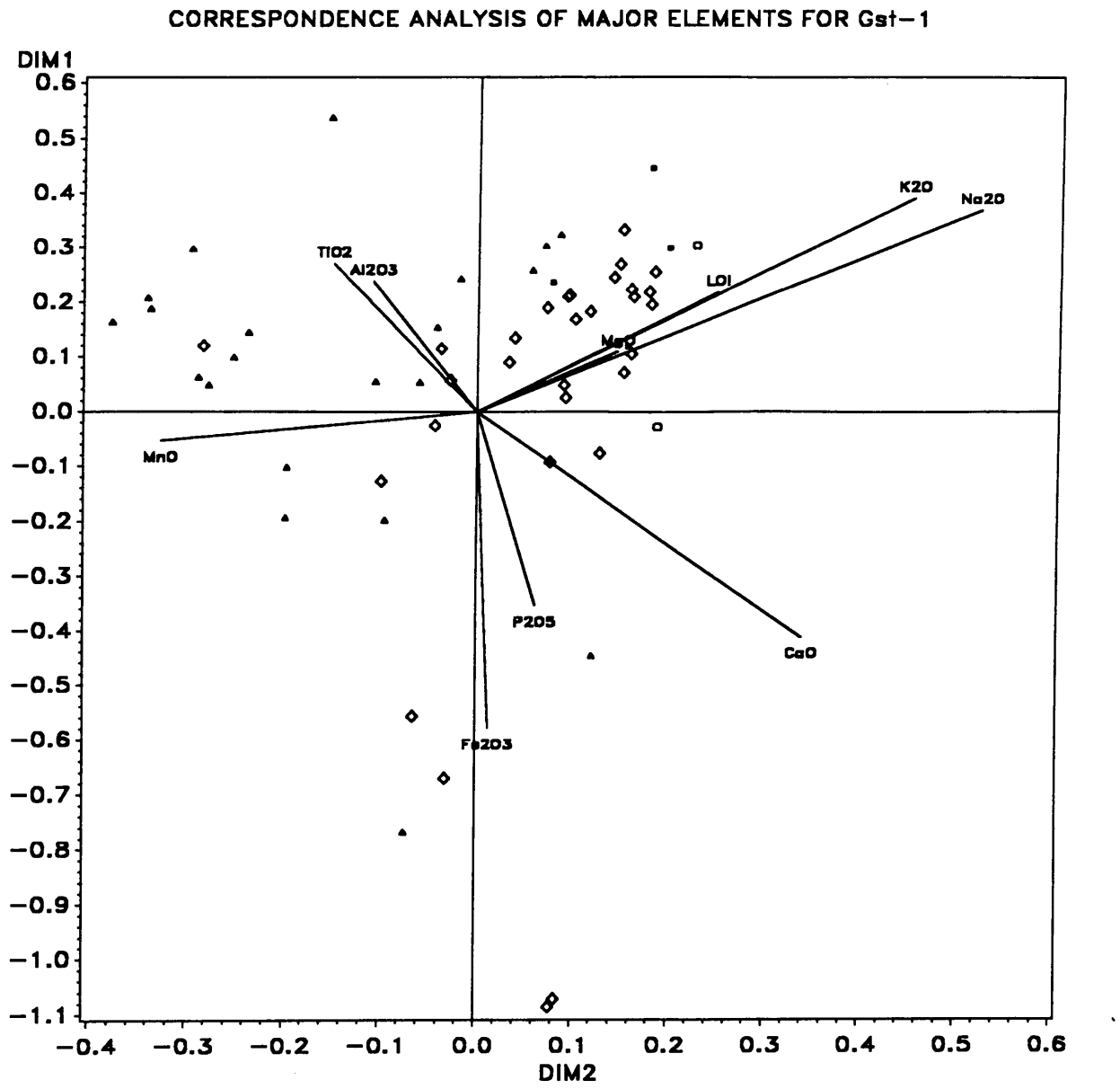

Figure 3.3.8.6: Correspondence analysis of major elements (except SiO_2) of shales from the Strubenkop Formation. Symbols for sampling areas: ● (red) = eastern Transvaal; ○ (red) = northeastern Transvaal; □ (violet) = eastern fragments; ◇ (green) = central Transvaal; ▲ (blue) = western Transvaal; † (blue) = western fragments; ‡ (blue) = northwestern Transvaal; ★ (yellow) = Botswana. Definition of sampling areas is shown in Figure 1.5.1. DIM 1 and DIM 2 are the values of the factor loadings of the samples and variables for the first and second factor (see Chapter 2.3.2). Angles between lines connecting a variable and the point (0,0) are proportional to the product moment correlation coefficient of these variables.

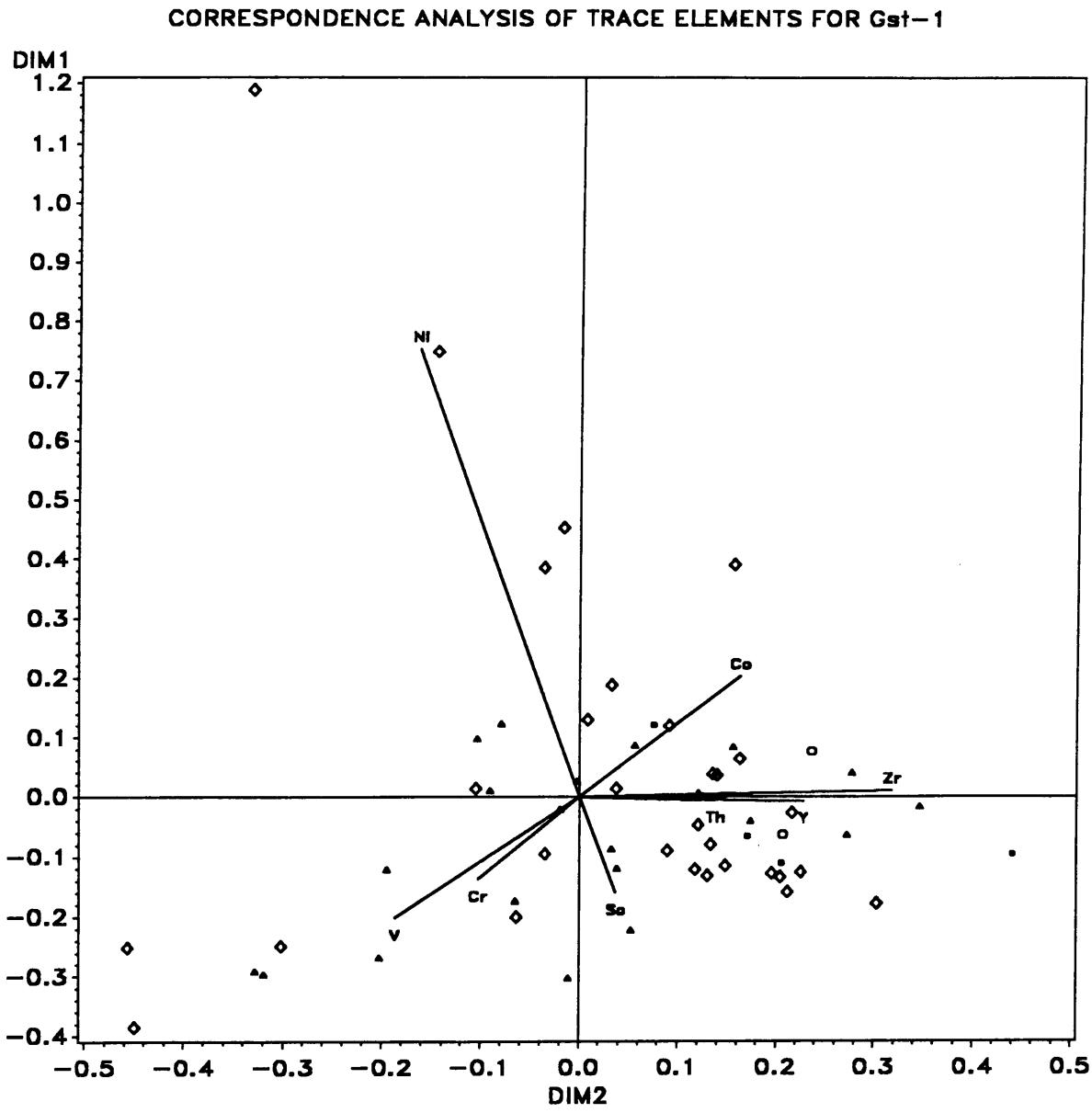

Figure 3.3.8.7: Correspondence analysis of selected trace elements of shales for the Strubenkop Formation. Symbols for sampling areas: ● (red) = eastern Transvaal; ○ (red) = northeastern Transvaal; □ (violet) = eastern fragments; ◇ (green) = central Transvaal; ▲ (blue) = western Transvaal; † (blue) = western fragments; ‡ (blue) = northwestern Transvaal; ★ (yellow) = Botswana. Definition of sampling areas is shown in Figure 1.5.1. DIM 1 and DIM 2 are the values of the factor loadings of the samples and variables for the first and second factor (see Chapter 2.3.2). Angles between lines connecting a variable and the point (0,0) are proportional to the product moment correlation coefficient of these variables.

The western Transvaal geochemical profile (Fig. 3.3.8.3) depicts the lower part of the Strubenkop Formation in this area (see Fig. 1.5.9 for location of the profile), and has an approximate thickness of 40 m (out of ca. 100 m total thickness). The profile contains two lithotypes, shale (open circle) and high-Fe shale with more than 15 wt.% Fe_2O_3(t) (filled square). TiO_2, Al_2O_3 and Fe_2O_3 are considerably enriched compared to average shale estimates (Table 3.2.1b), the other major elements are relatively strongly depleted. Al_2O_3 and Fe_2O_3 show, to a certain degree, an opposing trend (negative correlation), if minor variations are taken into account. Two samples in the middle of the profile are enriched in K_2O and Na_2O compared to the other samples of the profile. These high-K-Na samples are also relatively enriched in CaO and Cr, and seem to be depleted in Zr, TiO_2 and Th, although the depletion of the latter two elements is indistinct. The CIA drops sharply in these same two samples, but is nevertheless considerably higher (> 80) than values given for average shales (ca. 70-75) (Nesbit and Young, 1982). All other samples have a CIA of > 90. The profile is separated into a high-K/Rb lower portion and a low-K/Rb upper part. Cr/Th and Th/Sc exhibit an opposing trend.

The central Transvaal geochemical profile (Fig. 3.3.8.4) from Pretoria East (see Fig. 1.5.9 for location of the profile) has an approximate thickness of 40 m and contains two rocktypes, high-Fe shales (> 15 wt.% Fe_2O_3) and shales (< 15 wt.% Fe_2O_3). The profile is thought to represent the middle part of the Strubenkop Formation. It should be noted that the two high-Fe samples at the bottom of the profile (> 60 wt.% Fe_2O_3), were not taken into account for the calculation of average element contents of the shales of the Strubenkop Formation (Table 3.3.8.1). The position of a mafic sill is marked in the middle of the profile. The geochemistry of samples in close proximity to the sill is shown in Figure 3.3.8.5, and is not shown in this profile (Fig. 3.3.8.4). K_2O and Zr increase upwards, the CIA decreases upwards throughout the Pretoria East profile (Fig. 3.3.8.4). The two ironstone samples (> 60 wt.% Fe_2O_3) have high concentrations of P_2O_5, Cr and Th, and are relatively depleted in TiO_2, Al_2O_3, Zr and SiO_2. A comparison of the Scheerpoort (Fig. 3.3.8.2) and the Pretoria East profiles (Fig. 3.3.8.4) is difficult due to the uncertainties of their stratigraphic correlation. As ironstones were not encountered in the Scheerpoort profile, possibly due to an insufficient sample density, it is questionable if a thorough comparison can be carried out with the available data. However, the decrease of the CIA and the increase of Th/Sc in the

upper part of the Scheerpoort profile and upwards throughout the Pretoria East profile is worth mentioning.

Figure 3.3.8.5 shows some element variations of Strubenkop shales in contact with a mafic sill. Mafic sills and dykes occur frequently throughout the stratigraphy of the Pretoria Group (see Chapter 1.3). Element variations in sedimentary rocks in contact with these mafic sills and dykes can be expected to some degree. It is beyond the scope of this investigation to examine in detail the geochemical changes, and their extent in the sedimentary rocks due to contact metamorphic reactions with such local intrusives. However, it was thought neccessary to establish element variations of sedimentary rocks in contact with a mafic intrusive body in such an exemplary case as the well exposed sill and contact zone in the Strubenkop Formation. The strike of the sill is parallel to that of the shale beds, but the dip of the sill is almost vertical in contrast to the dip of the sedimentary bedding of about 30°N. The scale used in Figure 3.3.8.5 reflects distances measured in the field, independent of the differences in dip. If the absolute and relative element contents (i.e., compared to average shale estimates **and** average element content of the Strubenkop Formation), are taken into consideration, a significant increase of MgO, Zn and especially Ni is observed towards the contact. The absolute enrichment of these elements is higher in samples stratigraphically above the sill. This observation gives some reason to consider the variability shown by Sn and Cu as being also related to the intrusion, although the Cu-pattern is ambiguous. The other elements exhibit no obvious deviations related to the sill.

Correspondence analysis for major elements of the shales of the Strubenkop Formation (Fig. 3.3.8.6) discriminates between western and central Transvaal samples. Eastern and northeastern Transvaal samples fall in the same field as the central Transvaal samples. Correspondence analysis of selected trace elements (Fig. 3.3.8.7) shows no cluster related to sampling area.

3.3.9 Daspoort Formation

The major element geochemistry of the Daspoort Formation quartzites (Table 3.3.9.1)

Element	n	MEAN	STD ±	GM	MEDIAN	RANGE	VC
SiO_2	59	93.27	7.75	92.9	96.19	62.68 - 99.61	0.08
TiO_2	59	0.17	0.16	-	0.16	<LLD - 0.83	0.94
Al_2O_3	59	2.60	3.58	1.43	1.26	0.14 - 18.34	1.38
Fe_2O_3*	59	1.78	2.67	0.98	0.76	0.22 - 12.37	1.50
MnO	59	0.01	0.01	-	0.01	<LLD - 0.05	1.00
MgO	59	0.13	0.35	-	<LLD	<LLD - 1.39	2.69
CaO	59	0.05	0.13	-	0.02	<LLD - 0.87	2.60
Na_2O	59	0.25	0.88	-	0.03	<LLD - 4.73	3.52
K_2O	59	0.58	0.91	-	0.25	<LLD - 4.58	1.57
P_2O_5	59	0.06	0.16	-	0.03	<LLD - 1.14	2.67
H_2O^-	59	0.07	0.11	0.04	0.03	0.01 - 0.54	1.57
LOI	59	0.59	0.67	0.42	0.39	0.12 - 3.35	1.14
Zn	59	11	15.1	-	6	<3 - 105	1.37
Cu	59	4.4	14.7	-	<LLD	<3 - 95	3.34
Ni	59	7.5	15.0	-	5	<3 - 102	2.00
Co	59	3.7	3.8	-	4	<3 - 26	1.03
Ga	59	2.9 *)	6.2	-	<LLD	<3 - 31	2.14
Mo	59	7.6	2.6	-	8	<2 - 13	0.34
Nb	59	3.0	3.3	-	3	<2 - 16	1.10
Zr	59	120	143.0	86	66	26 - 975	1.19
Y	59	11	19.8	-	7	<2 - 149	1.80
Sr	59	27	69.5	9.6	7	2 - 438	2.57
Rb	59	19	34.8	-	9	<2 - 184	1.83
U	59	1.4 *)	3.0	-	<LLD	<5 - 13	2.14
Th	59	2.3 *)	4.7	-	<LLD	<5 - 18	2.04
Pb	59	6.5	19.6	-	<LLD	<5 - 141	3.02
Cr	59	174	55.1	164	185	58 - 338	0.32
V	59	31	24.7	-	24	<14 - 151	0.80
Ba	59	199	222.1	123	124	20 - 1243	1.12
Sc	59	2.3 *)	4.8	-	<LLD	<8 - 22	2.09
As	59	0.9 *)	3.0	-	<LLD	<10 - 11	3.33
S	59	84	176.1	-	<LLD	<50 - 891	2.10
Sb	59	0.4 *)	1.8	-	<LLD	<8 - 8	4.50
Sn	59	1.4 *)	4.0	-	<LLD	<8 - 16	2.86
B	9	45	41.1	32	32	10 - 129	0.91

Table 3.3.9.1: Average element concentrations of sandstones from the Daspoort Formation (n = number of samples; 'MEAN' = arithmetic mean; 'STD ±' = 1 σ standard deviation; 'GM' = geometric mean; 'MEDIAN' = median; 'VC' = variation coefficient; average major element concentrations are reported in weight %, average trace element concentrations in ppm; 'Fe_2O_3*' is all Fe expressed as Fe_2O_3; *) = arithmetic mean below detection limit; LLD = lower limit of detection)

Table 3.3.9.2: Average ratios of Daspoort Formation sandstones

(NOTE: ratios are not corrected, i.e. a sample was excluded from calculation of the average ratio if one or both elements are below the detection limit; n.c. = not calculated)

Ratio	n	MEAN	STD ±	GM	RANGE	VC
CIA	59	74.6	7.3	73.8	44.5 - 93.4	0.10
SiO_2/Al_2O_3	59	114	136.9	65	3.5 - 706	1.20
lg SiO_2/Al_2O_3	59	1.81	n.c.	n.c.	n.c.	n.c.
K_2O/Na_2O	45	10.5	12.6	6.0	0.3 - 72.7	1.20
lg Na_2O/K_2O	45	-0.78	n.c.	n.c.	n.c.	n.c.
Ti/Zr	58	10.6	7.3	7.9	0.7 - 26.2	0.69
Ti/Cr	58	5.9	4.6	4.2	0.5 - 25.4	0.78
Al/Zr	59	155	173.4	88	3.5 - 810	1.12
Al_2O_3/TiO_2	58	27.3	31.8	12.5	0.8 - 127.3	1.17
Al_2O_3/K_2O	53	5.5	4.2	4.8	1.9 - 28.0	0.76
K/Rb	50	256	198	229	106 - 1550	0.77
K/Ba	53	28	23	21	2.9 - 108	0.82
K/Sr	53	423	349	286	10 - 1826	0.83

exhibits a considerably higher average SiO_2-content than average sandstones (Table 3.2.1c). The other major elements are accordingly depleted, with CaO and MgO showing strong depletion. Co, Mo, Nb and especially Cr are enriched, Ga, Zr, Y and Rb depleted compared to average sandstone estimates (Table 3.2.1d).

Shale beds with a thickness of a few cm to dm occur locally in the Daspoort Formation quartzites. The average geochemistry of the shales (Appendix 2a) shows enrichment of SiO_2 and depletion of varying degrees for all other major elements, with CaO and Na_2O strongly depleted compared to average shale estimates (Table 3.2.1b). Zr, Cr, B and Mo are enriched, Zn, Co, Sr, Rb, Pb and V are depleted compared to average shale estimates (Table 3.2.1d). K_2O/Na_2O and SiO_2/Al_2O_3 are enriched compared to, respectively, Post-Archaean Average Shale (Taylor and McLennan, 1985) and Pontiac Average Metamorphic Shale (Feng et al., 1993); Th/U is depleted compared to Post-Archaean Average Shale (Taylor and McLennan, 1985). The element ratios Cr/V and Ni/Co resemble Late Archaean Average Shale (Taylor and McLennan, 1985), although they are slightly elevated, and the V/Ni-ratio exceeds the average values reported for Post-Archaean Average Shale, Late Archaean Average Shale, and Early Archaean Average Shale (Taylor and McLennan, 1985).

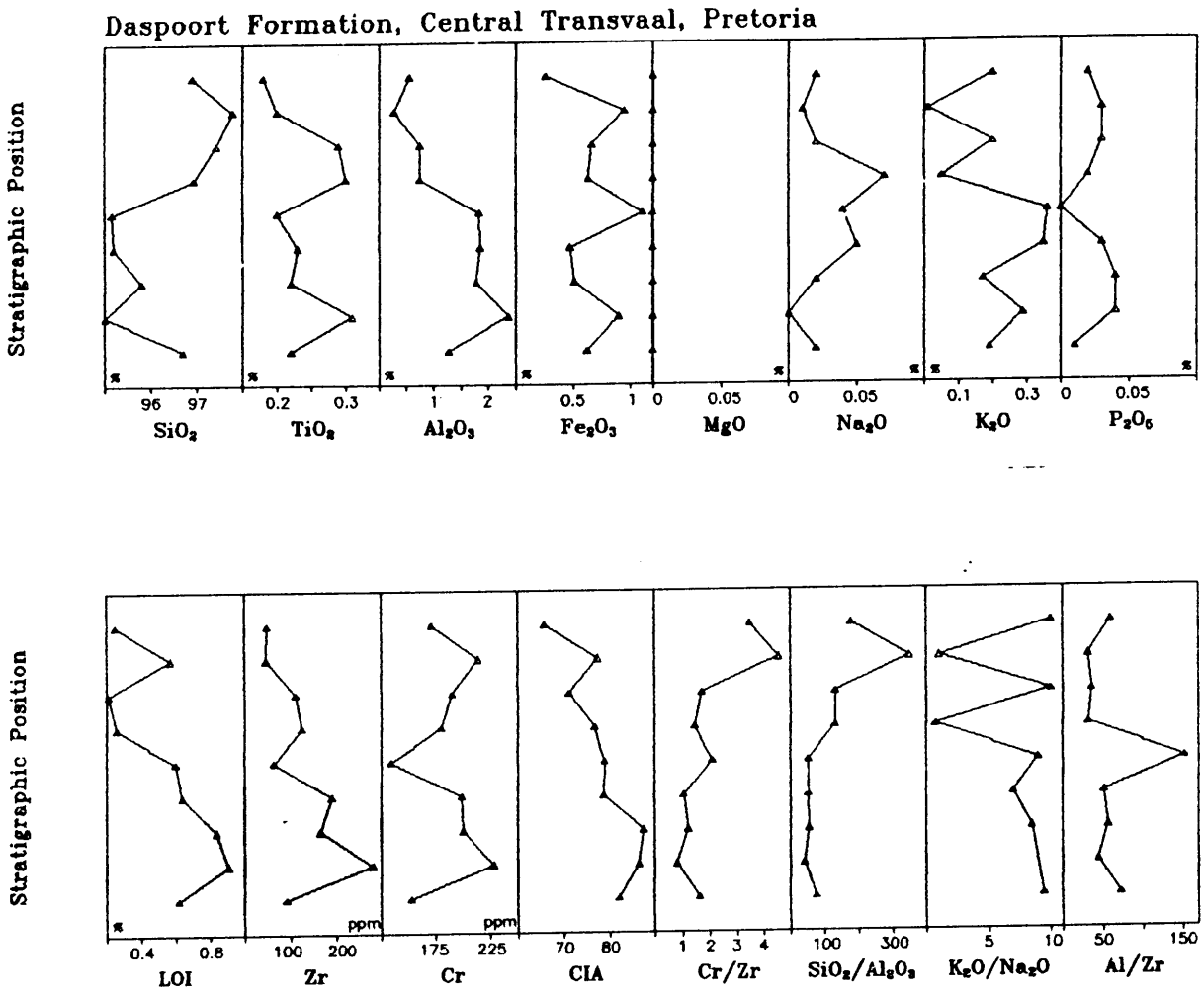

Figure 3.3.9.1: Geochemical profile of the Daspoort Formation, Pretoria, central Transvaal. Lithological type: Δ = sandstone. Vertical scale = ± 70 m in total.

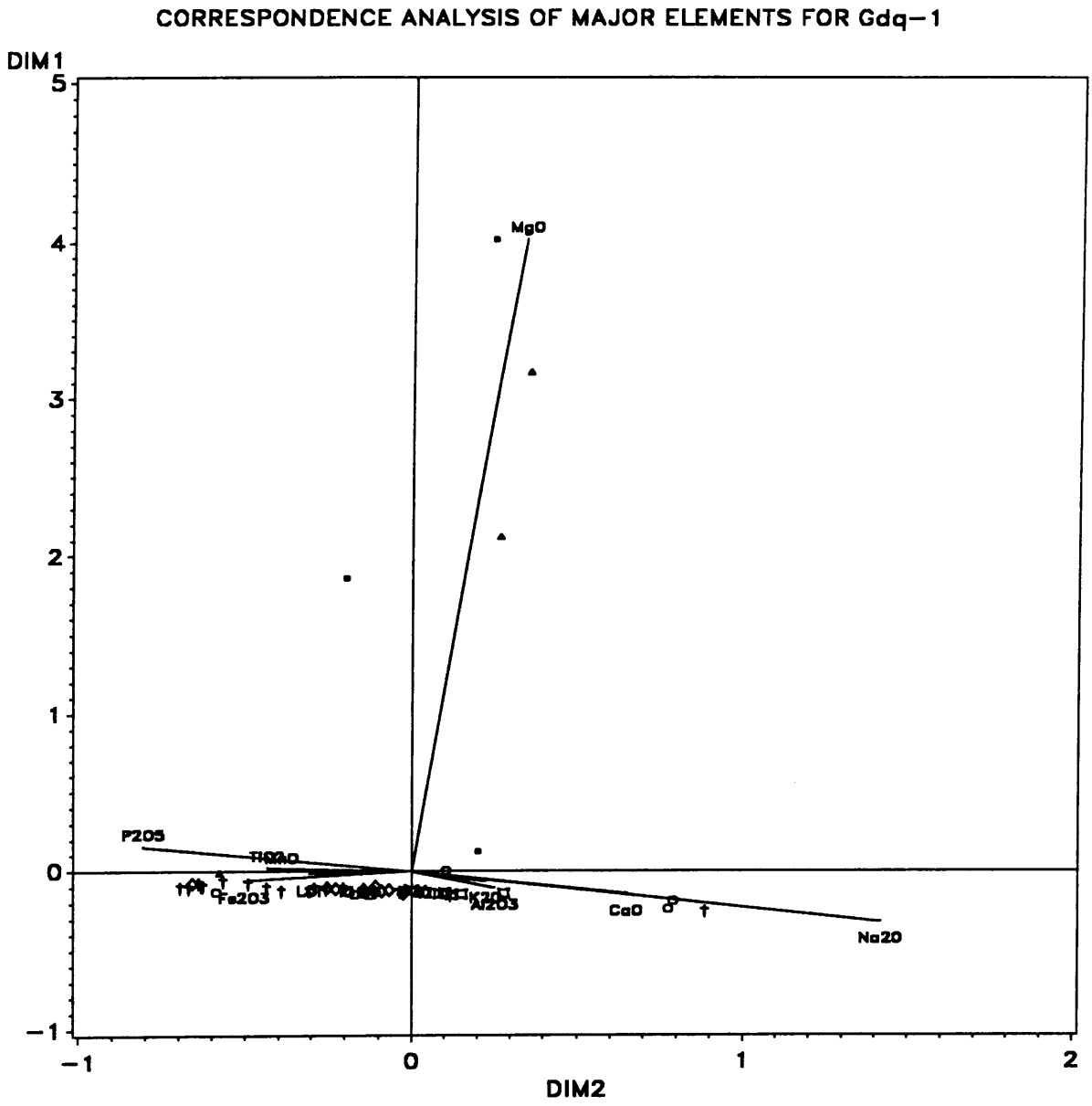

Figure 3.3.9.2: Correspondence analysis of major elements (except SiO_2) of sandstones from the Daspoort Formation. Symbols for sampling areas: ● (red) = eastern Transvaal; ○ (red) = northeastern Transvaal; □ (violet) = eastern fragments; ◇ (green) = central Transvaal; ▲ (blue) = western Transvaal; † (blue) = western fragments; ‡ (blue) = northwestern Transvaal; ★ (yellow) = Botswana. Definition of sampling areas is shown in Figure 1.5.1. DIM 1 and DIM 2 are the values of the factor loadings of the samples and variables for the first and second factor (see Chapter 2.3.2). Angles between lines connecting a variable and the point (0,0) are proportional to the product moment correlation coefficient of these variables.

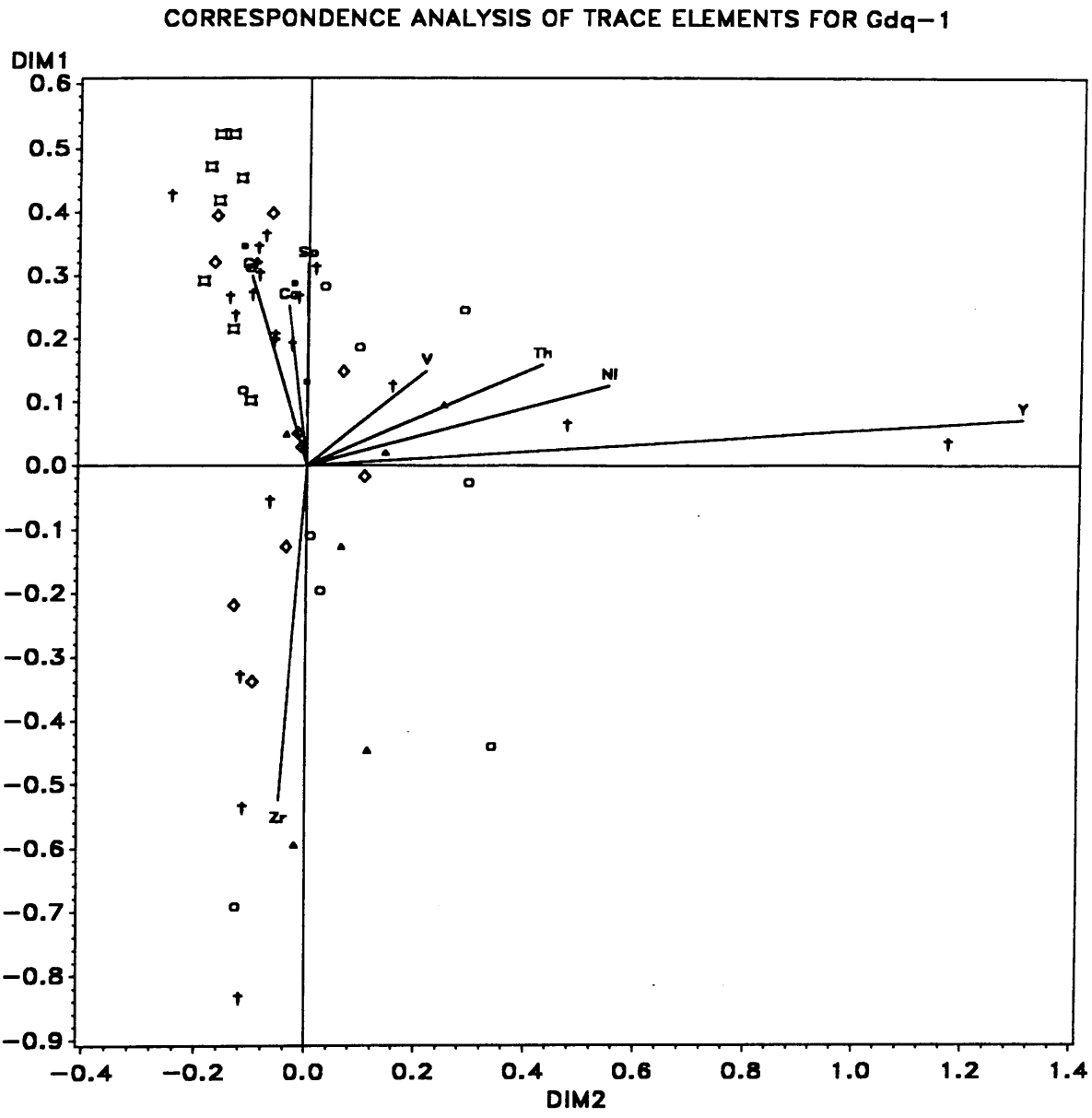

Figure 3.3.9.3: Correspondence analysis of selected trace elements of sandstones from the Daspoort Formation. Symbols for sampling areas: ● (red) = eastern Transvaal; ○ (red) = northeastern Transvaal; □ (violet) = eastern fragments; ◇ (green) = central Transvaal; ▲ (blue) = western Transvaal; † (blue) = western fragments; ‡ (blue) = northwestern Transvaal; ★ (yellow) = Botswana. Definition of sampling areas is shown in Figure 1.5.1. DIM 1 and DIM 2 are the values of the factor loadings of the samples and variables for the first and second factor (see Chapter 2.3.2). Angles between lines connecting a variable and the point (0,0) are proportional to the product moment correlation coefficient of these variables.

One complete geochemical profile (Fig. 3.3.9.1) was taken from the central Transvaal (see Fig. 1.5.10 for location of profile). Only quartzitic rocks of more than 95 wt.% SiO_2 occurred. The thickness of the profile is approximatly 70 m. The major elements MgO, Na_2O, K_2O, and CaO (not shown) are strongly depleted. Zr decreases upwards throughout the profile, except for the lowermost sample. Cr is strongly enriched compared to average sandstone estimates (Table 3.2.1d).

Correspondence analysis of the major elements of all the sandstones/quartzites sampled from the Daspoort Formation reveals a high degree of geochemical conformity in the sample set (Fig. 3.3.9.3). Correspondence analysis of selected trace elements exhibits a cluster for the eastern fragments samples, but reveals no pattern for the other sample areas.

3.3.10 Silverton Formation

The major element geochemistry of the Silverton Formation shales (Tables 3.3.10.1, 3.3.10.2 and 3.3.10.4) is similar to Post-Archaean Average Shale (Taylor and McLennan, 1985) and the North American Shale Composite (Gromet et al., 1984). Deviations from these estimates (Table 3.2.1b) are generally smaller than differences between these estimates themselves. If the other estimates listed in Table 3.2.1b are taken into account, only K_2O is somewhat depleted. Cr, Sc and B show elevated average contents compared with average shale estimates (Table 3.2.1d), and Cu, Co, Zr, Li and Sr are depleted. The increase/depletion of trace elements is only minor, and might not be significant. The REE (Table 3.3.10.4) show a slight enrichment of La, strong depletion of Ce and slight depletion of the HREE, except for Gd. Σ REE is depleted, and the LREE/HREE ratio is enriched compared to Post-Archaean Average Shale (Taylor and McLennan, 1985). The Th/Sc-ratio (Table 3.3.10.3) is intermediate between values given for Post-Archaean Average Shale and Archaean Average Shale (Taylor and McLennan, 1985); K_2O/Na_2O is enriched compared to Post-Archaean Average Shale. The Cr/V ratio resembles Post-Archaean Average Shale, V/Ni exceeds all average shale estimates (Table 3.2.1e), and Ni/Co is similar to Late Archaean Average Shale (Taylor and McLennan, 1985), although slightly elevated.

Element	n	MEAN	STD ±	GM	MEDIAN	RANGE	VC
SiO_2	203	60.49	7.02	60.04	61.18	29.08 - 89.23	0.12
TiO_2	203	0.69	0.24	-	0.67	<LLD - 1.76	0.35
Al_2O_3	203	15.75	3.85	14.96	15.34	0.32 - 25.37	0.24
Fe_2O_3*	203	6.86	3.53	5.94	6.60	0.50 - 35.64	0.52
MnO	203	0.09	0.07	-	0.06	<LLD - 0.60	0.78
MgO	203	3.24	2.95	2.35	2.54	0.11 - 20.66	0.91
CaO	203	1.73	3.08	-	0.64	<LLD - 27.45	1.78
Na_2O	203	1.25	1.24	-	0.89	<LLD - 5.92	0.99
K_2O	203	2.44	1.14	1.82	2.59	0.01 - 5.46	0.47
P_2O_5	203	0.09	0.08	-	0.07	<LLD - 0.81	0.89
H_2O^-	203	0.87	1.14	0.49	0.44	0.04 - 6.92	1.31
LOI	203	6.04	5.38	-	4.65	-0.05 - 31.00	0.89
Zn	203	87	55.8	70	75	7 - 414	0.64
Cu	203	30	33.9	19	22	<3 - 263	1.13
Ni	203	63	31.2	53	60	<3 - 160	0.50
Co	203	16	11.7	12	13	<3 - 70	0.73
Ga	203	21	10.4	19	20	<3 - 140	0.50
Mo	203	1.4 *)	2.6	-	<LLD	<2 - 18	1.86
Nb	203	12	3.1	11	12	4 - 22	0.26
Zr	203	142	42.3	134	141	7 - 263	0.30
Y	203	28	11.6	26	25	<2 - 96	0.41
Sr	203	82	58.3	64	64	3 - 342	0.71
Rb	203	124	58.1	88	138	<2 - 228	0.47
U	203	3.5 *)	3.9	-	<LLD	<5 - 13	1.11
Th	203	13	5.2	11	12	<5 - 31	0.40
Pb	203	19	15.7	15	16	<5 - 100	0.83
Cr	203	145	82.6	123	120	<14 - 528	0.57
V	203	145	78.7	132	126	30 - 599	0.54
Ba	203	848	1108.4	563	659	<16 - 10786	1.31
Sc	203	19	7.6	17	18	<8 - 50	0.40
As	203	3.8 *)	11.4	-	<LLD	<10 - 66	3.00
S	203	1807	4733.1	336	220	<50 - 30176	2.62
Sb	203	1.2 *)	4.7	-	<LLD	<8 - 50	3.92
Sn	203	2.5 *)	7.2	-	<LLD	<8 - 82	2.88
B	39	152	256.4	85	123	4 - 1670	1.69

Table 3.3.10.1: Average element concentrations of shales from the Silverton Formation

(n = number of samples; 'MEAN' = arithmetic mean; 'STD ±' = 1 σ standard deviation; 'GM' = geometric mean; 'MEDIAN' = median; 'VC' = variation coefficient; average major element concentrations are reported in weight %, average trace element concentrations in ppm; 'Fe_2O_3*' is all Fe expressed as Fe_2O_3; *) = arithmetic mean below detection limit; LLD = lower limit of detection)

Table 3.3.10.2: Average major element concentrations of shales from the Silverton Formation recalculated to 100 % volatile-free.

Element	n	MEAN	STD ±	RANGE
SiO2	203	65.27	6.27	42.68 - 93.03
TiO2	203	0.74	0.24	<LLD - 1.94
Al2O3	203	16.98	3.95	0.32 - 26.87
Fe2O3*	203	7.36	3.61	0.52 - 35.76
MnO	203	0.08	0.09	<LLD - 0.77
MgO	203	3.57	3.52	0.12 - 30.46
CaO	203	1.93	3.83	<LLD - 39.67
Na2O	203	1.34	1.29	<LLD - 5.91
K2O	203	2.63	1.22	0.01 - 5.90
P2O5	203	0.10	0.09	<LLD - 0.93

Table 3.3.10.3: Average ratios of shales from the Silverton Formation

(NOTE: ratios corrected as described in Chapter 3.1.2)

Ratio	n	MEAN	STD ±	GM	RANGE	VC
CIA	203	68.4	14.9	65.9	7.7 - 91.9	0.22
Fe/V	203	389	577	315	22 - 8309	1.48
K_2O/Na_2O	201	9.8	21.1	2.5	0.01 - 192	2.15
SiO_2/Al_2O_3	203	5.2	14.1	4.0	2.2 - 198	2.71
Cr/Th	202	13.5	12.3	10.6	1.3 - 95.8	0.91
Th/Sc	201	0.77	0.39	0.67	0.11 - 2.50	0.51
Cr/Zr	203	1.32	2.61	0.93	0.10 - 36.00	1.98
Co/Th	201	1.63	1.78	1.04	0.12 - 8.62	1.09
Al_2O_3/TiO_2	202	23.7	4.6	23.1	8.1 - 34.1	0.19
Al_2O_3/K_2O	203	19.7	53.0	8.2	3.0 - 361.5	2.69
K/Rb	203	177	80	168	42 - 950	0.45
K/Ba	203	34	21	27	0.6 - 172	0.62
Ti/Ni	202	106	152	74	11 - 1399	1.43
Cr/V	203	1.11	0.71	0.94	0.03 - 8.40	0.64
V/Ni	203	3.33	4.57	2.48	0.51 - 44.67	1.37
Ni/Co	203	5.32	4.34	4.35	0.50 - 33.78	0.82
Zr/Nb	203	12.4	3.3	11.9	1.4 - 25.8	0.27
Th/U	193	2.23	0.85	2.06	0.50 - 5.21	0.38
Ba/Rb	203	12	29	6	1.5 - 337	2.42
Ba/Sr	203	17	36	9	0.3 - 433	2.12
Ba/Th	203	68	94	48	3.2 - 981	1.38
Al/Zr	203	622	198	593	242 - 1210	0.32
Ti/Zr	202	30.7	10.5	29.2	16.2 - 69.4	0.34

Table 3.3.10.4: Average element concentrations and ratios of selected shale samples of the Silverton Formation

(n = number of samples; 'MEAN' = arithmetic mean; 'STD ±' = 1 σ standard deviation; 'GM' = geometric mean; 'MEDIAN' = median; 'VC' = variation coefficient; average major element concentrations (i.e. FeO to S_{XRF}) are reported in weight %, average trace element concentrations in ppm; n.c. = not calculated; subscript N = concentration normalised to chondrite; Ce/Ce* = $Ce_N/[(La_N + Pr_N)/2]$; Σ REE = sum of REE in ppm; NOTE: ratios corrected as described in Chapter 3.1.2; LLD = lower limit of detection)

ELEMENT	n	MEAN	STD ±	GM	MEDIAN	RANGE	VC
FeO	20	2.72	3.04	0.93	1.37	0.10 - 8.80	1.12
Fe_2O_3	20	2.90	2.54	1.61	2.02	0.03 - 7.75	0.88
CO_2	20	0.87	1.45	0.42	0.37	0.07 - 5.24	1.67
C_{org}	20	2.21	4.22	0.23	0.11	0.01 - 12.64	1.91
H_2O^+	20	3.22	1.25	2.96	3.58	1.40 - 4.95	0.39
S_{leco}	20	1470	4050	-	45	<10 - 17900	2.76
S_{xrf}	20	1665	3742	467	283	<50 - 16570	2.25
Li	20	41	27.7	33	35	7 - 124	0.68
La	20	44.6	36.4	37.0	34.4	12.1 - 185	0.82
Ce	20	42.2	25.4	32.6	40.3	2.4 - 103	0.60
Pr	20	9.3	8.0	7.5	6.2	2.8 - 39.7	0.86
Nd	20	31.4	28.5	24.5	21.8	7.6 - 138	0.91
Sm	20	5.6	4.2	4.7	4.1	2.2 - 21.1	0.75
Eu	20	1.03	0.67	0.90	0.85	0.5 - 3.4	0.65
Gd	20	4.6	3.3	3.9	3.3	2.2 - 17.3	0.72
Tb	20	0.66	0.44	0.58	0.50	0.3 - 2.3	0.66
Dy	20	3.9	2.5	3.4	3.1	1.9 - 13.1	0.64
Er	20	2.2	1.4	1.9	1.9	0.9 - 7.0	0.64
Tm	20	0.31	0.18	0.27	0.25	0.1 - 0.9	0.58
Yb	20	2.2	1.1	2.0	2.0	1.0 - 6.0	0.50
La/Sc	20	2.65	2.25	2.17	2.16	0.42 - 11.56	0.85
Th/La	20	0.42	0.17	0.39	0.39	0.14 - 0.90	0.41
Ba/La	20	41.9	88.9	21.5	17.1	7.8 - 411.4	2.12
LREE/HREE	20	13.61	5.56	12.35	13.73	4.09 - 23.11	0.41
K2O/ΣREE	20	218	113	193	190	58 - 493	0.52
Gd_N/Yb_N	20	1.59	0.40	1.54	1.60	0.93 - 2.34	0.25
La_N/Sm_N	20	5.07	1.15	4.93	5.08	2.42 - 7.21	0.23
Ce/Ce*	20	0.531	0.273	0.436	0.622	0.093 - 0.866	0.51
Eu/Eu*	20	0.636	0.142	0.623	0.619	0.488 - 1.103	0.22
C_{org}/S	20	29.5	65.7	4.6	2.8	0.1 - 290	2.23
ΣREE	20	147.7	97.8	126.8	112.7	38.5 - 494.2	0.66

In the eastern and northeastern Transvaal sampling areas, the Silverton Formation is subdivided into the lower Boven Shale Member, the medial Machadodorp Volcanic Member, and the upper Lydenburg Shale Member. The Boven Shale Member (Tables 3.3.10.5 and 3.3.10.6) is enriched in SiO_2 and depleted in Fe_2O_3(t), MnO, MgO, CaO and K_2O compared to average shale estimates. The trace element B is strongly enriched, Sc moderately so, and Zn, Cu, Ni and Co slightly depleted in the Boven shales. All REE are enriched with the exception of Ce, which is strongly depleted. The enrichment factor of the REE, calculated from the average contents, against the North American Shale composite (Gromet et al., 1984) decreases from 2.5 for La to 1.1 for Yb. Σ REE, LREE/HREE and La/Sc are strongly enriched in the Boven Shale Member compared to Post-Archaean Average Shale (Taylor and McLennan, 1985).

The Lydenburg Shale Member (Tables 3.3.10.7 and 3.3.10.8) major element geochemistry shows enrichment of SiO_2, and depletion of Al_2O_3, K_2O, and, to a minor degree, TiO_2 compared to average shale estimates (Table 3.2.1b). Cu and Co are also depleted compared to average shale estimates (Table 3.2.1d). The REE are generally depleted, with strong depletion of Ce, Er, Tm and Yb, but no depletion/enrichment of La, compared to Post-Archaean Average Shale (Taylor and McLennan, 1985) and North American Shale Composite (Gromet et al., 1984). The REE average contents and Σ REE resemble Archaean Average Shale (Taylor and McLennan, 1985), with the exception of La. Eu/Eu* is significantly increased compared to Post-Archaean Average Shale (Taylor and McLennan, 1985), but does not reach the value of Archaean Average Shale (Taylor and McLennan, 1985). La/Sc is depleted compared to Post-Archaean Average Shale (Taylor and McLennan, 1985). K_2O/Na_2O is slightly elevated compared to Post-Archaean Average Shale (Taylor and McLennan, 1985). However, if the geometric mean of the K_2O/Na_2O-ratio is taken as a fair estimate of the mean, which has to be considered due to the high variation coefficient pointing to a strongly skewed distribution, the average K_2O/Na_2O-ratio matches the estimate for Post-Archaean Average Shale (Taylor and McLennan, 1985). Th/Sc and Cr/V ratios have averages between Post-Archaean Average Shale and Archaean Average Shale (Taylor and McLennan, 1985), Ni/Co lies between the estimates for Early Archaean Average Shale and Late Archaean Average Shale(Taylor and McLennan, 1985), and V/Ni exceeds all reported values (Table 3.2.1e).

Element	n	MEAN	STD ±	GM	MEDIAN	RANGE	VC
SiO_2	29	63.06	3.80	62.96	62.43	57.42 - 75.28	0.06
TiO_2	29	0.70	0.11	0.69	0.72	0.41 - 0.90	0.16
Al_2O_3	29	18.05	3.40	17.75	17.17	13.97 - 25.37	0.19
Fe_2O_3*	29	5.27	2.45	4.47	5.75	0.85 - 10.36	0.47
MnO	29	0.04	0.06	-	0.03	<LLD - 0.28	1.50
MgO	29	1.66	1.17	1.12	1.71	0.11 - 4.55	0.71
CaO	29	0.32	0.52	-	0.05	<LLD - 1.86	1.63
Na_2O	29	1.34	1.35	-	0.86	<LLD - 4.97	1.01
K_2O	29	2.80	0.88	2.64	2.78	1.03 - 4.48	0.31
P_2O_5	29	0.06	0.03	-	0.05	<LLD - 0.12	0.50
H_2O^-	29	0.64	0.47	0.50	0.48	0.09 - 2.13	0.73
LOI	29	5.25	1.84	4.96	4.72	1.88 - 9.91	0.35
Zn	29	73	61.5	48	62	7 - 246	0.84
Cu	29	35	26.6	28	30	7 - 136	0.76
Ni	29	49	33.9	35	46	3 - 134	0.69
Co	29	7.9	5.1	5.9	8.0	<3 - 16	0.65
Zr	29	175	48.5	169	155	81 - 263	0.28
Rb	29	133	43.5	118	142	9 - 206	0.33
Th	29	17	5.5	16	16	8 - 26	0.32
Pb	29	26	22.8	19	23	<5 - 95	0.88
Cr	29	132	42.2	126	126	65 - 225	0.32
V	29	121	21.6	119	128	71 - 152	0.18
Sc	29	20	4.5	20	20	11 - 28	0.23
S	29	960	2620.5	206	159	<50 - 13693	2.73
B	12	261	445.0	160	128	106 - 1670	1.71
La	5	78.6	60.7	65.3	59.4	31.8 - 185	0.77
Ce	5	49.9	33.0	42.6	34.2	22.7 - 103	0.66
Pr	5	17.1	13.2	13.8	13.7	5.1 - 39.7	0.77
Nd	5	60.0	45.9	47.8	49.4	15.6 - 138	0.77
Sm	5	10.0	6.7	8.4	8.5	3.2 - 21.1	0.67
Eu	5	1.8	1.0	1.6	1.6	0.7 - 3.4	0.56
Gd	5	7.9	5.5	6.8	7.0	3.2 - 17.3	0.70
Tb	5	1.2	0.68	1.0	1.1	0.6 - 2.3	0.57
Dy	5	6.6	3.8	5.9	5.8	3.7 - 13.1	0.58
Er	5	3.7	1.9	3.4	3.4	2.0 - 7.0	0.51
Tm	5	0.52	0.23	0.49	0.50	0.3 - 0.9	0.44
Yb	5	3.5	1.5	3.3	3.2	2.0 - 6.0	0.43

Table 3.3.10.5: Average element concentrations of shales from the Boven Shale Member

(n = number of samples; 'MEAN' = arithmetic mean; 'STD ±' = 1 σ standard deviation; 'GM' = geometric mean; 'MEDIAN' = median; 'VC' = variation coefficient; average major element concentrations are reported in weight %, average trace element concentrations in ppm; 'Fe_2O_3*' is all Fe expressed as Fe_2O_3; *) = arithmetic mean below detection limit; LLD = lower limit of detection)

Table 3.3.10.6: Average ratios of shales from the Boven Shale Member

(NOTE: ratios corrected as described in Chapter 3.1.2)

Ratio	n	MEAN	STD ±	GM	RANGE	VC
CIA	29	75.7	9.4	75.1	53.8 - 86.6	0.12
K_2O/Na_2O	28	12.0	17.1	3.7	0.2 - 48.3	1.43
SiO_2/Al_2O_3	29	3.6	0.8	3.6	2.4 - 5.1	0.22
Cr/Th	29	9.1	4.9	8.1	3.5 - 21.9	0.54
Th/Sc	29	0.86	0.33	0.80	0.32 - 1.63	0.38
Cr/Zr	29	0.82	0.39	0.75	0.39 - 1.66	0.48
Co/Th	29	0.62	0.47	0.44	0.12 - 1.78	0.76
K/Rb	29	204	147	185	130 - 950	0.72
Cr/V	29	1.10	0.32	1.06	0.66 - 2.03	0.29
V/Ni	29	6.13	9.06	3.42	0.86 - 44.67	1.48
Ni/Co	29	7.76	7.35	5.01	0.50 - 33.78	0.95
Ti/Zr	29	25.1	4.9	24.6	18.9 - 35.8	0.20
La/Sc	5	4.18	4.18	3.09	1.22 - 11.56	1.00
LREE/HREE	5	14.44	6.10	13.39	7.67 - 20.88	0.42
Gd_N/Yb_N	5	1.74	0.54	1.66	0.93 - 2.34	0.31
La_N/Sm_N	5	4.97	0.95	4.90	3.83 - 6.26	0.19
Ce/Ce*	5	0.38	0.26	0.32	0.16 - 0.79	0.68
Eu/Eu*	5	0.61	0.05	0.61	0.53 - 0.66	0.08
Σ REE	5	240.7	151.7	208.6	99.1 - 494.2	0.63

Sandstones occur locally in the Silverton Formation. The average geochemistry of sandstones from the Silverton Formation is given in Appendix 2a. The sandstones have a fairly variable geochemistry, with SiO_2-contents ranging from 57 - 98 wt.%. Other major and trace elements vary accordingly.

Figure 3.3.10.1 shows a composite geochemical profile of the Silverton Formation in the eastern and northeastern Transvaal (see Fig. 1.5.11 for location of the various field profiles). The profile for the Boven Shale Member (Vsib) was sampled on the Long Tom Pass east of Lydenburg and has an approximte thickness of 200 m including diabase sills. The profile describes the lower part of the approximately 300 m thick Boven Shale Member. The profile of the Machadodorp Volcanic Member was sampled north of Ga-Mabotsa in the northeastern Transvaal and describes a complete profile with an approximate thickness of 250 m. The

Element	n	MEAN	STD ±	GM	MEDIAN	RANGE	VC
SiO_2	33	65.12	4.06	65.00	65.57	54.98 - 73.01	0.06
TiO_2	33	0.66	0.10	0.65	0.66	0.45 - 0.97	0.15
Al_2O_3	33	15.65	2.70	15.45	15.09	12.03 - 23.15	0.17
Fe_2O_3*	33	6.32	1.85	5.94	6.42	0.88 - 11.76	0.29
MnO	33	0.09	0.04	0.08	0.08	0.01 - 0.17	0.44
MgO	33	2.28	0.73	2.12	2.42	0.69 - 3.76	0.32
CaO	33	1.33	0.78	-	1.19	<LLD - 2.78	0.59
Na_2O	33	1.72	0.89	1.41	1.51	0.01 - 4.21	0.52
K_2O	33	2.80	0.83	2.68	2.66	1.38 - 4.53	0.30
P_2O_5	33	0.10	0.09	0.07	0.06	0.01 - 0.31	0.90
H_2O^-	33	0.65	0.66	0.42	0.39	0.08 - 2.50	1.02
LOI	33	2.77	1.86	2.37	2.50	1.00 - 10.95	0.67
Zn	33	95	68.4	80	76	20 - 401	0.72
Cu	33	30	46.6	16	16	<3 - 263	1.55
Ni	33	52	22.7	47	57	12 - 107	0.44
Co	33	12	6.7	11	12	<3 - 31	0.56
Zr	33	152	37.7	147	158	73 - 209	0.25
Rb	33	148	38.7	143	146	77 - 228	0.26
Th	33	15	5.3	14	14	7 - 31	0.35
Pb	33	26	17	21	22	<5 - 97	0.65
Cr	33	138	45.4	131	129	75 - 231	0.33
V	33	117	28.0	114	106	75 - 193	0.24
Sc	33	19	7.1	17	19	<8 - 35	0.37
S	33	394	979.5	190	147	<50 - 5680	2.49
La	5	38.2	17.9	35.3	34.5	20.1 - 68.4	0.47
Ce	5	34.6	20.0	27.8	38.5	6.6 - 60.4	0.58
Pr	5	6.9	3.8	6.2	5.9	3.3 - 13.3	0.55
Nd	5	21.4	14.0	18.3	18.0	7.6 - 45.1	0.65
Sm	5	4.2	1.7	4.0	3.6	2.7 - 7.2	0.41
Eu	5	0.98	0.21	0.96	1.0	0.8 - 1.3	0.21
Gd	5	3.4	1.0	3.3	3.1	2.6 - 5.1	0.29
Tb	5	0.48	0.15	0.46	0.5	0.3 - 0.7	0.31
Dy	5	2.8	0.69	2.7	2.6	1.9 - 3.8	0.25
Er	5	1.4	0.42	1.4	1.4	0.9 - 2.0	0.30
Tm	5	0.2	0.07	0.19	0.2	0.1 - 0.3	0.35
Yb	5	1.5	0.40	1.5	1.6	1.0 - 2.0	0.27

Table 3.3.10.7: Average element concentrations of shales from Lydenburg Shale Member

(n = number of samples; 'MEAN' = arithmetic mean; 'STD ±' = 1 σ standard deviation; 'GM' = geometric mean; 'MEDIAN' = median; 'VC' = variation coefficient; average major element concentrations are reported in weight %, average trace element concentrations in ppm; 'Fe_2O_3*' is all Fe expressed as Fe_2O_3; *) = arithmetic mean below detection limit; LLD = lower limit of detection)

Table 3.3.10.8: Average ratios of shales from the Boven Shale Member

(NOTE: ratios corrected as described in Chapter 3.1.2)

RATIO	NO.	MEAN	STD ±	GM	RANGE	VC
CIA	33	65.4	8.2	64.9	55.0 - 88.4	0.13
K_2O/Na_2O	33	3.2	4.9	1.9	0.5 - 22.0	1.53
SiO_2/Al_2O_3	33	4.3	0.9	4.2	2.6 - 6.1	2.09
Cr/Th	33	10.5	4.5	9.6	3.8 - 21.9	0.43
Th/Sc	33	0.85	0.36	0.77	0.27 - 1.73	0.42
Cr/Zr	33	0.95	0.36	0.89	0.52 - 1.85	0.38
Co/Th	33	0.97	0.67	0.79	0.21 - 3.44	0.69
K/Rb	33	159	35	156	82 - 276	0.22
Cr/V	33	1.21	0.43	1.15	0.57 - 2.32	0.36
V/Ni	33	2.78	2.09	2.42	1.28 - 12.92	0.75
Ni/Co	33	5.20	5.19	4.41	2.56 - 33.11	1.00
Ti/Zr	33	27.2	5.9	26.6	19.1 - 41.4	0.22
La/Sc	5	2.12	0.61	2.04	1.64 - 3.06	0.29
LREE/HREE	5	17.09	5.44	16.41	11.32 - 23.11	0.32
Gd_N/Yb_N	5	1.85	0.26	1.84	1.48 - 2.11	0.14
La_N/Sm_N	5	5.66	0.56	5.64	4.69 - 6.05	0.10
Ce/Ce*	5	0.49	0.24	0.41	0.10 - 0.68	0.49
Eu/Eu*	5	0.81	0.18	0.79	0.63 - 1.10	0.22
Σ REE	5	116.1	55.5	107.3	68.8 - 209.6	0.48

profile of the Lydenburg Shale Member was sampled on the Watervalsrivier Pass northwest of Lydenburg and has an approximate thickness of 400 m including diabases, and describes the uppermost part of the approximately 700 m thick Lydenburg Shale Member.

The three profiles contain three lithological units, shales, high-Mg-Ca-Na shales and volcanic rocks. The Boven Shale Member profile shows a generally low variability for most elements and ratios. Na_2O, Zr and Th decrease upwards in the profile, except for the three uppermost samples. The Machadodorp Volcanic Member has a fairly high variability, which is not only caused by differences in lithology. Defined stratigraphic patterns are not obvious. The Lydenburg Shale Member depicts both high and low variability, depending on the respective element or ratio. The occurrence of systematic stratigraphic changes can be inferred on a general basis for SiO_2 and SiO_2/Al_2O_3 (increase upwards), and for TiO_2, Al_2O_3 and CIA (decrease upwards), although outlier values and/or partial trends make the identification

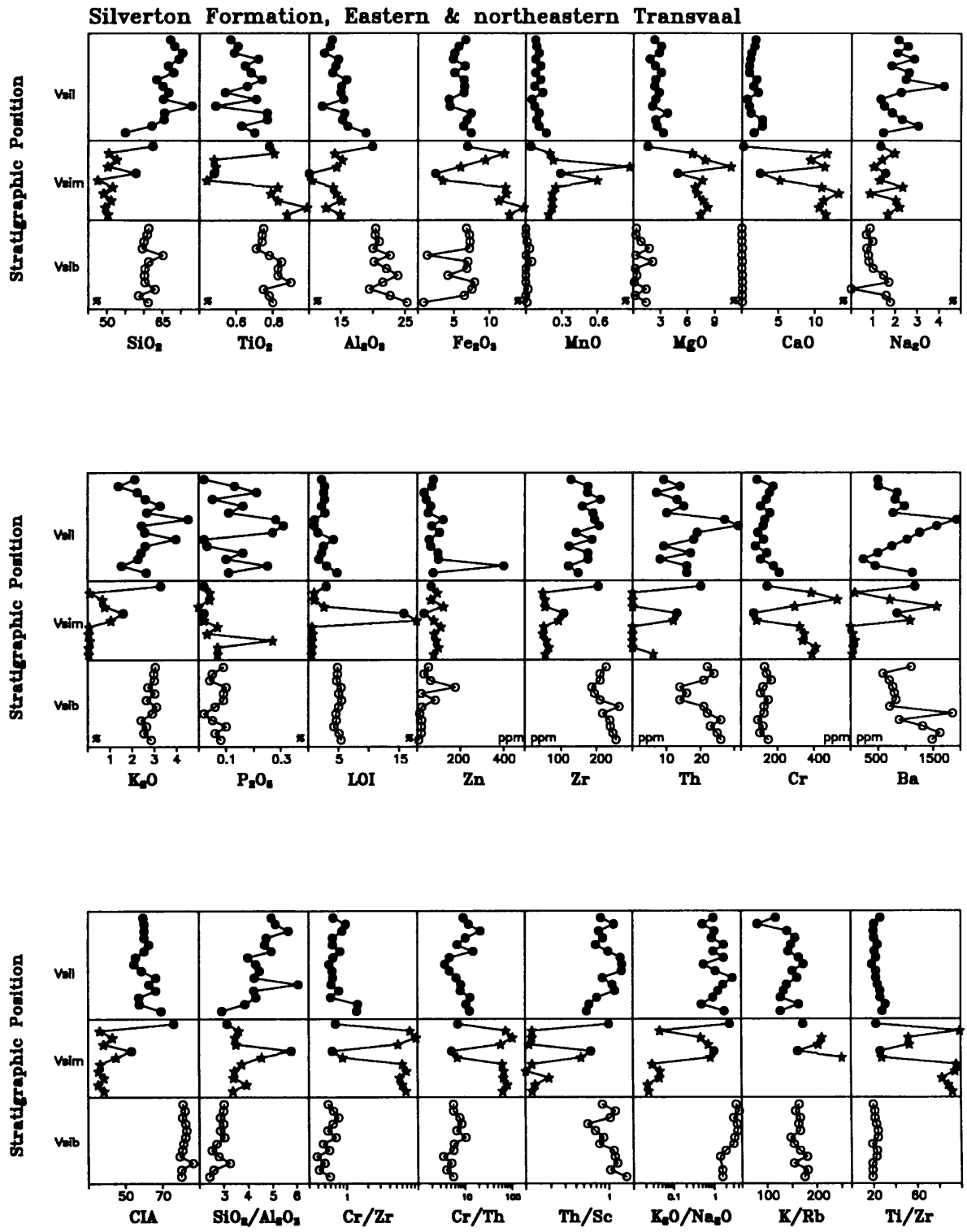

Figure 3.3.10.1: Geochemical profile of the Silverton Formation, eastern and northeastern Transvaal. Vsib: Boven Shale Member, Long Tom Pass, eastern Transvaal; Vsim: Machadodorp Volcanic Member, Ga-Mabotsa, northeastern Transvaal; Vsil: Lydenburg Shale Member, Watervalsrevier Pass, eastern Transvaal. Lithological types: ★ = volcanic rocks; ○ = shale; ● = high-Mg-Ca-Na shale. Vertical scale is variable: Vsib = ± 200 m in total; Vsim = ± 250 m in total; Vsil = ± 400 m in total.

difficult and questionable. Fairly well defined partial trends occur for Ba (middle part, increase upwards) and Cr/Th (lower part, decrease upwards) in the Lydenburg Shale Member.

The Boven and Lydenburg Shale Members can be discriminated by using Al_2O_3, MnO, MgO, CaO, CIA and SiO_2/Al_2O_3. For Na_2O, TiO_2, Zr and SiO_2, a separation effect can be inferred, but is less well defined than with the former elements/ratios. The shale and volcanic rock samples are obviously different for a number of elements and ratios (SiO_2, MgO, CaO, K_2O, Zr, Th, Cr, CIA, Cr/Zr, Cr/Th, Th/Sc, and Ti/Zr). The Ti/Zr-ratio deserves some attention, as the shale samples of all three members exhibit similar values, of about 20. The Ti/Zr-ratio exceeds 50 for all the volcanic rocks samples, except one with values similar to the shales. The latter sample has an unusual geochemistry, with LOI > 15 wt.%, and is also similar to shales in its Cr/Zr, Cr/Th, Th/Sc, Th, Cr and CaO contents.

The borehole STRAT 2 (see Fig. 1.5.11 for location of the borehole) is described in detail by Key (1983). The geochemical profile presented here (Fig. 3.3.10.2, 3.3.10.3 and 3.3.10.4) covers the lower and middle part of the approximately 600 m thick Silverton Formation in Botswana. The core contains several rocktypes: shale, graphitic shale, pyritic shale, shale with veins, calcareous shale, sandstones and an unusual crimson-coloured unit at 250 m depth. The latter unit has a thickness of 1.5 m and was analysed chemically in 5 - 10 cm batches. Only three representative samples of this unit are shown in the profile. A more detailed petrographic description of this unit follows in Chapter 4.5. The oxidation base of the STRAT 2 borehole lies at 20 m. The profile can be divided into the following stratigraphic units from base to top:

(1) lowermost shale beds,
(2) sandstone beds,
(3) pyritic shale beds,
(4) graphitic shale beds, and
(5) upper shale beds (Fig. 4.5.1).

The geochemical patterns of the profile are complex and difficult to summarize. Due to extreme values for one or a few samples (e.g., Fe_2O_3(t), MgO, and SiO_2, Fig. 3.3.10.2), the true variability or systematic changes of some elements may be masked. For example, the

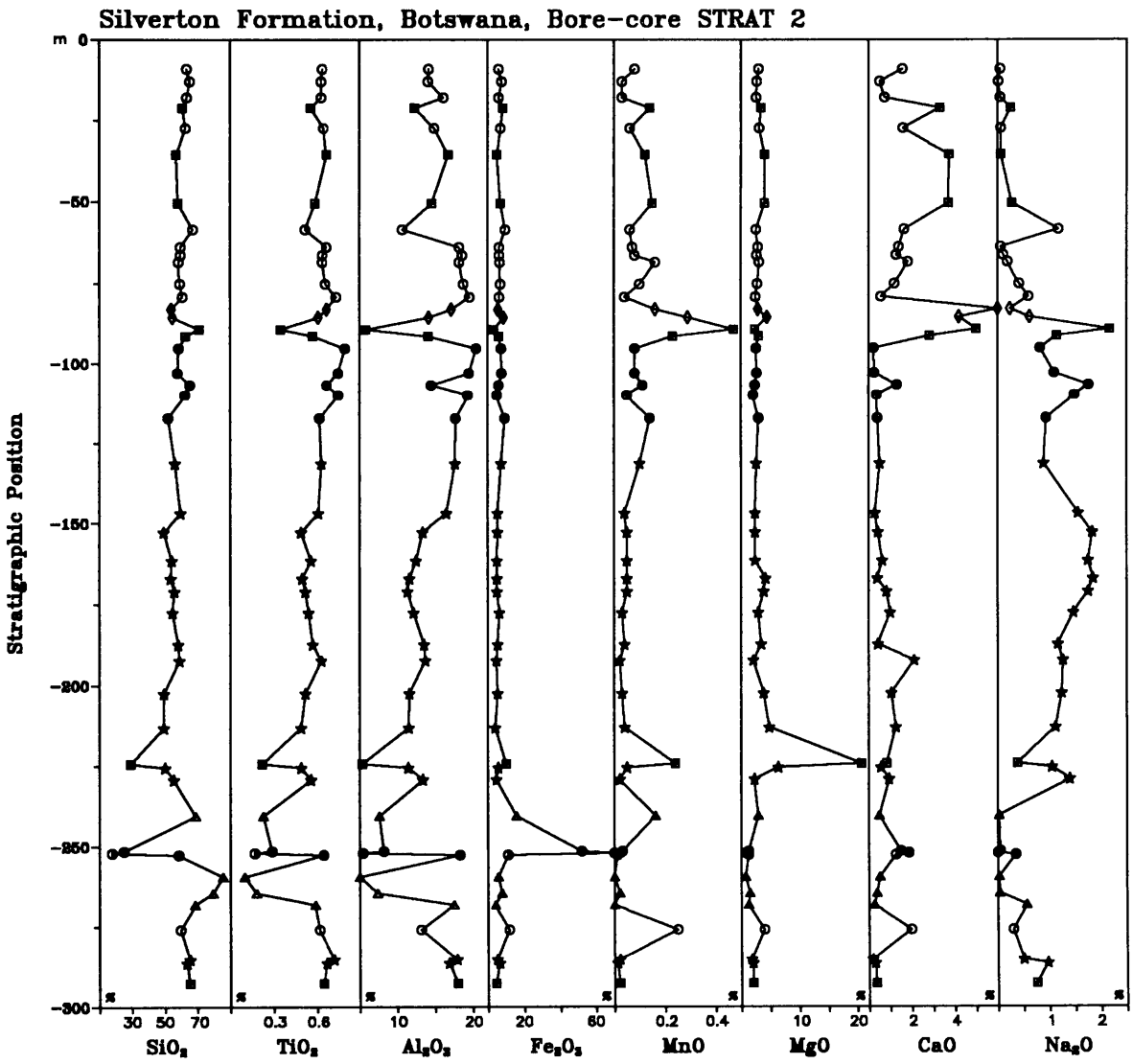

Figure 3.3.10.2: Geochemical profile of the lower part of the Silverton Formation, borehole STRAT 2, Botswana. Lithological types: ○ = shale; ★ = pyritic shale; ● = graphitic shale; ■ = shale with veinlets; ◇ = calcareous shale; Δ = sandstone; ◑ = crimson-coloured unit.

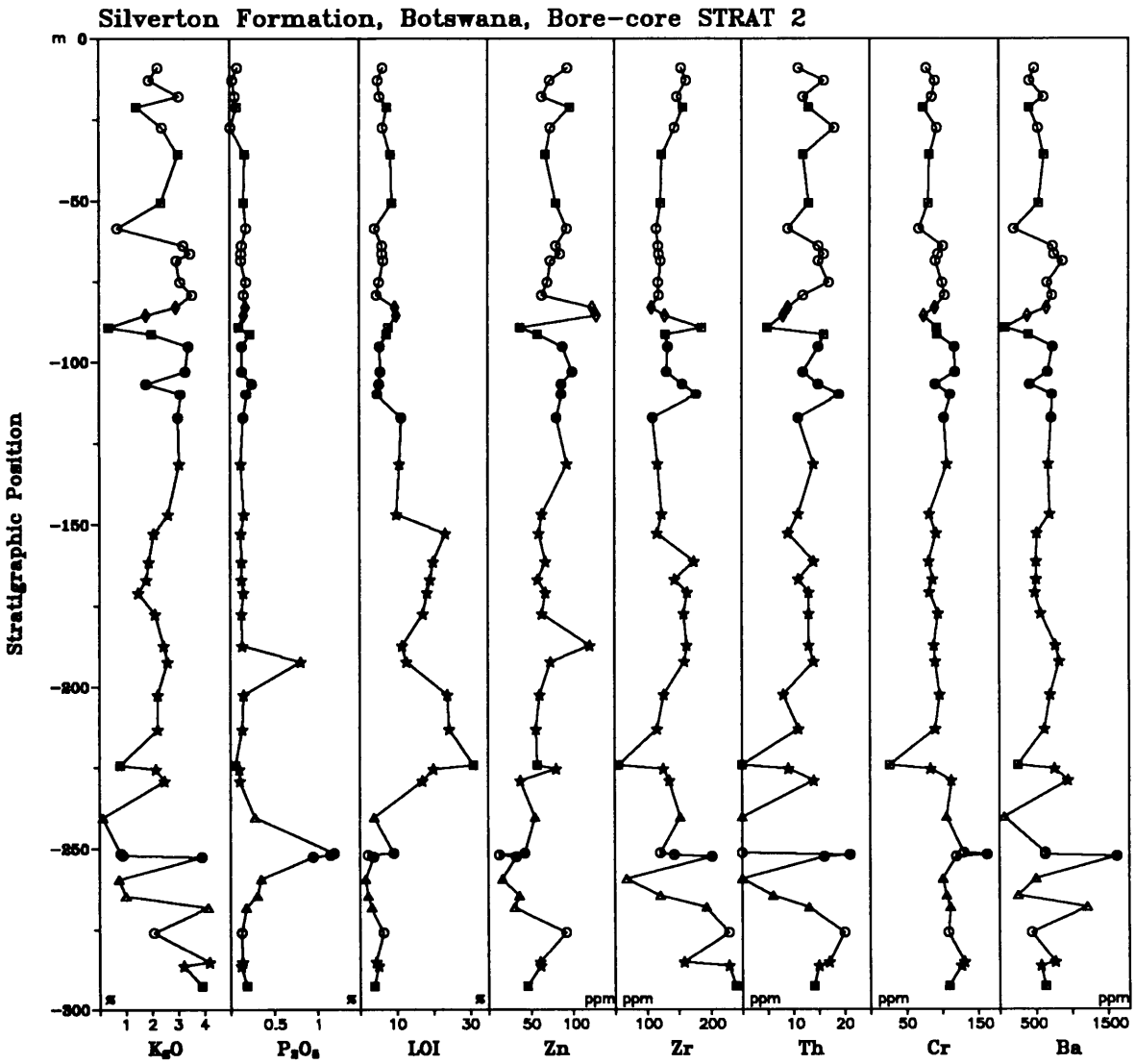

Figure 3.3.10.3: Geochemical profile of the lower part of the Silverton Formation, borehole STRAT 2, Botswana. Lithological types: ○ = shale; ★ = pyritic shale; ● = graphitic shale; ■ = shale with veinlets; ◇ = calcareous shale; Δ = sandstone; ◑ = crimson-coloured unit.

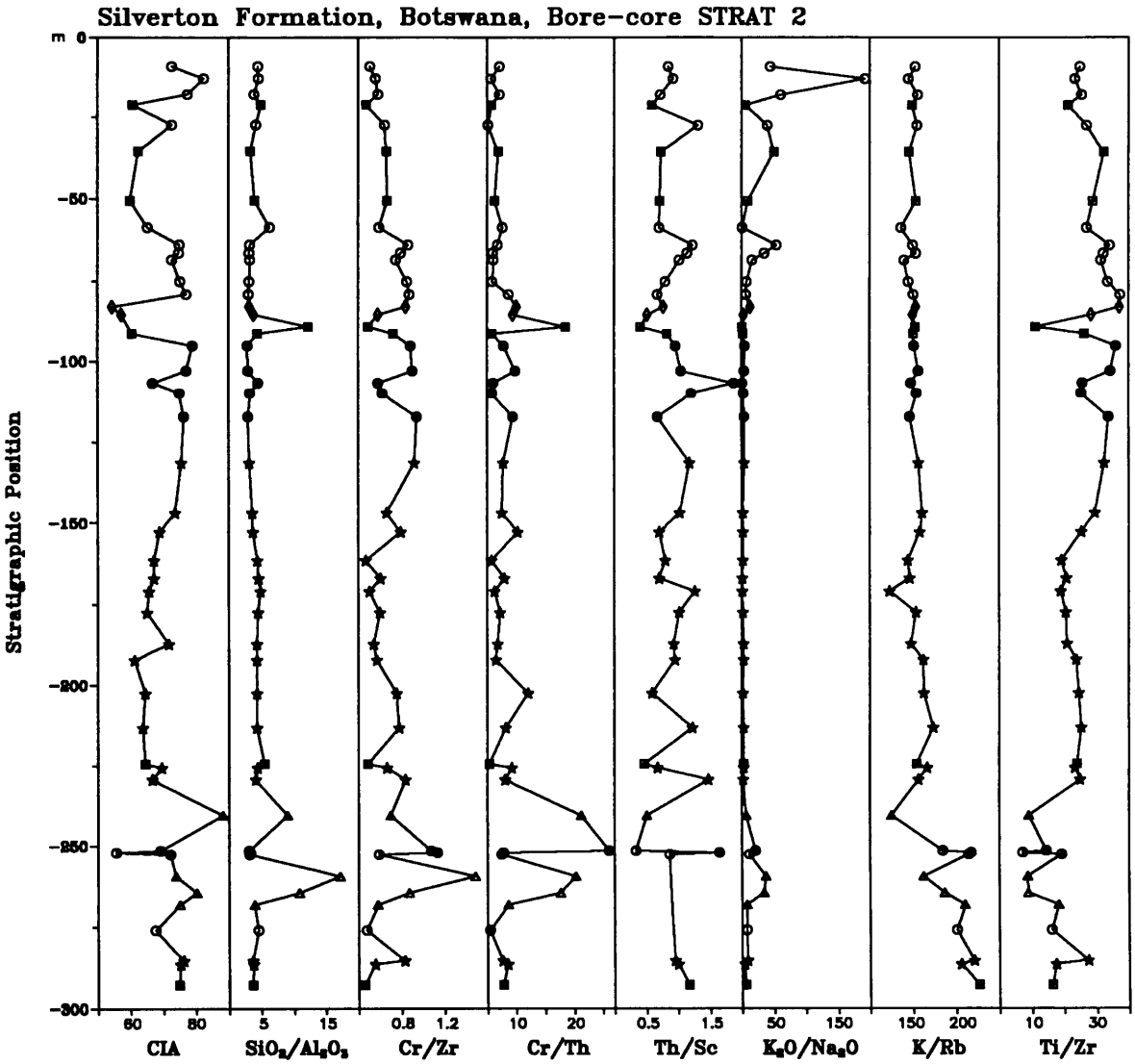

Figure 3.3.10.4: Geochemical profile of the lower part of the Silverton Formation, borehole STRAT 2, Botswana. Lithological types: ○ = shale; ★ = pyritic shale; ● = graphitic shale; ■ = shale with veinlets; ◇ = calcareous shale; Δ = sandstone; ◑ = crimson-coloured unit.

increase of SiO_2 from about 50 wt.% at the base of the pyritic shale beds to about 70 wt.% at the top of the profile is difficult to identify due to the scale used for SiO_2. However, some trends could be established: Al_2O_3 increases from the base of the pyritic shale beds towards the top of the graphitic shale beds, and then declines towards the top of the profile. TiO_2 has a similar pattern from the base of the pyritic shale beds towards the top of the graphitic shales, but is fairly constant in the uppermost part of the profile. The Al_2O_3 and TiO_2 patterns are masked due to a sharp decrease of both elements in calcareous shale samples at the base of the uppermost shale beds of the profile. Na_2O increases in the pyritic and graphitic shale beds. K/Rb decreases generally from the base of the profile towards the top of the pyritic shale beds, and is fairly stable in the upper parts of the profile.

The LES borehole geochemical profile (see Fig. 1.5.11 for location of the profile) from Botswana (Fig. 3.3.10.5) describes the upper 250 m of the Silverton Formation in Botswana. The samples were divided into several lithological types, shales, calcareous shales, carbonates, high-Fe-Mg shales, and sandstones. The profile shows high variability in the upper part of the profile, where sandstones are interlayered with high-Fe-Mg shales. The latter shales also have extraordinarily high contents of Cr. The variability in the lower and middle parts of the profile can be related easily to lithological differences. The carbonates are geochemically most mature (i.e., high CaO, MgO and LOI with corresponding depletion of other major elements) at the base of their occurrence (ca. 360 m depth). The carbonates then become more immature upward in the profile and change successively into calcareous shales. As the CIA has to be corrected for carbonate-CaO (Nesbit and Young, 1982), a calculation of CIA was omitted for calcareous samples.

The central Transvaal (see Fig. 1.5.11 for location of profile) geochemical profile (Fig. 3.3.10.6) contains two units, shale and high-Mg-Ca-Na shale. The profile includes the whole Silverton Formation in the area (east of Pretoria), and has an approximate thickness of 600 m including diabases. Trends can be noted for Th/Sc and P_2O_5, both increasing towards the top of the profile. However, the concentrations of P_2O_5 are too low to place much weight on this observation. The systematic change of Th/Sc cannot be confirmed by other scource rock indicators like the Cr/Th and Cr/Zr ratios. The occurrence of high-Mg-Ca-Na samples in the upper part of the profile, accompanied by a shale sample with a relatively high SiO_2-content, is worth mentioning.

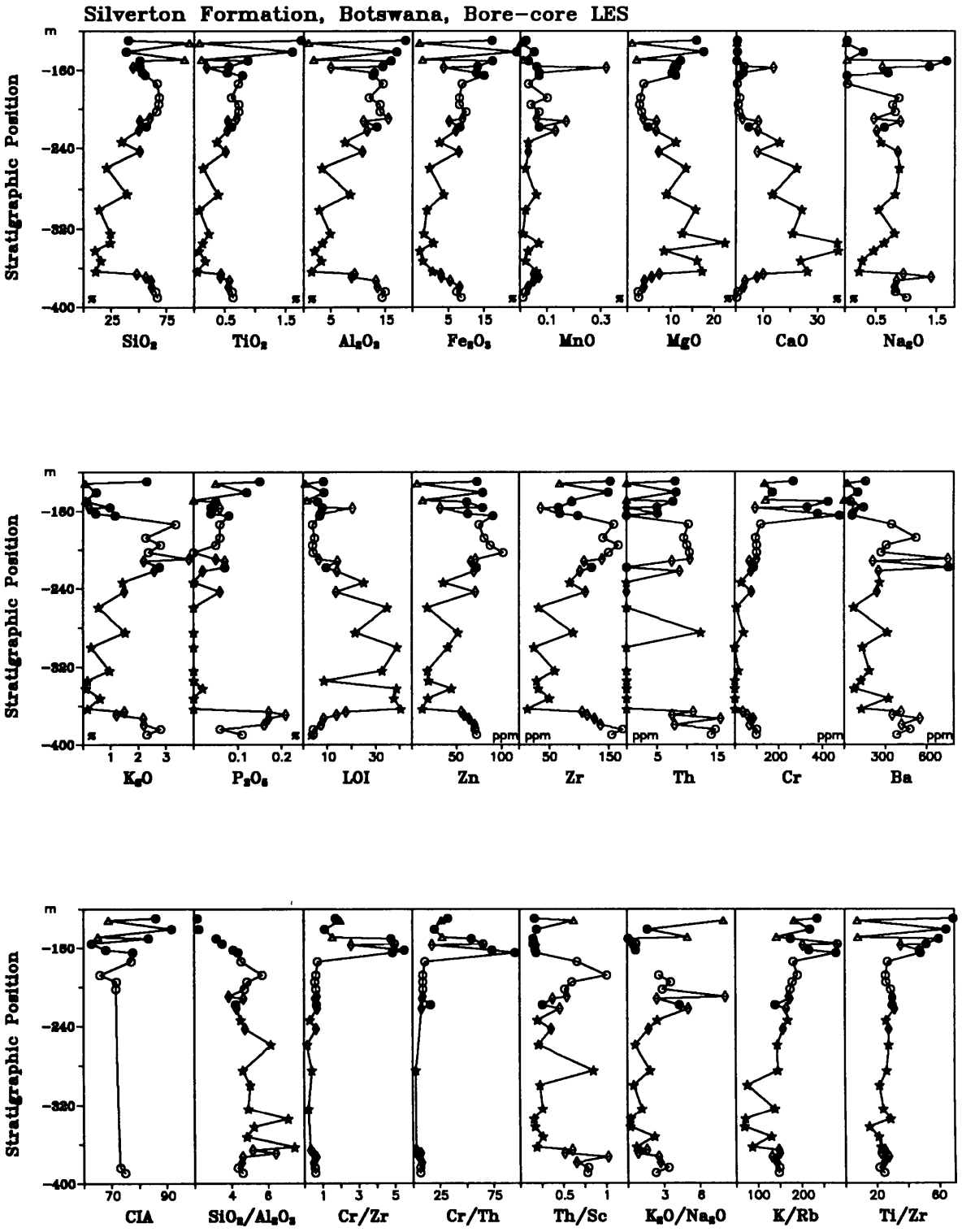

Figure 3.3.10.5: Geochemical profile of the upper part of the Silverton Formation, borehole LES, Botswana. Lithological types: ★ = carbonate; Δ = sandstone; ○ = shale; ◇ = calcareous shale; ● = high-Fe-Mg-shale. NOTE: Uppermost 120 m of drillhole (quartzites from the Magaliesberg Formation) were not analysed.

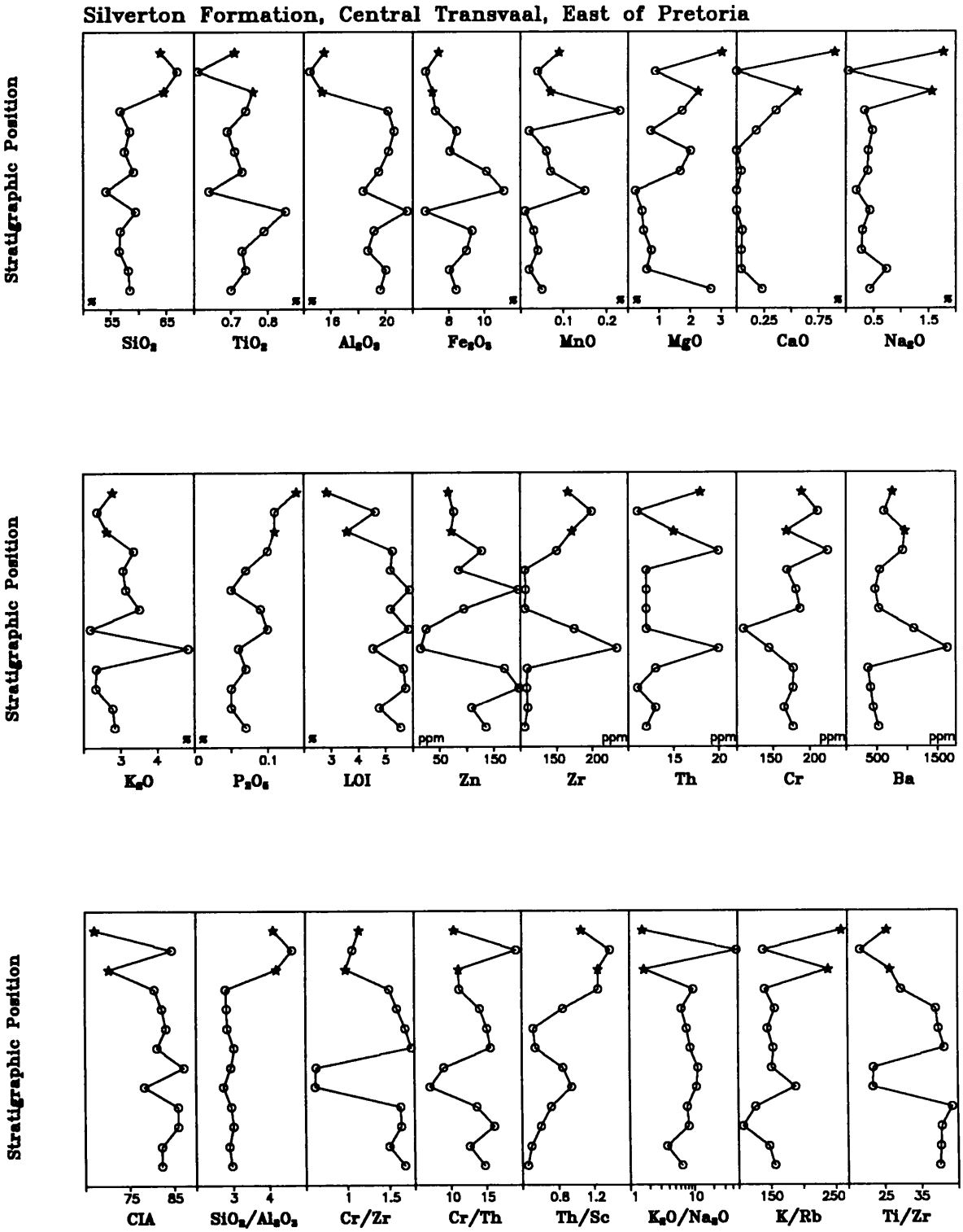

Figure 3.3.10.6: Geochemical profile of the Silverton Formation, east of Pretoria, central Transvaal. Lithological types: ★ = high-Mg-Ca-Na shale; ○ = shale. Vertical scale = ± 600 m in total.

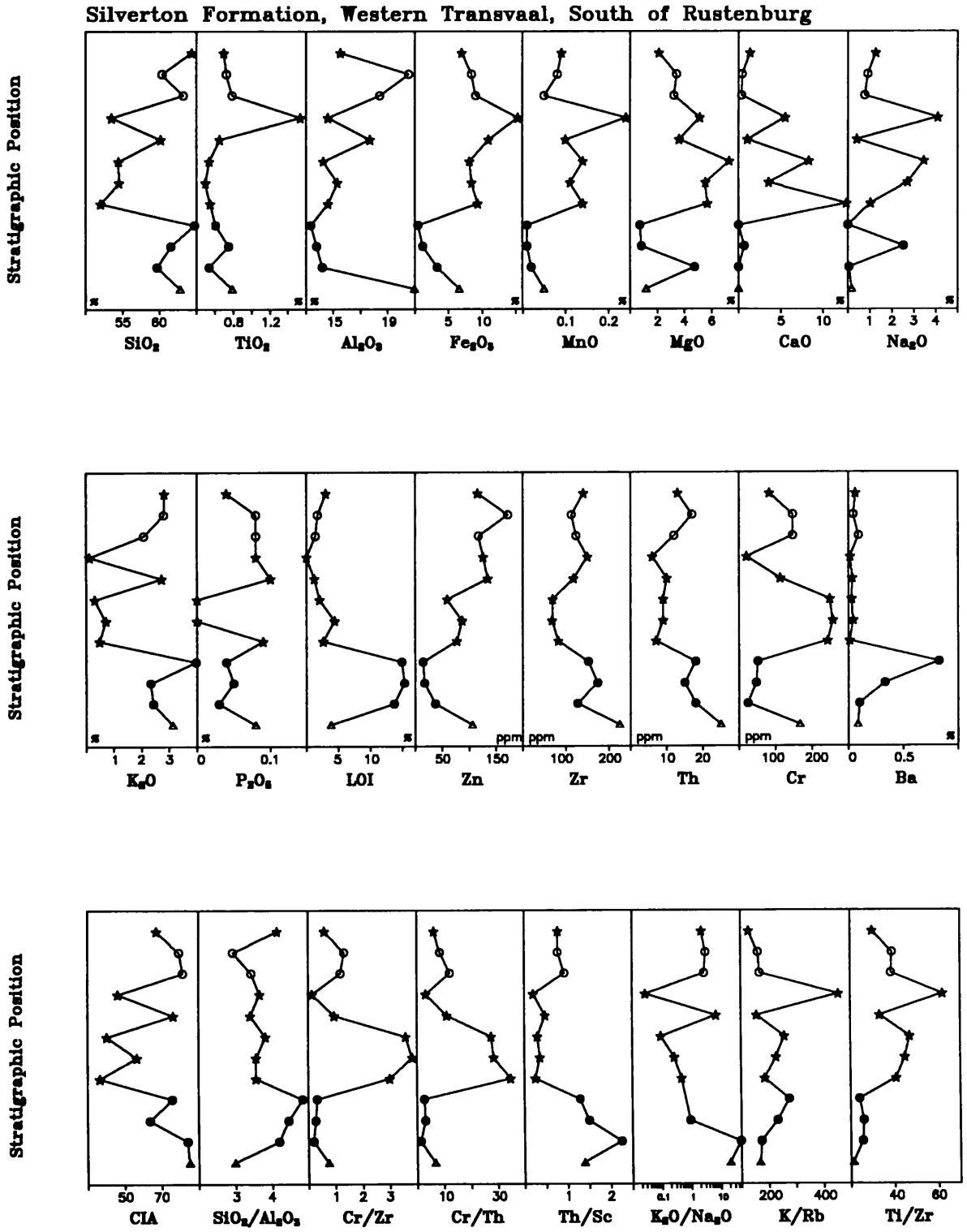

Figure 3.3.10.7: Geochemical profile of the Silverton Formation, south of Rustenburg, western Transvaal. Lithological types: ★ = high-Mg-Ca-Na shale; ○ = shale; Δ = andalusite shale; ● = graphitic shale. Vertical scale = ± 700 m in total.

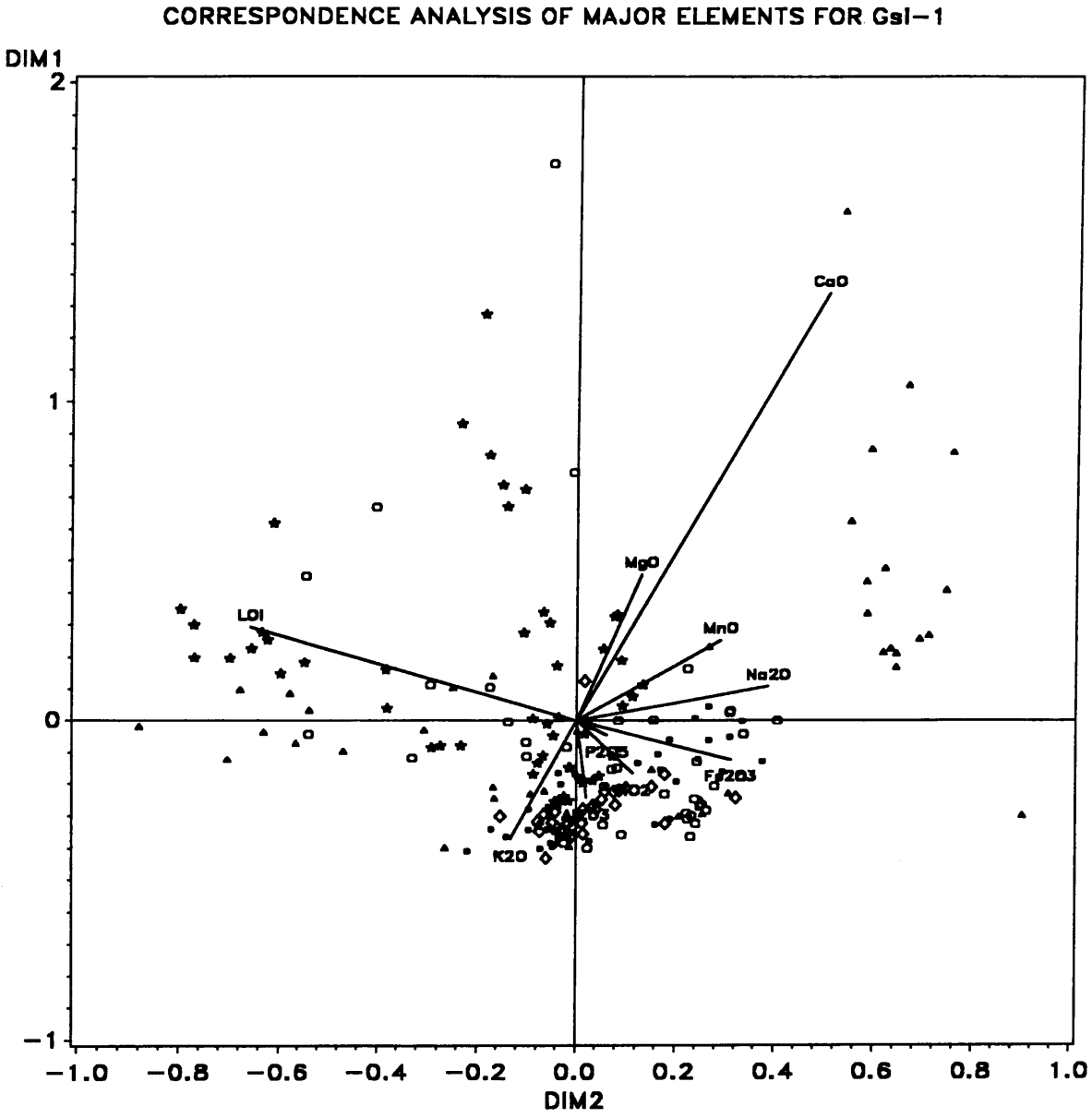

Figure 3.3.10.8: Correspondence analysis of major elements (except SiO_2) of shales from the Silverton Formation. Symbols for sampling areas: ● (red) = eastern Transvaal; ○ (red) = northeastern Transvaal; □ (violet) = eastern fragments; ◇ (green) = central Transvaal; ▲ (blue) = western Transvaal; † (blue) = western fragments; ‡ (blue) = northwestern Transvaal; ★ (yellow) = Botswana. Definition of sampling areas is shown in Figure 1.5.1. DIM 1 and DIM 2 are the values of the factor loadings of the samples and variables for the first and second factor (see Chapter 2.3.2). Angles between lines connecting a variable and the point (0,0) are proportional to the product moment correlation coefficient of these variables.

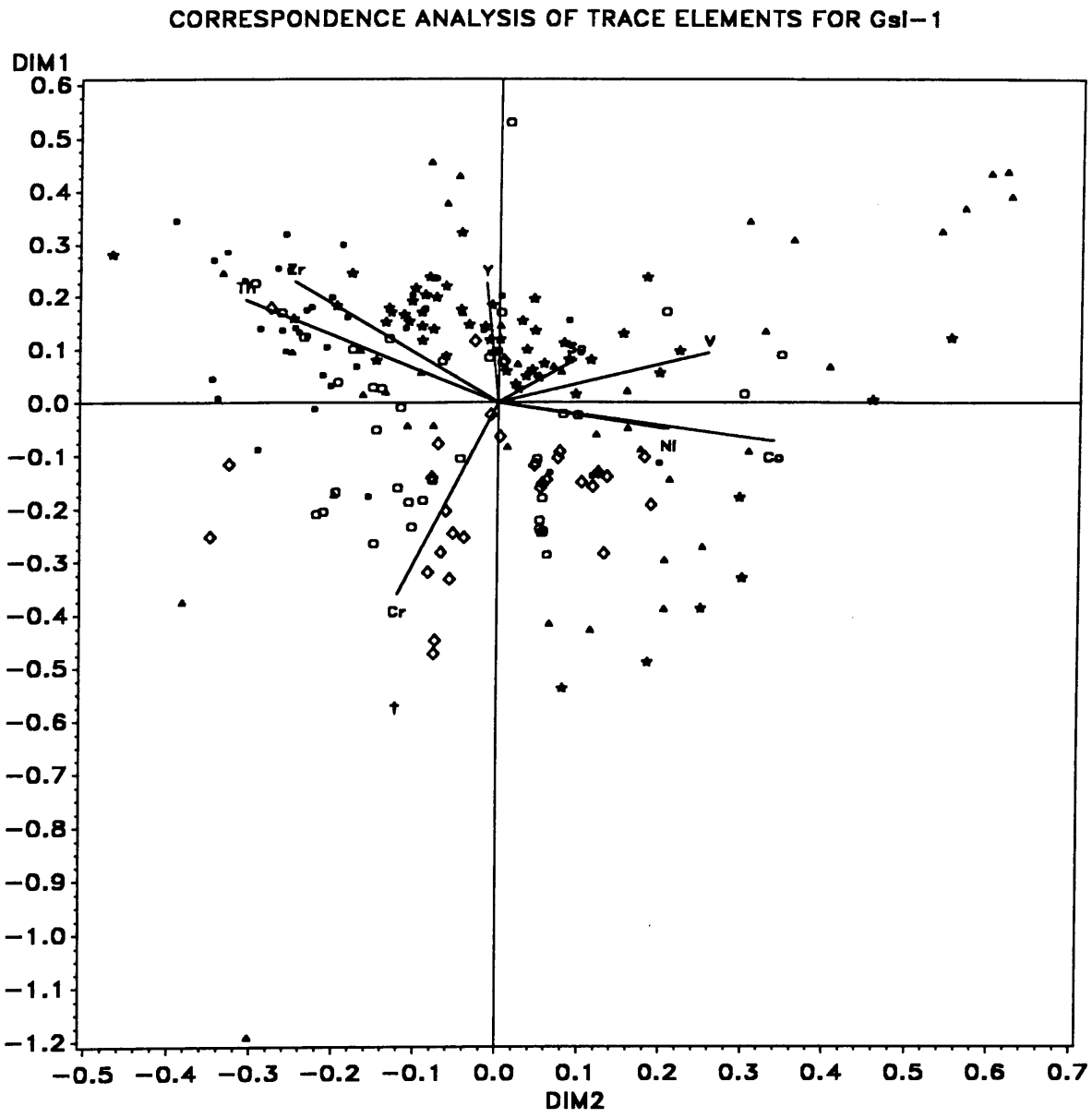

Figure 3.3.10.9: Correspondence analysis of selected trace elements of shales from the Silverton Formation. Symbols for sampling areas: ● (red) = eastern Transvaal; ○ (red) = northeastern Transvaal; □ (violet) = eastern fragments; ◇ (green) = central Transvaal; ▲ (blue) = western Transvaal; † (blue) = western fragments; ‡ (blue) = northwestern Transvaal; ★ (yellow) = Botswana. Definition of sampling areas is shown in Figure 1.5.1. DIM 1 and DIM 2 are the values of the factor loadings of the samples and variables for the first and second factor (see Chapter 2.3.2). Angles between lines connecting a variable and the point (0,0) are proportional to the product moment correlation coefficient of these variables.

The western Transvaal (see Fig. 1.5.11 for location of profile) geochemical profile (Fig 3.3.10.7) has an approximate thickness of 700 m including diabases, and contains four lithological types, shale, andalusite shale, graphitic shale and high-Mg-Ca-Na shale. Trends and systematic changes of the geochemistry are difficult to define, except for Zn, which increases upwards throughout most of the profile. K/Rb and K_2O/Na_2O are negatively correlated, whereas Cr/Zr and Cr/Th as well as $Fe_2O_3(t)$ and MnO are positively correlated. The high-Mg-Ca-Na samples of the western Transvaal profile have low SiO_2-contents, in contrast to the high-Mg-Ca-Na samples of the Lydenburg Shale Member of the eastern Transvaal, which are relatively high in SiO_2 compared to the underlying Boven Shale Member (Fig. 3.3.10.1).

Correspondence analysis was performed for major (Fig. 3.3.10.8) and selected trace elements (Fig. 3.3.10.9) of the Silverton Formation shale samples. The major element plot gives a good indication of the importance of the observed lithological types (Chapter 4.4). The high-Mg-Ca-Na shales of the western Transvaal sampling area (blue filled triangles on the far right side of the plot) provide a distinct group, whereas the high-Mg-Ca-Na shale samples from the eastern and northeastern Transvaal sampling areas are closer to the centre around the position of $Fe_2O_3(t)$ and Na_2O. Graphitic and pyritic shales plot close to LOI, the calcareous shales in the area between LOI and CaO-MgO. The correspondence analysis of selected trace elements discriminates the sample areas to a certain degree, but outlier values and overlapping fields may question the validity of this interpretation. If the outlier values are ignored, fairly well defined fields can be inferred for the central, northeastern, eastern and Botswana sampling areas.

3.3.11 Magliesberg Formation

The major element geochemistry of the Magaliesberg Formation sandstones (Table 3.3.11.1) shows enrichment of SiO_2 and depletion of all other major elements compared to average sandstone estimates (Table 3.2.1c). Notably, MgO, CaO and Na_2O are strongly depleted. Ni, Co, Cr, Mo and Nb are strongly enriched, Ga, Rb, Y, Zr, and B more or less strongly depleted compared to average sandstone estimates (Table 3.2.1d). Zn is moderately depleted,

Element	n	MEAN	STD ±	GM	MEDIAN	RANGE	VC
SiO_2	56	93.29	6.64	93.04	96.26	75.69 - 99.98	0.07
TiO_2	56	0.16	0.16	-	0.14	<LLD - 0.76	1.00
Al_2O_3	56	3.03	3.51	-	1.61	<LLD - 14.84	1.16
Fe_2O_3*	56	1.14	1.49	0.79	0.59	0.25 - 10.25	1.31
MnO	56	0.01	0.01	-	<LLD	<LLD - 0.04	1.00
MgO	56	0.24	0.46	-	<LLD	<LLD - 1.74	1.92
CaO	56	0.04	0.09	-	<LLD	<LLD - 0.51	2.25
Na_2O	56	0.14	0.41	-	0.04	<LLD - 2.74	2.93
K_2O	56	0.69	0.81	-	0.34	<LLD - 3.30	1.17
P_2O_5	56	0.03	0.03	-	0.02	<LLD - 0.11	1.00
H_2O^-	56	0.11	0.12	0.06	0.05	0.01 - 0.44	1.09
LOI	56	0.79	0.93	0.42	0.43	0.04 - 4.42	1.18
Zn	56	9.9	8.2	8.1	7	3 - 52	0.83
Cu	56	4.9	12.5	-	<LLD	<3 - 58	2.57
Ni	56	7.5	8.1	-	5	<3 - 38	1.08
Co	56	3.9	3.4	-	4	<3 - 18	0.87
Ga	56	1.9 *)	3.0	-	<LLD	<3 - 9	1.58
Mo	56	7.4	3.4	-	8	<2 - 14	0.46
Nb	56	3.2	4.0	-	3	<2 - 25	1.25
Zr	56	144	165	91	74	25 - 733	1.15
Y	56	8.3	6.3	-	7	<2 - 26	0.76
Sr	56	21	32	11	9	2 - 203	1.52
Rb	56	22	24	-	14	<2 - 94	1.09
U	56	1.3 *)	2.7	-	<LLD	<5 - 11	2.08
Th	56	2.2 *)	3.8	-	<LLD	<5 - 14	1.73
Pb	56	6.5	7.0	-	5	<5 - 22	1.08
Cr	56	157	57	-	167	<14 - 326	0.36
V	56	24	15	-	23	<14 - 75	0.63
Ba	56	250	305	-	96	<16 - 1039	1.22
Sc	56	2.3 *)	4.5	-	<LLD	<8 - 17	1.96
As	56	0.4 *)	1.9	-	<LLD	<10 - 10	4.75
S	56	62	148	-	<LLD	<50 - 1008	2.39
Sb	56	1.0 *)	2.9	-	<LLD	<8 - 11	2.90
Sn	56	0.5 *)	2.2	-	<LLD	<8 - 12	4.40
B	10	9.4	7.2	6.6	7	1 - 22	0.77

Table 3.3.11.1: Average geochemistry of sandstones from the Magaliesberg Formation

(n = number of samples; 'MEAN' = arithmetic mean; 'STD ±' = 1 σ standard deviation; 'GM' = geometric mean; 'MEDIAN' = median; 'VC' = variation coefficient; average major element concentrations are reported in weight %, average trace element concentrations in ppm; 'Fe_2O_3*' is all Fe expressed as Fe_2O_3; *) = arithmetic mean below detection limit; LLD = lower limit of detection)

Table 3.3.11.2 : Average ratios of Magaliesberg Formation sandstones

(NOTE: ratios are not corrected, i.e. a sample was excluded from calculation of the average ratio if one or both elements are below the detection limit; n.c. = not calculated)

Ratio	n	MEAN	STD ±	GM	RANGE	VC
CIA	50	75.4	10.7	74.7	52.6 - 100	0.14
SiO_2/Al_2O_3	50	105	135	50	5.1 - 521	1.29
lg SiO_2/Al_2O_3	50	1.70	0.55	n.c.	0.71 - 2.72	0.32
K_2O/Na_2O	46	14.6	14.8	8.0	0.4 - 59.0	1.01
lg Na_2O/K_2O	46	-0.90	0.54	n.c.	-1.77 - 0.40	0.60
Ti/Zr	55	9.8	9.7	6.4	0.9 - 39.3	0.99
Ti/Cr	54	7.4	8.7	3.9	0.4 - 35.0	1.18
Al/Zr	50	132	115	94	18 - 617	0.87
Al_2O_3/TiO_2	50	30.0	25.1	19.3	1.1 - 124.3	0.84
Al_2O_3/K_2O	49	5.8	3.6	4.9	1.5 - 15.8	0.62
K/Rb	43	246	88	229	62 - 439	0.36
K/Ba	52	25	18	20	4 - 96	0.72
K/Sr	53	310	249	219	28 - 1147	0.80

Sc moderately enriched, but as the average Sc-content is considerably below the detection limit, this observation must be regarded with great caution. However, the association of enriched elements (i.e., Cr, Ni, and Co) may indicate that the calculated average Sc-content reflects a true enrichment. Sc, along with Cr, Ni, and Co, is thought to reflect a mafic source rock contribution (e.g., Condie and Wronkiewicz, 1990; Taylor and McLennan, 1985).

Shales are locally intercalated with the Magaliesberg Formation sandstones (Button, 1973; Schreiber, 1990). Two types of shales are distinguished here geochemically: (1.) a 'normal' shale, and (2.) a shale containing high amounts of Cr and various other trace elements. 36 samples of the second type of shale were sampled near Bronkhorstspruit and are described separately. Seven sandstone specimens sampled from sandstone beds overlying and underlying the Bronkhorstspruit shales were also excluded from the main Magaliesberg sandstone data set as they contain unusually high base metal contents (for example, up to 1305 ppm Pb, and up to 174 ppm Zn, see Appendix 2a).

Element	n	MEAN	STD ±	GM	MEDIAN	RANGE	VC
SiO_2	22	60.31	6.92	59.94	60.37	49.91 - 77.61	0.12
TiO_2	22	0.82	0.23	0.79	0.76	0.35 - 1.30	0.28
Al_2O_3	22	20.34	5.09	19.73	18.60	10.15 - 32.19	0.25
Fe_2O_3*	22	5.39	2.69	4.49	5.79	0.98 - 10.58	0.50
MnO	22	0.03	0.03	-	0.03	<LLD - 0.07	1.00
MgO	22	1.75	0.98	1.50	1.35	0.55 - 3.59	0.56
CaO	22	0.19	0.28	-	<LLD	<LLD - 0.81	1.47
Na_2O	22	0.38	0.48	0.20	0.13	0.04 - 1.68	1.26
K_2O	22	4.86	1.54	4.60	5.08	2.10 - 7.89	0.32
P_2O_5	22	0.07	0.04	0.05	0.06	0.01 - 0.14	0.57
H_2O^-	22	0.83	0.93	0.54	0.51	0.08 - 4.35	1.12
LOI	22	4.37	1.58	4.08	4.20	1.48 - 8.27	0.36
Zn	22	56	26	48	58	11 - 92	0.46
Cu	22	22	16	19	18	9 - 80	0.73
Ni	22	37	17	33	32	14 - 83	0.46
Co	22	11	7.4	8.7	9	<3 - 29	0.67
Ga	22	27	7.3	26	27	9 - 40	0.27
Mo	22	1.3 *)	2.0	-	<LLD	<2 - 7	1.54
Nb	22	14	4.0	13	13	8 - 26	0.29
Zr	22	308	156	279	236	171 - 701	0.51
Y	22	33	11	32	32	16 - 56	0.33
Sr	22	82	50	66	80	17 - 191	0.61
Rb	22	191	77	176	182	59 - 380	0.40
U	22	7.9	6.3	-	6.5	<5 - 19	0.80
Th	22	18	6.0	17	19	7 - 27	0.30
Pb	22	19	13	14	17	<5 - 48	0.68
Cr	22	261	183	224	206	106 - 918	0.70
V	22	126	40	119	120	37 - 193	0.32
Ba	22	904	328	848	880	399 - 1698	0.36
Sc	22	17	7.4	15	17	<8 - 31	0.44
As	22	-	-	-	-	<10	-
S	22	719	1172	230	161	<50 - 4030	1.63
Sb	22	0.55 *)	2.6	-	<LLD	<8 - 12	4.73
Sn	22	2.5 *)	4.2	-	<LLD	<8 - 12	1.68
B	4	82	99	44	46	10 - 225	1.21

Table 3.3.11.3: Average element concentrations of shales from the Magaliesberg Formation (n = number of samples; 'MEAN' = arithmetic mean; 'STD ±' = 1 σ standard deviation; 'GM' = geometric mean; 'MEDIAN' = median; 'VC' = variation coefficient; average major element concentrations are reported in weight %, average trace element concentrations in ppm; 'Fe_2O_3*' is all Fe expressed as Fe_2O_3; *) = arithmetic mean below detection limit; LLD = lower limit of detection. NOTE: shale samples from Bronkhorstspruit are excluded from this data set; see Tables 3.3.11.6 and 3.3.11.7)

Table 3.3.11.4: Average major element concentrations of shales from the Magaliesberg Formation Lower Shales Member recalculated to 100 % volatile-free.

Element	n	MEAN	STD ±	RANGE
SiO_2	22	64.02	6.73	53.75 - 79.82
TiO_2	22	0.87	0.25	0.36 - 1.40
Al_2O_3	22	21.69	5.76	10.44 - 35.65
Fe_2O_3*	22	5.71	2.86	1.09 - 11.45
MnO	22	0.03	0.03	<LLD - 0.07
MgO	22	1.84	1.01	0.58 - 3.75
CaO	22	0.20	0.29	<LLD - 0.85
Na_2O	22	0.40	0.50	0.01 - 1.73
K_2O	22	5.17	1.63	2.24 - 8.21
P_2O_5	22	0.07	0.01	0.01 - 0.15

Table 3.3.11.5: Average ratios of shales from the Magaliesberg Formation

(NOTE: ratios corrected as described in Chapter 3.1.2)

Ratio	n	MEAN	STD ±	GM	RANGE	VC
CIA	22	76.1	7.0	75.8	62.06 - 88.62	0.09
Fe/V	22	319	166	264	48 - 618	0.52
K_2O/Na_2O	22	39.3	32.9	23.0	1.4 - 102.9	0.84
SiO_2/Al_2O_3	22	3.2	1.29	3.0	1.6 - 7.7	0.40
Cr/Th	22	15.3	10.1	13.1	5.4 - 43.7	0.66
Th/Sc	22	1.18	0.64	1.05	0.41 - 3.13	0.54
Cr/Zr	22	1.09	1.07	0.80	0.22 - 4.99	0.98
Co/Th	22	0.70	0.50	0.54	0.13 - 1.80	0.71
Al_2O_3/TiO_2	22	25.4	4.1	25.1	18.7 - 35.3	0.16
Al_2O_3/K_2O	22	4.5	1.6	4.3	2.8 - 8.7	0.36
K/Rb	22	223	52	217	126 - 374	0.23
K/Ba	22	48	18	45	19 - 82	0.38
Ti/Ni	22	162	86	142	65 - 321	0.53
Cr/V	22	2.04	1.03	1.88	1.28 - 4.94	0.51
V/Ni	22	4.03	1.97	3.60	1.64 - 7.86	0.49
Ni/Co	22	4.06	2.02	3.58	1.29 - 9.37	0.50
Zr/Nb	22	23.6	12.9	21.1	10.8 - 57.1	0.55
Th/U	22	2.28	0.93	2.07	0.37 - 4.41	0.41
Ba/Rb	22	5.5	3.7	4.8	2.3 - 20.1	0.67
Ba/Sr	22	19.0	18.8	12.8	3.9 - 69.6	0.99
Ba/Th	22	55.3	27.8	49.6	23.3 - 143.2	0.50
Al/Zr	22	403	142	375	174 - 643	0.35
Ti/Zr	22	18.7	7.2	16.9	6.2 - 30.0	0.39

Element	n	MEAN	STD ±	GM	MEDIAN	RANGE	VC
SiO_2	36	45.29	14.88	43.04	40.03	22.82 - 76.12	0.33
TiO_2	36	1.91	0.81	1.70	2.01	0.46 - 3.86	0.42
Al_2O_3	36	24.13	8.04	22.63	24.47	8.04 - 38.42	0.33
Fe_2O_3*	36	15.92	10.52	13.14	11.99	3.77 - 45.08	0.66
MnO	36	0.01	0.01	-	0.01	<LLD - 0.03	1.00
MgO	36	0.16	0.15	-	0.16	<LLD - 0.51	0.94
CaO	36	<0.01	0.01	-	<LLD	<LLD - 0.05	-
Na_2O	36	0.28	0.21	-	0.26	<LLD - 0.69	0.75
K_2O	36	1.76	1.40	1.25	1.53	0.08 - 5.69	0.80
P_2O_5	36	0.15	0.19	-	0.10	<LLD - 0.94	1.27
H_2O^-	36	3.37	3.25	2.36	2.00	0.59 - 13.32	0.96
LOI	36	6.70	1.87	6.42	6.47	2.91 - 10.08	0.28
Zn	36	364	342	237	226	41 - 1285	0.94
Cu	36	70	62	58	56	22 - 359	0.89
Ni	36	64	29	57	60	19 - 129	0.45
Co	36	2.9	3.3	-	<LLD	<3 - 19	1.14
Ga	36	31	13	-	36	<LLD - 51	0.42
Mo	36	1.1 *)	1.7	-	<LLD	<2 - 6	1.55
Nb	36	8.7	2.1	8.4	9	5 - 15	0.24
Zr	36	164	48	157	155	67 - 281	0.29
Y	36	35	11	34	33	20 - 76	0.31
Sr	36	90	50	72	91	7 - 193	0.56
Rb	36	66	47	52	56	4 - 187	0.71
U	36	13	13	-	10	<5 - 71	1.00
Th 1)	36	1.7 *)	4.1	-	<LLD	<5 - 20	2.41
Pb	36	422	877	202	208	34 - 5238	2.08
Cr	36	515	201	475	477	182 - 1084	0.39
V	36	390	188	359	360	149 - 1240	0.48
Ba	36	249	143	211	226	47 - 642	0.57
Sc	36	67	18	65	69	29 - 116	0.27
As	36	8.8 *)	13.3	-	<LLD	<10 - 66	1.51
S	36	291	236	242	235	50 - 1264	0.81
Sb	36	12	17	-	9	<8 - 83	1.42
Sn	36	0.4 *)	2.2	-	<LLD	<8 - 13	5.50
B	n.d.	-	-	-	-	-	-

Table 3.3.11.6: Average element concentrations of Bronkhorstspruit shales

(n = number of samples; 'MEAN' = arithmetic mean; 'STD ±' = 1 σ standard deviation; 'GM' = geometric mean; 'MEDIAN' = median; 'VC' = variation coefficient; average major element concentrations are reported in weight %, average trace element concentrations in ppm; 'Fe_2O_3*' is all Fe expressed as Fe_2O_3; *) = arithmetic mean below detection limit; LLD = lower limit of detection; n.d. = not determined. 1) Th was corrected for concentrations < LLD before calculation of mean)

Table 3.3.11.7: Average ratios of the Bronkhorstspruit shales

(NOTE: ratios corrected as described in Chapter 3.1.2)

Ratio	n	MEAN	STD ±	GM	RANGE	VC
CIA	36	92.4	4.2	92.3	81.8 - 99.6	0.05
K_2O/Na_2O	33	14.4	23.6	6.7	1.2 - 120	1.64
SiO_2/Al_2O_3	36	2.4	1.9	1.9	0.9 - 7.5	0.79
Cr/Th	36	97.5	42.0	87.2	13.1 - 217.2	0.43
Th/Sc	36	0.10	0.11	0.09	0.04 - 0.69	1.10
Cr/Zr	36	3.25	1.20	3.02	1.03 - 6.27	0.37
Al_2O_3/TiO_2	36	13.8	4.0	13.3	7.0 - 28.4	0.29
Al_2O_3/K_2O	36	33.6	77.7	18.1	4.6 - 477	2.31
K/Rb	36	206	39	201	87 - 303	0.19
Cr/V	36	1.43	0.51	1.32	0.38 - 2.50	0.36
V/Ni	36	7.08	3.73	6.28	2.78 - 16.07	0.53
Ni/Co	36	18.6	9.6	16.2	4.4 - 43.1	0.52
Zr/Nb	36	19.1	4.2	18.7	13.4 - 29.3	0.22
Al/Zr	36	821	281	762	238 - 1289	0.34
Ti/Zr	36	71.6	25.4	64.8	11.7 - 97.4	0.36

The 'normal' group of Magaliesberg Formation shales (Tables 3.3.11.3, 3.3.11.4 and 3.3.11.5) are enriched in Al_2O_3 and K_2O. MgO, P_2O_5, and Fe_2O_3(t) are moderately, and CaO and Na_2O are strongly depleted compared to average shale estimates (Table 3.2.1b). Zn, Cu, Ni and Co are depleted, Ga, Zr, Y, Rb, U, Th, Ba and Cr are enriched compared to average shale estimates (Table 3.2.1d). K_2O/Na_2O is significantly higher than either Post-Archaean Average Shale or Archaean Average Shale (Taylor and McLennan, 1985), whereas Th/U is depleted compared to these estimates (Table 3.2.1e). Cr/V and Ni/Co resemble Late Archaean Average Shale (Taylor and McLennan, 1985), although they are slightly elevated. V/Ni is significantly higher than the estimates for Post-Archaean Average Shale, Early Archaean Average Shale or Late Archaean Average Shale (Taylor and McLennan, 1985).

The Magaliesberg Formation near Bronkhorstspruit consists of mature sandstones, which contain shale lenses up to 1 m thick and several hundred metres long (Reczko et al., 1992). The major element geochemistry of the Bronkhorstspruit shales (Table 3.3.11.6) is unusual, with strong depletion of SiO_2, MnO, MgO, CaO, Na_2O, and more moderate depletion of potassium. TiO_2, Al_2O_3 and Fe_2O_3(t) are strongly enriched compared to average shale estimates (Table 3.2.1b). Zn, Pb, Cr, V, Sc, Sb and U are also strongly enriched, whereas

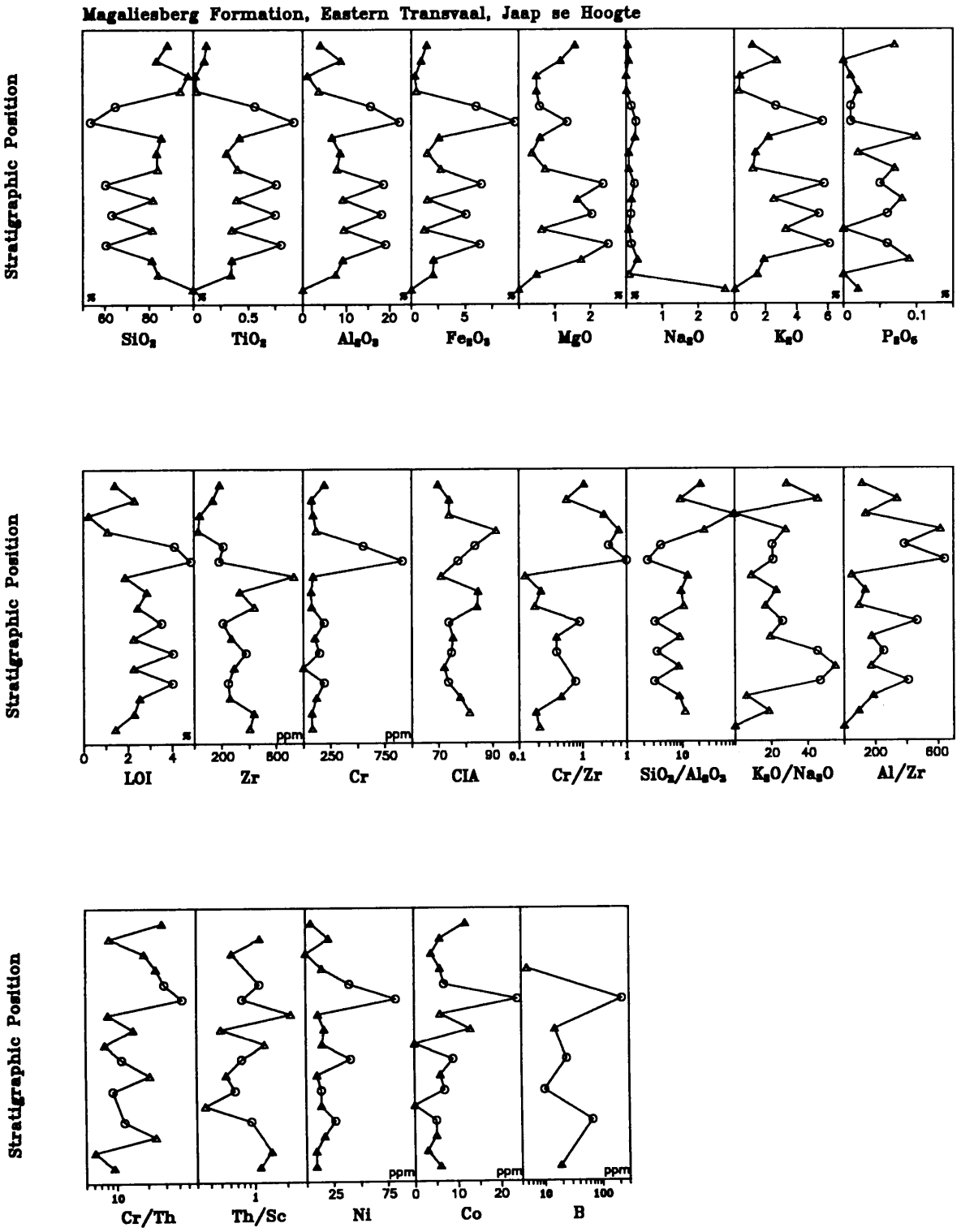

Figure 3.3.11.1: Geochemical profile of the Magaliesberg Formation, Jaap se Hoogte, eastern Transvaal. Lithological types: ○ = shale; Δ = sandstone. Vertical scale = ± 500 m in total.

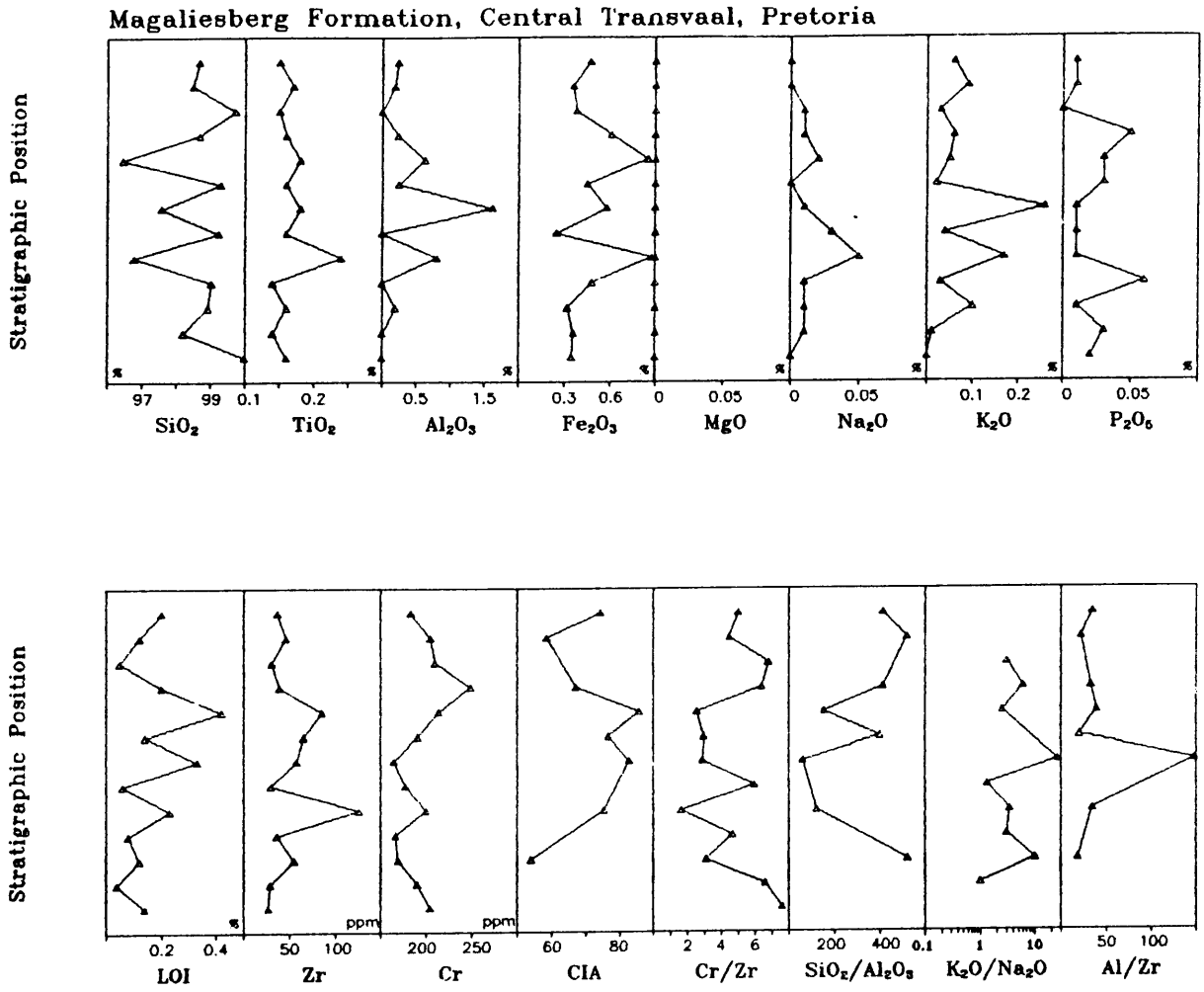

Figure 3.3.11.2: Geochemical profile of the Magaliesberg Formation, Pretoria, central Transvaal. Lithological types: Δ = sandstone and quartzite. Vertical scale = ± 200 m in total.

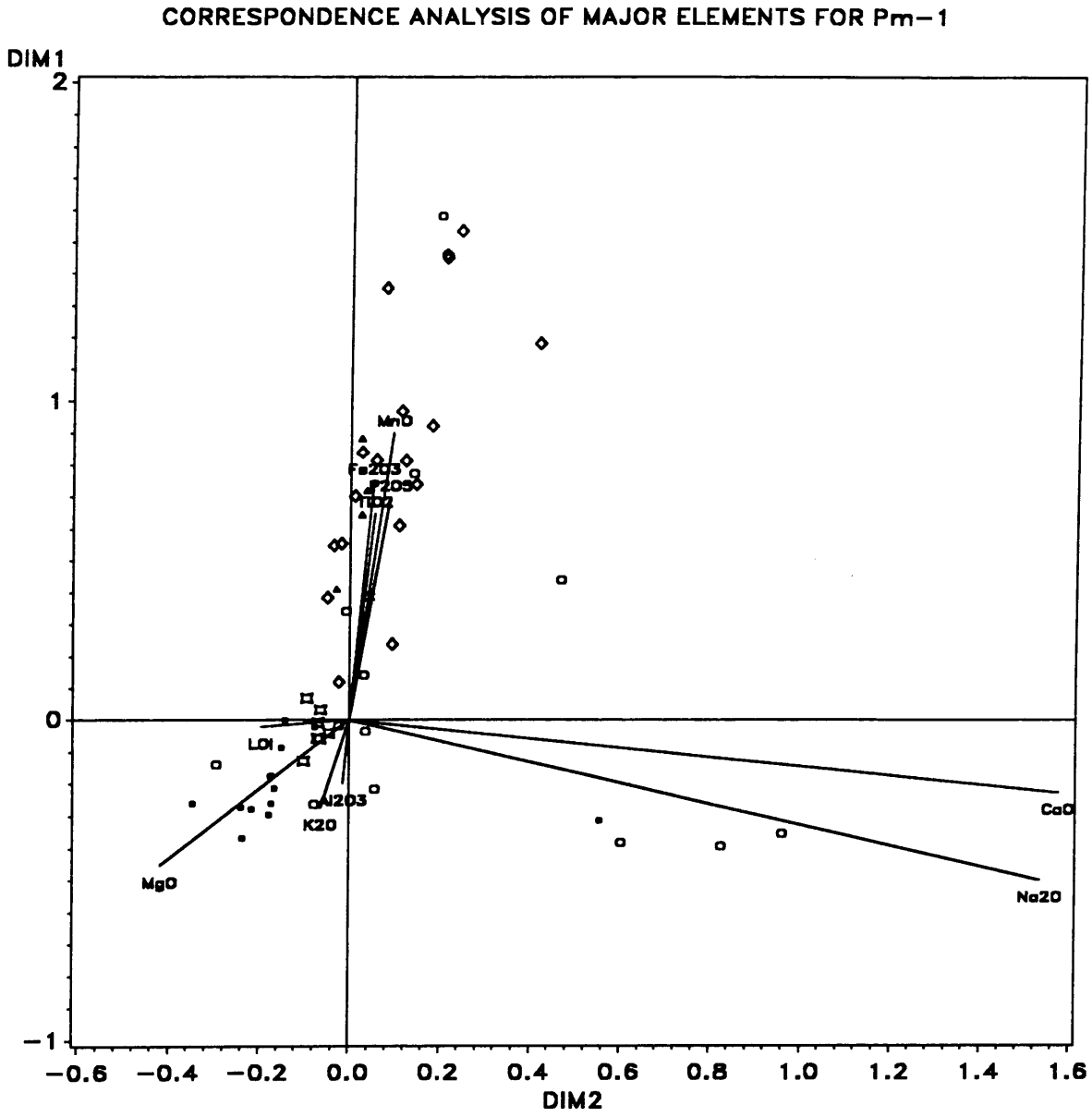

Figure 3.3.11.3: Correspondence analysis of major elements (except SiO_2) of sandstones from the Magaliesberg Formation. Symbols for sampling areas: ● (red) = eastern Transvaal; ○ (red) = northeastern Transvaal; □ (violet) = eastern fragments; ◇ (green) = central Transvaal; ▲ (blue) = western Transvaal; † (blue) = western fragments; ‡ (blue) = northwestern Transvaal; ★ (yellow) = Botswana. Definition of sampling areas is shown in Figure 1.5.1. DIM 1 and DIM 2 are the values of the factor loadings of the samples and variables for the first and second factor (see Chapter 2.3.2). Angles between lines connecting a variable and the point (0,0) are proportional to the product moment correlation coefficient of these variables.

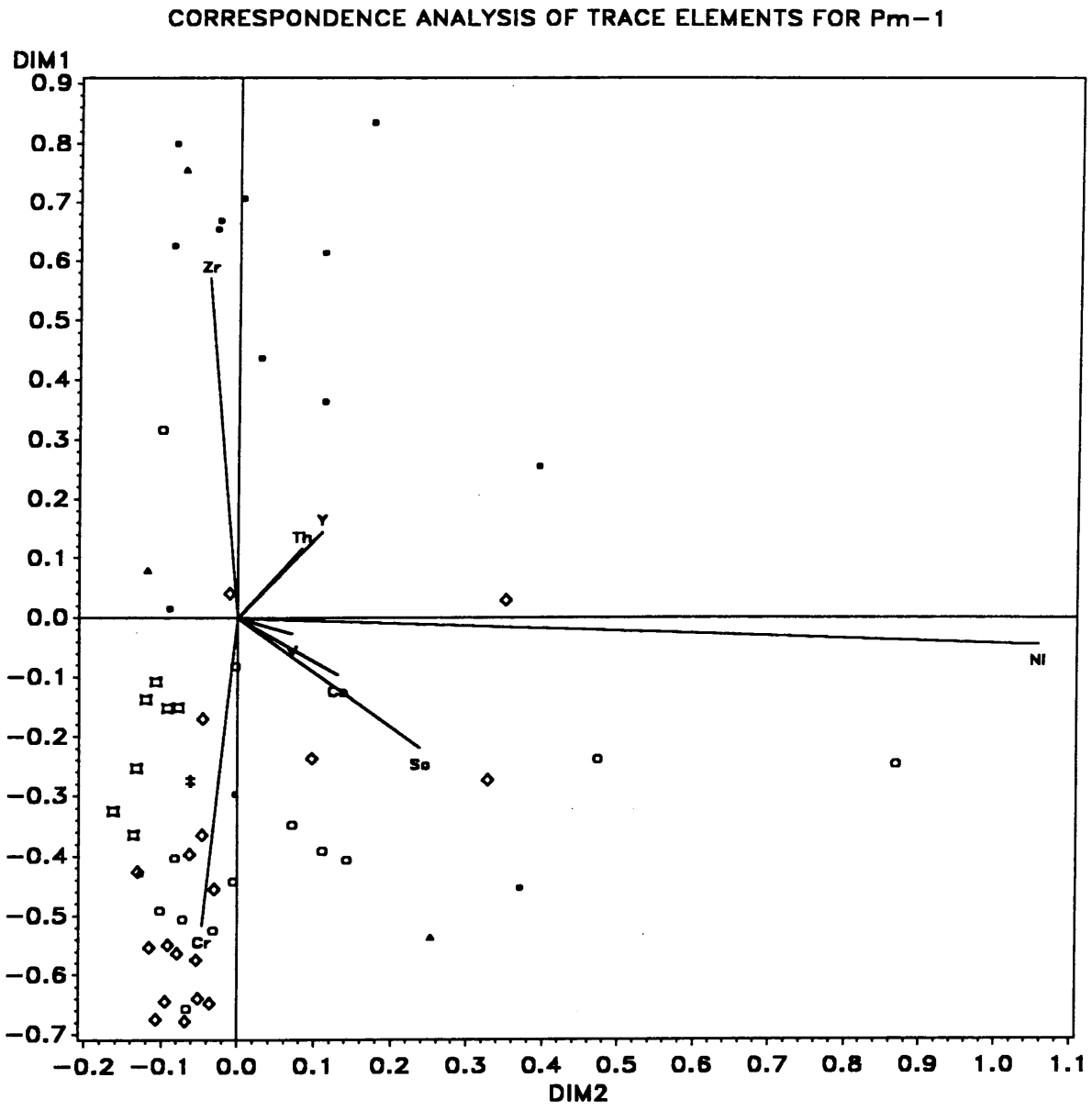

Figure 3.3.11.4: Correspondence analysis of selected trace elements of sandstones from the Magaliesberg Formation. Symbols for sampling areas: ● (red) = eastern Transvaal; ○ (red) = northeastern Transvaal; □ (violet) = eastern fragments; ◇ (green) = central Transvaal; ▲ (blue) = western Transvaal; † (blue) = western fragments; ‡ (blue) = northwestern Transvaal; ★ (yellow) = Botswana. Definition of sampling areas is shown in Figure 1.5.1. DIM 1 and DIM 2 are the values of the factor loadings of the samples and variables for the first and second factor (see Chapter 2.3.2). Angles between lines connecting a variable and the point (0,0) are proportional to the product moment correlation coefficient of these variables.

Co, Rb, Th and Ba are depleted compared to average shale estimates (Table 3.2.1d). Cr/V closely resembles Late Archaean Average Shale (Taylor and McLennan, 1985); K_2O/Na_2O and V/Ni exceed all values reported from average shale estimates (Table 3.2.1e).

Two complete geochemical profiles of the Magaliesberg Formation were taken, in the eastern and central Transvaal sampling areas (Fig. 1.5.12). The eastern Transvaal geochemical profile (Fig. 3.3.11.1) contains two rocktypes, shale (open circle) and sandstone (open triangle). The thickness of the profile is approximately 500 m, including several diabase intrusions with at least 100 m thickness in total. Shale samples are over-represented in the profile, as shales occur mostly in beds a few cm to dm thick. The main lithology of the profile is sandstone. The profile shows variable element patterns, mainly due to the lithological differences. Exceptions are the Cr, Ni, Co and B-contents of the uppermost shale samples. The Cr/Th and Cr/Zr-ratios of the sandstone samples overlying these uppermost shales are also elevated. Th/Sc does not reflect the change in trace element geochemistry indicated by Cr/Th and Cr/Zr.

The central Transvaal geochemical profile (Fig. 3.3.11.2) has an approximate thickness of 200 m and contains only sandstones (open triangles). The geochemical variability is low for all elements, if the scale is considered. The sandstones are quartzitic and very mature, with all samples containing more than 96 wt.% SiO_2.

Correspondence analysis was performed on the sandstones, for major elements except SiO_2 (Fig. 3.3.11.3) and selected trace elements (Fig. 3.3.11.4). The correspondence analysis for the major elements exhibits well defined clusters for the sampling areas. Eastern and northeastern Transvaal samples cluster together in the lower part of the diagram, western and central Transvaal samples in the upper part. Samples of the eastern fragments lie in an intermediate position between these two groups. A systemetic change of the geochemistry is therefore inferred in an east-west direction. Samples with relatively high CaO and Na_2O-contents are restricted to the northeastern Transvaal (3 samples) and eastern Transvaal (1 sample) sampling areas.
Correspondence analysis of selected trace elements (Fig. 3.3.11.4) generally confirms the regional control on geochemical variation indicated by correspondence analysis of the major

elements. The central Transvaal, eastern fragments and eastern Transvaal samples exhibit well defined clusters and depict further, to a certain extent, the above mentioned east-west trend. The northeastern Transvaal samples scatter throughout the diagram, but appear to be more related to the central Transvaal samples if they are evaluated according to their position relative to the 'DIM 1'-axis. The 'DIM 1' is analogous to the first factor in factor analysis, which accounts for the highest percentage of the variance of the variables. For the Magaliesberg Formation sandstones, 'DIM 1' accounts for 81.9 % of the variance.

3.3.12 Post-Magaliesberg Formations

The stratigraphic units overlying the Magaliesberg Formation have a variable regional development. In the eastern and northeastern Transvaal and the eastern fragments sampling areas, the Post-Magaliesberg portion of the Pretoria Group is subdivided from bottom to top into Vermont, Lakenvlei, Nederhorst, Steenkampsberg, and Houtenbek Formations. In the central Transvaal sampling area, only the Rayton Formation overlies the Magaliesberg Formation (SACS, 1980), and in Botswana only the Woodlands Formation is found in this stratigraphic position (Key, 1983). The Makeckaan Formation from the eastern fragment sampling area and undifferentiated sedimentary units overlying the Magaliesberg Formation in the western fragment sampling area (Rooiberg Fragment: Leeuwpoort and Smelterskop Formations) were sampled and analysed to some extent (Appendix 1a and 2a), but were not evaluated in detail due to their uncertain correlation with the Pretoria Group (Eriksson et al., 1993a). The Dullstroom Formation was excluded from the present investigation as new research points to a correlation with the Rooiberg Group (e.g., Eriksson et al., 1993).

The Rayton Formation consists mainly of coarser-grained rudaceous and arenaceous rocks interlayered with shales and volcanics. Van der Neut (1990) investigated the sedimentology of the Rayton Formation in the Pretoria area, and reported an approximate thickness of 500 m. The Woodlands Formation is generally poorly exposed, and has a thickness of up to 1200 m (Key, 1983). The characteristic lithology of the Woodlands Formation is a fine-grained, mature, cross-bedded sandstone (Key, 1983). However, the borehole STRAT 3, which disects the upper 300 m of the Woodlands Formation, contains mainly conglomerates and

Element	n	MEAN	STD ±	GM	MEDIAN	RANGE	VC
SiO_2	14	89.63	9.71	89.05	91.17	60.46 - 99.28	0.11
TiO_2	14	0.34	0.27	0.28	0.27	0.10 - 1.20	0.79
Al_2O_3	14	4.77	4.28	3.24	4.29	0.80 - 16.50	0.90
Fe_2O_3*	14	2.12	2.91	1.17	0.94	0.28 - 11.09	1.37
MnO	14	0.02	0.02	0.02	0.02	0.01 - 0.08	1.00
MgO	14	0.10	0.30	-	<LLD	<LLD - 1.12	3.00
CaO	14	0.08	0.17	0.03	0.03	0.01 - 0.65	2.13
Na_2O	14	0.06	0.06	0.04	0.04	0.01 - 0.23	1.00
K_2O	14	1.25	0.97	0.88	1.16	0.18 - 3.36	0.78
P_2O_5	14	0.04	0.06	0.03	0.03	0.01 - 0.24	1.50
H_2O^-	14	0.15	0.28	0.07	0.07	0.01 - 1.09	1.87
LOI	14	1.07	1.19	0.75	0.86	0.19 - 4.99	1.11
Zn	14	49	112	17	12	4 - 427	2.29
Cu	14	14	34	-	<LLD	<3 - 125	2.43
Ni	14	11	21	-	5	<3 - 84	1.91
Co	14	5.0	6.5	-	4	<3 - 25	1.30
Ga	14	4.9	5.9	-	5	<3 - 21	1.20
Mo	14	6.4	2.7	-	8	<2 - 9	0.42
Nb	14	5.6	3.4	4.8	4	2 - 14	0.61
Zr	14	149	81	126	145	44 - 272	0.54
Y	14	14	8.3	12	13	5 - 31	0.59
Sr	14	19	19	14	10	4 - 71	1.00
Rb	14	43	33	31	42	9 - 115	0.77
U	14	1.1 *)	2.3	-	<LLD	<5 - 6	2.09
Th	14	1.7 *)	3.0	-	<LLD	<5 - 9	1.76
Pb	14	34	45	-	16	<5 - 161	1.32
Cr	14	153	43	146	158	58 - 211	0.28
V	14	63	88	40	30	12 - 345	1.40
Ba	14	292	217	223	177	67 - 688	0.74
Sc	14	1.7 *)	6.4	-	<LLD	<8 - 24	3.77
As	14	-	-	-	-	-	-
S	14	33 *)	64	-	<LLD	<50 - 220	1.94
Sb	14	-	-	-	-	-	-
Sn	14	-	-	-	-	-	-
B	6	9.7	4.6	8.8	9.0	5 - 16	0.47

Table 3.3.12.1: Average element concentrations of sandstones from the Rayton Formation (n = number of samples; 'MEAN' = arithmetic mean; 'STD ±' = 1 σ standard deviation; 'GM' = geometric mean; 'MEDIAN' = median; 'VC' = variation coefficient; average major element concentrations are reported in weight %, average trace element concentrations in ppm; 'Fe_2O_3*' is all Fe expressed as Fe_2O_3; *) = arithmetic mean below detection limit; LLD = lower limit of detection)

Table 3.3.12.2 : Average ratios of Rayton Formation sandstones

(NOTE: ratios are not corrected, i.e. a sample was excluded from calculation of the average ratio if one or both elements are below the detection limit; n.c. = not calculated)

Ratio	n	MEAN	STD ±	GM	RANGE	VC
CIA	14	71.7	9.1	71.1	43.4 - 81.2	0.13
SiO_2/Al_2O_3	14	43.7	40.2	27.5	3.7 - 119.7	0.92
lg SiO_2/Al_2O_3	14	1.44	0.46	n.c.	0.56 - 2.08	0.32
K_2O/Na_2O	14	31.3	27.4	22.2	2.0 - 112.0	0.88
lg Na_2O/K_2O	14	-1.35	0.41	n.c.	-2.05 - -0.30	n.c.
Ti/Zr	14	15.2	10.2	13.2	6.6 - 47.3	0.67
Ti/Cr	14	18.8	30.8	11.4	3.9 - 124.0	1.64
Al/Zr	14	165	127	136	42 - 575	0.77
Al_2O_3/TiO_2	14	13.2	5.8	11.7	3.7 - 22.3	0.44
Al_2O_3/K_2O	14	3.8	1.0	3.7	2.6 - 6.5	0.26
K/Rb	14	238	39	235	166 - 302	0.16
K/Ba	14	41	23	33	3.6 - 88	0.56
K/Sr	14	838	764	533	55 - 2615	0.91

volcanics (Key, 1983). As the unconformity between Pretoria and Waterberg Groups is not exposed in the drilling area, the possibility exists that the upper part of the Woodlands Formation is in fact the basal portion of the Waterberg Group (D. P. Piper, 1992, pers. comm.). 13 sandstone samples of the Rayton Formation were analysed from the central Transvaal sampling area and 1 sample of the Woodlands Formation from borehole STRAT 3. These 14 samples are treated together, under the heading of the Rayton Formation in this thesis.

The average Rayton Formation sandstone/quartzite (Table 3.3.12.1 and 3.3.12.2) has a similar major element composition to the carbonate-free recalculated average sandstone estimate of Clarke (1924) (Table 3.2.1c), with the exception of MgO, CaO, and Na_2O, which are depleted. Compared to other estimates of average sandstone (Table 3.2.1c), SiO_2 is enriched and most other major elements more or less depleted. Ni, Co, Mo, Nb, Cr and Ba are enriched, Ga, Zr, Y and B depleted, compared to average sandstones (Table 3.2.1d). The average contents of V, Zn, Cu and Pb are moderately to strongly enriched due to a small number of samples with extremely high contents.

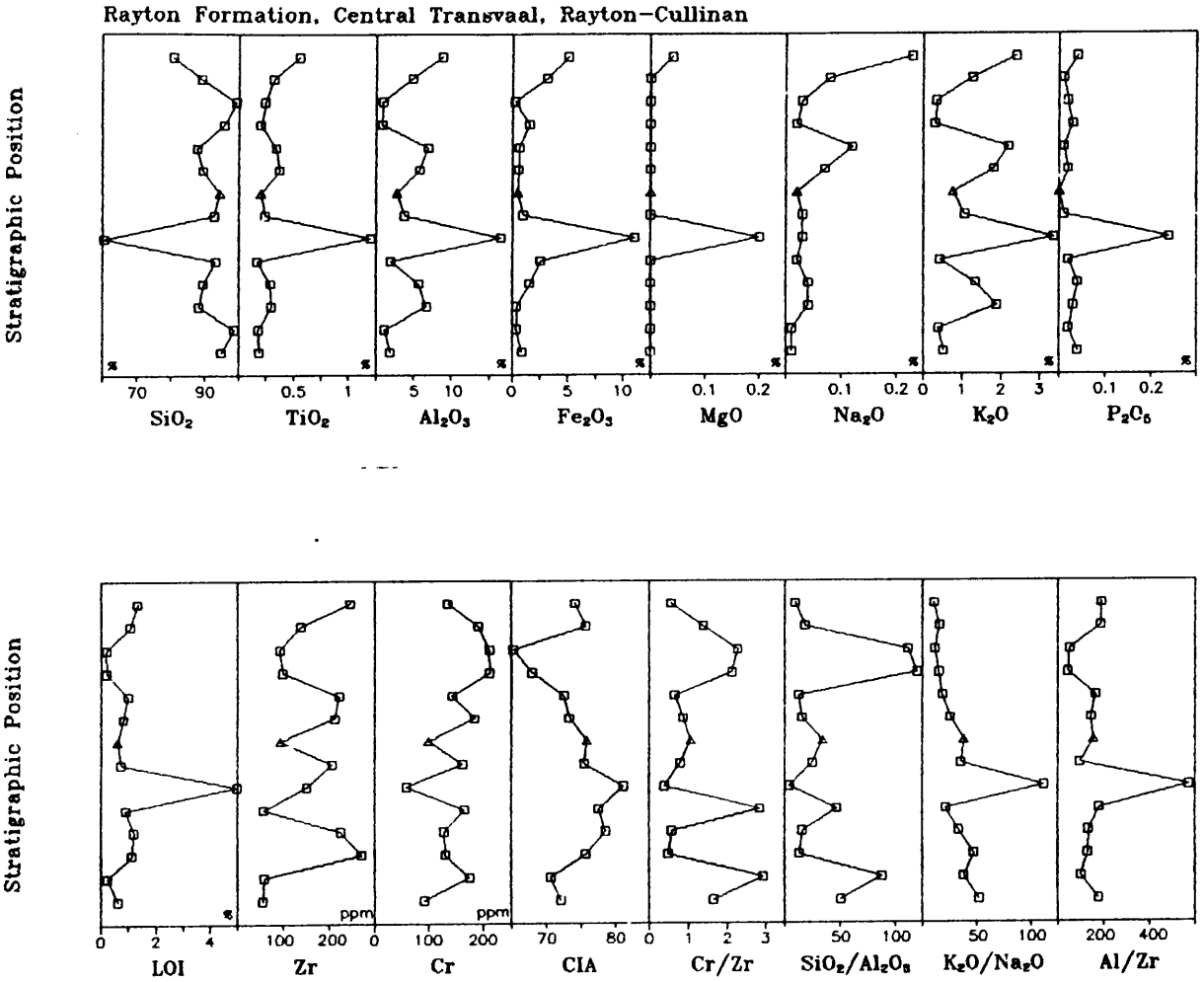

Figure 3.3.12.1: Geochemical profile of the Rayton Formation, Rayton-Cullinan, central Transvaal. Lithological types: Δ = conglomerate; □ = sandstone. Vertical scale = ± 400 m in total.

A geochemical profile of the Rayton Formation was taken in the Rayton/Cullinan area (Fig. 3.3.12.1). The profile has an approximate thickness of 400 m and describes the upper part of the Rayton Formation. Two rocktypes were encountered, sandstone and conglomerate. The profile exhibits relatively stable patterns for most elements and ratios, except for one unusual sandstone sample (6th from base) with a geochemistry similar to shales. The K_2O/Na_2O-ratio decreases throughout the profile, except for the unusual sandstone sample.

The Post-Magaliesberg Formations in the eastern Transvaal have an approximate thickness of 2400 m, including diabase sills, and are up to 1700 m thick, including diabase sills, in the northeastern Transvaal (Schreiber, 1990). As the frequency and thickness of diabase sills increase with stratigraphic height in the Pretoria Group (e.g., Button, 1973; Schreiber, 1990), the thicknesses stated above would have to be corrected by several hundred metres.

The major element geochemistry of the Vermont Formation (Tables 3.3.12.3, 3.3.12.4 and 3.3.12.6) shows an enrichment of MgO, and depletion of TiO_2, Al_2O_3, P_2O_5 and Fe_2O_3(t) compared to average shale estimates (Table 3.2.1b). CaO and Na_2O have average contents similar to average shale estimates, but the calculated mean is biased by samples with extremely high contents of these elements (CaO: 9.43 w.t.%; Na_2O: 3.43 w.t.%). Median and geometric mean of CaO and Na_2O point to depletion of these elements, but the sample size ($n = 12$) is too small to generalize about either depletion or 'normal' contents. The trace elements U and Ba are slightly enriched, Zn, Cu, Ni, Co and V are depleted compared to average shale estimates (Table 3.2.1d). La is slightly enriched, Ce, Sm and the HREE slightly depleted. Eu is strongly depleted. K_2O/Na_2O and La/Sc (Table 3.3.12.5) are enriched compared to Post-Archaean Average Shale (Taylor and McLennan, 1985), Th/U is depleted. The ratios Cr/V, V/Ni and Ni/Co resemble Late Archaean Average Shale (Taylor and McLennan, 1985). LREE/HREE is slightly higher, and Eu/Eu* significantly depleted compared to Post-Archaean Average Shale (Taylor and McLennan, 1985).

A geochemical profile (see Fig. 1.5.14 for location) of the lower part of the Vermont Formation has an approximate thickness of 200 m, including diabase sills, and contains 3 rock units, shale, high-Mg shale and high Mg-Ca-Na shale. The variability of major and trace elements is low in most shale samples, but rather high in the two other lithological

Element	n	MEAN	STD ±	GM	MEDIAN	RANGE	VC
SiO_2	12	61.91	4.99	61.71	62.90	49.36 - 67.25	0.08
TiO_2	12	0.47	0.16	0.43	0.48	0.11 - 0.70	0.34
Al_2O_3	12	15.19	3.92	14.35	16.31	4.06 - 18.83	0.26
Fe_2O_3*	12	5.16	1.51	4.91	5.19	1.97 - 7.46	0.29
MnO	12	0.09	0.13	0.05	0.04	0.01 - 0.45	1.44
MgO	12	6.74	6.85	5.27	4.58	2.46 - 27.41	1.02
CaO	12	1.18	2.64	0.22	0.35	0.01 - 9.43	2.24
Na_2O	12	0.91	1.06	0.46	0.22	0.10 - 3.43	1.17
K_2O	12	3.85	1.71	2.82	4.28	0.07 - 5.83	0.44
P_2O_5	12	0.06	0.04	-	0.06	<LLD - 0.12	0.67
H_2O^-	12	1.14	2.00	0.42	0.38	0.04 - 7.19	1.75
LOI	12	3.10	1.54	2.69	3.32	0.87 - 5.94	0.50
Zn	12	67	17	65	66	45 - 107	0.25
Cu	12	17	24	7.2	6.5	<3 - 82	1.41
Ni	12	46	32	40	37	15 - 136	0.70
Co	12	12	3.7	12	13	6 - 20	0.31
Ga	12	20	6.0	19	22	5 - 26	0.30
Mo	12	0.5 *)	1.7	-	<LLD	<2 - 6	3.40
Nb	12	12	3.2	12	13	5 - 16	0.27
Zr	12	199	113	172	156	43 - 434	0.57
Y	12	30	9.7	28	30	11 - 47	0.32
Sr	12	105	86	65	106	5 - 279	0.82
Rb	12	155	65	123	169	7 - 228	0.42
U	12	6.3	4.4	-	6.5	<5 - 13	0.70
Th	12	15	4.9	15	15	9 - 25	0.33
Pb	12	20	8.7	17	21	<5 - 33	0.44
Cr	12	103	43	86	112	<14 - 146	0.42
V	12	61	20	58	57	32 - 107	0.33
Ba	12	873	427	787	817	353 - 1946	0.49
Sc	12	16	5.6	15	15	8 - 25	0.35
As	12	-	-	-	-	-	-
S	12	94	74	67	85	25 - 220	0.79
Sb	12	-	-	-	-	-	-
Sn	12	3.1 *)	6.1	-	<LLD	<8 - 19	1.97
B	4	103	66	64	127	7 - 151	0.64

Table 3.3.12.3: Average element concentrations of shales from the Vermont Formation

(n = number of samples; 'MEAN' = arithmetic mean; 'STD ±' = 1 σ standard deviation; 'GM' = geometric mean; 'MEDIAN' = median; 'VC' = variation coefficient; average major element concentrations are reported in weight %, average trace element concentrations in ppm; 'Fe_2O_3*' is all Fe expressed as Fe_2O_3; *) = arithmetic mean below detection limit; LLD = lower limit of detection)

Table 3.3.12.4: Average major element concentrations of Vermont Formation shales recalculated to 100 % volatile-free.

Element	n	MEAN	STD ±	RANGE
SiO_2	12	64.72	3.53	57.26 - 68.79
TiO_2	12	0.49	0.18	0.12 - 0.78
Al_2O_3	12	15.92	4.21	4.36 - 19.87
Fe_2O_3*	12	5.42	1.71	2.12 - 8.65
MnO	12	0.09	0.13	0.01 - 0.48
MgO	12	7.10	7.36	2.48 - 29.44
CaO	12	1.22	2.69	0.01 - 9.60
Na_2O	12	0.93	1.08	0.10 - 3.57
K_2O	12	4.04	1.85	0.08 - 6.22
P_2O_5	12	0.06	0.04	<LLD - 0.12

Table 3.3.12.5: Average ratios of the Vermont Formation shales

(NOTE: ratios corrected as described in Chapter 3.1.2)

Ratio	n	MEAN	STD ±	GM	RANGE	VC
CIA	12	68.6	12.6	67.2	35.1 - 85.6	0.18
Fe/V	12	610	155	591	360 - 861	0.25
K_2O/Na_2O	12	15.3	16.4	6.1	0.4 - 53.6	1.07
SiO_2/Al_2O_3	12	4.8	3.1	4.3	2.9 - 14.5	0.65
Cr/Th	12	7.6	4.5	6.2	1.6 - 16.2	0.59
Th/Sc	12	1.10	0.52	0.99	0.48 - 2.08	0.47
Cr/Zr	12	0.61	0.31	0.53	0.20 - 1.03	0.51
Co/Th	12	0.90	0.41	0.82	0.40 - 1.67	0.46
Al_2O_3/TiO_2	12	34.0	8.3	33.2	23.5 - 54.5	0.24
Al_2O_3/K_2O	12	8.9	15.6	5.1	2.8 - 58.0	1.75
K/Rb	12	211	92	191	68 - 420	0.44
K/Ba	12	38	18	30	1.7 - 66	0.47
Ti/Ni	12	70	25	66	30 - 118	0.36
Cr/V	12	1.69	0.61	1.56	0.44 - 2.70	0.36
V/Ni	12	1.54	0.43	1.47	0.60 - 2.13	0.28
Ni/Co	12	3.74	1.88	3.33	1.15 - 8.50	0.50
Zr/Nb	12	15.7	6.1	14.7	8.6 - 27.1	0.39
Th/U	12	2.23	1.03	2.04	1.00 - 5.01	0.46
Ba/Rb	12	10.2	13.5	6.4	2.2 - 50.4	1.32
Ba/Sr	12	21.5	22.9	12.2	1.4 - 70.6	1.07
Ba/Th	12	60.0	28.3	54.1	22.1 - 114.5	0.47
Al/Zr	12	463	134	441	230 - 639	0.29
Ti/Zr	12	16.5	7.1	15.1	7.5 - 28.3	0.43

Table 3.3.12.6: Average element concentrations and ratios of selected shale samples of the Vermont Formation.

(n = number of samples; 'MEAN' = arithmetic mean; 'STD ±' = 1 σ standard deviation; 'GM' = geometric mean; 'MEDIAN' = median; 'VC' = variation coefficient; average major element concentrations (i.e. FeO to S_{XRF}) are reported in weight %, average trace element concentrations in ppm; n.c. = not calculated; subscript N = concentration normalised to chondrite;
Ce/Ce* = $Ce_N/[(La_N + Pr_N)/2]$; Σ REE = sum of REE in ppm; NOTE: ratios corrected as described in Chapter 3.1.2; LLD = lower limit of detection)

Element	n	MEAN	STD ±	GM	MEDIAN	RANGE
FeO	5	2.09	0.89	1.92	2.13	0.96 - 3.03
Fe_2O_3	5	2.39	1.67	1.75	3.02	0.47 - 4.14
CO_2	5	0.12	0.06	0.10	0.15	0.04 - 0.18
C_{org}	5	0.004	0.006	-	<LLD	<0.001 - 0.01
H_2O^+	5	2.58	1.28	2.34	1.78	1.44 - 4.15
S_{leco}	5	0.002	0.002	-	0.001	<0.001 - 0.005
S_{xrf}	5	0.006	-	-	-	-
Li	5	123	93	66	111	3 - 259
La	5	45.2	14.9	43.4	42.9	27.8 - 69.0
Ce	5	53.5	16.7	51.2	63.2	31.2 - 69.5
Pr	5	7.7	3.2	7.2	6.9	4.3 - 12.9
Nd	5	25.6	10.8	23.9	25.0	13.0 - 42.8
Sm	5	4.4	1.4	4.3	4.1	3.3 - 6.8
Eu	5	0.66	0.20	0.64	0.6	0.5 - 1.0
Gd	5	3.5	1.1	3.4	3.1	2.7 - 5.3
Tb	5	0.58	0.13	0.57	0.5	0.5 - 0.8
Dy	5	3.5	0.75	3.4	3.2	2.9 - 4.7
Er	5	2.1	0.37	2.1	2.0	1.7 - 2.6
Tm	5	0.34	0.06	0.34	0.3	0.3 - 0.4
Yb	5	2.4	0.39	2.3	2.3	2.0 - 2.9
La/Sc	5	3.63	1.41	3.41	3.58	1.99 - 5.75
Th/La	5	0.39	0.12	0.38	0.34	0.28 - 0.58
Ba/La	5	19.5	7.2	18.6	17.1	14.0 - 31.9
LREE/HREE	5	12.8	2.6	12.6	12.8	9.4 - 16.1
K2O/ΣREE	5	278	77	270	259	211 - 408
Gd_N/Yb_N	5	1.18	0.17	1.17	1.09	1.06 - 1.48
La_N/Sm_N	5	6.43	0.79	6.39	6.39	5.30 - 7.48
Ce/Ce*	5	0.65	0.19	0.63	0.76	0.39 - 0.79
Eu/Eu*	5	0.50	0.04	0.50	0.49	0.46 - 0.57
C_{org}/S	5	0.90	0.26	0.88	0.90	0.71 - 1.08
ΣREE	5	149.5	44.6	144.4	149.5	99.6 - 218.7

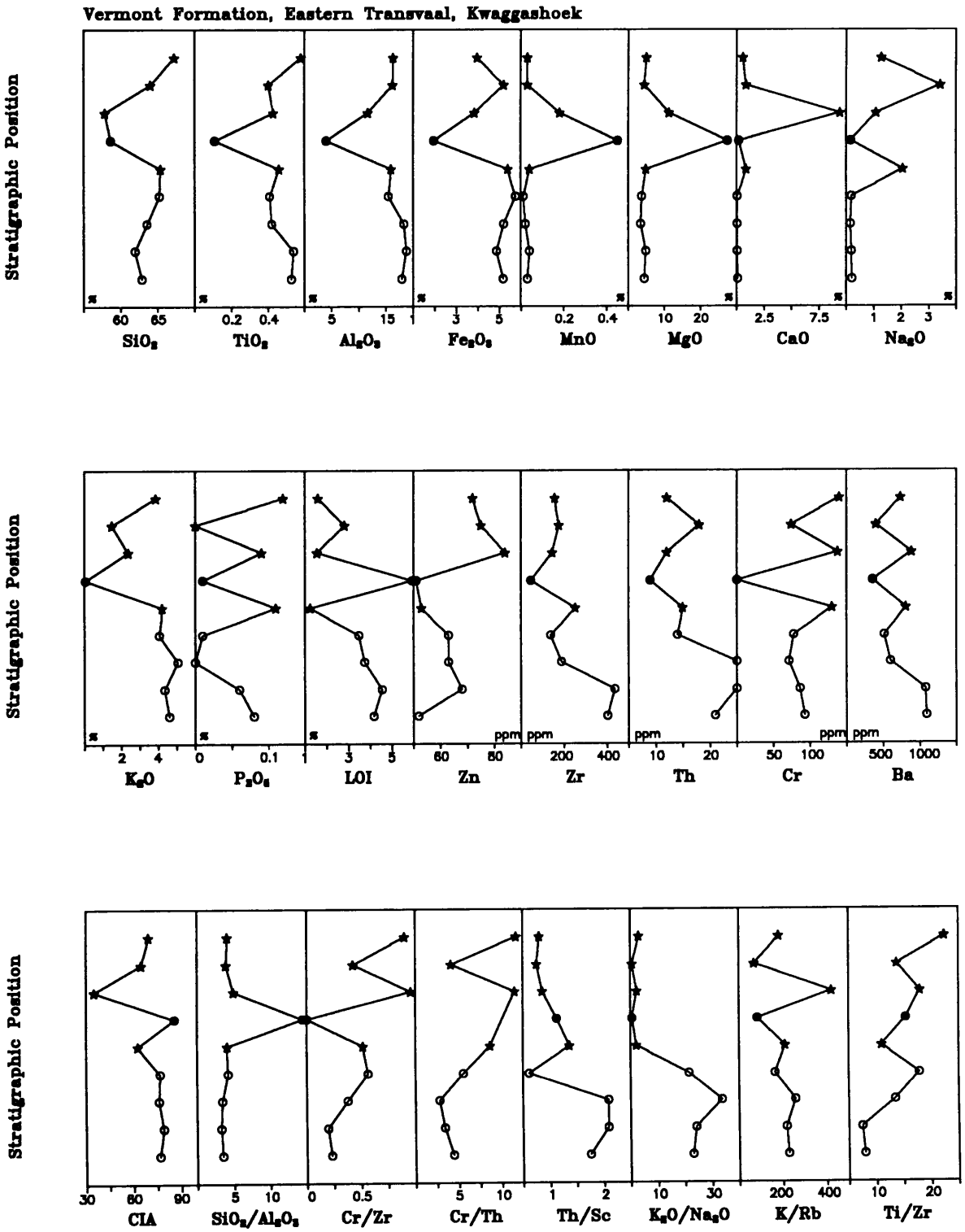

Figure 3.3.12.2: Geochemical profile of the Vermont Formation, Kwaggashoek, eastern Transvaal. Lithological types: ○ = shale; ● = high-Mg-shale; ★ = high-Mg-Ca-Na-shale. Vertical scale = ± 200 m in total.

groups. Zr-contents decline throughout the lower and middle part of the profile, and are stable in the upper part. Ti/Zr increases from bottom to top, although the pattern is somewhat irregular. K_2O/Na_2O discriminates between the shales (open circles) in the lower part of the profile and the other units in the upper part.

The Lakenvlei Formation sandstones (Tables 3.3.12.7 and 3.3.12.8) are depleted in CaO, $Fe_2O_3(t)$, TiO_2 and P_2O_5 compared to the carbonate-free recalculated average sandstone estmate of Clarke (1924). Other major element averages are similar to this estimate. The average Na_2O-content is elevated by 8 samples with contents of up to 4 wt.%, whereas most samples have contents considerably smaller than 0.3 wt.% (median: 0.11 wt.%), and thus are depleted compared to average sandstone estimates. However, compared to other Pretoria Group sandstones, the Lakenvlei Formation is enriched in Na_2O, and has a relatively high percentage of samples with significant amounts of Na_2O. The trace elements Ni, Co, Mo, Th, U, Cr, Ba and Sc are enriched, Zn, Ga, Zr, Y, and Rb are depleted compared to average sandstone estimates (Table 3.2.1d).

The Nederhorst Formation shale geochemistry is shown in Tables 3.3.12.9 and 3.3.12.10. A comparison with average shale estimates (Table 3.2.1b) proves difficult as most shales are calcareous or metamorphic equivalents of marls (i.e. calc-silicate rock). Accordingly, CaO and MgO are significantly enriched compared to average shale estimates. SiO_2, TiO_2, Al_2O_3, Fe_2O_3 and Na_2O are depleted. The average K_2O-content is elevated by a single sample with more than 9 wt.% K_2O. As the median of K_2O is only 1.20 wt.%, K_2O is considered to be depleted compared to average shale estimates. Zr and V are strongly, and Zn, Ni, and Co moderately depleted compared to average shale estimates (Table 3.2.1d). Cu seems to be strongly enriched. However, the average Cu-content is biased by a sample containing 995 ppm Cu. As the median of Cu is 18 ppm, and the geometric mean 31 ppm, Cu seems to be depleted rather than enriched compared to average shale estimates. It should be mentioned, that Sb and Sn have relatively high average contents. The K_2O/Na_2O-ratio (Table 3.3.12.11) is increased compared to Post-Archaean Average Shale (Taylor and McLennan, 1985), whereas the Th/U ratio is decreased. The ratios Cr/V, V/Ni, and Ni/Co resemble Late Archaean Average Shale (Taylor and McLennan, 1985), although they are slightly elevated compared to the latter.

Element	n	MEAN	STD ±	GM	MEDIAN	RANGE	VC
SiO_2	27	88.94	6.30	88.73	89.87	75.31 - 98.21	0.07
TiO_2	27	0.08	0.04	-	0.08	<LLD - 0.15	0.50
Al_2O_3	27	5.53	3.52	3.87	5.19	0.06 - 12.63	0.64
Fe_2O_3*	27	0.97	0.55	0.85	0.88	0.36 - 2.68	0.57
MnO	27	0.03	0.06	-	0.01	<LLD - 0.24	2.00
MgO	27	0.31	0.35	-	0.19	<LLD - 1.58	1.13
CaO	27	0.17	0.44	-	0.01	<LLD - 2.12	0.26
Na_2O	27	0.63	0.92	0.18	0.11	0.01 - 4.07	1.46
K_2O	27	1.62	1.75	-	1.01	<LLD - 7.01	1.08
P_2O_5	27	0.03	0.03	-	0.01	<LLD - 0.12	1.00
H_2O^-	27	0.10	0.06	0.08	0.08	0.03 - 0.26	0.60
LOI	27	0.93	0.97	0.63	0.59	0.21 - 4.54	1.04
Zn	27	9.6	3.5	9.0	9	4 - 21	0.37
Cu	27	2.4 *)	4.2	-	<LLD	<3 - 17	1.75
Ni	27	12	25	-	6	<3 - 133	2.08
Co	27	5.6	3.4	-	5	<3 - 14	0.61
Ga	27	4.5	4.5	-	5	<3 - 16	1.00
Mo	27	8.4	3.3	-	8	<2 - 14	0.39
Nb	27	2.2	2.0	-	3	<2 - 5	0.91
Zr	27	80	43	67	82	9 - 198	0.54
Y	27	12	10	-	10	<2 - 41	0.83
Sr	27	40	54	18	11	4 - 205	1.35
Rb	27	48	44	-	41	<2 - 166	0.92
U	27	1.3 *)	2.5	-	<LLD	<5 - 7	1.92
Th	27	3.7 *)	4.1	-	5	<5 - 13	1.11
Pb	27	8.2	14.5	-	<LLD	<5 - 49	1.77
Cr	27	131	49	121	137	49 - 215	0.37
V	27	20	12	-	21	<14 - 38	0.60
Ba	27	474	525	241	233	16 - 1886	1.11
Sc	27	3.2 *)	4.9	-	<LLD	<8 - 13	1.53
As	27	-	-	-	-	-	-
S	27	48	47	-	57	<50 - 121	0.98
Sb	27	-	-	-	-	-	-
Sn	27	-	-	-	-	-	-
B	8	96	191	27	23	5 - 563	1.99

Table 3.3.12.7: Average element concentrations of the Lakenvlei Formation sandstones

(n = number of samples; 'MEAN' = arithmetic mean; 'STD ±' = 1 σ standard deviation; 'GM' = geometric mean; 'MEDIAN' = median; 'VC' = variation coefficient; average major element concentrations are reported in weight %, average trace element concentrations in ppm; 'Fe_2O_3*' is all Fe expressed as Fe_2O_3; *) = arithmetic mean below detection limit; LLD = lower limit of detection)

Table 3.3.12.8 : Average ratios of Lakenvlei Formation sandstones

(NOTE: ratios are not corrected, i.e. a sample was excluded from calculation of the average ratio if one or both elements are below the detection limit; n.c. = not calculated)

Ratio	n	MEAN	STD ±	GM	RANGE	VC
CIA	27	63.5	17.4	61.0	23.7 - 92.6	0.27
SiO_2/Al_2O_3	27	87.4	309.1	22.9	6.0 - 1628	3.54
lg SiO_2/Al_2O_3	27	1.36	0.51	n.c.	0.78 - 3.21	n.c.
K_2O/Na_2O	26	17.36	19.0	4.7	0.02 - 86.0	1.10
lg Na_2O/K_2O	26	-0.67	1.06	n.c.	-1.94 - 1.72	n.c.
Ti/Zr	26	6.8	4.1	5.9	1.9 - 21.8	0.60
Ti/Cr	26	5.0	4.2	3.4	0.4 - 18.4	0.84
Al/Zr	27	362	217	306	35 - 1108	0.60
Al_2O_3/TiO_2	26	78	69	59	3 - 384	0.89
Al_2O_3/K_2O	26	10.2	17.0	5.2	1.8 - 81.5	1.67
K/Rb	26	307	333	243	42 - 1891	1.09
K/Ba	26	31	18	27	8 - 98	0.58
K/Sr	26	857	1064	384	16 - 4379	1.24

The geochemistry of Nederhorst Formation sandstones (Appendix 2a) shows enrichment of SiO_2 and MgO compared to the carbonate-free recalculated average sandstone of Clarke (1924) (Table 3.2.1c). Other major elements are more or less depleted, with strong depletion of TiO_2, CaO, and Na_2O. The trace elements Zn, Ga, Zr, Y, Sr, Rb and B are depleted, Co, Mo, Th, Cr, Ba and Sc are enriched compared to average sandstones (Table 3.2.1d). Nb and U are also enriched, but some doubt is cast on the validity of this observation as both average and median are below the detection limit and the sample number is small (n = 5). The average Ni-content is high due to one sample with a relatively high content (37 ppm).

The Steenkampsberg Formation sandstones (Tables 3.3.12.12 and 3.3.12.13) are strongly enriched in SiO_2 compared to average sandstones (Table 3.2.1c), and are depleted in all other major elements, except MgO. The trace elements Co, Mo, Nb, Th and Cr are enriched, Zn, Ga, Zr, Y, Rb and Pb are depleted compared to average sandstone estimates (Table 3.2.1d). A complete geochemical profile was taken on the Steenkampsberg Pass (Fig. 3.3.12.3, see Fig. 1.5.17 for location of profile). The profile has an approximate thickness of 600 m (including diabase sills) and can be compared to profile 4 of Schreiber (1990, p. 194). Two

Element	n	MEAN	STD ±	GM	MEDIAN	RANGE	VC
SiO_2	14	46.54	10.33	45.46	42.67	31.62 - 60.25	0.22
TiO_2	14	0.40	0.16	0.36	0.42	0.11 - 0.67	0.40
Al_2O_3	14	12.85	5.78	11.09	13.22	1.93 - 20.65	0.45
Fe_2O_3*	14	4.89	2.29	4.34	4.32	1.25 - 8.57	0.47
MnO	14	0.10	0.06	0.08	0.08	0.03 - 0.24	0.60
MgO	14	13.07	6.57	11.41	13.90	5.57 - 22.34	0.50
CaO	14	11.87	9.33	6.71	13.85	0.56 - 23.96	0.79
Na_2O	14	0.25	0.24	0.17	0.10	0.07 - 0.79	0.96
K_2O	14	3.27	3.57	-	1.20	<LLD - 9.08	1.09
P_2O_5	14	0.11	0.04	0.10	0.12	0.03 - 0.16	0.36
H_2O^-	14	0.54	0.76	0.26	0.20	0.05 - 2.34	1.41
LOI	14	5.82	4.89	-	4.72	<LLD - 17.78	0.84
Zn	14	71	43	59	58	17 - 158	0.61
Cu	14	120	273	31	18	9 - 995	2.28
Ni	14	43	20	37	40	9 - 81	0.47
Co	14	12	6.3	9.5	12	<3 - 22	0.53
Ga	14	17	8.5	14	16	<3 - 35	0.50
Mo	14	-	-	-	-	-	-
Nb	14	11	4.1	11	12	5 - 19	0.37
Zr	14	103	58	87	102	16 - 243	0.56
Y	14	30	40	20	21	4 - 167	1.33
Sr	14	103	69	74	84	6 - 232	0.67
Rb	14	122	123	36	65	<2 - 307	1.01
U	14	3.8 *)	4.0	-	<LLD	<5 - 9	1.05
Th	14	13	7.3	11	14	<5 - 23	0.56
Pb	14	21	35	12	13	<5 - 140	1.67
Cr	14	128	69	99	122	<14 - 267	0.54
V	14	79	42	68	73	19 - 168	0.53
Ba	14	480	475	236	381	<16 - 1618	0.99
Sc	14	19	8.7	18	15	13 - 44	0.46
As	14	13	29	-	<LLD	<10 - 112	2.23
S	14	168	181	98	85	<50 - 650	1.08
Sb	14	5.0 *)	8.0	-	<LLD	<8 - 26	1.60
Sn	14	5.6 *)	7.8	-	<LLD	<8 - 17	1.39
B	7	87	99	57	55	19 - 300	1.14

Table 3.3.12.9: Average element concentrations of Nederhorst Formation shales

(n = number of samples; 'MEAN' = arithmetic mean; 'STD ±' = 1 σ standard deviation; 'GM' = geometric mean; 'MEDIAN' = median; 'VC' = variation coefficient; average major element concentrations are reported in weight %, average trace element concentrations in ppm; 'Fe_2O_3*' is all Fe expressed as Fe_2O_3; *) = arithmetic mean below detection limit; LLD = lower limit of detection)

Table 3.3.12.10: Average major element concentrations of Nederhorst Formation shales recalculated to 100 % volatile-free.

Element	n	MEAN	STD ±	RANGE
SiO_2	14	49.50	8.74	38.72 - 61.59
TiO_2	14	0.42	0.16	0.14 - 0.75
Al_2O_3	14	13.55	5.92	2.40 - 23.18
Fe_2O_3*	14	5.18	2.32	1.55 - 8.71
MnO	14	0.11	0.08	0.03 - 0.30
MgO	14	14.35	7.81	5.67 - 27.77
CaO	14	13.16	10.65	0.57 - 28.40
Na_2O	14	0.26	0.24	0.07 - 0.80
K_2O	14	3.37	3.64	<LLD - 9.23
P_2O_5	14	0.11	0.04	0.03 - 0.16

Table 3.3.12.11: Average ratios of the Nederhorst Formation shales

(NOTE: ratios corrected as described in Chapter 3.1.2)

Ratio	n	MEAN	STD ±	GM	RANGE	VC
CIA	14	37.4	21.8	29.6	4.4 - 63.6	0.58
Fe/V	14	456	114	443	268 - 711	0.25
K_2O/Na_2O	14	12.5	16.3	-	0.41 - 60.53	1.30
SiO_2/Al_2O_3	14	4.8	3.6	4.1	1.7 - 16.4	0.75
Cr/Th	13	9.9	3.8	9.3	5.1 - 19.2	0.38
Th/Sc	14	0.83	0.43	0.70	0.11 - 1.69	0.52
Cr/Zr	14	1.32	0.44	1.20	0.37 - 1.75	0.33
Co/Th	14	0.99	0.59	0.82	0.17 - 2.40	0.60
Al_2O_3/TiO_2	14	31.3	5.7	30.7	17.6 - 41.0	0.18
Al_2O_3/K_2O	13	179.4	394	14.2	2.1 - 1072	2.20
K/Rb	13	164	76	142	42 - 256	0.46
K/Ba	13	46	36	24	1.0 - 106	0.78
Ti/Ni	14	58	8.5	58	48 - 74	0.15
Cr/V	14	1.65	0.62	1.52	0.42 - 3.18	0.38
V/Ni	14	1.88	0.42	1.83	1.04 - 2.55	0.22
Ni/Co	14	4.58	3.25	3.73	1.13 - 11.71	0.71
Zr/Nb	14	8.5	2.3	8.1	2.67 - 12.79	0.27
Th/U	11	2.54	0.94	2.40	1.50 - 4.61	0.37
Ba/Rb	13	10.4	14.0	5.9	2.1 - 42.5	1.35
Ba/Sr	14	9.8	23.8	3.3	0.3 - 92.0	2.43
Ba/Th	13	33.7	25.3	23.4	1.7 - 89.9	0.75
Al/Zr	14	687	96	679	384 - 758	0.14
Ti/Zr	14	25.9	6.6	25.0	10.6 - 41.2	0.25

Element	n	MEAN	STD ±	GM	MEDIAN	RANGE	VC
SiO_2	20	94.80	5.60	94.63	96.55	78.05 - 99.86	0.06
TiO_2	20	0.15	0.18	0.08	0.07	0.01 - 0.68	1.20
Al_2O_3	20	2.47	3.13	-	1.27	<LLD - 11.57	1.27
Fe_2O_3*	20	0.64	0.43	0.55	0.43	0.33 - 1.88	0.67
MnO	20	<0.01	0.01	-	<LLD	<LLD - 0.01	-
MgO	20	0.42	0.59	-	0.15	<LLD - 1.89	1.41
CaO	20	0.07	0.23	-	<LLD	<LLD - 0.99	3.29
Na_2O	20	0.09	0.26	-	0.02	<LLD - 1.18	2.89
K_2O	20	0.50	0.76	-	0.30	<LLD - 2.95	1.52
P_2O_5	20	0.02	0.03	-	0.01	<LLD - 0.07	1.50
H_2O^-	20	0.05	0.02	0.04	0.05	0.01 - 0.10	0.40
LOI	20	0.48	0.45	0.34	0.34	0.05 - 1.87	0.94
Zn	20	6.4	2.2	-	6.5	<3 - 12	0.34
Cu	20	0.6 *)	1.5	-	<LLD	<3 - 5	2.50
Ni	20	2.5 *)	3.7	-	<LLD	<3 - 11	1.48
Co	20	4.2	1.3	4.0	4.0	3 - 7	0.31
Ga	20	1.7 *)	3.0	-	<LLD	<3 - 11	1.77
Mo	20	9.4	3.8	-	10	<2 - 15	0.40
Nb	20	2.9	4.2	-	<LLD	<2 - 15	1.45
Zr	20	123	134	84	75	23 - 581	1.09
Y	20	4.2	3.7	-	5	<2 - 11	0.88
Sr	20	21	58	-	5	<2 - 260	2.76
Rb	20	20	24	-	15	<2 - 92	1.20
U	20	0.4 *)	1.6	-	<LLD	<5 - 7	4.00
Th	20	3.1 *)	5.1	-	<LLD	<5 - 16	1.65
Pb	20	2.7 *)	3.1	-	<LLD	<5 - 8	1.15
Cr	20	182	38	178	185	109 - 233	0.21
V	20	29	31	-	23	<14 - 151	1.07
Ba	20	136	225	-	62	<16 - 852	1.65
Sc	20	2.0 *)	4.0	-	<LLD	<8 - 11	2.00
As	20	0.8 *)	3.6	-	<LLD	<10 - 16	4.50
S	20	2.7 *)	11.9	-	<LLD	<50 - 53	4.41
Sb	20	-	-	-	-	-	-
Sn	20	1.7 *)	4.3	-	<LLD	<8 - 13	2.53
B	7	24	49	8.8	6.0	3 - 135	2.04

Table 3.3.12.12: Average element concentrations of Steenkampsberg Formation sandstones

(n = number of samples; 'MEAN' = arithmetic mean; 'STD ±' = 1 σ standard deviation; 'GM' = geometric mean; 'MEDIAN' = median; 'VC' = variation coefficient; average major element concentrations are reported in weight %, average trace element concentrations in ppm; 'Fe_2O_3*' is all Fe expressed as Fe_2O_3; *) = arithmetic mean below detection limit; LLD = lower limit of detection)

Table 3.3.12.13 : Average ratios of Steenkampsberg Formation sandstones

(NOTE: ratios are not corrected, i.e. a sample was excluded from calculation of the average ratio if one or both elements are below the detection limit; n.c. = not calculated)

Ratio	n	MEAN	STD ±	GM	RANGE	VC
CIA	18	78.7	8.0	78.3	65.0 - 97.5	0.10
SiO_2/Al_2O_3	18	129.9	178.1	63.4	6.8 - 652.7	1.37
lg SiO_2/Al_2O_3	18	1.80	0.55	n.c.	0.83 - 2.82	n.c.
K_2O/Na_2O	17	14.0	12.8	6.9	0.33 - 38.0	0.91
lg Na_2O/K_2O	17	-0.84	0.66	n.c.	-1.58 - 0.48	n.c.
Ti/Zr	20	6.8	4.0	5.7	1.3 - 18.2	0.59
Ti/Cr	20	4.7	5.2	2.7	0.3 - 19.2	1.11
Al/Zr	18	167	193	86	3.2 - 721	1.16
Al_2O_3/TiO_2	18	36.4	44.1	17.0	0.4 - 152.5	1.21
Al_2O_3/K_2O	17	7.3	4.8	6.1	3.1 - 19.0	0.66
K/Rb	14	197	76	180	50 - 297	0.39
K/Ba	14	47	29	38	4 - 120	0.62
K/Sr	17	573	536	270	14 - 1799	0.94

lithotypes were encountered, cm-thick micaceous beds associated with quartz veins and low-angle thrust faults, and sandstones. The latter are subdivided into 'normal' sandstones, and sandstones in close proximity to the veins, thrust faults and/or diabase sills. The geochemical pattern of the lower 6 sandstone samples is generally stable, whereas the upper samples show some degree of variability. Although the subdivision of the sandstones could not be verified unambiguously by geochemical means, some relatively high element contents (e.g., TiO_2, MgO, K_2O, Zr) seem to be related to the sandstones close to post-genetic features. Cr and Cr/Zr generally decline throughout the profile.

The Houtenbek Formation sandstones (Appendix 2a) are strongly enriched in SiO_2 and depleted in other major elements compared to average sandstone estimates (Table 3.2.1c). Due to the low sample number (n = 5), enrichment and depletion of some trace elements cannot be evaluated properly (e.g., Nb, Th, and U). However, it appears that Cr and Mo may be enriched, and Zn, Ga, Zr, Y, Rb, B, and Sr may be depleted. A geochemical profile of the Houtenbek Formation (Fig. 3.3.12.4, see Fig. 1.5.18 for location of profile) has an approximate thickness of 200 m and can be compared with profile 1 of Schreiber (1990, p.

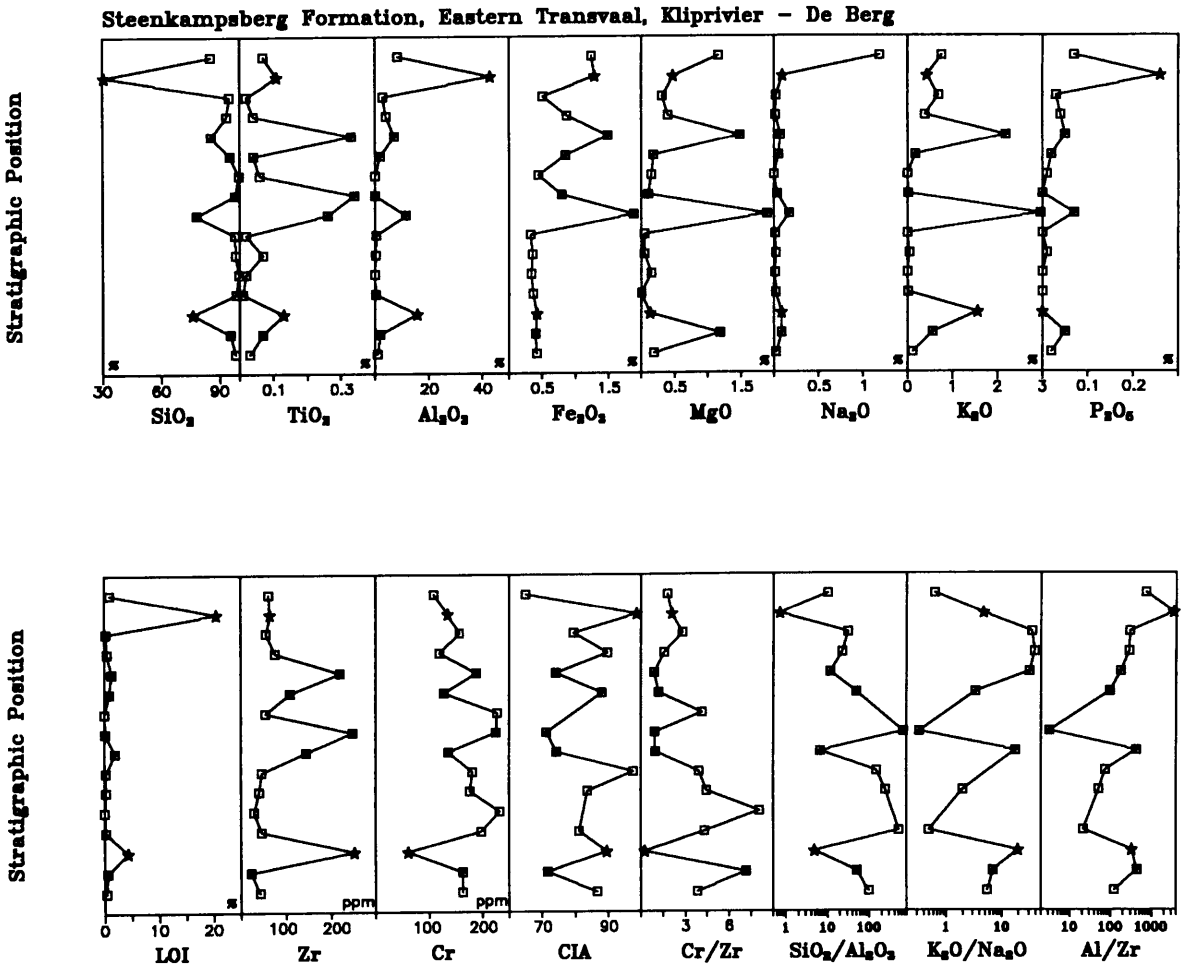

Figure 3.3.12.3: Geochemical profile of the Steenkampsberg Formation, Kliprivier - De Berg, eastern Transvaal. Lithological types: ★ = micaceous beds associated with veins and/or faults; □ = sandstone; ■ = sandstones in close proximity to veins, faults and sills/dykes. Vertical scale = ± 600 m in total.

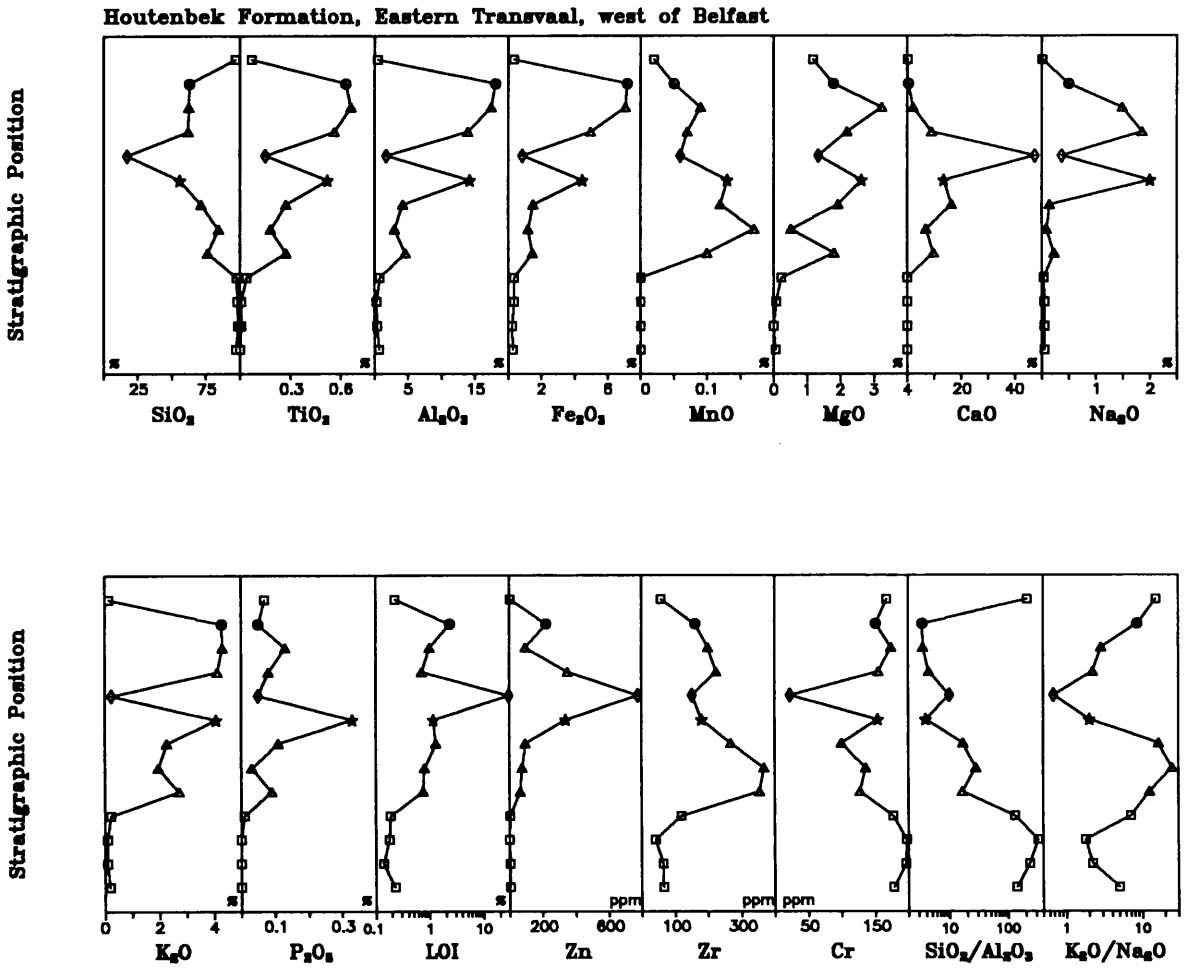

Figure 3.3.12.4: Geochemical profile of the Houtenbek Formation, west of Belfast, eastern Transvaal. Lithological types: ★ = high-Na shale/chert/carbonate; □ = sandstone; Δ = shale/chert/carbonate; ◇ = carbonate; ● = black hornfels. Vertical scale = ± 200 m in total.

204). Five lithotypes were encountered, sandstone, carbonate, a chert/carbonate/shale association, a high-Na chert/carbonate/shale association and black hornfels. The variability in the profile is mainly caused by lithological changes. However, SiO_2/Al_2O_3 decreases upwards throughout the profile, with exception of the uppermost sandstone sample. Al_2O_3, TiO_2 and Fe_2O_3 increase gradually from the base of the chert/carbonate/shale association towards the black hornfels. MnO and Zr increase strongly above the lower sandstone samples, and decrease gradually towards the top of the profile. The exceptionally high Zn-content of the carbonate sample (diamond)($\approx$ 700 ppm), which is accompanied by Zn-contents of $>$ 300 ppm in the two adjacent samples, should be noted.

3.4 Averages and systematic geochemical variations in Pretoria Group rocks

3.4.1 Geochemistry of Pretoria Group sedimentary rocks

3.4.1.1 Average Pretoria Group Shale estimate

The major element geochemistry of the Pretoria Group shales (Tables 3.4.1.1, 3.4.1.2 and 3.4.1.3) shows a moderate enrichment of Al_2O_3 and a moderate depletion of MnO and Na_2O compared to average shales (Table 3.2.1b). K_2O, TiO_2, MgO and CaO are moderately depleted compared to average shale estimates. If CaO is compared to carbonate-bearing average shale estimates (Table 3.2.1b), the Average Pretoria Group Shale estimate can be considered as CaO-depleted. A comparison of arithmetic mean, median and geometric mean of the average major element estimate of Pretoria Group shales casts some doubt on the suitability of the arithmetic mean as an estimate for the central value. For example, the average CaO-content of the Pretoria Group shales is strongly depleted in most formations (see Chapter 3.3). Only the Silverton, Vermont, Nederhorst and Houtenbeck Formations contain shales with considerable amounts of CaO, with shales of the Nederhorst Formation being strongly enriched and Silverton Formation shales being moderately enriched compared to the carbonate-free recalculated average shale estimates (Table 3.2.1b). Shales of other formations are strongly depleted in CaO. The average Pretoria Group CaO-content of shales decreases from 0.96 to 0.72, if the Nederhorst Formation samples, which comprise only 2.2

	n	MEAN	STD ±	GM	MEDIAN	RANGE	VC
SiO_2	640	58.77	8.11	58.13	58.84	16.08 - 92.02	0.14
TiO_2	640	0.72	0.22	-	0.71	<LLD - 1.90	0.31
Al_2O_3	640	18.95	5.50	17.93	19.01	0.32 - 37.51	0.29
Fe_2O_3*	640	8.27	5.15	7.14	7.80	0.50 - 64.31	0.62
MnO	640	0.05	0.08	-	0.03	<LLD - 1.01	1.60
MgO	640	2.10	3.07	-	1.16	<LLD - 27.41	1.46
CaO	640	0.96	2.92	-	0.12	<LLD - 27.45	3.04
Na_2O	640	0.70	0.88	-	0.41	<LLD - 5.92	1.26
K_2O	640	3.02	1.44	-	3.04	<LLD - 9.08	0.48
P_2O_5	640	0.12	0.13	-	0.09	<LLD - 2.30	1.08
H_2O^-	640	0.85	1.18	0.49	0.46	0.03 - 12.71	1.39
LOI	640	5.07	3.38	-	4.64	-0.05 - 31.00	0.67
Zn	640	76	69	58	68	5 - 981	0.91
Cu	640	41	55	27	31	<3 - 995	1.34
Ni	640	67	53	54	57	<3 - 717	0.79
Co	640	14	11	10	12	<3 - 75	0.79
Ga	640	25	9.0	23	25	<3 - 140	0.36
Mo	639	1.7	2.9	-	<LLD	<2 - 19	1.71
Nb	640	15	5.8	14	15	<2 - 89	0.39
Zr	640	174	79	161	160	7 - 978	0.45
Y	640	33	22	30	28	<2 - 426	0.67
Sr	640	95	95	71	78	3 - 1772	1.00
Rb	640	151	69	117	160	<2 - 477	0.46
U	640	6.3	5.0	-	7	<5 - 31	0.79
Th	640	18	6.9	16	18	<5 - 52	0.38
Pb	640	24	30	17	19	<5 - 474	1.25
Cr	640	174	95	151	162	<14 - 918	0.55
V	640	155	79	140	146	19 - 694	0.51
Ba	640	899	1133	657	702	<16 - 14706	1.26
Sc	640	19	8.5	17	17	<8 - 83	0.45
As	640	8.3	24.1	-	<LLD	<10 - 460	2.90
S	640	829	2850	215	180	<50 - 30176	3.44
Sb	640	1.7	4.9	-	<LLD	<8 - 50	2.88
Sn	640	2.6	5.9	-	<LLD	<8 - 82	2.27
B	174	98	141	69	72	4 - 1670	1.44

Table 3.4.1.1: Average element concentrations of Pretoria Group shales

(n = number of samples; 'MEAN' = arithmetic mean; 'STD ±' = 1 σ standard deviation; 'GM' = geometric mean; 'MEDIAN' = median; 'VC' = variation coefficient; average major element concentrations are reported in weight %, average trace element concentrations in ppm; 'Fe_2O_3*' is all Fe expressed as Fe_2O_3; *) = arithmetic mean below detection limit; LLD = lower limit of detection)

Table 3.4.1.2: Average major element concentrations of Pretoria Group shales recalculated to 100 % volatile-free.

Element	n	MEAN	STD ±	RANGE
SiO_2	639	62.71	7.87	17.23 - 93.77
TiO_2	639	0.77	0.23	<LLD - 1.98
Al_2O_3	639	20.23	5.85	0.32 - 39.17
Fe_2O_3*	639	8.80	5.40	0.52 - 68.91
MnO	639	0.06	0.08	<LLD - 1.11
MgO	639	2.28	3.47	<LLD - 30.46
CaO	639	1.06	3.39	<LLD - 39.67
Na_2O	639	0.75	0.93	<LLD - 5.91
K_2O	639	3.22	1.51	<LLD - 9.23
P_2O_5	639	0.13	0.14	<LLD - 2.51

Table 3.4.1.3: Average ratios of the Pretoria Group shales

(NOTE: ratios corrected as described in Chapter 3.1.2)

Ratio	n	MEAN	STD ±	GM	RANGE	VC
CIA	639	76.4	13.6	74.4	4.4 - 99.5	0.18
Fe/V	639	411	365	356	16 - 8309	0.89
K_2O/Na_2O	621	23.6	57.9	-	0 - 445	2.45
SiO_2/Al_2O_3	639	3.9	8.2	3.2	1.0 - 198	2.10
Cr/Th	637	11.8	12.0	9.4	0.27 - 146.9	1.02
Th/Sc	636	1.10	0.61	0.94	0.11 - 6.51	0.56
Cr/Zr	639	1.18	1.59	0.95	0.06 - 36.00	1.35
Co/Th	637	1.07	1.36	0.67	0.08 - 15.03	1.27
Al_2O_3/TiO_2	638	27.1	6.5	26.3	8.1 - 72.1	0.24
Al_2O_3/K_2O	638	18.8	78.9	7.6	2.1 - 1072	4.20
K/Rb	638	187	422	165	42 - 10722	2.26
K/Ba	638	36	19	30	0.2 - 174	0.53
Ti/Ni	638	100	122	76	6 - 1399	1.22
Cr/V	639	1.22	0.66	1.09	0.03 - 8.40	0.54
V/Ni	639	3.43	4.52	2.59	0.22 - 56.67	1.32
Ni/Co	639	6.93	7.54	5.04	0.50 - 79.60	1.09
Zr/Nb	639	12.7	6.9	11.6	1.4 - 81.5	0.54
Th/U	621	2.50	1.05	2.29	0.37 - 6.60	0.42
Ba/Rb	638	9.5	25.5	5.5	1.2 - 346	2.68
Ba/Sr	639	17	31	9.3	0.1 - 433	1.82
Ba/Th	638	59	92	41	0.8 - 1135	1.56
Al/Zr	639	631	211	590	51 - 1268	0.33
Ti/Zr	638	26.9	8.9	25.4	3.7 - 69.4	0.33

Element	n	MEAN	STD ±	GM	MEDIAN	RANGE	VC
FeO	50	3.01	3.16	-	2.09	<LLD - 11.85	1.05
Fe_2O_3	50	3.66	2.97	2.01	2.96	0.01 - 9.10	0.81
CO_2	50	0.52	0.97	0.27	0.31	0.04 - 5.24	1.87
C_{org}	50	0.97	2.84	-	0.05	<LLD - 12.64	2.93
H_2O^+	50	3.96	1.44	3.64	4.22	1.40 - 6.51	0.36
S_{ico}	50	0.07	0.27	-	0.003	<LLD - 1.79	3.86
S_{xrf}	50	0.09	0.25	0.03	0.02	<LLD - 1.66	2.78
Li	50	55	49	35	43	1 - 259	0.89
La	50	49.5	33.8	42.1	43.6	12.1 - 185	0.68
Ce	50	58.6	29.3	49.1	60.4	2.4 - 155	0.50
Pr	50	10.3	9.1	8.3	8.2	2.6 - 51.1	0.88
Nd	50	35.5	33.9	27.6	26.1	6.8 - 204	0.96
Sm	50	6.2	5.4	5.1	4.9	2.2 - 35.1	0.87
Eu	50	1.17	1.15	0.95	0.90	0.4 - 7.9	0.98
Gd	50	4.9	4.4	4.1	3.7	2.2 - 29.4	0.90
Tb	50	0.74	0.59	0.64	0.60	0.3 - 4.1	0.80
Dy	50	4.3	3.1	3.8	3.7	1.9 - 21.8	0.72
Er	50	2.4	1.5	2.1	2.0	0.9 - 10.7	0.63
Tm	50	0.34	0.20	0.31	0.30	0.1 - 1.4	0.59
Yb	50	2.5	1.3	2.3	2.3	1.0 - 9.3	0.52
La/Sc	50	3.34	3.06	2.63	2.68	0.42 - 19.40	0.92
Th/La	50	0.48	0.26	0.43	0.43	0.14 - 1.55	0.54
Ba/La	50	33.9	71.5	19.2	16.5	5.3 - 411.4	2.11
LREE/HREE	50	13.6	5.6	12.5	13.0	3.7 - 31.0	0.41
K2O/ΣREE	50	215	106	190	193	58 - 493	0.49
Gd_N/Yb_N	50	1.54	0.49	1.47	1.42	0.93 - 3.34	0.32
La_N/Sm_N	50	5.30	1.16	5.16	5.47	2.42 - 7.75	0.22
Ce/Ce*	50	0.66	0.25	0.58	0.75	0.09 - 1.08	0.38
Eu/Eu*	50	0.62	0.12	0.61	0.62	0.37 - 1.10	0.19
C_{org}/S	50	14.19	44.29	2.71	2.40	0.09 - 289.9	3.12
Σ REE	50	176.4	109.3	153.0	163.8	38.5 - 608.7	0.62

Table 3.4.1.4: Average element concentrations and ratios of selected shale samples of the Pretoria Group

(n = number of samples; 'MEAN' = arithmetic mean; 'STD ±' = 1 σ standard deviation; 'GM' = geometric mean; 'MEDIAN' = median; 'VC' = variation coefficient; average major element concentrations (i.e. FeO to S_{XRF}) are reported in weight %, average trace element concentrations in ppm; n.c. = not calculated; subscript N = concentration normalised to chondrite; Ce/Ce* = $Ce_N/[(La_N + Pr_N)/2]$; Σ REE = sum of REE in ppm; NOTE: ratios corrected as described in Chapter 3.1.2; LLD = lower limit of detection)

% of the sample set (14 out of 640 samples), are excluded. CaO has a median of 0.12 wt.%, i.e., about 50 % of the samples have a CaO-content of equal or lower than 0.12 wt.%.

Hence, the Average Pretoria Group Shale can be regarded as strongly depleted in CaO.
If the above considerations regarding the central value are applied to all major elements, the following classification would result for the Pretoria Group Shale Average: SiO_2, Fe_2O_3(t) and P_2O_5 have contents similar to average shale estimates (Table 3.2.1b), Al_2O_3 is moderately enriched, TiO_2 and K_2O are moderately depleted, MgO, CaO, Na_2O and MnO are strongly depleted. The average LOI is moderately lower than most average shale estimates, but higher than the Average Russian Early Proterozoic Metamorphic Shale estimate of Ronov and Migdisov (1971). However, these enrichment/depletion comparisons are difficult to verify as distribution, median, geometric mean and standard deviation of average shale estimates are not reported from their respective literature sources (see Table 3.2.1a). It is possible that the elements classified as strongly depleted in the Pretoria Group (i.e., MgO, CaO, Na_2O and MnO) are similarily distributed in the average shale estimates, i.e., it is uncertain, if the mean values reported for the average shale estimates represent stable estimates of the central value or if these mean values are biased similarly to the Average Pretoria Group Shale estimate. In the latter case, an enrichment/depletion classification, which considers extreme values, would be incorrect. However, an enrichment/depletion classification corrected for extreme values is widely confirmed by the results of the geochemistry of the Pretoria Group formations (Chapter 3.3). Some contents of MgO and CaO used in calculating the Average Pretoria Group Shale estimate are comparable to average shale estimates, and these comparable cases can be put down to two specific types of shales, the high-Mg-Ca-Na shales and calcareous shales. Both shale types are restricted to the Silverton and the post-Magaliesberg formations, where they occur together with other types of shales with varying compositions. To a certain degree, an exception to this pattern can be found for shales from the Botswana sampling area, which seem generally to be enriched in MgO compared to other sampling areas.

The trace element geochemistry of the Average Pretoria Group Shale (Tables 3.4.1.1 and 3.4.1.4) shows enrichment of Ga, Y, U, Th, Cr, Ba, and Sc, and depletion of Zn, Cu, Co, Sr, As and Sn compared to average shale estimates (Table 3.2.1d). Both enrichment and

depletion is moderate for all the elements listed. B has similar contents to the average shale estimate of Turekian and Wedepohl (1961), but is strongly enriched compared to Average Canadian Proterozoic Shale (Cameron and Garrels, 1980).

The CO_2-content of Pretoria Group shales (Table 3.4.1.4) is generally low, confirming the depletion of CaO. C_{ORG} has a high average content (0.97 wt.%), but a low median (0.05 wt.%), pointing to a skewed or polymodal distribution in the Pretoria Group shales. The significant difference of mean and median is caused by 3 samples from the Silverton Formation (out of a total of 50 samples analysed for C_{ORG}) having exceptionally high C_{ORG} contents (up to 12.64 wt.%). The accuracy of sulphur analysis by XRF is generally confirmed by the results of the analysis by LECO, although significant differences are observed for lower concentrations.

The average REE contents (Table 3.4.1.4) of the Average Pretoria Group Shale are similar to average shale estimates, with the exception of La, which is enriched. Pr is slightly enriched, Er and Yb are slightly depleted compared to average shale estimates. The Σ REE is similar to Post-Archaean Average Shale (Taylor and McLennan, 1985).
The La/Sc-ratio is slightly increased compared to Post-Archaean Average Shale (Taylor and McLennan, 1985), but has a significantly higher variability. Th/La is slightly, LREE/HREE and K_2O/Na_2O are strongly enriched compared to Post-Archaean Average Shale (Taylor and McLennan, 1985). Th/U is strongly depleted compared to Archaean Average Shale and Post-Archaean Average Shale (Taylor and McLennan, 1985). The ratios Cr/V, V/Ni and Ni/Co of the Average Pretoria Group Shale give ambiguous results. The Cr/V-average lies in an intermediate position between Late Archaean Average Shale and Post-Archaean Average Shale (Taylor and McLennan, 1985), and Ni/Co lies in the intermediate position between Late Archaean Average Shale and Early Archaean Average Shale (Taylor and McLennan, 1985). V/Ni exceeds the values reported for Post-Archaean Average Shale, Late Archaean Average Shale and Early Archaean Average Shale (Taylor and McLennan, 1985).

Element	n	MEAN	STD ±	GM	MEDIAN	RANGE	VC
SiO_2	335	89.64	10.41	88.94	94.26	46.08 - 99.98	0.12
TiO_2	335	0.19	0.20	-	0.12	<LLD - 1.20	1.05
Al_2O_3	335	4.43	5.12	-	2.31	<LLD - 27.45	1.16
Fe_2O_3*	335	2.41	3.60	1.29	1.13	0.22 - 35.73	1.49
MnO	335	0.02	0.04	-	0.01	<LLD - 0.39	2.00
MgO	335	0.33	0.60	-	0.04	<LLD - 4.64	1.82
CaO	335	0.11	0.40	-	0.01	<LLD - 4.60	3.64
Na_2O	335	0.26	0.82	-	0.04	<LLD - 6.84	3.15
K_2O	335	0.95	1.32	-	0.36	<LLD - 8.61	1.39
P_2O_5	335	0.05	0.09	-	0.02	<LLD - 1.14	1.80
H_2O^-	335	0.13	0.22	-	0.06	<LLD - 2.56	1.69
LOI	335	1.09	1.26	0.62	0.57	0.02 - 9.40	1.16
Zn	335	15	29	-	8	<3 - 427	1.93
Cu	335	9.3	29.2	-	<LLD	<3 - 357	3.14
Ni	335	13	22	-	5	<3 - 156	1.69
Co	335	4.7	4.4	-	4	<3 - 33	0.94
Ga	335	4.4	6.8	-	<LLD	<3 - 33	1.55
Mo	335	7.5	5.5	-	7	<2 - 86	0.73
Nb	335	3.8	4.2	-	3	<2 - 25	1.11
Zr	335	124	120	89	81	5 - 975	0.97
Y	335	11	15	-	7	<2 - 149	1.36
Sr	335	25	43	-	9	<2 - 438	1.72
Rb	335	39	56	-	15	<2 - 343	1.44
U	335	1.9	3.4	-	<LLD	<5 - 14	1.79
Th	335	3.4	5.5	-	<LLD	<5 - 29	1.62
Pb	335	8.4	21.5	-	<LLD	<5 - 253	2.56
Cr	335	160	55	-	161	<14 - 382	0.34
V	335	40	41	-	28	<14 - 345	1.03
Ba	335	282	368	-	124	<16 - 2305	1.31
Sc	335	3.6	6.1	-	<LLD	<8 - 31	1.69
As	335	1.5	6.7	-	<LLD	<10 - 69	4.47
S	335	152	780	-	<LLD	<50 - 13000	5.13
Sb	335	0.6	2.2	-	<LLD	<8 - 15	3.67
Sn	335	1.6	6.1	-	<LLD	<8 - 58	3.81
B	80	41	76	18	15.5	1 - 563	1.85

Table 3.4.1.5: Average element concentrations of Pretoria Group sandstones

(n = number of samples; 'MEAN' = arithmetic mean; 'STD ±' = 1 σ standard deviation; 'GM' = geometric mean; 'MEDIAN' = median; 'VC' = variation coefficient; average major element concentrations are reported in weight %, average trace element concentrations in ppm; 'Fe_2O_3*' is all Fe expressed as Fe_2O_3; *) = arithmetic mean below detection limit; LLD = lower limit of detection)

Table 3.4.1.6 : Average ratios of Pretoria Group sandstones

(NOTE: ratios are not corrected, i.e. a sample was excluded from calculation of the average ratio if one or both elements are below the detection limit; n.c. = not calculated)

Ratio	n	MEAN	STD ±	GM	RANGE	VC
CIA	326	75.3	12.6	74.1	23.7 - 100	0.17
SiO_2/Al_2O_3	326	86.4	144.9	37.4	1.9 - 1628	1.68
lg SiO_2/Al_2O_3	326	1.57	0.58	n.c.	0.29 - 3.21	n.c.
K_2O/Na_2O	274	16.7	22.9	7.5	0.02 - 183	1.37
lg Na_2O/K_2O	274	-0.88	0.66	n.c.	-2.26 - 1.72	n.c.
Ti/Zr	320	10.7	12.4	7.3	0.7 - 149.9	1.16
Ti/Cr	319	8.0	10.2	4.5	0.3 - 124.0	1.28
Al/Zr	326	212	187	137	3 - 1108	0.88
Al_2O_3/TiO_2	312	36.8	38.4	22.2	0.4 - 383.7	1.04
Al_2O_3/K_2O	304	11.7	27.7	6.0	0.7 - 254.3	2.37
K/Rb	279	223	162	197	31 - 1891	0.73
K/Ba	300	33	35	23	2 - 293	1.06
K/Sr	307	503	643	273	9 - 6144	1.28

3.4.1.2 Average Pretoria Group Sandstone estimate

The Average Pretoria Group Sandstone (Tables 3.4.1.5 and 3.4.1.6) is enriched in $Fe_2O_3(t)$, depleted in TiO_2, K_2O, P_2O_5, and moderately depleted in Al_2O_3, compared to the carbonate-free recalculated average sandstone estimate of Clarke (1924) (Table 3.2.1c). Na_2O and CaO are strongly depleted. Compared to other average sandstones (Table 3.2.1c), SiO_2 is strongly enriched and the other major elements more or less depleted.

The trace elements Ga, Zr, Y and Rb are depleted, Ni, Co, Nb, V and Ba are enriched compared to average sandstone estimates (Table 3.2.1d). Cr and Mo are strongly enriched compared to average sandstone estimates. U, Th, Sc and Sb are enriched from a statistical point of view, but uncertainties remain due to analytical limits, i.e., mean and median are below the detection limit.

Table 3.4.1.7: Average geochemistry of Pretoria Group Carbonate rocks and conglomerates

(concentrations are reported as mean ± 1 δ standard deviation; major elements: wt.%, trace elements: ppm)

Element	CARBONATES (n = 11)		CONGLOMERATES (n = 37)	
	MEAN ± STD	RANGE	MEAN ± STD	RANGE
SiO_2	23.23 ± 11.29	10.41 - 42.97	75.07 ± 17.97	53.40 - 99.13
TiO_2	0.22 ± 0.15	0.05 - 0.53	0.33 ± 0.28	<LLD - 0.85
Al_2O_3	3.80 ± 2.33	1.47 - 8.61	8.37 ± 7.50	<LLD - 19.14
$Fe_2O_3(t)$	2.18 ± 1.21	0.71 - 4.42	6.45 ± 5.48	0.23 - 25.45
MnO	0.04 ± 0.02	0.01 - 0.07	0.09 ± 0.09	<LLD - 0.47
MgO	11.59 ± 6.63	0.36 - 22.46	2.92 ± 2.28	<LLD - 6.32
CaO	27.02 ± 10.11	13.24 - 47.29	1.91 ± 2.29	<LLD - 9.14
Na_2O	0.52 ± 0.26	0.10 - 0.89	0.41 ± 0.53	<LLD - 2.05
K_2O	0.61 ± 0.50	0.10 - 1.53	0.92 ± 0.92	<LLD - 2.78
P_2O_5	0.01 ± 0.02	<0.01 - 0.05	0.42 ± 1.97	<LLD - 12.09
H_2O^-	0.13 ± 0.21	0.01 - 0.75	0.13 ± 0.17	<LLD - 0.86
LOI	30.13 ± 9.70	8.55 - 40.30	3.07 ± 2.41	0.11 - 9.82
Zn	94 ± 226	9 - 775	42 ± 38	<3 - 101
Cu	6.7 ± 10.4	<3 - 28	39 ± 58	<3 - 273
Ni	12 ± 11	<3 - 35	60 ± 60	<3 - 190
Co	4.6 ± 3.1	<3 - 11	18 ± 17	<3 - 49
Ga	3.0 ± 3.9	<3 - 10	8.9 ± 8.8	<3 - 24
Mo	0.7 ± 1.7	<2 - 5	2.6 ± 3.5	<2 - 12
Nb	5.3 ± 3.2	<2 - 11	6.5 ± 5.7	<2 - 17
Zr	62 ± 43	13 - 151	85 ± 75	2 - 390
Y	10 ± 4.7	4 - 18	14 ± 11	<2 - 29
Sr	60 ± 43	33 - 184	81 ± 144	3 - 853
Rb	37 ± 25	12 - 87	48 ± 49	<2 - 166
U	2.4 ± 5.0	<5 - 16	2.9 ± 4.4	<5 - 15
Th	2.3 ± 4.2	<5 - 12	5.0 ± 5.6	<5 - 15
Pb	18 ± 16	5 - 60	15 ± 10	<5 - 35
Cr	9.8 ± 13.9	<14 - 39	283 ± 180	46 - 751
V	33 ± 16	17 - 58	89 ± 61	16 - 190
Ba	313 ± 356	68 - 1299	442 ± 564	<16 - 2599
Sc	24 ± 6.3	14 - 34	12 ± 10	<8 - 33
As	<LLD	-	10 ± 16	<10 - 84
S	811 ± 505	203 - 2044	684 ± 1524	<50 - 7367
Sb	<LLD	-	1.4 ± 3.7	<8 - 15
Sn	1.0 ± 3.3	<8 - 11	4.0 ± 6.6	<8 - 22
B	12 (n = 1)	-	n. a.	-

3.4.1.3 Averages of other sedimentary rocks

The average geochemical composition of carbonate rocks and conglomerates from the Pretoria Group are given in Table 3.4.1.7. More detailed descriptive statistics of carbonate rocks and conglomerates are given in Appendix 2a. Carbonate rocks were sampled in the Silverton and Houtenbeck Formations. They have a variable geochemistry, shown by the considerable range of CaO and MgO. The contents of elements typical of clastic sedimentary rocks like Al_2O_3, SiO_2 and TiO_2 are enriched compared to the average carbonate estimate of Turekian and Wedepohl (1961). Fe_2O_3(t) and Na_2O are also enriched, MnO and P_2O_5 are strongly depleted. Co, Ba, Nb, Pb, V and Zr are enriched, Rb and Sc are strongly enriched compared to the average carbonate estimate of Turekian and Wedepohl (1961). Ni and Y are depleted, Sr strongly so.

The geochemistry of the Pretoria Group conglomerates is highly variable due to the lithological variability of the clasts. Chert clasts are most common, but several samples with volcanic rock, jasper, shale and high-P (phoshate or apatite) clasts are included in the sample set. The average Cr-content (ϕ 283 ppm) is exceptionally high compared to either average shale or average sandstone estimates. As, Ba, S and Cu are strongly enriched in individual samples compared to these estimates and to the averages for Pretoria Group shales and sandstones.

3.4.2 Geochemistry of the Pretoria Group volcanic rocks

3.4.2.1 Hekpoort Volcanics

39 samples of the Hekpoort Formation volcanic rocks, taken from localities throughout the Transvaal Basin, were analysed for major and trace elements. The volcanic rocks were subdivided into three sub-groups: (1) lava, (2) pale grey to greenish coloured, brittle volcanic rocks with unusually high contents of Al_2O_3 and K_2O and a bedding-parallel orientation of abundant muscovite or sericite, and (3) the 'felsic rock' of Key (1983) from boreholes in the Botswana sampling area. According to the SiO_2-alkali classification plot after Le Maitre

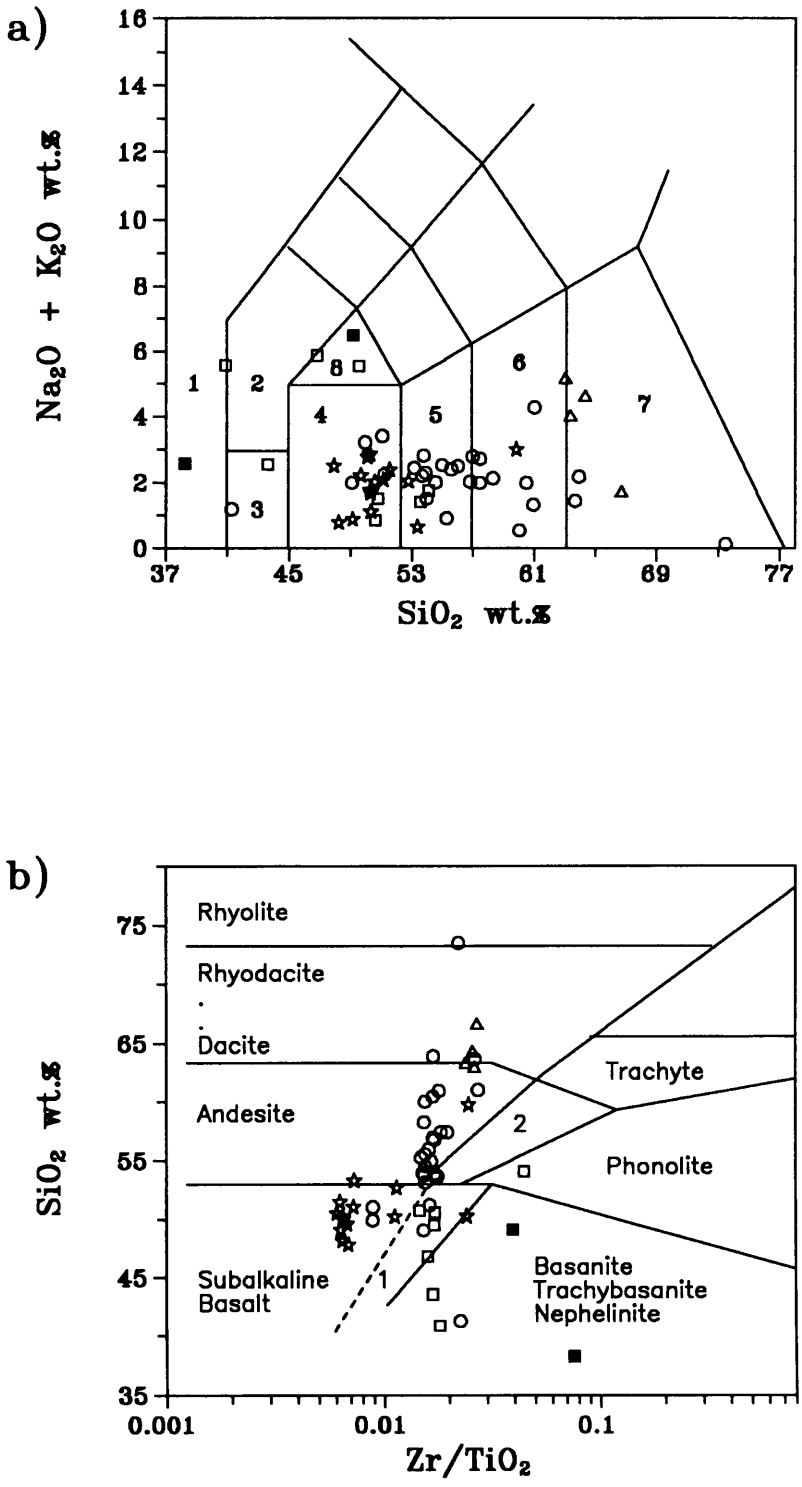

Figure 3.4.2.1: a) SiO_2-alkali classification plot for volcanic rocks (after Le Maitre, 1984). **b)** SiO_2-Zr/TiO_2 classification plot for volcanic rocks (after Winchester and Floyd, 1977). Hekpoort volcanics: □ = high-Al-K volcanic rocks; ○ = lavas; Δ = 'felsic rock'; ★ = Machadodorp volcanics; ■ = Tuffaceous material in the Timeball Hill Formation Lower Shale Member.

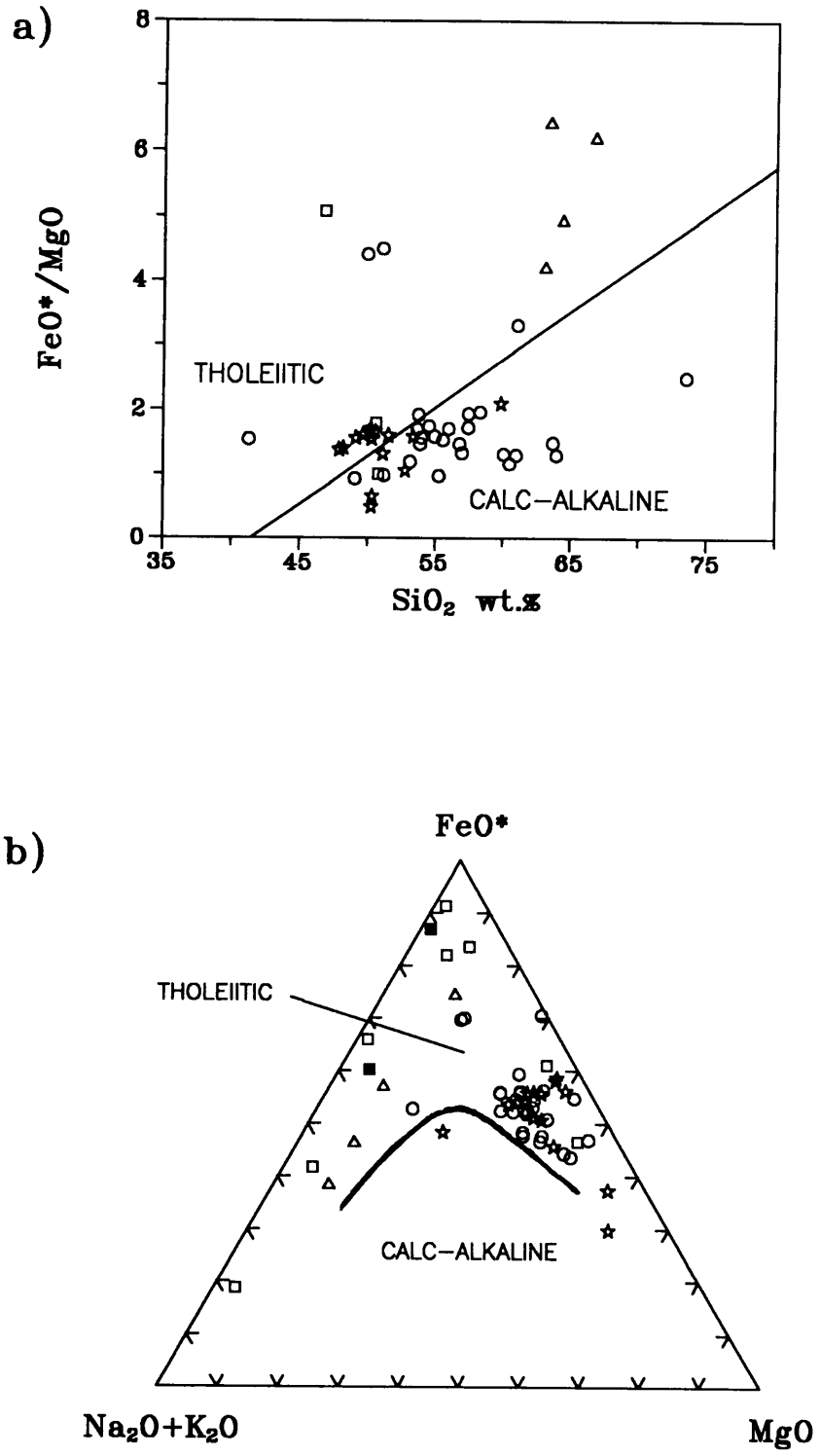

Figure 3.4.2.2: a) SiO_2-FeO*/MgO classification plot for volcanic rocks (after Gill, 1981). **b)** Na_2O+K_2O-FeO*-MgO ternary classification plot for volcanic rocks (after von Gruenewaldt and Harmer, 1993). Hekpoort volcanics: □ = high-Al-K volcanic rocks; ○ = lavas; Δ = 'felsic rock'; Machadodorp volcanics = ★; Tuffaceous material in the Timeball Hill Formation Lower Shale Member = ■.

(1984), the rock types of the Hekpoort volcanics vary from dacites to foidites (Fig. 3.4.2.1a), with most samples falling into the basaltic andesite (or andesitic basalt) field (n=13). Andesites (n=9), dacites (n=6) and basalts (n=6) follow in frequency. The 'felsic rock' plots in the dacite field, the high-Al-K volcanic rocks (subgroup 2 above) have a generally more mafic character than the lavas. The classification after Winchester and Floyd (1977) leads to similar results, with the lavas plotting mainly in the andesite field and the high-Al-K volcanics plotting in the alkaline basalt and basanite fields (Fig 3.4.2.1b), although the geochemical discrimination of the three subgroups is improved compared to Le Maitre's classification (Fig. 3.4.2.1a). The 'felsic rock' of Key (1983) plots in the andesite and dacite fields. The geochemical variability of the Hekpoort samples studied here, with the identification of rock types varying from felsic to mafic, is greater than that of previous studies (e.g., Sharpe et al., 1983; Schreiber, 1990). The distribution of rock types can be classified as 'continuous' (Vivallo and Claesson, 1987), but not as bimodal. However, the lavas (sub-group 1 above) show little geochemical variability as pointed out by Sharpe et al. (1983) and Harmer and von Gruenewaldt (1991), and are thus neither bimodally nor continuously distributed.

Most Hekpoort lavas fall into the calc-alkaline field, but the high-Al-K volcanics and 'felsic rocks' fall into the tholeiite field, when using a SiO_2-$FeO_{(t)}$/MgO classification plot after Gill (1981) (Fig. 3.4.2.2a). However, most samples of the Hekpoort volcanic rocks plot in the tholeiite field of the modified AFM-diagram of von Gruenewaldt and Harmer (1993)(Fig. 3.4.2.2b). The Hekpoort lavas cluster in both plots close to the demarcation line of the tholeiite and calc-alkaline fields.

A comparison of the geochemistry of the Hekpoort lavas and high-Al-K-volcanics (Tables 3.4.2.1 and Tables 3.4.2.2) exhibits some significant geochemical differences, apart from the enrichment of Al_2O_3 and K_2O in the latter sub-group. TiO_2, Fe_2O_3 and LOI are enriched in the high-Al-K volcanics, and all other major elements depleted compared to the lavas. This enrichment/depletion pattern is compatible with a change in geochemistry due to strong weathering. However, K_2O shows a threefold enrichment in the high-Al-K volcanics compared to the Pretoria Group shales, whereas TiO_2 is enriched by only ~30%. This pattern is contradictory to the weathering hypothesis, as K_2O has a mobility considerably greater than TiO_2 in a weathering environment (Nesbit et al., 1980; Loughan, 1969). Hence,

it seems propable that considerable amounts of K were added to the system. The trace elements Zr, Ni, Ga, Mo, Rb, U, Cr, V and Sc are strongly enriched in the high-Al-K volcanics compared to the Hekpoort lavas. Other trace elements are slightly enriched, with the exception of Sr, Zn and Cu, which are depleted. Ratios of immobile elements (e.g., Cr/Th and Th/Sc) exhibit changes, which could have been due to preferential enrichment or to primary compositional differences.

A comparison of the Hekpoort lavas analysed here (Table 3.4.2.1 and 3.4.2.2) with previously published data (sumarized by Schreiber, 1990, p. 228, Table 9) shows a general similarity of the previous estimates and the present estimate. The estimates of Button (1973) and Schreiber (1990) have slighly enriched Al_2O_3, Na_2O and K_2O and lower P_2O_5 and LOI contents compared to the estimate in Table 3.4.2.1.
The Hekpoort lavas have SiO_2, TiO_2 and CaO contents similar to Average Cenozoic Andesite (Chase, 1967), but Fe_2O_3(t), MgO and K_2O contents resemble Average Continental Tholeiite (Manson, 1967). The trace element contents of Cr, Co and Ni are similar to those of Average Basalt (Turekian and Wedepohl, 1961), Cu, Ba, Nb, V and Zr resemble Average Oceanic Andesite (Taylor and White, 1965), and Pb, Sn, Th and Zn have contents similar to Average Andesite (Vinogradov, 1962). Sr is strongly depleted and U is enriched in the Hekpoort volcanics compared to these estimates.

3.4.2.2 Machadodorp Volcanics

The Machadodorp lavas are restricted to the eastern and northeastern Transvaal sampling areas (see Fig. 1.5.1). The Machadodorp lavas fall, with few exceptions, in the basalt field of the classification plots of Winchester and Floyd (1977) and Le Maitre (1984) (Fig. 3.4.2.1 a and b), and in the tholeiite field of the classification plots of Gill (1981) and von Gruenewaldt and Harmer (1993).

Average SiO_2-contents are similar to Average Continental Tholeiite (Manson, 1967). The exceptionally low TiO_2-contents also point to a continental environment, as the Average Continental Tholeiite (Manson, 1967) is somewhat depleted compared to Average Oceanic

Table 3.4.2.1	Hekpoort Fm. Tuffs (n=8)	Hekpoort Fm. Lavas (n=27)	Hekpoort Fm. All Volc. (n=39)	Machadodorp Volc. All Volc. (n=15)
SiO_2	48.72 ± 4.66	56.21 ± 5.90	55.51 ± 6.81	51.01 ± 2.83
TiO_2	0.90 ± 0.35	0.69 ± 0.54	0.74 ± 0.48	0.77 ± 0.17
Al_2O_3	22.73 ± 9.80	13.56 ± 2.35	15.87 ± 6.02	14.44 ± 0.88
$Fe_2O_3(t)$	13.87 ± 8.43	10.56 ± 2.63	10.87 ± 4.69	10.94 ± 2.65
MnO	0.08 ± 0.10	0.15 ± 0.04	0.13 ± 0.07	0.25 ± 0.18
MgO	2.76 ± 3.70	5.94 ± 1.87	4.79 ± 2.85	7.36 ± 1.90
CaO	1.06 ± 1.99	6.07 ± 2.47	4.43 ± 3.34	10.51 ± 1.61
Na_2O	0.44 ± 0.42	1.15 ± 0.69	0.91 ± 0.71	1.53 ± 0.89
K_2O	2.69 ± 1.73	0.97 ± 0.74	1.60 ± 1.44	0.41 ± 0.75
P_2O_5	0.07 ± 0.08	0.14 ± 0.11	0.12 ± 0.10	0.08 ± 0.06
H_2O^-	0.58 ± 0.51	0.39 ± 0.37	0.46 ± 0.40	0.50 ± 0.88
LOI	5.74 ± 1.92	3.90 ± 5.07¶)	4.31 ± 4.34	1.57 ± 1.24
Zn	57 ± 56	76 ± 19	69 ± 32	98 ± 30
Cu	60 ± 81	96 ± 84	103 ± 112	72 ± 45
Ni	243 ± 210	140 ± 51	151 ± 114	116 ± 23
Co	43 ± 45	40 ± 9.9	39 ± 22	38 ± 13
Ga	25 ± 10	16 ± 5.0	19 ± 7.3	16 ± 4.1
Mo	3.0 ± 3.7	1.3 ± 2.0	1.9 ± 2.5	0.5 ± 1.5
Nb	11 ± 2.7	8.8 ± 2.9	9.8 ± 3.3	6.1 ± 3.0
Zr	172 ± 64	106 ± 42	129 ± 57	68 ± 29
Y	33 ± 12	26 ± 12	28 ± 12	29 ± 9.2
Sr	74 ± 50	122 ± 95	105 ± 86	85 ± 41
Rb	130 ± 76	47 ± 38	75 ± 64	15 ± 27
U	4.9 ± 4.1	2.8 ± 3.7	3.7 ± 4.0	1.3 ± 2.7
Th	11 ± 6.5	8.0 ± 4.7	9.5 ± 4.7	2.6 ± 5.9
Pb	18 ± 7.6	15 ± 6.3	16 ± 6.8	5.7 ± 5.0
Cr	663 ± 346	463 ± 298	471 ± 320	324 ± 112
V	361 ± 165	196 ± 69	225 ± 116	247 ± 69
Ba	515 ± 364	380 ± 249	438 ± 291	343 ± 448
Sc	35 ± 13	23 ± 8.8	24 ± 12	38 ± 9.7
As	< LLD*)	9.3 ± 41.8	6.8 ± 32.9	< LLD*)
S	363 ± 131	265 ± 236	430 ± 932	170 ± 119

Table 3.4.2.1: Average element concentrations of Pretoria Group volcanic rocks.

(Averages are reported as mean ± 1 δ standard deviation; major elements are reported in weight percent, trace elements in ppm; *) : all analyses below detection limit; ¶) : Mean without extreme value (28.16 wt.%) is 2.97 wt.%)

Table 3.4.2.2: Average ratios of Pretoria Group volcanic rocks.

(Average are reported as mean plus/minus 1 δ standard deviation; §) : Th and U corrected for missing values)

Table 3.4.2.2	Hekpoort Fm. Tuffs (n=8)	Hekpoort Fm. Lavas (n=27)	Hekpoort Fm. All Volc. (n=39)	Machadodorp Volc. All Volc. (n=15)
K_2O/TiO_2	2.76 ± 0.96	1.60 ± 1.24	2.16 ± 1.54	0.73 ± 1.44
P/TiO_2	0.15 ± 0.12	0.23 ± 0.22	0.20 ± 0.20	0.10 ± 0.07
Zr/Ti	0.034 ± 0.017	0.029 ± 0.007	0.031 ± 0.010	0.016 ± 0.010
Cr/Zr	4.85 ± 4.16	5.08 ± 3.67	4.59 ± 3.77	5.63 ± 2.34
Cr/Th	76.6 ± 73.9	56.8 ± 46.0	55.2 ± 52.6	62.5 ± 25.9§)
Th/Sc	0.39 ± 0.22	0.47 ± 0.42	0.59 ± 0.55	0.22 ± 0.25§)
Co/Th	5.81 ± 6.35	4.86 ± 1.76	4.61 ± 3.20	7.27 ± 2.98§)
Cr/V	2.23 ± 1.71	2.56 ± 1.64	2.33 ± 1.62	1.30 ± 0.32
Th/U	1.65 ± 0.60	1.12 ± 0.35	1.53 ± 0.58	2.01 ± 1.50§)
al_{NIGGLI}	55.5 ± 17.8	37.2 ± 5.5	43.6 ± 13.3	33.5 ± 4.3
c_{NIGGLI}	2.7 ± 5.1	15.0 ± 5.2	10.9 ± 8.1	22.0 ± 3.0
fm_{NIGGLI}	33.2 ± 20.4	39.8 ± 7.2	36.6 ± 12.4	37.7 ± 5.5
alk_{NIGGLI}	8.7 ± 5.3	8.0 ± 3.1	8.8 ± 4.3	6.8 ± 2.7
si_{NIGGLI}	107 ± 24	136 ± 42	136 ± 43	101 ± 16

Tholeiite (Engels et al., 1965). However, it should be noted that the Machadodorp lavas are also depleted compared to Average Continental Tholeiite (Manson, 1967). The low P_2O_5-content of the Machadodorp lavas, significantly depleted compared to both Average Continental Tholeiite (Manson, 1967) and Average Oceanic Tholeiite (Engels et al., 1965), would suggest an opposing conclusion, i.e., the possibility of an oceanic environment, as P_2O_5 is depleted in Average Oceanic Tholeiite compared to Average Continental Tholeiite. The average MgO-content of the Machadodorp lavas is compatible with the Average Oceanic Tholeiite (Engels et al., 1965). MnO is increased and Na_2O decreased compared to both Average Continental Tholeiite (Manson, 1967) and Average Oceanic Tholeiite (Engels et al., 1965). Zr, Sr, Ni and Cr have average contents similar to Averge Oceanic Tholeiite (Engels et al., 1965), whereas U, Th, Y and Ba average contents are compatible with the Average Basalt of Turekian and Wedepohl (1961).

Previous Average Machadorp Lava major element estimates (Button, 1973; Schreiber, 1990) are similar to the estimate of the present investigation (Table 3.4.2.1), which is remarkable as the sample numbers are small (Button, 1973: n = 3; Schreiber, 1990: n = 10; this investigation: n = 15). Hence, the geochemical variability of the Machadodorp lavas is considered to be generally low.

3.4.3 Stratigraphic variations of the geochemistry of shales and sandstones

The stratigraphic variation of the geochemistry of shales and sandstones is shown in Figures 3.4.3.1 a-e. The average content for each respective stratigraphic position was taken from Chapter 3.3. The resulting geochemical profiles assume an average thickness of 5400 m for the Pretoria Group. The Post-Magaliesberg formations' averages were taken from the eastern and northeastern Transvaal and the eastern Fragment sampling area stratigraphy. Shale averages are connected with a solid line, sandstone averages with a dashed line. The description of the profiles attempts to compare trends rather than to emphazise an individual element pattern.

The Rooihoogte and Timeball Hill Formation average shales have a similar content for a number of elements and ratios (SiO_2, TiO_2, Fe_2O_3(t), K_2O, LOI, Zr, Th, Sc, Nb, Y, V, Pb, Rb, B, CIA, K/Rb, Al_2O_3/TiO_2, SiO_2/Al_2O_3, Ti/Zr and Cr/Th), i.e., they show a generally low variability when considered together as one group. Major enrichment/depletion patterns are observed for MnO, MgO, CaO, Na_2O, P_2O_5, H_2O-, Ni, Zn, Co, Ba, Sr, Mo, As, Sb, Sn, K_2O/Na_2O, Co/Th, Ni/Co, Th/U and Ba/Th in these two formations. Other elements and ratios show minor degrees of variability in this stratigraphic position.

The transition from Timeball Hill Formation to Hekpoort Formation shales is marked by a change in geochemical pattern of varying degrees. TiO_2, CaO, Al_2O_3, Y, Ni, V, B, As,

---

Figure 3.4.3.1 a-e: Stratigraphic variability of average element concentrations and ratios of Pretoria Group shales and sandstones. Shale averages connected by solid line, sandstone averages by dashed line. Vrs = Rooihoogte Formation; Vt = Timeball Hill Formation; Vh = Hekpoort Formation; Vdw - Vdq = Dwaalheuwel to Daspoort Formations; Vsi = Silverton Formation; Vm = Magaliesberg Formation; Post-Vm = post-Magaliesberg formations. Shown stratigraphic thicknesses are proportional to average thickness of unit (average thicknesses are listed in meters in brackets behind symbol). Symbols: ○ = Rooihoogte Fm. (250); □ = Lower Timeball Hill Fm. (600); Δ = Timeball Hill Quartzite (200); ◇ = Upper Timeball Hill Fm. (600); ★ = Boshoek Fm. (70); ◔ = Hekpoort Fm. (600); ◙ = Dwaalheuwel Fm.(100); ◆ = Strubenkop Fm. (200); ● = Daspoort Fm. (100); ■ = Silverton Fm. (900); ▲ = Magaliesberg Fm. (300); ◑ = Vermont Fm. (300); ◨ = Lakenvlei Fm. (200); ◭ = Nederhorst Fm. (200); ◈ = Steenkampsberg Fm. (500); ◆ = Houtenbek Fm. (200).

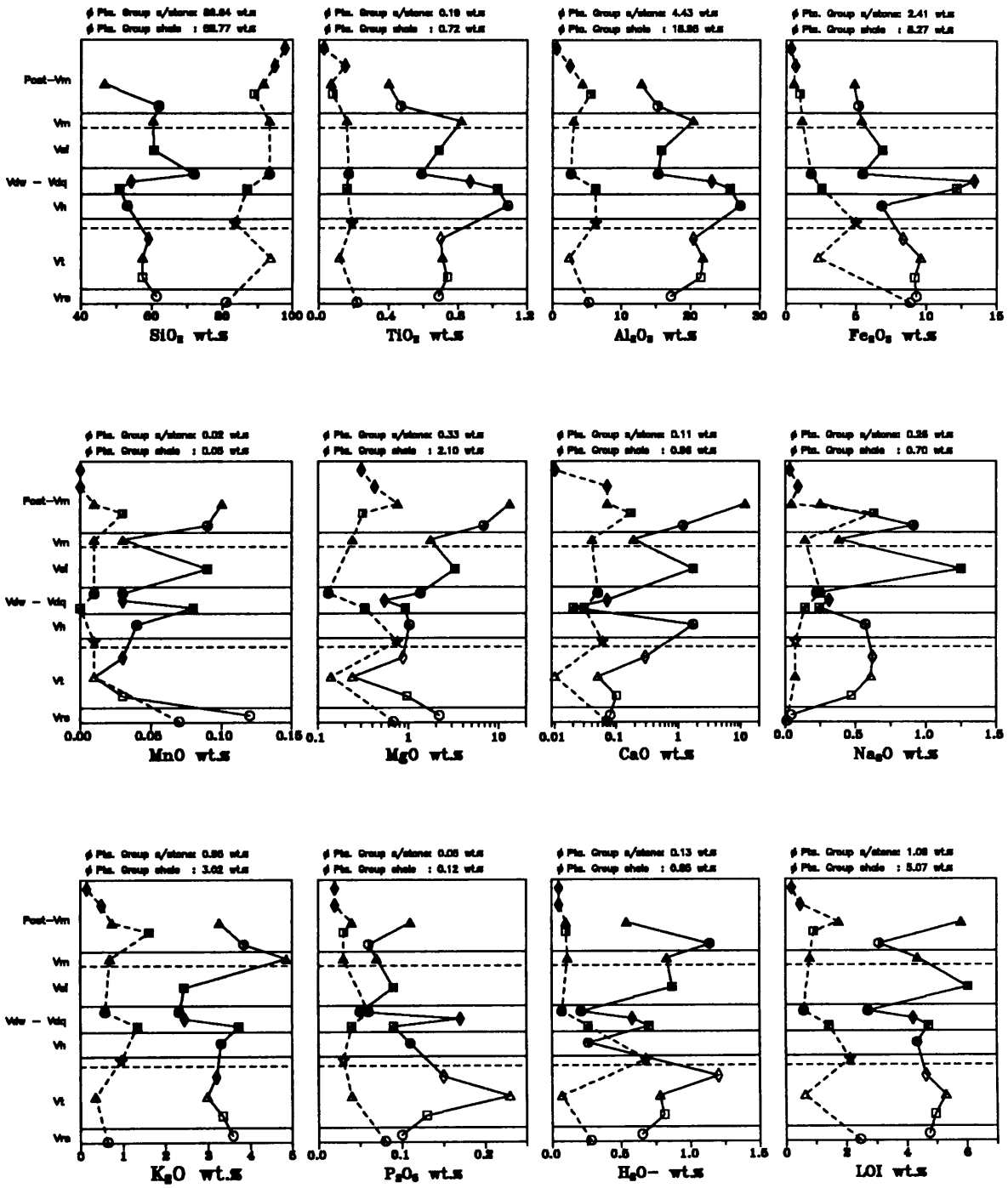

Figure 3.4.3.1 a: Stratigraphic variability of average element concentrations and ratios of Pretoria Group shales and sandstones. Shale averages connected by solid line, sandstone averages by dashed line. For further details see caption on page 232.

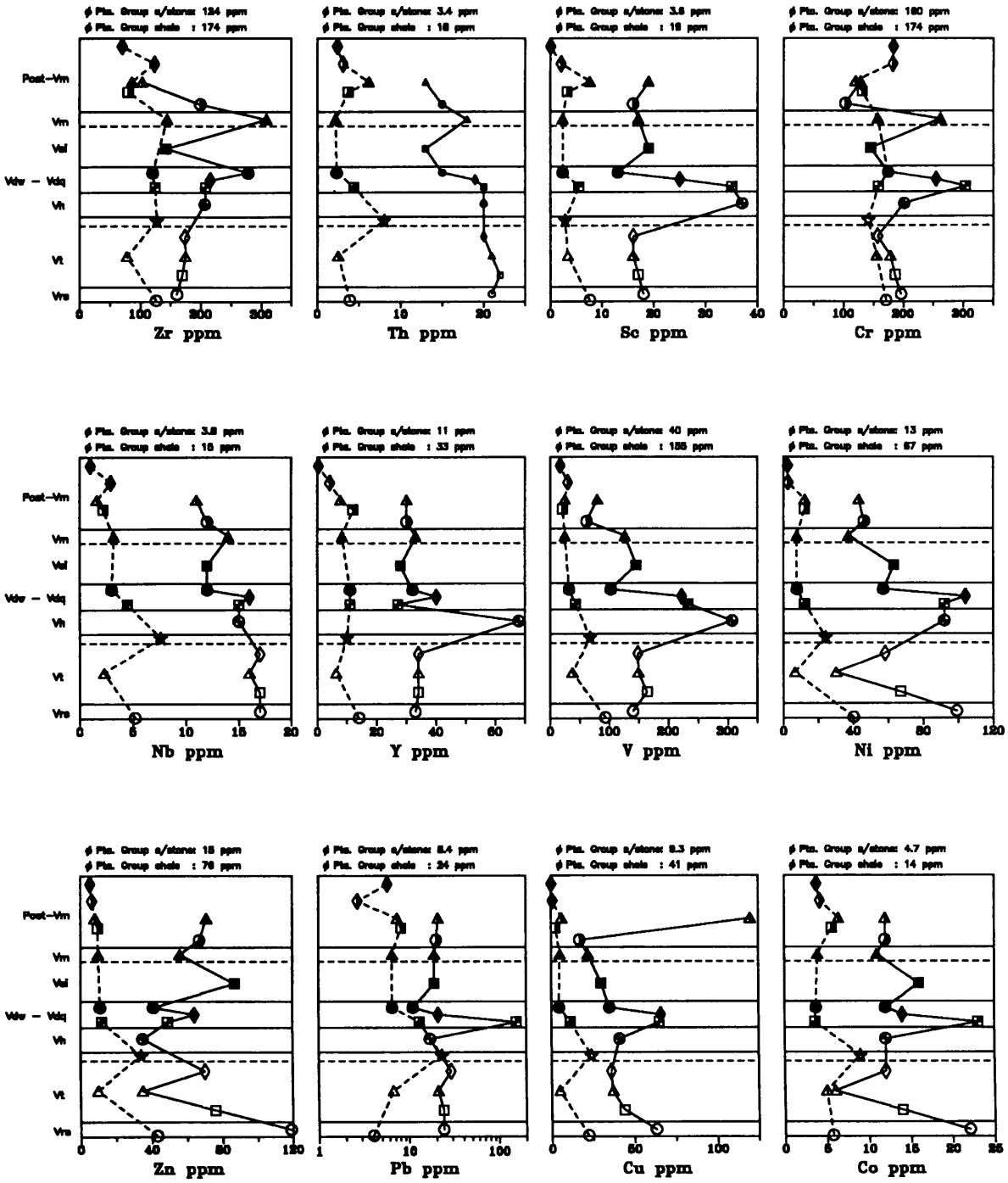

Figure 3.4.3.1 b: Stratigraphic variability of average element concentrations and ratios of Pretoria Group shales and sandstones. Shale averages connected by solid line, sandstone averages by dashed line. For further details see caption on page 232.

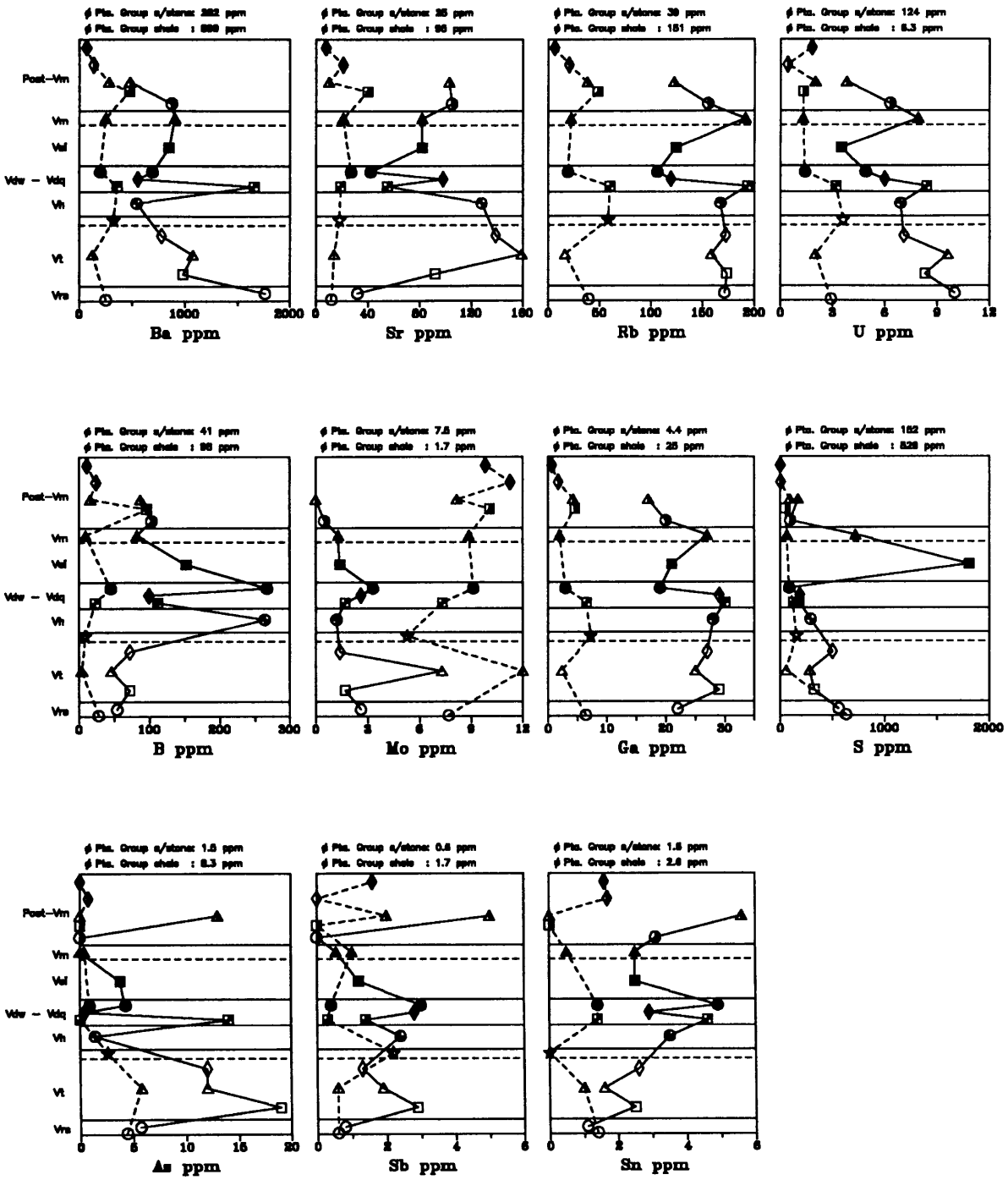

Figure 3.4.3.1 c: Stratigraphic variability of average element concentrations and ratios of Pretoria Group shales and sandstones. Shale averages connected by solid line, sandstone averages by dashed line. For further details see caption on page 232.

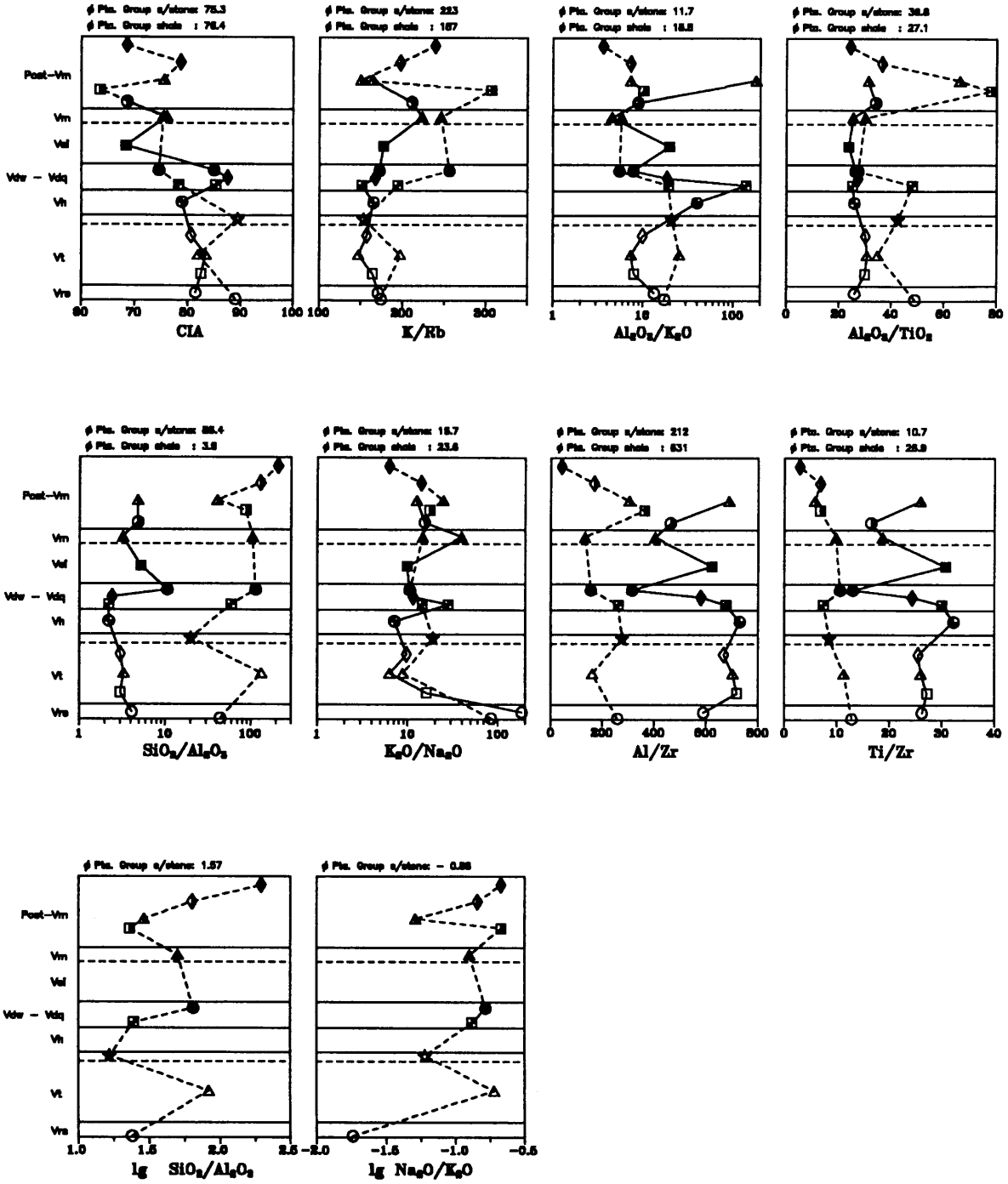

Figure 3.4.3.1 d: Stratigraphic variability of average element concentrations and ratios of Pretoria Group shales and sandstones. Shale averages connected by solid line, sandstone averages by dashed line. For further details see caption on page 232.

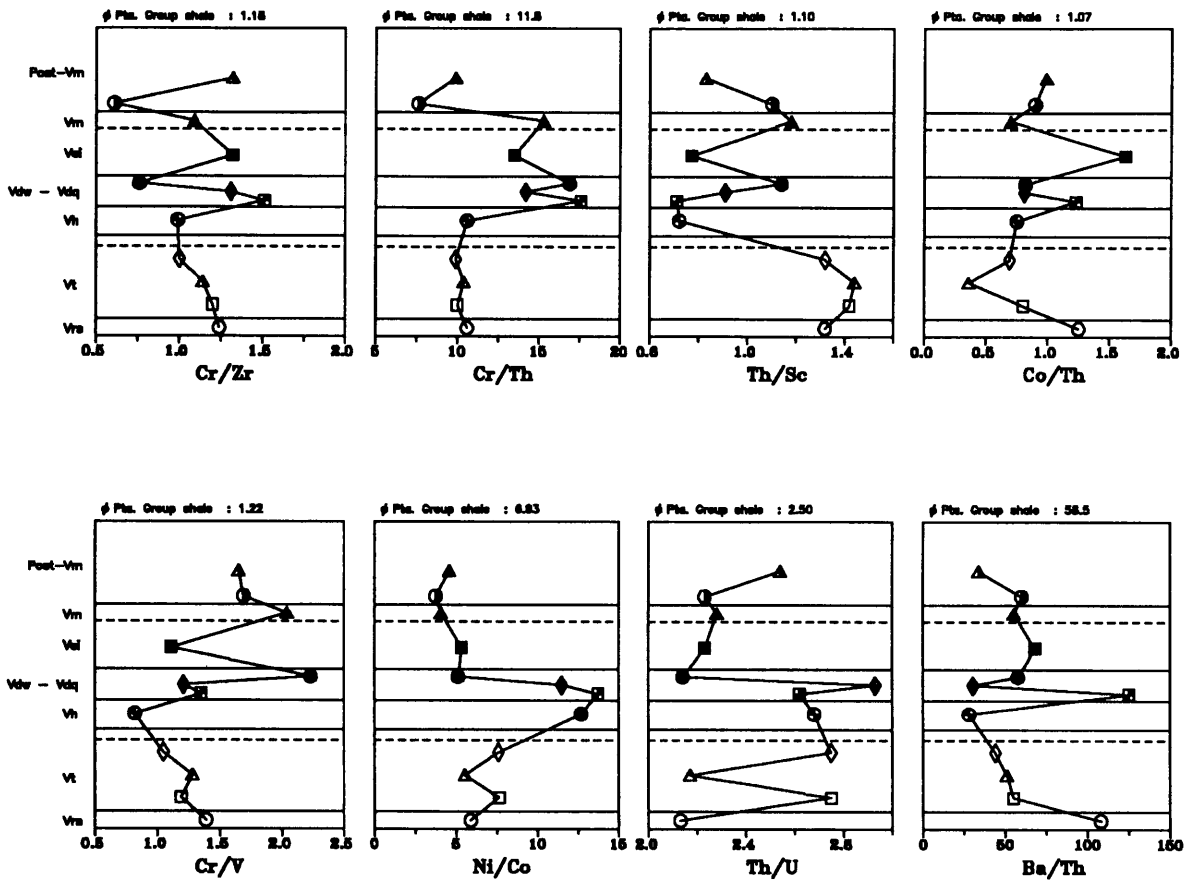

Figure 3.4.3.1 e: Stratigraphic variability of average element concentrations and ratios of Pretoria Group shales and sandstones. Shale averages connected by solid line, sandstone averages by dashed line. For further details see caption on page 232.

Al_2O_3/K_2O, Th/Sc and Ni/Co exhibit strong enrichment/depletion in the Hekpoort Formation shales compared to the underlying Timeball Hill Formation shales. The interval from Hekpoort to Daspoort Formation is distinguished by several peak contents (SiO_2, Fe_2O_3(t), MnO, P_2O_5, LOI, Cr, Co, Pb, Ba, As) and systematic changes (i.e., depletion/enrichment) in this interval for TiO_2, Al_2O_3, Sc, V, S, Ti/Zr, Al/Zr and Cr/V in the shales. The Hekpoort - Daspoort interval generally exhibits a high geochemical variability. The Daspoort Formation shales divide the profiles into a lower and upper part for SiO_2, Nb, Zr, Ga, SiO_2/Al_2O_3 and Ni/Co. The separation into these lower and upper parts is caused by a repitition in pattern after a significant change in the Daspoort Formation shales (e.g., SiO_2), discrimination due to different contents in lower and upper parts (e.g., Nb) or by a change in pattern, i.e., systematic change in either the lower or upper part of the profile and a stable pattern (e.g. Ni/Co) or high variability (e.g., Zr) in the other (i.e., lower or upper) part of the profile.

The Silverton Formation shales are unusual as only a few elements and ratios fit into a well defined systematic trend (TiO_2, Cu, Rb, Ga, SiO_2/Al_2O_3 and Th/U) from the underlying Daspoort Formation shales to the overlying Magaliesberg Formation shales. The Magaliesberg and Post-Magaliesberg Formation shales exhibit various systematic depletion/enrichment trends (TiO_2, Al_2O_3, MgO, CaO, Na_2O, K_2O, Zr, Th, Nb, Rb, U, Mo, Ga, Sn, K/Rb, Al_2O_3/K_2O, Al/Zr and Th/Sc).

Well defined systematic trends in the shales comprising the whole or major parts of the profile are rare. SiO_2 shows a general depletion trend from the Rooihoogte towards the Dwaalheuwel Formation and from the Daspoort Formation towards the top of the profile (i.e., Nederhorst Formation). Fe_2O_3(t) decreases from bottom to top, with the exception of the Dwaalheuwel and Strubenkop Formations, which are strongly enriched. MgO decreases in the lowermost part of the profile (Rooihoogte Formation to Timeball Hill Quartzites) and generally increases from there towards the top of the profile. Zr increases from the Rooihoogte towards the Strubenkop Formation shales, but has highly variable average contents above the Strubenkop Formation. Nb decreases generally throughout the profile, with strong depletion in the Daspoort Formation and minor depletion in the rest of the profile. The element pairs (respectively ratio pairs) Al_2O_3-TiO_2, Th-Nb, Sc-V, K_2O-Rb, P_2O_5-

Sr and Al/Zr - Ti/Zr seem to be correlated to each other. The two extreme Ba-contents correspond to either the highest Zn-content (Rooihoogte Formation) or highest Pb-content (Dwaalheuwel Formation).

The sandstone averages exhibit a more stable stratigraphic pattern compared to the shale averages, which might be due to the scale used in Figures 3.4.3.1 a-e. The average major and trace element contents generally decrease towards the top of the profile. This might be due to an increase in the maturity of the sandstones, which is inferred due to a general enrichment of SiO_2 towards the top of the Pretoria Group profile. However, the Timeball Hill Quarzite, Daspoort Formation and Magaliesberg Formation sandstones are an exception to this overall SiO_2-trend. Fe_2O_3(t) exhibits a well defined nonlinear depletion trend from bottom to top, with exception of the Timeball Hill Quarzites. This trend is repeated by Ni, V and Zn. It should be noted that the P_2O_5-content of the shales of the Timeball Hill Formation Quarzite Member is exceptionally high, which corresponds to a phosphatic conglomerate sample found at this stratigraphic level, but the corresponding sandstone average is depleted compared to the underlying Rooihoogte Formation sandstones.

The relations of stratigraphically corresponding shale and sandstone averages are erratic for most elements and ratios. This might be due to the scale used in Figures 3.4.3.1 a-e, as the average sandstone element contents are normally an order of magnitude lower than the shale averages. A well defined correlation of average sandstone and average shale pattern is shown by Mo and K_2O/Na_2O. The potentially interesting comparison of the CIA averages of Pretoria Group sandstones and shales gives ambiguous results. Similar CIA averages of comparable shales and sandstones are observed only in the Timeball Hill Formation Quarzite Member and the Magaliesberg Formation. The Rooihoogte Formation sandstones exhibit an increase of CIA compared to Rooihoogte Formation shales, other sandstones are depleted compared to their stratigraphic shale equivalent. This difference in CIA for compatible sandstone and shale averages is highest in the Daspoort Formation.

In many geochemical publications, the absolute differences of mean values for variable stratigraphic heights are utilised to characterise a change of factors (i.e., source rocks, tectonic setting, palaeoenvironmental setting) which determine the geochemistry of

sedimentary rocks. For example, Condie and Wronkiewicz (1990) compare mean values of ratios from Kaapvaal sedimentary rocks, including Pretoria Group shales, and interpret absolute differences of ratio means as representing compositional changes of source rocks with changes in stratigraphic height and tectonic setting. The approach of Condie and Wronkiewicz (1990) is discussed critically in Chapter 2.1.2 for various reasons. Similarly, Taylor and McLennan (1985) compare mean values of average shale estimates of several aeons (i.e., > 3.0 Ga, 3.0 - 2.5 Ga, 2.5 - 1.7 Ga, 1.7 - 0.6 Ga, 0.6 - 0.0 Ga), and draw far reaching conclusions with respect to changes in crustal composition, without establishing a significant difference between their mean values.

A statistical approach to compare mean values is described in Chapter 2.2.1. Fourteen elements and ratios were tested using one-way analysis of variance and the LSD-test to investigate the significance of changes of mean values with stratigraphic height in the Pretoria Group. For this purpose, all measured values were transformed to their logarithms to satisfy the prerequisites of one-way analysis of variance (see Chapter 2.2.1). It must be mentioned that analysis of variance is aided by an equal size of data sets to be compared (Garrett, 1983). The difference of numbers of samples in the data sets to be compared is proportional to two types of errors: (1) the unwarranted rejection of the null hypothesis (i.e., for analysis of variance, $\mathbf{H_0}$ **is:** $\bar{x}_1 = \bar{x}_2 = \ldots = \bar{x}_k = \bar{x}$, where $\bar{x}_1$ to $\bar{x}_k$ are the mean values of the **k** data sets and $\bar{x}$ is the overall mean), which is called **α-error**, and, (2) the unwarranted retention of the null hypothesis, which is called **ß-error** (Sachs, 1982, 1992). The number of shale samples taken in the different formations is thought to be too variable for a straightforward approach. Hence, formation data sets were combined into subgroups to provide for more similarity in the sample size. The combination resulted in the definition of five subgroups: (1) Rooihoogte Formation and Timeball Hill Formation Lower Shale Member (n = 163), (2) Timeball Hill Formation Upper Shale Member (n = 124), (3) Hekpoort, Dwaalheuwel and Strubenkop Formations (n = 75), (4) Silverton Formation (n = 203), and, (5) Magaliesberg and post-Magaliesberg Formations (n = 55). It is obvious that the differences in sample sizes are by no means satisfactory to exclude either α or ß-errors after the combination into subgroups. All results obtained by one-way analysis of variance of the stratigraphically sorted groups must thus be interpreted with caution. It should also be mentioned that the transformation of values to their logarithms results in a comparison of geometric means. The

Table 3.4.3.1: Statistical summary of one-way analysis of variance for stratigraphically defined sub-groups of Pretoria Group shales. (SS: sum of squares; df: degrees of freedom; MS: mean sum of squares; $F' = MS_{between}/MS_{within}$; see Chapter 2.2.1 for detailed description of procedure. Significance level of rejection of H_0 for all elements > 99.99 %)

Element	Effect	SS	df	MS	F'
Al_2O_3	between	3.026	4	0.756	35.518
	within	13.097	615	0.021	
Fe_2O_3	between	5.175	4	1.294	22.999
	within	34.597	615	0.056	
SiO_2	between	0.193	4	0.048	12.026
	within	2.468	615	0.004	
MgO	between	61.257	4	15.314	72.627
	within	128.836	611	0.211	
K_2O	between	6.391	4	1.598	9.332
	within	105.141	614	0.171	
Nb	between	3.334	4	0.833	56.507
	within	9.07	615	0.015	
Th	between	7.392	4	1.848	48.134
	within	23.611	615	0.038	
Cr	between	4.644	4	1.161	19.613
	within	36.407	615	0.059	
Sc	between	3.01	4	0.753	20.295
	within	22.808	615	0.037	
CIA	between	1.905	4	0.476	38.798
	within	7.536	614	0.012	
SiO_2/Al_2O_3	between	4.313	4	1.078	40.081
	within	16.519	614	0.027	
Cr/Th	between	2.811	4	0.703	10.714
	within	40.139	612	0.066	
Th/Sc	between	9.370	4	2.343	42.975
	within	33.361	612	0.055	
Ni/Co	between	5.043	4	1.261	13.193
	within	58.68	614	0.096	

mean square of sums (MS, see Chapter 2.2.1) is thus not equivalent to the variance, but to the squared dispersion factor (see Chapter 2.1.2).

The results of one-way analysis of variance are compiled in Table 3.4.3.1. The results for the LSD-test are given in Appendix 2d, and are represented in a simplified graphical manner in Figures 3.4.3.2 a-n for elements and ratios. The results are interpreted tentatively as

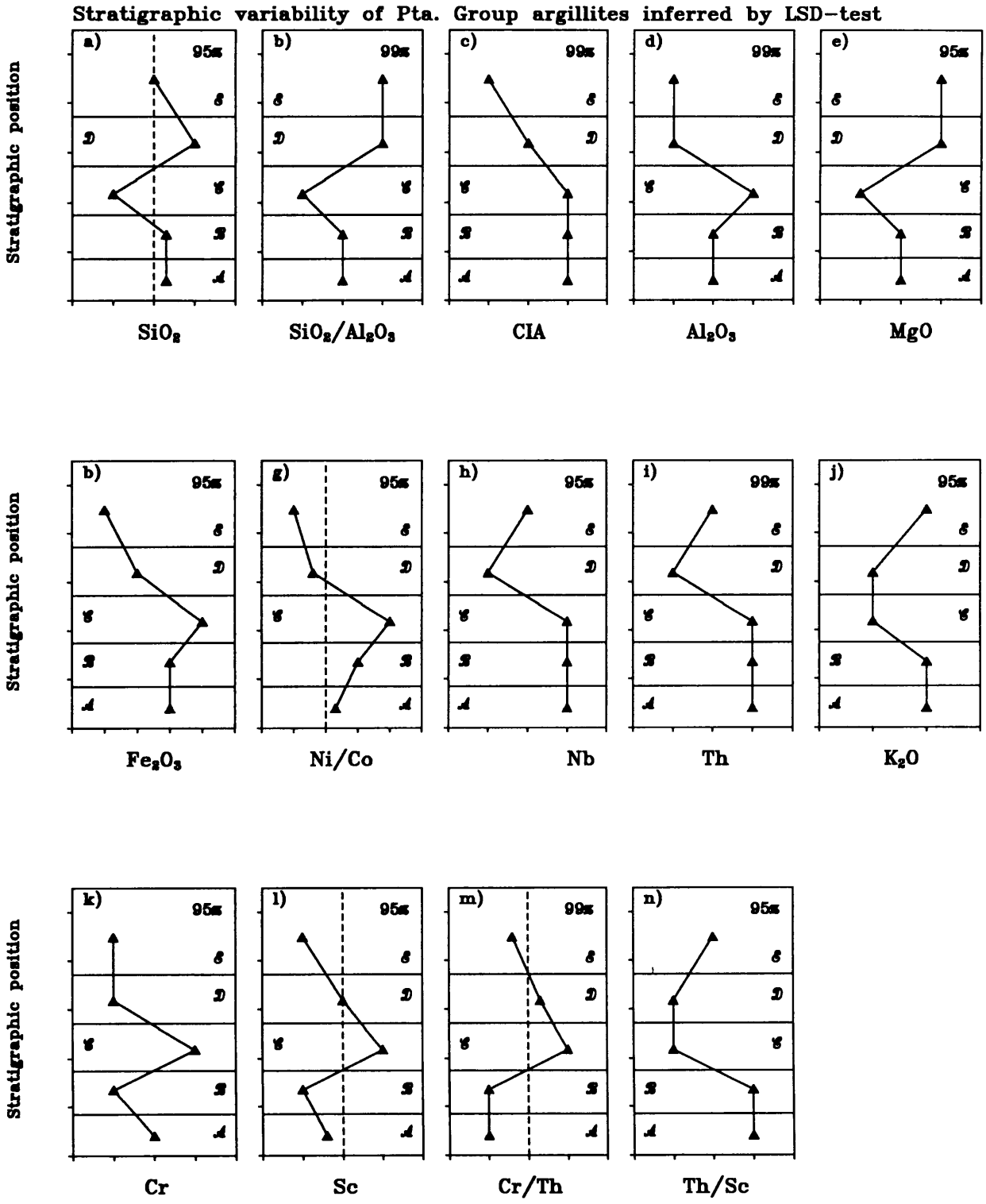

Fig. 3.4.3.2: Stratigraphic variability of Pretoria Group argillites inferred by LSD-test. (Stylised letters: A = Rooihoogte and Lower Timeball Hill Formations; B = Upper Timeball Hill Formation; C = Hekpoort, Dwaalheuwel and Strubenkop Formations; D = Silverton Formation; E = Magaliesberg and post-Magaliesberg Formations. Ordinate: stratigraphic height of the Pretoria Group, one tic mark represents 1000 m; Abscissa: results of the LSD-test, a horizontal difference of one tic mark or more represents a significant difference between sub-groups (e.g., Fe2O3: C > A = B > D > E), significance level of shown differences are shown in the upper right corner of plot.)

emphasizing the geochemical differences between the Silverton Formation and underlying and overlying formations, as well as confirming the unusual character of the geochemistry of the Hekpoort-Dwaalheuwel-Strubenkop subgroup. The high significance level for rejecting H_0 (in all cases > 99.99 %) constrains the possibility that a ß-error occurs, but emphazises the risk of an α-error for the approach used.

3.4.4 Regional variation in the geochemistry of shales

The average shale estimate of the main sampling areas (Botswana, western Transvaal, central Transvaal, eastern Transvaal and northeastern Transvaal, see Figure 1.5.1 for geographical definition of sampling areas) is shown in Tables 3.4.4.1 and 3.4.4.2. A simple comparison of the arithmetic means leads to the identification of three trends:

(1) an east-west depletion/enrichment trend (i.e., Botswana -> WTvl -> CTvl -> ETvl -> NETvl) for As and K_2O/Na_2O, which are both enriched towards the west, and for alk_{NIGGLI}, which is enriched towards the east.

(2) a north-south depletion/enrichment trend (i.e., Botswana & NETvl = northern sampling areas -> WTvl & CTvl & ETvl = southern sampling areas) for Zr and Ni/Co, which are enriched in the southern sampling areas.

(3) a more complicated 'radial' depletion/enrichment trend with depletion/enrichment from western & eastern sampling areas towards the central sampling area. For example, Botswana -> WTvl -> CTvl <- ETvl <- NETvl for Al_2O_3, al_{NIGGLI}, $Fe_2O_3(t)$, Sr, Sb and CIA, which are enriched towards the central sampling areas, or, alternatively, MnO and Ba/Th, which are enriched towards the Botswana and northeastern Transvaal sampling areas in relation to the central Transvaal sampling area. This 'radial' trend includes a distinct north-south enrichment/depletion trend for Al_2O_3 and Ba/Th, but not for the other elements/ratios mentioned.

These enrichment/depletion trends are only defined by differences in the arithmetic mean values, irrespective of the actual differences of the averages and the standard deviation. Hence, statistical tests are neccessary to verify these trends.

AREA	Botswana	WTvl	CTvl	ETvl	NETvl
SIZE	(n = 124)	(n = 127)	(n = 133)	(n = 150)	(n = 71)
SiO_2	57.96 ± 6.74	59.54 ± 8.22	57.83 ± 8.04	58.16 ± 9.76	61.37 ± 5.98
TiO_2	0.67 ± 0.19	0.81 ± 0.33	0.73 ± 0.16	0.69 ± 0.21	0.70 ± 0.16
Al_2O_3	16.77 ± 4.01	19.64 ± 7.25	20.32 ± 4.13	19.50 ± 6.07	16.98 ± 3.52
Fe_2O_3(t)	8.24 ± 2.71	8.83 ± 6.08	9.87 ± 7.83	7.14 ± 3.44	6.87 ± 2.65
MnO	0.08 ± 0.11	0.06 ± 0.07	0.03 ± 0.04	0.05 ± 0.07	0.06 ± 0.08
MgO	3.56 ± 3.17	1.60 ± 2.47	0.78 ± 0.75	2.85 ± 4.60	1.95 ± 1.24
CaO	1.01 ± 2.11	1.19 ± 2.80	0.16 ± 0.25	1.43 ± 4.44	1.40 ± 3.36
Na_2O	0.47 ± 0.51	0.87 ± 1.36	0.44 ± 0.30	0.76 ± 0.77	1.30 ± 1.02
K_2O	2.83 ± 1.02	2.48 ± 1.63	3.11 ± 1.24	3.43 ± 1.66	2.84 ± 1.22
P_2O_5	0.13 ± 0.11	0.10 ± 0.07	0.17 ± 0.22	0.11 ± 0.11	0.07 ± 0.06
H_2O	0.63 ± 0.90	0.40 ± 0.46	1.47 ± 1.21	0.84 ± 1.59	1.09 ± 1.11
LOI	7.44 ± 5.15	4.17 ± 2.92	4.90 ± 1.23	4.49 ± 2.12	4.45 ± 3.94
Zn	104 ± 117	62 ± 55	73 ± 44	72 ± 53	84 ± 38
Cu	41 ± 39	49 ± 47	41 ± 30	45 ± 92	23 ± 21
Ni	84 ± 63	67 ± 45	75 ± 75	54 ± 32	54 ± 20
Co	19 ± 13	15 ± 13	13 ± 11	11 ± 9.1	15 ± 7.4
Ga	21 ± 5.5	25 ± 13	26 ± 5.3	26 ± 9.8	24 ± 6.4
Mo	2.1 ± 3.6	2.3 ± 2.5	1.9 ± 3.1	1.0 ± 2.6	1.2 ± 2.3
Nb	14 ± 4.3	13 ± 3.9	18 ± 9.5	14 ± 4.2	12 ± 2.8
Zr	146 ± 36	181 ± 71	181 ± 62	188 ± 93	150 ± 41
Y	30 ± 9.5	36 ± 37	34 ± 16	36 ± 24	24 ± 6.0
Sr	52 ± 24	99 ± 79	122 ± 155	116 ± 82	93 ± 51
Rb	146 ± 51	122 ± 78	157 ± 55	165 ± 76	142 ± 58
U	7.2 ± 4.7	4.8 ± 4.4	6.6 ± 5.3	7.5 ± 5.4	4.1 ± 4.4
Th	17 ± 6.9	15 ± 6.5	19 ± 6.1	19 ± 7.8	15 ± 4.8
Pb	25 ± 18	19 ± 13	25 ± 35	30 ± 46	20 ± 13
Cr	159 ± 79	157 ± 102	212 ± 83	166 ± 97	155 ± 52
V	143 ± 73	194 ± 111	165 ± 74	133 ± 63	138 ± 36
Ba	991 ± 1804	732 ± 952	772 ± 531	966 ± 828	1152 ± 1473
Sc	18 ± 6.8	22 ± 13	16 ± 6.1	19 ± 7.3	21 ± 5.1
As	9.7 ± 18.4	8.1 ± 15.2	6.9 ± 12.8	5.8 ± 15.1	1.4 ± 4.4
S	2661 ± 5749	617 ± 1497	260 ± 511	252 ± 640	567 ± 1720
Sb	1.0 ± 3.2	2.1 ± 5.0	3.4 ± 7.1	1.2 ± 4.0	0.4 ± 1.9
Sn	1.4 ± 3.8	3.9 ± 6.1	2.4 ± 8.3	2.9 ± 5.4	2.0 ± 4.5
B	87 ± 61[1]	39 ± 43[§]	67 ± 29[♀]	130 ± 209[#]	n. a.

Table 3.4.4.1: Average element concentrations of Pretoria Group shales from selected sampling areas. (Mean values are reported as mean ± 1 δ standard deviation. WTvl = western Transvaal; CTvl = central Transvaal; ETvl = eastern Transvaal; NETvl = northeastern Transvaal. ¶: n = 65; §: n = 11; ♀: n = 28; #: n = 70. n.a.: not analysed)

Table 3.4.4.2: Average ratios of Pretoria Group shales from selected sampling areas.

(NOTE: ratios corrected as described in Chapter 3.1.2)

AREA	Botswana	WTvl	CTvl	ETvl	NETvl
n	(n = 124)*	(n = 127)*	(n = 133)*	(n = 150)*	(n = 71)
SiO_2/Al_2O_3	3.8 ± 1.7	5.5 ± 17.9	3.1 ± 1.3	3.7 ± 3.3	3.8 ± 0.9
Al_2O_3/TiO_2	25.8 ± 7.4	25.7 ± 7.2	28.4 ± 5.1	28.9 ± 5.9	25.0 ± 4.9
Al_2O_3/K_2O	8.4 ± 13.7	34.6 ± 78.1	10.8 ± 22.5	27.9 ± 142.3	10.7 ± 20.6
K_2O/Na_2O	69.0 ± 111	14.3 ± 34.5	13.8 ± 28.6	13.1 ± 15.9	3.9 ± 3.6
Cr/Th	11.9 ± 13.5	11.9 ± 10.0	12.1 ± 6.3	9.8 ± 7.0	11.1 ± 5.1
Th/Sc	1.06 ± 0.52	0.92 ± 0.59	1.31 ± 0.58	1.14 ± 0.67	0.79 ± 0.34
Cr/Zr	1.16 ± 0.83	1.27 ± 3.22	1.31 ± 0.76	0.99 ± 0.58	1.07 ± 0.42
Co/Th	1.46 ± 1.83	1.41 ± 1.96	0.83 ± 0.88	0.66 ± 0.57	1.12 ± 0.68
CIA	75.4 ± 12.5	76.8 ± 17.1	82.5 ± 5.2	74.1 ± 15.9	69.6 ± 11.7
K/Rb	164 ± 26	178 ± 67	164 ± 30	241 ± 866	183 ± 106
K/Ba	39 ± 22	33 ± 19	37 ± 14	36 ± 23	30 ± 15
Cr/V	1.12 ± 0.39	0.96 ± 0.84	1.32 ± 0.35	1.36 ± 0.74	1.15 ± 0.42
V/Ni	2.07 ± 1.00	4.21 ± 4.00	3.19 ± 1.95	4.12 ± 7.29	3.52 ± 5.30
Ni/Co	5.41 ± 4.18	6.87 ± 6.20	8.83 ± 10.43	8.26 ± 9.00	4.30 ± 3.43
Th/U	2.13 ± 0.86	2.53 ± 1.07	2.67 ± 1.09	2.50 ± 1.11	2.50 ± 0.85
Zr/Nb	10.8 ± 3.2	13.8 ± 5.4	11.4 ± 4.5	14.2 ± 9.1	12.4 ± 3.2
Ba/Rb	6.6 ± 9.0	12.4 ± 23.2	8.0 ± 29.9	9.2 ± 24.6	14.8 ± 42.1
Ba/Th	68 ± 141	51 ± 71	43 ± 34	57 ± 66	86 ± 135
Al/Zr	634 ± 180	616 ± 216	646 ± 204	614 ± 234	626 ± 166
Ti/Zr	28.6 ± 8.2	28.7 ± 11.6	25.8 ± 6.9	24.2 ± 8.1	28.8 ± 6.9
al_{NIGGLI}	53.8 ± 10.9	60.6 ± 16.1	64.0 ± 8.4	58.5 ± 14.3	55.9 ± 8.9
c_{NIGGLI}	2.9 ± 5.8	2.9 ± 6.6	0.5 ± 0.7	2.8 ± 7.7	4.1 ± 8.5
fm_{NIGGLI}	30.8 ± 10.9	23.7 ± 13.8	22.6 ± 10.6	23.5 ± 11.1	22.6 ± 6.8
alk_{NIGGLI}	12.5 ± 3.9	12.9 ± 6.4	12.9 ± 4.2	15.1 ± 5.8	17.4 ± 5.6
si_{NIGGLI}	167 ± 79	179 ± 125	164 ± 60	166 ± 126	176 ± 35
qz_{NIGGLI}	17.1	27.3	11.7	5.5	5.9

As the variation coefficients of Al_2O_3 in the regional sampling subgroups point to approximately normal distributions of Al_2O_3, a test comparing the variation coefficients can be performed (see Chapter 2.1.3). The test results are given in Table 3.4.4.3. The test results distinguish the western Transvaal and eastern Transvaal Al_2O_3-distributions as having different parent distributions, but fail to discriminate between the Al_2O_3-distributions of the northeastern, Botswana and central Transvaal sample sets. However, this test compares the variability in two sets of samples, and, for example, can be utilized to test two independant sample subsets from the same sampling area having similar means on correspondence of the underlying parent distribution, but is not suitable to postulate significant differences between means. The multiple comparison of means requires a different type of test to establish a significant difference between mean values and, thereby, between respective sample sets.

The regional data sets described above were tested with one-way analysis of variance on

Table 3.4.4.3: Variation coefficent test for regional differences of the parent distributions of Al_2O_3 (upper right triangle of matrix: n.s = a difference of the underlying parameters of the variation coefficients has to be rejected; $z' > z_{0.05}$ = a difference of the underlying parameters of the variation coefficients has to be assumed with a 5 % error probability; lower left triangle of matrix: values for z', calculated after equation (2.19), Chapter 2.1.3; critical limit for $z_{0.05}$ = 1.96.

	Bots	WTvl	CTvl	ETvl	NETvl
Bots	********	$z' > z_{0.05}$	n.s	$z' > z_{0.05}$	n.s
WTvl	4.70	********	$z' > z_{0.05}$	$z' > z_{0.05}$	$z' > z_{0.05}$
CTvl	1.84	6.31	********	$z' > z_{0.05}$	n.s
ETvl	3.07	1.97	4.94	********	$z' > z_{0.05}$
NETvl	1.38	5.59	0.19	4.16	********

differences of their mean values, and, if the null hypothesis had to be rejected on the chosen significance level (1 % error probability), the LSD-test was performed to determine the sampling areas differing from each other for a respective element. The results of analysis of variance are compiled in Appendix 2d. It should be mentioned that, on the basis of comparing **F'** values, the test results for the 26 tested elements on regional differences are less significant than the results for stratigraphic differences, although a comparison is difficult due to sample sizes and their differences. However, one-way analysis of variance could establish significant differences of the respective mean values for 24 of the tested elements (the null hypothesis had to be retained only for Pb and Sb). The test results of the LSD-test are shown in Table 3.4.4.4. The results of the LSD-test are represented graphically in Figures 3.4.4.1 a - c in the form of rough isopleth maps. If the results of the statistical approach (i.e., one-way analysis of variance plus LSD-test) are compared with the results of a simple evaluation of arithmetic mean values, a number of discrepancies are obvious. Only K_2O/Na_2O, Zr and Fe_2O_3 have similar patterns in both approaches. It should be emphazised that both approaches may be biased to a certain degree by the sampling design, i.e. preferential sampling of a formation in a region. A two-way analysis of variance was not attempted, as the sample sizes of the respective subgroups would have become too small and,

Table 3.4.4.4: Statistical summary of the LSD-test and the F'-ratios for regionally defined sub-groups of Pretoria Group shales. (Results of LSD-test: relationships of mean values inferred by the LSD-test; Signif. LSD: significance level of predicted relationships; ANOVA F': $MS_{between}/MS_{within}$; see Chapter 2.2.1 for detailed descrption of procedure. Significance level of rejection of H_0 for all elements > 99 %)

Element	Results of LSD-test	Signif. LSD	ANOVA: F'
Al_2O_3	B < C = E; N < C	95 %	5.342
Fe_2O_3	E = N = W < C; E = N < B	95 %	7.984
MgO	C = W < E = N < B	99 %	44.934
MnO	C < W; W < N; E < B	95 %	9.464
K_2O	W < N = B = C = E	99 %	8.497
Zn	W < E = C < N = B	95 %	15.605
Cu	N < E = B = W; E < C	95 %	9.4
Co	E < C = W < N = B	95 %	14.274
Ba	W < B < N; W < E = C	95 %	6.618
S	E < C = N = W < B	95 %	45.546
As	N < W = B; C = E < B	95 %	4.223
Sr	B < W = E = N; W < C	95 %	17.568
Zr	B = N < W = E = C	95 %	6.64
V	E < N = B < C = W	95 %	14.351
Th	W = N = B < E = C	99 %	8.684
Cr	W = B = N = E < C	99 %	11.886
Sc	C < B < N; B = E; N = W	95 %	6.925
CIA	N < W = B; W < C	95 %	7.417
K_2O/Na_2O	N < W < E = C < B	95 %	18.291
Cr/Th	E < N; E = W = B < C	95 %	4.185
Cr/Zr	W = E < C; W < B; W < N	95 %	8.744
Th/Sc	N = W < B = E < C	95 %	15.095
Ba/Th	W = C = B < N; E < N; W < N	95 %	5.528
Ni/Co	N < B = W = E; N < C; B < C	95 %	6.386

more importantly, too different in size. The sample sizes of the regions chosen for one-way analysis of variance are similar (see Table 3.4.4.1), with the exception of the northeastern sampling area.

Correspondence analysis of major and selected trace elements was performed for all shale samples (Fig. 3.4.4.2 and 3.4.4.3). Correspondence analysis of the major elements generally infers a high degree of uniformity, with most samples clustering parallel to the 'dim 2'-axis close to the Al_2O_3-position (the Al_2O_3-line and symbol is in fact overprinted, Fig. 3.4.4.2). A fairly well defined cluster of western Transvaal samples lies on the extension of the MnO-line, although the cluster comprises only 11% of the western Transvaal samples (14 out of 127). Correspondence analysis of selected trace elements exhibits a high degree of variability, independant of the respective sample area. Clusters defining sampling areas are not apparent.

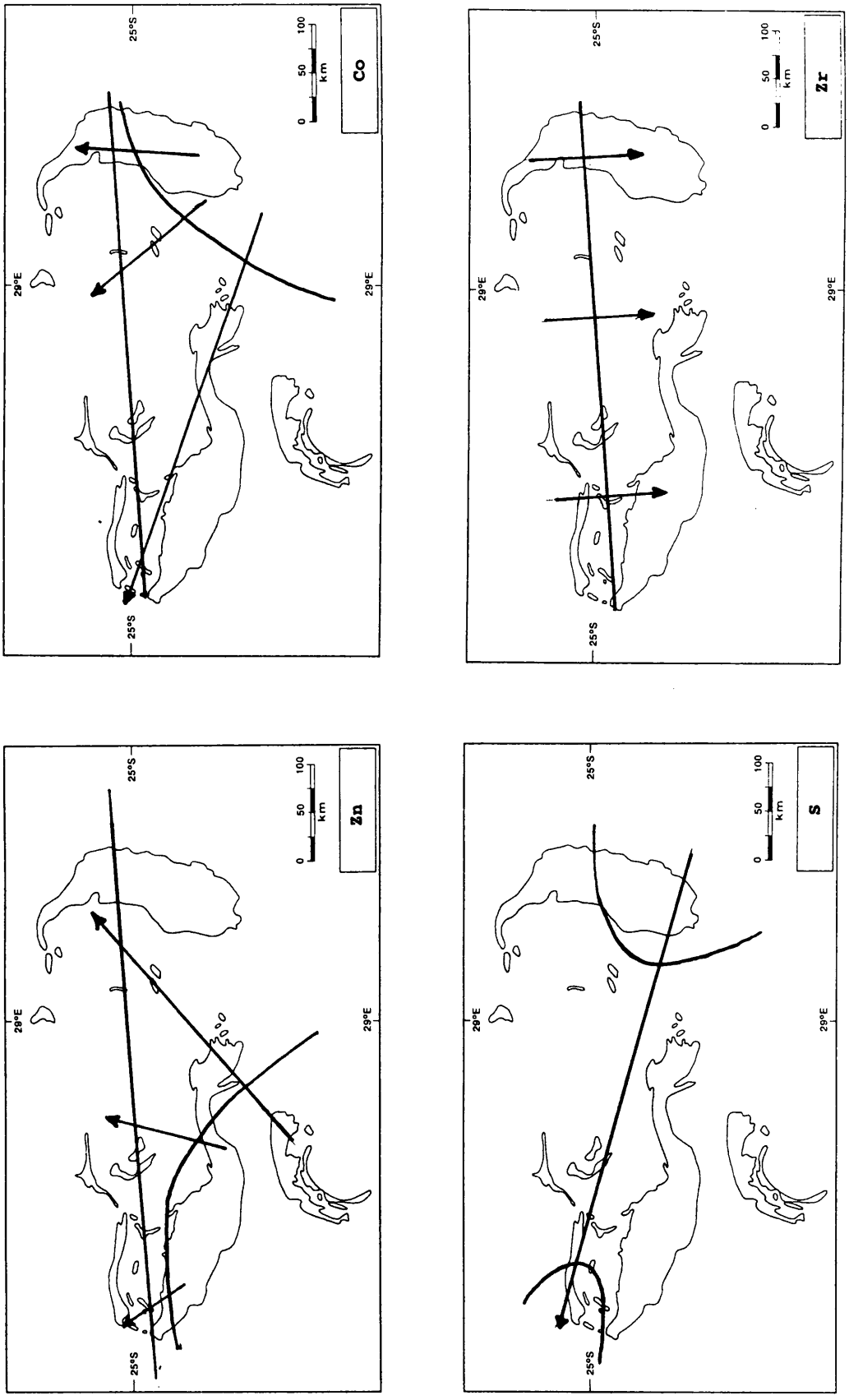

Figure 3.4.4.1a: Differences of regional element concentrations inferred by one-way analysis of variance and the LSD-test. Arrows indicate direction of increase. Lines are approximate boundaries separating areas with a signifficant difference in element concentration.

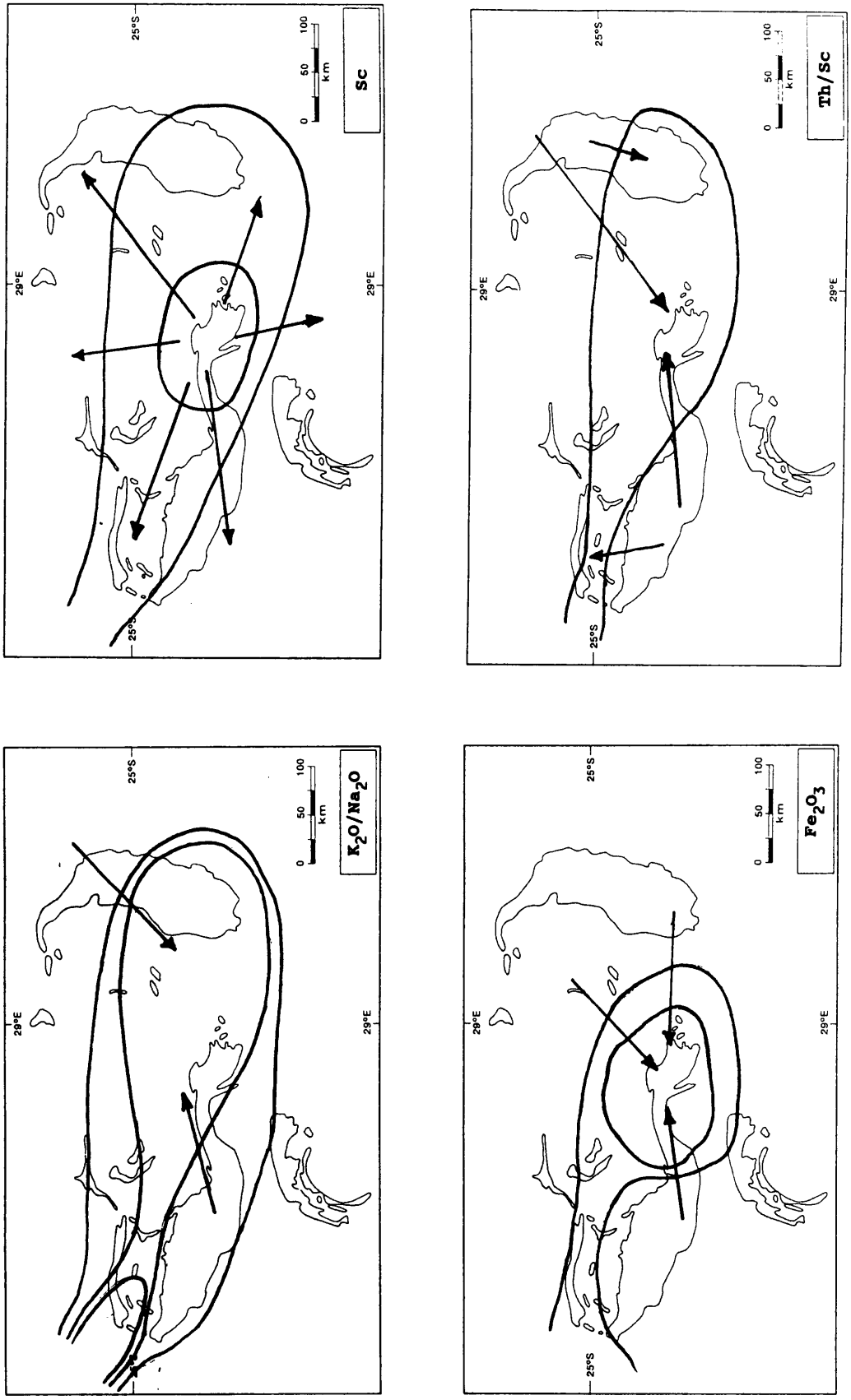

Figure 3.4.4.1b: Differences of regional element concentrations inferred by one-way analysis of variance and the LSD-test. Arrows indicate direction of increase. Lines are approximate boundaries separating areas with a signifficant difference in element concentration.

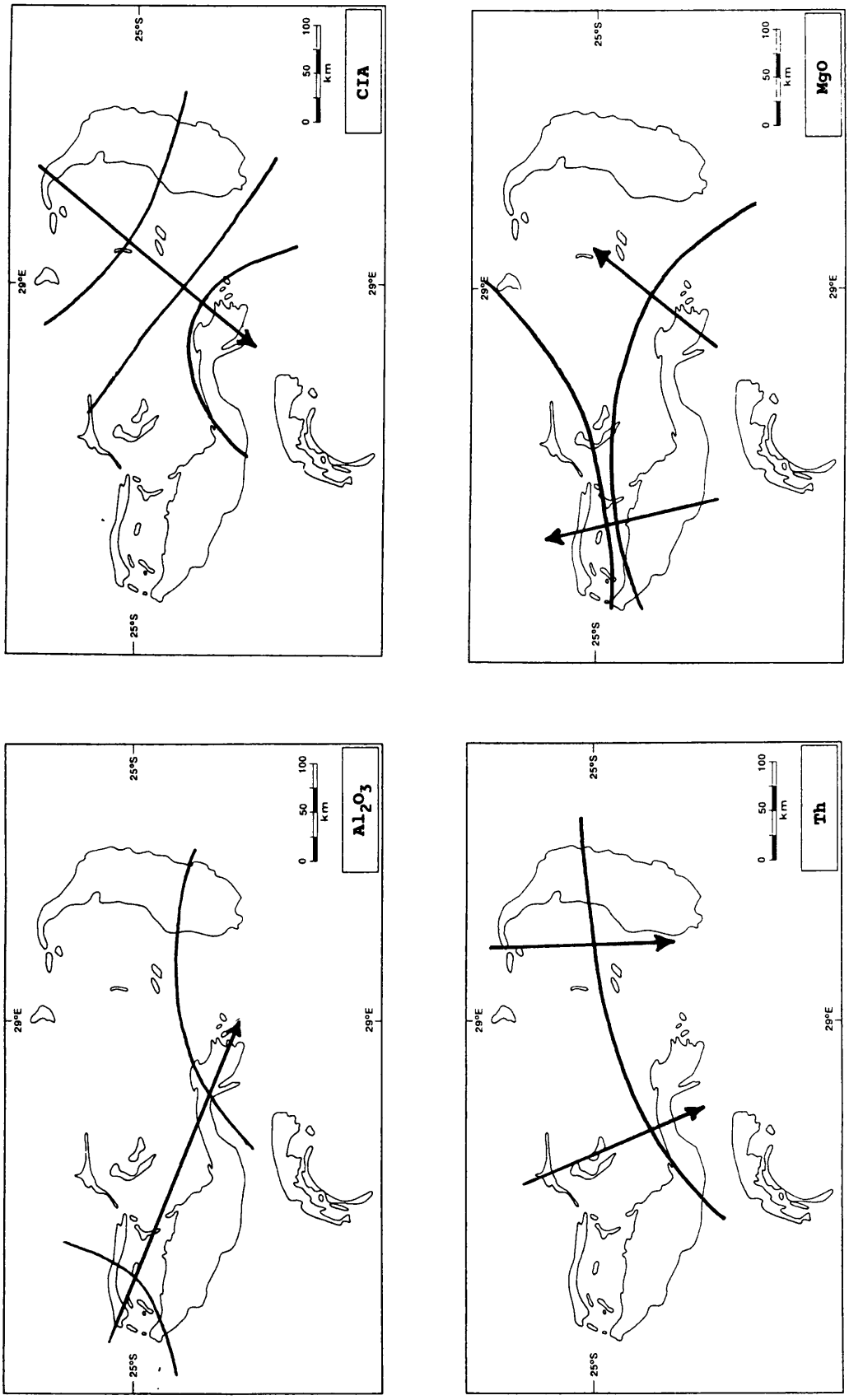

Figure 3.4.4.1c: Differences of regional element concentrations inferred by one-way analysis of variance and the LSD-test. Arrows indicate direction of increase. Lines are approximate boundaries separating areas with a signifficant difference in element concentration.

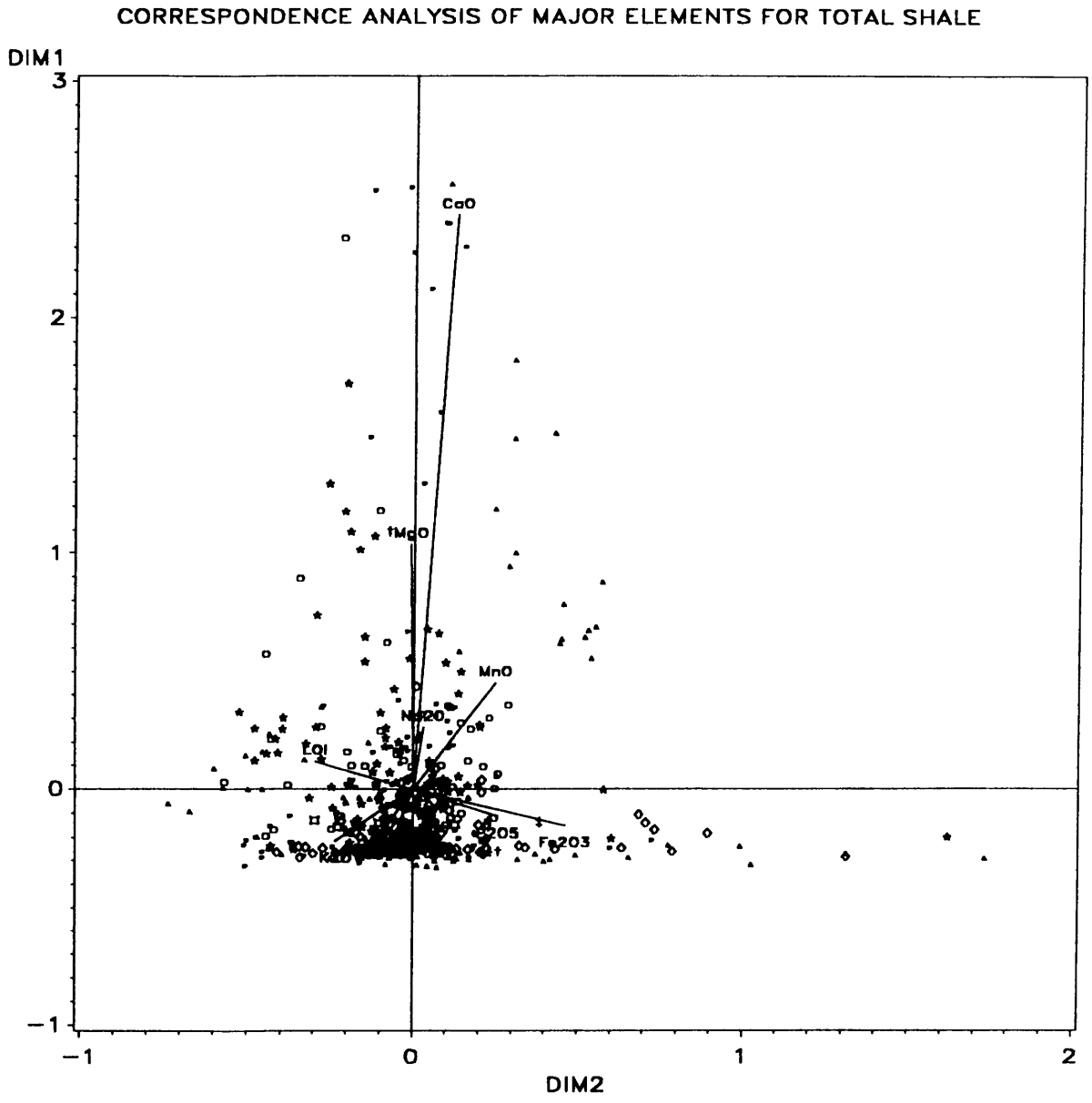

Figure 3.4.4.2: Correspondence analysis of major elements (except SiO_2) of Pretoria Group shales. Symbols for sampling areas: ● (red) = eastern Transvaal; ○ (red) = northeastern Transvaal; □ (violet) = eastern fragments; ◇ (green) = central Transvaal; ▲ (blue) = western Transvaal; † (blue) = western fragments; ‡ (blue) = northwestern Transvaal; ★ (yellow) = Botswana. Definition of sampling areas is shown in Figure 1.5.1. DIM 1 and DIM 2 are the values of the factor loadings of the samples and variables for the first and second factor (see Chapter 2.3.2). Angles between lines connecting a variable and the point (0,0) are proportional to the product moment correlation coefficient of these variables.

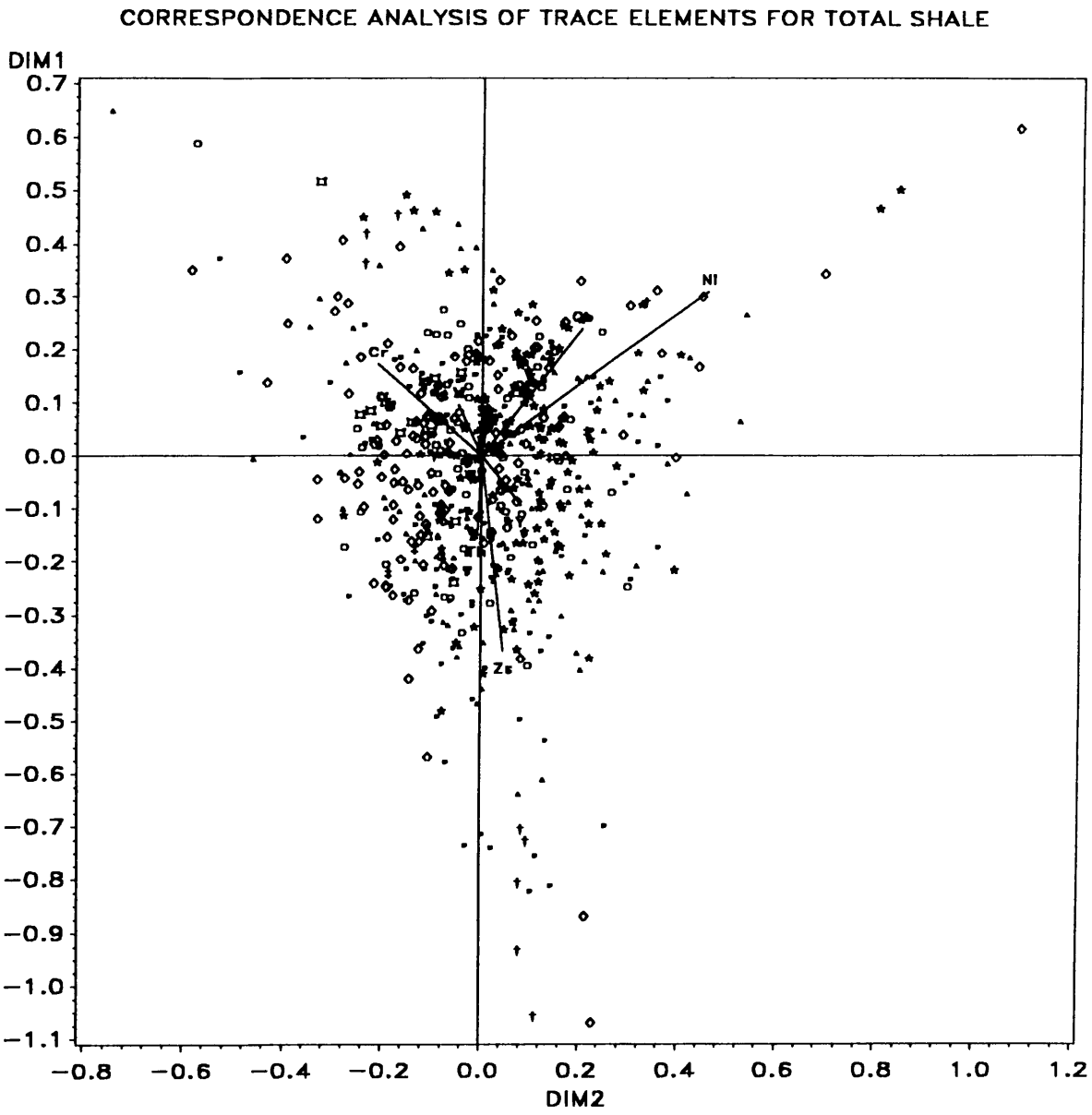

Figure 3.4.4.3: Correspondence analysis of selected trace elements of Pretoria Group shales. Symbols for sampling areas: ● (red) = eastern Transvaal; ○ (red) = northeastern Transvaal; □ (violet) = eastern fragments; ◇ (green) = central Transvaal; ▲ (blue) = western Transvaal; † (blue) = western fragments; ‡ (blue) = northwestern Transvaal; ★ (yellow) = Botswana. Definition of sampling areas is shown in Figure 1.5.1. DIM 1 and DIM 2 are the values of the factor loadings of the samples and variables for the first and second factor (see Chapter 2.3.2). Angles between lines connecting a variable and the point (0,0) are proportional to the product moment correlation coefficient of these variables.

CHAPTER 4: DISCUSSION OF RESULTS

4.1 Provenance of the Pretoria Group sedimentary rocks

The provenance of Pretoria Group argillites and sandstones was previously discussed by Condie and Wronkiewicz (1990), Wronkiewicz and Condie (1990), Schreiber (1990) and Schreiber et al. (1991, 1992). Schreiber (1990) and Schreiber et al. (1992) infer predominantly granitic source rocks for shales with local contributions from mafic sources, based on low Cr/Zr-ratios (i.e., averages for formations sorted according to regions lie between 0.5 and 2.7) and an Al_2O_3-TiO_2 classification plot after McLennan et al. (1979). Condie and Wronkiewicz (1990) propose a granitic provenance for Pretoria Group argillites, based on low Cr/Th-ratios compared to older Kaapvaal sedimentary rocks. Furthermore, they conclude that the low Th/Sc, Co/Th and Cr/Th-ratios exclude the possibility of appreciable recycling (< 20 %) of older Kaapvaal sedimentary rocks into the Pretoria Group sedimentary rocks. Wronkiewicz and Condie (1990) come to similar conclusions, based on La-Th-Sc and Th-Hf-Co ternary diagrams, although they suggest lesser contributions of basaltic and/or komatiitic source material were possible. The enrichment of Th compared to the North American Shale Composite (Gromet et al., 1984) is cited as a possible reflection of a Th-enriched granitic source, with an estimated Th-content of 35 to 40 ppm (Wronkiewicz and Condie, 1990).

The distribution of mudrocks analysed in this investigation on a La-Th-Sc ternary diagram is shown in Figure 4.1.1 A-D, for the shale samples that were analysed for La. These samples occupy the same field as samples reported by Condie and Wronkiewicz (1990). However, the Lower Timeball Hill shales of the eastern Transvaal sample area (Figure 4.1.1 C) have a variation which encompasses the whole field of variation of the Pretoria Group shales. In addition, the Lower Timeball Hill shales from both the central and eastern Transvaal sampling areas show a systematic trend from inferred felsic sources at the base towards more mafic sources at the top of the succession. This is contradictory to a more or less stable Th/Sc-ratio (see also Fig. 3.3.2.2).

REE, Th and Sc are thought to to be a good reflection of different source rocks due to their low seawater/crust distribution coefficients and low seawater residence times (Taylor and

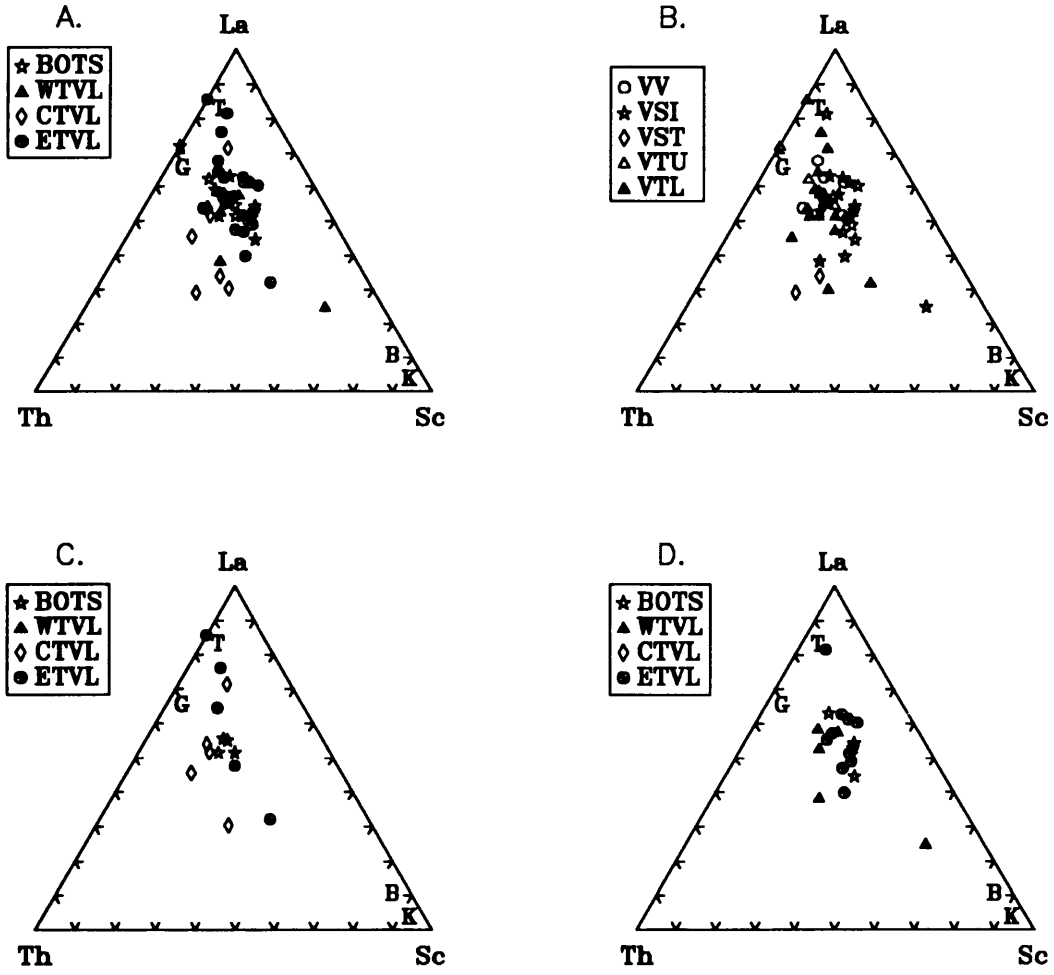

Figure 4.1.1 A-D: La-Th-Sc ternary diagrams after Bhatia (1983) and Wronkiewicz and Condie (1990). **A.**: all Pretoria Group samples analysed for La. Symbols (see box left of diagram) refer to sampling area (see also Fig. 1.5.1): BOTS = Botswana, WTVL = western Transvaal, CTVL = central Transvaal, ETVL = eastern Transvaal. **B.**: as A, symbols (see box left of diagram) refer to stratigraphic position: VV = Vermont Formation, VSI = Silverton Formation, VST = Strubenkop Formation, VTU = Upper Timeball Hill Shale Member, VTL = Lower Timeball Hill Shale Member. **C.**: Timeball Hill Formation Lower Shale Member, symbols (see box left of diagram) refer to sampling area. **D.**: Silverton Formation, symbols (see box left of diagram) refer to sampling area. Capital letters refer to position of average basalt (B), komatiite (K), tonalite (T) and granite (G).

McLennan, 1985). However, a comparison of Eh-pH-diagrams of Th, Sc and La (Brookins, 1988) and recent natural aqueous environments (Garrels and MacKenzie, 1971), show a greater field of solubility for La than for Th and Sc. Fractionation of REE within residual systems (e.g., soils) is reported by Nesbitt (1979). The REE-contents and patterns of shales further depend on the interaction of the aqueous phase and the sediment during deposition (Ruhlin and Owen, 1986). So called 'hydrothermal sediments' can have La contents of up to several hundred ppm La (Ruhlin and Owen, 1986), thus exceeding the average values of theoretical end-member compositions of Pongola and Transvaal source rocks (Wronkiewicz and Condie, 1990) many times. REE-contents can, furthermore, be subject to diagenetic changes (e.g., Valeton, 1988), which can distort the relative abundances of REE to each other and, thereby, the original REE-pattern (German and Elderfield, 1990). Another problem concerning the suitability of La as a source rock indicator is the preferential enrichment of La reported for some basaltic lavas (Robertson and Fleet, 1976; Hellmann et al., 1979).

Several Lower Timeball Hill and Silverton Formation samples have La-contents exceeding 100ppm (see Chapters 4.4 and 4.5). This strong enrichment of La, normally accompanied by a pronounced negative Ce anomaly, is thought to reflect hydrothermal activity related to the extrusion of the Bushy Bend and Machadodorp volcanics (Eriksson et al., under review; Reczko et al., under review). The suitability of La as a reliable source rock indicator is thus questioned, as the absolute La contents used for the La-Th-Sc ternary diagram may be prone to changes independent of the actual source rock. The application of La-Th-Sc diagrams should therefore be omitted from provenance studies of Pretoria Group shales. It should be mentioned that Bhatia and Crook (1986) have successfully used the La-Th-Sc ternary diagram for the discrimination of plate tectonic settings of greywackes, i.e., relatively unweathered, rapidly deposited sediments.

A further indication of the unsuitability of REE as source rock indicators for the Pretoria Group shales is seen by the application of the discrimination diagrams of Bhatia (1985) to these samples (Fig. 4.1.2 a-f). Bhatia (1985) found indicative trends in shales, especially for K_2O/Na_2O versus REE parameter plots. The Pretoria Group samples scatter throughout these diagrams (Fig. 4.1.2 a-f) and have a considerably larger variability compared to the shale samples described by Bhatia (1985).

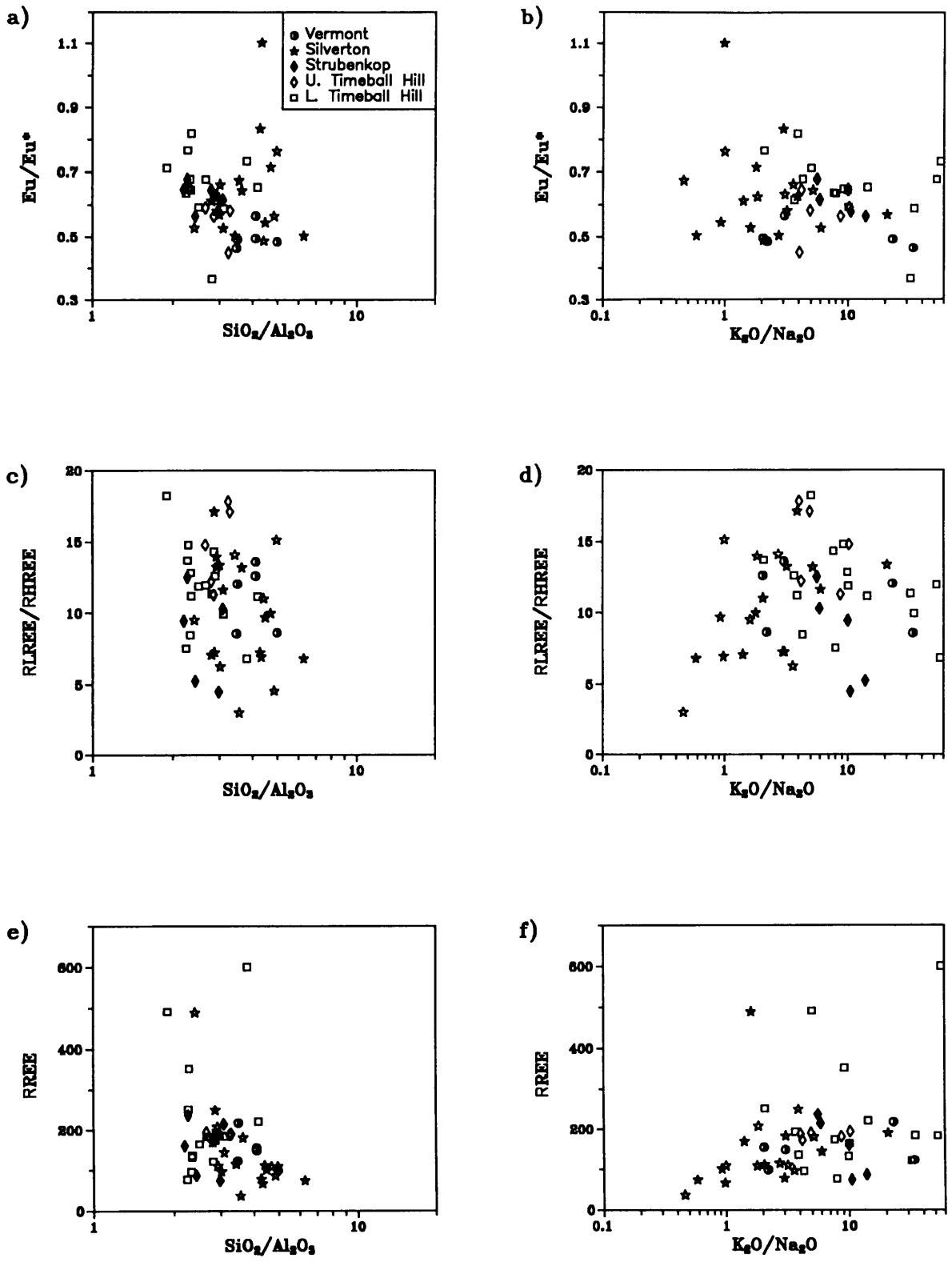

Figure 4.1.2 a-f: Pretoria Group argillites: REE-parameters versus SiO_2/Al_2O_3 and K_2O/Na_2O. Symbols: ★ = Silverton Fm.; □ = Lower Timeball Hill shales; ○ = Vermont Fm.; ◇ = Upper Timeball Hill shales; ◆ = Strubenkop Fm.

Another approach for estimating the provenance of mudrocks (and sandstones) was provided by Roser and Korsch (1988). They applied discriminant analysis of major elements (Al_2O_3, TiO_2, $Fe_2O_3(t)$, MgO, CaO, Na_2O, K_2O) to a sample set of known provenance, and were able to improve the correct classification of an independent control group to 85 %, using a calculated discriminant function. Roser and Korsch (1988) differentiate between primarily mafic (P1), intermediate (P2), felsic (P3) and recycled (P4) provenances.

The application of Roser and Korsch's (1988) discriminant function to Pretoria Group argillites is shown in Figures 4.1.3 a-i. The plots point to predominantly mafic and intermediate sources for the lower part of the Pretoria Group (Rooihoogte to Strubenkop Formation), a mixed mafic/recycled provenance for the Daspoort Formation, a predominantly recycled provenance with major contributions from mafic, intermediate and felsic sources for the Silverton Formation, and a recycled provenance with minor contributions from intermediate and felsic sources for the Magaliesberg and Vermont Formations. The classification plots after Roser and Korsch (1988) point to a stratigraphic variation (base to top) from mafic-intermediate, to recycled sources, with some minor contributions from felsic sources in the upper part of the Pretoria Group. An evaluation of the Nederhorst argillite samples with the discriminance plot after Roser and Korsch (1988) had to be omitted, as these predominantly calcareous samples fall outside the margins of the diagram. The application of the discriminance plot of Roser and Korsch (1988) and its implications for the provenance of Pretoria Group mudrocks, contrast with the interpretation of the previously referenced authors (see above), who infer predominantly felsic sources for the Pretoria Group mudrocks.

Condie and Wronkiewicz (1990) used ratios of the elements Cr, Th, Sc, Zr, La, Co and Yb, which are thought to be fairly immobile and thus indicative of a specific source, for the estimation of provenances of South African Archaean and Proterozoic shales, including Pretoria Group samples from the Timeball Hill (not differentiated), Strubenkop and Silverton Formations. Their approach is based on systematic changes of Cr/Th, Co/Th, Th/Sc, Cr/Zr, La/Sc, Cr/Zr, Cr/V, La/Th and La/Yb in magmatic source rocks (granite, tonalite, basalt and komatiite). Th/Sc and, especially, Cr/Th are pointed out by Condie and Wronkiewicz (1990) as sensitive indicators of source rock compositions, and/or relative changes of

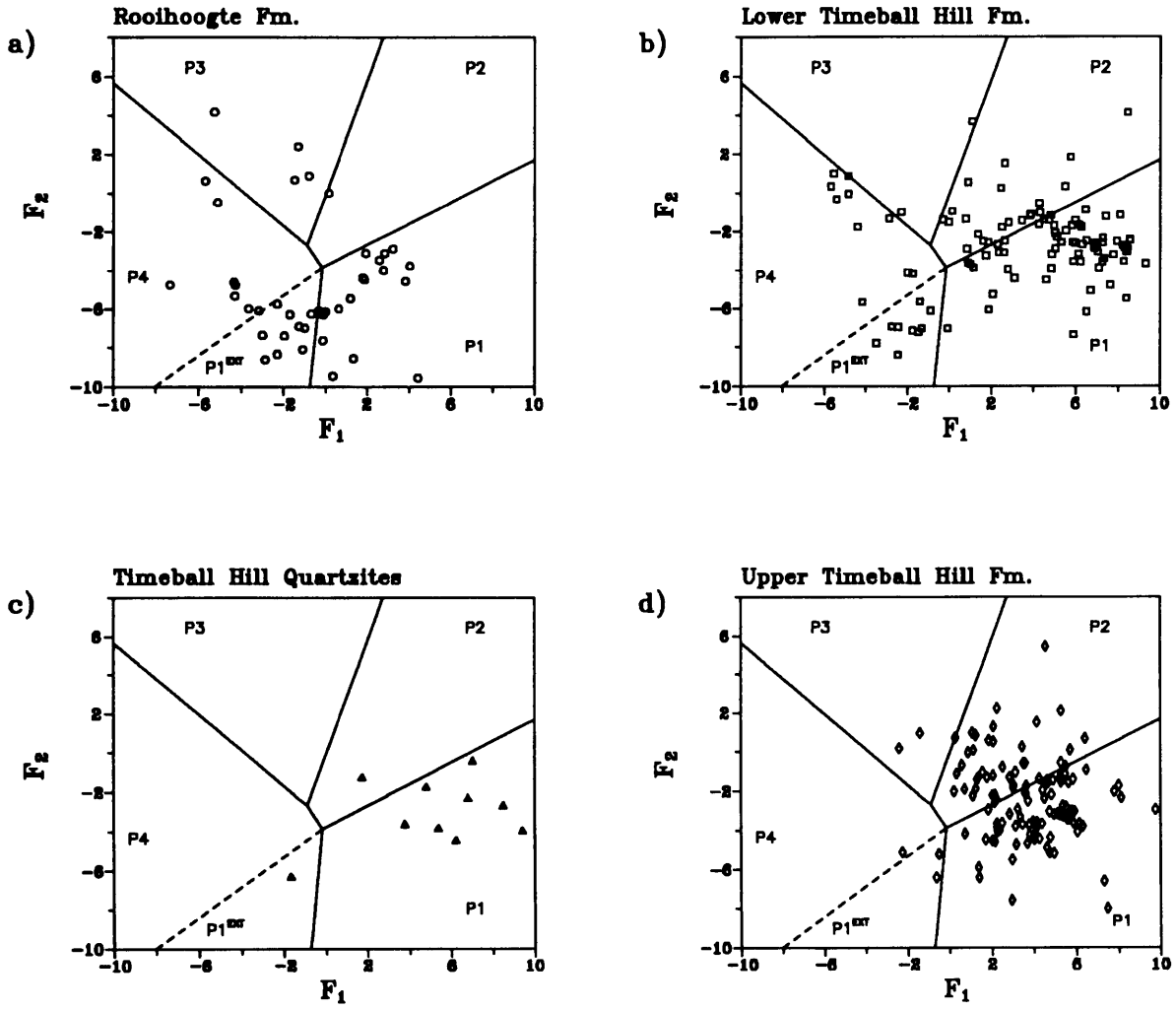

Fig. 4.1.3 a-i: Discriminance plots of Pretoria Group shales after Roser and Korsch (1988). Shales were recalculated to 100 % volatile-free before the discriminant function was applied. P_1: mafic provenance (P_1^{EXT} mafic provenance with high concentrations of Fe_2O_3* and MgO in the sample); P_2: intermediate provenance; P_3: felsic provenance; P_4: recycled sedimentary.

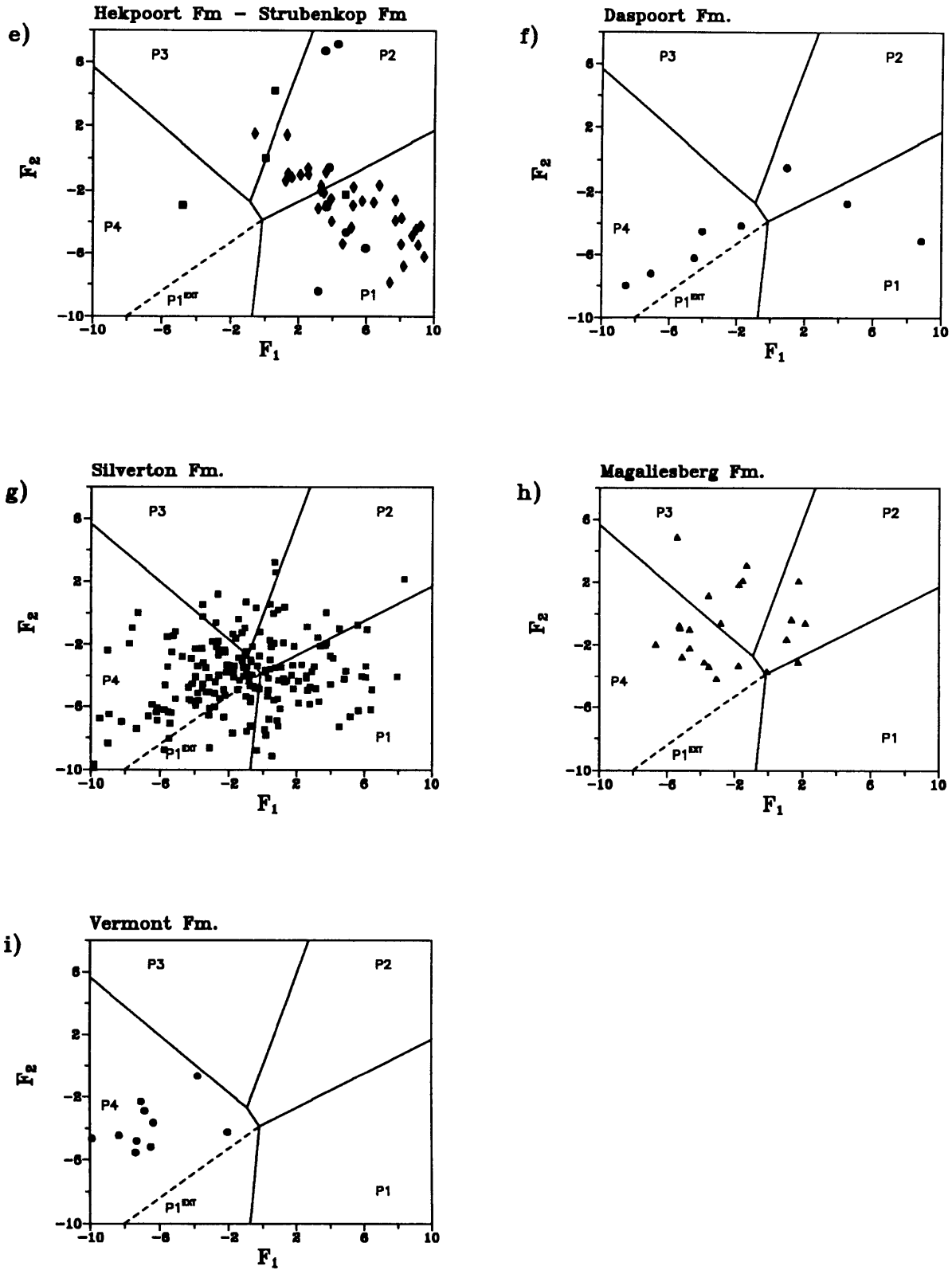

Fig. 4.1.3 a-i (continued): Discriminance plots of Pretoria Group shales after Roser and Korsch (1988). (Symbols for Figure 4.1.3 e: ● = Hekpoort Fm., ■ = Dwaalheuwel Fm., ◆ = Strubenkop Fm.)

Table 4.1.1: Felsic-mafic mixing ratios for Cr/Th, Th/Sc and Cr/Zr.

Calculated from Archaean mafic and felsic end member compositions inferred by Taylor and McLennan (1985, p. 181). Felsic end-member composition: Cr 30 ppm, Sc 5 ppm, Th 6.8 ppm, Zr 200 ppm; Mafic end-member composition: Cr 330 ppm, Sc 40 ppm, Th 0.8 ppm, Zr 50 ppm; values in brackets are average ratios from basalts and tonalites given by Condie and Wronkiewicz (1990).

Mixing ratio Felsic : Mafic	Cr/Th	Th/Sc	Cr/Zr
0 : 100	413 (500)	0.02 (0.02)	6.6 (5.5)
10 : 90	214	-	4.6
20 : 80	135	-	3.4
25 : 75	111	0.07	2.9
30 : 70	92	-	-
33.3 : 66.6	82	0.10	2.3
40 : 60	66	-	1.91
50 : 50	47	0.17	1.44
60 : 40	34	-	1.07
66.6 : 33.3	27	0.29	0.87
70 : 30	24	-	0.77
75 : 25	20	0.39	0.65
80 : 20	16	0.47	0.53
90 : 10	10	0.81	0.32
100 : 0	4.4 (6.5)	1.36 (1.3)	0.15 (0.3)

provenance in the stratigraphic column. Condie and Wronkiewicz (1990) find a 'significant' change in provenance, i.e., from mafic/komatiitic sources to granitic sources, towards the younger sedimentary assemblages (Pretoria, Waterberg and Soutpansberg Groups). Schreiber et al. (1992) found a predominantly granitic provenance, with locally important basaltic contributions, based on Cr/Zr-ratios of shales. Schreiber et al. (1992) interpreted average

Cr/Zr-ratios of 0.5 to 2.7 (averages given are regional averages of formations) as resembling more closely the average Cr/Zr-ratios of tonalites (ϕ 0.3) than basalts (average Cr/Zr-ratio of ϕ 5.5; Condie and Wronkiewicz, 1990). The provenance estimations of Pretoria Group argillites which use these ratios (e.g., Schreiber et al., 1992; Condie and Wronkiewicz, 1990) are thus based on a linear development of the ratios from ultramafic to felsic provenances and their mixtures. However, a linear development is impossible, due to the combination of inferred negative correlations of the respective elements building a ratio, and due to the differences of an order of magnitude or more in absolute end-member contents of the respective elements. An evaluation of the ratios given by Condie and Wronkiewicz (1990) was not possible, as they omit to give the average element contents of their inferred magmatic endmember compositions. The references given by Condie and Wronkiewicz (1990) for the reported average ratios are inconclusive, in so far as they do not include any statistical parameters concerning the reported ratios or related element contents. A personal request to Professor Condie, to obtain the statistics of the magmatic end-member compositions, was unsuccessful (K.C. Condie, pers. comm., 1993).

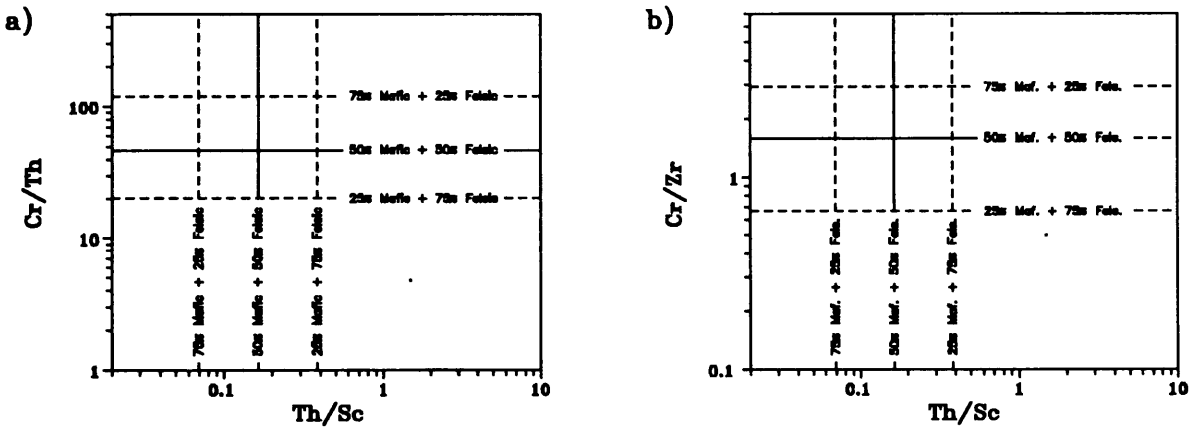

Fig. 4.1.4 a-z: Th/Sc, Cr/Th and Cr/Zr discrimination diagrams of Pretoria Group argillites. Symbols for sampling areas: ● = eastern Transvaal; ○ = northeastern Transvaal; □ = eastern fragments; ◇ = central Transvaal; ▲ = western Transvaal, western fragments and northwestern Transvaal; ★ = Botswana. Definition of sampling areas is shown in Fig. 1.5.1. Figures 4.1.4 a and b define fields for provenance composition by using mixing ratios of Table 4.1.1, Pretoria Group shales are shown in Figures 4.1.4 c-z.

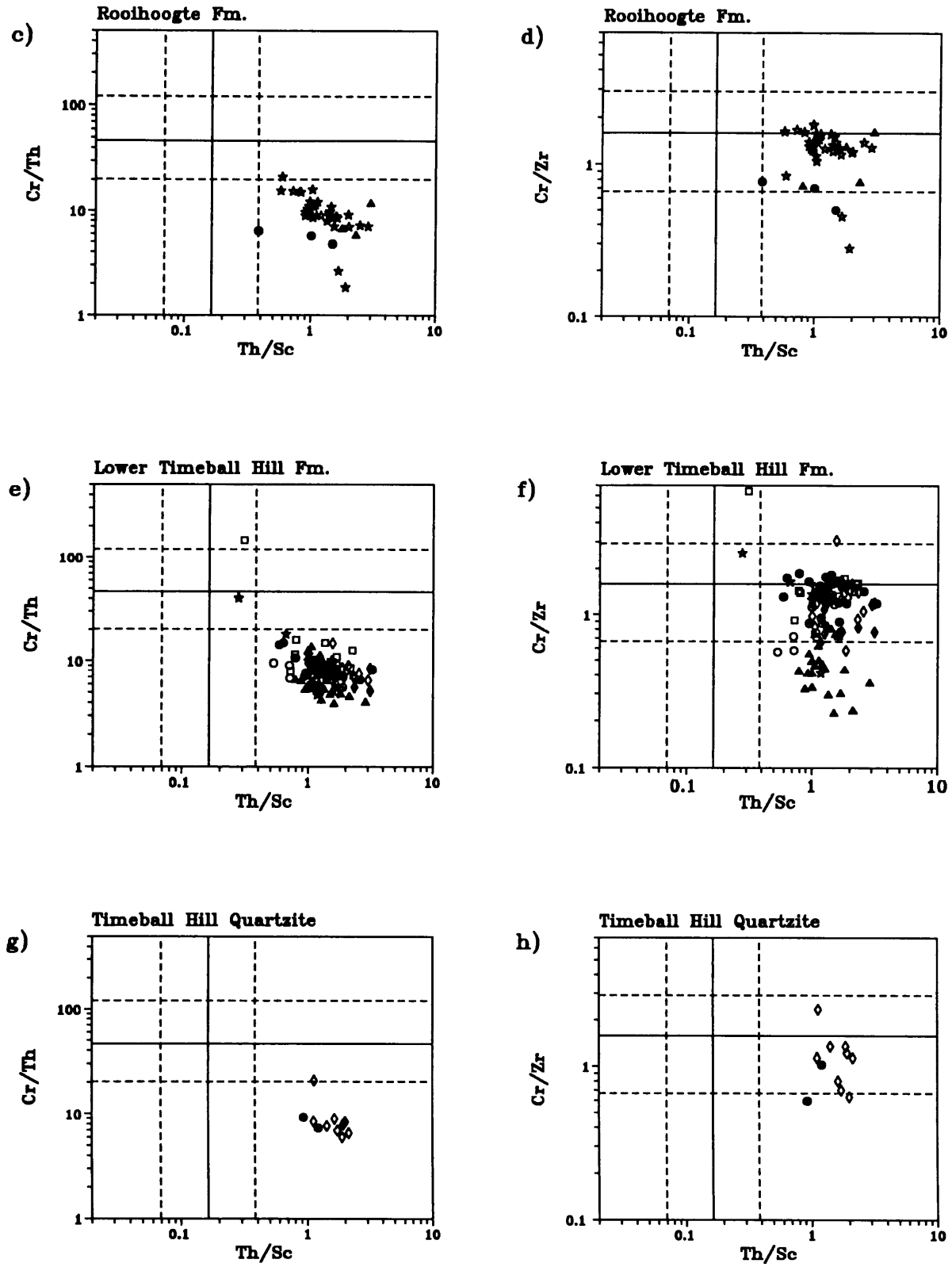

Fig. 4.1.4 a-z (continued): Th/Sc, Cr/Th and Cr/Zr discrimination diagrams of Pretoria Group argillites.

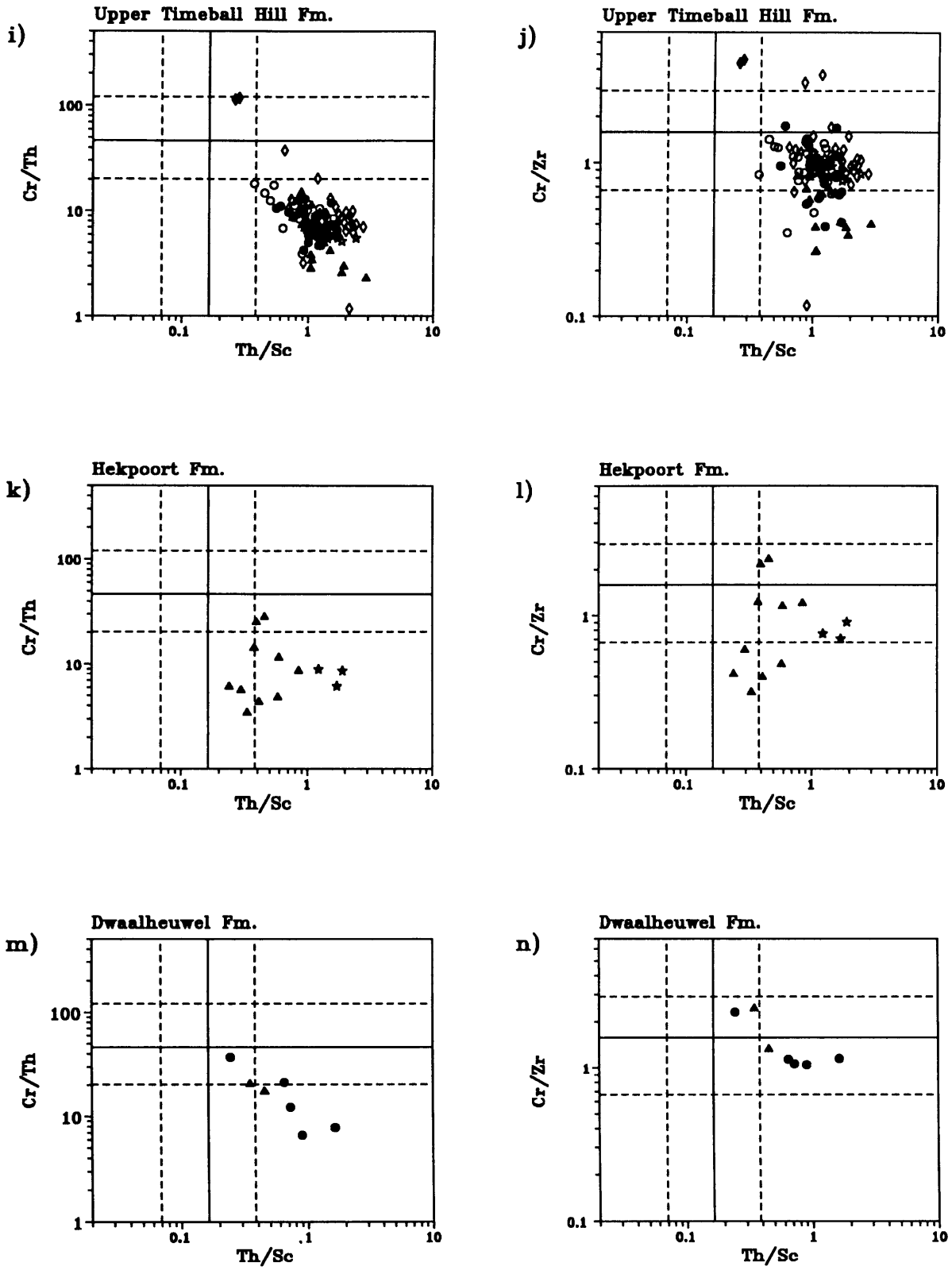

Fig. 4.1.4 a-z (continued): Th/Sc, Cr/Th and Cr/Zr discrimination diagrams of Pretoria Group argillites.

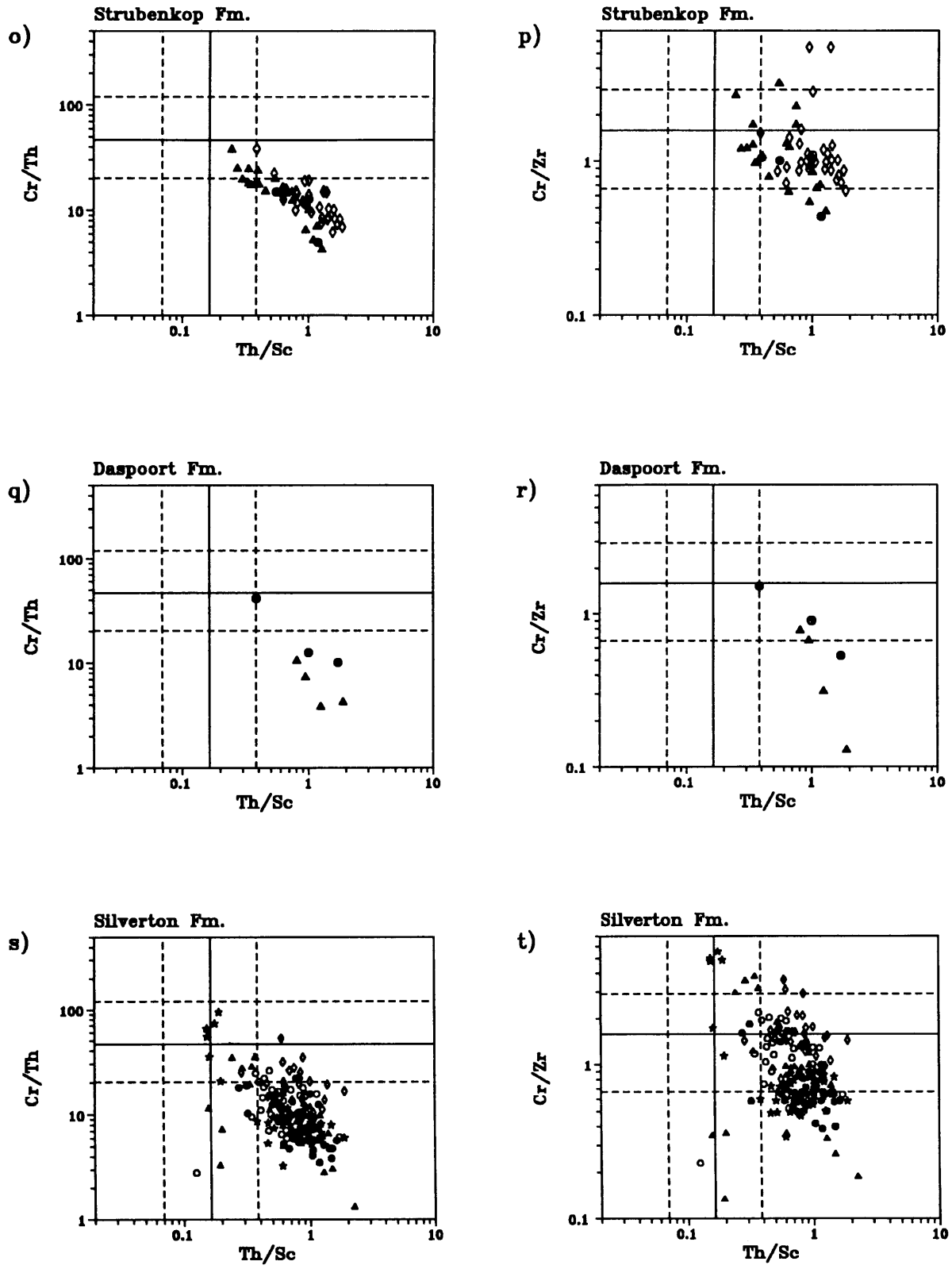

Fig. 4.1.4 a-z (continued): Th/Sc, Cr/Th and Cr/Zr discrimination diagrams of Pretoria Group argillites.

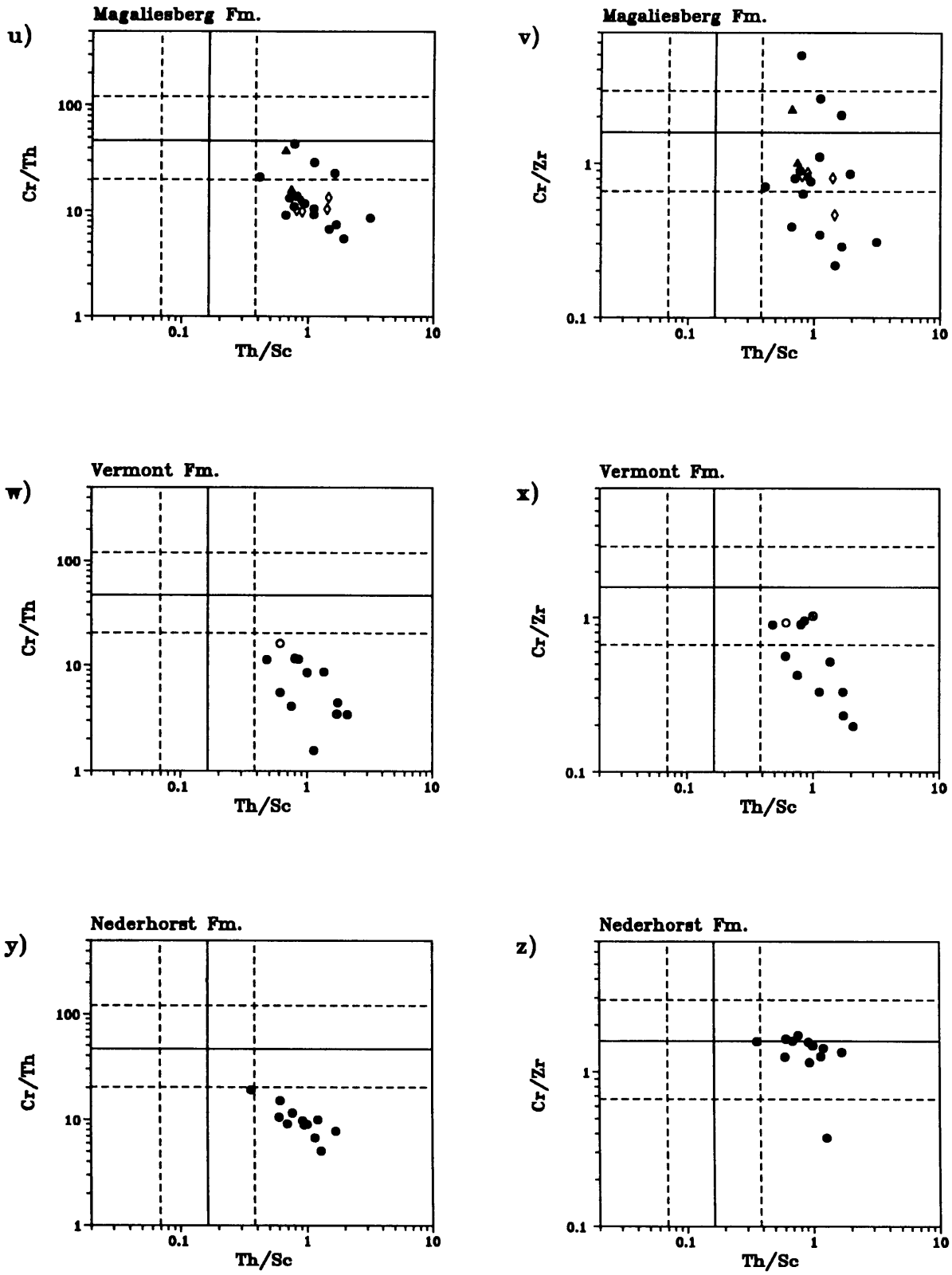

Fig. 4.1.4 a-z (continued): Th/Sc, Cr/Th and Cr/Zr discrimination diagrams of Pretoria Group argillites.

An estimation of the effects of mixing are shown for Cr/Th, Th/Sc and Cr/Zr in Table 4.1.1. The inferred effects of mixing felsic and mafic source materials are based on Archaean mafic and felsic end-member compositions proposed by Taylor and McLennan (1985). The good correlations between values given by Condie and Wronkiewicz (1990) for basalt and tonalite with the proposed end-member values in Table 4.1.1 are noteworthy. If non-linear development of ratios due to mixing, as illustrated here, is considered, the Cr/Zr-ratios reported by Schreiber et al. (1990) would rather infer a provenance with mafic contributions between 20 and 70 % for the Pretoria Group shales. Based on Table 4.1.1, fields of average provenance composition can be assigned to Th/Sc-Cr/Th and Th/Sc-Cr/Zr diagrams (Fig. 4.1.4 a-z). Pretoria Group argillites analysed in this thesis have Cr/Th and Th/Sc ratios falling into the felsic provenance field with less than 25 % mafic contribution, whereas Cr/Zr ratios show a greater variability with an average of 25 - 50 % mafic contribution (Fig. 4.1.4 c-z). It must be noted that the Cr/Zr-ratio generally shifts towards more felsic values from the base to the top of the Pretoria Group. The Silverton Formation shows a bimodal Cr/Zr-distribution with two more or less defined clusters lying close to the 25 % and 50 % mixing lines, respectively (Fig. 4.1.4 t).

An interpretation of significant mafic source rock contributions, averaging 25 - 50 %, based on the Cr/Zr-ratio is contradicted by Cr/Th and Th/Sc-ratios, which point to smaller contributions (< 25 %) from mafic sources. One possibility to explain the ambiguity of these ratio plots (Fig. 4.1.4 c-z) is preferential enrichment of Cr, Th and Sc compared to Zr. The enrichment or depletion of elements in Pretoria Group argillites and sandstones is compiled in Table 4.1.2, based on data given in Chapters 3.3 and 3.4. Wronkiewicz and Condie (1990) mention an enrichment of Th for Pretoria Group argillites compared to North American Shale Composite (Gromet et al., 1984). They propose a Th-rich granitic source to explain the enrichment of Th. However, Wronkiewicz and Condie (1990) fail to acknowledge an apparent increase of Cr and Sc for the same Pretoria Group shales, which can be inferred from their published averages. The combination of the enrichment of Cr, Sc and Th makes the interpretation of a high-Th granitic source somewhat arbitrary. The enrichment of Al_2O_3 and of trace elements thought to have a low mobility (e.g., Cr, Th and Sc) and the more or less strong depletion of alkali and alkali-earth elements and some mobile trace elements (e.g., Zn, Cu and Co) in Pretoria Group shales (Table 4.1.2), favour the incorporation of altered, i.e. weathered, material into the argillites. Mineralogical

	SHALE		SANDSTONE	
FORMATION	Enrichment	Depletion	Enrichment	Depletion
Vrs	(Si),(Fe) **Cr,Ba**,U,**Ni**,Th	**Ca,Na,** Sr,As	Fe,Zn,Cu,Ni,Mo,Nb, Cr,V,Ba,Sc,Co	Mg,Ca,Na,K Ga,Zr,Y
Vtl	Al Ga,U,Th,Cr	Mg,Ca,Na Co,Sr		
Vtq	Al,P,(Fe) Cr,Mo,Th,U,Ba	**Mg,Ca,Mn**,Na Zn,Ni,Co	Si Ni,Cr,Mo,Co	all maj. but Fe Zr,Y,Rb,B
Vtu	Al,Ga,U,Th (Cr),(Pb)	Ca,Mg,Na (Zn),(Cu),(Co)		
Vb			Zn,Cu,Pb,Co,U Ba,Mo,Cr,Ni	**Ca,Na**,Mg,K Zr,Y
Vh	**Al**,Ti,Cr,**Ni,V,Sc,** **Y,B**,U,Th,Ga	Si,Mg,Mn,Na Zn,Co,As,(Pb)		
Vdw	**Al**,Fe,**Cr**,Ni,Ga,U, Th,Rb,Pb,V,Ba,Sc	**Si,Ca**,Na,Mg Zn,Sr	(Si),**Cr,Nb,Mo,Ba** Ni,V,U	**Na,Ca** Zr,Y
Vst	Al,Fe,**Cr,Ni,** Ga,V,**Sc**,Th,U,Y	**Ca**,Na,Mg,Mn,Si,K Zn,Co,Rb,Sr		
Vdq	Si Zr,Cr,B,Mo	all maj., **Ca,Na** Zn,Co,Sr,Rb,Pb,V	**Si** **Cr**,Co,Mo,Nb	all maj, **Ca,Mg** Ga,Zr,Y,Rb
Vsi	Cr,Sc,B	(K) Cu,Co,Zr,Li,Sr		
Vm	Al,K,Cr,Zr,Ga,Y, Rb,U,Th,Ba	**Ca,Na**,Mg,P,Fe Zn,Cu,Ni,Co	Si,**Cr,Ni,Co**,Mo,Nb (Sc)	all maj., **Mg,Ca,** **Na**,Ga,Rb,Y,Zr,B
Vv	MgO U,Ba	Al,Ti,P,Fe Zn,Cu,Ni,Co,V		
Vlq			(Na),Cr,Ni,Co,Mo, Th,U,Ba,Sc	Ca,Fe,Ti,P Zn,Ga,Zr,Y,Rb
Vn	Ca,Mg (Cu),(Sb),(Sn)	Si,Ti,Al,Fe,Na **Zr**,**V**,Zn,Ni,Co	Si,Mg,Cr,Co,Mo,Th Ba,Sc,(Ni)	**Ti,Ca,Na**,Zn,Ga, Zr,Y,Sr,Rb,B
Vsq			**Si** Cr,Co,Mo,Nb,Th	all maj. but Mg Zn,Ga,Zr,Y,Rb, Pb
Vht			**Si** Cr,Mo	all majors,Zn, Ga,Zr,Y,Rb,B,Sr
Vry			(Si),Cr,Ni,Co,Mo Nb,Ba	Mg,Ca,Na Ga,Zr,Y,B
Pta. Group	Al Ga,Y,U,Th,Ba Cr,Sc,(?B)	Mn,Na,Ca,(K) (Mg),(Ti) Zn,Cu,Co,Sr,As	Fe,(Si), **Cr,Mo**,Ni,Co,V,Nb, Ba,?Sc,?U,?Th,?Sb	**Ca,Na** Ti,K,P,(Al) Ga,Zr,Y,Rb

Table 4.1.2: Enrichment/depletion trends of average element concentrations of Pretoria Group sedimentary rocks (compiled after Chapter 3.3 and 3.4) compared to average shale and sandstone estimates (Chapter 3.2). Bold: major enrichment/depletion; brackets: minor enrichment/depletion; ?: uncertain enrichment/depletion trend. Formation codes as in Table 3.1.5; Vb = Boshoek Formation, Vh = Hekpoort Formation, Vht = Houtenbek Formation.

Table 4.1.3a: Average element contents of the Hekpoort volcanics and the Hekpoort palaeosol. (1) Button 1979: Waterval Boven palaeosol; 2) Button 1973: Hekpoort lava from Waterval Boven; 3) Sharpe et al. 1983: Average Hekpoort volcanics from the eastern Transvaal. All Fe is reported as Fe_2O_3.

	ϕ Hekpoort Palaeosol[1)] n = 13, ETvl	Hekpoort Lava 1[2)], n = 1, ETvl	ϕ Hekpoort Lava 2[3)], n = 30, volatile free, ETvl	Hekpoort Palaeosol[1)], n = 13, volatile free, ETvl	Enrichment-factor: Palaeosol -> Lava 1	Enrichment-factor: vol.-free Palaeosol -> Lava 2
SiO_2	50.03	57.28	57.27	52.03	0.87	0.91
TiO_2	1.45	0.67	0.60	1.51	2.16	2.52
Al_2O_3	28.79	15.41	15.13	29.94	1.87	1.98
Fe_2O_3(t)	7.01	9.89	8.78	7.29	0.71	0.83
MnO	0.09	0.15	0.13	0.09	0.60	0.69
MgO	0.75	5.65	5.48	0.78	0.13	0.14
CaO	0.11	6.46	6.77	0.11	0.02	0.02
Na_2O	0.46	1.43	2.15	0.48	0.32	0.22
K_2O	7.42	1.39	1.14	7.72	5.34	6.77
P_2O_5	0.06	0.08	0.10	0.06	0.75	0.60
H_2O^-	0.37	0.29	-	-	1.28	-
LOI	4.59	1.90	-	-	2.42	-
Zn	21	n.d.	70	-	-	0.30
Cu	89	n.d.	61	-	-	1.46
Ni	153	n.d.	90	-	-	1.70
Zr	256	n.d.	123	-	-	2.08
Sr	57	n.d.	208	-	-	0.27
Rb	299	n.d.	64	-	-	4.67
Cr	152	n.d.	278	-	-	0.55
Ba	403	n.d.	236	-	-	1.71

components indicating strong alteration/weathering (e.g., kaolinite) are abundant in the shales (Chapter 3.1.6). The occurrence and preservation of palaeosols in the Pretoria Group (Button, 1979; Reczko et al., 1992) further point to the important role of weathering in the genesis of the Pretoria Group (see also Chapter 4.2).

The estimation of provenance of sedimentary rocks by geochemical means is complicated by the differences in mobility of the elements. Lelong et al. (1976) provide some data on the

Table 4.1.3b: Average element contents of the Tertiary Iceland-Faearoe palaeosol and its parent basalt. (1) Nilsen and Kerr (1978); all Fe is reported as Fe_2O_3; IFP = Iceland-Faeearoe palaeosol, PB = parent basalt, v-f = volatile-free.)

	ϕ Iceland-Faeroe Palaeosol[1] n=17	Parent Basalt[1] of IFP,n=1	ϕ IFP[1], recalc. volatile free	Parent Basalt[1] of IFP, recalc. v-f	Enrichment-factor: IFP -> PB	Enrichment-factor: IFP (v-f) -> PB (v-f)
SiO_2	42.35	48.40	49.72	50.52	0.88	0.98
TiO_2	2.64	1.00	3.10	1.04	2.64	2.98
Al_2O_3	18.28	15.60	21.46	16.28	1.17	1.32
Fe_2O_3(t)	16.81	9.97	19.74	10.41	1.69	1.90
MnO	0.06	0.17	0.07	0.18	0.35	0.39
MgO	1.65	7.10	1.94	7.41	0.23	0.26
CaO	1.37	11.30	1.61	11.80	0.12	0.14
Na_2O	1.75	2.10	2.06	2.19	0.83	0.94
K_2O	0.14	0.06	0.16	0.06	2.33	2.67
P_2O_5	0.12	0.10	0.14	0.10	1.20	1.40
H_2O^-	6.54	2.40	-	-	2.73	-
LOI	7.97	1.10	-	-	7.25	-
Zn	n.d.	n.d.	-	-	-	-
Cu	180	100	-	-	1.80	-
Ni	48	70	-	-	0.69	-
Zr	158	50	-	-	3.16	-
Sr	82	200	-	-	0.41	-
Rb	n.d.	n.d.	-	-	-	-
Cr	68	300	-	-	0.23	-
Ba	11	20	-	-	0.55	-

'average' mobility of ions and oxides in selected weathering environments, thus also showing relative differences in mobility due to climate and type of source rock for so-called 'immobile' elements like Cr. Valeton (1988) compares boehmite-bauxite and diaspore-bauxite; both are products of extreme weathering, thereby indicating a preferential enrichment of Cr compared to Th in the diaspore-bauxite as opposed to the boehmite-bauxite. However, Th is enriched compared to Cr in diagenetically recrystallized, redeposited kaolinite-rich soils (flint clay facies) as opposed to redeposited kaolinite-rich soils (laterite derived facies), with absolute enrichment of both Cr and Th in the flint clay facies (Valeton, 1988). Preferential enrichment of Cr compared to Th and Sc is inferred for the Proterozoic

metasediments of the Wanni and Highland Complexes from Sri Lanka (Prame and Pohl, 1994). Condie and Wronkiewicz (1990) interpret the enrichment of Cr/Th of Pretoria Group shales compared to the estimated ratio of the upper continental crust (ϕ 3 -5), as reflecting preferential enrichment of Cr caused by adsorption of Cr on clay minerals during weathering or deposition. A further cause of distortion in the application of Cr and Zr as source rock indicator elements is the possible incorporation of chromite and/or zircon as a heavy mineral phase into the sediment (Laskowski and Kröner, 1985).

An estimation of preferential enrichment of either Cr, Th, Sc and/or Zr is difficult to obtain for Precambrian sedimentary rocks. Table 4.1.3 a compares the geochemistry of the Waterval Boven palaeosol at the top of the Hekpoort Formation (Button, 1979) with Hekpoort volcanics from the Waterval Boven district (Button, 1973) and from the broader eastern Transvaal region (Sharpe et al., 1983). The enrichment factors, defined by average element concentration of the palaeosol divided by the average concentration of the volcanics, give the following enrichment/ depletion order:

ENRICHMENT		STABLE		DEPLETION
K > > Ti > Al	<--	Si > Fe	-->	P, Mn > Na > Mg > Ca
Rb > > Zr > Ba, Ni > Cu	<--		-->	Cr > Zn > Sr

The surprisingly strong enrichment of potassium is seen in nearly all Precambrian and many Palaeozoic palaeosols (Retallack, 1986), and is explained by either diagenetic enrichment due to illitization of clay minerals with depth (Retallack, 1986), or by the lack of vascular land plants, which deplete the soil of potassium (Weaver, 1969). The slight depletion of iron is to be expected, if the simplified weathering model of Holland (1984) is applied to the Waterval Boven palaeosol. As a diabase sill immediately overlies the palaeosol profile (Retallack and Krinsley, 1993), the enrichment of Ni, Ba and Cu might be of a secondary nature (see Chapter 3.3.8). Nevertheless, the depletion of Cr is enigmatic and unexpected, considering the low mobility of Cr in a lateritic weathering environment (e.g., Valeton, 1988; Guilbert and Park, 1986).
Table 4.1.3 b gives the geochemistry of a Tertiary in-situ laterite and its parent basalt (Nilsen and Kerr, 1978). The ensuing enrichment/depletion order is:

ENRICHMENT		STABLE		DEPLETION
Ti > K > Fe	<--	P > Al > Si > Na	-->	Mn > Mg > Ca
Zr > Cu	<--		-->	Ni > Ba > Sr > Cr

The Tertiary laterite depicts a similar enrichment/depletion order to the Waterval Boven palaeosol, with exception of Na, which seems to more stable in the Tertiary laterite, and Ni and Ba, which are depleted instead of enriched. Ti is significantly more enriched than Al in both palaeosols. Zr shows relatively strong enrichment in both palaeosols. Cr is even more depleted in the Tertiary laterite than in the Waterval Boven palaeosol.

It is not intended here to propose a general depletion of Cr under extreme weathering conditions, or in the particular case of weathering conditions in the Precambrian. The two case studies of enrichment/depletion trends were undertaken to emphasize the necessity of considering preferential enrichment and/or fractionation of source rock indicator elements used in this and other studies. Even if the relative insensitivity of certain elements , e.g., Cr, Th, Sc and Zr, to weathering, alteration and metamorphism is correct (e.g., Condie and Wronkiewicz, 1990), i.e., if these elements show a corresponding enrichment/depletion trend, the preservation of the primary source rock ratios would further presuppose an approximately equal degree of enrichment/depletion of these elements. The latter prerequisite is difficult to test, as, (1) the climate influences the relative degree of mobility, i.e., degree of enrichment/depletion of the respective element (Lelong et al.,1976); (2) the mobility of elements depends on source rocks and host minerals; and (3) the type and length of weathering of a specific source rocks is essentially unknown, especially for the Precambrian. Further distortions of the primary source rock ratios can be caused by enrichment due to flocculation of clay minerals with adsorption of Cr during weathering or deposition, or by the introduction of detrital heavy minerals into the sediment (see discussion above).

A superficial test of preferential enrichment of Cr, Th, Sc and Zr in Precambrian sedimendary rocks can be performed, if the ratios of Cr/Th, Cr/Zr and Th/Sc are calculated from Archaean Average Shale (Taylor and McLennan, 1985; Table 3.2.1d) and are compared to the crustal composition of the Archaean, which is thought to be represented by a composition with a 1 : 2 ratio of felsic and mafic end-members (Taylor and McLennan,

Table 4.1.4: Corrected felsic-mafic mixing ratios for Cr/Th, Th/Sc and Cr/Zr.

(Calculated from Archaean mafic and felsic end-member compositions inferred by Taylor and McLennan (1985, p. 181); correction based on 1:2 felsic-mafic composition of Average Archaean Crustal Composition (Taylor and McLennan, 1985) and on the inferred preferential enrichment of Zr and Th over Cr and Sc in Archaean Average Shale compared to Average Archaean Crustal Composition (see text). Archaean Average Shale: Cr 205 ppm, Sc 20 ppm, Th 6.3 ppm, Zr 120 ppm (Taylor and McLennan, 1985).)

Mixing ratio Felsic : Mafic	Cr/Th	Th/Sc	Cr/Zr
0 : 100	164	0.06	4.9
10 : 90	85	-	3.4
20 : 80	54	-	2.5
25 : 75	44	0.22	2.2
30 : 70	37	-	-
33.3 : 66.6	32.5	0.32	1.70
40 : 60	26.2	-	1.42
50 : 50	18.7	0.54	1.07
60 : 40	13.5	-	0.79
66.6 : 33.3	10.7	0.91	0.64
70 : 30	9.5	-	0.57
75 : 25	7.9	1.23	0.48
80 : 20	6.4	1.48	0.39
90 : 10	4.0	2.55	0.24
100 : 0	1.8	4.28	0.11

1985). From this test, it emerges that the Cr/Th (32.5), Th/Sc (0.32) and Cr/Zr (1.71) ratios of Archaean Average Shale (Taylor and McLennan, 1985) would have to be interpreted as having mafic contributions between 30 % (Th/Sc) and 60 % (Cr/Zr) according to Table 4.1.1. The ratios thus indicate a more felsic composition than that proposed by Taylor and McLennan (1985). Hence, a preferential enrichment of Th and Zr over Cr and Sc could be inferred for the Archaean, presupposing that the estimations of Archaean crustal composition, felsic and mafic end-member composition and Average Archaean Shale are correct. It must

be acknowledged, however, that the calculation of ratios from average estimates is problematic. Taylor and McLennan (1985) report only the average Th/Sc-value of Archaean Average Shale (Table 3.2.1e). However, the Th/Sc average of Archaean Average Shale (ϕ 0.43) is higher than the ratio calculated from the average element contents, thus indicating an even more pronounced felsic provenance contribution for Archaean Average Shale. Nevertheless, the differences in interpretation of the actual Th/Sc-average and the calculated average are negligible, i.e., both averages point to source rocks with more than 20 % and less than 30 % mafic contribution. The geochemistry of the Archaean Pongola Supergroup and Lower Transvaal Sequence argillites (Wronkiewicz and Condie, 1990) seems to confirm a preferential enrichment of Th over Cr, if mafic and ultramafic sources are concluded (Wronkiewicz and Condie, 1990). The enrichment factor of Th ($\approx$ 8) compared to the Archaean mafic end-member composition exceeds the enrichment factor of Cr ($\approx$ 3) significantly.

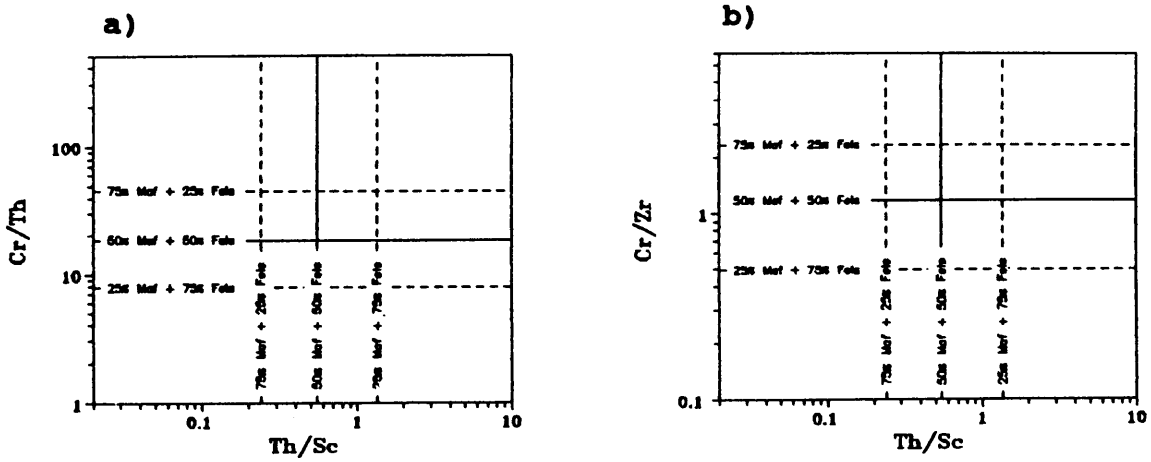

Fig. 4.1.5 a-z: Th/Sc, Cr/Th and Cr/Zr discrimination diagrams of Pretoria Group argillites. Symbols for sampling areas: ● = eastern Transvaal; ○ = northeastern Transvaal; □ = eastern fragments; ◇ = central Transvaal; ▲ = western Transvaal, western fragments and northwestern Transvaal; ★ = Botswana. Definition of sampling areas is shown in Fig. 1.5.1. Figures 4.1.5 a and b define fields for provenance composition by using the 'corrected' mixing ratios of Table 4.1.4; Pretoria Group shales are shown in Figures 4.1.5 c-z.

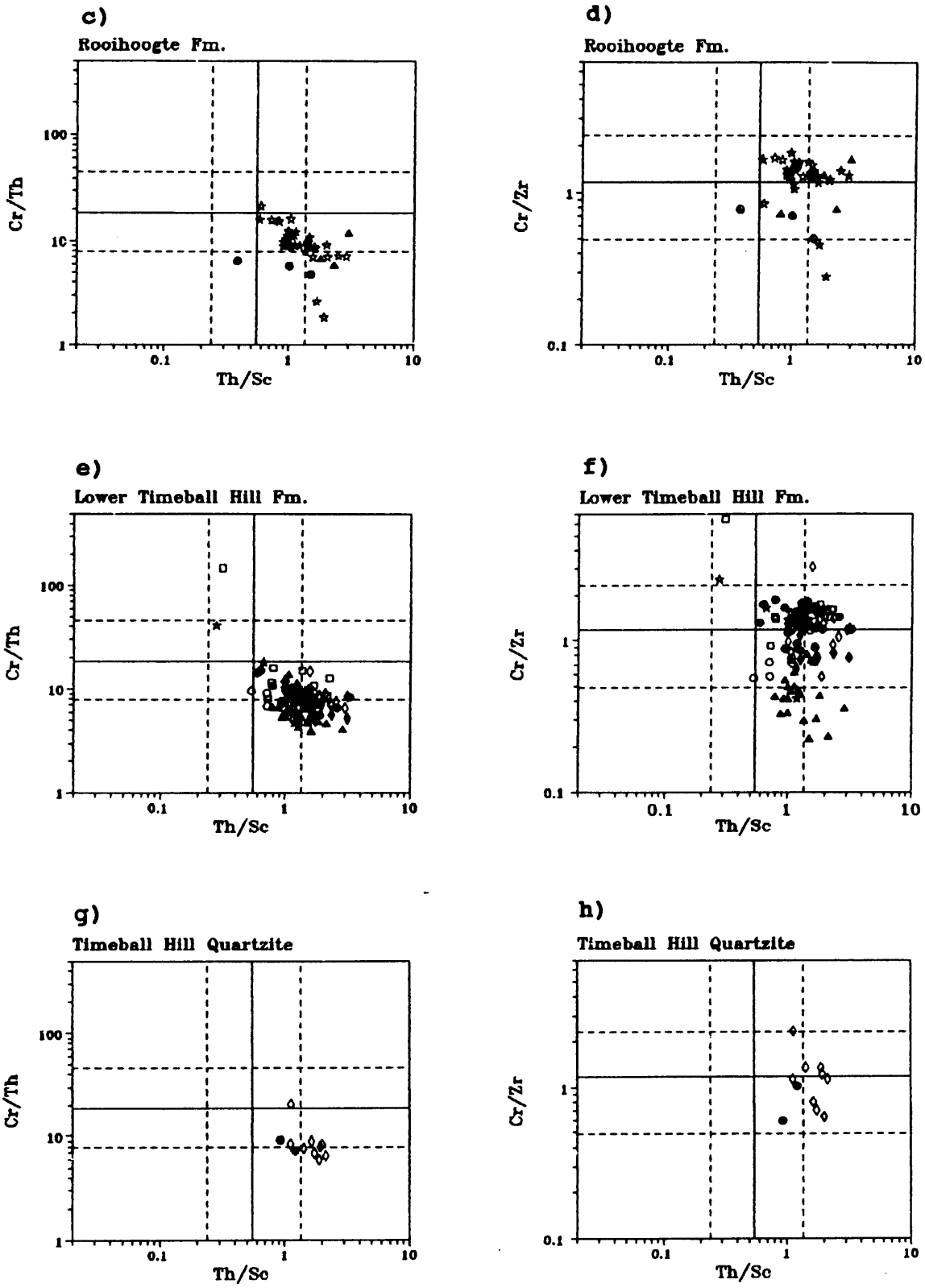

Fig. 4.1.5 a-z (continued): Th/Sc, Cr/Th and Cr/Zr discrimination diagrams of Pretoria Group argillites.

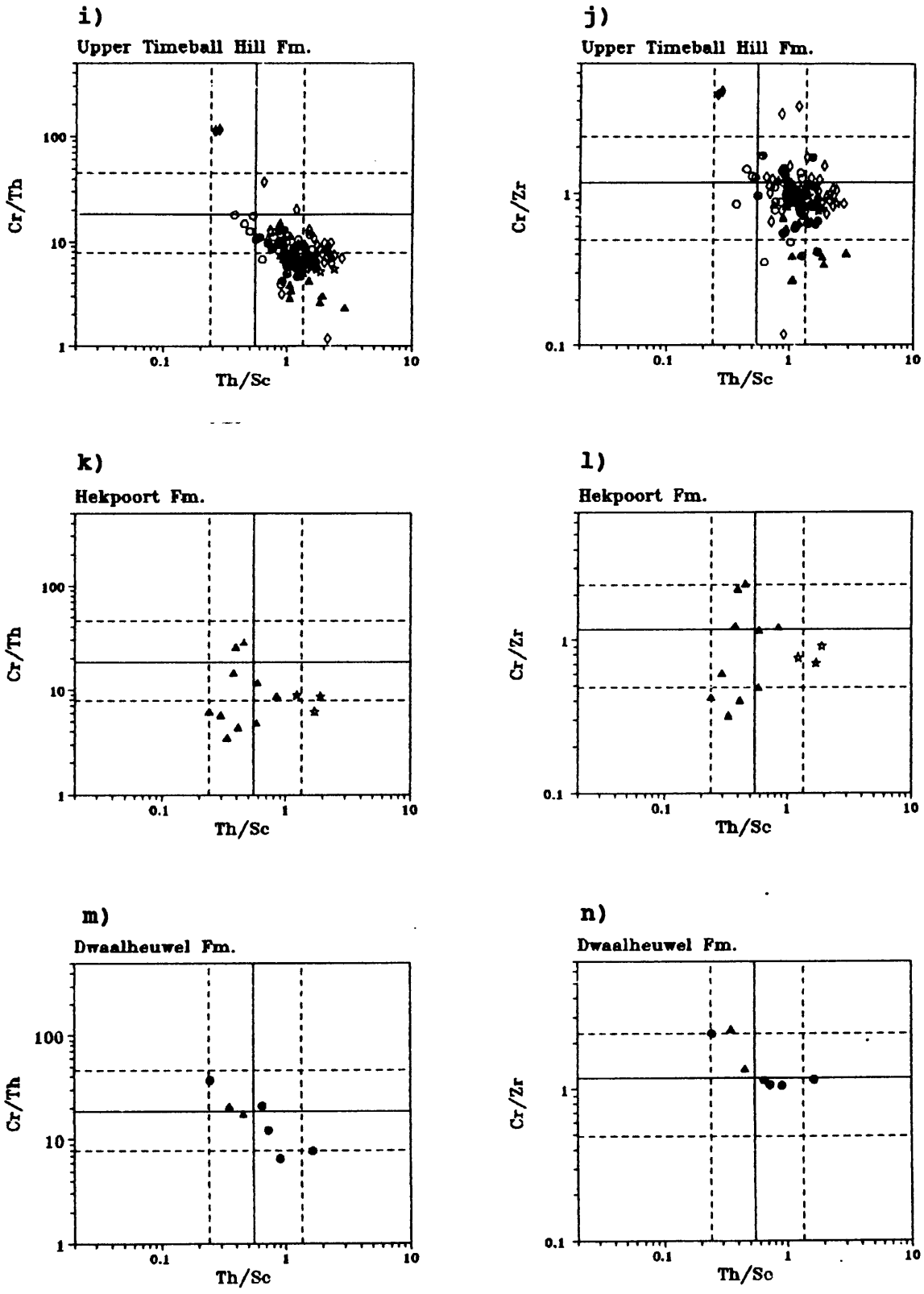

Fig. 4.1.5 a-z (continued): Th/Sc, Cr/Th and Cr/Zr discrimination diagrams of Pretoria Group argillites.

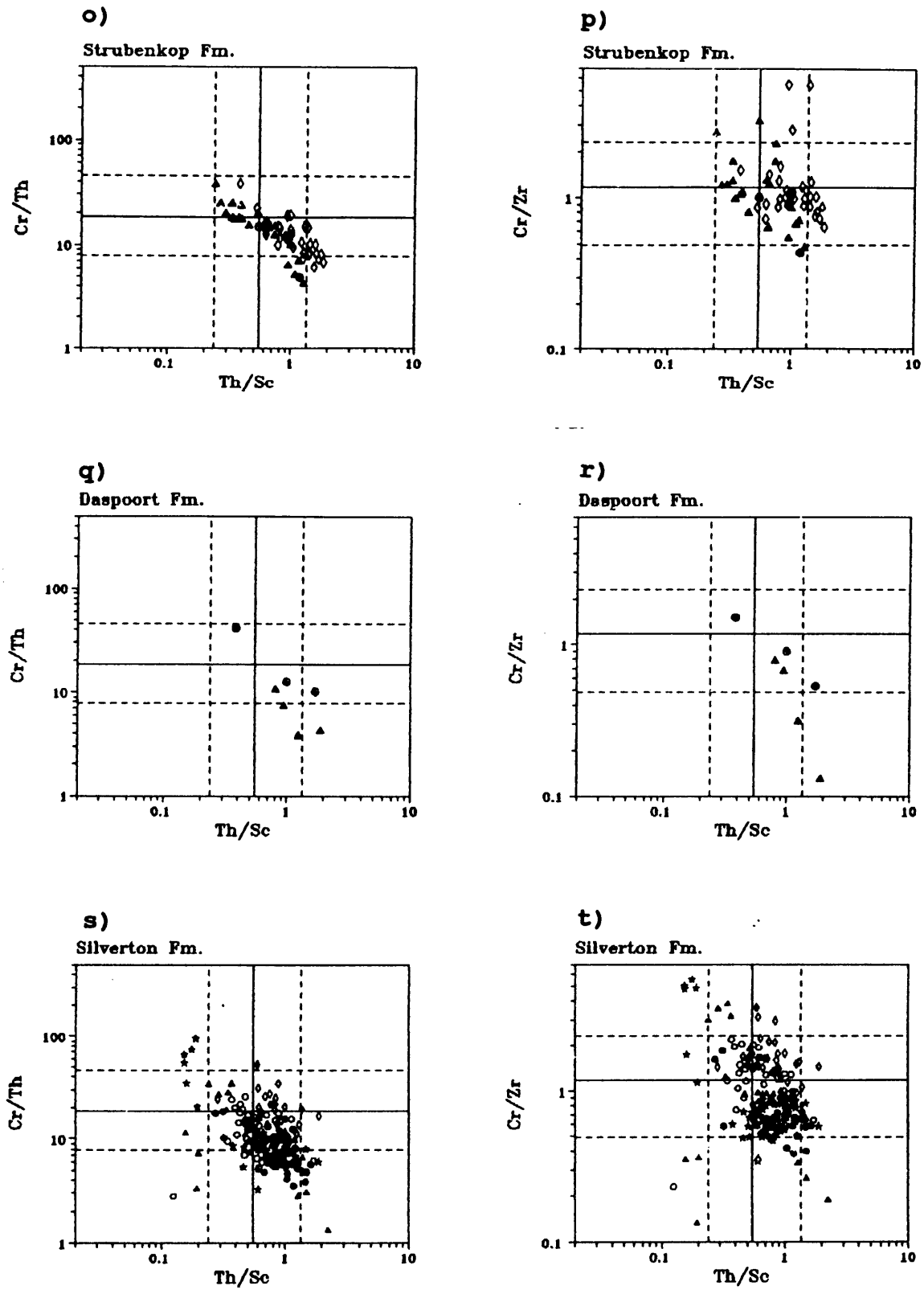

Fig. 4.1.5 a-z (continued): Th/Sc, Cr/Th and Cr/Zr discrimination diagrams of Pretoria Group argillites.

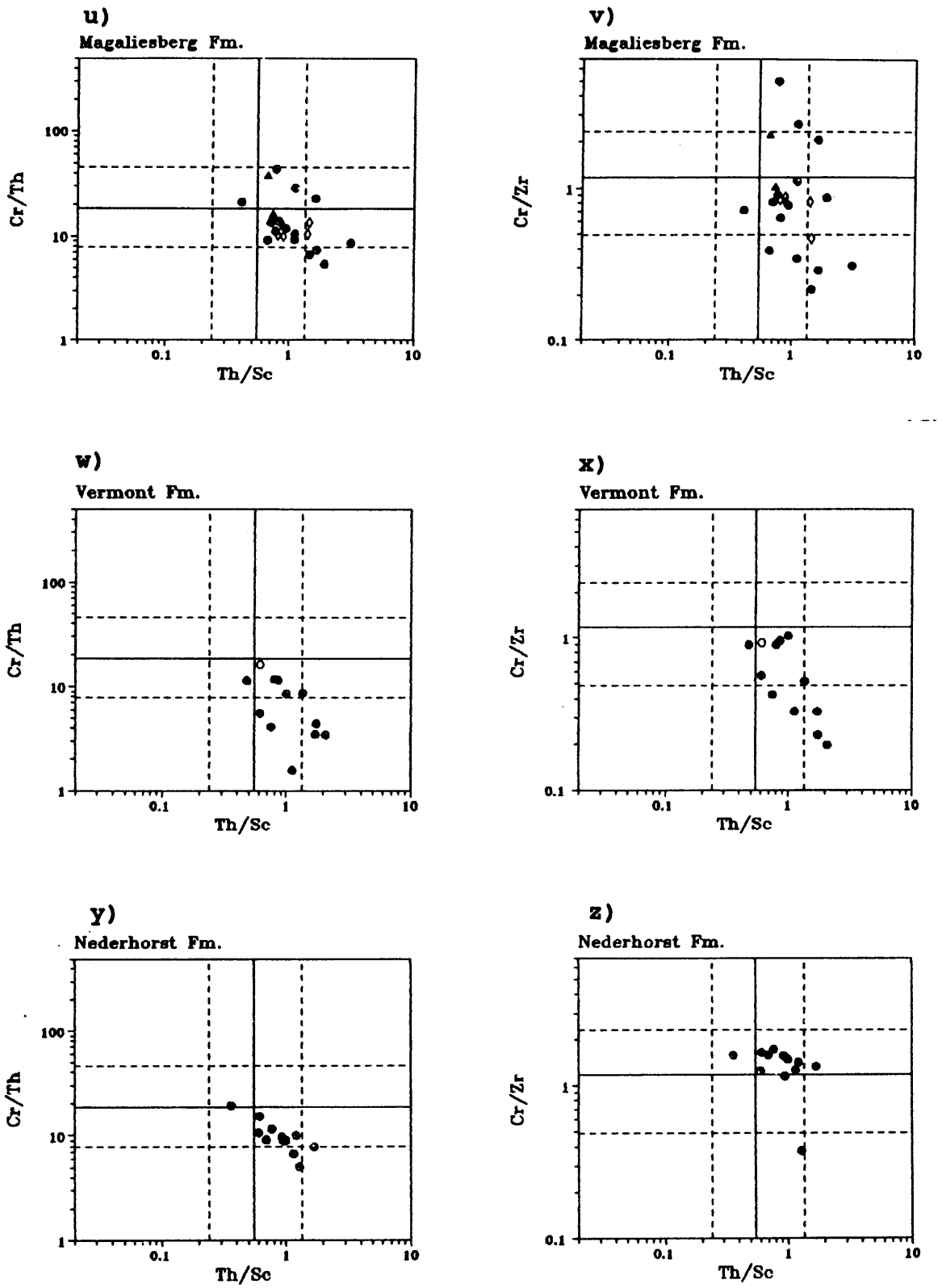

Fig. 4.1.5 a-z (continued): Th/Sc, Cr/Th and Cr/Zr discrimination diagrams of Pretoria Group argillites.

Table 4.1.4 lists corrected felsic-mafic mixing ratios, based on the assumption that the preferential enrichment of Th and Zr over Cr and Sc is expressed by the relationship of Archaean crustal composition and Archaean Average Shale (Taylor and McLennan, 1985). The new provenance mixing-ratios can be used for the development of redefined Th/Sc-Cr/Th and Th/Sc-Cr/Zr provenance classification diagrams (Fig. 4.1.5 a and b). An application of these two classification plots to Pretoria Group argillites (Fig. 4.1.5 c-z) shows a significant improvement in the internal correlation of the plots compared to the earlier classification plots (Fig. 4.1.4 a-z). However, some doubts concerning reliability remain, due to the ambiguity of the plots for the Rooihoogte, Lower Timeball Hill and Nederhorst Formations (Fig. 4.1.5 c,d,z).

The application of both uncorrected and corrected provenance classification diagrams to Pretoria Group volcanic rocks (Fig. 4.1.6 a-d) illustrates an excellent agreement of the corrected mixing ratios (Fig. 4.1.6 c and d) with results obtained from the classification diagrams of Le Maitre (1984) and Winchester and Floyd (1979) (Fig. 3.4.2.1 a and b), but patterns are distorted for the uncorrected mixing ratios (Fig. 4.1.6 a and b). This result is somewhat surprising, as a reverse relationship would be expected. It should be emphasized that the hypothesis of predominantly mafic and ultramafic source rocks for the Pongola Supergroup and the Lower Transvaal sequence argillites (Condie and Wronkiewicz, 1990) is confirmed by the corrected classification diagrams, but has to be rejected for the uncorrected mixing ratios.

The provenance of Pretoria Group sandstones is discussed by Schreiber et al. (1991) in some detail. Mainly based on petrographic evidence like heavy mineral content, relative potassium feldspar and plagioclase contents, grain size and shape of mineral constituents, Schreiber et al. (1991) suggest derivation of the Pretoria Group sandstones from the Archaean basement of the Kaapvaal craton and from second cycle sedimentary sources. Penecontemporaneous volcanic sources and an increase of reworked older sedimentary rocks are thought to be of some importance during Pre-Magaliesberg times (Schreiber et al., 1991).

The Pretoria Group sandstones are depleted in Zr and strongly enriched in Cr (Table 4.1.2). A predominantly granitic provenance of the sandstones is not compatible with this

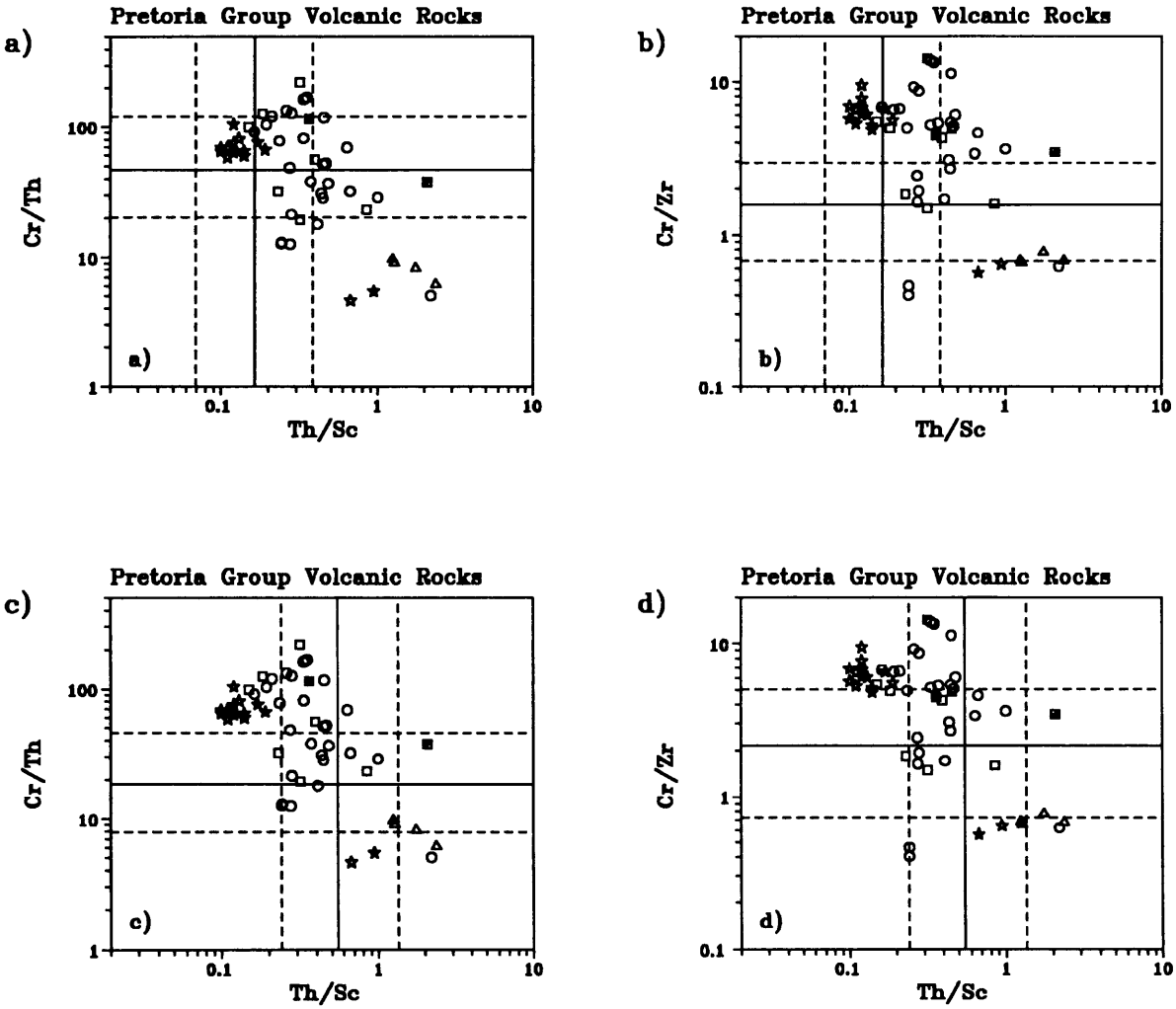

Figure 4.1.6 a-d: Th/Sc, Cr/Th and Cr/Zr discriminance diagrams applied to volcanic rocks of the Pretoria Group. Figure 4.1.6 a and b: discriminant fields after Fig. 4.1.4 a and b ('uncorrected' ratios); Figure 4.1.6 c and d: discriminant fields after Fig. 4.1.5 a and b ('corrected' ratios). Symbols: ★ = Machadodorp volcanics; □ = high-Al-K volcanic rocks from the Hekpoort Fm.; ○ = Hekpoort lavas; ■ = Timeball Hill Fm. tuffs.

enrichment/depletion pattern. The positive correlation of SiO_2 and Cr in the sandstones (Chapter 3.1.5) suggests an addition of Cr in detrital form, possibly as chromite. The occurrence of chromite is restricted to mafic and ultramafic igneous rocks (Schröcke and Weiner, 1981). Chromite is resistant to the effects of weathering (Schröcke and Weiner, 1981). Cr-rich quartzites from the Archaean Prince Albert Group at Laughland Lake, Canada, are interpreted as containing weathered residual material from ultramafic rocks (Henderson and Schau, 1983). As is the case with the Pretoria Group sandstones, the Cr-rich Prince Albert Group sandstones are enriched in Ni, a further indication of mafic provenance contributions (Laskowski and Kröner, 1985; Taylor and McLennan, 1985). The comparatively high Cr-content of conglomerates (see Chapter 3.4.1.3) is a further strong indication that mafic and/or ultramafic source rocks have contributed material, at least locally.

The application of Roser and Korsch's (1988) classification diagram to Pretoria Group sandstones (Fig. 4.1.7 A-L) indicates a provenance mainly consisting of recycled sedimentary sources (P4-field), with minor contributions from mafic sources in the lower part of the Pretoria Group ($P1^{EXT}$-field). The fields occupied by comparable argillites (Fig. 4.1.3 a-i) and sandstones (Fig. 4.1.7 A-L) are slightly different, with exception of the Timeball Hill Quartzite (Klapperkop Member), which exhibits significant differences for sandstones compared with shales (Fig. 4.1.3c and 4.1.7b). These small differences in inferred provenance of penecontemporaneous sandstones and argillites indicated by the classification diagrams of Roser and Korsch (1988) might be due to transport fractionation of clay and sand-sized material.

The influence of transport fractionation on the resulting geochemistry of shale-sandstone assemblages was adressed by van de Kamp et al. (1976), Swayer (1986) and, more recently, Garcia et al. (1991). The latter were successfully able to apply Al_2O_3-Zr-TiO_2 ternary diagrams to demonstrate the influence of transport fractionation for Palaeozoic shale - sandstone/greywacke assemblages with granitic provenances. The fractionation of Zr in the transport process is thought to be reflected by an enrichment of Zr, relative to Al_2O_3 and TiO_2, in the sandstone/greywackes compared to the shales, and by a linear dependency of associated shale - sandstone/greywacke assemblages in the Al_2O_3-Zr-TiO_2 ternary diagram. Garcia et al. (1991) based their approach on three basic assumptions, apart from the

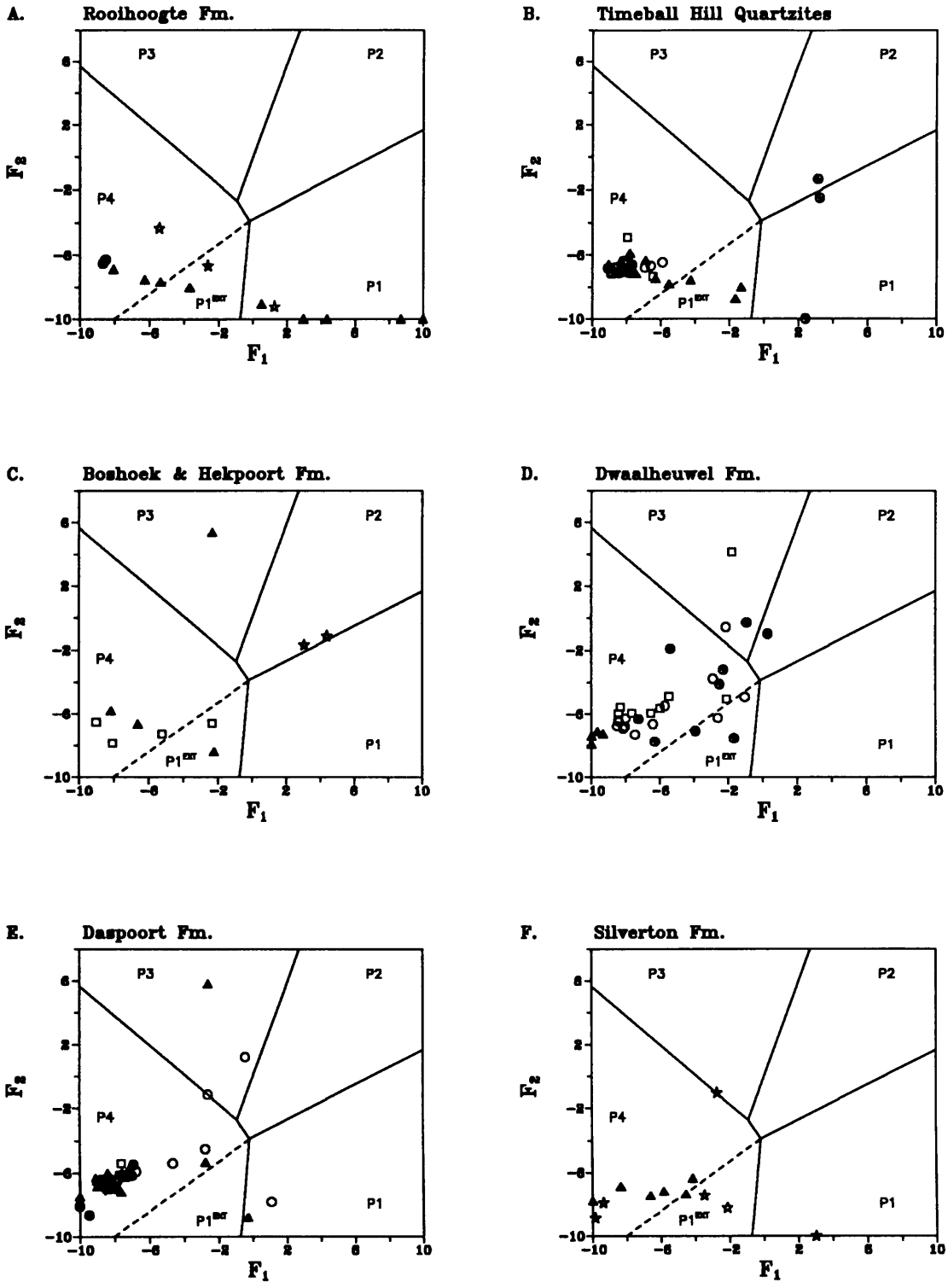

Fig. 4.1.7 A-L: Discriminance plots of Pretoria Group sandstones after Roser and Korsch (1988). Sandstones were recalculated to 100 % volatile-free before the discriminant function was applied. P_1: mafic provenance (P_1^{EXT} mafic provenance with high concentrations of Fe_2O_3* and MgO in the sample); P_2: intermediate provenance; P_3: felsic provenance; P_4: recycled sedimentary. Symbols represent sampling areas: ● = eastern Transvaal; ○ = northeastern Transvaal; □ = eastern fragments; ◇ = central Transvaal; ▲ = western Transvaal, western fragments and northwestern Transvaal; ★ = Botswana. Definition of sampling areas is shown in Fig. 1.5.1.

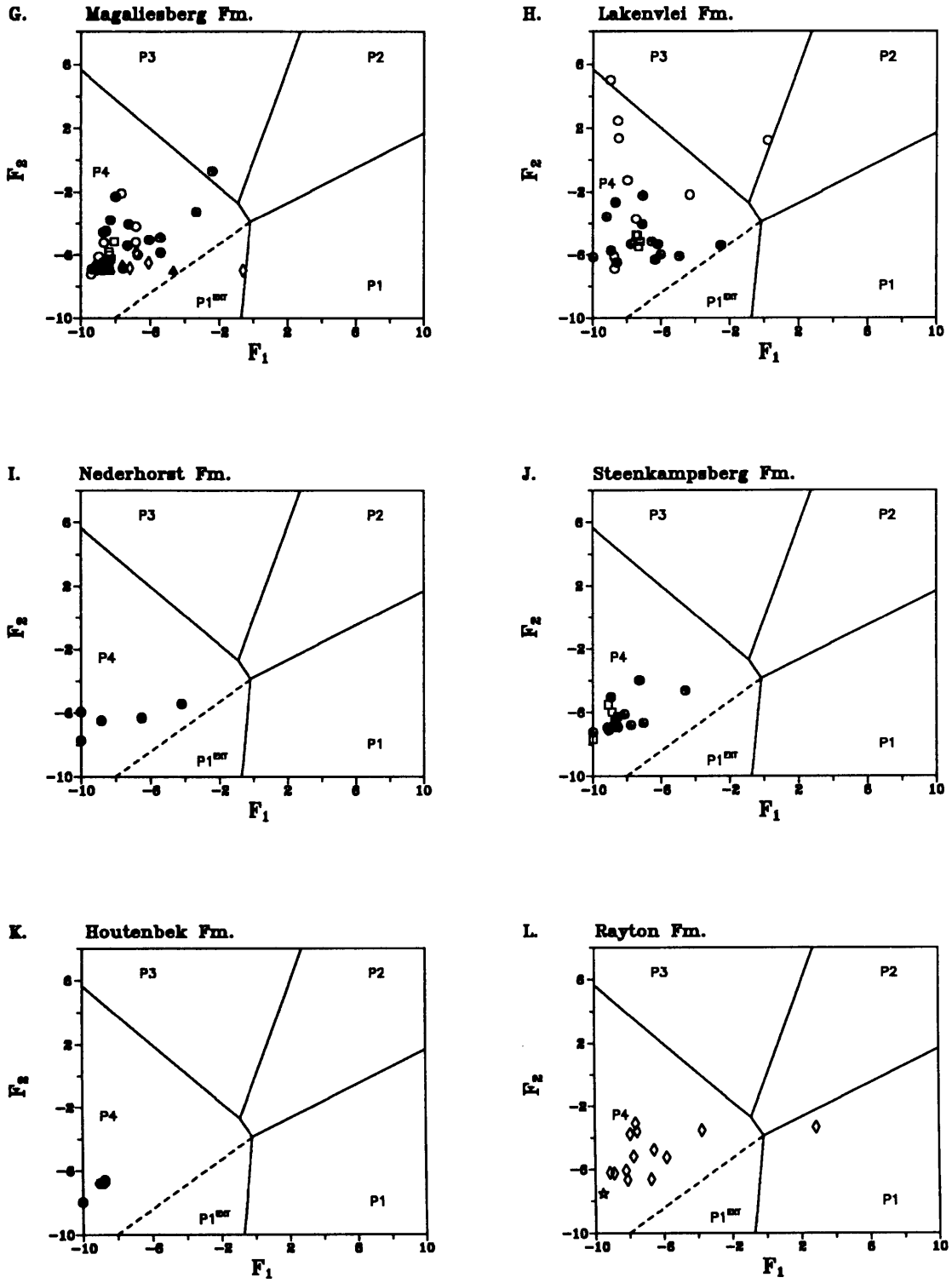

Fig. 4.1.7 A-L (continued): Discriminance plots of Pretoria Group sandstones after Roser and Korsch (1988).

prerequisite of immobility of Al, Ti and Zr in the weathering process: (1) a fractionation of zircon in the sedimentary process leads to the enrichemnt of Zr in the heavy mineral fraction of sandstones; (2) weathering processes enrich TiO_2 in the clay fraction and (3) the degree of fractionation between TiO_2 and Zr depends on the maturity of the resulting sedimentary assemblage. These assumptions are questionable for mafic source rocks, which can exhibit a positive correlation of TiO_2 and Zr (Merkle and v. Gruenewaldt, 1986). Figure 4.1.8 A-F shows Al_2O_3-Zr-TiO_2 ternary diagrams of associated Pretoria Group shale-sandstone assemblages. The plots of Rooihoogte and Magaliesberg Formations and Timeball Hill Quarzites (Fig. 4.1.8 A,B,E) point to transport fractionation of Zr to a certain degree. The influences of transport sorting are spurious or ambiguous for the combined Dwaalheuwel-Strubenkop and Vermont-Lakenvlei Formations and have to be rejected for the Daspoort Formation. More or less variable patterns within Al_2O_3-Zr-TiO_2 plots can be inferred to reflect: (1) rapid accumulation of the sedimentary assemblage and/or (2) simultaneous contribution of different sources and/or (3) a higher number of sorted sedimentary end-members (Garcia et al., 1991). A further complication occurs for sandstone- shale/greywacke assemblages, which have higher or similar Al_2O_3/TiO_2-ratios in sandstones to those in shales (Garcia et al., 1991). As the Pretoria Group sandstones generally have higher Al_2O_3/TiO_2-ratios than their compatible shales (Fig. 3.4.3.1d, Table 3.4.1.5), some distortion in the Al_2O_3-Zr-TiO_2 pattern must be expected for Pretoria Group shale - sandstone assemblages. However, the simultaneous contribution of different sources inferred by the corrected Th/Sc-Cr/Th and Th/Sc-Cr/Zr classification diagrams (Fig. 4.1.5 A-Z) might have had an effect as well.

The fractionation of Cr during the transport process can be tested with Al_2O_3-Cr-TiO_2 diagrams shown in Figure 4.1.9 A-F. The relationship of Cr in the Pretoria Group sandstone-shale assemblages is similar to the Zr-relationships in the Palaeozoic sandstone-shale assemblages described by Garcia et al. (1991), i.e., a relative enrichment in the sandstones of the respective element. For this reason, the application of Al_2O_3-Cr-TiO_2 plots of Pretoria Group shale-sandstone assemblages was thought to provide some information on the hypothesis of the presence of detrital chromite in the sandstones (see above). The Al_2O_3-Cr-TiO_2 diagrams show an apparent fractionation trend for Rooihoogte and Magaliesberg Formations and for the Timeball Hill Quartzite Member (Fig. 4.1.9 A,B,E). The pattern of

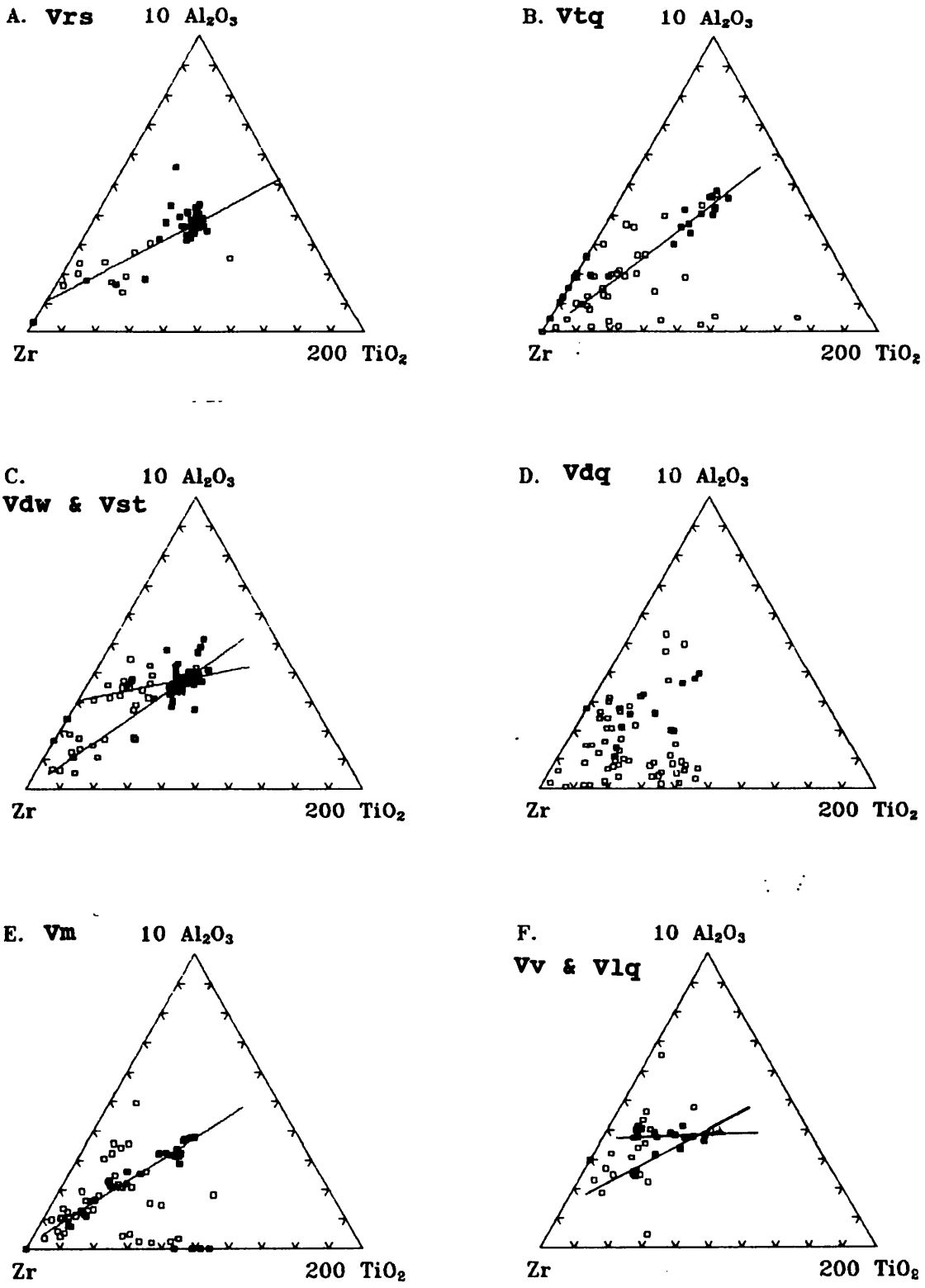

Fig. 4.1.8 A-F: Al_2O_3-Zr-TiO_2 ternary diagram for shales and sandstones after Garcia et al. (1991). Symbols: ■ = shales; □ = sandstones. A. = Rooihoogte Fm.; B. = Timeball Hill Quartzite (Klapperkop Member); C. = Dwaalheuwel and Strubenkop Fms.; D. = Daspoort Fm.; E. = Magaliesberg Fm.; F. = Vermont and Lakenvlei Fms.. Lines show inferred sandstone-shale relationship.

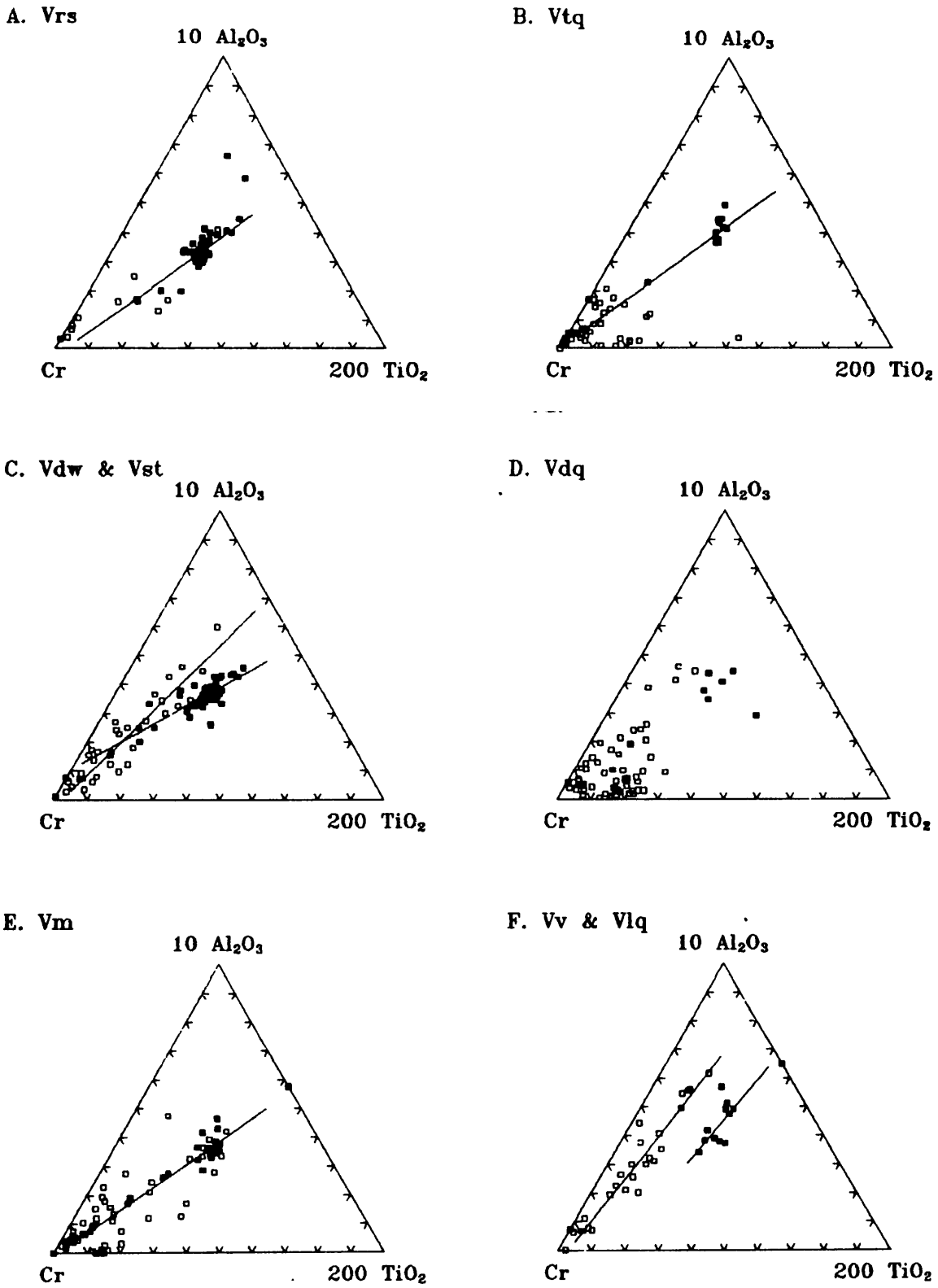

Fig. 4.1.9 A-F: Al_2O_3-Cr-TiO_2 ternary diagram for shales and sandstones. Symbols: ■ = shales; □ = sandstones.

A. = Rooihoogte Fm.; B. = Timeball Hill Quartzite (Klapperkop Member); C. = Dwaalheuwel and Strubenkop Fms.; D. = Daspoort Fm.; E. = Magaliesberg Fm.; F. = Vermont and Lakenvlei Fms.. Lines show inferred sandstone-shale relationship.

the combined Dwaalheuwel-Strubenkop association points to a relation of sandstones and shales, although the presence of two trends complicates the interpretation. The Dwaalheuwel and Strubenkop Formations are thought to be facies equivalents (Eriksson et al., 1993). A slight change in source rocks and/or a change in the accumulation rate can be inferred from this Dwaalheuwel - Strubenkop Al_2O_3-Cr-TiO_2 plot (Fig. 4.1.9 C). The Daspoort Formation sandstones scatter without revealing any apparent trend (Fig. 4.1.9 D). The Al_2O_3-Cr-TiO_2 plot of the combined Vermont-Lakenvlei association shows two distinct trends, for shales (Vermont Fm.) and sandstones (Lakenvlei Fm.), thus emphazising a genetic difference between the two formations. The Lakenvlei Formation contains highly feldspathic sandstones indicative of rapid accumulation. It is thus concluded that the Vermont and Lakenvlei Formations are not facies equivalents and that the change in lithology might be due to increased tectonic activity such as uplift of the source terrains. The patterns of the Al_2O_3-Zr-TiO_2 and Al_2O_3-Cr-TiO_2 (Fig. 4.1.8 and Fig. 4.1.9) can be explained by the contribution of different source rocks and some degree of transport fractionation. A change in accumulation rate due to a change in the prevailing tectonic activity may be important for successive shale-sandstone assemblages.

The geochemistry of the Pretoria Group sedimentary rocks contains contrasting signals for the estimation of their provenance. In the foregoing discussion it was attempted to include all information obtained in this investigation; a more conclusive interpretation would have resulted in concealing the critical observations and argueing along the path of the prevailing scientific opinion as expressed in the literature. An especially critical point seems to be the behaviour of Th in the sedimentary process. The postulated preferential enrichment of Th over Cr in shales is concluded from the abundances of Cr and Th in the inferred Archaean crustal composition (Taylor and McLennan, 1985) and Archaean shale estimates (e.g., Taylor and McLennan, 1985; Wronkiewicz and Condie, 1987, 1989, 1990). However, the results obtained by independent methods (e.g., Roser and Korsch's (1988) discriminance diagram using several major elements, and the ternary diagrams after Garcia et al., 1991) seem to confirm the modified Th/Sc-Cr/Th and Th/Sc-Cr/Zr provenance estimation diagrams defined here.The provenance of Pretoria Group sedimentary rocks can be explained by contributions from a complex source terrain with predominantly granitic and sedimentary sources as well as, possibly, ultramafic sources. The latter could have provided the detrital chromite in the

sandstones. Alternatively, the chromite could have been inherited from Cr-rich sedimentary sources, similar to the chromite-rich Archaean shales as inferred by Laskowski and Kröner (1985). Sedimentary sources are postulated for the Pretoria Group as they are generally poorer in detrital zircon than granites and could thus explain the low Zr-contents in the sandstones examined in this study. Furthermore, Archaean shales (Wronkiewicz and Condie, 1987, 1989, 1990) are low in Ti, despite their inferred mafic provenance, a feature shared by the Pretoria Group shales and sandstones. Sedimentary sources could also account for the mafic provenance patterns observed in the Pretoria Group up to the stratigraphic level of the Strubenkop Formation, if the mafic pattern of the sedimentary source areas was inherited by the Pretoria Group. The apparent increase in recycled sedimentary material towards the top of the Pretoria Group may point to a 'cannibalistic' behaviour, with partial erosion and sedimentation of previously-deposited Pretoria Group rocks. Penecon-temporaneous volcanic sources are inferred for the Dwaalheuwel and Strubenkop Formations, which may contain weathered and eroded Hekpoort volcanics, and for the Silverton Formation, which has abundant tuffaceous material interlayered with detrital clay minerals, at least in its upper parts (see Chapter 4.4). The evidence of significant contributions of penecontemporaneous volcanic sources is spurious for the other formations of the Pretoria Group. The widespread occurrence of volcanism throughout the Pretoria Group is discussed in Chapter 4.4, but is thought to have had only insignificant effects on the general provenance patterns observed in the geochemistry discussed here.

4.2 Palaeoclimatic indications inferred from the geochemistry of the Pretoria Group sedimentary rocks

The degree of chemical weathering in the provenance area can be estimated by the 'Chemical Index of Alteration' (CIA) of shales (Nesbitt and Young, 1982), which is defined as:

$$CIA = [(\text{mol. } Al_2O_3)/\text{mol.}(Al_2O_3 + CaO^* + Na_2O + K_2O)] * 100,$$

where CaO^* is the amount of CaO incorporated in the silicate fraction of the shales. As the CO_2-content was not determined for most of the samples, a correction for calcareous material

was not possible when the CIA was calculated. However, the error is thought to be small for most shale samples, as CO_2-contents are generally low (median = 0.31 w.t.%, see Chapter 3.4.1.1), with the exception of the Nederhorst Formation and a few calcareous shale samples of the Silverton Formation. Average shale estimates have a CIA of 70-75, modern residual clays and Amazon cone muds have values of 80-100, Pleistocene varved and glacial clays values of 60-65, and Pleistocene tills and Archaean shield sediments of north-western Ontario CIA values of $\approx$ 50 (Nesbitt and Young, 1982). Based on this approach, several workers have given interpretations of the syndepositional palaeoclimate of the Pretoria Group sedimentary rocks (e.g., Wronkiewicz and Condie, 1990; Schreiber, 1990; Schreiber et al., 1992). Due to a comparable CIA of Timeball Hill and Silverton Formation shales and the North American Shale Composite (Gromet et al., 1984), Wronkiewicz and Condie (1990) conclude a 'climate similar to those representative of the average Phanerozoic', a definition thought to be, at the least, unclear. However, the CIA of the Strubenkop Formation argillites (ϕ 89) is interpreted as characteristic of sediments derived from chemically weathered detritus (Wronkiewicz and Condie, 1990). Schreiber (1990) and Schreiber et al. (1992) describe high CIA values for the Timeball Hill and Strubenkop Formations, and gradually declining values from the Strubenkop to the Post-Magaliesberg Formations. The high and seemingly stable CIA-values in the lower part of the Pretoria Group (up to and including the Strubenkop Formation) are interpreted as indicating a stable palaeoclimate (Schreiber et al., 1992) with inferred humid conditions (Schreiber, 1990). The decline of the CIA in the upper part of the Pretoria Group is interpreted as being due to basement uplift and/or increased continental rifting, which was also apparently responsible for an increase of arkose deposition and penecontemporaneous volcanic activity, thus causing an increased supply of fresh or less weathered material (Schreiber et al., 1992).

Eriksson (1992) infers, on the basis of the polar wandering curve for the Kaapvaal Craton from 2300 to 1850 Ma (also discussed in Eriksson et al., 1993), the possibility of nival climatic conditions for the lower part of the Pretoria Group (up to Hekpoort Formation). Sedimentological evidence for glaciation is found, especially in the Boshoek Formation, which contains diamictites and varved shales (Button, 1973; P.G. Eriksson, pers. comm., 1994). Fine laminae of alternating siltstone and mudstone in the argillites of the Timeball Hill Formation are interpreted as varves deposited in glacial lakes (Eriksson, 1992).

The interpretations of the syndepositional palaeoclimate of the Pretoria Group are thus at variance with each other, due to variable geochemical and sedimentological data. However, the interpretations based on geochemical evidence also differ from each other, although to a lesser degree. As the geochemical interpretations of the syndepositional palaeoclimate are largely based on the CIA, and its comparisons with values given by Nesbitt and Young (1982), the significance of the CIA and possible interpretational pitfalls are discussed briefly.

The interpretative utility of the CIA as a palaeoclimate indicator is restricted in an active tectonic environment (Wronkiewicz and Condie, 1987). Orogenic tectonics and/or basement uplift can change the detrital component provided to a particular basin, i.e., less weathered material is provided to the basin and the CIA is subsequently lowered in the resulting argillites. Schreiber et al. (1992) ascribe the decrease of the CIA of Pretoria Group argillites with increasing stratigraphic height to increased tectonic activity, thus inferring, indirectly, limited applicability of the CIA as a palaeoclimate indicator for the upper part of the Pretoria Group. Both penecontemporaneous climate and tectonic activity seem to influence the resulting CIA pattern of shales, i.e. fresh or less weathered rocks are provided if tectonic activity and, consequently, erosion rates increase or if chemical weathering is absent in the source area; thus a qualitative interpretation of the palaeoclimate is only feasible if the CIA indicates chemical weathering, in other words if the CIA is at least greater than 75. It must be mentioned in this context, that although intense chemical weathering is reported most frequently from tropical climates with humid and hot conditions, it is also reported from glacial environments, though at reduced rates (Reynolds and Johnson, 1972). The latter observation is significant once a time-factor is introduced. The generation of weathering products from a given source rock is accordingly not only a function of climatic and tectonic conditions in the source area, but also dependent on the time this source rock is exposed to weathering.

Another problem of geochemical indicators of the palaeoclimate, is the addition or subtraction of elements during diagenesis, metasomatism and metamorphism. Nesbitt and Young (1989) interpret the enrichment of potassium in the Hekpoort palaeosol (see also Chapter 4.1) as an indication of K-metasomatism, where potassium was introduced after deposition by percolating solutions. Pore fluids in subsiding marine basins are rich in sodium

and marine sediments can thus undergo Na-metasomatism, which results in the generation of albite (Nesbitt and Young, 1989). Both types of metasomatism would shift the CIA towards lower values.

Chemical analyses of Gulf Coast oil wells show a relatively uniform chemistry with depth, thus indicating a closed system and only minor changes due to diagenesis (Weaver, 1989). Only Mg, Na and CO_2 seem to have a limited ability to move from mudrocks into sandstones (Weaver, 1989); however, an effect on the CIA of Pretoria Group shales due to this reaction can be neglected, as the Pretoria Group sandstones are depleted in Na. Ronov et al. (1977) were able to show that the concentration of all elements except the volatile elements in shales remains nearly invariant during low and medium-grade metamorphism. A pronounced effect on the geochemistry of the Pretoria Group shales due to metamorphism can thus be excluded, as only the CIA of originally calcareous shales might be misinterpreted due to the loss of CO_2, and the incorporation of Ca into silicates like tremolite (Turner, 1981).

Figure 4.2.1 A shows the stratigraphic variation of the CIA in the Pretoria Group argillites. Calcareous samples are identified by a CIA below 30, and were found only in the Silverton and Nederhorst Formations. The plot generally confirms the stratigraphic pattern of the mean values shown in Figure 3.4.3.1 d. The lower part of the Pretoria Group up to the Daspoort Formation has relatively high CIA-values, normaly exceeding 75. The Silverton Formation has a high variability, with non-calcareous shales having a CIA as low as 30. The Post-Magaliesberg Formations tend to have generally lower CIA-values than the pre-Silverton formations. Figures 4.2.1 B and D illustrate, to a certain degree, a positive correlation of CIA values with the immobile elements Ti and Zr, although the correlations are less well defined in the higher CIA range. Figure 4.2.1 C shows the expected negative correlation between MgO and CIA. Mg is thought to be more mobile in the weathering environment than Ca (Anderson and Hawkes, 1958), but can be reincorporated into clay minerals when chlorite is formed (Nesbitt and Young, 1989). Chlorite is formed as a by-product of the illitization of smectites (Weaver, 1989) and, more importantly, by the conversion of kaolinite during burial, according to the reaction:

$$Mg_5Al_2Si_3O_{10}(OH)_8 + 10\ H^+ = Al_2Si_2O_5(OH)_4 + 1\ SiO_2(c) + 5\ Mg^{2+} + 7\ H_2O,$$

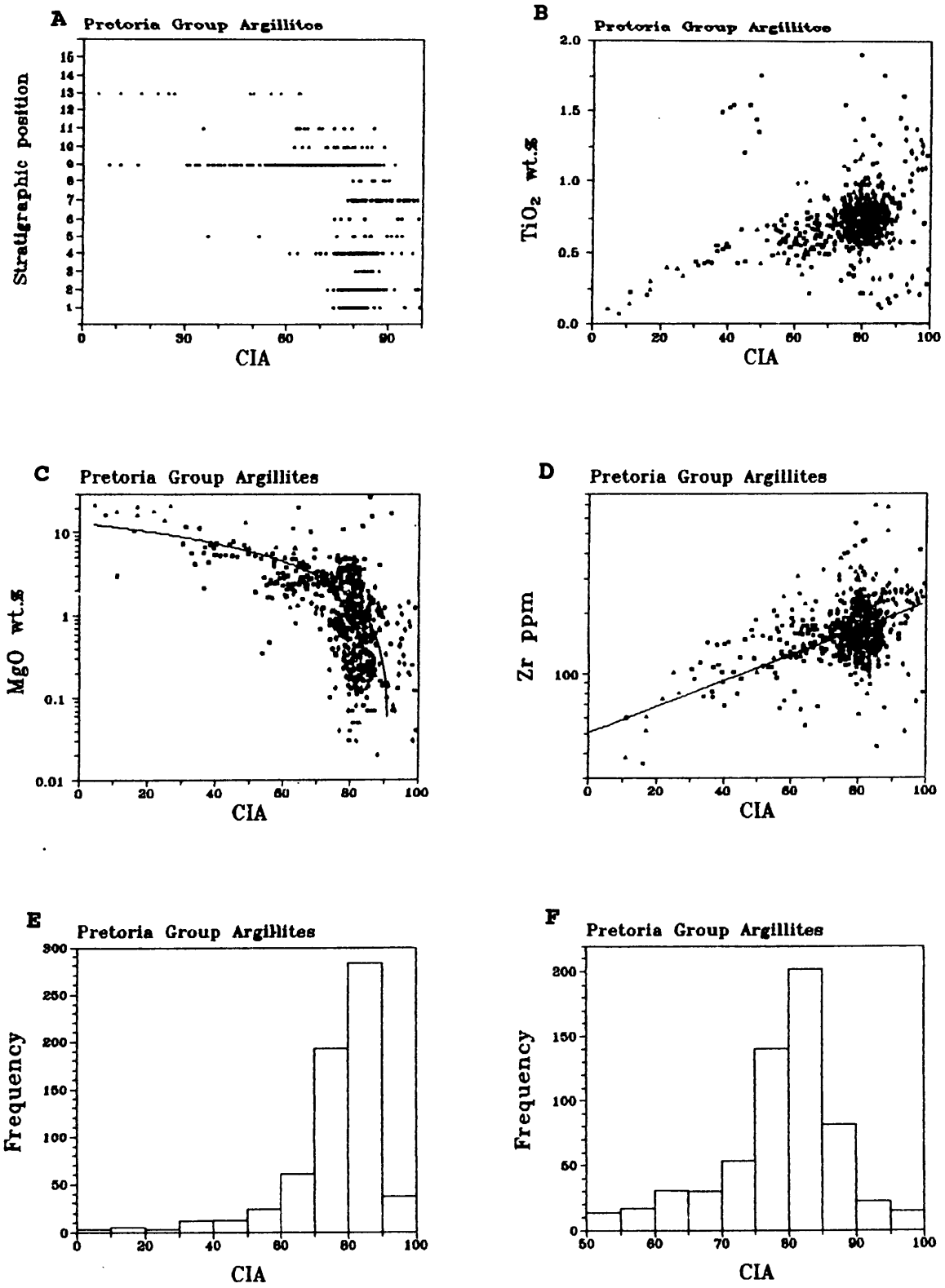

Figure 4.2.1 A-F: Stratigraphic variability of the CIA, distribution of CIA and the relationship of CIA and MgO, TiO_2 and Zr in Pretoria Group shales. Ordinate of Figure 4.2.1 A: 1 = Rooihoogte Fm.; 2 = Lower Timeball Hill Fm.; 3 = Timeball Hill Quartzites; 4 = Upper Timeball Hill Fm. and Boshoek Fm.; 5 = Hekpoort Fm.; 6 = Dwaalheuwel Fm.; 7 = Strubenkop Fm; 8 = Daspoort Fm.; 9 = Silverton Fm.; 10 = Magaliesberg Fm.; 11 = Vermont Fm.; 12 = Lakenvlei Fm.; 13 = Nederhorst Fm.; 14 = Steenkampsberg Fm.; 15 = Houtenbek Fm.. Lines shown in Figures 4.2.1 C and D are linear regression curves with CIA as independent variable. Ordinate in Figures 4.2.1 E and F is number of samples.

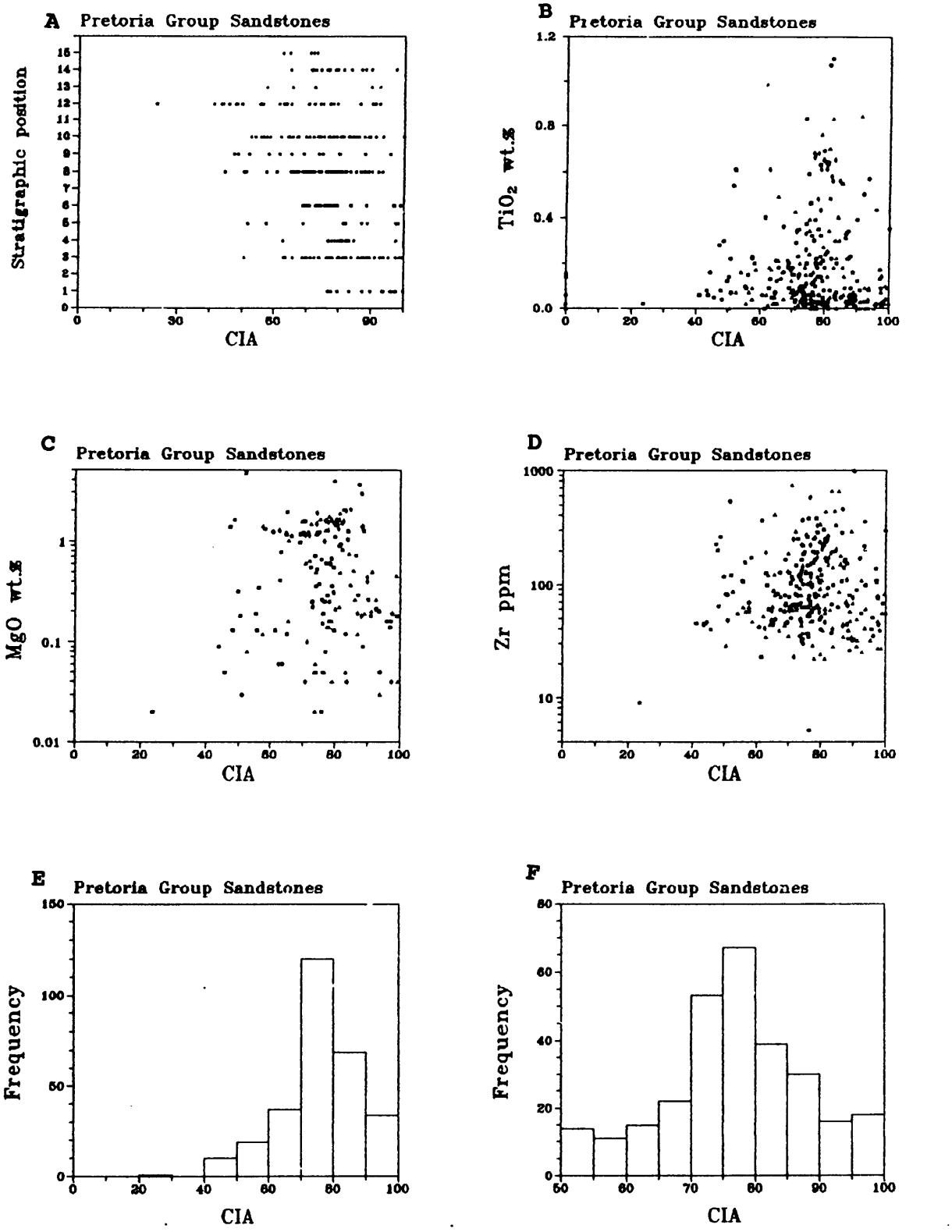

Figure 4.2.2 A-F: Stratigraphic variability of the CIA, distribution of CIA and the relationship of CIA and MgO, TiO_2 and Zr in Pretoria Group sandstones. Ordinate of Figure 4.2.1 A: 1 = Rooihoogte Fm.; 2 = Lower Timeball Hill Fm.; 3 = Timeball Hill Quartzites; 4 = Upper Timeball Hill Fm. and Boshoek Fm.; 5 = Hekpoort Fm.; 6 = Dwaalheuwel Fm.; 7 = Strubenkop Fm; 8 = Daspoort Fm.; 9 = Silverton Fm.; 10 = Magaliesberg Fm.; 11 = Vermont Fm.; 12 = Lakenvlei Fm.; 13 = Nederhorst Fm.; 14 = Steenkampsberg Fm.; 15 = Houtenbek Fm.. Ordinate in Figures 4.2.1 E and F is number of samples.

where the reaction will proceed from right to left if the temperature increases (Nesbitt and Young, 1989; Weaver, 1989). The strong negative correlation between CIA and MgO (Fig. 4.2.1 C) favours the removal of MgO from the source rock during weathering processes. It should be emphazised that the MgO-content declines sharply at a CIA of about 75, thus indicating the importance of small changes in CIA at this level. Although chlorite is a common mineral in the Pretoria Group shales, the formation of Mg-chlorite from kaolinite seems to have been largely prohibited (see Chapter 4.4). The distribution of the CIA (Fig. 4.1.2 E and F) shows that most Pretoria Group argillite samples ($\approx$ 70 %) have a CIA greater than 75.

The Pretoria Group sandstones (Fig. 4.2.2 A-F) have a more variable CIA-distribution than their penecontemporaneous shales (Fig. 4.2.1 A). The CIA of sandstones shows neither a correlation with the immobile elements Ti and Zr (Fig. 4.2.2 B and D), nor with the mobile element Mg (Fig. 4.2.2 C). It is thus doubtful, if the CIA can be applied to the Pretoria Group sandstones, or, more generally, to any sandstones at all. The porosity and permeability of sandstones make them susceptible to percolating solutions, which have the potential to precipitate clay minerals independently of the prevailing palaeoclimate. Authigenic clay minerals are a common constituent of sandstones (Weaver, 1989). Hence, the CIA should not be applied to sandstones. It should be emphazised, that the CIA is intended as an alteration index for shales (Nesbitt and Young, 1982).

McLennan et al. (1983) introduced another approach for determining palaeoweathering conditions, using upper crust normalized element distribution spidergrams. Figures 4.2.3 A and C show the patterns of the formation averages of Pretoria Group shale formations; Figure 4.2.3 B is a reproduction of the Toorongo Granodiorite weathering profile (Nesbitt et al., 1980), sorted according to the degree of weathering. Cations of alkali and alkali-earth elements with relatively large ionic radii, such as Rb and Ba, seem to be fixed in weathering profiles, whereas smaller cations such as Na, Sr and Ca are selectively leached from the weathering profile (Wronkiewicz and Condie, 1987). This mechanism is relative, as, for example, Ba has a smaller ionic radius than K (e.g., Seim and Tischendorf, 1990), which is thus more readily leached from the profile. However, the solubility of alkali and alkali-earth elements in a weathering profile seems to decrease with increasing ionic radii within

each group, i.e., from Na^+ to Rb^+ in the alkali element group and from Ca^{2+} to Ba^{2+} in the alkali-earth element group. Mg^{2+} seems to fit this trend, but can also be reintroduced or fixed in the weathering profile (see discussion above). A comparison of Pretoria Group shale averages with the Toorongo weathering profile confirms the similarity of the lower Pretoria Group formations (up to the Daspoort Formation) with highly weathered material, except for the shales of the Hekpoort Formation. The post-Daspoort Formations have patterns similar to slightly weathered or fresh rocks. It must be noted that potassium is not as strongly depleted in the average values as expected, if strong weathering conditions are assumed.

A viable alternative explanation for the relatively elevated potassium levels might be the occurrence of K-metasomatism. Apart from the Waterval Boven Hekpoort palaeosol, strong enrichment of potassium is noted for sandstones in the Hekpoort Formation in Botswana (Figure 3.3.6.1), argillites immediately overlying the Hekpoort Formation in the western Transvaal (Fig. 3.3.6.2), argillites in the Magaliesberg Formation near Pretoria (Samples UVM - 21, -306, -311, -321, -322, with K_2O-contents between 6 and 8 w.t.%; see Appendix 1a) and argillites and tuffs from the basal Lower Timeball Hill Formation in the Eastern Transvaal (Fig. 3.3.2.2). The Bushy Bend Lavas in the Potchefstroom Basin are reported to have K_2O-contents exceeding 5 w.t.%, but have otherwise a basaltic-andesitic signature (Eriksson et al., in press b), thus inferring alteration processes, which might be related to K-metasomatism. Another explanation for the relatively elevated K-contents might be the production of illite at the expense of kaolinite with increasing temperature (Nesbitt and Young, 1989). As the equilibrium between kaolinite and illite controls the K^+/H^+ of groundwater and interstitial waters, K^+/H^+ must decrease as temperature increases, thus shifting the reaction

$$KAl_3Si_3O_{10}(OH)_2 + H^+ + 0.5\ H_2O = 1.5\ Al_2Si_2O_5(OH)_4 + K^+$$

towards the left hand side (Nesbitt and Young, 1989). Hence, K_2O might have been added to the shales during diagenesis, if K-rich groundwaters and/or interstitial waters are presupposed. The introduction of K+ by solutions from external sources (i.e., K-metasomatism) would result in even larger quantities of illite being produced, up to the point of destroying all kaolinite (Nesbitt and Young, 1989).

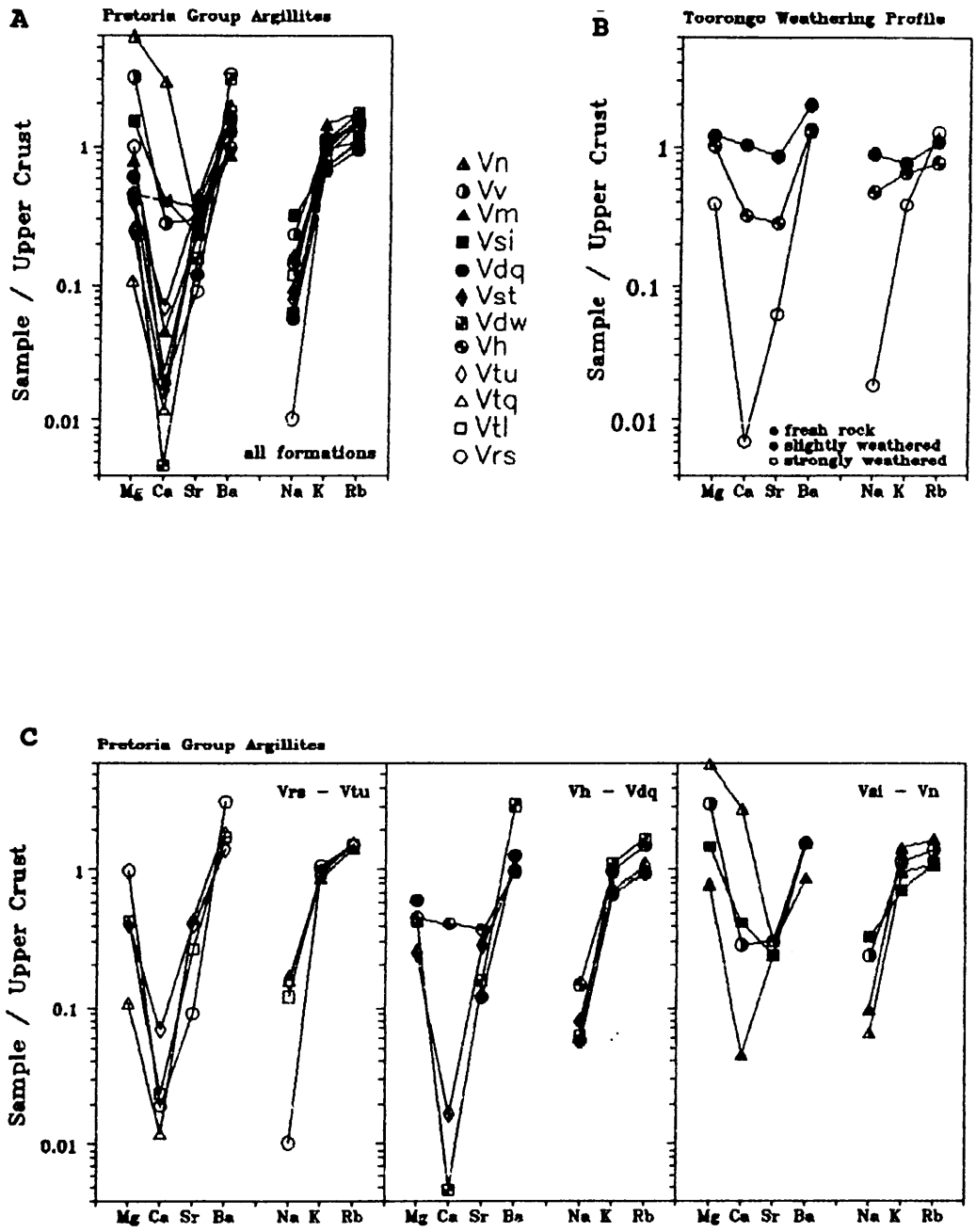

Figure 4.2.3 A - C: Upper Crust (Taylor and McLennan, 1985) normalised diagrams of average Pretoria Group shales (Fig. 4.2.3 A and C) and Upper Crust (ibid.) normalised diagram of the Toorongo weathering profile (data recalculated from Nesbitt et al., 1980)(Fig. 4.2.3 B). Symbols: ○ = Vrs = Rooihoogte Fm.; □ = Vtl = Lower Timeball Hill Fm.; Δ = Vtq = Timeball Hill Quartzite; ◇ = Vtu = Upper Timeball Hill Fm.; ◒ = Vh = Hekpoort Fm.; ◙ = Vdw = Dwaalheuwel Fm.; ◆ = Vst = Strubenkop Fm.; ● = Vdq = Daspoort Fm.; ■ = Vsi = Silverton Fm.; ▲ = Vm = Magaliesberg Fm.; ◑ = Vv = Vermont Fm.; ◭ = Vn = Nederhorst Fm..

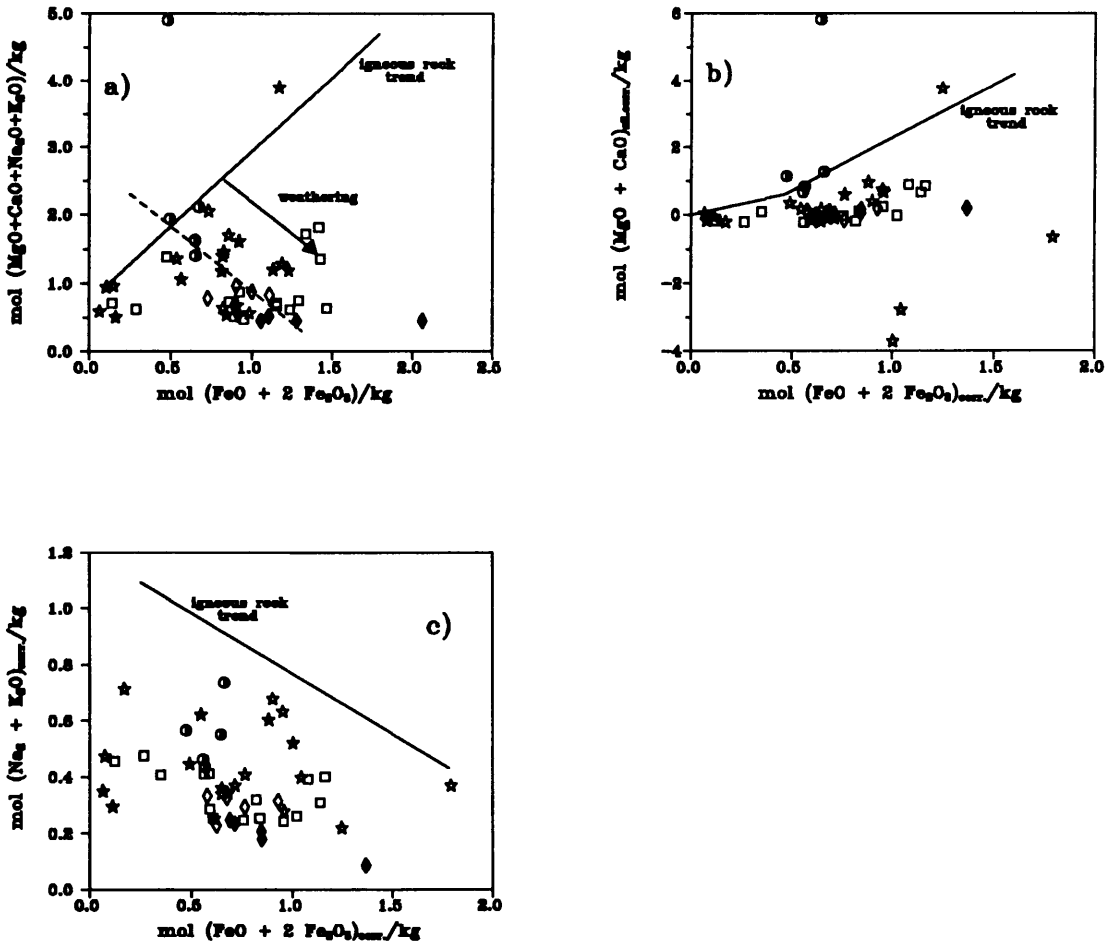

Figure 4.2.4 a-c: The relationships between the sums of the number of moles of (MgO + CaO + Na_2O + K_2O), $(Na_2O + K_2O)_{silicate\ corrected}$ and $(MgO + CaO)_{silicate\ corrected}$ and the number of moles of (FeO + 2 Fe_2O_3) and $(FeO + 2\ Fe_2O_3)_{silicate\ corrected}$ in Pretoria Group shales, compared to the igneous rock trend of Holland (1984). Symbols: ★ = Silverton Fm.; □ = Lower Timeball Hill Fm.; ◑ = Vermont Fm.; ♦ = Strubenkop Formation; ◇ = Upper Timeball Fm.. Calculations:

mol $(MgO + CaO)_{sil.corr.}$ = mol $(MgO + CaO - CO_2 - SO_3) \cdot 15.6/Al_2O_3$ wt.%

mol $(Na_2O + K_2O)_{corr.}$ = mol $(K_2O + Na_2O) \cdot 15.6/Al_2O_3$ wt.%

mol $(FeO + 2\ Fe_2O_3)_{corr.}$ = mol $(FeO + 2\ Fe_2O_3) \cdot 15.6/Al_2O_3$ wt.%

The indications of the contribution of strongly weathered source material to the Pretoria Group sedimentary rocks are strengthend further by the relative position of the Pretoria Group shales in Figures 4.2.4 a, b and c, compared to igneous rock element variation lines. The Pretoria Group shales deviate significantly from the igneous rock trend proposed by Holland (1984). Only samples from the Silverton and Vermont Formations plot close to the igneous rock trend in Figures 4.2.4 A and B. One sample of the Vermont Formation (top of Fig. 4.2.4 A and B) shows some evidence of a different type of alteration, causing the introduction of Mg into the rock. Figure 4.2.4 B further indicates an initial depletion of MgO and CaO, as the mol. $(MgO + CaO)_{sil.corr.}$ lies close to 0 for most samples. Negative values of the mol. $(MgO + CaO)_{sil.corr.}$ are only possible, if other carbonate minerals than calcite, dolomite or magnesite and/or considerable amounts of sulphides are present in the rock. However, the patterns shown in Figures 4.2.4 A-C presuppose igneous source rocks, and it is questionable if the diagrams can be applied in the presence of sedimentary or metamorphic source rocks.

Wronkiewicz and Condie (1990) interpret the comparatively low K/Rb-ratio of the Pretoria Group argillites as an indication of source rock weathering for the Pretoria Group. The relationships of K/Rb with CIA, Al_2O_3, MgO and Zr are shown in Figures 4.2.5 A-F for argillites (Fig. 4.2.5 A, C, E and F) and sandstones (Fig. 4.2.5 B and D). Obviously, a simple relationship between weathering and the K/Rb-ratio has to be excluded for the Pretoria Group sedimentary rocks. The K/Rb-ratio of Pretoria Group argillites, for nearly all samples, lies below the K/Rb-ratio of the North American Shale Composite (Gromet et al., 1984), which has an average K/Rb-ratio of 230 (Wronkiewicz and Condie, 1990) (Fig. 4.2.6 A). If the K/Rb - CIA relationship is investigated after separation of the samples into their respective formations (Fig. 4.2.6 A-H), fairly well established to excellent correlations can be observed up to the Strubenkop Formation, thus confirming a decrease of potassium relative to Rb as expected in a weathering profile (see Fig. 4.2.3 B). A weak negative correlation between K/Rb and CIA is also observed for the Magaliesberg Formation, if CIA-values above 75 only are taken into account. It is concluded, that the K/Rb-ratio can give an indication of source rock weathering, but a generalized application as proposed by Wronkiewicz and Condie (1990) seems to be unsupported by the above results. The K/Rb-distribution and, especially, its relationship to the CIA, in the Pretoria Group shales is

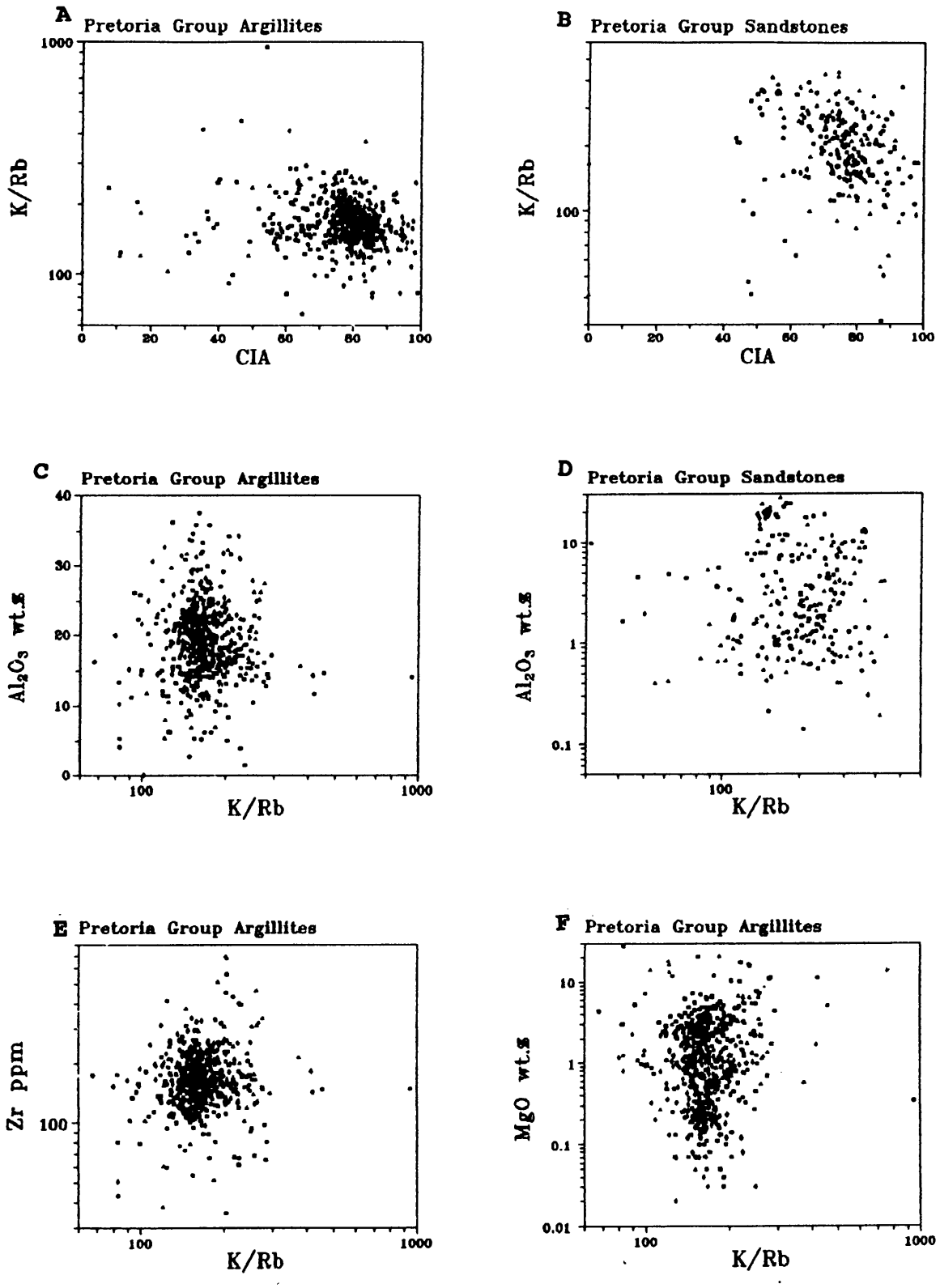

Fig. 4.2.5 A-F: The relationship between the K/Rb-ratio and CIA, Al_2O_3, Zr and MgO in Pretoria Group shales (Fig. 4.2.5 A, C and E) and sandstones (Fig. B, D and F).

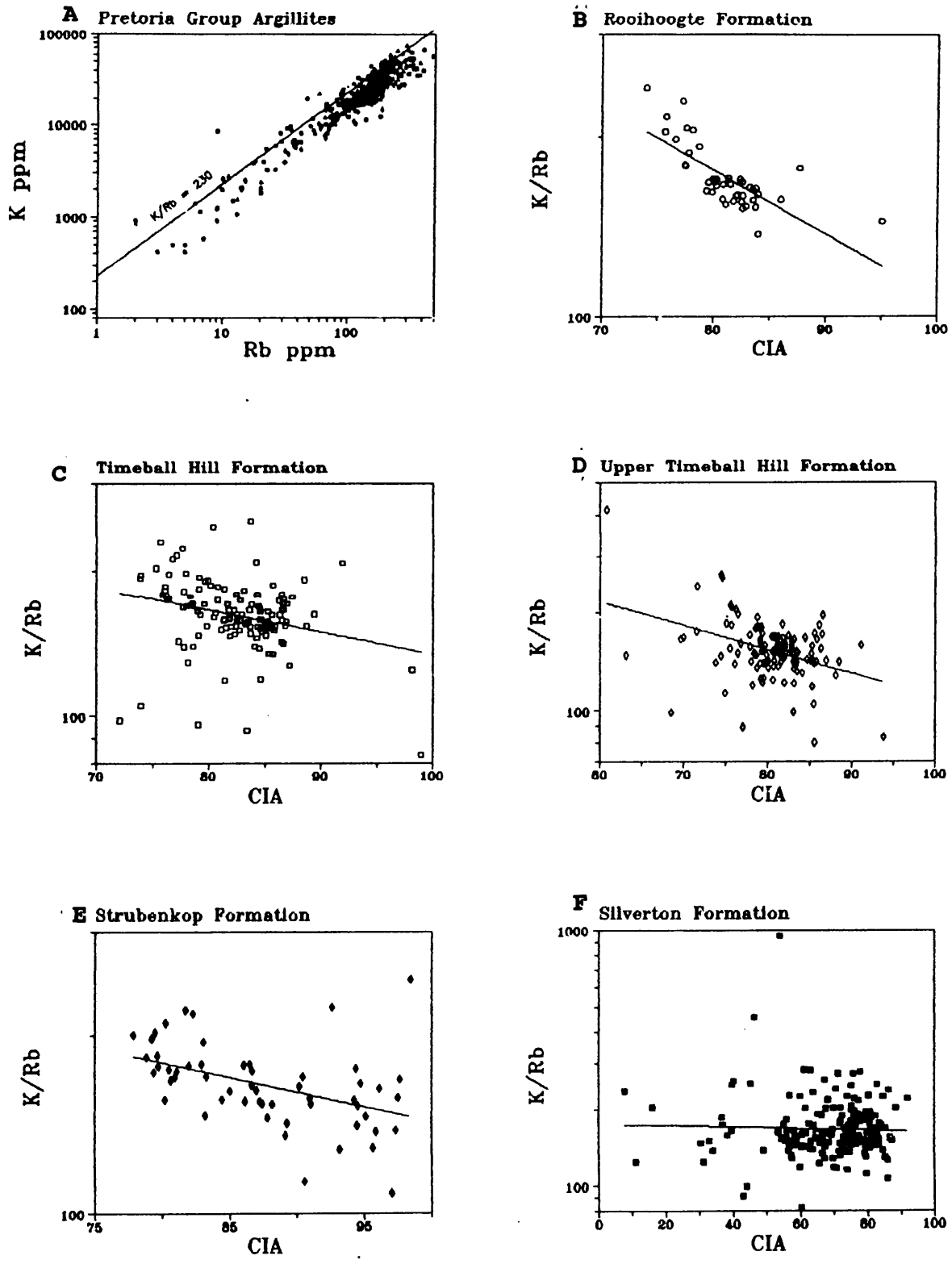

Fig. 4.2.6 A-H: The relationship between K and Rb (Fig. 4.2.6 A), and between the K/Rb-ratio and the CIA (Fig. 4.2.6 B-H) in Pretoria Group shales. Line in Figure 4.2.6 A represents the K/Rb-ratio of the North American Shale Composite (Gromet et al., 1984), lines in Figures 4.2.6 B-H represent exponential regression curves with CIA as independent variable.

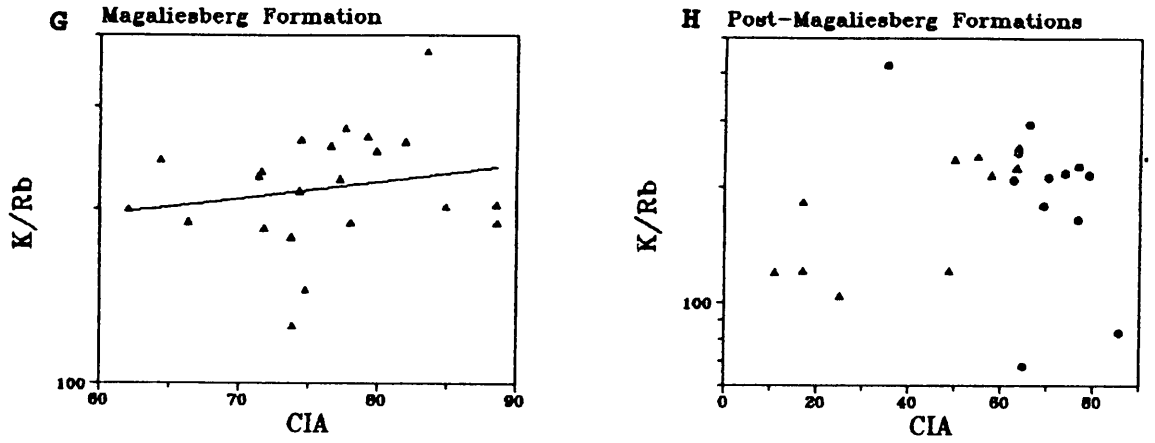

Fig. 4.2.6 A-H (continued): The relationship between K and Rb (Fig. 4.2.6 A), and between the K/Rb-ratio and the CIA (Fig. 4.2.6 B-H) in Pretoria Group shales.

interpreted as an additional confirmation of chemical weathering of source rock material for the lower part of the Pretoria Group.

The previous discussions in this chapter are centred around the question, whether intense source rock weathering occurred in the Pretoria Group provenance area. The evidence cited above definitely points to strong chemical weathering of the source rocks up to the Daspoort Formation, and indicates a geochemical change for the post-Daspoort Formations. This change might have various causes, i.e., tectonic activity with increased erosion rates (Schreiber et al., 1992), climatic changes and/or increase of penecontemporaneous volcanism with fresh volcanic material being mixed with detrital components. The latter effect has to be considered for the post-Daspoort Formations as tuffs and tuffaceous shale beds can be recognised frequently in these formations (Schreiber, 1990).

The strong chemical weathering signature of the Pretoria Group shales up to the Daspoort Formation is an indication of a humid-hot palaeoclimate having prevailed during deposition. However, the time-dependancy of weathering processes, discussed previously in this chapter, allows the possibility of other explanations for the geochemical weathering signature of the basal Rooihoogte and Timeball Hill Formations. The depositional hiatus between the deposition of the Chuniespoort and Pretoria Groups can be estimated as at least 100 Ma (Eriksson et al., in press a), thus giving sufficient time for deep chemical weathering

irrespective of the prevailing climate. Palaeokarst sinkholes in the Chuniespoort dolomite, genetically linked to the unconformity, are found frequently below the contact of the Pretoria Group (e.g., Crocker et al., 1988). The chemical weathering signature of the Rooihoogte and Timeball Hill Foramtions might thus be led back to weathering profiles related to the depositional hiatus. Hence, the geochemical signature pointing to chemical weathering might be misinterpreted, if a humid-hot synsedimentary palaeoclimate is inferred for the Rooihoogte and Timeball Hill Formations. Synsedimentary chemical weathering with an appropriate humid-hot climate is inferred for the Dwaalheuwel, Strubenkop and Daspoort Formations, as the restrictions discussed above do not seem to be applicable to these formations. Synsedimentary palaeoclimate cannot be inferred by applying the CIA to sandstones in the Pretoria Group.

4.3 Tectonic setting of the Pretoria Group as inferred from the geochemistry of sedimentary and volcanic rocks

The tectonic setting of the Pretoria Group as inferred from the geochemistry of sandstones was previously discussed by Schreiber et al. (1991, 1992). Their approach was based on a Fe_2O_3 + MgO -Na_2O - K_2O ternary diagram proposed by Blatt et al. (1980). The Fe_2O_3 + MgO -Na_2O - K_2O ternary diagram discriminates sandstones into ferromagnesian potassic, sodic and potassic sandstones. The ferromagnesian potassic sandstone group is thought to reflect an "exogeosynclinal" tectonic setting, i.e., "clastic wedges spread out over the edges of cratons from sources in peripheral folded mountains" (Blatt et al., 1980, p. 378), and comprises mostly lithic sandstones (Blatt et al., 1980). The sodic sandstones (mostly graywackes) point to deposition in an "eugeosynclinal" tectonic setting, and the potassic sandstones (mostly arkoses) are thought to reflect a "taphrogeosynclinal" tectonic setting, i.e., deep fault basins on the craton (Blatt et al., 1980). Schreiber et al.'s (1991, 1992) application of Blatt et al.'s (1980) approach shows most sandstone samples of the Pretoria Group falling into the ferromagnesian potassic and potassic sandstone groups, with pre-Magaliesberg Formation samples clustering in the former and post-Silverton Formation samples clustering in the latter group. Schreiber et al. (1992) interpret their results as evidence for stable cratonic conditions in the pre-Magaliesberg Formations times, and tectonic instability with concomitant uplift of source rocks, thought to be mainly of granitic composition, during the later stages of the Pretoria Group.

Figures 4.3.1 A-E shows the application of the Fe_2O_3 + MgO -Na_2O - K_2O ternary diagram to the present data set. The results of Schreiber et al. (1991, 1992) seem to be broadly confirmed, although differences are observed for the Boshoek, Dwaalheuwel and Daspoort Formations. The observed geochemistry of the present sample set (Fig. 4.3.1 A-E) is more variable than the data presented by Schreiber et al. (1991, 1992), and a differentiation into pre-Magaliesberg and post-Silverton Formation groups is ambiguous in the present sample set. Only 90 sandstone samples out of a data set of 334 sandstone samples qualified for inclusion in the diagram (fig. 4.3.1 A-E), as Blatt et al. (1980) exclude all sandstone samples with an Al_2O_3-content of less than 5 wt.% for incorporation into the Fe_2O_3 + MgO -Na_2O - K_2O ternary diagram.

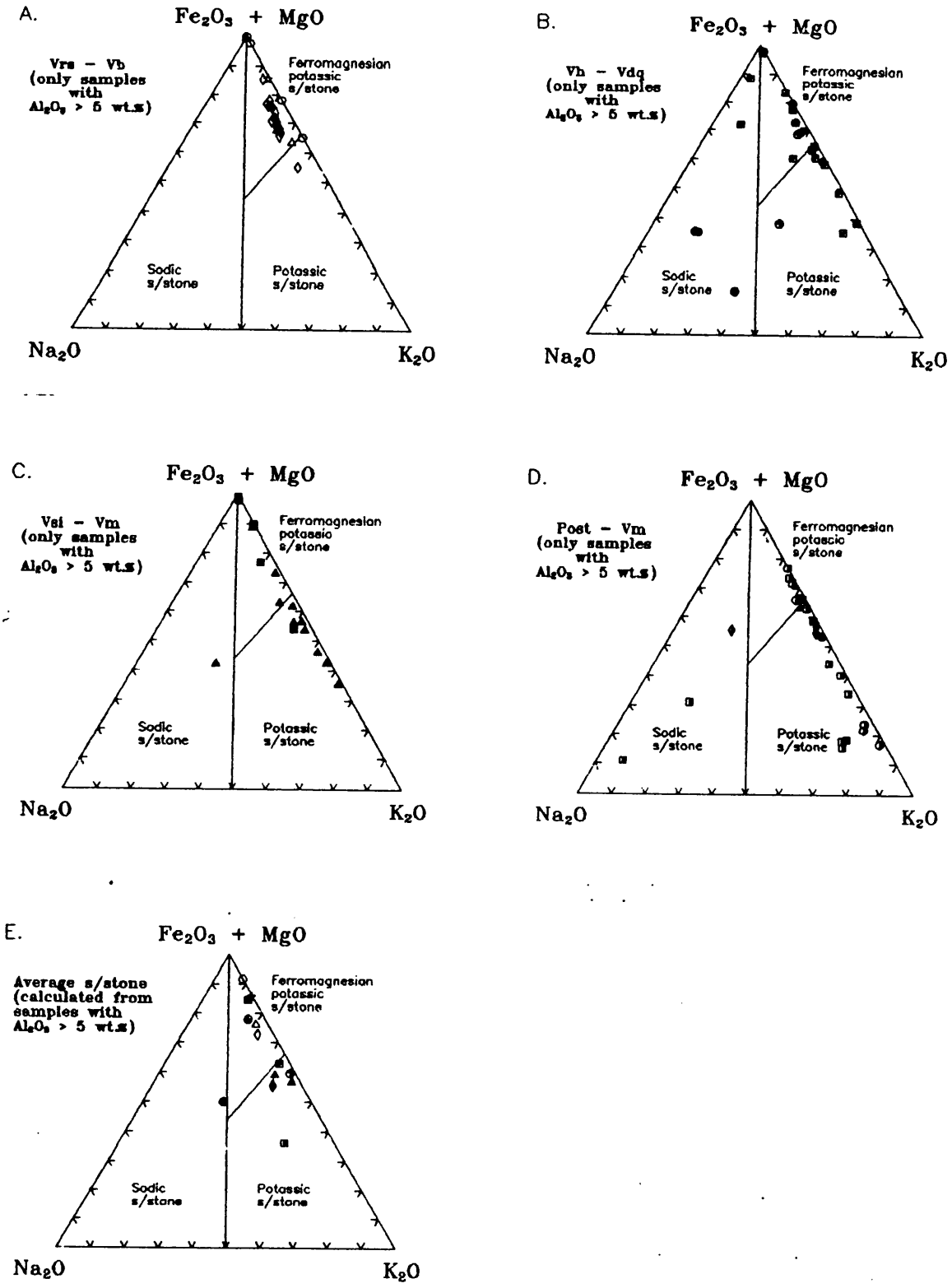

Figure 4.3.1 A-E: The tectonic setting discriminance diagram of Blatt et al. (1980) applied to Pretoria Group sandstones with Al_2O_3 > 5 wt.%. Ferromagnesian potassic sandstone field = 'exogeosynclinal'; potassic sandstone field = 'taphrogeosynclinal'; sodic sandstone field = 'eugeosynclinal'. Symbols: ○ = Rooihoogte Fm. (Vrs); Δ = Timeball Hill Quartzite; ◇ = Upper Timeball Hill Fm.; ★ = Boshoek Fm. (Vb); ◕ = Hekpoort Fm. (Vh); ◙ = Dwaalheuwel Fm.; ◆ = Strubenkop Fm.; ● = Daspoort Fm. (Vdq); ■ = Silverton Fm. (Vsi); ▲ = Magaliesberg Fm. (Vm); ◘ = Lakenvlei Fm.; ▲ = Nederhorst Fm.; ◆ = Steenkampsberg Fm.; ◆ = Houtenbek Fm.; ○ = Rayton Fm.; stratigraphic abbreviations used in diagrams are listed in brackets behind symbol legend.

The basin classification used by Blatt et al. (1980) seems somewhat antiquated and cannot be applied to a modern approach in basin analysis (e.g., Miall, 1984; Allen and Allen, 1990). For example, the classification of a foreland basin is at least unclear, if the above cited definitions of Blatt et al. (1980) of tectonic settings are applied. Furthermore, K_2O, Na_2O and MgO can be added or subtracted by processes like weathering, sorting during transport and/or diagenesis. Particularly diagenesis, including sodium and potassium metasomatism, can change the primary geochemistry of sandstones, and can thus lead to a distorted pattern in the Fe_2O_3+ MgO-Na_2O-K_2O ternary diagram (Blatt et al., 1980). Another restriction of the Fe_2O_3+ MgO-Na_2O-K_2O classification diagram is the exclusion of sandstones with less than 5 wt.% Al_2O_3 (Blatt et al., 1980), thus invoking doubts concerning the applicability of the diagram to more mature (i.e. quartz-rich) sandstone assemblages. According to the petrographic work of Schreiber et al. (1991, 1992), quartz arenites are the most abundant petrographic group in Pretoria Group sandstones. This is generally confirmed by the geochemical classification of Pretoria Group sandstones (see Chapter 4.4, Fig. 4.4.1), and can also be deduced from the small percentage of sandstones (< 30%, see above) containing more than 5 wt.% Al_2O_3. It is thus doubtful, if a meaningful result can be obtained for the tectonic setting by using Blatt et al.'s (1980) approach. The widespread occurrence of inferred potassium metasomatism in the Pretoria Group (see Chapter 4.2) suggests a related change in primary geochemistry, although an interpretational bias is improbable as both potassium-rich sandstones (i.e., arkoses) and potassium metasomatism favour a continental setting. Floyd et al. (1989) use the Fe_2O_3 + MgO-Na_2O-K_2O ternary diagram as a geochemical classification of petrography, but all their samples contain high Al_2O_3-contents. It will be shown later (Chapter 4.4), that in the case of the Pretoria Group, the application of the Fe_2O_3 + MgO-Na_2O-K_2O ternary diagram as a geochemical classification diagram for petrography would yield results which are contradicted by the classification diagram of Pettijohn et al. (1972) (Fig. 4.4.1).

Bhatia (1983) also related the geochemical composition of sandstones to various plate tectonic settings. Figures 4.3.2 A-E and 4.3.3 A-E show the position of Pretoria Group sandstone samples and average values in the classification diagrams suggested by Bhatia (1983). Most sandstone samples and averages plot in or close to the passive margin field (Fig. 4.3.2 A-E and Fig. 4.3.3 A-E). A notable exception is the samples and average value for the Upper

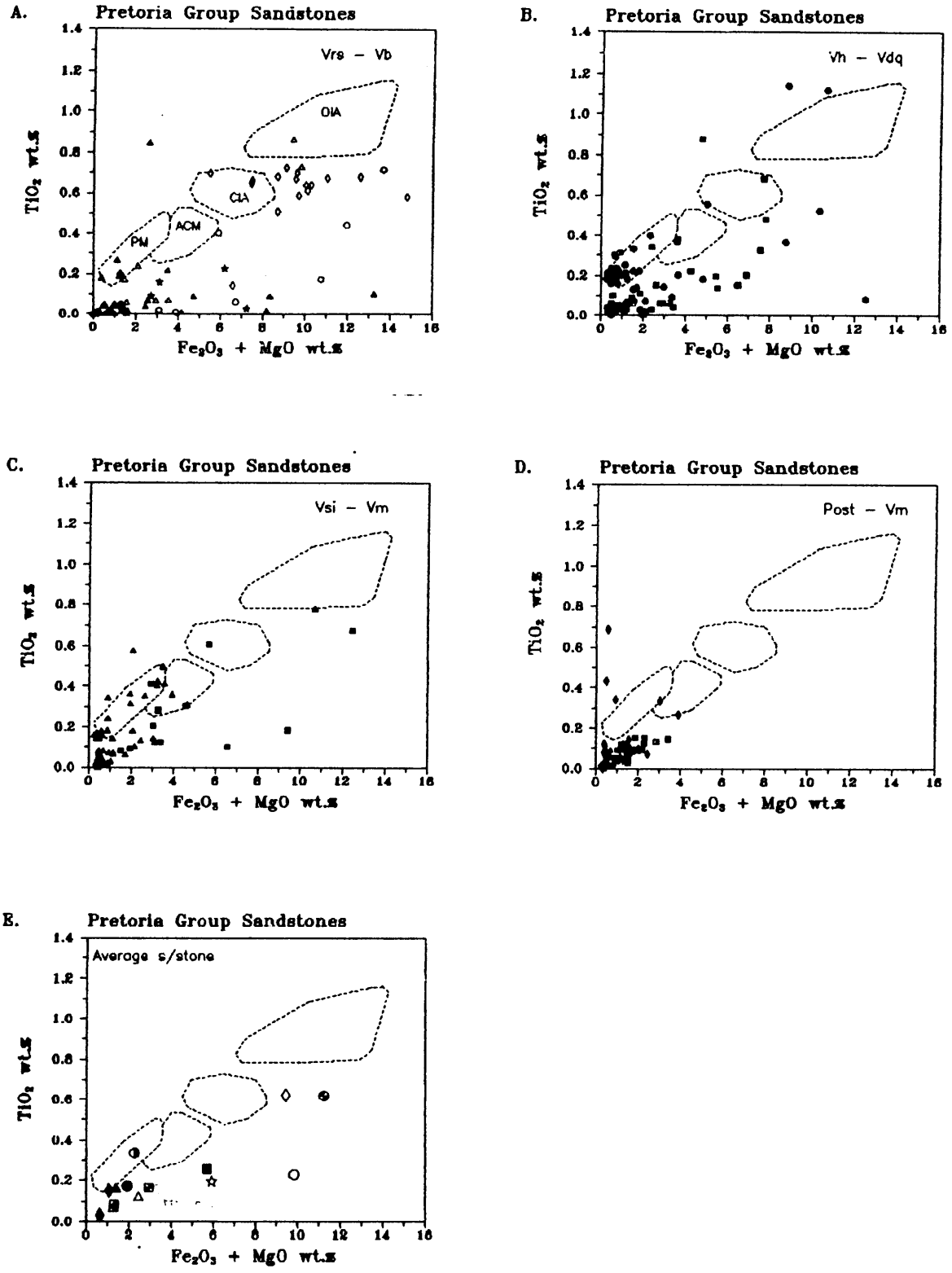

Fig. 4.3.2 A-E: TiO_2 - Fe_2O_3* + MgO tectonic setting discriminance diagram after Bhatia (1983) applied to Pretoria Group sandstones. Sandstones recalculated to 100% volatile-free. Symbols as in Figure 4.3.1. OIA = oceanic island arc; CIA = continental island arc; ACM = active continental margin; PM = passive margin. For stratigraphic abbreviations see Fig. 4.3.1.

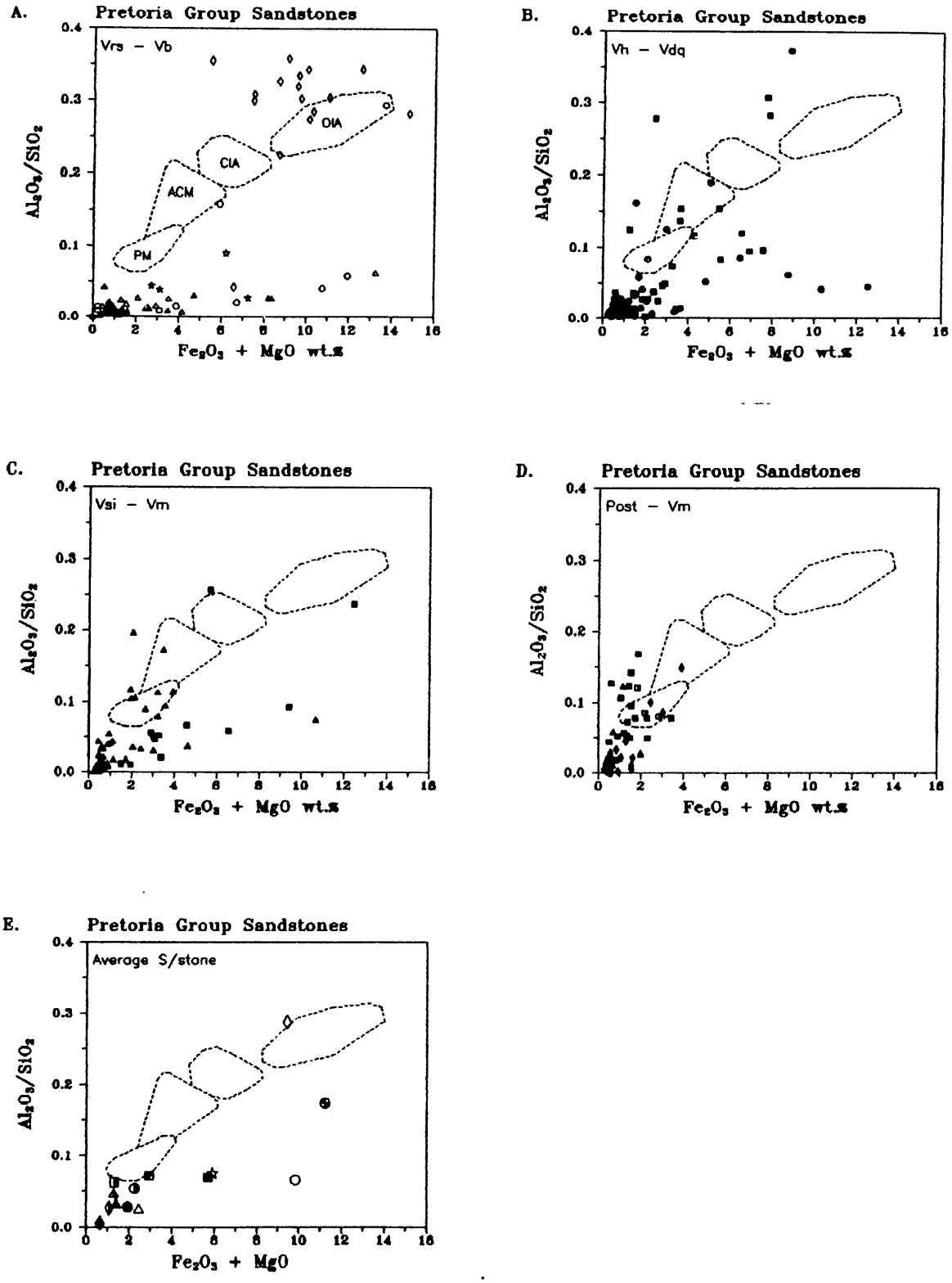

Fig. 4.3.3 A-E: Al_2O_3/SiO_2 - Fe_2O_3* + MgO tectonic setting discriminance diagram after Bhatia (1983) applied to Pretoria Group sandstones. Sandstones recalculated to 100% volatile-free. Symbols as in Figure 4.3.1. OIA = oceanic island arc; CIA = continental island arc; ACM = active continental margin; PM = passive margin. For startigraphic abbreviations see Fig. 4.3.1.

Timeball Hill Formation sandstones. However, these sandstone samples include the 'alternating shale and sandstone facies' (see Chapter 3.1.3), which might be not representative of a 'true' sandstone. Other sandstone averages deviating from the main field of composition of Pretoria Group sandstones are the Rooihoogte, Hekpoort, Boshoek and Silverton Formation averages. With the exception of the Hekpoort sandstones, these outliers have higher Fe_2O_3 + MgO contents without a concomitant increase of TiO_2 or Al_2O_3/SiO_2, and thus fall outside the areas defining Bhatia's (1983) tectonic classification groups. The increase of Fe_2O_3 + MgO is largely due to an increase in iron-content as the average MgO-content of the Pretoria Group sandstones does not exceed 1.5 wt.% (Chapter 3.3). As Rooihoogte, Boshoek and Hekpoort Formations were deposited in a palaeoenvironment related to erosional unconformities and/or soil development (Button, 1973; Button, 1979; Eriksson et al., 1993), the unusual geochemical pattern of these sandstones might be explained by the development of lateritic soils due to chemical weathering, and by the redistribution of genetically related iron minerals in the prevailing sedimentary environment. Alternatively, the unusual geochemistry might be due to the sample scale and palaeoenvironment, as defined by Ingersoll et al. (1993), who investigated the effect of depositional environment on the resultant sandstone petrofacies. Ingersoll et al. (1993) divided the depositional environment into three orders, namely, talus piles to small drainages (= first order), streams and rivers draining mountain ranges (= second order), and large rivers and the shelf environment (= third order). They (ibid.) were able to show that the sandstone petrography of first order sandstone assemblages is more dependent on the composition of their local sources than their plate tectonic setting. The variability of sandstone petrography decreases from first to third order assemblages, and only third order assemblages are able to provide an unambiguous interpretation of the plate tectonic setting (Ingersoll et al., 1993). Although Ingersoll et al. (1993) discuss a purely petrographic approach to interpreting the plate tectonic setting of sandstone assemblages, their results cannot be neglected in a geochemical investigation, as the geochemistry of sandstones is largely dependent on the petrographic composition. It is notable that Rooihoogte and Boshoek Formations show the highest variability of Pretoria Group sandstones in a quartz - feldspar - rock fragment diagram (Schreiber et al., 1991, 1992). The Rooihoogte, Boshoek and Dwaalheuwel Formations are interpreted as having been deposited in an alluvial fan palaeoenvironment (e.g., Eriksson et al., 1993; see also Chapter 1.3, Table 1.2.3), thus

representing a first order assemblage after Ingersoll et al. (1993). Hence, the exceptional geochemical pattern of these sandstones and their average values in Bhatia's tectonic discriminant diagram might be related to their depositional environment. An increase of iron in first order assemblages can be expected if iron-rich sources are present in the local provenance area, or if the iron-content is increased due to the local redistribution of iron-rich weathering residues. This model can also be applied to the sandstones of the Hekpoort Formation, which are thought to represent largely reworked volcanogenic material (Key, 1983; Nesbitt and Young, 1989). It is concluded that the geochemical approach of Bhatia (1983) can generally be applied to Pretoria Group sandstones, indicating thereby a passive margin tectonic setting for the Pretoria Group. The Rooihoogte, Boshoek, Hekpoort and Dwaalheuwel Formations are thought to represent first order sandstone assemblages, after Ingersoll et al. (1993), and have a distorted tectonic setting signature due to their inferred depositional palaeoenvironment.

Roser and Korsch (1986) discriminated the tectonic setting of mud to sand-sized material into three broad categories (passive margin, active continental margin and oceanic island arc margin), by using a simple SiO_2 - Na_2O/K_2O binary diagram. Figures 4.3.4 A-D show the position of Pretoria Group argillites and sandstones in this SiO_2 - Na_2O/K_2O binary diagram. It is apparent that most of the argillite samples (SiO_2 generally $<$ 70 wt.%) and nearly all the sandstone samples (SiO_2 generally $>$ 80 wt.%) occupy the passive margin field. Only the Silverton Formation shales (Fig. 4.3.4 C) have a transitional pattern with an equal number of samples in the passive margin and the active continental margin fields, as well as 17 samples falling into the oceanic island arc margin field. Roser and Korsch (1986) emphasize the transitional nature of their discriminantion approach, with a continuous development from mineralogically mature sedimentary rocks (passive margins), through quartz-intermediate assemblages (active continental margins), to quartz-poor volcanogenic sedimentary rocks (oceanic island arc margins). Implicit in this scheme is the possibility that the SiO_2 - Na_2O/K_2O distribution might not only depend on tectonic setting, but might also be influenced by the provenance (Roser and Korsch, 1986).

A geochemical comparison of Pretoria Group volcanic rocks (Chapter 3.4.2, Fig. 4.3.4 E and 4.3.5) shows a sharply defined separation between Hekpoort and Machadodorp volcanic

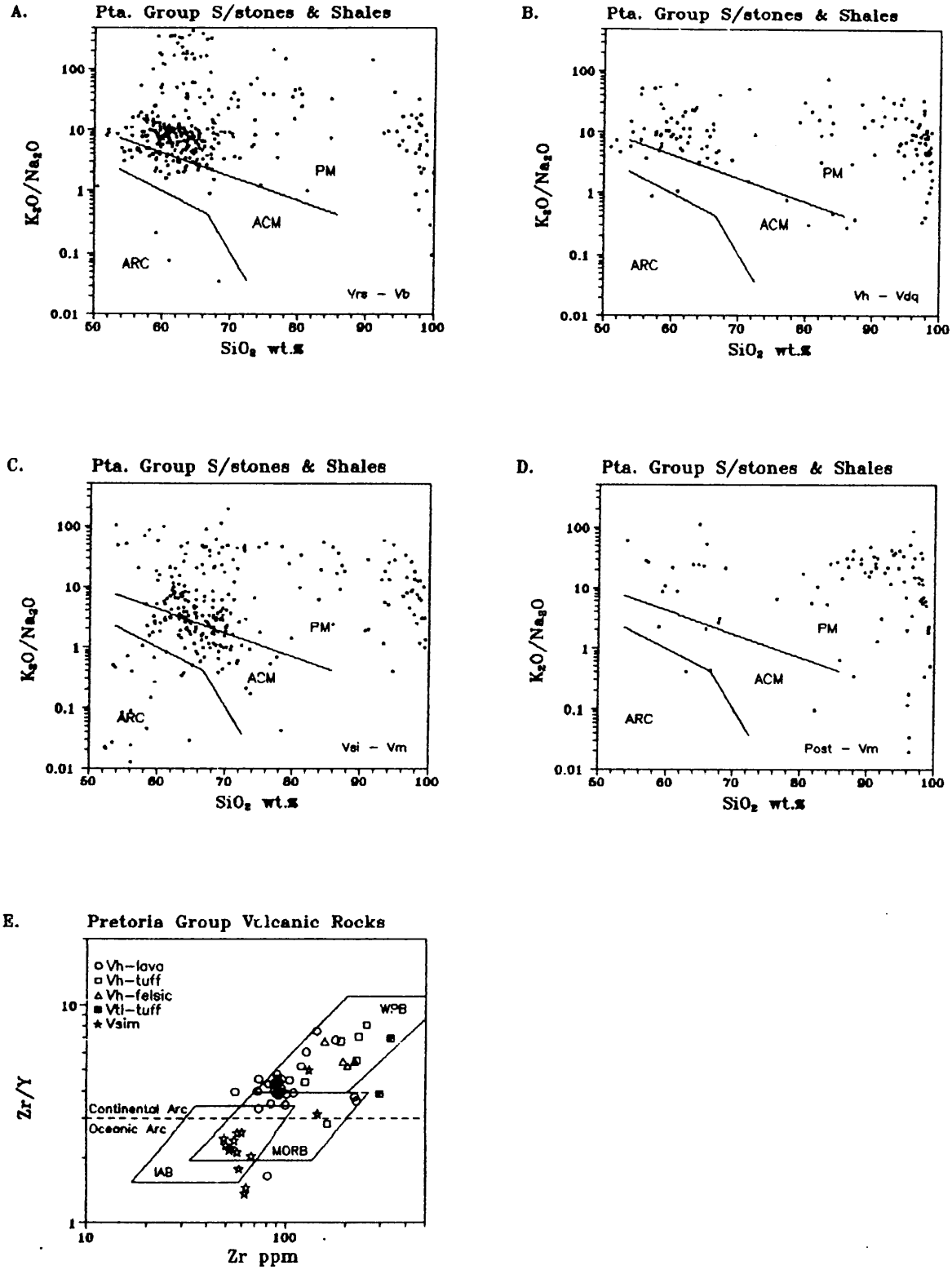

Figure 4.3.4 A-E: A.-D.: SiO2 - K2O/Na2O tectonic discriminance diagrams after Roser and Korsch (1986) applied to Pretoria Group sandstones and shales (recalculated to 100% volatile-free). A. Rooihoogte - Boshoek Formations; B. Hekpoort - Daspoort Formations; C. Silverton and Magaliesberg Formations; D. post-Magaliesberg Formations. Figure 4.3.4 E: Zr - Zr/Y tectonic setting discriminance diagram after Pearce and Norry (1978). WPB = within plate basalts; MORB = mid-ocean ridge basalts; IAB = island arc basalts. Symbols as in Fig. 4.3.5.; Vh = Hekpoort Fm., Vtl = Lower Timeball Hill Shale Member, Vsim = Machadodorp Volcanic Member.

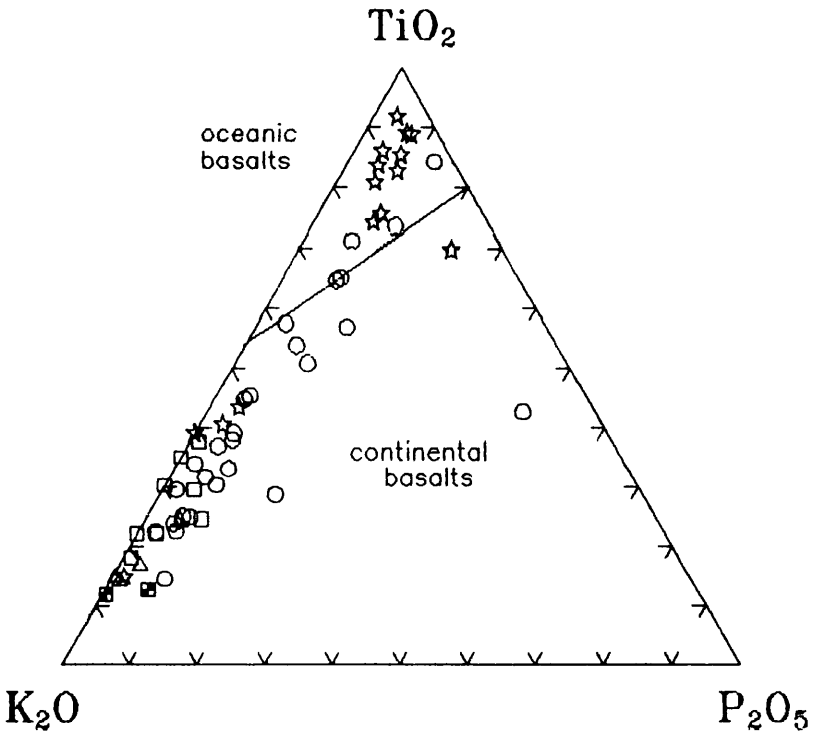

Fig. 4.3.5: TiO_2 - K_2O - P_2O_5 tectonic setting discriminance diagram for basalts (after Muller, 1983) applied to Pretoria Group volcanic rocks. ○ = Hekpoort lava; □ = high-Al-K volcanic rock from the Hekpoort Fm.; Δ = 'felsic' rock from the Hekpoort Fm.; ■ = tuffaceous material from the Lower Timeball Hill Fm.; ★ = Machadodorp volcanics.

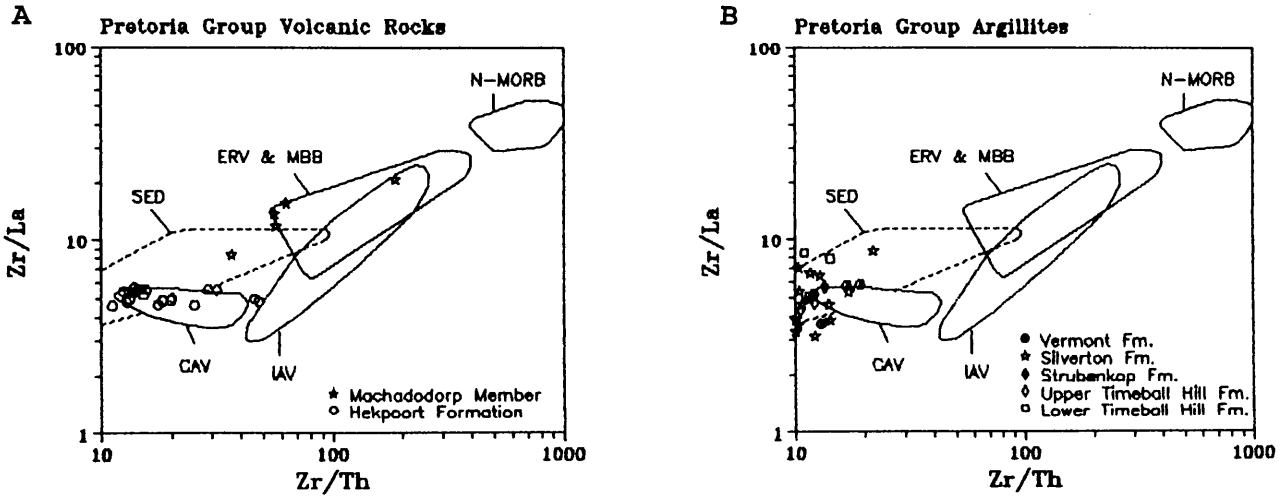

Fig. 4.3.6 A-C: Zr/Th - Zr/La tectonic setting discriminance diagram for volvanic rocks after Smith (1991). CAV = continental arc volcanics; ERV & MBB = ensialic rift volcanics and marginal basin basalts; N-MORB = normal mid-ocean ridge basalt; IAV = island arc volcanics; SED = sediments. A: Hekpoort (○) and Machadodorp (★) volcanic rocks, data were taken from Sharpe et al. (1983) and Crow and Condie (1990). B and C: sedimentary rocks of the Pretoria Group (symbols explained in Figure 4.3.6 B)

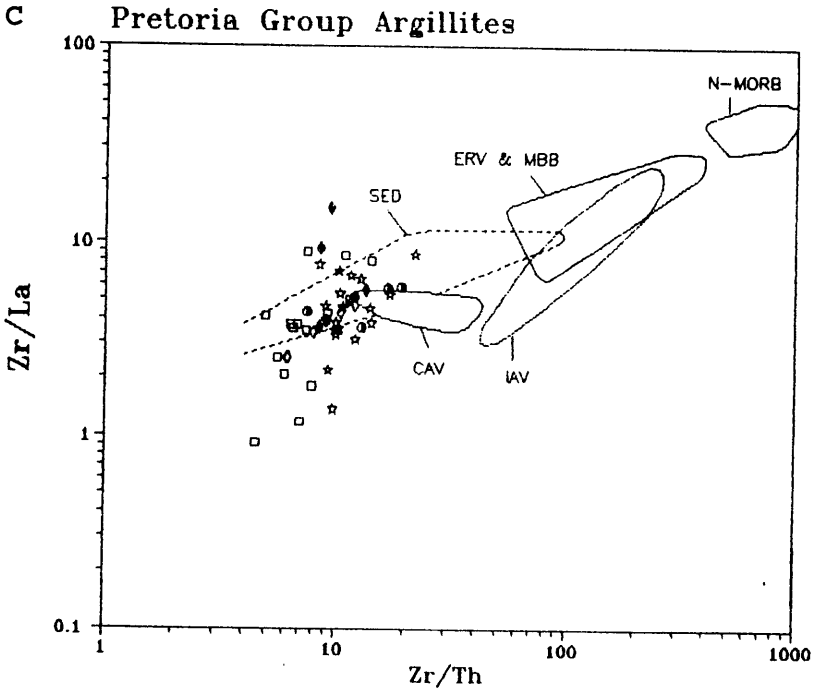

Fig. 4.3.6 A-C (continued): Zr/Th - Zr/La tectonic setting discriminance diagram for volcanic rocks after Smith (1991) (see p. 315).

rock samples. The Machadodorp volcanics have an oceanic basalt signature, whereas the Hekpoort volcanics have a continental basalt geochemistry. It is argued that the Silverton Formation shale samples falling into the oceanic island arc margin field of Roser and Korsch (1986) (Fig. 4.3.4 C) may include a strong volcanic component related to penecontemporaneous volcanism. These argillite samples are also clustered outside the main trend of the CIA - TiO_2 diagram (Fig. 4.2.1 B), with exceptionally high Ti-contents. The presence of tuffaceous shales and argilliceous tuffs in the Silverton Formation was previously reported by Eriksson et al. (1990) and Schreiber (1990). The variable SiO_2 - Na_2O/K_2O distribution of the Silverton shales, probably due to penecontemporaneous volcanism, poses intrinsic problems for the general applicability of the tectonic setting discrimination diagram of Roser and Korsch (1986). Eriksson et al. (1993; in press a) and Schreiber (1990) proposed an intracratonic rift setting for the Pretoria Group. Intracratonic rifts fall necessarily into the passive margin tectonic setting. As the geochemistry and petrography of rift-related sedimentary rocks can be influenced by penecontemporaneous volcanism, as proposed for the Silverton Formation, by proximity to active tectonic settings (e.g., Rio Grande rift, Potter, 1986) and by erosion of ancient active settings (e.g., Rio Conchos, Ingersoll et al., 1993),

the interpretation of plate tectonic settings of sedimentary basins should generally not be based on sedimentary compositions alone (Ingersoll et al., 1993). Floyd et al. (1989) applied discriminant scores calculated by Bhatia (1983) for Lewisian clastic metasediments from a rift setting, and concluded that the discriminant function proposed by Bhatia (1983) might not be able to discriminate between continental arc settings and rift-related depositional environments. The discriminant functions of Bhatia (1983) could not be applied to the Pretoria Group samples as the FeO-content was not analysed separately in the present investigation.

Although the geochemistry of Pretoria Group sedimentary rocks shows evidence for a passive margin tectonic setting, it may be instructive to discuss the geochemistry and possible settings of the volcanic rocks of the Pretoria Group in some detail. Figures 4.3.6 A - C show the position of Pretoria Group volcanic and sedimentary rocks in a Zr/Th - Zr/La discrimination diagram after Smith (1991). The Zr/Th - Zr/La discrimination diagram is thought to exemplify the relationship of large ion lithophile elements (LILE, Th), light rare earth elements (LREE, La) and high field strength elements (HFSE, Zr). Due to a highly variable La-content (see also Chapter 4.1, 4.2 and 4.5), the argillicous rocks of the Pretoria Group plot partly outside the sedimentary field proposed by Smith (1991)(Fig. 4.3.6 B and C). It is interesting to note that the geochemical composition of the sedimentary rocks is thought to be uncharacteristic of their tectonic setting in this approach. However, the plot can be applied to Hekpoort and Machadodorp volcanics (Fig. 4.3.6 A). As REE were not determined for volcanic rocks in the present investigation, the data plotted in Figure 4.3.6 A were taken from Sharpe et al. (1983) and Crow and Condie (1990). The Hekpoort samples fall into the continental arc field, the Machadodorp volcanics into the ensialic rift and marginal basin basalt field (Fig. 4.4.6 A).

The magmatism of continental arcs is related to partial melting in the over-riding plate and, possibly, in the subducted oceanic plate, when the latter reaches depth between 100 and 150 km (Allen and Allen, 1990). Rift basins owe their origin to either mechanical stretching of the lithosphere (passive rifting) or to a thermal disturbance involving the mantle (active rifting) (Allen and Allen, 1990). The plate tectonic setting of a continental arc is a convergent margin, the plate tectonic setting of a rift basin a divergent margin (Allen and

Allen, 1990). It might be argued that extensional arc settings (e.g., Dewey, 1980) match this pattern, i.e., roll-back of the subducting hinge leads to extensional tectonics in the overriding plate and produces a back-arc (= marginal) basin behind the continental arc. However, continental arc and marginal basin are penecontemporaneous features and lateral 'tectonic facies equivalents' on a convergent plate margin, whereas the Hekpoort volcanism preceeds the Machadodorp volcanism and Hekpoort and Machadodorp volcanics were deposited in vertical succession in the same basin. Furthermore, the Pretoria Group is devoid of orogenic features, which would be expected from the compressional stages of convergent margin development (Allen and Allen, 1990). A retro-arc foreland basin setting (e.g., Biddle et al., 1986), as proposed for the Transvaal Supergroup by Winter (1989), can account for the continental arc signiture of the Hekpoort volcanism; however, it is not compatible with either Machadodorp volcanic rock geochemistry and its implications, the subsidence history, sedimentation and depositional palaeoenvironment of the Transvaal Supergroup and, more specifically, the Pretoria Group (e.g., Tankard et al., 1983; Eriksson et al., 1993), nor with the lack of structural evidence supporting this model.

The geochemistry and magma evolution of the Hekpoort volcanics were previously discussed by Sharpe et al. (1983), Myers et al. (1987), Condie and Crow (1990), Crow and Condie (1990), Harmer and v. Gruenewaldt (1991) and v. Gruenewaldt and Harmer (1993). Sharpe et al. (1983) consider the genesis of Hekpoort volcanics as having been a stepwise procedure of partial melting → assimilation → fractionation → extrusion involving compositionally homogenous mantle and lower crust. Myers et al. (1987) report geochemical similarities of Kaapvaal volcanics, including the Hekpoort volcanics, from the Archaean (≈ 3.0 Ga) to the Phanerozoic (≈ 180 Ma), and favour a model in which most of these volcanic suites were derived by melting within a modally metasomatized sub-continental lithosphere. Crow and Condie (1990), Harmer and v. Gruenewaldt (1991) and v. Gruenewaldt and Harmer (1993) suggest an ancient (i.e., older than 3.0 Ga) subduction-zone component in the lower crust or upper mantle below the Transvaal Basin, as the most likely source for the Hekpoort volcanics. Crow and Condie (1990) further relate the geochemistry of the Machadodorp volcanics to a mantle source different to the Hekpoort volcanics source, and infer strong similarities between the Machadodorp volcanics and MORB. Harmer and v. Gruenewaldt (1991) and v. Gruenewaldt and Harmer (1993) interpret the consistency of the trace element

patterns of the Hekpoort (and correlated Ongeluk) volcanics as evidence against crustal magma contamination of a homogeneous mantle source during ascent through the continental crust. In contrast, Condie and Crow (1990) successfully model the Hekpoort volcanics as having been derived by assimilation-fractional crystallisation of Al-undepleted komatiite with Archaean granitoids. Condie and Crow (1990) point out that a magma derivation from subcontinental lithosphere is unlikely for the Archaean and Early Proterozoic volcanics of the Kaapvaal Craton, as South African ultramafic xenoliths from kimberlites, thought to represent the subcontinental lithosphere, are too depleted in major elements like Fe, Ca and Ti to serve as basaltic sources. Condie and Crow (1990) also relate the Machadodorp volcanics to their contaminated komatiite model.

However, the MORB-like signature of the Machadodorp volcanics (Crow and Condie, 1990; see also Fig. 4.3.4 E and Fig. 4.3.5) makes an assimilated-fractional crystallisation model (DePaolo, 1981) with a komatiitic source and a crustal contaminant unlikely, as can also be deduced from the Ti - Zr diagram shown in Fig. 4.3.7 A and B. It is apparent from Figures 4.3.7 A and B that the Machadodorp volcanics can be modelled simply, as a partial melt of material with mantle composition, to account for their MORB-type signature. MORB-type magmas are enriched in incompatible and compatible elements, except Mg, compared to primitive mantle (Hofmann, 1988; Floyd, 1991), although elements behaving incompatibly in the mantle have stable ratios in mantle processes (Hatton and Sharpe, 1988). The Ti - Zr ratio observed in the Machadodorp volcanics (Fig. 4.3.7 A and B) is similar to various mantle ratios, thus strengthening the interpretation that the bulk of the Machadodorp volcanics are MORB-type basalts; this is also inferred by the distribution of other trace elements like flat LREE-patterns (Crow and Condie, 1990) and MORB-normalised trace element patterns (v. Gruenewaldt and Harmer, 1993), except for an increase in K, Rb, Ba and Th, which can be led back to minor crustal contamination (Crow and Condie, 1990). MORB genesis is interpreted as decompressional partial melting of primitive mantle, due to upwelling of the asthenosphere in extensional tectonic settings, exemplified by mid-ocean ridges (White, 1991). Apart from mid-ocean ridges, asthenospheric upwelling is an important feature in all modern rift models (Allen and Allen, 1990; Latin et al., 1993). Upwelling mantle with a normal potential temperature of 1280° C crosses the dry solidus at about 50 km depth, and begins to melt (White, 1991). It is argued that the geochemical patterns of the

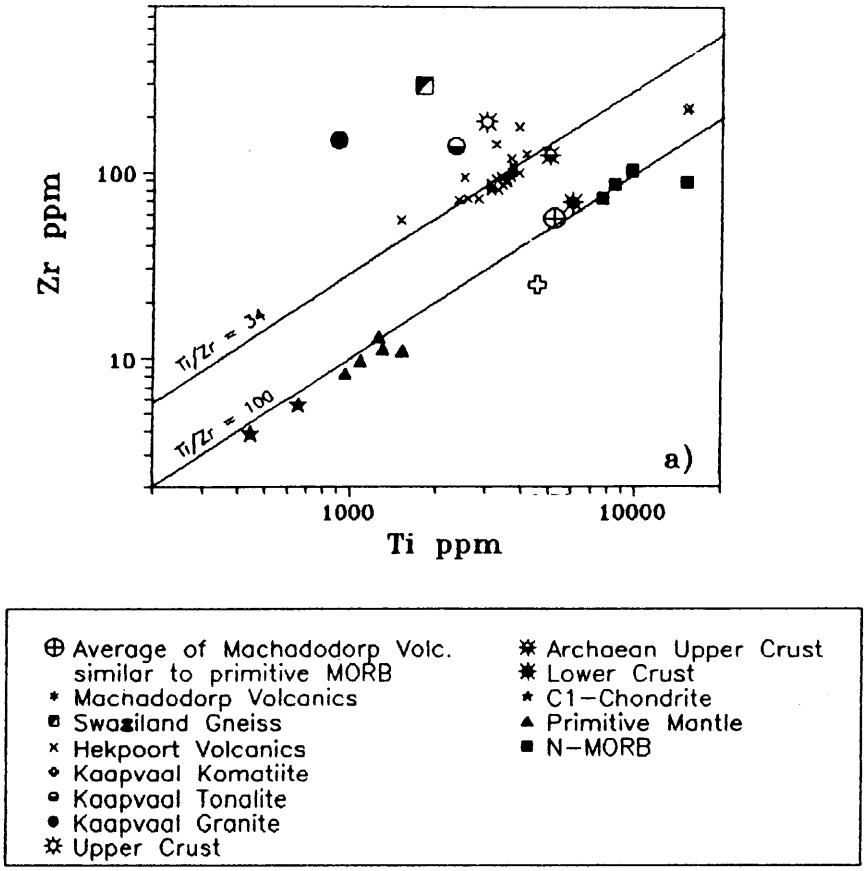

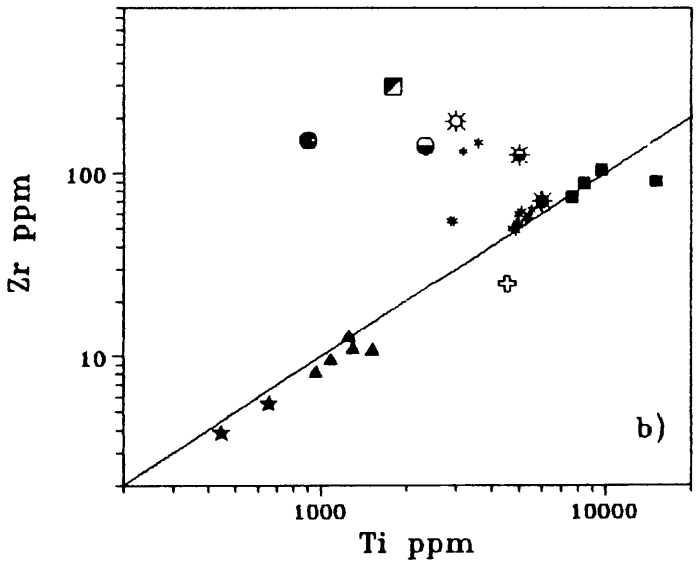

Fig. 4.3.7 A and B: The relationship of Zr and Ti in Hekpoort and Machadodorp volcanics compared to literature data of various crustal levels. Symbols are explained in box.

Data sources: Kaapvaal komatiite, tonalite and granite from Condie and Crow (1990); Upper Crust, Archaean Upper Crust and Lower Crust from Taylor and McLennan (1985); Primitive Mantle from Wood et al. (1979), Anderson (1983), Taylor and McLennan (1985), Hofmann (1988), Sun and McDonough (1989); N-MORB from Pearce (1983), Tarney (1984), Hofmann (1989), Sun and McDonough (1989); Swaziland Gneiss from Hatton and Sharpe (1988); C1-Chondrite from Taylor and McLennan (1985), Sun and McDonough (1989).

Hekpoort and Machadodorp volcanics are compatible with a rift tectonic setting.

Sharpe et al. (1983) were able to model the geochemistry of Hekpoort volcanics, by assuming a 5 - 8 % partial melt of mantle material, which was contaminated by crustal material with Swaziland Gneiss composition (82 % partial melt, 18 % contaminant), together with hornblende fractionation (Cawthorn and O'Hara, 1976) of the contaminated melt, removing 15 % olivine, 15 % orthopyroxene and 70 % hornblende. In addition, the application of an assimilated-fractional crystallization model, using a contaminated melt of the same composition, is able to produce the trace and major element patterns of the Hekpoort volcanics, except for the initial strontium ratio (Sharpe et al., 1983). The geochemistry of the Hekpoort volcanics can also be modelled successfully by assuming assimilated-fractional crystallisation of a parental magma of komatiitic composition and crustal contamination with rocks of granitoid composition (Condie and Crow, 1990).

A rift tectonic setting could thus explain the volcanic events in the Pretoria Group without requiring different magma sources (e.g., Crow and Condie, 1990), nor inferring an unusual lower crust/upper mantle composition (e.g. Harmer and v. Gruenewaldt, 1991). Upwelling of the asthenospere and related decompressional partial melting of mantle material, with crustal contamination during ascent of the magma, can explain the geochemical composition of both Hekpoort and Machadodorp volcanics, and is thus thought to represent a viable alternative genetic model for Pretoria Group volcanism. Partial melting of lower crustal material with a subduction zone component (e.g., Harmer and v. Gruenewaldt, 1991) or partial melting of modally metasomatized subcontinental lithosphere (e.g., Myers et al., 1987) can account for the composition of the Hekpoort volcanics, but not for the composition of the Machadodorp volcanics.

The geochemical signature of Pretoria Group sedimentary rocks is indicative of a passive margin tectonic setting, and thus compatible with a rift setting. It is concluded that asthenospheric upwelling and related processes in the mantle and lithosphere can be used as a simple explanation for the occurrence and composition of the Pretoria Group volcanism.

4.4 Palaeoenvironment, diagenesis and epithermal processes

4.4.1 The distribution of boron in Pretoria Group sedimentary rocks

The palaeoenvironment of the Pretoria Group has been the subject of controversial discussion in recent years, with two opposing interpretations prevailing, namely an epeiric marine palaeoenvironment and an intracratonic palaeoenvironment with predominantly fluvial-lacustrine settings (see Chapter 1.3 and Table 1.3 for references). As previous workers base their interpretation mainly on sedimentological data, one aim of this investigation was a thorough discussion of the palaeoenvironmental implications of the observed geochemistry of the sedimentary rocks of the Pretoria Group. The B content of Pretoria Group shales was utilized by Schreiber (1990), Eriksson (1992) and Eriksson et al. (1993) to infer a predominantly freshwater palaeoenvironment for Pretoria Group shales, except for the Silverton Formation, which is thought to show evidence of a marine transgression.

The relationship of depositional environment and geochemistry of sedimentary rocks is difficult to assess. Interpretations of source rocks, palaeoclimate and tectonic setting are based on abundances of elements thought to be relatively immobile and/or ratios of immobile to mobile elements (Chapter 4.1, 4.2 and Chapter 4.3). In contrast, the utilization of the geochemistry of sedimentary rocks to interpret depositional palaeoenvironments involves mainly mobile elements like Na, Mg, Ca, K (e.g., Spears, 1974), Ni, Cu, Zn, Rb and B (e.g., Zawada, 1988). The geochemical interpretation of depositional palaeoenvironment is based principally on absorption or adsorption of elements enriched in seawater onto clay minerals. It has to be emphasized in this context that the major part of most clay mineral associations has a detrital origin (i.e., as opposed to an authigenic origin), independent of the depositional environment (Chamley, 1989). Hence, the geochemical approach to palaeoenvironmental interpretation has several implicit problems: (1) The inherited detrital content of the discriminatory element in a sample is generally an unknown variable (e.g., Eriksson et al., under review a); (2) sedimentation rate and/or water temperature is known to increase/decrease sorption (Harder, 1959, 1963; Porrenga, 1967), but is also a generally unknown variable; (3) the distribution coefficients for a respective element in a clay mineral-seawater system may differ for different clay minerals (e.g., Porenga, 1967); and (4) the

effects of diagenesis, epithermal processes and/or metamorphism (i.e., post-depositional events) may change the absolute or relative contents of mobile elements in a specific clay mineral, and can therefore lead to depletion/enrichment of discriminatory elements in the whole rock sample.

Boron may serve as an example of the problems inherent in geochemically based palaeoenvironmental interpretations. Boron is thought to be a useful palaeosalinity indicator in sedimentary rocks, as river waters are 400 times lower in their boron contents than seawater (Harder, 1974c); in addition, a general positive relationship between boron content of sedimentary rocks and the salinity of their waters of deposition can be distinguished (e.g., Frederickson and Reynolds, 1960; Walker and Price, 1963). Once boron has been adsorbed onto clay mineral particles, it becomes fixated by hydrostatic bonding and thereafter is incorporated into the tetrahedral sheet structures of the clay minerals (Couch, 1971). The boron content normally correlates strongly with total clay content (e.g., Potter et al., 1963), and will tend to be concentrated within the illite fraction of the clay minerals (e.g., Fairchild et al., 1988), although muscovite-sericite, glauconite, lepidolite, montmorillonite and serpentinite may also have very high boron contents (Harder, 1974a). Due to the common preferential uptake of boron by illite, Reynolds (1965) gave the following equation to adjust the total boron content of a sample to boron bound in the illite fraction:

$$\text{ppm } B_{ILLITE} = \text{ppm } B_{\text{in sample}} * 7.7 \,/\, \text{wt.\% } K_2O_{\text{in sample}},$$

where 7.7 represents the theoretical K_2O-content of illite in weight percent. The total boron and adjusted boron contents are thought to be related to the palaeosalinity of the depositional waters with defined fields for marine (100-200 ppm B_{SAMPLE}; > 300 ppm B_{ILLITE}), brackish (80-110 ppm B_{SAMPLE}; 200-300 ppm B_{ILLITE}) and freshwater (10-50 ppm B_{SAMPLE}; < 200 ppm B_{ILLITE}) depositional environments (Reynolds, 1965, 1972). B_{SAMPLE} or B_{ILLITE}-contents have been applied successfully in several investigations to determine the depositional palaeoenvironment (e.g., Ernst et al., 1958; Frederickson and Reynolds, 1960; Ernst and Werner, 1964). However, the same approach failed in other investigations (e.g., Dewis et al., 1972; Baumann and Werner, 1973), thereby indicating that the relationship of B-contents of sedimentary rocks and palaeosalinity of the depositional palaeoenvironment is more

complex.

The boron content of a sedimentary rock is subject to a large number of influences other than the boron content and salinity of waters of deposition: clay content and clay mineralogy, inherited boron within detrital particles, rate of sedimentation, water temperature, organic matter content, detrital and authigenic tourmaline, diagenesis and metamorphism (Nel, 1968; Harder, 1974c and d; Schopf, 1980; Fairchild et al., 1988; Zawada, 1988; Eriksson et al., under review a). Poorly crystallised illites adsorb more boron than well crystallised illite (e.g., Porrenga, 1967). The incorporation of boron into the tetrahedral sheet structure of clay minerals (Couch, 1971) prevents loss of boron during low grade metamorphism (Harder, 1974e) and during moderate weathering (Fairchild et al., 1988), but implies a problem as inherited boron in detrital clay particles may mask the palaeosalinity of waters of deposition (Bouska, 1981). A slower rate of sedimentation will increase boron sorption, as will higher temperatures (Harder, 1959, 1963; Porrenga, 1967). Organic matter can also affect the uptake of boron by clay minerals, by forming an inhibiting protective covering on the particles (Landergren and Carvajal, 1969). Due to the resistance of the illite structure, diagenesis is likely to have only a small effect on boron contents of illites (Nel, 1968). However, illite may be only one of the constituents of the clay mineral assemblage, and thus the possibility of diagenetic loss of boron must be considered (Wedepohl, 1974). The presence of organic matter to hinder boron adsorption onto clay particles may also result in a greater diagenetic loss of this relatively mobile element (Eriksson et al., under review a).

The boron contents of Pretoria Group rocks are shown in Figures 4.4.1 and 4.4.2. The Pretoria Group shales have an average boron content of 98 ppm (n = 174), sandstones of 41 ppm (n = 80), carbonate rocks of 72 ppm (n = 9) and andesitic tuffs interbedded with argilliceous material from the Hekpoort Formation of 186 ppm (n = 6) (see also Chapter 3.4). The Pretoria Group shales have a somewhat lower average boron content than other average boron estimates for shales (Harder, 1974d: 100 ppm for all shales, 120 ppm for post-Precambrian shales; Shaw and Bugry, 1966: 160 ppm); however, they are considerably enriched compared to Average Canadian Proterozoic shale (Cameron and Garrels, 1980), which has an average boron content of only 25 ppm. It is doubtful if the mean boron concentration of Pretoria Group shales reflects an appropriate estimate of the central value

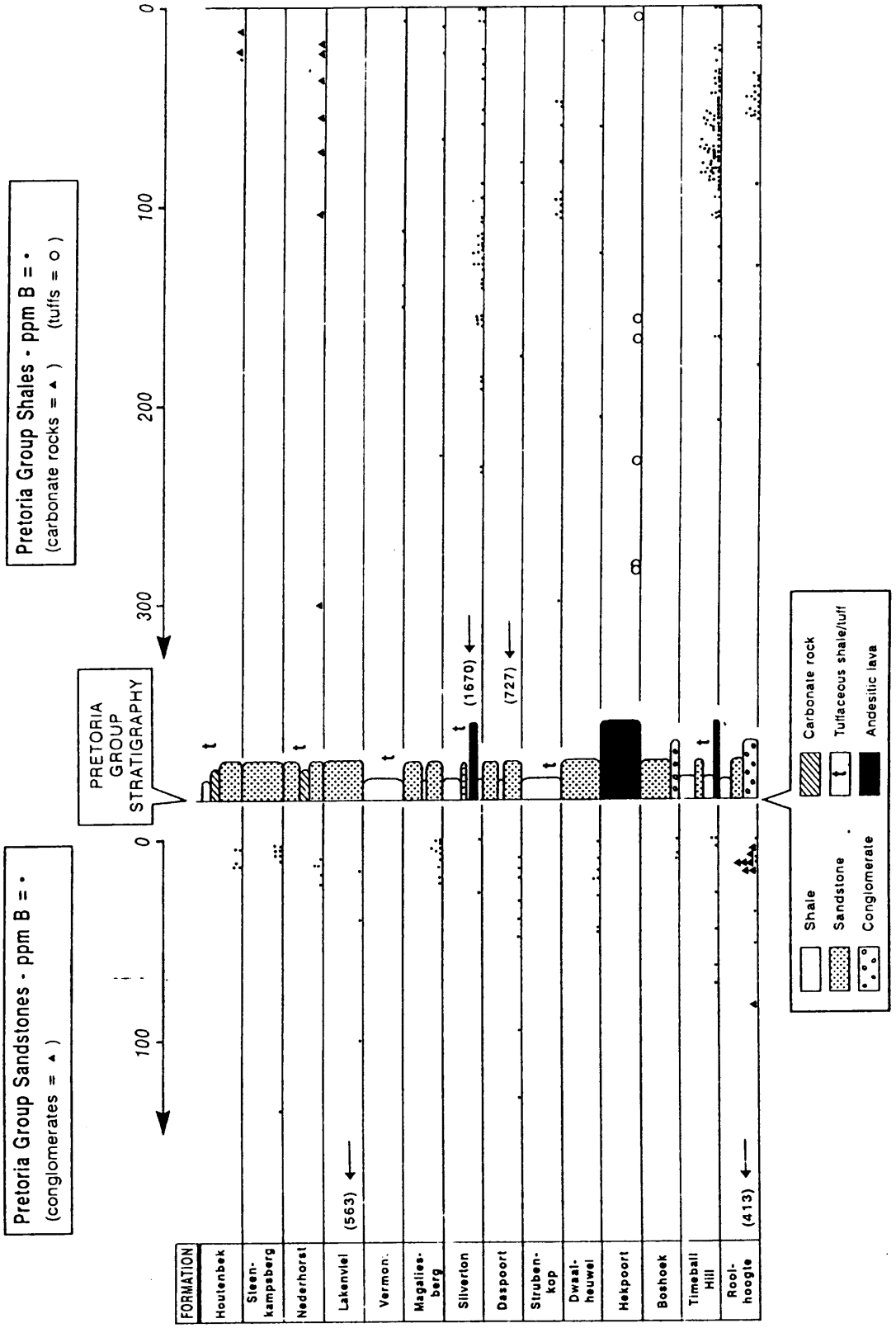

Fig. 4.4.1: Boron values determined for the Pretoria Group, plotted against stratigraphic height. True values of thicknesses of stratigraphic units not shown. Modified after Eriksson et al. (under review a).

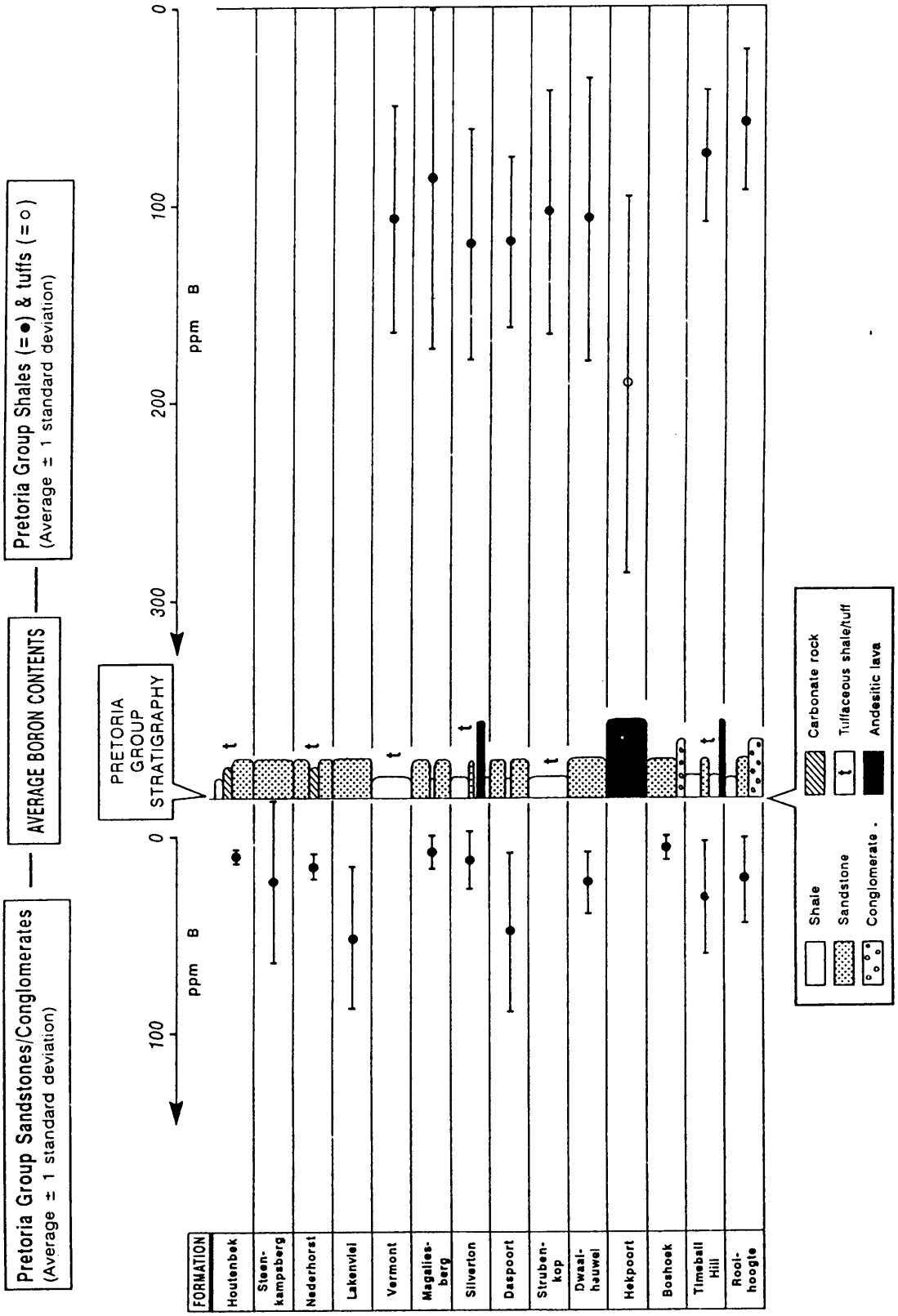

Fig. 4.4.2: Average boron contents (± 1 σ standard deviation) of shales, sandstones and tuffs (Hekpoort Formation only) within the stratigraphic units of the Pretoria Group. Note that boron values too large to be plotted on Figure 4.4.1 (and shown there in brackets) were not used in the determination of the averages and standard deviations shown here. Modified after Eriksson et al. (under review a).

of the boron distribution, as the standard deviation exceeds the arithmetic mean (i.e., the variation coefficient is greater than 1)(Table 3.4.1.1). The median of the boron distribution of Pretoria Group shales lies at 72 ppm, the geometric mean at 69 ppm (Table 3.4.1.1), thus indicating that the average boron concentration is depleted compared to average shales (see above), but not as strongly depleted as Canadian Average Proterozoic Shales (Cameron and Garrels, 1980). The average boron concentration of Pretoria Group sandstones is higher than the 30 ppm B estimate for quartzose sandstones and the 35 ppm B estimate for wackes reported by Harder (1974d). However, the average boron concentration of Pretoria Group sandstones is biased by a small number of extremely high B-contents (up to 563 ppm boron). The median boron concentration of Pretoria Group sandstones is 15.5 ppm, the geometric mean 18 ppm (Table 3.4.1.4), thus implying some depletion compared to average sandstone estimates. Andesitic lavas have average boron concentrations between 20 and 40 ppm (Harder, 1974b), with andesitic tuffs reaching concentrations of up to 2100 ppm in individual samples (Lisitsyn and Khitrov, 1962). The Pretoria Group andesitic tuff average of 186 ppm far exceeds that of the sedimentary rocks and is significantly higher than andesite averages. The Pretoria Group carbonates analysed for boron (Fig. 4.4.1) have relatively high average boron contents compared to Harder's (1974d) average of 20 ppm B for carbonates.

Figure 4.4.2 shows the Pretoria Group boron averages and the 1 σ standard deviation sorted according to stratigraphic height. The mean boron concentrations of Pretoria Group shales exhibit a reasonably well defined increase in boron content from the basal Rooihoogte Formation up to the Silverton Formation, after which there are too few values to discriminate further. Anomalously high boron values occur within the carbonate rocks of the Nederhorst Formation, where they are interbedded with thin fine-grained material thought to represent tuffaceous material (Schreiber, 1990). Anomalously high boron values are also found at the transition of Rooihoogte and Timeball Hill Formations, and in the Daspoort, Silverton, Dwaalheuwel and Lakenvlei Formations (Fig. 4.4.1).

As discussed previously, the boron content of shales depends largely on the relative abundance of illite. The illite content of the Pretoria Group shales is difficult to assess with the methods used in this investigation (XRD, see Chapter 3.1.6) as illite, muscovite, biotite and other micas are all characterised by a peak of approximately 10 Å in the X-ray

diffraction pattern. However, a more detailed investigation of the clay mineralogy would have difficulty in distinguishing between primary illite, i.e. illite present during the depositional process, and secondary illite, i.e. illite formed from smectite, kaolinite and/or mixed-layer clay minerals upon burial, diagenesis and/or metasomatism (Weaver, 1989; Nesbit and Young, 1989). Although the boron content of primary illite is unlikely to be affected by diagenesis or low grade metamorphism (Harder, 1974e), a thorough investigation of the relationship of boron contents of secondary illite compared to the boron contents of their precursors has not been published. The genesis of secondary illite is discussed controversially (see Weaver, 1989, p. 418 ff for a detailed discussion), and proposed reaction mechanisms vary from dissolution precipitation to solid-state transformation. As the Pretoria Group shales do not contain expandable clay layers (Chapter 3.1.6), it is concluded that smectites and/or mixed-layer clay minerals, if present primarily, were transformed into illite and/or chlorite upon burial. The transformation of illite into K-feldspar (Nesbit and Young, 1989) seems to have been unimportant for Pretoria Group shales, as K-feldspar was only detected in one shale sample of the Nederhorst Formation (sample number ET-341). It should be noted that the boron content of this sample is only 19 ppm, although the potassium content is 5.62 wt.%. The relationship of boron and potassium in Pretoria Group shales is shown in Figure 4.4.3 B. Although the samples scatter considerably, a weak negative correlation of K_2O and B can be seen for the bulk of the shale samples in Figure 4.4.3 B. A primarily negative correlation of potassium and boron in Pretoria Group shales can also be deduced from the comparison of mean K_2O and B contents (Fig. 3.4.3.1a and c). The potassium content of Pretoria Group shales can be assumed to be dependent on the total mica mineral group content, i.e. illite and mica group minerals. Hence, the reverse stratigraphic distribution of K_2O (Fig. 3.4.3.1a) and B (Fig. 4.4.2) could be explained by assuming changing proportions of illite and mica group minerals, with an increase of the illite fraction compared to the mica fraction, and an overall decreasing total mica content with increasing stratigraphic height. As boron is preferentially enriched in illite, the boron content increases with stratigraphic height, although potassium is somewhat depleted (Fig. 3.4.3.1a). However, this interpretation is in conflict with the clay mineral assemblage of Pretoria Group shales. The mineralogy of Pretoria Group shales is compiled in Tables 3.1.6 a-c. The shales can be divided into two major petrographic groups due to their clay mineralogy, (a) shales with abundant mica and kaolinite group minerals, which prevail in the lower part of the Pretoria

Group up to the Strubenkop Formation, and, (b) shales with abundant mica and plagioclase, in the Silverton and Vermont Formations. It has to be stressed that chlorite is only common in the Botswana sampling area, where the subdivision cannot be applied as kaolinite group minerals are common constituents throughout the profile. At temperatures between 200 to 350 C°, kaolinite is normally transformed to pyrophyllite, due to dewatering, or to a K-hydromica (i.e., illite), if the $[K^+]/[H^+]$ ratio of interstitial waters is high (Weaver, 1989). The abundance of kaolinite in the Pretoria Group shales is somewhat enigmatic, if a minimum burial temperature of 300 C° is assumed (Button, 1979), but can readily be explained by retrograde diagenesis of pyrophyllite during late stage ascent to the surface. Kaolinite is thought to be concentrated in shales of continental facies and/or with a relatively short transport distance (e.g., Rösler and Lange, 1976; Chamley, 1989). The abundance of kaolinite strongly supports a continental affinity for the Pretoria Group shales, combined with chemical weathering of the source rocks. As moderate chemical weathering in the provenance area would already transform mica minerals into illite, chlorite, smectite and/or mixed-layer clay minerals, the concomitant detrital input of kaolinite and mica minerals is improbable for detritus from a homogeneously weathered source area.

As already discussed in Chapter 4.2, interstitial and ground waters of continental origin tend to enrich sedimentary rocks in potassium during diagenesis and metasomatism, due to the transformation of either kaolinite or smectite into illite (Weaver, 1989; Nesbit and Young, 1989). Pretoria Group shales show some evidence for the post-depositional enrichment of potassium, i.e. the strong enrichment of potassium in the Hekpoort palaeosol (Table 4.1.3a) and the potassium patterns in upper crust-normalised spidergrams, which deviate significantly from the expected pattern (Chapter 4.2, Fig. 4.2.3). These upper crust-normalised diagrams (Fig. 4.2.3) suggest an average enrichment of the potassium content of Pretoria Group shales by a factor of 2 to 4 compared to weathered shales of otherwise similar chemical composition (Nesbitt et al., 1980).

An interpretation of the K_2O-B relationship must thus consider the diagenetic and/or metasomatic neoformation of illite. The K_2O-B relationship can be explained by two possible models: (1) the illitisation process added potassium and released boron relative to the primary shale composition; (2) the low boron content of the primary clay mineral assemblage was

maintained and the potassium content increased more strongly than in model (1). The latter model infers a primary positive correlation of boron and potassium, whereas the former model is difficult to evaluate. The strongly positive correlation of B_{SAMPLE} and B_{ILLITE} (Fig. 4.4.3 A) is compatible with both models, as a decreasing potassium content increases the factor '**7.7 / wt.% K_2O**' (Reynolds, 1965) and thus leads to an increase of the B_{ILLITE} value, i.e. the B_{SAMPLE} - B_{ILLITE} relationship shown in Figure 4.4.3 A seems to be an auto-correlation. This is confirmed by strongly positive correlations of various elements and their respective "adjusted content in illite" (e.g., Cr, Ba, La, V, Zn, not shown here). However, the empiric B_{SAMPLE} - B_{ILLITE} power regression curve calculated from the present data set (Fig. 4.4.3 A) is similar to a theoretical power regression curve calculated from empirical values defining the freshwater, brackish and marine palaeoenvironments (Reynolds, 1965, 1972), and exhibits a correct internal correlation, i.e. the curve transects the fields defined by the empirical values for the different palaeoenvironments examined by Reynolds (1965, 1972). Hence, a relationship of B-content and palaeoenvironment cannot be excluded, but is difficult to substantiate.

Figure 4.4.3 E and F show the relationship of Cr and B_{ILLITE}, which are negatively correlated. As chromium is thought to be at least partly of a detrital nature (Chapter 4.1), and may thus be considered to represent a weathering residue as does kaolinite, an increase of Cr accompanying the kaolinitic phase is expected. The mica and kaolinite assemblage of the lower Pretoria Group samples (up to Strubenkop Formation) are actually enriched in Cr compared to the plagioclase and mica assemblage of upper Pretoria Group samples (Fig. 4.4.3 E, note main field of occurrence of Silverton Formation samples, ■, in Fig. 4.4.3 E, which are representative of the 'upper Pretoria Group' in the above context).
The MgO and MgO+CaO+Na_2O - B_{ILLITE} relationships (Fig. 4.4.3 C and D) are interpreted as a further confirmation of a geochemical discrimination of "Upper" (post-Daspoort Formations) and "Lower" (Rooihoogte and Timeball Hill Formations) Pretoria Group as defined by mineralogy. The differentiation of lower (main abundance between solid lines) and upper (main abundance between dashed lines) Pretoria Group samples is especially evident in the B_{ILLITE}-MgO+CaO+Na_2O diagram (Fig. 4.4.3 D). The lower Pretoria Group distribution shows a negative correlation between B_{ILLITE} and MgO+CaO+Na_2O, whereas the upper Pretoria Group shales exhibit a strongly positive correlation. The Dwaalheuwel to

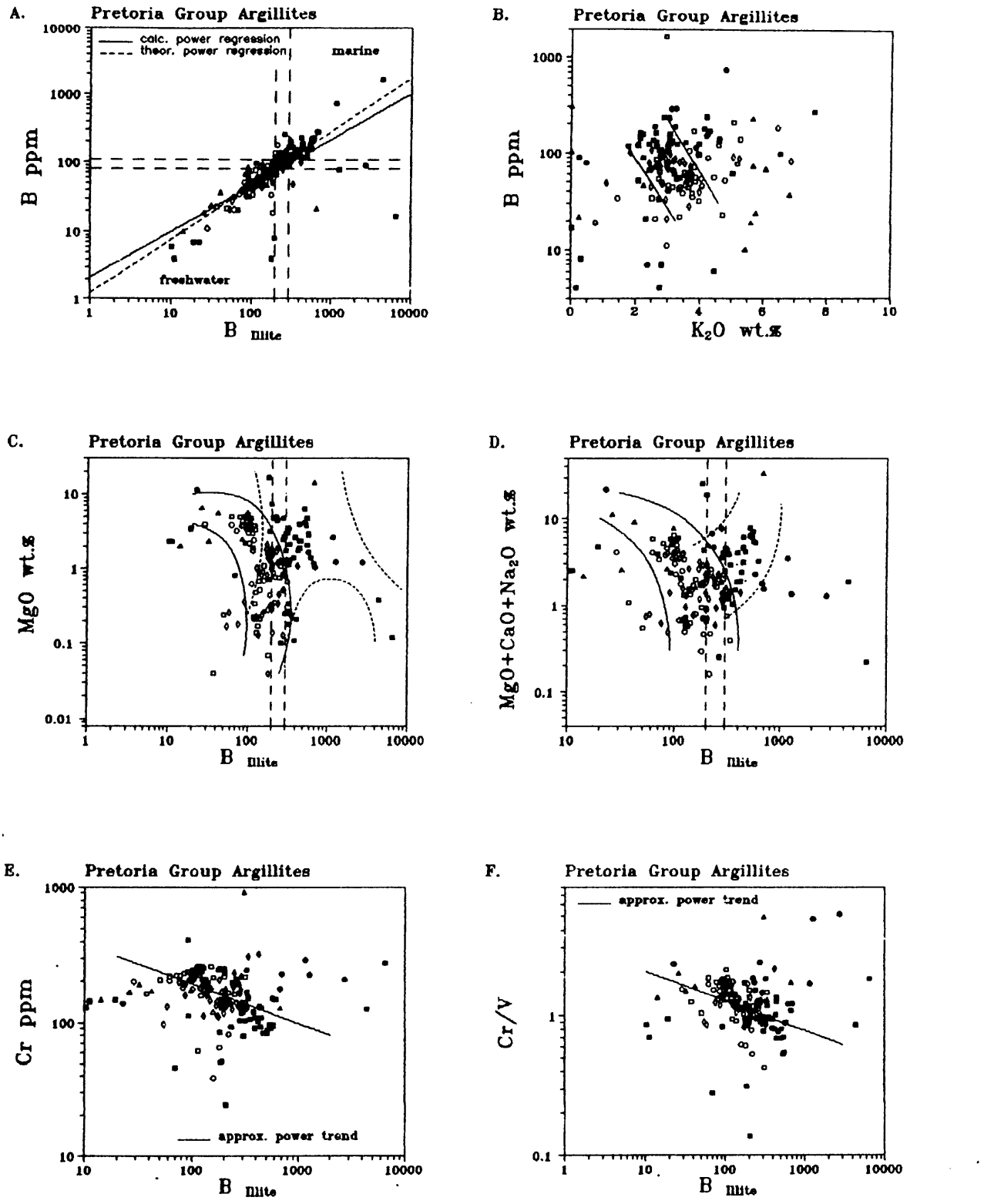

Fig. 4.4.3 A-F: The relationship of B_{SAMPLE} and B_{ILLITE} to various elements, ratios and sums of elements in Pretoria Group argillites. For explanation see text. Symbols: ○ = Vrs = Rooihoogte Fm.; □ = Lower Timeball Hill Fm.; Δ = Timeball Hill Quartzite; ◇ = Upper Timeball Hill Fm.; ◔ = Hekpoort Fm.; ◙ = Dwaalheuwel Fm.; ◆ = Strubenkop Fm.; ● = Daspoort Fm.; ■ = Silverton Fm.; ▲ = Magaliesberg Fm.; ◑ = Vermont Fm.; ◭ = Nederhorst Fm..

Daspoort Formation shales have an intermediate position, the Hekpoort Formation shales are strongly enriched in B_{ILLITE}. It should be noted that the high MgO-contents in the Lower Pretoria Group field represent samples from the Botswana sampling area, thus pointing to Mg-chlorite as principal Mg-mineral. The Upper Pretoria Group samples have generally higher MgO-contents than Lower Pretoria Group samples. The MgO content of recent seawater is about 300 times higher than river waters (Seim and Tischendorf, 1990), although it has to be emphasized that a considerable uncertainty exists about the MgO-content of ancient seawater (Holland, 1984). A widespread phenomenon recorded at the freshwater-saline boundary is the exchange of cations, namely river-supplied Ca adsorbed on clay minerals is replaced by Na, K, and Mg at the contact with saline water (Chamley, 1989). However, this process cannot account for the differences in MgO-contents observed in the "Lower" and "Upper" Pretoria Group. Eriksson et al. (1990) interpret the occurrence of shales with high MgO, CaO and Na_2O-contents in the Silverton Formation as indicative of tuffaceous material interlayered with the shales. As the presence of volcanogenic material is known to increase boron contents of shales (Bouska, 1981), the increase of boron with stratigraphic height (Fig. 4.4.2) might also be indicative of an increase in penecontemporaneous volcanism (Eriksson et al., under review a). This hypothesis is supported by the concomitant occurrence of anomalously high boron values and volcanic rocks in the Pretoria Group succession (transition zone of Rooihoogte and Timeball Hill Formations: Bushy Bend Lava; Hekpoort Lavas; Silverton Formation: Machadodorp volcanics; Nederhorst Formation: carbonates interlayered with tuffaceous beds) and/or widespread hydrothermal activity (basal Timeball Hill Formation shales)(Eriksson et al., under review a; Reczko et al., in press).

4.4.2 The REE geochemistry of Pretoria Group shales

The chondrite-normalised (normalised to C1-chondrite average of Taylor and McLennan, 1981) REE-patterns of 50 Pretoria Group shale samples are shown in Figures 4.4.4 A-E and 4.4.5 A-E. As only a limited number of REE-analyses could be performed because of financial constraints, REE-contents were only determined for the major shale units in the Pretoria Group, namely Lower and Upper Timeball Hill, Strubenkop, Silverton and Vermont

Formations. Lower Timeball Hill Formation and Silverton Formation samples were analysed for three sampling areas to account for lateral variations, and all samples sets (i.e., 10 sets of 5 samples) were taken at locations where an inferred complete stratigraphic profile was sampled, thus covering the respective formation from base to top. Due to the restrictions, western and central Transvaal sampling areas were combined into one areal group ("CTvl" = central Transvaal, for REE comprising western and central Transvaal sampling areas as defined in Chapter 1.2).

The REE-patterns of the Pretoria Group are characterised by highly variable REE-patterns, with, (1) a number of samples having moderate to large negative Ce-anomalies; (2) individual samples showing middle HREE-depletion leading to 'bowed' chondrite-normalised HREE-patterns; and, (3), defined lateral variations from sampling profile to sampling profile of REE-variability, with samples of the Botswana sampling area showing a low variability compared to samples of the other sampling areas (Fig. 4.4.4 A-E and 4.4.5 A-E). The Lower Timeball Hill Formation in the eastern Transvaal sampling area and the Lydenburg Shale Member of the Silverton Formation (only defined in the eastern Transvaal sampling area) are further distinguished by an unusual Eu-pattern, as most samples exhibit no or only slightly negative Eu-anomalies. Figures 4.4.6 A-F show the mean and geometric mean REE-concentrations of shale-dominated formations and of the total Pretoria Group sample set, normalised to chondrite, as well as the range of variation defined by the 1 σ dispersion factor (see Chapter 2.1.2). The standard deviation was thought to be unrepresentative of the REE-variation as the variability of REE is high, and variation coefficients point to non-normal distributions (see Chapter 3.3 and 3.4). The average REE contents and the range of variation shown in Figures 4.4.6 A-F confirms generally the conclusions drawn from Figures 4.4.4 A-E and 4.4.5 A-E, with the negative Ce-anomaly distinguished as the prominent feature. Figures 4.4.7 A-F show REE-patterns of average Pretoria Group shales normalised to chondrite (Taylor and McLennan, 1981) and North American Shale Composite (Gromet et al., 1984), grouped according to the formations (Fig. 4.4.7 A and B), sampling areas (Fig. 4.4.7 C and D) and total average (Fig. 4.4.7 E and F); these figures strengthen the inferred unusual REE-pattern for the Pretoria Group. The La-content of Pretoria Group samples is enriched by a factor of up to 2 compared to North American Shale Composite (Gromet et al., 1984), the Ce-content is strongly depleted compared to La and other LREE (Fig. 4.4.7 A-F). The middle HREE-depletion ('bowed' pattern) can be observed in all chondrite-

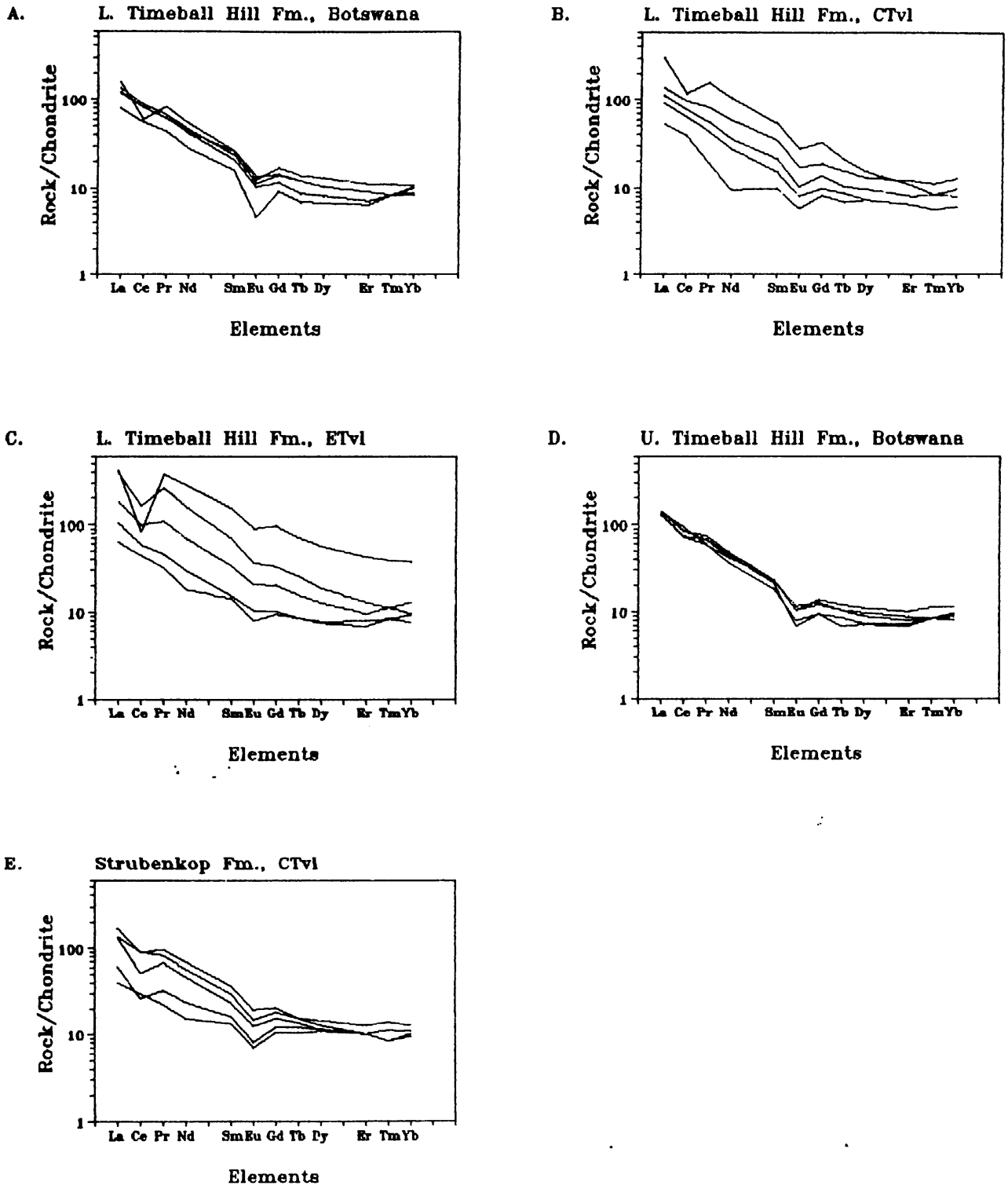

Fig. 4.4.4 A-E: Chondrite-normalised REE-patterns of Timeball Hill and Strubenkop Formation argillite samples. Normalisation-factors are taken from Taylor and McLennan (1981).

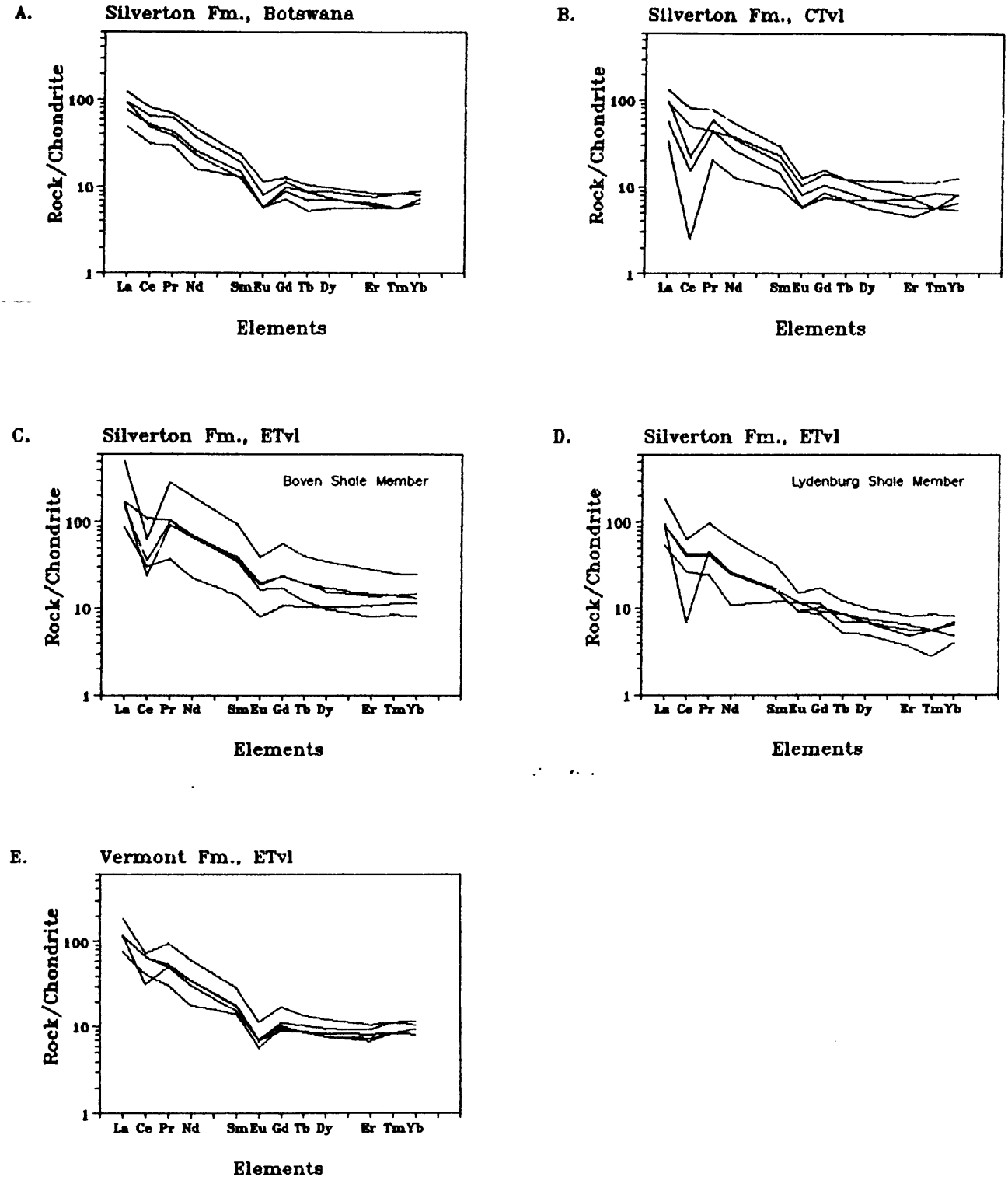

Fig. 4.4.5 A-E: Chondrite-normalised REE-patterns of Silverton and Vermont Formation argillite samples. Normalisation-factors are taken from Taylor and McLennan (1981).

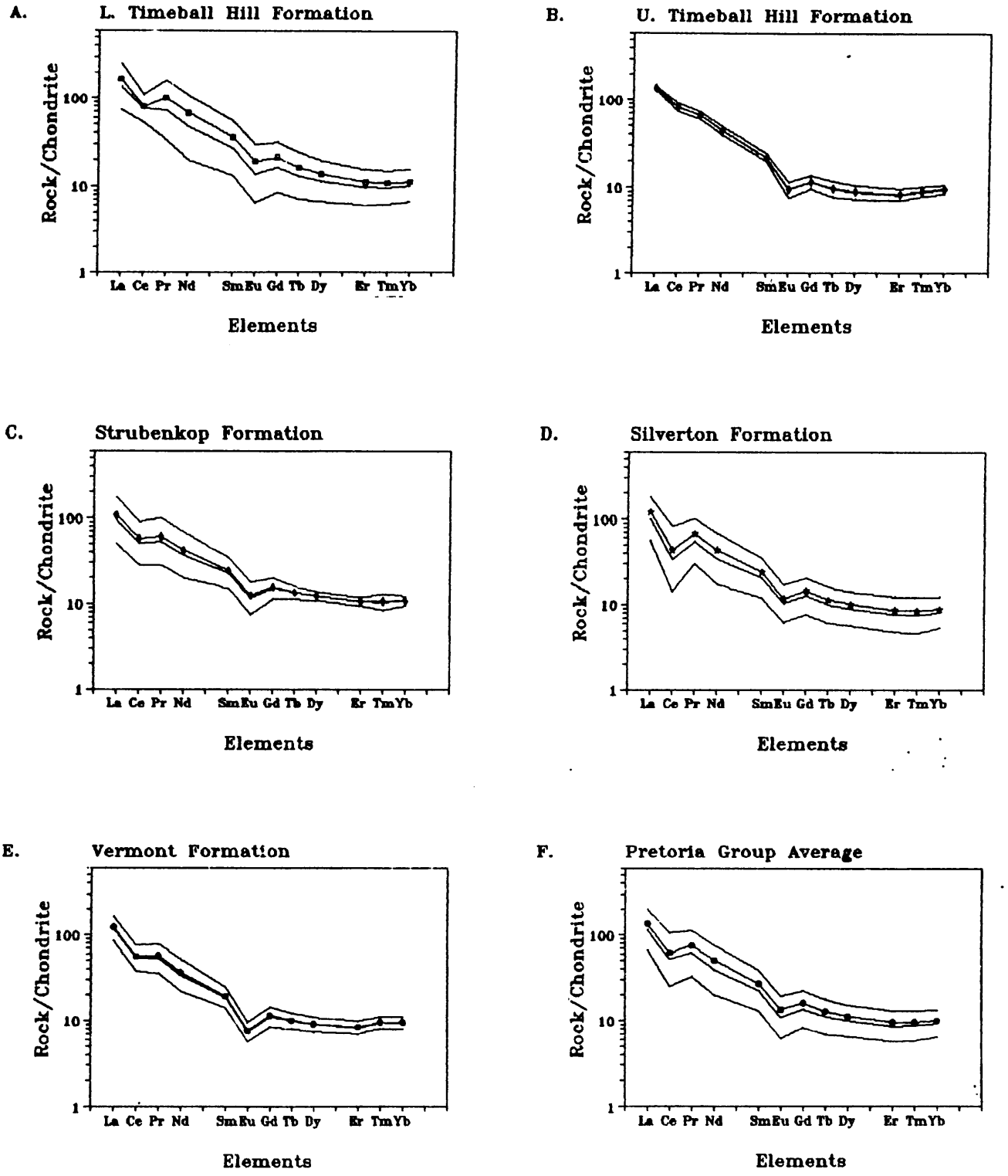

Fig. 4.4.6 A-F: Chondrite-normalised REE-patterns of average Pretoria Group argillites, shown as geometric mean multiplied/divided by the 1 δ dispersion factor (lines without symbols) and arithmetic mean (lines with symbols). Normalisation-factors taken from Taylor and McLennan (1981).

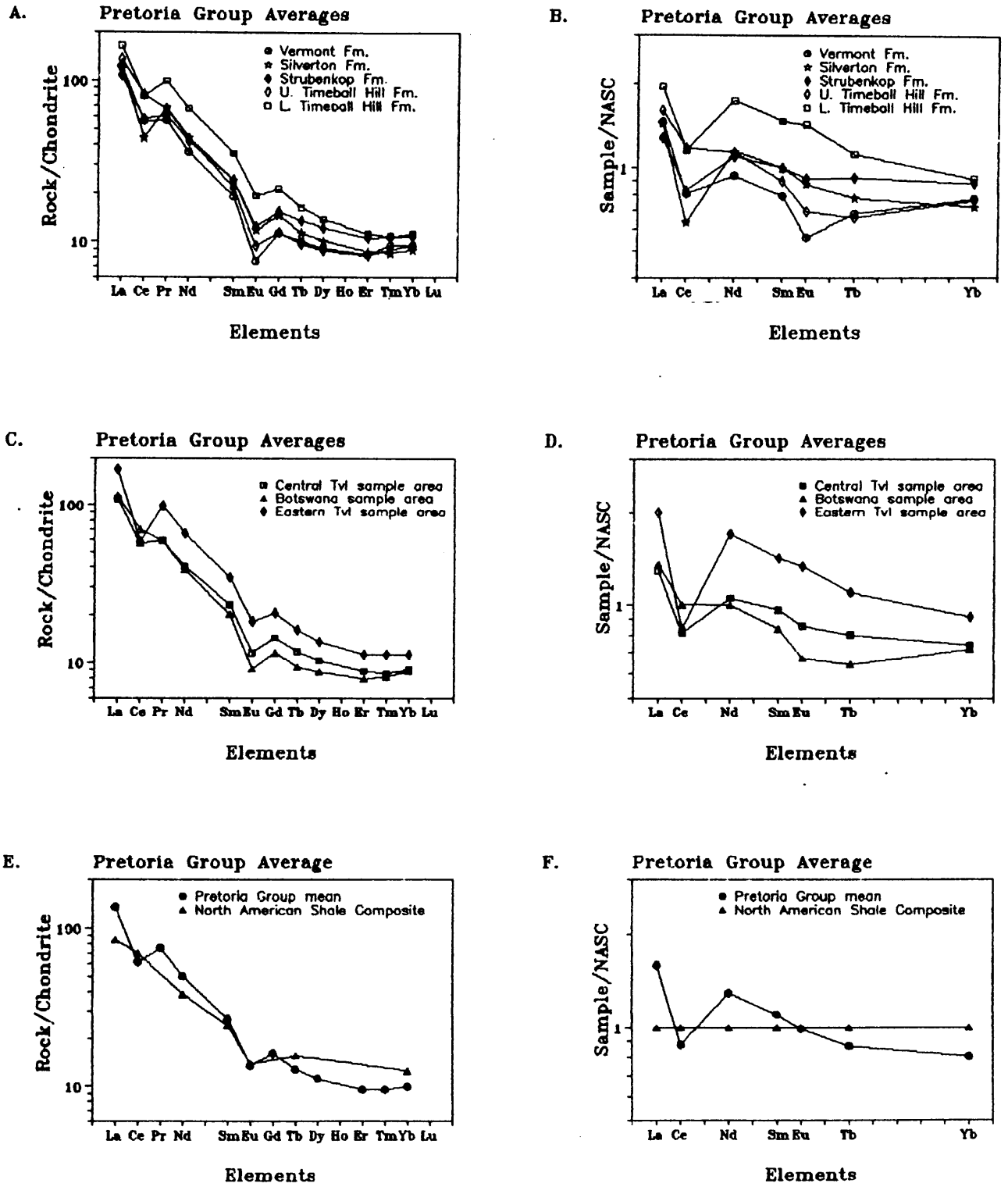

Fig. 4.4.7 A-F: Chondrite and NASC-normalised REE-patterns of average Pretoria Group argillites (geometric mean values). Average values according to stratigraphy, geography and total data set. Normalising-factors taken from Taylor and McLennan (1981) and Gromet et al. (1984). Please note middle HREE-depletion compared to NASC in Figure 4.4.7 E.

normalised REE-averages (Fig. 4.4.7 A, C and E).

As the Ce-anomaly of average terrigenous particulate input is thought to equal 1 (McLennan, 1989; Condie, 1991), the more or less pronounced negative Ce-anomalies in Pretoria Group shales might point to depositional or post-depositional processes. To the best knowledge of the author, negative Ce-anomalies have not been reported up to now from Early Proterozoic shales. The occurrence of negative Ce-anomalies is reported, amongst others, from seawater (e.g., Elderfield and Greaves, 1982), weathering profiles (e.g., Nesbit, 1979), organic material (e.g., Fleet, 1984), hydrothermal sediments (e.g., Ruhlin and Owen, 1986), deep-sea sediments (e.g., Piper, 1974), hydrothermaly altered basalts (e.g., Ludden and Thompson, 1978), metabasalts (e.g., Hellman et al., 1977) and ophiolites (e.g., Menzies et al., 1977). A REE-anomaly is defined by the deviation of an element from an otherwise linear REE-pattern, and is thus a relative expression of the deviation from a supposedly linear REE-trend. Mathematically, a REE-anomaly is calculated by the ratio of the chondrite-normalised concentration of the respective element to a theoretical concentration calculated from the respective chondrite-normalised neighbouring elements (e.g., the Ce-anomaly is calculated as $Ce/Ce^* = Ce_N/[(La_N+Pr_N)/2]$ or $Ce/Ce^* = Ce_N/[(2La_N+Nd_N)/3$; in the present investigation the Ce-anomaly was calculated by using the first equation, following a suggestion by Murray and Leinen, 1993). While discussing the mobility of REE of volcanic rocks, Hellman et al. (1979) differentiated five major types of REE mobility, namely

(1) gross REE and selective LREE enrichment;
(2) REE redistribution around a primary mean;
(3) gross REE depletion;
(4) selective HREE depletion; and,
(5) selective REE mobility.

Pronounced REE-anomalies are explained by

(A) selective REE mobility (type 5 above), with preferential depletion/enrichment of only one REE by a leaching, oxidation or scavenging process, or
(B) relatively less/more depletion/enrichment compared to the other REE (type 1 or 3 above) (Hellman et al., 1979).

The negative Ce-anomaly in Pretoria Group shales may include both A and B-type Ce-anomalies. Large Ce-anomalies in the Lower Timeball Hill Formation occur in samples with

the highest REE-contents (Fig. 4.4.4 A-C), and the average Ce-concentration of the Lower Timeball Hill Formation shales is enriched, although only slightly so, compared to North American Shale Composite (Gromet et al., 1984) (Fig. 4.4.7 B). Hence, the Ce-anomaly of the Lower Timeball Hill Formation shales can be explained by a B-type anomaly. A similar interpretation can be arrived at for the Silverton Formation shales of the central Transvaal sampling area (Fig 4.4.5 B), which show an increasing Ce-anomaly with decreasing REE-contents. However, the Ce-anomalies of the other sample sets (Fig 4.4.4 D, E and 4.4.5 A, C, D, E) show no systematic change of Ce/Ce* associated with a variable REE-content, thus pointing to an A-type anomaly.

Ce is different from the other REE as it possesses a Ce(IV) valence in addition to the trivalent condition normal for the REE (Brookins, 1988). The negative Ce-anomaly of seawater is thought to reflect the oxidation of Ce^{3+} to Ce^{4+} and precipitation from solution as CeO_2, which is adsorbed onto clay or organic particle coatings (Fleet, 1984). A number of observations suggest that removal of Ce from seawater probably occurs in the open ocean rather than in estuarine or shelf waters, as inferred by investigations cited in Fleet (1984). A major sink of Ce is thought to be iron manganese nodules, which normally show a pronounced positive Ce-anomaly (Fleet, 1984). However, coatings and adsorbed phases on suspended particles in the open ocean also have pronounced positive Ce-anomalies, and the uptake of REE from seawater onto suspended particles seems to be a major process controlling the REE composition and fractionation of both deep ocean surface sediments and seawater (Sholkovitz et al., 1994). Deep-sea sediments have a highly variable REE-pattern, with both strongly positive and negative Ce-anomalies reported (e.g., Ruhlin and Owen, 1986; Kunzendorf et al., 1993; Murray and Leinen, 1993). Metalliferous ridge crest hydrothermal sediments seem to have derived their REE mainly from seawater via scavenging, and thus normally exhibit a pronounced negative Ce-anomaly (e.g., Ruhlin and Owen, 1986; German and Elderfield, 1990).

Negative Ce-anomalies of sedimentary rocks related to a seawater source can only be preserved if the processes controlling the Ce-anomaly in the seawater also prevail in the pore waters of the underlying sediments (German and Elderfield, 1990). As the negative Ce-anomaly of recent seawater is a result of the generally oxidizing conditions of the recent

hydrosphere and atmosphere, primary Ce-anomalies are only preserved in recent sediments underlying zones of oxic diagenesis (German and Elderfield, 1990). Fryer (1977 a,b) suggested an enrichment of Ce^{3+} in the Precambrian oceans due to low oxygen-fugacity, which, implicitly, can explain the lack of negative Ce-anomalies in the Precambrian sedimentary record. Hence, it seems to be unlikely that the Ce-anomalies of the Pretoria Group shales can be led back to a seawater source, as, (1) the Pretoria Group shales were apparently laid down in a nearshore environment with only intermediate water depth, where modern waters and sediments lack a pronounced Ce-anomaly (Fleet, 1984); (2) the organic-rich black shales from the base of the Silverton Formation (up to 12 wt.% C_{ORG}) can be assumed to represent reducing diagenetic conditions, as can the shales from the base of the Lower Timeball Hill Formation, which have a black colouration due to abundant Fe^{2+} oxides; and, (3) Precambrian seawaters are thought to be enriched in Ce^{3+}, and thus scavenging from or equilibration with seawater cannot account for the negative Ce-anomaly observed in the Pretoria Group shales.

Although negative Ce-anomalies are reported from weathering profiles, the resulting Ce-anomalies are relatively small (Humphries, 1984), and would produce a B-type negative Ce-anomaly with preferential enrichment of other LREE compared to Ce (Nesbit, 1979). Residual material has a slightly positive Ce-anomaly (Nesbit, 1979). The fractionation of REE in a weathering profile is thought to have only minor effects for the sedimentary record, as most sedimentary rocks result from a mechanical mixing of detritus and hence tend to be homogenised (Nesbit, 1979). Accordingly, the observed Ce-anomalies of Pretoria Group shales cannot be ascribed exclusively to weathering, although weathering might be considered as an explanation for the negative Ce-anomalies of the stronly LREE-enriched Lower Timeball Hill Formation shales.

REE-contents and patterns can also be influenced by biogenic flux transporting the REE to the sea floor, although this does not seem to be a dominant process regulating the REE-abundance of recent sediments (Murray and Leinen, 1993). Plankton has REE-patterns similar to seawater, thus implying equilibration or scavenging processes from a seawater source (Elderfield et al., 1981). As discussed above, a Ce-depleted seawater source seems unlikely for the Pretoria Group sediments. However, diagenetic processes due to a strongly

reducing environment may have fractionated the REE and caused preferential depletion of Ce. Figures 4.4.11 C-F show the realtionships of S, C_{ORG}, Ce, La and Ce/Ce*. It is evident that Ce is strongly depleted with decreasing S/C_{ORG} atomic ratio, whereas La is not depleted. Ce/Ce* shows a positive correlation with the S/C_{ORG} ratio in the excess-carbon field, i.e., the negative Ce-anomaly becomes smaller with increasing S/C_{ORG}. The relationship of C_{ORG} and REE is rather complicated as inferred by simple C_{ORG}-REE plots (not shown here), which exhibit no apparent dependency. The lack of simple C_{ORG}-REE relationships may be explained by dilution, i.e., apart from the inferred diagenetic processes, the detrital REE input may be relatively depleted in shales with abundant carbon. However, C_{ORG}-rich shales show no significant depletion of La compared to shales with low C_{ORG}-contents or shales with a S/C_{ORG} ratio similar to 'normal' recent conditions (Fig. 4.4.11 C, E). Ce may thus have suffered preferential depletion (A-type Ce/Ce*) in Pretoria Group shales with excess carbon-contents, possibly involving dissolution processes during diagenesis.

Another group of rocks exhibiting large negative Ce-anomalies are hydrothermaly altered basalts and metalliferous shales ("hydrothermal sediments") from mid-ocean ridges. The deficiency of Ce compared to other LREE is explained by equilibration of REE with and/or scavenging of REE from seawater (e.g., Ludden and Thompson, 1979; Humphries, 1984; Ruhlin and Owen, 1986). However, hydrothermal sediments show a decrease in Ce-anomaly with distance from the ridge (Ruhlin and Owen, 1986), thus pointing to a preferential enrichment of Ce compared to the other REE. The occurrence of strong positive Ce-anomalies in individual sample sets (e.g., Kunzendorf et al., 1993) and the mineralogy of hydrothermal sediments, i.e. oxides, suggests the possibility of an alternative interpretation. Graf (1978) demonstrated an Archaean-type REE-pattern in the Ordovician age Algoma-type iron-formation deposit of Bathurst, thereby indicating that the REE-pattern is not related to seawater chemistry but rather to the nature of water-rock reactions in hydrothermal systems. Hopf (1993) described preferential depletion of Ce compared to other REE from hydrothermally altered rhyolites from New Zealand. Notably, Hopf (1993) further reported altered rocks with strong middle HREE depletion, which could be modelled succesfully by using fluid/rock ratios as low as 9, thus contradicting the conclusion of Michard (1989), that hydrothermal activity is only expected to change the REE contents of solid rocks if fluid/rock ratios are very high. Interstitial metalliferous sediments, umbers, and pillow lavas from the

Troodos Ophiolite, Cyprus, show evidence of extensive hydrothermal alteration and show REE-patterns distinguished by large negative Ce-anomalies and positive Yb-anomalies; in other words, they have a 'bowed' middle REE-pattern, and seem further enriched in LREE (Robertson and Fleet, 1976). Hellman et al. (1979) have related the positive Yb-anomalies reported by Robertson and Fleet (1976) to "the result of a poorly understood metasomatic process". LREE-concentrations of hydrothermal vent fluids are strongly enriched compared to natural waters (Owen and Olivarez, 1988), and thus comprise a medium which is potentially able to change REE-concentrations and patterns via water-rock reactions as suggested by Graf (1978).

Figures 4.4.8 A-F show the relationship between Al_2O_3, chondrite-normalised La and Ce, the theoretical chondrite-normalised concentration of Ce and La being calculated as

(1) $Ce^* = (La_N + Pr_N) / 2$, and

(2) $La^* = (3\ Pr_N) - (2\ Nd_N)$

Al_2O_3 was chosen as aluminium is assumed to be relatively immobile in the sedimentary cycle. It has to be emphasized that the samples analysed for REE show only minor dilution by quartz, but have an otherwise variable mineralogy (see Chapter 3.1.6). The observed sample distribution is plotted with a polynomial regression curve (Fig. 4.4.8 A-D). As the La- and Ce-anomalies are defined as La_N/La^* and Ce_N/Ce^* respectively , the vertical distances of the polynomial best fits of La_N and La* (Fig. 4.4.8 E) and Ce_N and Ce* (Fig. 4.4.8 F) are proportional to the respective anomaly. La shows no defined anomaly, with the possible exception of a small positive La-anomaly relative to small Al_2O_3-contents (Fig. 4.4.8 E). Two fields of large Ce-anomalies are distinguished relative to Al_2O_3: (1) between 12 and 16 wt.% Al_2O_3 and (2) for Al_2O_3-concentrations larger than 24 wt.% (Fig. 4.4.8 F). Field (1) comprises only samples from the Silverton Formation, namely, carbon-rich shales from the western Transvaal sampling area ($C_{ORG} >$ 12 wt.%), high Mg-Ca-Na shales from the western Transvaal sampling area, and high Mg-Ca-Na shales from the Lydenburg Shale Member (eastern Transvaal sampling area). Field (2) comprises samples from the basal Lower Timeball Hill Formation and one sample from the Boven Shale Member (Silverton Formation, eastern Transvaal sampling area). Field (2) samples are strongly enriched in LREE, except Ce, compared to North American Shale Composite (Gromet et al., 1984). The LREE-enrichment cannot be ascribed solely to a concomitant increase of clay minerals

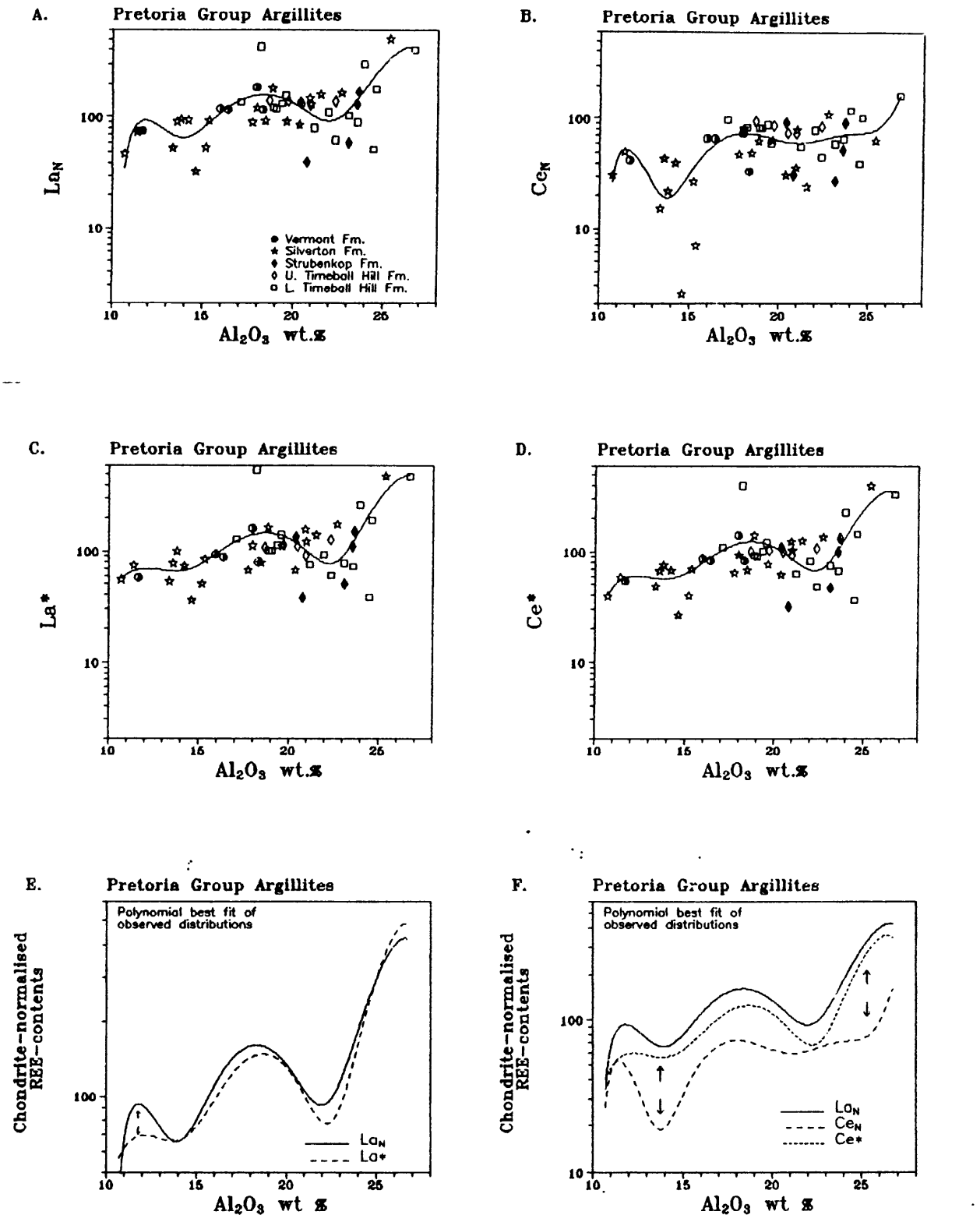

Fig. 4.4.8 A-F: The relationship of chondrite-normalised La and Ce (Fig. 4.4.8 A and B), and theoretical La and Ce concentration (Fig. 4.4.8 C and D, for calculation and definition see p. 338 and 342) to Al_2O_3. Lines represent polynomial regression curves. Figures 4.4.8 E and F are a comparison of regression curves from Figures 4.4.8 A-D. Arrows indicate the position of REE-anomalies relative to Al_2O_3. Symbols as given in Figure 4.4.8 A.

(expressed as Al_2O_3-enrichment), as the LREE-enrichment exceeds the Al_2O_3-enrichment by an order of magnitude. As noted above, residual materials of a weathering profile (kaolinite) have weak positive Ce-anomalies and are slightly depleted in LREE (Nesbit, 1979). Hence, a mechanism unrelated to weathering is implied by the observed enrichment of LREE and the concomitant development of large negative Ce-anomalies. Strong enrichment of Al_2O_3 is observed in tuffaceous material of both Lower Timeball Hill and Hekpoort Formations (see Fig. 3.3.6.1 and 3.3.2.2), pointing to alteration processes. It is proposed here, that the concomitant enrichment of Al_2O_3 and LREE as well as the observed large Ce-anomalies in field (2), can be explained by hydrothermal/metasomatic alteration. Field (1) contains mainly high-Mg-Ca-Na shales (5 out of 7 samples), which are thought to represent tuffaceous shales (Eriksson et al., 1990). It has to be emphasized, that the occurrence of large negative Ce-anomalies is not restricted to the mentioned fields (1 and 2). Negative Ce-anomalies are not correlated with Al_2O_3-contents, and the definition of the fields was performed to find similarities of rocks with exclusively large negative Ce-anomalies relative to Al_2O_3, with the aim to define a mechanism explaining the observed patterns. However, the Al_2O_3-REE plots are thought to point to a relationship of negative Ce-anomalies with volcanism and hydrothermal/metasomatic alteration.

Figures 4.4.9 A and B show hydrothermal sediments from the East Pacific Ocean Ridge normalised to chondrite (Taylor and McLennan, 1981) and North American Shale Composite (Gromet et al., 1984). Figures 4.4.9 D shows four selected Pretoria Group samples normalised to North American Shale Composite (Gromet et al., 1984), emphazising the similarity of individual Pretoria Group shales with hydrothermal sediments (Fig. 4.4.9 B). These Pretoria Group shales have a flat REE-pattern (Fig. 4.4.9 C), if normalized to the hydrothermal sediment sample 598-1/2-96/98 of Ruhlin and Owen (1986); in other words, the REE are similarily fractionated in Pretoria Group shales and hydrothermal sediments. However, it can be shown that the Pretoria Group shales are different from either mid ocean ridge sediments or deep-sea sediments (Fig. 4.4.9 E). The bulk of the Pretoria Group samples fall in the field defined by Red Sea sediments, whereas samples with large Ce-anomalies (Ce/La is proportional to Ce/Ce*) are not defined by the fields given by Kunzendorf et al. (1988). It should be noted, in this context, that the Machadodorp volcanics mainly fall in the Red Sea volcanics field when plotted in a Zr/Th-Zr/La plot (Fig. 4.3.6 A).

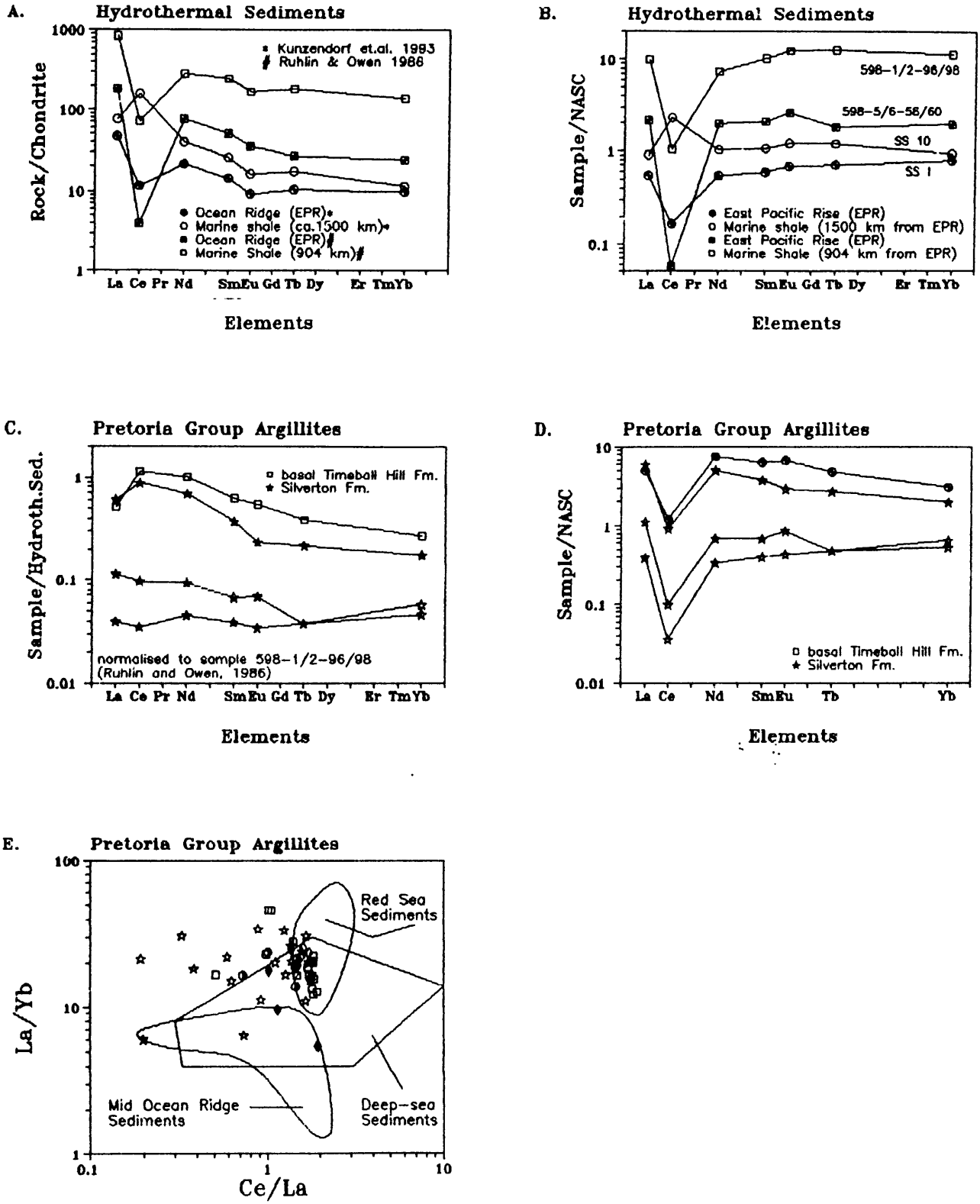

Fig. 4.4.9 A-E: Comparison of Pretoria Group argillites with 'hydrothermal sediments'. A and B: Chondrite and NASC-normalised REE-patterns of 'hydrothermal sediment' samples reported by Ruhlin and Owen (1986) and Kunzendorf et al. (1993). Position of samples relative to East Pacific Rise (EPR) given in the lower part of Figures 4.4.9 A and B. Identification number of samples in Figure 4.4.9 B. C and D: Selected Pretoria Group argillite samples normalised against NASC and 'hydrothermal sediment' sample 598-1/2-96/98 of Ruhlin and Owens (1986). E: Distribution of Pretoria Group argillites in the Ce/La - La/Yb diagram of Kunzendorf et al. (1988). Symbols of Figure 4.4.9 E as in Figure 4.4.8 A.

The Ce/La-La/Yb plot (Fig. 4.4.9 E) points to relatively stable La/Yb ratios, and preferential depletion of Ce (A-type Ce-anomaly) as an important process controlling the REE-pattern. It must be mentioned here that REE-mobility during high-temperature alteration of sea-floor basalt is stronly dependent on mineralogical constraints, as the presence of chlorites seems to stabilize the REE-content and pattern (Ludden and Thompson, 1979). This capacity of chlorite may explain the differences in REE-pattern of shales from the Botswana sampling area, with a low variability and only individual samples exhibiting a negative Ce-anomaly, as opposed to the higher variabilities and frequent negative Ce-anomalies observed in shales from the central and eastern sampling areas.

Figures 4.4.10 A-D are an attempt at a synthesis of the implications of B and REE-contents. Humphries (1984) implies an association of REE and alkali contents, if hydrothermal alteration/metasomatism has influenced the abundance of REE. Boron is known to be transported by alteration fluids, as is demonstrated by tourmalinization adjacent to hydrothermally influenced mineralization areas (Guilbert and Park, 1986). As it was previously argued that the negative Ce-anomaly may have been caused by fractionation of REE due to hydrothermal/metasomatic alteration, a negative correlation between Ce/Ce* and alkalis as well as boron, and a positive correlation between alkalis (expressed as K_2O + Na_2O wt.%) and boron could be expected. The predicted relationships can be observed in the Pretoria Group shales in Figures 4.4.10 B, C and D, although it has to be pointed out that the correlations are rather broad. However, considering the mobility of boron and alkalis, the influence of an underlying detrital REE-pattern and the differences in the clay mineral assemblages, the relationships of Ce/Ce*, boron and alkalis are interpreted as evidence for alteration processes influencing the abundance and patterns of REE, boron and alkalis.

4.4.3 Palaeoenvironment, petrography and provenance

Plots utilising correspondence analysis of Pretoria Group shales (Chapter 3.3) exhibit a certain degree of geochemical discrimination of sampling areas for the Lower and Upper Timeball Hill and the Strubenkop Formations (Fig. 3.3.2.6, 3.3.4.6 and 3.3.8.6). Whereas the sampling areas of both Timeball Hill shale members can be discriminated with trace

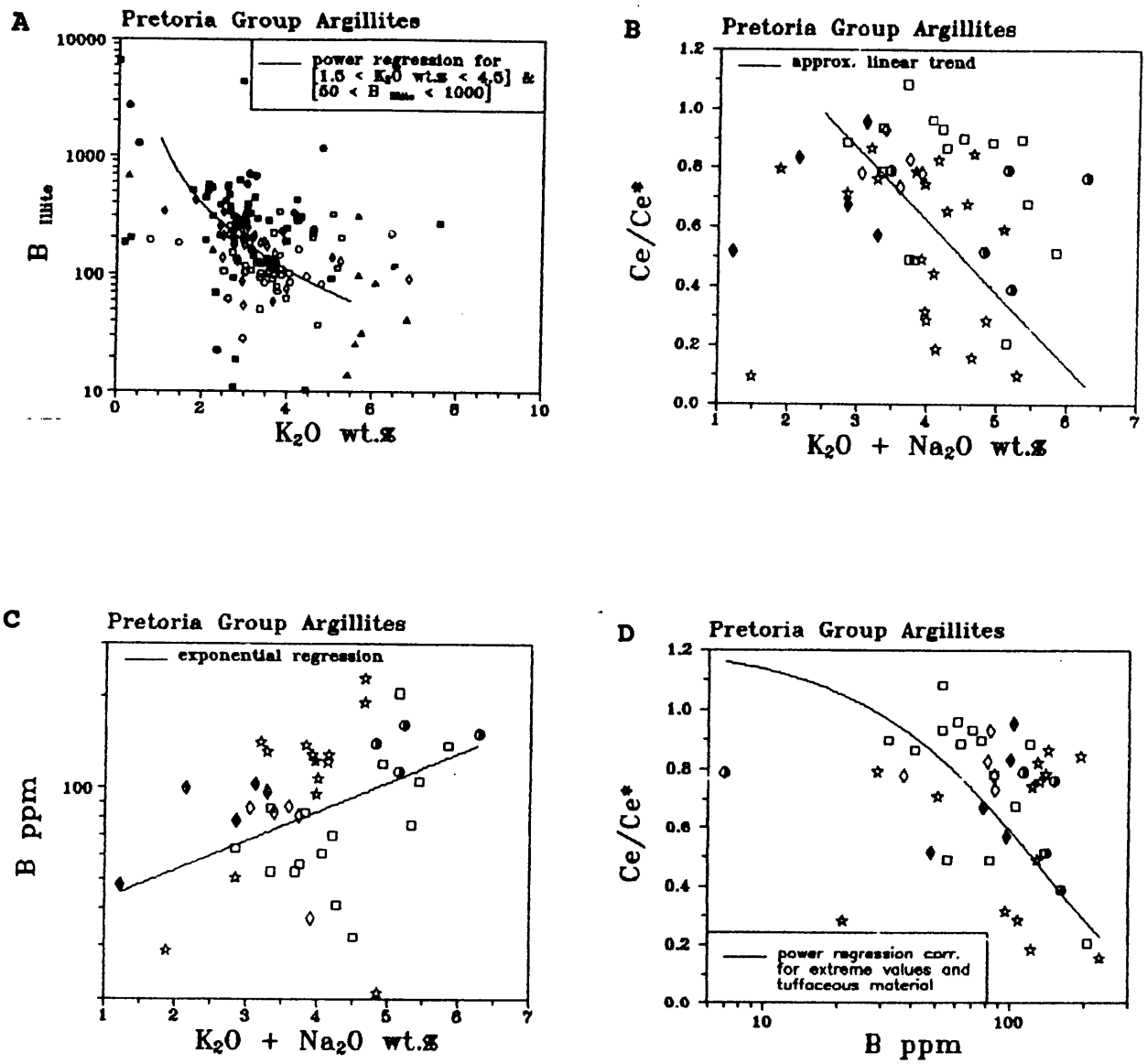

Fig. 4.4.10 A-D: The relationships of B_{ILLITE} and K_2O (A), Ce/Ce* and $K_2O + Na_2O$ (B), B_{SAMPLE} and $K_2O + Na_2O$ (C), and Ce/Ce* and B_{SAMPLE} (D). Lines and curves are calculated regression curves. The curve of Figure 4.4.10 B is an estimation drawn by hand ('approx. linear trend'). Symbols of Fig. 4.4.10 A: ○ = Rooihoogte Fm.; □ = Lower Timeball Hill Fm.; Δ = Timeball Hill Quartzite; ◇ = Upper Timeball Hill Fm.; ◔ = Hekpoort Fm.; ◘ = Dwaalheuwel Fm.; ◆ = Strubenkop Fm.; ● = Daspoort Fm.; ■ = Silverton Fm.; ▲ = Magaliesberg Fm.; ◑ = Vermont Fm.; ◭ = Nederhorst Fm.. Legend of Fig. 4.4.10 B-D shown in box of Fig. 4.4.10 B.

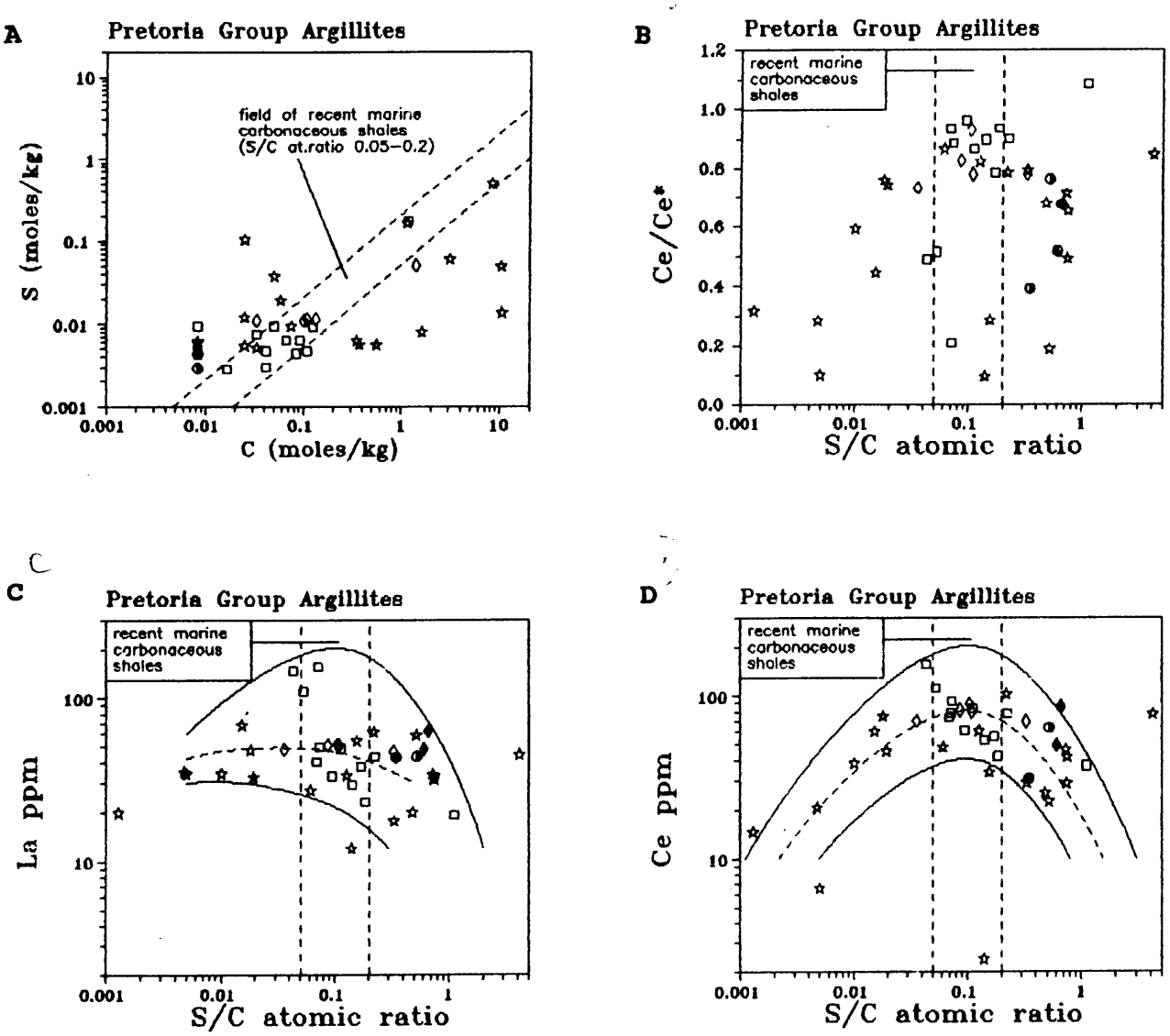

Fig. 4.4.11 A-D: The relationships of S in mol and C in mol (A), and Ce/Ce*, Ce and La and the S/C atomic ratio (B, C and D). Symbols: see box in Fig. 4.4.11 A. Field of S/C atomic ratio for recent marine carbonaceous shales after Williams (1978).

elements (Fig. 3.3.2.6 and 3.3.4.6), the Strubenkop Formation shales are discriminated by their major element relationships (Fig. 3.3.8.6). The degree of discrimination of correspondence analysis plots decreases from the Lower Timeball Hill Formation towards the Strubenkop Formation, i.e., in stratigraphic order, and shows no discrimination of sampling areas for the Silverton Formation shales (Fig. 3.3.10.8 and 3.3.10.9). However, correspondence analysis of major elements of Silverton Formation shales (Fig. 3.3.10.8) can be utilized as a petrographic tool, which discriminates between carbonaceous shale (close to LOI), calcareous shale (between LOI and MgO/CaO), high Mg-Ca-Na shale (between MgO/CaO and Fe_2O_3) and 'normal' shale (close to Al_2O_3) end-members.

Figures 4.4.12 A-F are enlargements of the source rock discriminance plots developed in Chapter 4.1 (Fig. 4.1.4 E, F, I, J, O and P). Although the discriminatory character of Figures 4.4.12 A-F is weak, i.e., the respective fields of sampling areas overlap, differences in the bulk areal compositions are evident.

Shales are accumulations of fine-grained weathering products and authigenic clay minerals, with a vast predominance of the former (Chamley, 1989). Clay mineral assemblages tend to be homogenised during the sedimentary process (Nesbit, 1979), and thus constitute excellent indicators of bulk provenance (Condie and Wronkiewicz, 1990). However, the trace element patterns of Cr, Th, Sc, Zr, Y and V of shales from the lower part of the Pretoria Group (up to Strubenkop Formation) point to local sources with small but defined differences in provenance. This is compatible with the observed clay mineralogy, i.e., the abundance of kaolinite favours a relatively short transport distance (e.g., Rösler and Lange, 1976; Chamley, 1989). Furthermore, strong coast-parallel currents must have been lacking in the lower part of the Pretoria Group depository as these currents would have lead to a more homogenised provenance pattern. An epeiric sea environment with open sea conditions to the south of the preserved main Transvaal basin and Potchefstroom sub-basin (Tankard et al., 1982) would be expected to have produced some evidence of lateral geochemical homogenisation of shales. It can be argued that the Lower Pretoria Group shales up to the Strubenkop Formation were actually homogenised to a certain degree, although this argument would infer significant differences in the respective provenance areas. However, as the abundance of kaolinite provides further evidence for short transport and, thus, local sources,

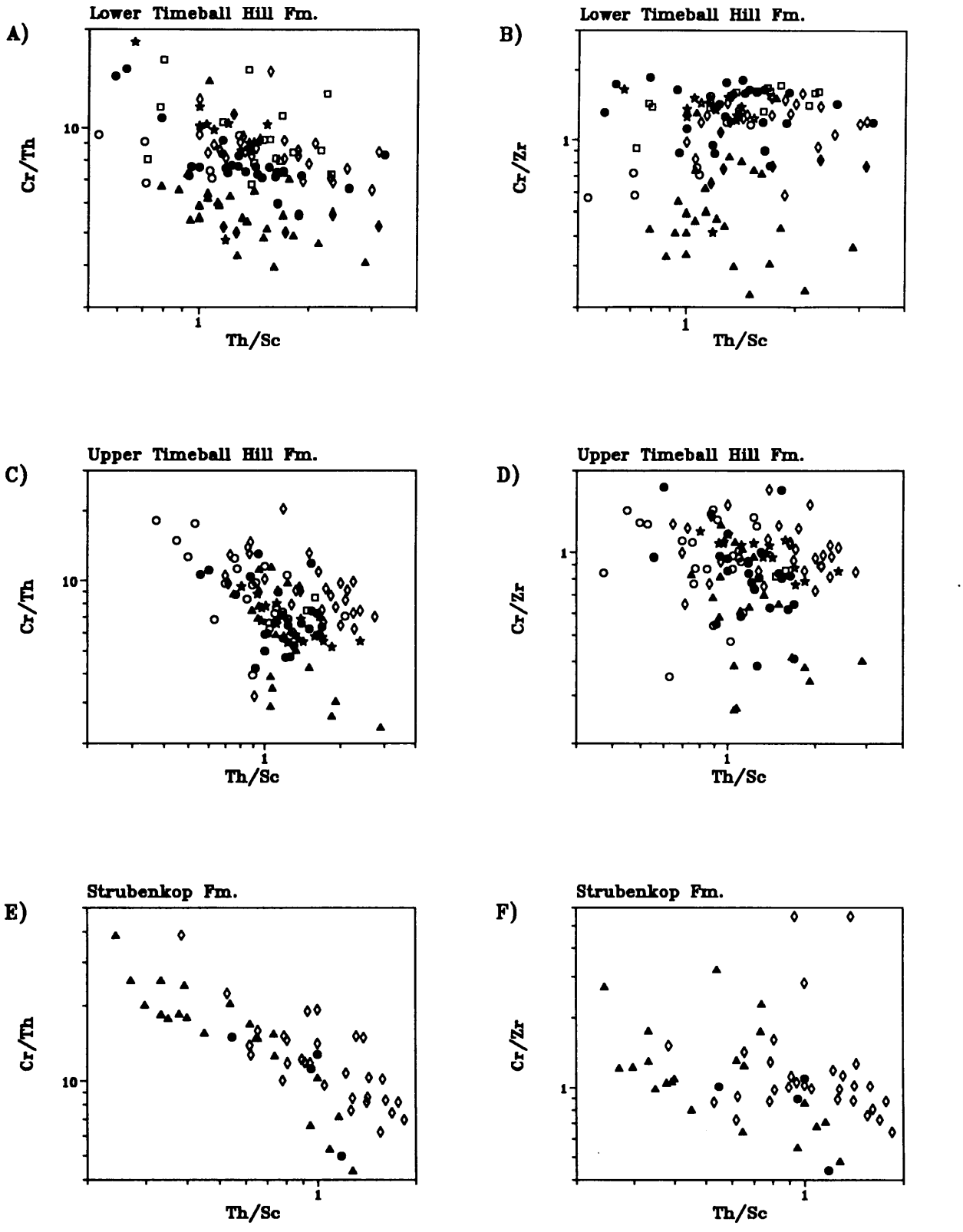

Fig. 4.4.12 A-F: Enlargements of source terrain discriminance plots shown in Figures 4.1.4 E, F, I, J, O and P. Symbols: ○ = northeastern Transvaal; □ = eastern fragments; ◇ = central Transvaal; ● = eastern Transvaal; ▲ = western Transvaal, western fragments and northwestern Transvaal; ★ = Botswana.

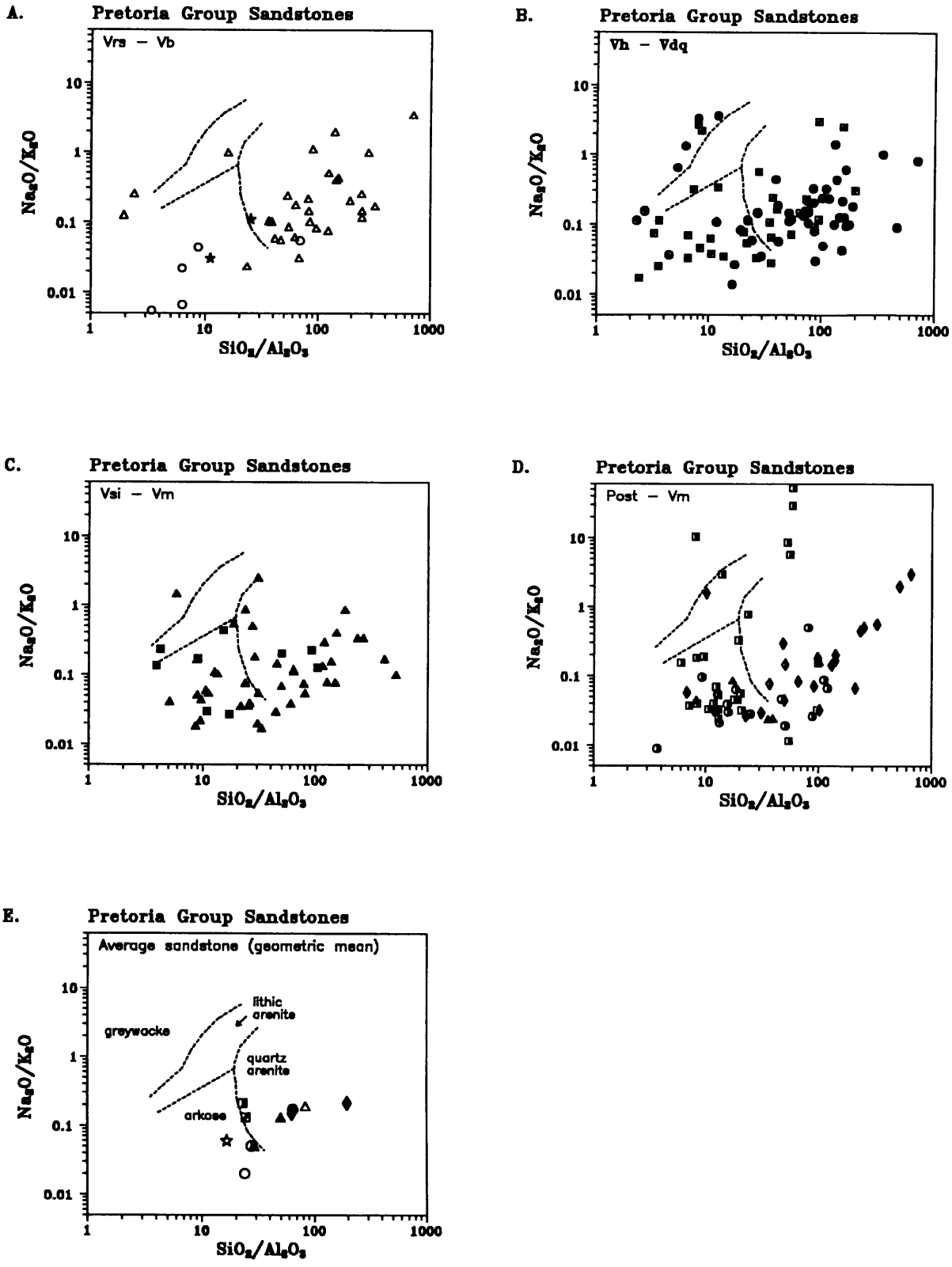

Figure 4.4.13. A-E: SiO2/Al2O3 versus Na2O/K2O diagram for petrographic classification (modified after Pettijohn et al., 1973; fields after Floyd et al., 1989). Symbols: ○ = Rooihoogte Fm. (Vrs); Δ = Timeball Hill Quartzite; ★ = Boshoek Fm. (Vb); ◔ = Hekpoort Fm (Vh); ◘ = Dwaalheuwel Fm.; ● = Daspoort Fm. (Vdq); ■ = Silverton Fm. (Vsi); ▲ = Magaliesberg Fm. (Vm); ◘ = Lakenvlei Fm.; ◭ = Nederhorst Fm.; ◆ = Steenkampsberg Fm.; ◆ = Houtenbek Fm.; ◑ = Rayton Fm.; "Post - Vm" = post-Magaliesberg formations.

an epeiric sea environment with open open sea conditions to the south (Tankard et al., 1982) is unlikely. Nevertheless, a marine environment restricted to an intracratonic structural basin cannot be excluded.

Figures 4.4.13 A-E show petrographic sandstone classification diagrams after Pettijohn et al. (1972) and Floyd et al. (1989). It is obvious that the bulk of Pretoria Group sandstone samples fall in either the quartz arenite or the arkosic sandstone field. The average composition of Rooihoogte, Rayton and Nederhorst Formation sandstones is arkosic (Fig. 4.4.13 E); other sandstone averages show mature quartzose compositions. It should be mentioned that very mature sandstones, i.e., those with SiO_2-contents close to 100 wt.%, might have Na_2O, K_2O or Al_2O_3-contents below the detection limit, and thus cannot be shown in these diagrams. The dominant quartzose-arkosic nature of the sandstones strongly suggests a continental or marginal continental tectonic setting of the sandstones (see Chapter 4.3). Correspondence analysis of trace elements of sandstones shows a generally weak discrimination of sampling areas (Fig. 3.3.3.6, 3.3.7.4, 3.3.9.3 and 3.3.11.4). The best areal discrimination is observed for Magaliesberg Formation sandstones, with successively weaker areal discrimination for Timeball Hill Quartzite, Dwaalheuwel and Daspoort Formations, with the latter showing no discriminatory element pattern at all. Geochemical patterns discussed in Chapter 4.3 point to first order sandstone assemblages, i.e., alluvial fan or fluvial environments, for the Rooihoogte, Boshoek, Hekpoort and Dwaalheuwel Formations. It is thus surprising that the Dwaalheuwel Formation sandstones show only a weak areal signiture compared to other Pretoria Group sandstones. However, the thickness relationships of Dwaalheuwel Formation and underlying Hekpoort volcanics seem to be inversely proportional, as can be inferred from Schreiber (1990), and the Dwaalheuwel Formation might thus be the result, at least partly, of extensive reworking of Hekpoort volcanic rocks. This model infers a relatively homogeneous geochemical provenance pattern for the Dwaalheuwel Formation and can account for the comparatively weak areal signature of the Dwaalheuwel Formation. The relatively stronger areal signatures of Timeball Hill Quartzite and Magaliesberg Formation suggest some modification of existing sedimentological models (e.g., Eriksson, 1973; Button, 1973; Eriksson et al., 1991, 1993). Local sources seem to be more important than is implied by the sedimentological models. Both Timeball Hill Quartzite and Magaliesberg Formation rocks were deposited during regressions (Eriksson and

Clendenin, 1990; Eriksson et al., under review b), which can be concluded independently of the marine/lacustrine-fluvial controversy. However, reworking processes can hardly account for the observed geochemical pattern, and the evidence for local sources implies that fluvial processes might have been more influential than previously thought. Eriksson et al. (under review b) come to similar conclusions for the Magaliesberg Formation, although the facies relationships in time and space of this formation are far more complex than inferred solely by the geochemistry of sandstones.

The discussion of depositional and post-depositional processes influencing the geochemistry of the Pretoria Group sedimentary rocks can be summarized as follows:

(1) The abundance and relationships of boron in Pretoria Group shales point to various possible influences, namely palaeoenvironment, varying clay mineral assemblages, penecontemporaneous volcanism and/or post-depositional processes.

(2) Apart from detrital input, the REE-abundance and patterns of Pretoria Group shales seem to be strongly dependent on post-depositional processes and clay mineralogy. Both diagenesis and hydrothermal/metasomatic alteration or a more complex relationship between them and the clay mineral assemblage may explain REE-patterns, which are unusual for Early Proterozoic sedimentary rocks.

(3) Relationships of boron, REE and alkalis emphasize the importance of post-depositional processes.

(4) Neither boron nor REE abundances unequivocally support either epeiric marine or predominantly fluvial-lacustrine depositional models.

(5) The clay mineral assemblage and the trace element signatures of Pretoria Group shales and sandstones provide some evidence for the occurrence of local provenance signatures, thus supporting an intracratonic structural basin setting, but cannot solve the marine/lacustrine-fluvial controversy.

(6) Generally low MgO and CaO contents of Pretoria Group shales favour a freshwater setting. However, the mobility of MgO and CaO in the sedimentary cycle makes such a conclusion somewhat spurious.

4.5 Economic geology

The Pretoria Group contains various types of known mineralization: fault-bounded hydrothermal Au-deposits related to the intrusion of diabase sills or the Bushveld Complex (e.g., Hammerbeck, 1976; Harley and Charlesworth, 1993; Boer et al., 1993), andalusite deposits in shales within the Bushveld metamorphic aureole (Hammerbeck, 1976), and oolitic ironstones (Schweigart, 1965). This discussion will centre on possible base-metal mineralization in the Pretoria Group, in the light of lithostratigraphic, geochemical, inferred palaeoenvironmental and structural analogies to classic stratiform sulphide deposits.

Stratiform base-metal sulphide occurrences can be divided into two main groups: the volcanogenic exhalative deposits related to island arc margins, and the continental rift- and shelf carbonate- related exhalative sedimentary deposits (Maynard, 1983). The inferred intracratonic setting and rift association, as well as the mainly clastic sedimentary assemblage of the Pretoria Group (Eriksson et al., 1993, Chapter 4.3), makes a comparison with the exhalative volcanogenic group of Maynard (1983) improbable. However, a comparison with the Guilbert and Park (1986) model of base-metal deposit genesis in intracratonic rift basins, or aulacogens, with active volcanism and terrigenious sedimentation, seems to be justifiable for the Pretoria Group. In such a setting, the metal-/sulphide-carrying brines can be derived by active hot springs related to volcanism (e.g., Leblanc and Billaud, 1978), or they may simply be basin brines from deeper parts of the basin, or related to deep fracture systems (Guilbert and Park, 1986). The environment envisioned by Guilbert and Park (1986) is compatible with the exhalative sedimentary group of Maynard (1983) and the distal environments of Gilmour (1976).

The highest sulphur contents in Pretoria Group sedimentary rocks are found in pyritic black shales of the Silverton Formation in the Botswana and western Transvaal sampling areas. The sulphur contents reach up to 3 wt.% and average 1.6 wt.% (n =15). Figure 4.5.1 shows a simplified stratigraphic profile of the Silverton Formation in Botswana, compiled from drillhole data provided by Key (1983) and Piper and Kreimeyer (1992), and field observations during this study.

The pyritic black shale facies is underlain by sandstones and siltstones (Fig. 4.5.1). An unusual ferruginous unit, with crimson colouration and about 1.5 m in thickness, occurs in the middle part of these grey-coloured sandstone beds (marked by a black line in Fig. 4.5.1). A detailed profile of the ferruginous unit (Fig. 4.5.2 A) shows sedimentological features such as traction carpets, cross-lamination and graded bedding, which are compatible with deposition as a complex, surging, high-density turbidity current (Lowe, 1982, Fig. 4.5.2 B). The ferruginous unit consists of fine-grained oolitic ironstones, chert/quartz grains (forming the traction carpets) and a cobble bed with ironstone, mudstone and pyrite clasts.
Microscopic investigation of the pyrite clasts, which are up to 3 cm in diameter, reveals an unusual association, with goethitic/hematitic iron oolites imbedded in a pyrite matrix (Fig. 4.5.3 A-D and 4.5.4 A-D). The iron oolites exhibit further evidence for a polycyclic development (Fig. 4.5.4 A-D), indicating turbulent water conditions alternating with prolonged periods of relative quiescence during their genesis. As the rims of the ooids are not altered, diagenetic origin of the sulphide can be excluded. Hence, a syngenetic origin of oolites and sulphide mineralisation is probable, with 'freezing' of the ooids in rapidly precipitating pyrite. Pyritic and other sedimentary clasts (incl. oolites) were then probably redeposited together by a high-density turbidity current. The rapid precipitation of pyrite points to exhalative processes, which provided, at least, substantial amounts of sulphur.

The profile of the Silverton Formation in the Botswana sampling area (see Fig. 1.5.1 for location of area) has similarities with the sedimentary facies patterns encountered in stratiform sulphide deposits of the exhalative sedimentary group. These deposits regularly exhibit facies associations of carbonaceous sediments, carbonates and tuffaceous shales (Stanton, 1972), and are thus similar to the facies association observed in the Silverton Formation (Fig. 4.5.1). In the western Transvaal sampling area, the Silverton shales grade from a kaolinite/andalusite-rich basal shale unit to a thin carbonaceous chert breccia and sandstone unit, which is followed by carbonaceous and tuffaceous shales of several hundred meters thickness. Carbonaceous shales overlying the breccia/sandstone unit are enriched in sulphur (up to 0.5 wt.%), thereby suggesting an excellent stratigraphic correlation with the Bostswana sampling area. The Silverton Formation pyritic shale facies of the Botswana sampling area and carbonaceous/tuffaceous Silverton shales of the western Transvaal sampling area were laid down in a northwest-southeast striking trough (Eriksson et al., 1991,

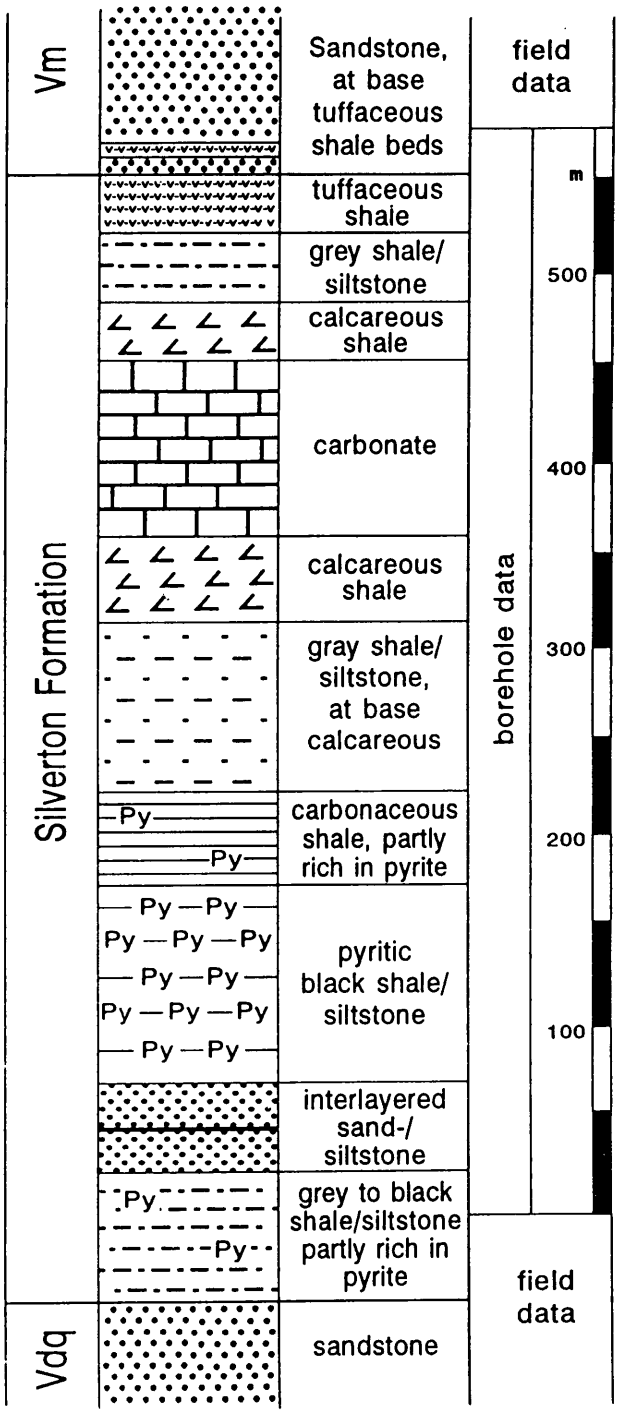

Fig. 4.5.1: Simplified stratigraphic profile of the Silverton Formation in Botswana. Black line in "interlayered sand-/siltstone" facies marks location of crimson-coloured unit. Vdq = Daspoort Fm., Vm = Magaliesberg Fm..

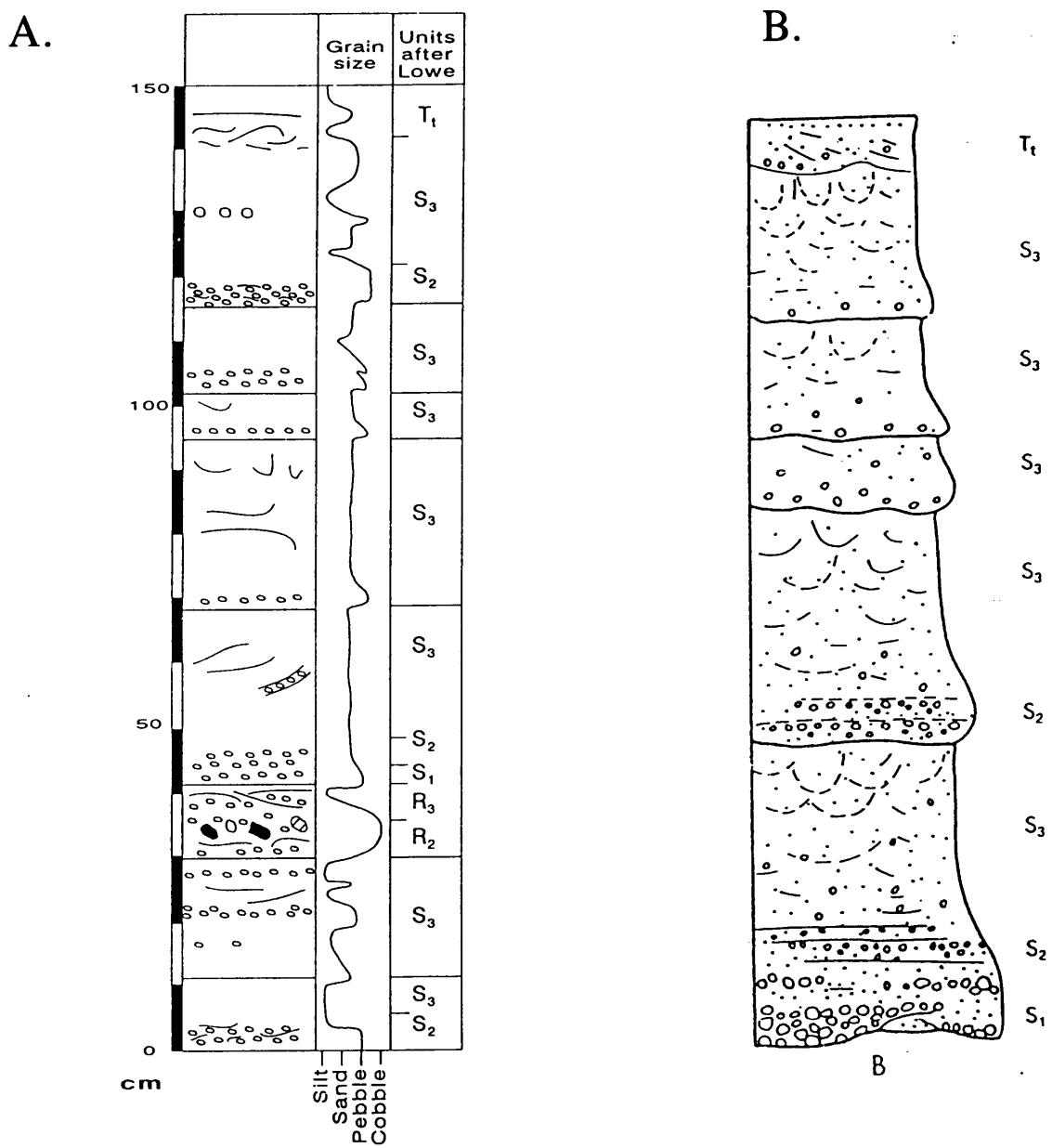

Fig. 4.5.2: A. Profile of a crimson-coloured ferruginous unit in the Silverton Formation, occurring in drillhole STRAT 1 from Botswana. B. Schematic features commonly found in deposits of complex, surging, high-density turbidity currents (modified after Lowe, 1982).

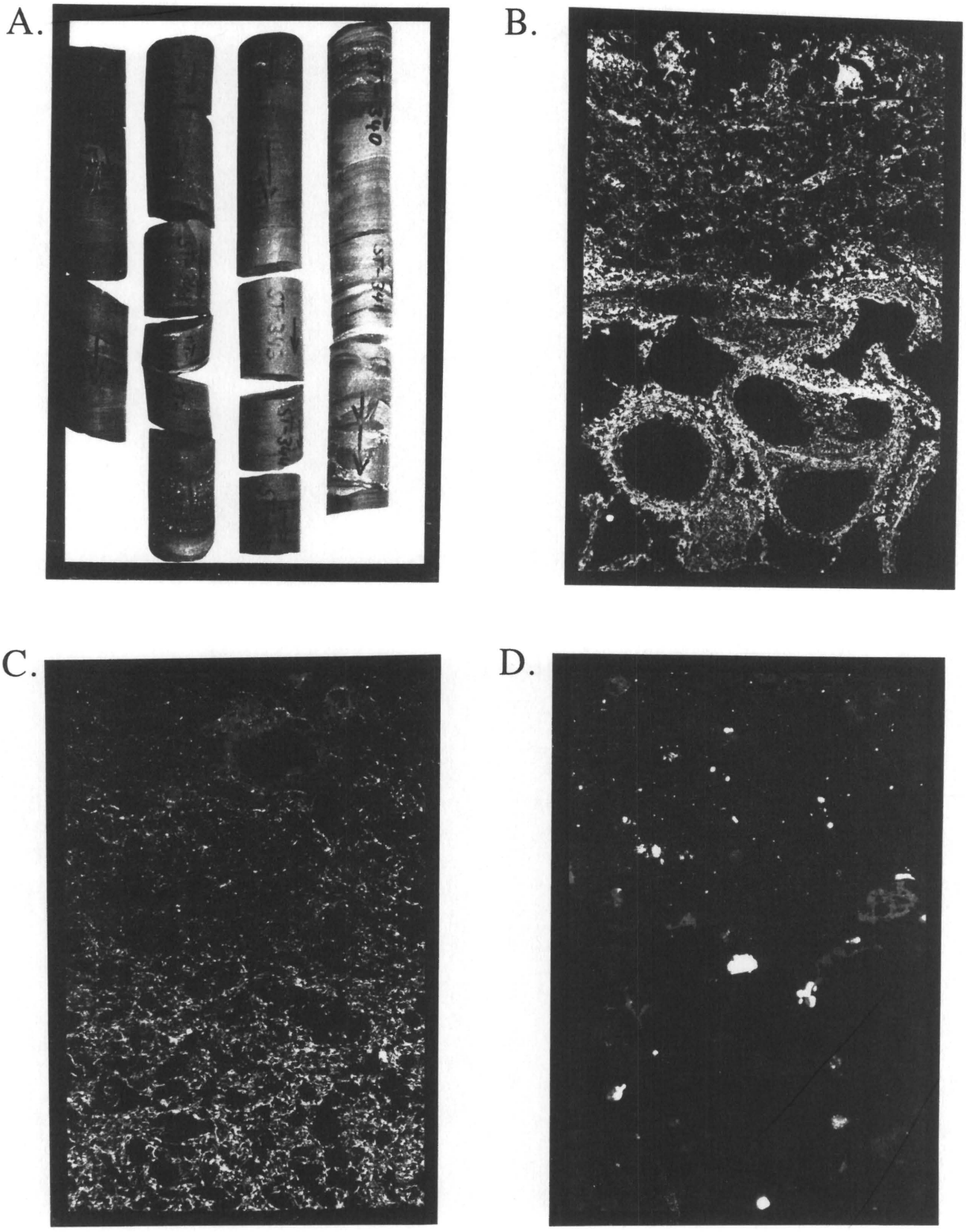

Fig. 4.5.3: A. Crimson-coloured unit from bore-core STRAT 3. Length of core shown = ± 1.5 m. Base of section is in the lower right corner, top of section in the upper left corner. Cobble bed with pyrite clasts is at the base of the shown section (= lower right corner). Diameter of core (A.) = 54 mm; height of photographs B.-D. = 870 μm B. - D.: Upward-fining cycle from the bottom of Figure 4.5.3 B to top of Figure 4.5.3 D.

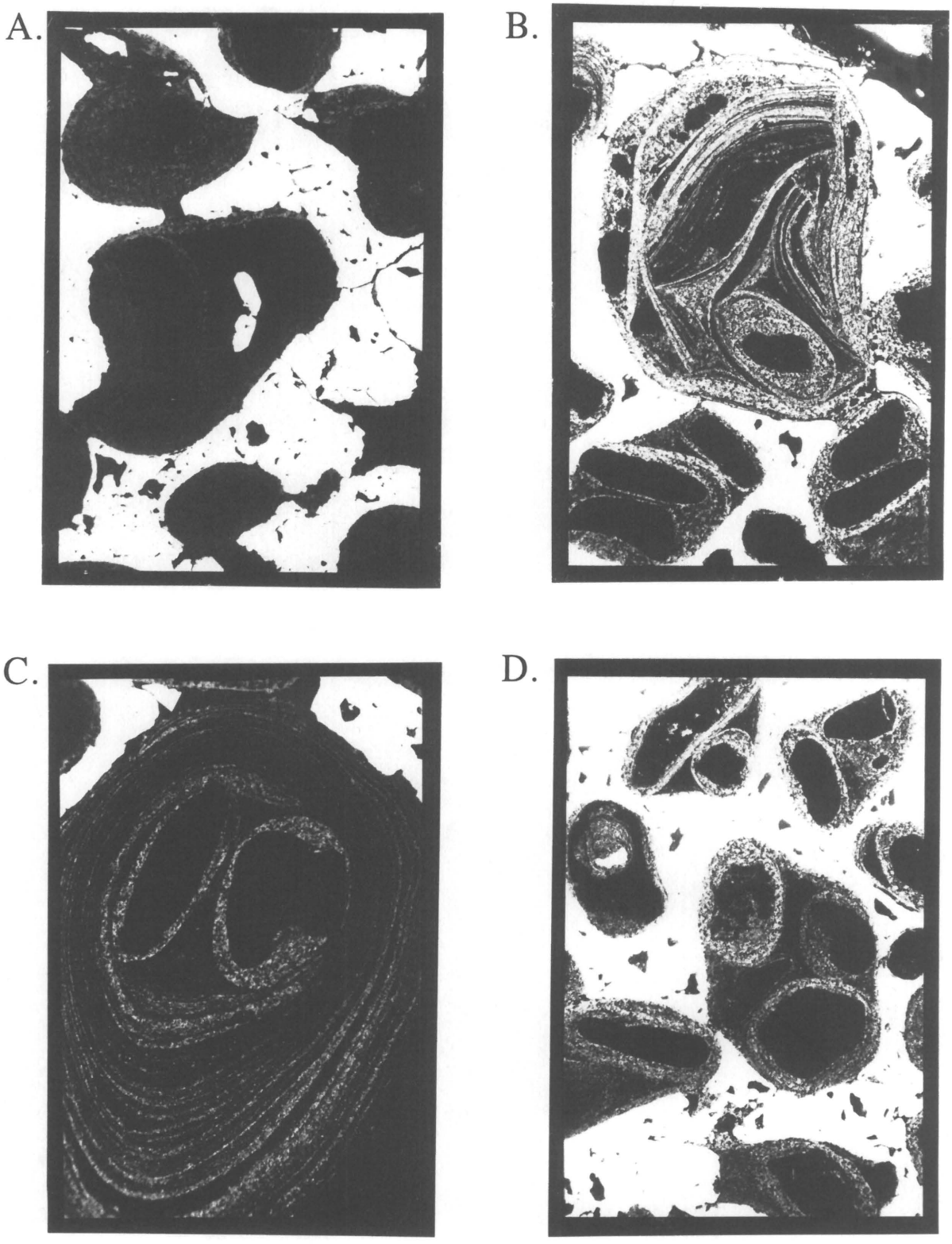

Fig. 4.5.4 A-D: Hematitic/goethitic iron oolites imbedded in pyrite matrix. Polished section photographs from a pyrite clast in a cobble bed in the inferred high-density turbidity current deposit, Silverton Formation (see Fig. 4.5.2 A). Height of photographs = 870 μm.

see Fig. 4.5.5), which is associated with a parallel-striking major fault system (Eriksson and Reczko, in press; see Fig. 4.5.6). The exhalative sulphides described from the Botswana drillholes are found in the vicinity of the intersection of this fault-system with the Thabazimbi-Murchinson lineament, an east-west striking fault-system which is thought to have controlled the northern margin of the Transvaal basin during Pretoria Group times (Eriksson et al., 1993; Eriksson and Reczko, in press). Large (1988) related SEDEX-type deposits in a rift tectonic setting to a tensional pulse in the post-rift thermal subsidence stage. The tensional pulse is normally accompanied by volcanic activity and elevated rates of subsidence (Large, 1988). In the Pretoria Group, the transition from mechanical rifting to thermal subsidence is thought to occur at the base of the Silverton Formation (e.g., Eriksson et al., 1993). The extrusion of the medial Machadodorp Volcanic Member of the Silverton Formation might indicate a tensional pulse as proposed by Large (1988).

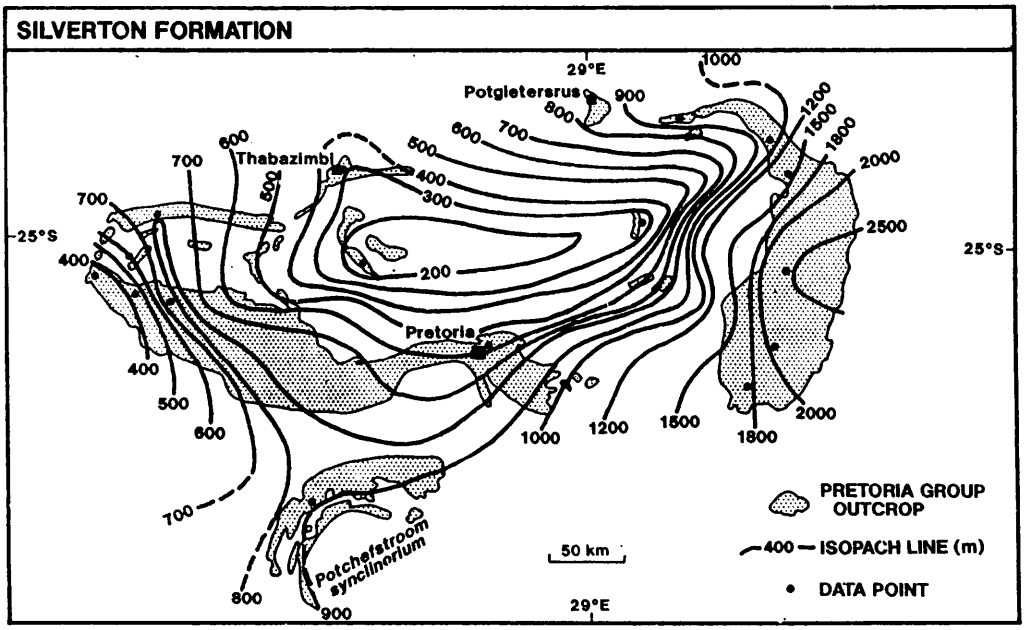

Figure 4.5.5: Isopach map showing thickness of the Silverton Formation in the main Transvaal basin (modified after Eriksson et al., 1990). Note inferred NW-SE striking trough in the western Transvaal.

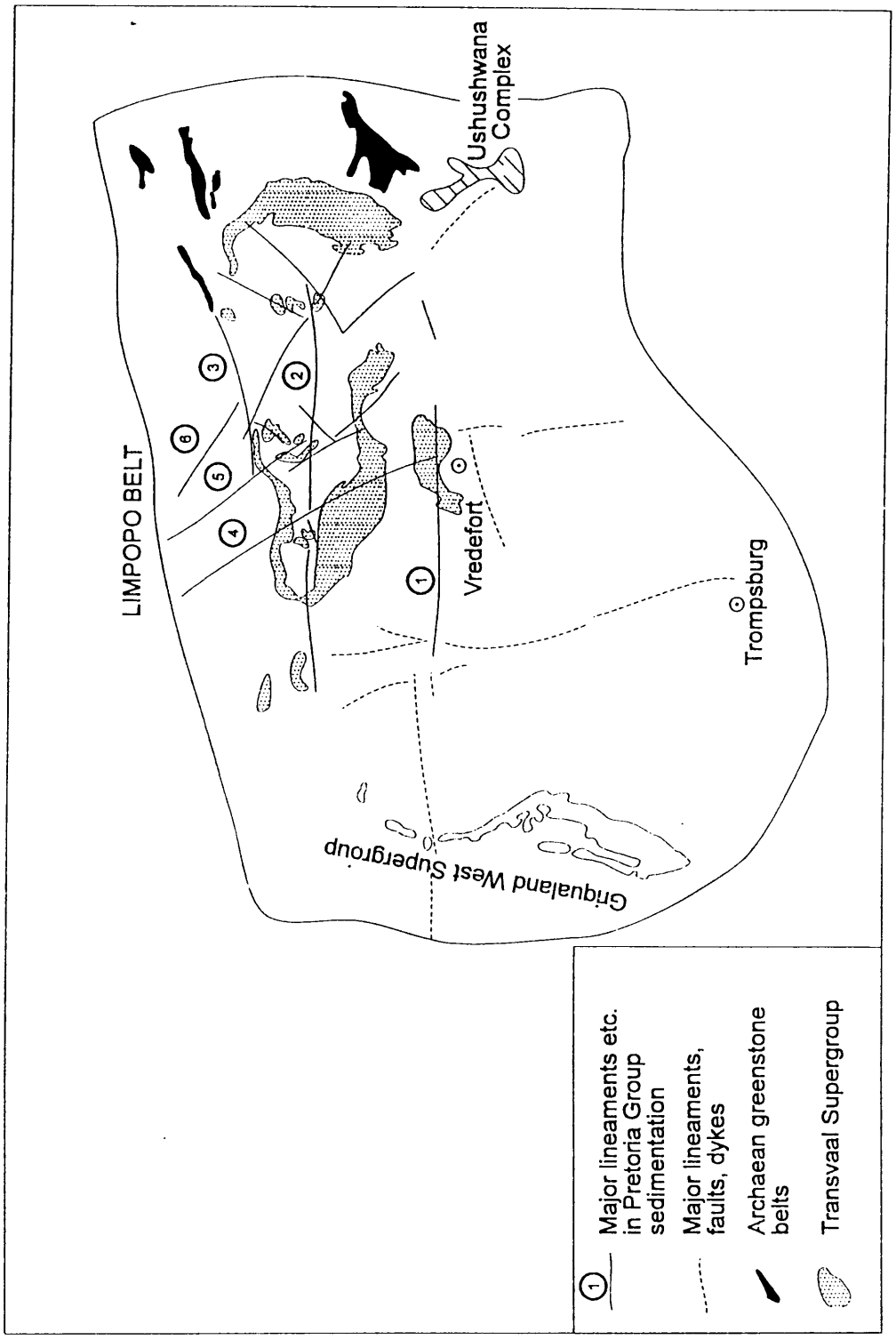

Figure 4.5.6: Main fault systems in the Transvaal basin active during Pretoria Group deposition (modified after Corner, 1991, and Eriksson and Reczko, in press)

Another shale unit with potential base-metal mineralization may be the base of the Lower Shale Member of the Timeball Hill Formation, which also has an associated black shale facies. The colouration of these black shales is thought to be secondary, caused by the replacement of pyrite with Fe^{2+}-oxides during hydrothermal alteration (Eriksson et al., in press c). Pyritic shales are found locally at this stratigraphic position (Schweigart, 1963). A strong increase of As-contents of shales (up to 460 ppm, see Table 3.3.2.1) at this stratigraphic level also points to the influence of hydrothermal processes (Feely et al., 1991). The associated Bushy Bend Lava Member underlies these pyritic shales (Eriksson et al., in press c) and thins from a maximum of 90 m in the Potchefstroom Synclinorium towards the north. In the eastern Transvaal basin, the Bushy Bend Lava Member is assumed to be represented by a highly altered tuff, $\leq$ 0.5 m thick, interbedded with black shales of the basal Timeball Hill Formation (see Chapter 3.3.2 and Fig. 3.3.2.2). These tuffs contain high amounts of Cr, Zn, Cu, Co, Ni and As, and have a PGE-content of up to 1 g/t (see Chapter 3.3.2; Schreiber, 1990).

Figures 4.5.7 A-C show geochemical profiles from drillholes in the uppermost part of the rudaceous Rooihoogte Formation and the base of the Timeball Hill Formation in Botswana (for other element contents of the relevant drillhole samples, see Fig. 3.3.1.1, 3.3.1.2 and 3.3.2.1 in Chapters 3.3.1 and 3.3.2). The lithology of the profiles is described in some detail by Key (1983). Petrographic features of the basal Timeball Hill samples in the drillhole 'GOSSAN 2' (Fig. 4.5.7 A) include weathered pyrite cubes at the top of beds and local pyrite vugs due to weathering of pyrite (Key, 1983). The basal Timeball Hill samples in these profiles exhibit a considerable enrichment of Zn, Cu, Pb and Ba. It has to be mentioned that the Zn-pattern may be complicated, due to recent mobility and related enrichment at the oxidation base in the drillhole cores (Fig. 4.5.7 A to C). However, elevated Zn-contents, of up to 1600 ppm, are observed at comparable stratigraphic levels (for example in the Polo Ground Quartzite Member, the uppermost arenaceous unit of the Rooihoogte Formation (Key, 1983)), and are thus interpreted as synsedimentary or early post-depositional enrichments. The volcanoclastic composition of siltstones underlying the Polo Ground Member (Key, 1983) further strengthens an inferred relationship of sulphide mineralisation, base-metal enrichment and penecontemporaneous volcanism. The extrusion of the Bushy Bend lavas in the Potchefstroom sub-basin can thus be correlated stratigraphically with the

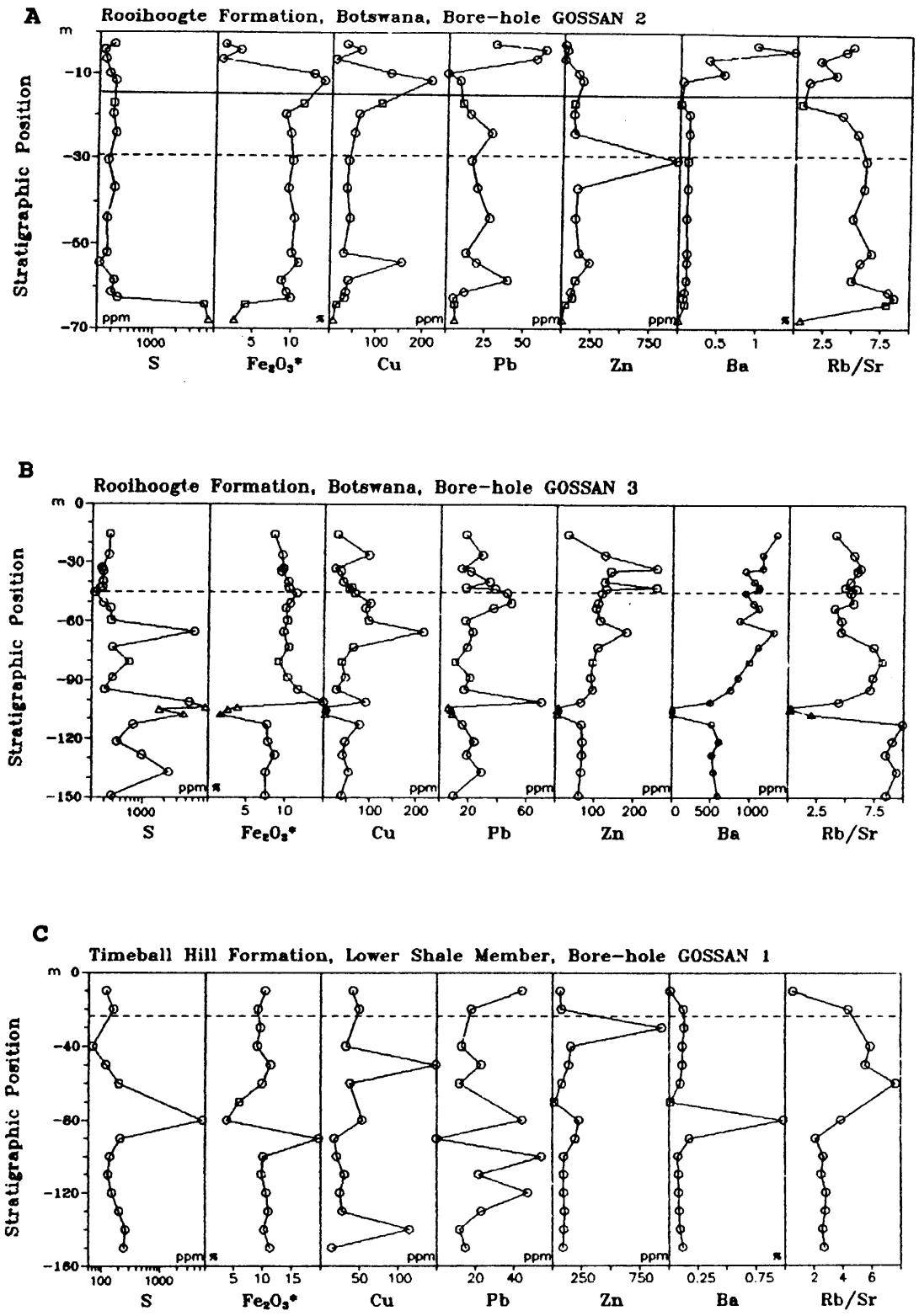

Figure 4.5.7 A-C: Geochemical profiles of the Rooihoogte and Timeball Hill Formations from Botswana drillhole cores. Symbols: ○ = shale; □ = sandstone; Δ = conglomerate. Dashed lines = oxidation base of drillhole. Solid line in Fig. 4.5.7 A is the inferred contact of Rooihoogte and Timeball Hill Formations

occurrence of tuffs, widespread hydrothermal alteration of shales, volcanoclastic detritus, sulphide mineralisation and base-metal enrichment at the level of the base of the Timeball Hill Formation in the main Transvaal basin.

The lithological associations described for the basal Timeball Hill shales and for the Silverton Formation shales are, to a certain degree, favourable for the genesis of stratiform sulphide deposits. Both described units contain sedimentary rocks deposited in a reducing palaeoenvironment, and were associated with penecontemporaneous volcanism and hydrothermal alteration processes. The Silverton Formation massive sulphides (Fig. 4.5.4 A-D) are compatible with brine discharge, which was, at least, rich in sulphur. Associated with the generally carbonaceous shales of the Silverton Formation are abundant andesitic tuffaceous shales and/or volcanics. The abundant carbon, the presence of stromatolitic carbonates and of inferred high-density turbidity current deposits in the Silverton Formation (Fig. 4.5.2), and the facies association of the Timeball Hill Formation (Schreiber, 1990; Eriksson et al., 1993), both support a shallow to intermediate water-depth not far from the shoreline (Eriksson et al., in press c), in the sense of Stanton (1972). The principal geological features typical of the setting of stratiform sulphide deposits (Stanton, 1972; Maynard, 1983; Guilbert and Park, 1986) thus seem to be present in the Pretoria Group. Furthermore, the inferred rift-related tectonic setting of the Silverton Formation, and the association of volcanism and massive sulphide occurrences in this formation is thought to be compatible with the geological setting of many SEDEX-mineralisation occurrences (Large, 1988).

The geochemistry of the basal Timeball Hill Formation (Fig. 4.5.7 A-C) leads to further speculation. The association there of a substantial increase in Ba, Cu and Zn(-Pb) is typical of some stratiform base-metal sulphide deposits (Stanton, 1972). Widepread hydrothermal/metasomatic processes (Chapter 4.4) provide an appropriate potential mechanism of metal-rich fluid transportation and resultant mineralisation. Although the occurrence of inferred hydrothermal/metasomatic processes generally does not seem to be restricted to a specific stratigraphic unit, geochemical indications of hydrothermal/metasomatic processes are most pronounced at stratigraphic levels where more or less extensive penecontemporaneous volcanism is observed. However, as

hydrothermal/metasomatic activity seems to be extensive both laterally and vertically, i.e., more than one alteration episode can be assumed, a renewed mobilisation of base-metals due to later-stage epithermal processes cannot be excluded.

CHAPTER 5: CONCLUSIONS

5.1 Summary of discussion

The discussion of the implications of the geochemistry of the sedimentary rocks of the Pretoria Group (see Chapter 4) can be summarized as follows:

(1) Source rocks:

Abundances and relationships of elements thought to be representative of certain specific source rocks (i.e., Cr, Th, Sc and Zr) point to a complex source terrain for the Pretoria Group sedimentary rocks, with predominantly granitic and sedimentary sources, as well as, possibly, ultramafic sources. The sedimentary sources proposed here may have been rich in elements typical of mafic to ultramafic sources (i.e., Cr and Sc), and the fairly high abundance of these elements in Pretoria Group sedimentary rocks thus may have been partly inherited from their sedimentary sources. Furthermore, transport fractionation seems to have influenced the evolving geochemical patterns of shales and sandstones. A critical point in the evaluation of provenance by geochemical means is the assumption that 'immobile' provenance indicator elements like Th, Zr, Cr and Sc have a similar geochemical behaviour in the sedimentary process. It is shown that this assumption may be misleading in the interpretation of source rocks of Precambrian age. REE cannot be utilized for provenance estimations of Pretoria Group sedimentary rocks.

(2) Syndepositional palaeoclimate:

The syndepositional palaeoclimate is thought to have been humid-hot, at least for the middle part of the Pretoria Group (Hekpoort to Daspoort Formations). The lower part of the Pretoria Group (up to Timeball Hill Formation) shows a similar geochemical pattern to the middle part, but the palaeoclimate cannot be interpreted without reasonable doubt in the same way as for the middle part of the group. Chemical weathering profiles related to the depositional hiatus between the underlying Chuniespoort Group and the Pretoria Group (at least 100 Ma) may have been reworked and redeposited in early Pretoria Group times. The palaeoclimate of the

post-Daspoort formations is difficult to interpret due to penecontemporaneous volcanism (Silverton Formation) and, possibly, increased rates of tectonic activity (Schreiber, 1990). Generally, the geochemistry of Pretoria Group sedimentary rocks shows ample evidence of non-metamorphic alteration processes, although a differentiation into syn- and post-depositional processes is difficult.

(3) Tectonic setting:

The geochemical signature of Pretoria Group sedimentary rocks is indicative of a divergent margin tectonic setting, and thus compatible with a rift tectonic setting. Asthenospheric upwelling and processes in the mantle and lithosphere related to a rift tectonic setting are thought to provide a simple explanation for the occurrence and compsition of Pretoria Group volcanic rocks.

(4) Depositional palaeoenvironment, diagenesis and epithermal processes:

The abundance and relationships of boron and REE point to a strong influence of post-depositional processes, namely diagenesis and/or hydrothermal alteration on the observed geochemistry. Trace element patterns and clay mineral assemblages support the occurrence of local sources and, thereby, relatively short transport distances for at least the lower part of the Pretoria Group sedimentary assemblage (up to Daspoort Formation). The described geochemistry thus provides some evidence for an intracratonic structural basin setting, but cannot solve the marine/lacustrine controversy.

(5) Economic geology:

Widespread hydrothermal/metasomatic processes provide an appropriate potential mechanism for metal-rich fluid transportation and, possibly, resultant mineralisation. The occurrence of massive sulphides, penecontemporaneous volcanic activity and the inferred tectonic setting give a theoretically favourable environment for base-metal deposits.

5.2 Genesis of the Pretoria Group basin - a brief attempt at a model

The sedimentary basin classification of Miall (1984) includes five types of basins, namely

A. Divergent margin basins;

B. Convergent margin basins;

C. Transform and transcurrent fault basins;

D. Basins developed during continental collision and suturing;

E. Cratonic basins.

This classification scheme is based on three criteria (Miall, 1984):

1. the type of crust on which the basin rests,
2. the position of the basin relative to plate margins, and,
3. where the basin lies close to a plate margin, the type of plate interaction occurring during sedimentation.

Allen and Allen (1990) proposed a simplified classification of sedimentary basins, mainly based on the primary tectonic mechanisms:

a. Basins generated due to lithospheric stretching;

b. Basins generated by flexure on continental and oceanic lithosphere;

c. Strike-slip or megashear-related basins.

Miall's (1984) criteria of basin classification can easily be applied to the Pretoria Group. The Pretoria Group was deposited on continental crust, in an interior position on the Kaapvaal craton. The sedimentary assemblage constituting the Pretoria Group is markedly undeformed, i.e., a primary deflection of the lithosphere by applied force systems (Allen and Allen, 1990) seems to be unlikely. Hence, the basin types "convergent margin basins" (B.), "basins developed during continental collision" (D.) in the sense of Miall (1984), and "basins generated by flexure" (b.) in the sense of Allen and Allen (1990) must be discarded as viable genetic alternatives.

Due to the location of the Pretoria Group in the interior of the Kaapvaal craton, a passive margin setting (sub-type of the "divergent margin basins" of Miall (1984) and "basins generated by lithosperic stretching" of Allen and Allen (1990)) has to be rejected as well. Obviously, the sedimentary rocks deposited in a passive margin tectonic setting must be

incorporated into the continental crust by a collisional (= orogenic) event, if they are now located in the craton interior. It seems somewhat arbitrary, that many Proterozoic basin-fills comprising unfolded sedimentary assemblages are ascribed to a passive margin setting, as structural evidence does not support this assumption. The geological record of the Phanerozoic gives ample evidence for the mechanism of basin development on platforms and cratons. Independent of the marine and/or lacustrine facies associations, preservable sedimentary basins on platforms and cratons (if not related to a collisional event) are associated with stretched lithosphere or related to strike-slip movement, i.e. structural basins. The rate of sea-level rise and fall is an important factor controlling the vertical and horizontal character of a sedimentary assemblage. However, sequence stratigraphic concepts stress equally the importance of subsidence rates and rates of sedimentary input (e.g. Wilgus et al., 1988; Allen and Allen, 1990; Posamentier et al., 1993).

The relationship of intracratonic sags (i.e. the "cratonic basins" of Miall (1984)) and "failed rifts/aulacogens" proposed by Allen and Allen (1990) (Fig. 5.1) allows the combination of the basin types A. ("divergent margin basins") and E. ("cratonic basins") of Miall (1984) into a single group, namely, the basin type "basins generated by lithospheric stretching" of Allen and Allen (1990), with the aim of simplifying the interpretational approach. The exclusion of various basin types and sub-types leaves three viable alternatives for the classification of the Pretoria Group basin:

I. Intracratonic sag
II. Failed rift/aulacogen
III. Strike-slip/megashear-related basin.

Generally, strike-slip/megashear-related basins are small (only a few tens of kilometers across), i.e. locally restricted occurrences prevail (Miall, 1984). The size of the Transvaal basin thus makes a pure strike-slip character for the Pretoria Group basin unlikely. However, divergent-oblique strike-slip movement may accompany rifting processes (Miall, 1984).

If strechting of the lithosphere is accepted as the primary mechanism of subsidence for the Pretoria Group basin, only intracratonic sags and failed rifts/aulacogens remain as possible basin types. The geometry of the main occurrences of the Pretoria Group (Transvaal and

Potchefstroom basin), i.e. oval to circle-shaped with a maximum length to width ratio of 2.5 : 1, favour an intracratonic sag basin (if it is assumed that these basins did not extend into the Kanye basin), as rift basins have normally a length to width ratio from 3 : 1 up to 10 : 1 (Chain and Michailov, 1989). However, more complicated rift settings can have a lower length to width ratio than 3 : 1 (e.g. North Sea Graben). The sedimentology, and the volcanic and sedimentary geochemistry of the Pretoria Group generally favour a rift setting (e.g., Schreiber, 1990; Eriksson et al., 1993; v. Gruenewaldt and Harmer, 1993; see Chapter 4.3), possibly including the development of half-grabens (e.g., Eriksson 1990, see Fig. 1.2.4) and synsedimentary uplifts (Eriksson et al., 1988). Deep-reaching fault systems influencing the sedimentation of the Pretoria Group (see Fig. 4.5.5) are regarded as partial evidence of tensile stresses overcoming rock strength and causing brittle fracture of the crust (Eriksson and Reczko, in press). Hence, 'true' rifting in the sense of Allen and Allen (1990) has taken place in the Pretoria Group basin, opposed to the development of intracratonic sags, where the deviatoric stresses are too weak to cause brittle failure (Allen and Allen, 1990). Reczko et al. (1994) proposed an asymmetrical stretching model for the Transvaal and Potchefstroom basins in Pretoria Group times, based on the model of Coward (1986) (Fig. 5.1). This model can account for the length/width ratio, erosional/weathering episodes in the Pretoria Group (e.g., base of the Boshoek Formation and top of the Hekpoort Formation (Button, 1973, 1979)) and the thinning of the Silverton Formation towards the Potchefstroom basin. More significantly, this model allows for the development of sub-basins, thermal domes and an inversion of older extensional faults (Eriksson et al., 1988; Eriksson et al., 1990b; Reczko et al., 1994). However, the final stages of the Pretoria Group basin development shown in Figure 5.1 are based on insufficient data (geophysical interpretations of a seismic line taken near Pretoria, R. C. Hinds, pers. comm., 1994), and thus are somewhat speculative, i.e. the compressional event may have taken place after the mafic phase of the Bushveld Complex. It has to be remembered in this context that the intrusion of the Bushveld Complex and related structural displacements are a major obstruction in resolving the problems related to the development of the Pretoria Group or, more generally, the Transvaal Supergroup.

The tectonic setting of the Pretoria Group proposed here is compatible with the preservation probabilities for major tectonic realms reported by Veizer (1988). The preservation

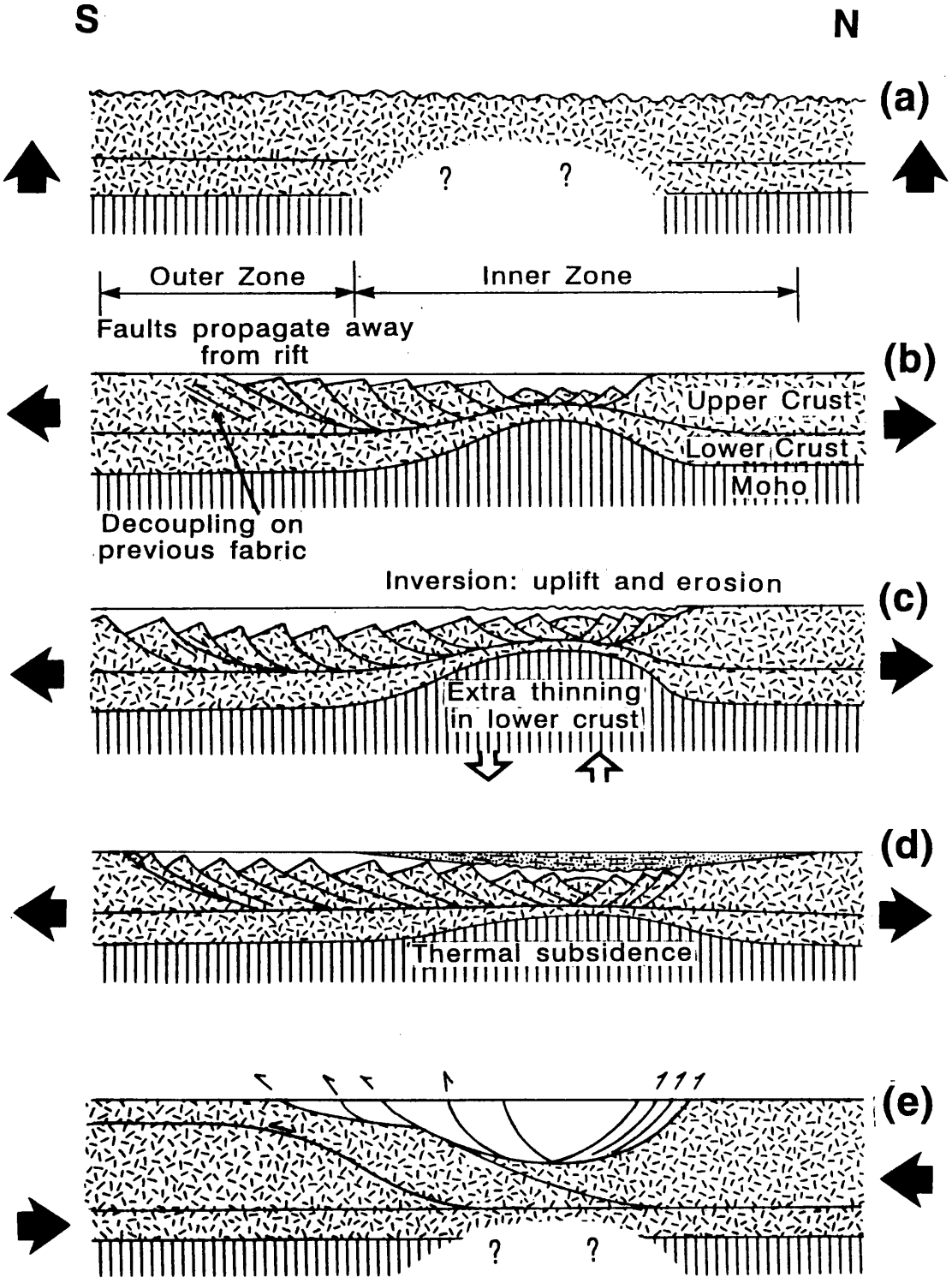

Fig. 5.1: Basin development in the Transvaal and Potchefstroom basins during Pretoria Group times (modified after Reczko et al., 1994).

probabilities provided by Veizer (1988) can also be utilized indirectly to speculate about the provenance of the Pretoria Group. As greenstone belt environments would have been rapidly recycled, they are under-represented in the geological record and, compared to cratonic regions, must have been present to an extent much greater than is apparent from present exposures (McLennan and Taylor, 1988). The enrichment of elements like Cr, Ni and Sc in late Archaean sedimentary rocks compared to Pretoria Group and Waterberg sedimentary rocks (Wronkiewicz and Condie, 1987, 1989, 1990; Condie and Wronkiewicz, 1990) may thus be explained by an increased supply of eroded material from greenstone belts. As the deposition and sedimentation of the Pretoria Group is thought to have been controlled by reactivated lineaments (Thabazimbi-Murchison and Barberton-Sugarbush lineaments) related to greenstone belts (Eriksson and Reczko, in press), greenstone material could have provided some of the mafic provenance components found in the sedimentary rocks of the Pretoria Group (see Chapter 4.1). As the generation of greenstone belts as a major basin type decreased from the early Archaean to the late Archaean or, respectively, after the cratonisation of the crust, a decreasing amount of mafic provenance components would be expected from late Archaean to early Proterozoic sedimentary assemblages in South Africa, as the greenstone belts would have been either eroded or finally incorporated into the crust. However, an alternative model is also viable: all the greenstone belts would probably have been eroded or incorporated into the crust prior to or shortly after cratonisation, and the post-cratonisation sedimentary assemblages could have been related to reworked first-order sedimentary rocks rich in greenstone material. Recycling of these sedimentary sources could presumably have produced second-order sedimentary rocks with a strong remaining greenstone component; renewed and progressive recycling of the second-order assemblages could finally have led to dilution of the mafic components by other sources such as tonalite and/or granite.

ACKNOWLEDGEMENTS

The author wishes to thank the Foundation for Research Development (FRD) for a bursary and the University of Pretoria for further financial support which enabled this study. Dr. Martin Sharpe from Rocklabs CC, the staff of the Geological Survey of South Africa and Mr. Rolf Venter from the Atom Energy Corporation are thanked for their help with analysing the samples. Dr. Mike van der Linde (University of Pretoria) supported the utilization of the SAS software with his terrific programming skills. Dr. Dave Piper (British Geological Survey) provided the opportunity to take the bore-core samples from the Geological Survey of Botswana. The staff of the Geological Department of the University of Pretoria must be mentioned here for many helpful discussions and for providing literature. I want to thank especially Dr. Roland Merkle (University of Pretoria, Dept. of Geology) for the many discussions and references regarding the treatment of numerical data. Mrs. Sabine Verryn (University of Pretoria, Dept. of Geology) is acknowledged for performing the XRD analyses. Dr. Ron Hinds provided a personal computer, Ms. Hester Botha and Mr. Christoph Gauert helped editing an earlier version of the thesis. My special thanks are due to my promoters, Profs. Patrik G Eriksson and Carel P Snyman for their patience, discussions, valuable tips and an unbeatable support.

REFERENCES

Aitchison, J. (1986). The statistical analysis of compositional data. Methuen, New York.

Allen, P. A., and Allen, J. R. (1990). Basin Analysis: Principles and Applications. Blackwell, Oxford.

Anderson, D. H., and Hawkes, H. E. (1958). Relative mobility of the common elements in weathering of some schist and granite areas. Geochim. Cosmochim. Acta **14**, 204-210.

Anderson, D. L. (1983). Chemical composition of the mantle. J. Geophys. Res. **88**.

Backhaus, K., Erichson, B., Plinke, W., and Weiber, R. (1990). Multivariate Analysenmethoden. Springer, Berlin.

Baumann, A., and Werner, E. (1973). Geochemisch-paläogeographische Untersuchungen im süddeutschen Molassebecken. Z. dt. geol. Ges. **124**, 363-378.

Benzécri, J. P. (1973). L'Analyse des Données. Vol. 2: L' Analyse des Correspondances. Dunod, Paris.

Beukes, N. J. (1983). Palaeoenvironmental setting of the iron-formations in the depositional basin of the Transvaal Supergroup, South Africa. In: Iron Formations: Facts and Problems (Eds.: Trendall, A. F., and Morris, R. C.), 131-209. Elsevier, Amsterdam, Holland.

Beukes, N. J. (1986). The Transvaal Sequence in Griqualand West. In: Mineral Deposits of Southern Africa (Eds.: Anhaeusser, C. R. and Maske, S.), 819-828. Geological Society of South Africa, Johannesburg, South Africa.

Bhatia, M. R. (1983). Plate tectonics and geochemical composition of sandstones. J. Geol. **91**, 611-627

Bhatia, M. R. (1985). Rare earth element geochemistry of Australian Paleozoic graywackes and mudrocks: provenance and tectonic control. Sed. Geol. **45**, 97-113.

Bathia, M. R., and Crook, A. W. (1986). Trace element characteristics of graywackes and tectonic setting discrimination of sedimentary basins. Contrib. Mineral Petrol. **92**, 181-193.

Biddle, K. T., Uliana, M. A., Mithchum, R. M., Fitzgerald, M. G., and Wright, R. C. (1986). The stratigraphic and structural evolution of the central and eastern Magallanes Basin, southern South America. In: Foreland Basins, (Eds. Allen, P. A., and Homewood, P.), Spec. Publ. Int. Assoc. Sedim. **8**, 41-61.

Binder, F. (1962). Die log-normale Häufigkeitsverteilung. Radex-Rundschau 1962/2, 89-105.

Blatt, H., Middleton, G., and Murray, R. (1980). Origin of sedimentary rocks. 2nd ed., Prentice-Hall, Englewood Cliffs, NJ.

Böhmer, R. G. (1977). Die bepaling en verspreiding van spoorelemente in afsettingsgesteentes van die Groep Pretoria. D.Sc. thesis (unpubl.), Univ. of Pretoria, Pretoria, South Africa.

Boer, R. H., Meyer, F. M., Robb, L. J., Greney, J. R., and Vennemann, T. W. (1993). The nature of the gold mineralization in the Sabie-Pilgrim's Rest goldfield, eastern Transvaal, South Africa. Egru Inf. Circ. **262**, University of the Witwatersrand, Johannesburg, South Africa.

Bouska, V. (1981). Geochemistry of Coal. Elsevier, Amsterdam.

Brookins, D. G. (1988). Eh-pH Diagrams for Geochemistry. Springer, Berlin.

Butler, J. C. (1979). Numerical consequences of changing the units in which chemical analyses of igneous rocks are analysed. Lithos **12**, 33-39.

Butler, J. C., and Woronow, A. (1986). Discrimination among tectonic settings using trace element abundances of basalts. J. Geophys. Res. **91**, B 10289-10300.

Button, A. (1973). A regional study of the stratigraphy and development of the Transvaal Basin in the eastern and northeastern Transvaal. Ph.D. thesis (unpubl.), Univ. of the Witwatersrand, Johannesburg, South Africa.

Button, A. (1975). Stratigraphy and attitude of the floor of the Bushveld Complex in the eastern Transvaal. Inf. Circ. EGRU **96**, Univ. of the Witwatersrand, Johannesburg, South Africa.

Button, A. (1979). Early Proterozoic weathering profile on the 2200 M.Y. old Hekpoort Basalt, Pretoria Group, South Africa: Preliminary results. Inf. Circ. EGRU **133**, Univ. of the Witwatersrand, Johannesburg, South Africa.

Button, A. (1986). The Transvaal sub-basin of the Transvaal Sequence. In: Mineral Deposits of Southern Africa (Eds.: Anhaeusser, C. R. and Maske, S.), 811-817. Geological Society of South Africa, Johannesburg, South Africa.

Button, A., and Vos, R. G. (1977). Subtidal and intertidal clastic and carbonate sedimentation in a macrotidal environment: an example from the Lower Proterozoic of South Africa. Sedim. Geol. **18**, 175-200.

Cawthorn, R. J., and O'Hara, M. J. (1976). Amphibole fractionation in calcalkaline magma genesis. Am J. Sci. **276**, 309-329.

Cameron, E. M., and Garrels, R. M. (1980). Geochemical compositions of some Precambrian shales from the Canadian Shield. Chem. Geol. **28**, 181-197.

Chamley, H. (1989). Clay Sedimentology. Springer, Berlin.

Chayes, F. (1969). The chemical composition of cenozoic andesites. Proceedings of the Andesite Conference, Oregon Dept. Geol. Min. Ind. Bull. **65**, 1-11.

Clarke, F. W. (1924). Data of Geochemistry. Bull. U.S. Geol. Surv. 770, Washington, United States.

Cody, R. D. (1970). Anomalous boron content of two continental shales in eastern Colorado. J. Sedim. Petrol. **40**, 750-754.

Condie, K. C. (1991). Another look at rare earth elements in shales. Geochim. Cosmochim. Acta **55**, 2527-2531.

Condie, K. C., and Hunter, D. R. (1976). Trace element geochemistry of Archaean volcanic rocks from the Barberton region, South Africa. Earth Planet. Sci. Lett. **29**, 389-400.

Condie, K. C., and Crow, C. (1990). Early Precambrian within-plate basalts from the Kapvaal Craton in southern Africa: A case for crustally contaminated komatiites. J. Geol. **98**, 100-107.

Condie, K. C., and Wronkiewicz, D. J. (1990). The Cr/Th ratio in Precambrian pelites from the Kaapvaal Craton as an index of craton evolution. Earth. Planet. Sci. Let. **97**, 256-267.

Conover, W. J. (1980). Practical Nonparametric Statistics. Wiley, New York.

Couch, E. L. (1971). Calculation of paleosalinities from boron and clay mineral data. Bull. AAPG **55**, 1829-1837.

Coward, M. P. (1986). Heterogeneous stretching, simple shear and basin development. Earth Planet. Sci. Lett. **80**, 325-336.

Crocker, I. T., Martini, J. E. J., and Söhnge, A. P. G. (1988). The fluorspar deposits of the Republics of South Africa and Bophuthatswana. Handbook Geol. Surv. S. Afr. **11**, Pretoria, South Africa.

Crockett, R. N. (1969). The geological significance of the margin of the Bushveld Basin in Botswana. Ph.D. thesis (unpubl.), Univ. of London, London, U.K.

Crockett, R. N. (1972). The Transvaal System in Botswana: its geotectonic and depositional environment and special problems. Trans. Geol. Soc. S. Afr. **75**, 275-292.

Crow, C., and Condie, K. C. (1990). Geochemistry and origin of early Proterozoic volcanic rocks from the Transvaal and Soutpansberg successions, South Africa. Prec. Res. **47**, 17-26.

Davis, J. C. (1973). Statistics and Data Analysis in Geology. Wiley, New York.

Dewey, J. F. (1980). Episodicity, sequence, and style at convergent plate boundaries. In: The Continental Crust and its Mineral Deposits, (Ed. Strangeway, D. W.), Spec. Pap. Geol. Assoc. Canada **20**, 553-573.

Dewis, F. J., Levinson, A. A., and Bayliss, P. (1972). Hydrogeochemistry of the surface waters of the Mackenzie River drainage basin, Canada. IV. Boron-salinity clay mineralogy relationship in modern deltas. Geochim. cosmochim. Acta **36**, 1359-1375.

Doornbos, R., and Dijkstra, J. B. (1983). A multi sample test for equality of the coefficients of variation in normal distributions. Comm. Stat. Simul. Comp. **12**, 147-158.

Du Toit, A. L. (1954). The Geology of South Africa. Oliver and Boyd, Edinburgh, U.K.

Elderfield, H., and Greaves, M. J. (1982). The rare earth elements in sea water. Nature **296**, 214-219.

Elderfield, H., Hawkesworth, C. J., Greaves, M. J., and Calvert, S. E. (1981). Rare earth element geochemistry of oceanic ferromanganese nodules and associated sediments. Geochim. Cosmochim. Acta **45**, 513-528.

Engelbrecht, J. P. (1976). Meta-sediments of the Pretoria Group in the Enzelsberg area, Marico district. Trans. Geol. Soc. S. Afr. **79**, 61-71.

Engelbrecht, J. P. (1986). Die Bosveldkompleks en sy vloergesteentes in die omgewing van Nietverdiend, Wes-Transvaal. Ph.D. thesis (unpubl.), Univ. of Pretoria, Pretoria, South Africa.

Engel, A. E. J., Engel, C. G, and Havens, R. G. (1968). Chemical characteristics of oceanic basalts and the upper mantle. Bull. Geol. Soc. Am. **76**, 719-734.

Eriksson, K. A. (1973). The Timeball Hill Formation - a fossil delta. J. Sedim. Petrol. **43**, 1046-1053.

Eriksson, P. G. (1988a). The sedimentology of the Rooihoogte Formation, Transvaal Sequence. S. Afr. J. Geol. **91**, 477-489.

Eriksson, P. G. (1988b) A palaeoenvironmental review of The Pretoria Group, Transvaal Sequence. Geocongress '88 (Durban, South Africa): Abstracts, 187-190.

Eriksson, P. G. (1990). Rift-controlled sedimentation in the floor rocks of the Bushveld Complex. Geocongress '90 (Cape Town, South Africa): Abstracts.

Eriksson, P. G. (1992). On discriminating Precambrian marine and lacustrine basins: an example from the Early Proterozoic Pretoria Group. Geocongress '92 (Bloemfontein, South Africa): Abstracts, 113-115.

Eriksson, P. G., and Twist, D. (1986). A note on a lahar deposit in the Hekpoort Formation, Transvaal Sequence, near Pretoria. Trans. Geol. Soc. S. Afr. **89**, 415-418.

Eriksson, P. G., and Clendenin, C. W. (1990). A review of the Transvaal Sequence, South Africa. J.Afr.Earth Sci. **10**, 101-116.

Eriksson, P. G., and Reczko, B. F. F. (in press). Tectonic setting of the Pretoria Group, Transvaal Supergroup. Abstract Conf. 'Centennial Geocongress Geol. Soc. S. Afr.'.

Eriksson, P. G., Nixon, N., and Snyman, C. P. (1987). A study of upper Pretoria Group sedimentary rocks in contact with the Rustenburg Suite in the Buffelspoort Dam area, near Rustenburg. S. Afr. J. Geol. **90**, 124-136.

Eriksson, P. G., Meyer, R., and Botha, W. J. (1988). A hypothesis on the nature of the Pretoria Group basin. S. Afr. J. Geol. **91**, 490-497.

Eriksson, P. G., Labuschagne, H., and Engelbrecht, J. P. (1989). Stratigraphy, lithology and sedimentology of the Droogedal Formation, Transvaal Sequence, western Transvaal. S. Afr. J. Geol. **92**, 102-109.

Eriksson, P.G., Twist, D., Snyman, C. P., and Burger, L. (1990). The geochemistry of the Silverton Formation, Transvaal Sequence. S. Afr. J. Geol. **93**, 454-462.

Eriksson, P. G., Schreiber, U. M., and Van der Neut, M. (1991a). A review of the sedimentology of the Early Proterozoic Pretoria Group, Transvaal Sequence, South Africa: implications for tectonic setting. J. Afr. Earth Sci. **10**, 107-119.

Eriksson, P. G., Schreiber, U. M., and Van der Neut, M. (1991). A review of the sedimentology of the Early Proterozoic Pretoria Group, Transvaal Sequence, South Africa: implications for tectonic setting. Geocongress '91: Precambrian Sedimentary Basins of Southern Africa (Pretoria, South Africa), Abstracts, 12.

Eriksson, P. G., Schweitzer, J. K., Bosch, P. J. A., Schreiber, U. M., Van Deventer, J. L., and Hatton, C. J. (1993a). The Transvaal Sequence: an overview. J. Afr. Earth Sci. **16**, 25-51.

Eriksson, P. G., Schreiber, U. M., Van der Neut, M., Labuschagne, H., Van der Schyff, W., and Potgieter, G. (1993b). Alternative marine and fluvial models for the non-fossiliferous quartzitic sandstones of the Early Proterozoic Daspoort Formation, Transvaal Sequence of southern Africa. J. Afr. Earth Sci. **16**, 355-366.

Eriksson, P. G., Hattingh, P. J., and Altermann, W. (in press a). An Overview of the Transvaal Sequence and Bushveld Complex, South Africa. Min. Dep..

Eriksson, P. G., Engelbrecht, J. P., Res, M., and Harmer, R. E. (in press b). The Bushy Bend lavas, a new volcanic member of the Pretoria Group, Transvaal Sequence. S. Afr. J. Geol. **97**, 1-7.

Eriksson, P. G., Reczko, B. F. F., Merkle, R. K. W., Schreiber, U. M., Engelbrecht, J. P., Res, M., Snyman, C. P., and McNerney, N. (in press c). Early Proterozoic black shales of the Timeball Hill Formation, South Africa: Volcanogenic, biogenic and palaeoenvironmental influences. J. Afr. Earth Sci..

Eriksson, P. G., Reczko, B. F. F., and Piper, D. P. (under review a). The distribution of boron in the Early Proterozoic, Transvaal Supergroup, South Africa: geological implications. submitted to Geol. Mag.

Eriksson, P. G., Reczko, B. F. F., Boshoff, A. J., Schreiber, U. M., v. d. Neut, M., and Snyman, C. P. (under review b). Architectural elements from Lower Proterozoic braid-delta and high energy tidal flat deposits in the Magaliesberg Formation, Transvaal Supergroup, South Africa. submitted to Sed. Geol. (accepted for publication).

Ernst, W., and Werner, H. (1964). Anwendung der Bor-Methode in den geologischen Formationen zu ihrer besseren Unterteilung in wissenschaftlichem und praktischem Interesse sowie Untersuchungen über Bindung und Festlegung des Bors in natürlichen und künstlichen Sedimenten. Forsch.-Ber. Land Nordrhein.-Westf. **1433**, 1-27.

Ernst, W., Krejci-Graf, K., and Werner, H. (1958). Parallelisierung von Leithorizonten im Ruhrkarbon mit Hilfe des Borgehaltes. Geochim. Cosmochim. Acta **14**, 211-222.

Fairbridge, R. W. (1972). The encyclopedia of Geochemistry and Environmental Sciences. Van Nostrand Reinhold Company, New York.

Fairchild, I., Hendry, G., Quest, M., and Tucker, M. (1988). Chemical analysis of sedimentary rocks. In: Techniques in Sedimentology, (Ed. M. Tucker), Blackwell, Oxford, 274-354.

Feng, R., Kerrich, R., Maas, R. (1993). Geochemical, oxygen, and neodymium isotope compositions of metasediments from the Abitibi greenstone belt and Pontiac Subprovince, Canada: Evidence for ancient crust and Archaean terrane juxtaposition. Geochim. Cosmochim. Acta **57**, 641-658.

Fleet, A.J. (1984). Aqueous and sedimentay geochemistry of the rare earth elements. In: Rare Earth Element Geochemistry, (Ed. Henderson, P.), Developments in Geochemistry **2**, Elsevier, Amsterdam, 343-374.

Floyd, P. A., Winchester, J. A., and Park, R. G. (1989). Geochemistry and tectonic setting of Lewisian clastic metasediments from the Early Proterozoic Loch Maree Group of Gairloch, NW Scotland. Prec. Res. **45**, 203-214.

Floyd, P. A. (1991). Oceanic Basalts. Blackie - Van Nostrand Reinhold, Glasgow.

Frederickson, A. F., and Reynolds, R. C. (1960). How measuring palaeosalinity aids exploration. Oil and Gas J. **1**, 154-158.

Frick, C. (1967). The margin of the Bushveld Complex in the vicinity of De Berg, north of Dullstroom. M.Sc. thesis (unpubl.), Univ. of Pretoria, Pretoria, South Africa.

Friedrich, G. H., and Herzig, P. M. (1988). Base Metal Sulfide Deposits. Springer, Berlin - Heidelberg.

Fryer, B. J. (1977a). Trace element geochemistry of the Sokoman Iron Formation. Can. J. Earth Sci. **14**, 1598-1610.

Fryer, B. J. (1977b). Rare earth evidence in iron-formations for changing Precambrian oxidation states. Geochim. Cosmochim. Acta **41**, 361-367.

Füchtbauer, H. (1988). Sedimente und Sedimentgesteine. Schweitzerbart, Stuttgart.

Garcia, D., Coelho, J., and Perrin, M. (1991). Fractionation between TiO_2 and Zr as a measure of sorting within shale and sandstone series (Northern Portugal). Eur. J. Min. **3**, 401-414.

Garrels, R. M., and MacKenzie, F. T. (1971). Evolution of sedimentary rocks. Norton and Co., New York.

Garrett, R. G. (1983). Sampling Methodology. In: Handbook of Exploration Geochemistry, Vol. 2, (Ed. Govett, G. J. S.), Elsevier, Amsterdam, 83-110.

Garrett, R. G. (1993). Another cry from heart. Explore **81**, 9-14.

Gauert, C. D. K., de Waal, S. A., and Wallmach, T. (in press). The geology of the Uitkomst Complex, eastern Transvaal - Evidence for a magma conduit. Abstract Conf. 'Centennial Geocongress Geol. Soc. S. Afr.'.

German, C. R., and Elderfield, H. (1990) Application of the Ce anomaly as a paleoredox indicator: The ground rules. Paleoceanography **5**, 823-833.

Gill, J. B. (1981). Orogenic Andesites and Plate Tectonics. Springer, Berlin.

Gilmour, P. (1976). Some transitional types of mineral deposits in volcanic and sedimentary rocks. In: Handbook of Stratabound and Stratiform Ore Deposits, Vol. 1, (Ed. Wolf, K. H.), Elsevier, New York, 111-160.

Govett, G. J. S. (1983). Rock Geochemistry in Mineral Exploration. Handbook of Exploration Geochemistry, Vol. 3, Elsevier, Amsterdam.

Graf, J. L. (1978). Rare earth elements, iron formations and seawater. Geochim. Cosmochim. Acta **42**: 1845-1850

Gromet, L. P., Dymek, R. F., Haskin, L. A., and Korotev, R. L. (1984). The "North American shale composite": Its compilation, major and trace element characteristics. Geochim. Cosmochim. Acta **48**, 2469-2482.

Guilbert, J. M., and Park, C. F. (1986). Ore Deposits. Freeman and Co, New York.

Hammerbeck, E. C. I. (1976). Gold outside the Witwatersrand triad. In: Mineral Resources of the Republic of South Africa, Handbook 7, (Ed. C.B. Coetzee), Department of Mines, Geological Survey of South Africa, Pretoria, South Africa, pp 75-92

Harder, H. (1959). Beitrag zur Geochemie des Bors. Teil II: Bor in Sedimenten: Nachdrucke der Akademie der Wissenschaften Göttingen, II., Mathematisch-physikalische Klasse, II, **6**, p. 123.

Harder, H. (1963). Inwieweit ist das Bor ein marines Indexelement? Fortschr. Geol. Rheinl. Westf. **10**, 239.

Harder, H. (1974a). Boron: Abundance in rock-forming minerals, boron-minerals. In: Handbook of Geochemistry, Vol. II/I: Elements H (1) to Al (13), (Ed. K.H. Wedepohl), Springer, Heidelberg, p. 5-D-1 to 5-D-6.

Harder, H. (1974b). Boron: Abundance in common igneous rock types. In: Handbook of Geochemistry, Vol. II/I: Elements H (1) to Al (13), (Ed. K.H. Wedepohl), Springer, Heidelberg, p. 5-E-1 to 5-E-10.

Harder, H. (1974c). Boron: Abundance in natural waters and in the atmosphere. In: Handbook of Geochemistry, Vol. II/I: Elements H (1) to Al (13), (Ed. K.H. Wedepohl), Springer, Heidelberg, p. 5-I-1 to 5-I-3.

Harder, H. (1974d). Boron: Abundance in common sediments and sedimentary rock types. In: Handbook of Geochemistry, Vol. II/I: Elements H (1) to Al (13), (Ed. K.H. Wedepohl), Springer, Heidelberg, p. 5-K-1 to 5-K-13.

Harder, H. (1974e). Boron: Behaviour in metamorphic reactions. In: Handbook of Geochemistry, Vol. II/I: Elements H (1) to Al (13), (Ed. K.H. Wedepohl), Springer, Heidelberg, p. 5-N-1.

Harley and Charlesworth (1993). Formation of bedding-parallel, thrust-hosted gold deposits, Sabie-Pilgrim's Rest goldfield, eastern Transvaal: The role of fluid pressure. EGRU Inf. Circ. **263**, University of the Witwatersrand, Johannesburg, South Africa.

Harmer, R. E., and v. Gruenewaldt, G. (1991). A review of magmatism associated with the Transvaal Basin - implication for its tectonic setting. S. Afr. J. Geol. **94**, 104-122.

Hartzer, F. J. (1989). Stratigraphy, structure, and tectonic evolution of the Crocodile River Fragment. S. Afr. J. Geol. **92**, 110-124.

Hatton, C. J., and Sharpe, M.R. (1988). Significance and origin of boninite-like rocks associated with the Bushveld Complex. In: Bononites (Ed. Crawford, A.J.), 174-207, Unwin Hyman, London, U.K.

Hatton, C. J., and von Grünewaldt, G. (1990). Early Precambrian layered intrusions. In: Early Precambrian Basic Magmatism (Eds.: Hall, R.P. & Hughes, D.J.), 56-82, Blackie and Son, London, U.K.

Hellman, P. L., Smith, R. E., and Henderson, P. (1977). Rare Earth Element Investigation of the Cliefden Outcrop, N.S.W., Australia. Contrib. Mineral. Petrol. **65**, 155-164.

Hellman, P. L., Smith, R. E., and Henderson, P. (1979). The Mobility of Rare Earth Elements: Evidence and Implications From Selected Terrains Affected by Burial Metamorphism. Contrib. Mineral. Petrol. **71**, 23-44.

Henderson, P. (1984). Rare Earth Element Geochemistry. Developments in Geochemistry **2**, Elsevier, Amsterdam.

Hiemstra, S. A., and van Biljon, W. J. (1959). The geology of the upper Magaliesberg Stage and the lower Bushveld Complex in the vicinity of Steelpoort. Trans. Geol. Soc. S. Afr. **62**, 239-255.

Hill, M. (1975). Correspondence analysis: a neglected multivariate method. J. R. Statist. Soc., Ser. C, **23**, 340-354.

Hofmann, A. W. (1988). Chemical differentiation of the Earth: the relationship between mantle, continental crust, and oceanic crust. Earth Planet. Sci. Lett. **90**, 297-314.

Holland, H. D. (1984). The Chemical Evolution of the Atmosphere and Oceans. Princeton University Press, Princeton.

Hopf, S. (1993). Behaviour of rare earth elements in geothermal systems of New Zealand. J. Geochem. Explor. **47**, 333-357.

Humphries, S. E. (1984). The mobility of rare earth elements in the crust. In: Rare Earth Element Geochemistry, (Ed. Henderson, P.), Developments in Geochemistry **2**, Elsevier, Amsterdam, 317-342.

Ingersoll, R. V., Kretchmer, A. G., and Valles, P. K. (1993). The effect of sampling scale on actualistic sandstone petrofacies. Sedimentology **40**, 937-953.

Jöreskog, K. G., Klovan, J. E., and Reyment, R. A. (1976). Geological Factor Analysis. Elsevier, Amsterdam.

Key, R. M. (1983). The geology of the area around Gabarone and Lobatse, Kweneng, Kgatleng, Southern and South East Districts. District Memoir Geol.Surv. Botswana **5**.

Klop, A. A. C. (1978). The metamorphosed sediments of the Pretoria Group and the associated rocks northwest of Zeerust, western Transvaal. M.Sc. thesis (unpubl.), Univ. of Pretoria, Pretoria, South Africa.

Kunzendorf, H., Stoffers, P., and Gwozdz, R. (1988). Regional variations of REE patterns in sediments from active plate boundaries. Marine Geol. **84**, 191-199.

Kunzendorf, H., Glasby, G. P., Stoffers, P., and Plüger, W. L. (1993). The distributionof rare earth and minor elements in manganese nodules, micronodules and sediments along an east-west transect in the southern Pacific. Lithos **30**, 45-56.

Landergren, S., and Carvajal, M. C. (1969). Geochemistry of boron, III: The relationship between boron concentration in marine clay sediments expressed as an adsorption isotherm. Arkiv för Mineralogi och Geologi, **5**, 13.

Large, D. (1988). The Evaluation of Sedimentary Basins for Massive Sulfide Mineralization. in: Base Metal Sulfide Deposits (eds. Friedrich, G.H., and Herzig, P.M.), Springer, Berlin, 3-11.

Laskowski, N., and Kröner, A. (1985). Geochemical characteristics of Archaean and Late Proterozoic to Palaeozoic fine-grained sediments from southern Africa and significance for the evolution of the continental crust. Geol. Rundsch. **74**, 1-9.

Leblanc, M., and Billaud, P. (1978). A volcano-sedimentary copper deposit on a continental margin of upper Proterozoic age: Bleïda, Anti-Atlas, Morocco. Econ. Geol. **73**, 1101-1111.

Lelong, F., Tardy, Y., Grandin, G., Trescases, J. J., and Boulange, B. (1976). Pedogenesis, chemical weathering, and processes of formation of some supergene ore deposits. In: Handbook of Stratabound and Stratiform Ore Deposits, Vol. 6, (Ed. Wolf, K. H.), Elsevier, New York, 111-160.

Le Maitre, R. W. (1982). Numerical Petrology. Developements in Petrology 8, Elsevier, Amsterdam.

Le Maitre, R. W. (1984). A proposal by the IUGS sub-commision on the systematics of igneous rocks for a chemical classification of volcanic rocks based on the total alkali silica (TAS) diagram. Australian L. Earth Sci. **31**, 243-255.

Lisitsyn, A. E., and Khitrov, V. G. (1962). A microspectrochemical study of the distribution of boron in minerals of some igneous and metamorphic rocks in the Middle Urals. Geochemistry **3**, 293.

Loughan, F. C. (1969). Chemical Weathering of the Silicate Minerals. Elsevier, Amsterdam.

Lowe, D. R. (1982). Sediment gravity flows: II. Depositional models with special reference to the deposits of high-density turbidity currents. J. Sedim. Petrol. **52**, 279-297.

Ludden, J. N., and Thompson, G. (1978). Behaviour of rare earth elements during submarine weathering of tholeiitic basalts. Nature **274**, 147-149.

Ludden, J. N., and Thompson, G. (1979). An evaluation of the behaviour of the rare earth elements during the weathering of sea-floor basalt. Earth. Plet. Sci. Lett. **43**, 85-92.

Manson, V. (1967). Geochemistry of basaltic rocks: major elements. In: Basalts, (Eds. Hess, H. H., and Poldervaart, A.), Interscience Publishers, New York, 215-269.

Martini, J. E. J. (1990). An Early Proterozoic Playa in the Pretoria Group, Transvaal, South Africa. Prec. Res. **46**, 341-351.

Maynard, J. B. (1983). Geochemistry of sedimentary ore deposits. Springer, New York.

McLennan, S. M. (1989). Rare earth elements in sedimentary rocks: Influence of provenance and sedimentary processes. In: Geochemistry and Mineralogy of Rare earth elements, (Eds. Lipin, B. R., and McKay), Rev. Mineral. **21**, 169-200.

McLennan, S. M., and Taylor, S. R. (1988). Crustal evolution: Comments on "The Archean-Proterozoic transition: Evidence from the geochemistry of metasedimentary rocks from Guyana and Montana" by A. K. Gibbs, C. W. Montgomery, P. A. O'Day and E. A. Erslev. Geochim. Cosmochim. Acta **52**, 785-787.

McLennan, S. M., Fryer, B. J., and Young, G. M. (1979). Rare earth elements in Huronian (Lower Proterozoic) sedimentary rocks: composition and evolution of the post-Kenoran upper crust. Geochim. Cosmochim. Acta **43**, 375-388.

McLennan, S. M., Taylor, S. M., and Kröner, A. (1983). Geochemical evolution from Archean shales from South Africa: I. The Swaziland and Pongola Supergroups. Prec. Res. **22**, 93-124.

McNemar, Q. (1969). Psychological Statistics. Wiley, New York.

Meisch, A. T. (1969). The constant sum problem in geochemistry. In: Computer Applications in the Earth Sciences, (Ed. Merriam, D. F.), 161-176.

Meissner, K. H. (1987). Resources of brick clay, building sand and coarse aggregate in the Pretoria area. Bull. Geol. Surv. S. A. **84**, 33 pp.

Menzies, M., Blanchard, D., and Jacobs, J. (1977). Rare earth and trace element geochemistry of metabasalts from the Point Sal Ophiolite, California. Earth Plan. Sci. Lett. **37**, 203-215.

Merkle, R. K. W., and v. Gruenewaldt, G. (1986). Compositional variation of Co-rich pentlandite: Relation to the evolution of the Upper Zone of the Western Bushveld Complex, South Africa. Canad. Min. **24**, 529-546.

Miall, A. D. (1984). Principles of Sedimentary Basin Analysis. Springer, New York.

Michard, A. (1989). Rare earth element systematics in hydrothermal fluids. Geochim. Cosmochim. Acta **53**, 745-750.

Murray, R. W., and Leinen, M. (1993). Chemical transport to the seafloor of the equatorial Pacific Ocean across a latitudinal transect at 135°W: Tracking sedimentary major, trace, and rare earth element fluxes at the Equator and the Intertropical Convergence Zone. Geochim. Cosmochim. Acta **57**, 4141-4163.

Myers, R. E., Cawthorn, R. G., McCarthy, T. S., and Anhaeusser, C. R. (1987). Fundamental uniformity in trace element patterns of the volcanics of the Kaapvaal Craton from 3000 to 2100 Ma: evidence for the lithospheric origin of these continental tholeiites. In: Geochemistry and Mineralization of Proterozoic Volcanic Suites, (Eds. Pharao, T. C., Beckinsale, R. D., and Rickard, D.), Blackwell, Oxford, 315-326.

Nel, W. A. (1968). The estimation and distribution of boron in fine grained South African sediments. M.Sc. thesis (unpubl.), Univ. of Cape Town, Cape Town, South Africa.

Nesbit, H.W. (1979). Mobility and fractionation of rare earth elements during weathering of a granodiorite. Nature **279**, 206-210.

Nesbit, H. W., and Young, G. M. (1982). Early Proterozoic climates and plate motions inferred from major element chemistry of lutites. Nature **299**, 715-717.

Nesbit, H. W., and Young, G. M. (1989). Formation and diagenesis of weathering profiles. J. Geol. **97**, 129-147.

Nesbit, H. W., Markovics, G., and Price, R. C. (1980). Chemical processes affecting alkalies and alkaline earths during continental weathering. Geochim. Cosmochim. Acta **44**, 1659-1666.

Nilsen, T. H., and Kerr, D.R. (1978). Paleoclimatic and paleogeographic implications of a lower Tertiary laterite (latosol) on the Iceland-Faeroe Ridge, North Atlantic region. Geol. Mag. 115, 153-182.

Nixon, N., Eriksson, P. G., Jacobs, R., and Snyman, C. P. (1988). Early Proterozoic micro-algal structures in carbonaceous shales of the Pretoria Group, southwest of Potchefstroom. S. Afr. J. Sci. **84**, 592-595.

Owen, R. M., and Olivarez, A. M. (1988). Geochemistry of Rare Earth Elements in Pacific Hydrothermal Sediments. Marine Chem. **25**, 183-190.

Pearce, J. A. (1983). Role of the sub-continental lithosphere in magma genesis at active continental margins. In: Continental Basalts and Mantle Xenoliths, (Eds. Hawkesworth, C.J., and Norry, M. J.), Shiva Publ., Nantwich.

Pearce, J. A., and Norry, M. J. (1979). Petrogenic implications of Ti, Zr, Y, and Nb variations in volcanic rocks. Contrib. Mineral Petrol. **69**, 33-47.

Pearce, T. H., Gorman, B. E., and Birkett, T. C. (1975). The TiO_2-K_2O-P_2O_5 diagram: a method of discriminating between oceanic and non-oceanic basalts. Earth Planet. Sci. Lett. **24**, 419-426.

Pettijohn, F. J., Potter, P. E., and Siever, R. (1972). Sand and sandstone. Springer, New York.

Piper, D. Z. (1974). Rare earth elements in the sedimentary cycle: a summary. Chem. Geol. 14, 285-304.

Piper, D. P., and Kreimeyer, R. (1992). The Sengoma Quartzite Formation and the upper part of the Sengoma Argillite Formation at Tsinane Hill, Lobatse: Results from stratigraphic borehole LES1. Report Geological Survey Botswana (unpubl.), Lobatse, Botswana.

Porrenga, D. H. (1967). Influence of grinding and heating of layer silicates on boron sorption. Geochim. Cosmochim. Acta **31**, 309-312.

Posamentier, H. W., Summerhayes, C. P., Haq, B. U., and Allen, G. P. (Eds.)(1993). Sequence Stratigraphy and Facies Associations. Spec. Publ. Int. Assoc. Sedim. **18**, Blackwell, Oxford.

Potter, P. E. (1986). South America and a few grains of sand: part I - beach sands. J. Geol. **94**, 301-319.

Potter, P. E., Shimp, N. F., and Witters, J. (1963). Trace elements in marine and fresh-water argillaceous sediments. Geochim. Cosmochim. Acta **27**, 669-694.

Prame, W. K. B. N., and Pohl, J. (1994). Geochemistry of pelitic and psammopelitic Precambrian metasediments from southwestern Sri Lanka: implications for two contrasting source-terrains and tectonic settings. Prec. Res. **66**, 223-244.

Press, W. H., Flannery, B. P., Teukolsky, S. A., and Vetterling, W. T. (1988). Numerical Recipes. Cambridge University Press, Cambridge.

Reczko, B. F. F. (1992). The stratigraphy of the lower Pretoria Group in the Kanye basin and its relationships to the stratigraphy of the Transvaal basin. Report to Jwaneng Diamond Mine, DEBSWANA (unpubl.).

Reczko, B. F. F., Eriksson, P. G., and Snyman, C. P. (1992). Geochemistry of shales interbedded in the Magaliesberg Formation, Pretoria Group, near Pretoria: palaeoenvironmental and diagenetic implications. Geocongress '92 (Bloemfontein, South Africa): Abstracts, 305-307.

Reczko, B. F. F., Eriksson, P. G., and Snyman, C. P. (1994). Mississippi Valley-type F-Zn-Pb mineralization in the Transvaal Supergroup, Kaapvaal Craton. Conference 'Proterozoic Crustal Evolution & Metallogeny' (Windhoek, Namibia): Abstracts.

Reczko, B. F. F., Eriksson, P. G., and Snyman, C. P. (in press). Some evidence for the base-metal potential of the Pretoria Group: stratigraphic targets, tectonic setting and REE patterns. Min. Dep.

Retallack, G. J. (1986). The fossil record of soils. In: Paleosols - their recognition and interpretation, (Ed. Wright, V. P.), Princeton University Press, Princeton, 1-57.

Retallack, G. J., and Krinsley, D. H. (1993). Metamorphic alteration of a Precambrian (2.2 Ga) paleosol from South Africa revealed by backscattered electron imaging. Prec. Res. **63**, 27-41.

Reynolds, R. C. (1965). The concentration of boron in Precambrian seas. Geochim. Cosmochim. Acta **29**, 1-16.

Reynolds, R. C. (1972). Boron: Element and geochemistry. In: The encyclopedia of Geochemistry and Environmental Sciences, (Ed. R.W. Fairbridge), Van Nostrand Reinhold Company, New York, 88-99.

Reynolds, R. C., and Johnson, N. M. (1972). Chemical weathering inthe temperate glacial environment of the Northern Cscade Mountains. Geochim. Cosmochim. Acta **36**, 537-554.

Richards, R. J., and Eriksson, P. G. (1988). The sedimentology of the Pretoria Group in selected areas of the northern portion of the Rooiberg Fragment. S. Afr. J. Geol. **91**, 498-508.

Rhodes, R. C. (1971). Palaeocurrents in the Pretoria Group north of Marble Hall, Transvaal. Ann. Geol. Surv. S. Afr. **9**, 119-120.

Robertson, A. H. F., and Fleet, A. J. (1976). The origins of rare earth in metalliferous sediments of the Troodos Massif, Cyprus. Earth Planet. Sci. Lett. 28, 385-394.

Rollinson, H. R. (1992). Another look at the constant sum problem in geochemistry. Min. Mag. **56**, 469-475.

Ronov, A. B., and Migdisov, A. A. (1971). Geochemical history of the crystalline basement and the sedimentary cover of the Russian and North American platforms. Sedimentology **16**, 137-185.

Ronov, A. B., Migdisov, A. A., and Lobach-Zhuchenko, S. B. (1977). Regional metamorphism and sediment composition evolution. Geochem. Int. **14**, 90-112.

Roser, B. P., and Korsch, R. J. (1986). Determination of tectonic setting of sandstone-mudstone suites using SiO_2 content and K_2O/Na_2O ratio. J. Geol. **94**, 635-650.

Roser, B. P., and Korsch, R. J. (1988). Provenance signatures of sandstone-mudstone suites determined by using discriminant function analysis of major element data. Chem. Geol. **67**, 119-139.

Rösler, H. J., and Lange, Horst (1976). Geochemische Tabellen. Enke, Stuttgart.

Ruhlin, D. E., and Owen, R. M. (1986). The rare earth element geochemistry of hydrothermal sediments from the East Pacific Rise: Examination of a seawater scavenging mechanism. Geochim. Cosmochim. Acta 50, 393-400.

Sachs, L. (1982). Applied Statistics. Springer, New York.

Sachs, L. (1992). Angewandte StatistiK. Springer, Berlin.

Saunders, A. D., and Tarney, J. (1984). Geochemical characteristics of basaltic volcanism within back-arc basins. In: Marginal Basin Geology, (Eds. kokelaar, B. P., and Howells, M. F.), Geol. Soc. Spec. Publ. **16**, 59-76.

Sawyer, E. W. (1986). The influence of source rock type, chemical weathering and sorting on the geochemistry of clastic sediments from the Quetico Metasedimentary Belt, Superior Province, Canada. Chem. Geol. **55**, 77-95.

Schau, M., and Henderson, J. B. (1983). Archean chemical weathering at three localities on the Canadian Shield. Prec. Res. **20**, 189-224.

Schopf, T. J. (1980). Paleoceanography. Harvard University Press, Cambridge.

Schreiber, U. M. (1990). A palaeoenvironmental study of the Pretoria Group in the eastern Transvaal. Ph.D. thesis (unpubl.), Univ. of Pretoria, Pretoria, South Africa.

Schreiber, U. M., and Eriksson, P. G. (1992). The sedimentology of the post-Magaliesberg formations of the Pretoria Group, Transvaal Sequence, in the eastern Transvaal. S. Afr. J. Geol. **95**, 1-16.

Schreiber, U. M., Eriksson, P. G., Meyer, P. C., and Van der Neut, M. (1990). The sedimentology of the Boshoek Formation, Transvaal Sequence. S. Afr. J. Geol. **93**, 567-573.

Schreiber, U. M., Eriksson, P. G., Van der Neut, M., and Snyman, C. P. (1992). Sedimentary petrography of the Early Proterozoic Pretoria Group, Transvaal Sequence, South Africa: implications for tectonic setting. Sedim. Geol. **80**, 89-103.

Schröcke, H., and Weiner, K. L. (1981). Mineralogie. De Gruyter, Berlin.

Schweigart, H. (1963). Untersuchungen der Eisenerze der Pretoria Serie im Transvaal mit spezieller Berücksichtigung ihrer Genese. Ph.D. thesis (unpubl.), Ludwig-Maximilian-Universität München, München, Germany.

Schweigart, H. (1965). Genesis of the iron ores of the Pretoria Series, South Africa. Econ. Geol. **60**, 269-299.

Schweitzer, J. K. (1986). Field and geochemical investigations of the Dullstroom and Rooiberg volcanic rocks. Geocongress '86 (Johannesburg, South Africa): Abstracts, 873-876.

Schweitzer, J. K. (1992). Alteration processes within the volcanic floor and roof rocks of the Bushveld Complex. Geocongress '92 (Bloemfontein, South Africa): Abstracts, 857-859.

Seim, R. (1990). Geochemie der Sedimentite. In: Grundlagen der Geochemie, (Eds. Seim, R., and Tischendorf, G.), VEB Dt. Verlag für Grundstoffindustrie, Leipzig, 347-398.

Seim, R., and Tischendorf, G. (1990). Grundlagen der Geochemie. VEB Dt. Verlag für Grundstoffindustrie, Leipzig.

Sharpe, M. R. (1984). Petrography, classification and chronology of mafic sill intrusions beneath the eastern Bushveld Complex. Geol. Surv. S. Afr. Bull. **77**.

Sharpe, M. R., Brits, R., and Engelbrecht, J. P. (1983). Rare earth and trace element evidence pertaining to the petrogenesis of 2.3 Ga old continental andesites and other volcanic rocks from the Transvaal Sequence, South Africa. Inst. Geol. Res. Bushveld Complex, Research Report **40**, University of Pretoria, Hillcrest.

Shaw, D. M., and Bugry, R. (1966). A review of boron sedimentary geochemistry in relation to new analyses of some North American shales. Can. J. Earth Sci. **3**, 49.

Sholkovitz, E. R., Landing, W. M., and Lewis, B. L. (1994). Ocean particle chemistry: The fractionation of rare earth elements between suspended particles and seawater. Geochim. Cosmochim. Acta **58**, 1567-1579.

Smith, A. D. (1991). Reply to the comment by A. P. Boyle and R. K. Westhead. Min. Dep. **26**, 242-244.

South African Committee for Stratigraphy (SACS) (1980). Stratigraphy of South Africa, part 1: Lithostratigraphy of the Republic of South Africa, South West Africa/Namibia and the Republics of Bophuthatswana, Trankei and Venda. Handbook Geol. Surv. S. Afr. **8**.

Spears, D. A. (1974). Relationship between water-soluble cations and paleosalinity. Geochim Cosmochim. Acta **38**, 567-575.

Stanton, R. L. (1972). Ore Petrology. McGraw-Hill, New York

Sun, S. S., and McDonough, W. F. (1989). Chemical and isotopic systematics of ocean basalts: implications for mantle compositions and processes. In: Magmatism in the Ocean Basins, (Eds. Saunders, A. D., and Norry, M. J.), Geol. Soc. Spec. Publ. **42**, 313-345.

Tankard, A. J.; Jackson, M. P. A.; Eriksson, K. A.; Hobday, D. K.; Hunter, D. R.; Minter, W. E. L. (1982). Crustal Evolution of Southern Africa. Springer Verlag, New York.

Taylor, S. R., and White, A. J. R. (1965). Geochemistry of andesites and the growth of continents. Nature **208**, 271-273.

Taylor, S. R., and McLennan, S. M. (1981). The composition and evolution of the continental crust: rare earth element evidence from sedimentary rocks. Phil. Trans. Roy. Soc. **A301**, 381-?.

Taylor, S. R., and McLennan, S. M. (1985). The Continental Crust: its Composition and Evolution. Blackwell, Oxford.

Tucker, M. (1988). Techniques in Sedimentology. Blackwell, Oxford, 274-354.

Turekian, K. K., and Wedepohl, K. H. (1961). Distribution of the elements in some major units of the earth's crust. Geol. Soc. Am. Bull. **72**, 175-192.

Turner, J. T. (1981). Metamorphic Petrology. 2nd ed., McGraw-Hill, New York.

Valeton, I. (1988). Verwitterung und Verwitterungslgerstätten. In: Sedimente und Sedimentgesteine, (Ed. Füchtbauer, H.), Schweitzerbart, Stuttgart, 11-68.

Van Biljon, S. (1950). The transformation of the upper part of the Pretoria Series in the Bushveld Igneous Complex. Trans. Geol. Soc. S. Afr. **52**, 1-175.

Van de Kamp, P. C., Leake, B. E., and Senior, A. (1976). The petrography and geochemistry of some Californian arkoses with application to identifying gneisses of metasedimentary origin. J. Geol. **84**, 195-212.

Van Der Neut, M. (1990). Afsettingstoestande van die Pretoria Group grsteentes in die Pretoria-Bronkhorstspruit-Delmas gebied. M.Sc. thesis (unpubl.), Univ. of Pretoria, Pretoria, South Africa.

Veizer, J. (1988). Continental growth: Comments on "The Archean-Proterozoic transition: Evidence from the geochemistry of metasedimentary rocks from Guyana and Montana" by A. K. Gibbs, C. W. Montgomery, P. A. O'Day and E. A. Erslev. Geochim. Cosmochim. Acta **52**, 789-792.

Verryn, S. M. C., Merkle, R. K. W., and v. Gruenewaldt, G. (1991). Gold- and associated ore minerals of the Waaikraal Deposit, northwest of Brits, Bushveld Complex. Eur. J. Min. 3, 451-466.

Visser, D. J. L. (1957). The structural evolution of the union. Trans. Geol. Soc. S. Afr. **60**, 13-49.

Visser, J. N. J. (1969). "n Sedimentologiese studie van die Serie Pretoria in Transvaal. Ph.D. thesis (unpubl.), Univ. of Orange Free State, Bloemfontein.

Visser, J. N. J. (1971). The deposition of the Griquatown Glacial Member in the Transvaal Supergroup. Trans. Geol. Soc. S. Afr. **74**, 187-199.

Visser, J. N. J. (1972). The Timeball Hill Formation at Pretoria -a prograding shoreline deposit. Ann. Geol. Surv. S. Afr. **9**, 115-118.

Vivallo, W., and Claesson, L.-A. (1987). Intra-arc rifting and massive sulphide mineralization in an early Proterozoic volcanic arc, Skellefte district, northern Sweden. In: Geochemistry and Mineralization of Proterozoic Volcanic Suites, (Eds. Pharao. T. C., Beckinsale, R. D., and Rickard, D.), Blackwell, Oxford, 69-79.

Von Grünewaldt, G., and Harmer, R. E. (1993). Tectonic setting of Proterozoic Layered Intrusions with special reference to the Bushveld Complex. In: Proterozoic Crustal Evolution, (Ed. Condie, K. C.), Elsevier, Amsterdam, 181-213.

Wagner, P. A. (1928). The iron deposits of the Union of South Africa. Mem. 26, Geol. Surv. S. Afr., Pretoria, South Africa.

Walker, C. T., and Price, N. B. (1963). Departure curves for computing paleosalinity from boron in illites and shales. Bull. AAPG **47**, 833-841.

Wallmach, T., Hatton, C. J., and Droop, G. T. R. (1989). Extreme facies of contact metamorphism developed in calc-silicate xenoliths in the eastern Bushveld Complex. Canad. Min. **27**, 509-523.

Weaver, C. E. (1969). Potassium, illite and the ocean. Geochim. Cosmochim. Acta **31**, 2181-2196.

Weaver, C. E. (1989). Clays, Muds, and Shales. Developments in Sedimentology **44**, Elsevier, Amsterdam.

Wedepohl, K. H. (1969-1978). Handbook of Geochemistry. Springer, Heidelberg.

White, R. (1991). Structure of the oceanic crust from geophysical measurements. In: Oceanic Basalts, (Ed. Floyd, P. A.), Blackie - Van Nostrand Reinhold, Glasgow, 30-48.

Wilgus, C. K., Ross, C. A., Posamentier, H., and Kendall, C. G. St. C. (Eds.)(1988). Sea-level changes: An integrated approach. SEPM Spec. Publ. **42**, Tulsa.

Williams, N. (1978). Studies of the base metal sulfide deposits at McArthur River, Northern Territory, Australia: II. The sulfide-S and organic-C relationships of the concordant deposits and their significance. Econ. Geol. **73**, 1036-1056.

Winchester, J. A., and Floyd, P. A. (1977). Geochemical discrimination of different magma series and their differentiation products using immobile elements. Chem. Geol. **20**, 325-343.

Winter, H. De la R. (1989). A tectonic classification of certain South African depositional basins and criteria for recognition of major unconformity-bounded sequences. S. Afr. J. Geol. **92**, 167-182.

Winter, H. De la R. (1991). Basin Analysis. Short Course Notes, Geocongress '91: Precambrian Sedimentary Basins of Southern Africa (Pretoria, South Africa)

Wolf, K. H. (ed). Handbook of Stratabound and Stratiform Ore Deposits. Vol. 1, Elsevier, New York.

Wood, D. A., Joron, J. L., Treuil, M., Norry, M., and Tarney, J. (1979). Elemental and Sr isotope variations in basic lavas from Iceland and the surrounding ocean floor: The nature of mantle source inhomogeneites. Contrib. Mineral Petrol. **70**, 319-339.

Woronow, A. (1987). The statistical analysis of compositional data by John Aitchison (Book review). Math. Geol. **19**, 579-581

Wronkiewicz, D. J., and Condie, K. C. (1989). Geochemistry and provenance of sediments from the Pongola Supergroup, South Africa: Evidence for a 3.0-Ga-old continental craton. Geochim. Cosmochim Acta **53**, 1537-1549.

Wronkiewicz, D. J., and Condie, K. C. (1990). Geochemistry of Archean shales from the Witwatersrand Supergroup, South Africa: Source-area weathering and provenance. Geochim. Cosmochim Acta **51**, 2401-2416.

Wronkiewicz, D. J., and Condie, K. C. (1990). Geochemistry and mineralogy of sediments from the Ventersdorp and Transvaal Supergroups, South Africa: Cratonic evolution during the early Proterozoic. Geochim. Cosmochim. Acta **54**, 343-354.

Zawada, P. K. (1988). Trace elements as possible palaeosalinity indicators for the Ecca and Beaufort Group mudrocks in the southwestern Orange Free State. S. Afr. J. Geol. **91**, 18-26.